SOVIET PHYSICS

JETP

A translation of Zhurnal Éksperimental'noĭ i Teoreticheskoĭ Fiziki.

Vol. 12, No. 4 pp. 627-817 (Russ. orig. Vol. 39, No. 4, pp. 905-1174, Oct., 1960) April, 1961

INVESTIGATION OF THE EQUILIBRIUM CHARGE DISTRIBUTION IN A FAST ION BEAM

V. S. NIKOLAEV, I. S. DMITRIEV, L. N. FATEEEVA, and Ya. A. TEPLOVA

Institute of Nuclear Physics, Moscow State University

Submitted to JETP editor April 13, 1960

J. Exptl. Theoret. Phys. (U.S.S.R.) **39**, 905-914 (October, 1960)

The equilibrium distribution of charges in beams of light ions ($Z = 2 - 18$) and krypton ions that have passed through He, N_2, Ar, Kr, and a celluloid film, has been measured for velocities $v \sim 2.6 \times 10^8$ cm/sec and higher. Some new information has been obtained on the dependence of the mean charge $\bar{i}$ and the distribution width σ on the velocity of the ions, on the charge of their nucleus, and on the medium. Significant differences in the values of $\bar{i}$ in various gases have been found for all types of ions. Thus, for ions with $Z > 10$ the value of $\bar{i}$ in a celluloid film exceeds that in gases by 1.6 to 2.3 times. Appreciable deviations from a smooth dependence of $\bar{i}$ and σ on Z have been detected in the region $Z \sim 10 - 12$.

1. INTRODUCTION

AN investigation of the equilibrium distribution of charges in a beam of light ions with atomic numbers Z ranging from 5 to 10, passing through hydrogen, air, argon, and a celluloid film, has established[1] a monotonic dependence of the average charge $\bar{i}$ in the gases on Z, and has disclosed that $\bar{i}$ varies with the medium. Since a violation of the monotonic dependence of $\bar{i}$ on Z can be expected on going from one period in the periodic system to another, we have measured in the present investigation the equilibrium distribution of charges for a much larger number of ions, namely helium, lithium, boron, nitrogen, neon, sodium, magnesium, aluminum, phosphorus, argon, and krypton. To determine the variation of $\bar{i}$ with the medium, we measured the equilibrium distributions of these ions in helium, nitrogen, argon, krypton, and celluloid film. The results for the ions of helium, boron, nitrogen, and neon were obtained in a larger velocity interval than in reference 1. The measurements for ions with $Z > 10$ were made at a velocity $v = 2.6 \times 10^8$ cm/sec, and additional measurements at $v = 4.10 \times 10^8$ cm/sec have been made for sodium, phosphorus, and argon.

2. DESCRIPTION OF THE EXPERIMENT

Two multiply-charged ions were accelerated in a 72-cm cyclotron.[2] The extracted and focused ion beam was confined near the focus by two slits 1 cm wide, placed 30 cm apart. To obtain ions with different charges, a thin celluloid film approximately 2 $\mu g/cm^2$ thick was placed in the path of the beam near the first slit. On passing through the films, ions of initial charge i were transformed into ions with charges $i \pm 1$, $i \pm 2$, etc through electron loss and capture. At low velocities, a considerable number of such ions was obtained by charge exchange between the beam and the residual gas in the ion line past the focusing magnet.

Ions of a specified charge were deflected by an analyzing magnet into a special charge-exchange chamber 40 cm long equipped with input and output channels of 2×5 mm cross section and approximately 30 mm long. In the investigation of

the equilibrium distributions of the charges in gases, a channel 7 × 0.7 mm, 310 mm long, was placed in the charge-exchange chamber along the ion path, and the gas was fed continuously to the center of this channel. The average pressure in this channel was 200 — 800 times greater than the pressure in the volumes before and after the charge-exchange chamber, and could be set at the value necessary to establish equilibrium distribution. To monitor the equilibrium state, the measurements were performed at different initial charges and at several gas pressures that differed by 1.5 or 2 times. The thickness of the layer of nitrogen or heavier gas necessary to establish equilibrium distribution was on the order of 0.5×10^{16} molecules/cm^2 at an ion velocity $v \sim 3 \times 10^8$ cm/sec, and was one order of magnitude higher at $v \sim 10^9$ cm/sec. The corresponding thickness of the helium layer was $\sim 2 \times 10^{16}$ and 5×10^{17} molecules/cm^2, respectively. The impurities in the helium, nitrogen, and argon employed amounted to less than 0.5%. The krypton contained 7% of xenon. The fraction of the residual gas in the channel, at a pressure corresponding to the equilibrium state, did not exceed 0.5%.

To obtain equilibrium charge distribution for ions passing through a celluloid film, the channel along the path of the beam was replaced by one or two thin celluloid films placed 2 cm ahead of the exit channel of the charge-exchange chamber. The film thickness, measured with a microphotometer,[3] was $\sim 2 - 5$ μg/cm^2. The ion velocity changed little on going through such films, and consequently the charge distribution was hardly different after passing through one or two films, once equilibrium was reached.

A second analyzing magnet was used to investigate the ion charge distribution after passage through the charge-exchange chamber. The ions were recorded with 8 proportional counters, each registering ions of a specified charge. The counter system was separated from the high-vacuum part of the setup by a slit 0.08 mm wide and a 100 mm long, sealed with a celluloid film ~ 20 μg/cm^2 thick. The counters were filled with air to a pressure of 40 — 100 mm Hg.

When operating with lithium ions, which are always accompanied by nitrogen ions of twice the charge, the field intensity of the second analyzing magnet was chosen such that the counters that received the lithium ions were separated by intermediate counters which registered the nitrogen ions with odd charges. The number of these evenly-charged ions, recorded simultaneously with the lithium ions, was calculated from the measurement results and from the known distribution of the charges of the nitrogen ions. As a rule, the nitrogen-ion admixture did not exceed 1 — 5%.

The accuracy of the values obtained for the number of ions of charge i, Φ_i, depended essentially on the dispersion of the values of Φ_i obtained in measurements at different pressures and initial charges. The absolute error $\Delta\Phi_i$ did not exceed in most cases $0.01\sqrt{\Phi_i}$. For very small Φ_i, the error was due essentially to random pulses, whose level corresponded to $\Phi_i \sim (1 \text{ to } 5) \times 10^{-4}$.

The ion velocity was determined, accurate to 1.5 or 2%, from the intensity of the focusing-magnet field. In the final result, account was taken of the change in the particle velocity due to the passage through the films and the layers of gas. The reduction in the ion velocity did not exceed 0.8% in the film ahead of the first analyzing magnet, amounted to $\sim 0.2\%$ in the channel (after equilibrium state was reached), and amounted to 0.2 — 1.5% in the films placed in the charge-exchange chamber.

3. MEASUREMENT RESULTS FOR IONS WITH $Z \leq 10$

The results of the measurements of the equilibrium distribution of the charges of light ions ($Z \leq 10$) are listed in Tables I, II, and III and are shown in Fig. 1. These data, when used in conjunction with the interpolation method described earlier,[1] yield the equilibrium distribution of the charges for any intermediate ion velocity. In the case of the helium and lithium ions, in addition to the results given in Tables I and II, the equilibrium distributions of the charges were obtained for approximately the same velocities in a celluloid film, and yielded for $i > 0$ values of Φ_{i+1}/Φ_i which agreed with the results of references 1 and 4 for the helium ions, and of references 5 — 7 for the lithium ions. The results of our measurements for helium ions at a velocity near 4.1×10^8 cm/sec (in helium, nitrogen, and argon), which are not listed in Table I, are in complete agreement with the results of Allison.[4]

The values of Φ_1/Φ_0 are 1.2 — 1.5 times greater in the compared results than in references 4 and 5. The discrepancy is probably due to the fact that the values of Φ_0 were determined in the present investigation less accurately for the lightest ions, and are possibly somewhat underestimated.

The equilibrium distributions obtained in the

TABLE I. Equilibrium Distribution of the Charges of Helium Ions

Medium	10^{-8} v, cm/sec	Φ_0, %	Φ_1, %	Φ_2, %	$\bar{i}$	σ	Medium	10^{-8}, v cm/sec	Φ_0, %	Φ_1, %	Φ_2, %	$\bar{i}$	σ
He	5.67	6.4	61.4	32.2	1.26	0.56	Ar	5.67	1.3	42.9	55.8	1.54	0.52
	7.92	0.3	27.7	72.0	1.72	0 45		7.92	0.04	10.1	89.9	1.90	0.30
	11.67	—	4.0	96.0	1.96	0.20		11.67	0.01	4.4	95.6	1.96	0.21
	16.86	—	0.6	99.4	1.99	0.11		16.86	—	1.15	98.85	1.99	0.11
N_2	5.67	2.6	51.2	46.2	1.44	0.55	Kr	3.89	14	78	8	0.93	0.46
	7.92	0.05	17.3	82.7	1.83	0.38		5.67	1.4	49.1	49.5	1.48	0.53
	11.67	—	3.8	96.2	1.96	0.19		7.92	0.06	16.2	83.7	1.84	0.37
	16.86	—	0.75	99.25	1.99	0.095		11.67	0.01	7.6	92.4	1 92	0.26
								16.86	—	1.6	98.4	1.98	0.13

TABLE II. Equilibrium Distribution of the Charges of Lithium Ions

Medium	10^{-8} v, cm/sec $\varepsilon\kappa$	Φ_0, %	Φ_1, %	Φ_2, %	Φ_3, %	$\bar{i}$	σ
He	4.01	5	78	17	0.2	1.12	0.46
	5.69	1.4	47.9	47.8	2.9	1.52	0.58
	8.03	0.2	11.6	59.6	28.6	2.17	0.62
	11.64	—	0.5	18.0	81.5	2.81	0.41
N_2	4.01	3	70	27	0.2	1.25	0.50
	5.69	0.5	32.1	61.3	6.1	1.73	0.57
	8.06	0.03	5.3	51.2	43.5	2.38	0.59
	11.64	—	0.5	19.0	80.5	2.80	0.42
Ar	4.01	2	70	28	0.4	1.27	0.49
	5.69	0.3	25.5	66.0	8.2	1.82	0.56
	8.06	0.03	3.1	44.5	52.4	2.50	0.56
	11.64	—	0.6	22.1	77.3	2.77	0.44
Kr	4.01	3	81	16	0.1	1.14	0.42
	5.69	0.5	36.8	58.9	3.8	1.66	0.56
	8.03	0.1	7.2	58.0	34.7	2.28	0.57
	11.64	—	1.6	32.6	65.8	2.64	0.52

TABLE III. Equilibrium Distribution of the Charges of Boron Ions

Medium	10^{-8} v, cm/sec	Φ_0, %	Φ_1, %	Φ_2, %	Φ_3, %	Φ_4, %	Φ_5, %	$\bar{i}$	σ
He	2.75	12.6	62.9	23.7	0.8	—	—	1.13	0.61
	3.79	7.6	52.7	36.4	3.3	0.01	—	1.35	0.67
	7.00	0.1	5.3	38.1	52.2	4.3	0.03	2.55	0.67
	7.87	0.03	1.9	23.7	62.0	12.2	0.2	2.85	0.65
N_2	2.75	10.2	59.8	28.8	1.2	—	—	1.23	0.60
	3.78	4.2	41.9	47.5	6.3	0.05	—	1.56	0.68
	7.87	—	0.6	15.5	65.0	18.4	0.5	3.03	0.62
Ar	2.75	10.8	59.4	28.6	1.2	—	—	1.20	0.60
	3.78	3.6	42.2	47.9	6.2	0.06	—	1.57	0.67
	7.00	—	1.0	22.9	66.2	9.7	0.2	2.85	0.60
	7.87	—	0.3	11.0	67.5	20.7	0.5	3.10	0.59
Kr	2.75	16.2	63.1	20.3	0.4	—	—	1.05	0.58
	3.79	5.2	48.1	43.1	3.6	0.02	—	1.45	0.65
	7.00	—	1.3	24.5	66.7	7.4	0.1	2.80	0.58
	7.87	—	0.5	13.2	70.0	16.0	0.3	3.02	0.57
Celluloid film	2.72	8.1	48.6	36.6	6.6	0.07	—	1.42	0.74
	3.05	6.3	43.6	40.7	9.3	0.1	—	1.53	0.76
	3.77	2.5	28.1	48.7	20.1	0.6	—	1.88	0.77
	6.98	—	1.0	18.1	58.4	21.3	1.2	3.03	0.70
	7.63	—	0.4	10.8	53.3	32.5	3.0	3.27	0.70

present work for the charges of the ions of boron, nitrogen, and neon yield, wherever they can be compared with the earlier results,[1] average charge values which are as a rule two or three percent lower. Such a systematic difference is within the limits of possible errors of the calibration of the focusing magnet (approximately 1.5 — 2% in each case).

We know that most investigations of the equilibrium distribution of the charges of ions with $Z > 2$ have been devoted to the passage of nitrogen ions through solid substances. The measurements made in the present investigation on nitrogen ions in a celluloid film are in good agreement with the results of Stephens and Walker[8] and with the measurements of the average charge of nitrogen ions in

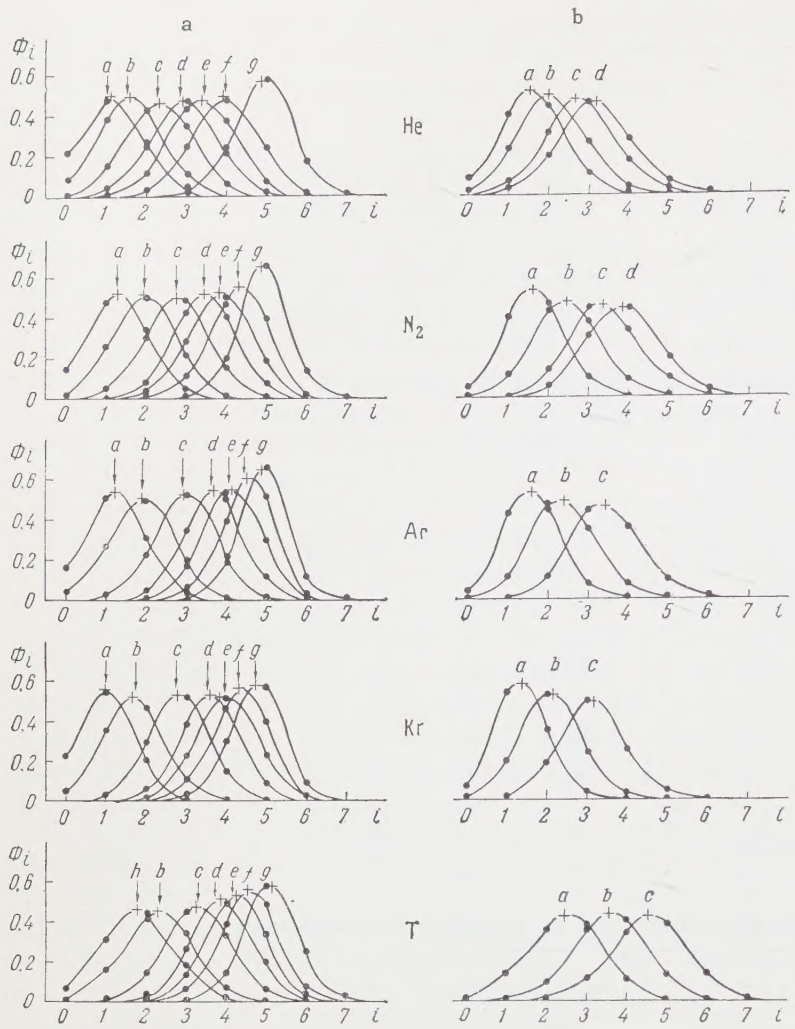

FIG. 1. Equlibrium distribution of the charges of ions of nitrogen (a) and neon (b) in helium, nitrogen, argon, krypton, and celloid film (T). The velocities (in multiples of 10^8 cm/sec) for nitrogen ions are 2.60 (a), 4.11 (b), 5.69 (c), 7.02 (d), 7.91 (e), 9.15 (f), 11.64 (g), and 3.04 (h); the values for the neon ions are 2.65 (a), 4.04 (b), 5.52 (c), 6.33 (d). The symbol plus at each distribution has $\bar{i}$ as its abscissa and the quantity $(2\pi\sigma^2)^{-1/2}$ as its ordinate.

nickel,[9] but the cited results display systematic deviations from those of other investigations,[10,11] which give values of $\bar{i}$ that are some ten percent higher. It is hardly possible to attribute such a discrepancy to a difference in the geometrical conditions, since our control measurements,[1] in which the geometric condition were varied, showed no noticeable changes in the equilibrium distributions. An estimate of the possible errors of the present experiment, and the good agreement between results obtained for other ions and previously known data, particularly with the results of all the investigations with helium ions, give grounds for assuming our results to be more correct for nitrogen ions in celluloid.

The experimental data obtained showed that the distribution of all the charges in all media is close to Gaussian

$$\Phi_i \approx (1/\sigma\sqrt{2\pi})\exp[-(i-\bar{i})^2/2\sigma^2],$$

and can be characterized essentially by two parameters: the average charge $\bar{i} = \sum_i \Phi_i i$ and the distribution width $\sigma = [\sum_i \Phi_i (i-\bar{i})^2]^{1/2}$. Exceptions are the cases when the distribution is highly asymmetrical relative to the average charge, owing to the fact that $\bar{i}$ is close either to zero or to Z. In this case σ^2 no longer determines the width of the Gaussian distribution, but yields, as always, the difference between the mean-squared charge $\overline{i^2} = \sum_i \Phi_i i^2$, which is used in the calculation of the average energy losses, and the quantity $\overline{i^2}$.

At a given ion velocity, the values of σ in different gases differ as a rule by not more than ten percent. When $v \lesssim (5 \text{ to } 7) \times 10^8$ cm/sec, the value of σ in celluloid is 10 — 20% greater than in gases. When v is increased, σ first increases but starts decreasing when $v > (5 \text{ to } 7) \times 10^8$ cm/sec. The maximum values of σ are 0.55, 0.6, 0.7, 0.8, and 0.9 for the ions of helium, lithium, boron, nitrogen, and neon respectively, i.e., they increase monotonically with increasing Z.

Unlike Hubbard and Lauer,[12] we observed in the present work considerable differences in the values of the mean ion charge in different gases (see Fig. 2). Although the ratio of the values of $\bar{i}$ in different media does not remain constant with

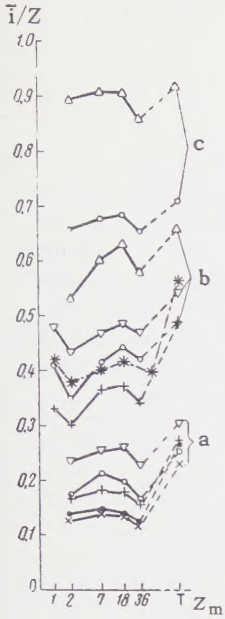

FIG. 2. Degree of ionization $\bar{i}/Z$ of the following ions: Δ – Li, ∇ – B, $\circ$ – N, + – Ni, $\bullet$ – P, and $\times$ – Ar in different gases (with atomic number Z_m) and in a celluloid film (T) at velocities $v = 3 \times 10^8$ (a), 6×10^8 (b), and 11×10^8 cm/sec (c). The values of $\bar{i}/Z$ in hydrogen are taken from reference 1. For comparison, we give the values of $\bar{i}/Z$ for the light group of uranium fission fragments (*) at $v = 14 \times 10^8$ cm/sec (reference 13).

changing velocity, the following regularities, which are common to all ions, can be noted. In the case of ions passing through a gas, the maximum of $\bar{i}$ is observed in nitrogen or argon, and the values of $\bar{i}$ in these gases do not differ by more than 5%. The average charge in helium is always smaller than the average charge in nitrogen, and the average charge in krypton is smaller than in argon. In the velocity range $(3.5 \text{ to } 10) \times 10^8$ cm/sec the minimum of $\bar{i}$ occurs in helium, and at $v \sim 3 \times 10^8$ cm/sec and $v \sim (11 \text{ to } 12) \times 10^8$ cm/sec it occurs in krypton. In most cases the difference between the maximum and minimum values of i in gases amounts to 20%. From a comparison of the results of our previous work[1] it follows that the average charge is greater in hydrogen than in helium. The average charge in a celluloid film is greater than the average charge in a gas for all ions except helium.

The dependence of $\bar{i}$ on the medium, obtained for multiply-charged ions of light elements, agrees qualitatively with the dependence of $\bar{i}$ on the medium for uranium fission fragments,[13] but the relative difference between the maximum and the minimum values of $\bar{i}$ is approximately twice as large in gases, while the relative difference between the maximum value of i in gases and the value of i in solids is much less than for fragments, diminishing rapidly with increasing charge of the nucleus.

That $\bar{i}$ is larger in solids than in gases in the case of multiply-charged ions of light elements has been established and briefly discussed earlier.[1] The smaller value of $\bar{i}$ in helium, compared with hydrogen, and the increase of $\bar{i}$ with increasing atomic number of the gas Z_m, can be qualitatively attributed, like the analogous dependence of $\bar{i}$ on Z_m for fragments,[14,15] to the different behavior of the electron loss and capture cross sections with varying Z_m. However, the dependence of $\bar{i}$ on Z_m in heavy gases contradicts the existing theoretical estimates.[14-16] According to these estimates, in which the statistical model of the atom is used, the average charge of the ions should increase or remain constant with increasing Z_m. Actually, however, when Z_m increases from 18 to 36, a substantial decrease in the average charge is observed, amounting to as much as 20% for ions of light elements at $v \sim 4 \times 10^8$ cm/sec. It should be noted that as the ion velocity is decreased, the relative value of this reduction becomes greater. At $v \sim 10^8$ cm/sec, for example, the average charge of nitrogen, neon, or argon ions in argon is half the charge in nitrogen or neon.[17] Thus, for multiply-charged ions of light elements the dependence of $\bar{i}$ on Z_m is determined essentially by factors which have been disregarded in the theoretical investigations that employ the statistical model of the atom, and consequently the accuracy of such calculations can hardly pretend to be more several times 10%.

As indicated earlier,[1] the degree of ionization $\bar{i}/Z$ of different ions in hydrogen, air, and argon can be represented approximately in the range $\bar{i}/Z \sim 0.2$ to 0.6 by a function of the parameter $vZ^{-\alpha}$, which is different for each gas. Examination of the experimental data of the present work has shown that this conclusion holds also for ions passing through helium and krypton. In all the gases employed, $\alpha = 0.45$, which agrees, within the limits of errors, with the previous value $\alpha \sim 0.4$.[1] This conclusion, which is apparently correct for any gas medium, can be explained by a simple application of the statistical model of the atom.[1] It is impossible, however, to represent in this form the average charge of different ions in celluloid film, even approximately, since the exponent α is in this case a function of both Z and v.

4. RESULTS OF MEASUREMENTS FOR IONS WITH Z > 10

The results of the measurements of the equilibrium distribution of the charges of ions with Z > 10 are shown in Figs. 3 and 4. Experimental data by other workers are available only for ions of sodium[7] and argon[17] at low energies, and can therefore not be compared directly with our results. A reasonable interpolation of these data is possible, however.

The dependence of the average ion charge on

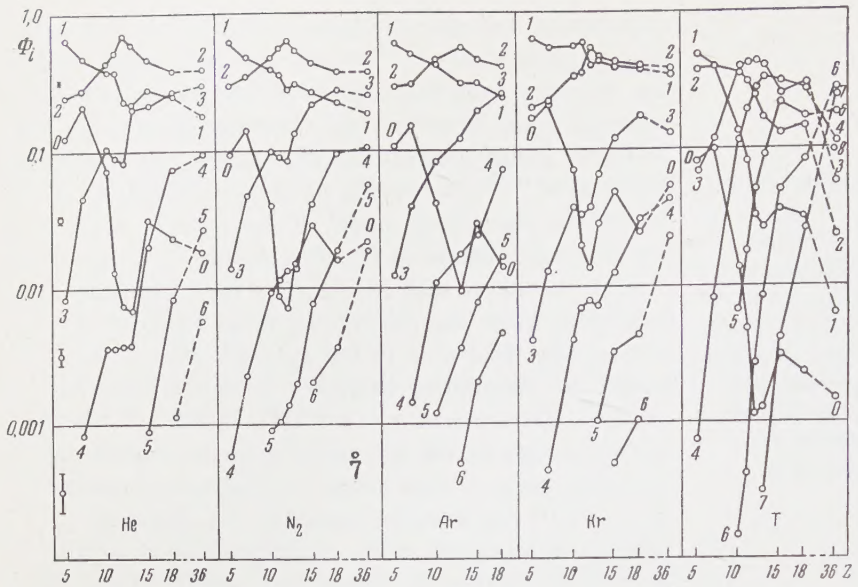

FIG. 3. Dependence of the relative amount Φ_i of ions of charge i on the charge of the ion nucleus, Z, in helium, nitrogen, argon, krypton, and celluloid film (T) at $v = 2.6 \times 10^8$ cm/sec. The errors in the values of Φ_i are indicated near the ordinate axis, while the values of i are marked on each curve.

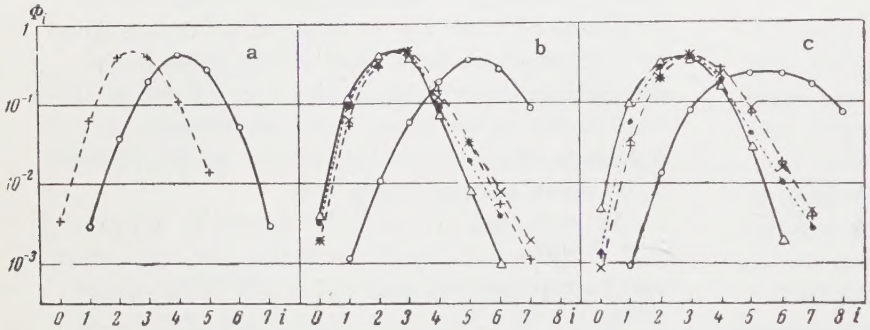

FIG. 4. Equilibrium distribution of charges in a beam of ions of sodium (a), phosphorus (b), and argon (c): Δ – in helium, + – in nitrogen, × – in argon, ● – in krypton, and ○ – in celluloid film. $v = 4.5 \times 10^8$ cm/sec for sodium ions and 4.05×10^8 cm/sec for phosphorus and argon.

the medium is approximately the same as for ions with $Z \leq 10$ at these velocities. The maximum of $\bar{i}$ for ions passing through gas occurred in nitrogen, but for magnesium and aluminum ions it occurred in helium. The minimum occurred in krypton, the difference between maximum and minimum being 15 – 20%. At $Z \gtrsim 10$, the difference between the average charge in celluloid and in gas begins to increase noticeably. Whereas this difference does not exceed 15% for the lighter ions at these velocities, it reaches approximately 50% for neon, approximately 60% for sodium, magnesium, aluminum, and argon, approximately 80% for phosphorus, and approximately 130% for krypton. It must be noted that at high velocities, as demonstrated by measurements with uranium fission fragments,[13] the excess of the average charge in solids over the average charge in gas is much less, and amounts to 40% for the light group of fragments ($Z \approx 38$ at $v \approx 14 \times 10^8$ cm/sec).

The average charge $\bar{i}$ increases in all substances with increasing Z for a fixed ion velocity. The degree of ionization $\bar{i}/Z$ (see Fig. 5) diminishes monotonically in gases. However, the rate of decrease of $\bar{i}/Z$ with increasing Z slows down near $Z = 10$. In a solid we observe an increase in $\bar{i}/Z$ in this region. In this connection, if $\bar{i}/Z$ is represented in a given gas as a function of $vZ^{-\alpha}$, then α will no longer be constant. We have $\alpha \sim 0$ for $Z \sim 10$ to 12 and $\alpha \sim 0.6$ for $Z \sim 13$ to 18.

An even greater deviation from a smooth depence on Z is observed in the values of Φ_i. If we plot Φ_i vs. Z (see Fig. 3), all values of Φ_0 and Φ_1 have clearly pronounced minima in all media near $Z = 12$. As the charge increases, the singularities in the indicated region of Z become less pronounced. The minima of Φ_0 and Φ_1 near $Z = 12$, and the slowing down of the increase in Φ_3 and Φ_4 in gases with increasing Z, observed near $Z = 12$, denote a reduction in the width σ of the equilibrium distribution in this region of Z. As can be seen from Fig. 6, σ has a minimum for magnesium ions. For $Z > 10$, the distribution width in celluloid film begins to increase over that in gases. For argon and krypton ions this difference reaches 40 and 50%, respectively.

Thus, an investigation of the equilibrium distribution of the charges of light ions has shown that in the vicinity $Z \sim 10$ to 12, where a new

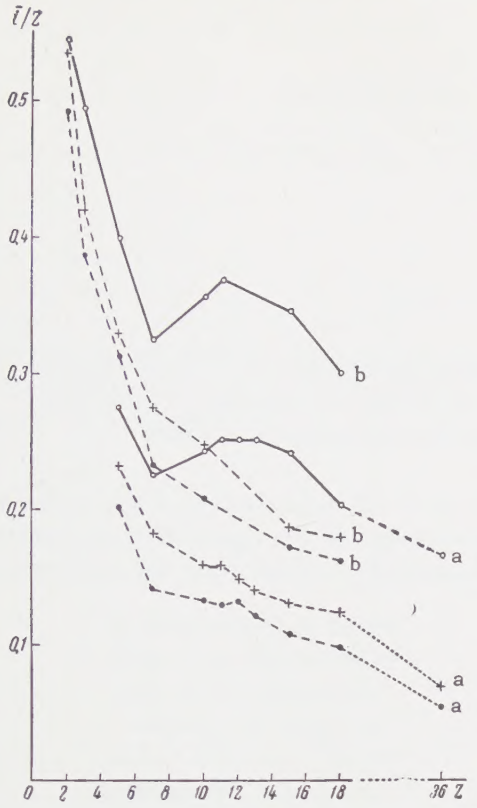

FIG. 5. Dependence of the degree of ionization $\bar{i}/Z$ on the charge Z of the ion nucleus: + – in N_2, ● – in krypton, o – in celluloid film at $v = 2.6 \times 10^8$ cm/sec (a) and $v = 4.1 \times 10^8$ cm/sec (b).

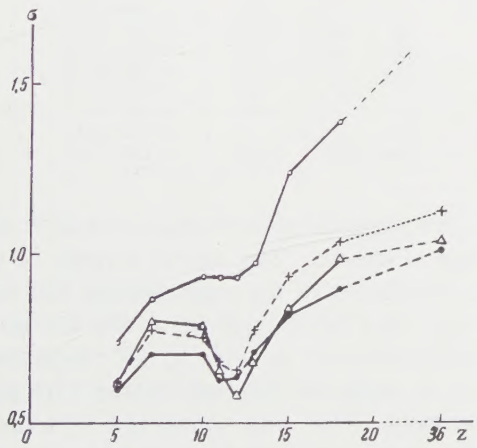

FIG. 6. Dependence of the width of equilibrium charge distribution, $\sigma = (i^2 - \bar{i}^2)^{1/2}$, on Z: Δ – in helium, + – in nitrogen, ● – in krypton, and o – in celluloid film at $v = 2.6 \times 10^8$ cm/sec.

electron shell begins to be filled at $v \sim 3 \times 10^8$ cm/sec, there are noticeable deviations from a smooth dependence of the quantities Φ_i, i, and σ on Z. It should be noted that these deviations are strongest in the distribution width σ in the case of gases and in the value of the average charge in the case of solids, and that this influences strongly the average energy losses.[18]

The equilibrium charge distributions of ions with $Z \geq 10$ passing through nitrogen, argon, and krypton, and of ions with $Z \geq 15$ passing through helium, deviate systematically from Gaussian in the region of large values of i, since the ratios Φ_i/Φ_{i+1} no longer increase with increasing i (see, for example, Fig. 4).

The constancy of Φ_i/Φ_{i+1} at large values of i can be attributed to the influence of collisions involving large changes in the charge, and are evidence that ions with $i > \bar{i} + 1$ are produced in these cases essentially by simultaneous loss of several electrons. No change to constant values of Φ_i/Φ_{i+1} was observed in the passage of ions through a celluloid film.

[1] Nikolaev, Dmitriev, Fateeva, and Teplova, JETP **33**, 1325 (1957), Soviet Phys. JETP **6**, 1019 (1958).

[2] Nikolaev, Dmitriev, Teplova, and Fateeva, Сб. Ускорители (Anthology 'Accelerators'), Atomizdat, 1960, in press.

[3] Dmitriev, Teplova, Nikolaev, and Fateeva, Приборы и техника эксперимента (Instrum. and Exptl. Techniques) **6**, 131 (1959).

[4] S. K. Allison, Revs. Mod. Phys. **30**, 1137 (1958).

[5] Teplova, Dmitriev, Nikolaev, and Fateeva, JETP **32**, 974 (1957), Soviet Phys. JETP **5**, 797 (1957).

[7] S. Devons and J. Towle, Proc. Phys. Soc. **A69**, 345 (1956).

[7] Leviant, Korsunskiĭ, Pivovar, and Podgornyĭ, Dokl. Akad. Nauk SSSR **103**, 403 (1955).

[8] K. G. Stephens and D. Walker, Proc. Roy. Soc. **A229**, 376 (1955).

[9] Reynolds, Scott, and Zucker, Phys. Rev. **95**, 671 (1954).

[10] Nikolaev, Fateeva, Dmitriev, and Teplova, JETP **32**, 965 (1957), Soviet Phys. JETP **5**, 789 (1957).

[11] Reynolds, Wyly, and Zucker, Phys. Rev. **98**, 474 (1955).

[12] E. L. Hubbard and E. J. Lauer, Phys. Rev. **98**, 1814 (1955).

[13] N. O. Lassen, Dan. Mat. Fys. Medd. **26**, 5 (1951).

[14] N. Bohr and J. Lindhard, Dan. Mat. Fys. Medd. **28**, 7 (1954).

[15] G. J. Bell, Phys. Rev. **90**, 549 (1953).

[16] R. L. Gluckstern, Phys. Rev. **98**, 1817 (1955).

[17] Stier, Barnett, and Evans, Phys. Rev. **96**, 973 (1953).

[18] Teplova, Nikolaev, Dmitriev, and Fateeva, Izv. Akad. Nauk SSSR Ser. Fiz. **23**, 894 (1959), Columbia Tech. Transl. p. 883.

Translated by J. G. Adashko
165

POLARIZATION OF 6.8-MEV PROTONS SCATTERED ON CARBON

M. V. PASECHNIK, N. N. PUCHEROV, B. F. ORLENKO, and V. S. PROKOPENKO

Institute of Physics, Academy of Sciences, U.S.S.R.

Submitted to JETP editor April 15, 1960

J. Exptl. Theoret. Phys. (U.S.S.R.) 39, 915-916 (October, 1960)

Experiments on double scattering of 6.8-Mev protons were performed. The large value of the polarization of protons scattered on carbon is evidence of the importance of spin-orbit interaction during scattering. An angular dependence on the polarization is noted.

EXPERIMENTS on the polarization of protons scattered elastically by atomic nuclei show that proton polarization can become considerable even at relatively low energies.[1,2] The present investigation was devoted to polarization of protons on carbon in the energy region near 7 Mev. The work was undertaken both to investigate the role of the spin-orbit interaction during elastic scattering and to construct a polarization instrument in which carbon is used as the second scatterer.

A beam of 6.8-Mev protons was produced in a cyclotron. After extraction from the accelerating chamber, focusing, rotation through 30°, and collimation, the protons impinged on a target located in a vacuum reaction chamber. The polarization was determined by double-scattering experiments. The second scatterer was also carbon. The second-scattering angle was 45°. The doubly-scattered protons were recorded with Ya-1 nuclear emulsions 200 μ thick. The emulsions were scanned under a microscope to select tracks of specified direction and magnitude. This served to segregate the group of protons that experienced double elastic coplanar scattering by carbon.

The construction of the instrument was such that simultaneous measurements could be made at six primary-scattering angles. This has reduced noticeably the operating time of the cyclotron, which is considerable in double-scattering experiments. The entire measuring apparatus was thoroughly adjusted, since geometrical inaccuracies could lead to false asymmetry.

The carbon targets were made in the form of polystyrol film filled with fine graphite powder. The target thickness was on the order of 10 mg/cm^2. The exposure time was from 2 to 10 hours, depending on the scattering angle, with the primary beam current on the order of 0.01 μa.

The right-left asymmetry after the second scattering was determined in the experiments. The results of the measurements are listed in the table. Knowledge of the right-left asymmetry makes it possible to determine the polarization,

Value of asymmetry in experiments on double scattering of 6.8-Mev protons on carbon; $e = (R - L)/(R + L)$; R and L are the numbers of tracks to the right and to the left.

$\theta°_{lab}$	R	L	e
45	2485	1664	0.198±0.02
65	245	123	0.332±0.10
80	520	642	—0.105±0.05
90	107	432	—0.606±0.09
100	1204	551	0.300±0.05
110	1827	690	0.451±0.04
120	137	20	0.742±0.15
135	2227	1659	0.146±0.02

provided the particle polarization in one of the scatterings is known. The use of targets of considerable thickness in the experiments did not enable us to take full advantage of the known data on the polarization of protons at 45° (references 3 and 4) or to calibrate the instrument with sufficient accuracy. This was connected with the considerable energy indeterminacy that arises in scattering of low-energy protons by a thick target. Account must be taken here of the rapid variation of the polarization with energy in the case of carbon.

The qualitative estimates made disclose a considerable polarization upon scattering of 6.8-Mev protons by carbon. This demonstrates the possibility of using carbon as an analyzer in the investigation of polarization in our energy range. To obtain accurate quantitative data we shall use thinner targets, particularly since experiments

have shown that this does not increase the exposure time excessively.

Estimates show that the angular dependence of the polarization in the scattering of protons by carbon is similar to that in diffraction. A comparison of the angular dependence of the polarization which we obtained for carbon with the data for aluminum[3] shows good agreement in quantities $A^{1/3} \sin(\theta_m/2)$, where θ_m is the angle at which the maximum or minimum takes place.

In conclusion, the authors express their gratitude to the cyclotron crew of the laboratory for performing the present work.

[1] L. Rosen and J. E. Brolley, Phys. Rev. **107**, 1454 (1957).

[2] V. P. Sorokin and A. Ya. Taranov, Dokl. Akad. Nauk SSSR **111**, 82 (1956), Soviet Phys.-Doklady **1**, 637 (1957).

[3] R. E. Warner and W. P. Alford, Phys. Rev. **114**, 1338 (1959).

[4] G. C. Phillips and P. D. Miller, Comptes Rendus du Congres International de Physique Nucleaire, Paris, (1959) p. 522.

Translated by J. G. Adashko
166

A STUDY OF THE VARIATION WITH TEMPERATURE OF THE SPONTANEOUS MAGNETIZATION OF CHROMIUM TELLURIDE

L. G. GAĬDUKOV, N. P. GRAZHDANKINA, and I. G. FAKIDOV

Institute of Metal Physics Academy of Sciences, U.S.S.R. and Sverdlovsk State Pedagogical Institute

Submitted to JETP editor April 27, 1960

J. Exptl. Theoret. Phys. (U.S.S.R.) 39, 917-922 (October, 1960)

The temperature variation of the spontaneous magnetization of chromium telluride (CrTe) in the magnetic transformation temperature region was determined by three different methods. The magnetocaloric effect and the magnetization were measured for various magnetic field strengths at various temperatures. The Curie temperature of chromium telluride was found to be +60°C by the method of thermodynamic coefficients. The results obtained are discussed in terms of the s-d exchange model of ferromagnetism.

GUILLAND[1], from a study of the absolute saturation magnetization of chromium telluride at low temperatures, has proposed that the reason for the small value of the magnetic moment of the chromium atom ($M = 2.39\ \mu_B$) is the existence in this compound of uncompensated antiferromagnetism (or ferrimagnetism). The fact that the spontaneous magnetization of ferrimagnets is different from zero is, according to Néel's model,[2] due to the non-equivalent magnetic moments of the transition metal ions situated in the different magnetic sublattices, which are oriented antiparallel to one another. In order to verify this hypothesis and to determine whether chromium telluride belongs to the ferromagnetic or ferrimagnetic class of substances, we have undertaken a detailed study of the temperature dependence of the spontaneous magnetization σ_S in the region of the Curie point. The curve of $\sigma_S/\sigma_0 = f(T/\Theta_f)$ obtained by Guilland cannot be used to judge the temperature behavior of the spontaneous magnetization in the direct vicinity of the Curie point Θ_f, and it requires refinement, since different data are given in two papers by this author.[3,4]

SPECIMEN FABRICATION AND MEASUREMENT PROCEDURE

Chromium telluride was obtained by melting together finely divided and carefully mixed chromium and tellurium powders in evacuated and sealed-off quartz ampoules. Electrolytic chromium was used as the starting material and had the following chemical composition: Cr — 99.9, Si — 0.03, Fe — 0.02, Cu — 0.0013, N — 0.015%. To remove hydrogen, the chromium was annealed under a high vacuum at 1000°C for 12 hours.

The chemical composition of the tellurium was as follows: Te > 99.999, Cu — 0.0001, Ag — 0.0002, Bi < 0.0001, Sb and As — 0.0001%. After fabrication the alloy was subjected to x-ray phase analysis, and the microstructure was studied; these showed the presence of traces of Te along with the principal phase CrTe. For measurements of the magnetocaloric effect and the magnetization, specimens in the form of balls were turned from the alloy obtained. The magnetocaloric effect was measured by a method similar to that described by Fakidov and Krasovskiĭ[5]. The magnetization isotherms were measured with the aid of a pendulum magnetic balance similar in construction to Domenicali's.[6] The maximum magnetic fields used in this case were 16 koe. The weights of the specimens were 0.022 to 0.030 g. The specimen was kept at constant temperature by a Heppler thermostat, which maintained the temperature constant within ±0.05°. The temperature was measured with a copper-constantan thermocouple and a potentiometer.

RESULTS

In order to obtain the most reliable data on the temperature variation of the spontaneous magnetization of chromium telluride, we measured the dependence of the magnetocaloric effect on the magnetic field strength both above and below the Curie point, and the magnetization isotherms of the compound in the region of the paraprocess. Curves showing the variation of the magnetocaloric effect ΔT with the square of the magnetization, taken at various temperatures, are shown in Fig. 1; by

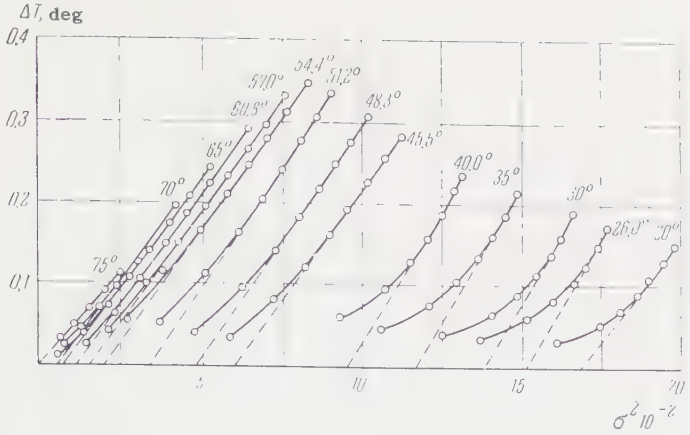

FIG. 1. The dependence of the magnetocaloric effect ΔT on the square of the specific magnetization for various temperatures.

extrapolating the straight-line portions of these curves to $\Delta T = 0$, the square of the spontaneous magnetization σ_s^2 is obtained.

The measurement of the magnetization isotherms in the paraprocess region allows the temperature variation of the spontaneous magnetization to be determined by two methods: "the method of the equal magnetization lines", developed by Weiss and Forer, and "the method of thermodynamic coefficients," which was used by Belov[7,8] in studies of a number of ferro- and ferrimagnetic substances. The data we obtained on the magnetization of chromium telluride as a function of magnetic field strength is presented in Fig. 2. This data is shown in the figure as curves of H/σ as

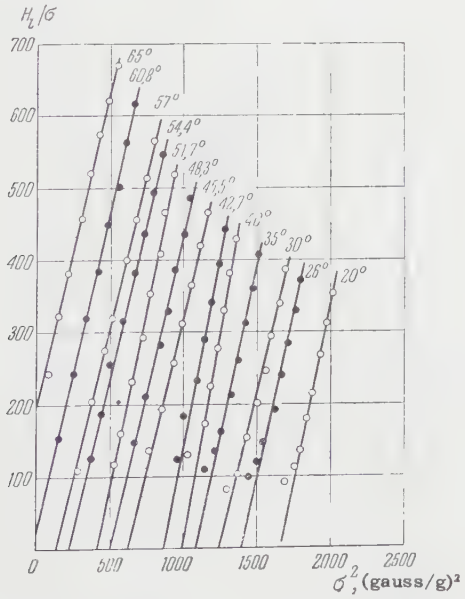

FIG. 2. Dependence of H_i/σ on σ^2 for chromium telluride. The field H is corrected by taking into account the demagnetizing factor of the specimen shape.

functions of σ^2, so that it is possible to compare the well known thermodynamic equation[9]

$$\alpha\sigma + \beta\sigma^3 = H \qquad (1)$$

with our results. The spontaneous magnetization was calculated with the aid of the thermodynamic coefficients α and β, the ratio of which is equal to the square of the spontaneous magnetization $\sigma_s^2 = -\alpha/\beta$.

It is seen from the graphs presented that the true magnetization of chromium telluride in the region of the Curie temperature can be adequately described by Eq. (1); this allows the values of the thermodynamic coefficients α and β and their temperature variations to be determined. It is found that, in the temperature range $|T - \Theta_f| \leq 14.5°$, the coefficient α changes linearly with temperature, with $d\alpha/dT = 40$, but the value of the coefficient β remains almost constant and lies within the limits 1 to 0.8. In accord with the conclusions of the thermodynamic theory, α is negative and β positive throughout the temperature range studied for $T < \Theta_f$. The Curie temperature determined from the condition $\alpha = 0$ is found to be 60°C, which is somewhat larger than the value $\Theta_f = 55°C$ we found from the magnetocaloric effect and the values $\Theta_f = 57.5°$ and $\Theta_f = 58.0°C$ found from the break in the curve of electrical resistance vs. temperature and from the maximum of the galvanomagnetic effect $(-\Delta R/R)$.

The temperature variation of the spontaneous magnetization of chromium telluride determined by the three methods described is shown in Fig. 3; the fairly good agreement of the results in the temperature region $T < \Theta_f$ can be seen. The destruction of the "remnants" of spontaneous magnetization occurs in the interval of temperature 30 to 40° above the Curie point, as is seen from the curves of $\sigma_s(T)$ derived from measurements of

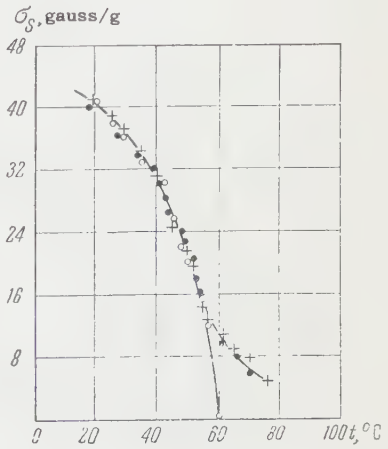

FIG. 3. The temperature variation of the spontaneous magnetization of chromium telluride: ● – from the "equal magnetization lines" method, + – from the data on the magnetocaloric effect, ○ – from "the method of thermodynamic coefficients."

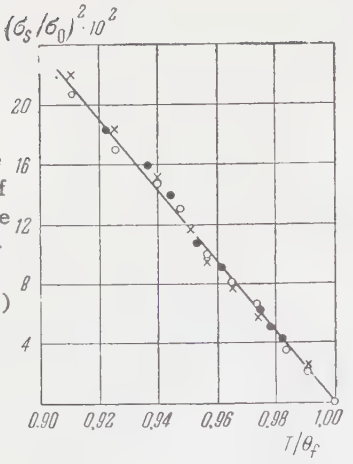

FIG. 4. The temperature variation of the square of the spontaneous magnetization of chromium telluride near to the Curie temperature. (The symbols used for the points correspond with those in Fig. 3.)

the magnetocaloric effect and by "the method of equal magnetization lines."

Making use of the magnetic equation of state

$$(\sigma_s/\sigma_0)^2 = \xi(1 - T/\Theta_f), \qquad (2)$$

we have determined the rate at which the spontaneous magnetization of chromium telluride changes with temperature near the Curie point. The coefficient ξ is equal to 2.40 to 2.46 according to the data in Fig. 4, where the temperature variation of the square of the relative spontaneous magnetization is plotted. The value of σ_0 for chromium telluride* was taken to be 79.5 gauss/g; the magnetic moment of the chromium ion is then $M_{eff} = 2.56\ \mu_B$, which is somewhat larger than the values of M_{eff} quoted by other authors.[1,10] The comparison of the curve we obtained, for the temperature variation of the spontaneous magnetization of CrTe, with the curves calculated theoretically on the basis of the Weiss theory, taking into account the spatial quantization of the magnetization vector, shows that the assumption $j = 3/2$ for CrTe reflects reality most closely. (Here j is the internal quantum number given by $j = L + S$, where L is the azimuthal or orbital quantum number, and S is the spin quantum number.) Guilland quotes for CrTe two different values: $j = 3$ (reference 3) and $j = 2$ (reference 4).

Measurements we have made on the temperature variation of the magnetic susceptibility of chromium telluride show that in the paramagnetic region the susceptibility obeys the Curie-Weiss law $\chi = C_M/(T - \Theta)$, with values for the constants C_M and Θ of 1.97 and 347°K, respectively; this agrees quite well with previously quoted data.[11,12] The value of the effective magnetic moment M_{eff}, calculated from our experimental data by the formula $M_{eff} = \sqrt{3kC_M/N\beta^2}$ is 3.97 μ_B; the theoretical value of M_{eff}, calculated assuming complete "freezing" of the orbital moment for $S = 3/2$, is 3.87 μ_B (k is the Boltzmann's constant).

*The value of σ_0 was determined from the experimental data of Lotgering and Gorter[12] on the magnetization at T = 20°K by a graphical extrapolation to infinitely large magnetic field strength with a hyperbolic law of approach to saturation $\sigma = \sigma_s(1 - 1/H)$. The agreement of the magnetization values we obtained with the data of reference 12 in the temperature region 77 to 400°K was very good.

DISCUSSION OF THE RESULTS

As is well known, the existence of uncompensated antiferromagnetism in a substance can be determined most directly by neutron diffraction studies, which allow the structure of the magnetic sublattices to be established. Insofar as such studies have not been made on CrTe to date, the possibility that this compound belongs to the ferrimagnetic class of substances (as Guilland proposes) is only one of several alternative causes of the small value of the magnetic moment of the chromium atom in CrTe. A simultaneous study of the various physical properties of this compound is necessary to answer this question simply.

1. Firstly, the observed decrease in the magnetic moment of Cr in the compound CrTe can be caused by the partial filling of the 3d band of Cr by the external electrons from Te which participate in the sharing of electrons in the crystal. Such a change of the electron energy spectrum of the transition metal inevitably results in heteropolar bonds, which should show up in the electrical and x-ray spectral properties of the compound. A study we made together with Kikoin of the electrical and galvanomagnetic properties of CrTe,[13] which established the existence of metallic conductivity in the compound, as well as studies of the fine structure of the K absorption spectra of Cr in CrTe made by Men'shikov and Nemnonov[14] on our specimens, showed the small participation of the d electrons of the transition metal in the chemical bond. This is indeed a confirmation of Pearson's ideas[15] on the existence of the p^3-electronic configuration in the transition metal compounds with the NiAs type of crystal structure.

2. The other reason for a reduced magnetic moment is the existence in the substance of magnetic subsystems. For semiconducting ferrimagnets (ferrites) these subsystems form two or more magnetic sublattices with different magnetizations. For metallic ferromagnets, according to the s-d exchange model[16], the subsystems are formed by the internal d and external s electrons. Thus, the resulting magnetization of the crystal as a whole is the sum of the magnetizations of the

lattice and of the conduction electrons. The spontaneous magnetization of metallic ferrimagnets can in the general case be due to magnetic subsystems of both types.

Because the mechanisms that give rise to spontaneous magnetization in ferro- and ferrimagnets are different, the character of the magnetic transformation is essentially different in these two classes of substances. As has been shown by theoretical[17] and experimental[7,8] work, the difference shows up especially in the different rates at which the spontaneous magnetization changes with temperature in the region of the Curie point, which is described by the coefficient ξ in Eq. (2). For ferrites ξ is much smaller than 3 and lies within the limits 0.1 to 0.7; for metallic ferromagnets, on the other hand, according to the calculation of Vonsovskiĭ and Vlasov,[17] one has $\xi > 3$. The empirical value we have obtained for chromium telluride is equal to the theoretical value of ξ for $j = 3/2$, calculated from the formulae of the "quasi-classical" theory of ferromagnetism, which does not take into account the spontaneous magnetization of the conduction electrons.

Summarizing all that has been said, it can be proposed that CrTe is apparently not a ferrimagnet, as Guilland surmised, but belongs to the ferromagnetic class of substances, in which the s-d exchange interaction is small. The absence of the hyperbolic change of susceptibility with temperature in the paramagnetic region, which is characteristic of ferrimagnets, as well as the much better agreement between the values of the magnetic moment determined from the paramagnetic measurements and from the magnetization at absolute saturation, as compared with ferrites and ferromagnetic metals, can be taken as a confirmation of this view.

According to Pearson's scheme for the hybridization of wave functions in NiAs type structures, the resonating p^3 bonds in CrTe require the existence of four uncompensated 3d electrons, which determine the value of the effective magnetic moment M_{eff}. Nevertheless, the number of magnetically active electrons estimated from the value of the effective magnetic moment we measured was found to be less than four. This discrepancy could be caused either by the sharing of some small fraction of the d electrons with the s electrons, or by the formation of an intrinsic d conduction band due to dd interaction. A final answer to this question could be obtained from a study of the x ray K and L emission spectra.

Neutron diffraction investigations of CrTe should be decisive in verifying the ideas expressed here on the ordering of the magnetic spin moments in this compound.

[1] C. Guilland and S. Barbezat, Compt. rend. **222**, 386 (1946); C. Guilland, Revs. Modern Phys. **25**, 119 (1953).

[2] L. Néel, Ann. Physik **3**, 137 (1948).

[3] C. Guilland, Compt. rend. **223**, 1110 (1946).

[4] C. Guilland, Compt. rend. **222**, 1224 (1946).

[5] I. G. Fakidov and V. P. Krasovskiĭ, JETP **36**, 1063 (1959), Soviet Phys. JETP **9**, 755 (1959).

[6] C. A. Domenicali, Rev. Sci. Instr. **21**, 327 (1950).

[7] Belov, Bol'shova, and Elkina, Izv. Akad. Nauk SSSR Ser. Fiz. **21**, 1047 (1957), Columbia Tech. Transl. p. 1051.

[8] K. P. Belov and A. N. Goryaga, Izv. Akad. Nauk SSSR Ser. Fiz. **21**, 1038 (1957), Columbia Tech. Transl. p. 1043.

[9] V. L. Ginzburg, JETP **17**, 833 (1947).

[10] I. Tsubokawa, J. Phys. Soc. Japan **11**, 662 (1956).

[11] H. Haraldsen and A. Neuber, Z. anorg. u. allgem. Chem. **234**, 353 (1937).

[12] F. K. Lotgering and E. W. Gorter, J. Phys. Chem. Solids **3**, 238 (1957).

[13] Fakidov, Grazhdankina, and Kikoin, Dokl. Akad. Nauk SSSR **68**, 491 (1949).

[14] A. Z. Men'shikov and S. A. Nemnonov, Физика металлов и металловедение (Metal Physics and Metallography) (in the press).

[15] W. B. Pearson, Canad. J. Phys. **35**, 886 (1957).

[16] S. V. Vonsovskiĭ and Ya. S. Shur, Ферромагнетизм (Ferromagnetism), OGIZ (1948).

[17] S. V. Vonsovskiĭ and K. B. Vlasov, JETP **25**, 327 (1953).

Translated by K. F. Hulme
167

ANGULAR DISTRIBUTIONS OF α PARTICLES FROM THE F^{19} (p, α) O^{16} REACTION

I. B. TEPLOV, O. P. SHEVCHENKO, and E. K. RUUGE

Institute for Nuclear Physics, Moscow State University

Submitted to JETP editor, May 6, 1960

J. Exptl. Theoret. Phys. (U.S.S.R.) 39, 923-928 (October, 1960)

A telescope of three proportional counters was used to measure angular distributions of α particles from the F^{19} (p, α)O^{16} reaction with formation of the O^{16} nucleus in the ground state. Measurements were made over the range of angles 20 — 160° for 11 energies of the incident protons between 5.1 and 6.5 Mev. All the angular distributions show a marked anisotropy. The results are discussed from the point of view of possible reaction mechanisms.

INTRODUCTION

THE investigation of angular distributions of particles formed in the F^{19} (p, α)O^{16} reaction for proton energies up to 2.6 Mev has been carried out by various authors.[1,2] The analysis of the results shows that in this energy range the main reaction mechanism is a process associated with formation of an intermediate compound nucleus. Ranken et al.[3] obtained excitation curves for the F^{19} (p, α)O^{16} reaction in the energy range from 1.2 to 5.5 Mev. The very evident resonance character of these curves shows that the formation of a compound nucleus continues to be the predominant reaction mechanism, at least up to proton energies ~5 Mev. For higher energies, the F^{19} (p, α)O^{16} reaction has been investigated only by Likely and Brady,[4] who measured angular distributions of the α-particle group corresponding to formation of the O^{16} nucleus in its ground state, for proton energies 16.0 and 18.5 Mev. At these energies one observes a series of maxima of the differential cross section in the angular distributions. Comparing the experimental data with the results of computation, the authors conclude that at these energies of the incident protons the predominant reaction mechanism is the capture by the proton of a triton from the F^{19} nucleus.

The purpose of the present work is to study the angular distribution of α-particles resulting from the F^{19} (p, α)O^{16} reaction for proton energies in the range 5.1 — 6.5 Mev.

EXPERIMENTAL METHOD

In our work we used protons with an energy ~6.6 Mev, obtained by accelerating molecular hydrogen in the 120-centimenter cyclotron of the Institute for Nuclear Physics of Moscow State University. The proton energy was changed by slowing the protons with aluminum foils 10.5 μ in thickness. To determine the energy of the incident particles, we measured the energy spectrum of protons elastically scattered by an aluminum foil (0.18 mg/cm^2 thick) at an angle of 90°. The mean proton energy was determined to an accuracy of ~50 kev.

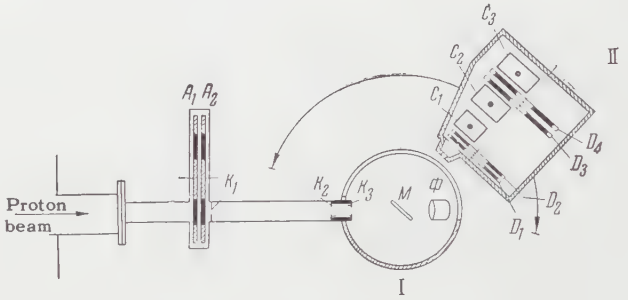

FIG. 1. Experimental set-up. I — vacuum chamber, II — chamber with counters. M — target; Φ — collector; D_1, D_2, D_3, D_4 — disks with aluminum foils; C_1, C_2, C_3 — proportional counters; K_1, K_2, K_3 — collimating slits; A_1, A_2 — disks with aluminum foils for varying the beam energy.

The arrangement of the apparatus used in the experiment is shown schematically in Fig. 1. The focused beam of protons taken out of the cyclotron, after passing through collimating slits (3 × 6 mm), impinged on a thin target set at an angle of 45°, placed at the center of a vacuum chamber 12.4 cm in diameter.

Particles formed in nuclear reactions emerged from the vacuum chamber through a slit which was covered by a 1.2 mg/cm^2 film of "lavsan" and were recorded by a telescope of three proportional counters; the first two counters were connected in coincidence and the third in anti-coincidence. The counters were kept in a special chamber which could be rotated about the target over the range of angles from 0 to 162°. The particles entered the counter chamber through an entrance window

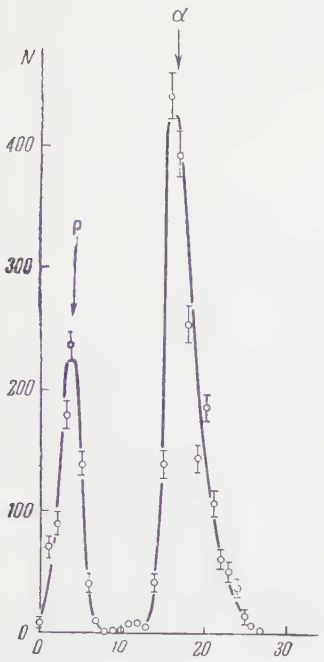

FIG. 2. Differential distribution of pulse heights (V) for particles emerging at an angle of 30° from an aluminum target, for E_p = 6.6 Mev (with no aluminum absorber in front of the first counter).

of mica 2 mg/cm² thick, the size of which was 3 × 6 in some experiments, and 2 × 4 mm in others. The chamber was filled with a mixture of argon (96%) and CO_2 (4%) to a pressure of 20 cm Hg. Inside the chamber, in front of the first counter, there were two disks by means of which one could insert in the path of the particles an aluminum absorber with any thickness from 0 to 540 μ in steps of 5.25 μ. The disks and the counter chamber could be rotated remotely.

To vary the width of the energy interval in which particles were recorded, two disks were placed between the second and third counters, with a set of aluminum foils 7 μ thick. In taking the energy spectra (cf., for example, Fig. 3), these foils were not used and the width of the energy interval was determined only by the distance between the first and second counters and by the gas pressure in the chamber. In measuring angular distributions the absorber thickness was chosen so that the energy interval recorded was greater than the energy spread of the group of particles under investigation.

To distinguish α particles from protons, a pulse height analyzer was placed ahead of the coincident circuit in the leads from the first counter. Figure 2 shows a differential pulse spectrum obtained with this analyzer for an aluminum target. Because of the great difference in specific ionization of protons and α particles, the peaks corresponding to inelastic scattering of protons by aluminum (left peak) and to α particles from the Al^{27} (p, α) Mg^{24} reaction (right peak) are well resolved. In measuring the α particles, the pulse height analyzer was used as an integral counter and the lower threshold was adjusted so that protons were not recorded.

The experimental equipment described made it possible to investigate the energy and angular distributions of particles with a range exceeding 30 μ of aluminum; this corresponds to a minimum energy of 1.7 Mev for protons and 6.7 Mev for α particles.

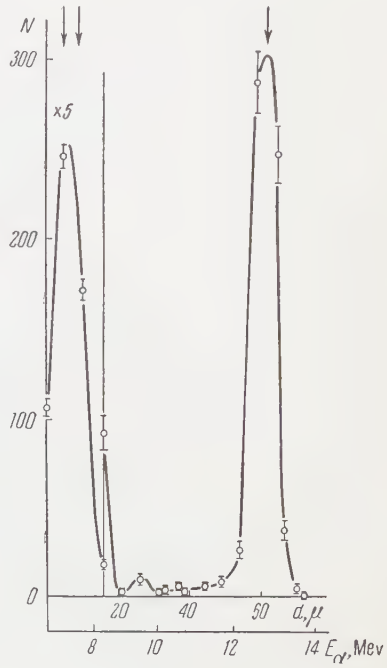

FIG. 3. Energy spectrum of α particles from the $F^{19}(p,\alpha)O^{16}$ reaction for E_p = 6.6 Mev. The upper scale on the abscissa gives the thickness d of aluminum absorber in front of the first counter, and the lower scale the energy of the α particles in Mev.

EXPERIMENTAL RESULTS

In Fig. 3 we show the distribution in range of α particles emerging at an angle of 30° from bombardment of a teflon target by protons of 6.6 Mev. The arrows show the expected location of the three groups of α particles produced in the F^{19} (p, α) O^{16} reaction. No α particles were observed from reactions on any other elements, since the α particles formed in most (p, α) reactions have an energy less than 6.7 Mev. The background at most angles did not exceed 1 — 2% and was somewhat higher at small and large angles. At 20° the background reached 10%, while for still smaller angles the background increased sharply because of the heavy loading of the counters by elastically scattered protons. Because of this the angular distributions were measured over the range of angles from 20 to 160°.

The angular distributions of the long-range α particles, which result from the F^{19} (p, α) O^{16} reaction corresponding to formation of the O^{16}

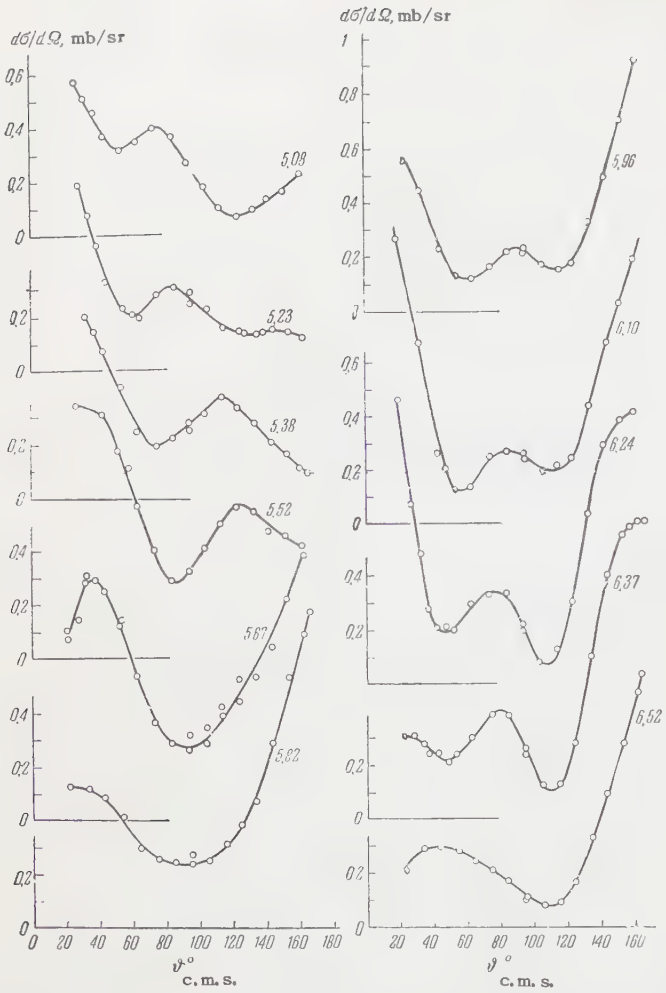

FIG. 4. Angular distributions (in the c.m.s.) for α particles from the $F^{19}(p,\alpha)O^{16}$ reaction, corresponding to the ground state of O^{16}. On the curves are shown the values of the mean energy of the protons in the target. The statistical errors are smaller than the size of the experimental points.

nucleus in its ground state (Q = 8.12 Mev), were measured for 11 values of the energy of bombarding protons from 5.15 to 6.68 Mev. The results obtained, transformed to the center of mass system, are shown in Fig. 4. In measuring the angular distributions we used a target of teflon (the simplest formula being CF_2) 1.6 mg/cm^2 in thickness. With the target set at an angle of 45°, this is equivalent to a loss of 140 kev for protons with 6 Mev energy. For protons with energies of 5.67 and 6.52 Mev the angular distributions were measured several times. For 6.52 Mev we also made control measurements with targets of CaF_2 and LiF prepared by evaporation in vacuum. The experimental data obtained in the various experiments are in good agreement with one another.

The values of the differential cross sections in millibarns per steradian recorded on the ordinates in Fig. 4 were obtained by comparing the results of the present work at an angle of 90° and proton energies of 5.08 and 5.23 Mev with the cross sections given by Ranken et al.[3]

DISCUSSION OF RESULTS

As we see from Fig. 4, all the observed angular distributions are markedly anisotropic. For proton energies of 5.08 up to 6.24 Mev, there is a rise in the differential cross section at small angles. For energies from 5.67 to 6.52 Mev the angular distributions reach a maximum at angles close to 180°. The presence of all these maxima is characteristic of direct processes: the ejection by the impinging proton of an α particle from the nucleus (so-called "knock-out"),[5] and pick up by the proton of a triton from the F^{19} nucleus[6] should lead to the occurrence of a maximum at small angles, while "heavy particle stripping" for light nuclei can lead to the appearance of a maximum at large angles. As already mentioned, the angular distributions of α particles from the F^{19} (p, α) O^{16} reaction measured by Likely and Brady[4] for protons with energies 16.0 and 18.5 Mev are explained well if one assumes that the main reaction mechanism at these energies is the pickup of a triton. One can draw no conclusion concerning the relative contribution of "heavy particle stripping" at these energies from the work of Likely and Brady, since they made their measurements only for angles less than 120°. However, "heavy particle stripping" seems to give a considerable contribution to the reaction C^{12} (α, p) N^{15} which was investigated by Nonaka et al.[8] for α particles with energies from 25 to 39 Mev (this is equivalent to protons with energies from 14.7 to 25.9 Mev for the inverse reaction). The angular distributions obtained by them for particles formed in this reaction have a maximum at small angles, while for energies of the α particles below 31 Mev (which corresponds to proton energies less than 1.95 Mev for the inverse reaction) there is observed a maximum at large angles, whose height is of the same order as that of the forward maximum.

Thus the presence of sharp maxima in the differential cross section is naturally explained by direct processes. Calculations show that one can obtain satisfactory agreement with all the observed angular distributions by using the simplest formula[7] for computing angular distributions in the processes of capture and "heavy particle stripping," if one takes account of interference between these processes. (As an example we show in Fig. 5 the results of computation of angu-

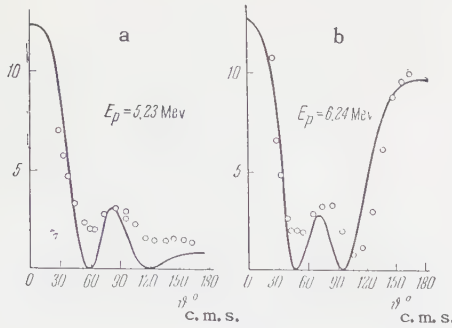

FIG. 5. Comparison of observed angular distributions with the distributions computed in case a for pickup (for interaction radius $R = 7.4 \times 10^{-13}$ cm); for case b – for pickup (for $R = 7.8 \times 10^{-13}$ cm) and for "heavy particle stripping" (for $R = 7.0 \times 10^{-13}$ cm), where interference has been taken into account.

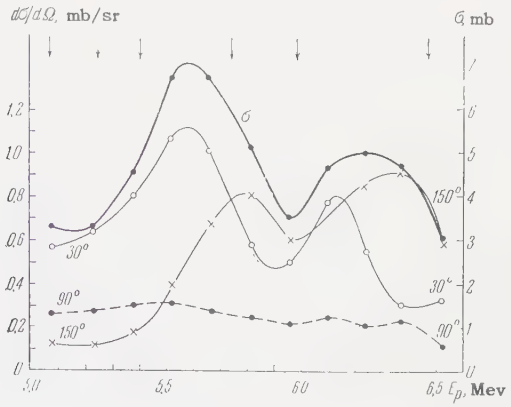

FIG. 6. Dependence of total cross section (solid curve) and differential cross section at angles of 30°, 90°, and 150° (dashed curves) on proton energy.

lar distributions for protons with energies 5.23 and 6.24 Mev.) However, such agreement can be obtained only if for the different proton energies we use different values of the parameters characterizing the radii of interaction in the processes of capture and "heavy particle stripping," and of the relative values of the amplitudes for these processes. This is related to the strong dependence of the observed angular distributions on the energy of the incident protons. In addition, when the energy is varied, the maxima in the angular distributions shift opposite in direction to that which one should get from the theory of direct processes. For example, when the proton energy is increased from 5.08 to 5.67 Mev, the maxima shift toward larger angles, whereas for the case of direct ejection and for the case of capture, the maxima should shift toward 0°. In order to explain the observed shift of the maximum, one must assume a very rapid fall-off in the parameter R with increasing energy, which it seems cannot be justified.

The strong dependence of the angular distributions on the energy of incident protons is an indication of the important role of reaction mechanisms associated with formation of a compound nucleus.[9] Further evidence in favor of this is that the change in total cross section with energy is not monotonic, as it should be for direct processes. In Fig. 6 we show the change in total cross section with energy and the excitation curves for the differential cross sections at angles 30°, 90° and 150°. The experimental curves shown on the figure (except for the excitation curve at 90°) have resonance character. It is true that the position of the two maxima observed does not coincide with that of the resonances obtained by Blaser et al.[10] for the F^{19} (p, n) Ne^{19} reaction, which are shown by the arrows on Fig. 6. In addition, the observed maxima in the excitation curves are too broad to be interpreted as resonances corresponding to individual levels in the intermediate nucleus. Nevertheless, the resonance structure of the excitation curves shows that in the (p, α) reaction in fluorine compound nucleus formation plays an important role.

Thus the measured angular distributions of α particles formed in the F^{19} (p, α) O^{16} reaction show apparently that in the range of proton energies from 5.1 to 6.5 Mev there is no single predominant reaction mechanism. In this energy interval there are sizable contributions both from direct processes and from reaction mechanisms associated with formation of a compound nucleus.

In conclusion the authors express their gratitude to B. V. Devichev for valuable assistance in carrying out the work and also to the operating group of the cyclotron.

[1] Isoya, Ohmura, and Momota, Nucl. Phys. **7**, 116 (1958).

[2] R. L. Clarke and E. B. Paul, Can. J. Phys. **35**, 155 (1957).

[3] Ranken, Bonner, and McCrary, Phys. Rev. **109**, 1646 (1958).

[4] J. G. Likely and F. P. Brady, Phys. Rev. **104**, 118 (1956).

[5] Austern, Butler, and McManus, Phys. Rev. **92**, 350 (1953).

[6] P. B. Daitch and J. B. French, Phys. Rev. **87**, 900 (1952).

[7] L. Madansky and G. E. Owen, Phys. Rev. **99**, 1608 (1955).

[8] Nonaka, Yamaguchi, Mikumo, Umeda, Tabata, and Hitaka, J. Phys. Soc. Japan **14**, 1260 (1959).

[9] R. M. Eisberg and N. M. Hintz, Phys. Rev. **103**, 645 (1956).

[10] Blaser, Boehm, Marmier, and Scherrer, Helv. Phys. Acta **24**, 465 (1951).

Translated by M. Hamermesh
168

ANGULAR AND MOMENTUM DISTRIBUTIONS OF RESIDUAL NUCLEI PRODUCED IN THE INELASTIC SCATTERING OF FAST PIONS AND PROTONS ON HELIUM

M. S. KOZODAEV, M. M. KULYUKIN, R. M. SULYAEV, A. I. FILIPPOV and Yu. A. SHCHERBAKOV

Joint Institute for Nuclear Research

Submitted to JETP editor May 11, 1960

J. Exptl. Theoret. Phys. (U.S.S.R.) **39**, 929-936 (October, 1960)

We investigate the angular and momentum distributions of residual nuclei produced as a result of quasi-free interaction of fast pions or protons with the nucleons of helium nuclei. It is found that the shape of the distributions can be explained within the framework of the Serber-Goldberger model by taking into account the transfer of additional momentum due to coupling. The possibility of determining the momentum distribution of the nucleons in the helium nucleus from the momentum spectrum of the residual nuclei is discussed. The momentum distribution of the nucleons can be satisfactorily described by a Gaussian function that decreases to the 1/e value at an energy $E_0 = (12 \pm 2)$ Mev.

INTRODUCTION

EXPERIMENTS with fast particles have demonstrated that the inelastic interaction between these particles and nuclei is essentially the result of several successive collisions of the incoming particle with individual nucleons of the nucleus. Such processes can be described by regarding the nucleons as free, and coupling can be accounted for in first approximation by introducing a certain intranuclear nucleon momentum distribution, for example, the degenerate Fermi-gas distribution (the Serber-Goldberger model[1-2]).

Of particular interest are the so called quasi-free collisions, which are accompanied by the knock-out of only one nuclear nucleon. A study of such processes can yield information on the intranuclear nucleon momentum distribution, since the kinematic characteristics of all three particles in the final state depend on the momentum of the nucleon inside the nucleus at the instant when it collides with a fast particle.

In references 3 — 5, the momentum distribution of the nucleons in the nuclei was investigated by an analysis of the energy spectra of inelastically scattered nucleons. This method, however, is not free of certain shortcomings, the most important among them being the impossibility of distinct separation of the quasi-free scattering processes.

The most direct connection exists between the intranuclear momentum of the nucleus and the momentum of the residual nucleus.[6,7] Within the framework of the model under consideration, the momentum of the residual nucleus should be equal in magnitude and opposite in direction to the momentum of the nucleons with which collision takes place; thus, the momentum spectrum of the residual nuclei should be a direct reflection of the internuclear momentum distribution of the nucleons. However, such a simplified interpretation of the spectra of the residual nuclei calls for an experimental verification. It may be useful in this connection to study the angular distributions of the residual nuclei, and to carry out experiments with different particles over a wide range of energies. To investigate the intranuclear momentum distributions of the nucleons over the residual nuclei, it is best to use the helium nucleus, which experiences, with a high degree of probability, quasi-free collisions when bombarded by fast particles.[8,9] Furthermore, the residual nuclei He^3 and H^3 are relatively easy to record.

Attempts to obtain information on the intranuclear motion of nucleons in the nucleus He^4 were undertaken in references 5 and 10. In spite of the high accuracy of the resultant inelastic proton scattering spectra, Hillman et al.[5] were unable to make a clearcut choice between the two compared parameters of the Gaussian distribution — 5 Mev and 18 Mev. Selove and Teem[10] investigated the momentum spectrum of deutrons in the capture of neutrons from the nucleus He^4 by protons. However, as indicated by the authors themselves, they were unable to obtain data on the nucleon momentum distribution, owing to the low energy of the incoming particles (95 Mev).

We report here the results of an investigation of the angular and momentum distributions of resid-

ual nuclei in quasi-free interactions of fast pions and protons with helium nucleons.

EXPERIMENTAL SETUP AND IDENTIFICATION OF INTERACTION EVENTS*

The experiments were made with high-pressure diffusion chambers exposed to the particle beams from the synchrocyclotron of the Joint Institute for Nuclear Research. The proton, positive-pion, and negative pion energies were 630 ± 15, 237 ± 7, 330 ± 6 Mev, respectively. Some 20,000 photographs were obtained in each of the proton and negative-pion beams, and approximately 10,000 were obtained in the positive-pion beam.

By observing the interactions in a diffusion chamber we could exclude events accompanied by cascades as well as events that could be attributed to the interaction between the incoming particle and a group of nucleons in the nucleus. Quasi-elastic interaction events were segregated by suitable angle and momentum correlation of the particles emitted after the interaction. Figure 1 shows a typical quasi-elastic scattering of a proton by a proton. The momentum of the H^3 and He^3 nuclei was determined in most cases from the range of these particles in the gas of the chamber. In those cases when the recoil nucleus did not stop in the sensitive volume of the chamber, its momentum was determined by calculation from the known momentum of the incoming particles and the angles of the scattered particles. This could be done only for H^3, for in this case the scattering angles of all the particles were known. The average accuracy of determination of the momenta of the residual nuclei was approximately 15%. The results of identification of the remaining reactions are listed in the table.

FIG. 1. Photograph of quasi-elastic scattering of a proton by a proton.

Number of events	Reaction	Serial number	Cross section 10^{-27} cm
1	$p+He^4 \to p+p+H^3$	88(2)*	29±3
2	$\pi^+ + He^4 \to \pi^+ + p + H^3$	51(1)	50±7
3	$\pi^- + He^4 \to \pi^- + p + H^3$	27(4)	13±3
4	$p+He^4 \to p+n+He^3$	136	46±4
5	$p+He^4 \to (\pi,N,N)+He^3$		
6	$\pi^+ + He^4 \to \pi^+ + n + He^3$	14	14±4
7	$\pi^- + He^4 \to \pi^- + n + He^3$	72(4)	34±4
8	$\pi^+(^-) + He^4 \to \pi^0 + p(n) + H^3(He^3)$	85 (2)	—

*The parentheses contain the number of cases in which the track of the residual nucleus is not seen and the direction of its emission is thus unknown.

It was impossible to separate reaction 4 from the quasi-free interaction accompanied by a creation of mesons and by the emission of a He^3 nucleus (reaction 5). Among the events classified as reactions 4 and 5 there could be also included two other processes,

$$p + He^4 \to \pi^+ + n + He^4, \qquad p + He^4 \to \pi^0 + p + He^4.$$

However, estimates based on Moulthrop's results[11] show that the contribution of these reactions is insignificant.

EXPERIMENTAL RESULTS

Figure 2 shows a histogram of the angular distribution of the residual nuclei from a quasi-free scattering of protons (reactions 1, 4, and 5). The angular distribution of the residual nuclei reactions 2, 3, 6, 7, and 8 is shown in Fig. 3. The statistical material available provides no indication whatever of the difference between the distributions for the residual nuclei from reactions with positive and negative pions. The results for both types of pions were therefore combined to improve the statistics.

*A detailed description of the experimental setup, data reduction, and identification of interaction events was given by us in references 8 and 9.

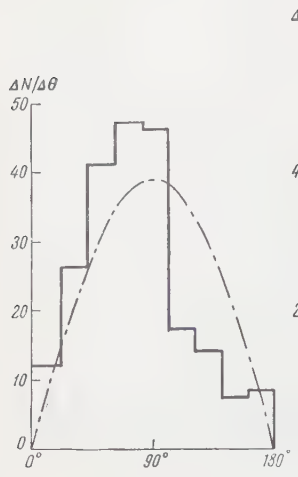

FIG. 2

FIG. 3

FIG. 2. Angular distribution of residual nuclei (in laboratory system) from the quasi-free proton-scattering reactions. Dash-dot curve – distribution calculated with allowance for the energy dependence of the nucleon-nucleon cross sections.

FIG. 3. Angular distribution of residual nuclei from the quasi-free interaction of positive and negative pions. Dash-dot curve – distribution calculated with allowance for the energy dependence of the meson-nucleon cross sections.

It follows from an examination of both histograms that the residual nuclei are emitted preferably in the forward hemisphere. If the anisotropy of the angular distribution is characterized by the quantity $\alpha = N_1/N_2$, where N_1 and N_2 are the numbers of nuclei emitted in the forward and backward hemispheres, we obtain the following values of α for the distributions indicated above:

$$\alpha_p = 2.17 \pm 0.15, \qquad \alpha_\pi = 1.26 \pm 0.13.$$

The momentum distributions of the residual nuclei are shown in Figs. 4 and 5. As in the preceding case, the histograms are plotted for the residual nuclei from reactions 1, 4, 5 and 2, 3, 6,

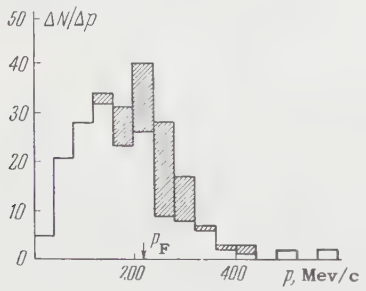

FIG. 4. Momentum distribution of residual nuclei from a quasi-free proton scattering reaction. The hatched areas indicate cases in which only the minimum value of the momentum is known. The arrow indicates the end-point momentum of the Fermi distribution.

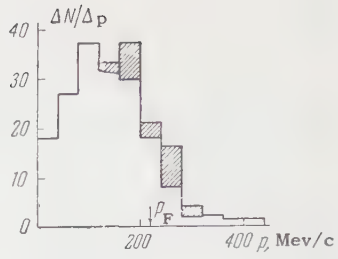

FIG. 5. Momentum distribution of residual nuclei from the quasi-free interaction of positive and negative pions. The notation is the same as in Fig. 4.

7 respectively. The data on reaction 8 were not included in the distribution because the ranges of the H^3 nuclei did not fit, as a rule, in the sensitive volume of the chamber. Both distributions are similar in form, although the nature and energy of the bombarding particles and the type of reaction were quite different. In no case is the form of the momentum distribution similar to the Fermi distribution for a degenerate gas at zero temperature, although the residual nuclei have momenta which are of the same order of magnitude as is usually ascribed to the intranuclear nucleons.

DISCUSSION OF RESULTS

A. Angular Distributions. An attempt can be made to understand the foregoing by considering the collision between a fast particle and the nucleus within the framework of the Serber-Goldberger model. According to this model, the momenta of the intranuclear nucleons are isotropically distributed in space. However, the angular distribution of the residual nuclei will in general not be isotropic, since it depends on many factors connected with the motion of the nucleons. Estimates show that the deformation of the angular distribution is due essentially to the dependence of the meson-nucleon or nucleon-nucleon cross section on the relative energy of the colliding particles. Figures 2 and 3 show the angular distributions of the residual nuclei calculated in this approximation. A Gaussian intranuclear nucleon momentum distribution $A \exp(-p^2/p_0^2)$ was assumed, with $p_0 = 150$ Mev/c. The integration was from 0 to $p_{max} = 300$ Mev/c. The energy dependence of the cross sections was approximated in the form $a + bE + cE^2$, where E is the kinetic energy of the incoming particles in the laboratory system of coordinates.

The calculated values of the anisotropic coefficients are found to be equal to 1 for the reactions 1, 4, and 5 and to 0.7 for the reactions 2, 3, 6, 7, and 8. In either case, the experimental distributions are shifted towards the smaller angles, compared with the calculated values. It can be assumed that this effect is due to the interaction be-

tween the knock-on nucleon and the residual nucleus.

By continuing the analysis on the basis of the Serber-Goldberger model we can obtain a simplified account of this interaction. It is reasonable to assume that the nucleon knocked out from the nucleus imparts to the latter a certain additional momentum $\Delta\mathbf{p}$ in the direction of its motion. The magnitude of this momentum can be estimated approximately from the energy and momentum conservation laws, by assuming that the knock-on nucleon acquires instantaneously a momentum $\mathbf{p}$, which produces the break in the bond. In this case the magnitude of the additional momentum $|\Delta\mathbf{p}|$ is a single-valued function of the masses of the particles that participate in the reaction, of the momentum $\mathbf{p}$ acquired by the nucleon, and also of the binding energy of the last nucleon in the nucleus.

In reactions 2 and 3 it was possible to measure the direction and magnitude of the momentum of the knock-on nucleon. The additional momentum vector $\Delta\mathbf{p}$ could thus be determined in each case. The picture of the interaction events was reconstructed in space to determine both the magnitude and the direction of the momentum of the residual nucleus prior to its interaction with the knock-on nucleon. The solid line of Fig. 6 shows the angular distribution of the H^3 nuclei from reactions 2 and 3. The histogram obtained after taking account of the interaction in the final states, is plotted dotted in the same figure. It is shifted backward somewhat compared with the experimentally-obtained distribution. The dash-dot line in the same figure is calculated with allowance for the energy dependence of the meson-nucleon cross sections. The intranuclear momentum distribution of the nucleons was taken in the same form as in the calculations,

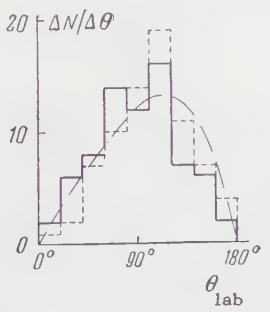

FIG. 6. Angular distribution of the H^3 nuclei from reactions 2 and 3. The dotted line shows the distribution corrected for the interaction between the nucleon and the residual nucleus. The dash-dot line shows the distribution calculated with allowance for the energy dependence of the meson-nucleon cross sections.

the results of which are shown in Fig. 2. It is seen that allowance for the interaction of the knock-on nucleon with the residual nucleus brings the experimental distribution closer to the calculated one.

This simple method of accounting for the interaction between the nucleon and the residual nucleus in the final state cannot be used for the remaining reactions, since the direction and the magnitude of the momentum of the nucleon knocked out from the nucleus are indeterminate. The form of the angular distribution can, generally speaking, be calculated for these reactions by the Monte-Carlo method. Such a calculation was made with a "Ural" electronic computer for reaction (1). No calculations were made for the other reactions, since their momentum spectra could not be fully analyzed, owing to the presence of a considerable number of events in which the momentum of the residual nucleus could not be measured.

The calculation was carried out in the following sequence. After "drawing" the probable magnitude and direction of the momentum $\mathbf{p}$ of the intranuclear nucleon, the magnitude and direction of the momenta of the colliding nucleons were obtained from kinematic calculations. Use was made here of known data on the differential cross sections of elastic pp scattering at different energies.[12] The initial momentum of the residual nucleus $\mathbf{p}'_{res}$ was assumed to be $\mathbf{p}'_{res} = -\mathbf{p}_N$. The calculation was concluded by finding the vector $\mathbf{p}_{res} = \mathbf{p}'_{res} + \Delta\mathbf{p}$, corresponding to the actual direction and magnitude of the momentum of the residual nucleus. The magnitude of the vector $\Delta\mathbf{p}$ was found by the method indicated above. The exclusion principle eliminated from further consideration the cases in which one of the colliding nucleons had a momentum less than 220 Mev/c (endpoint energy of the Fermi distribution for the helium nucleus). The angular distribution calculated in this manner is characterized by an anisotropic coefficient $\alpha_p^* = 1.25 \pm 0.15$, which agrees with the experimentally-obtained $\alpha_p = 1.5 \pm 0.2$.

It should be noted that the large value of α_p in the overall angular distribution of the residual nuclei from all the quasi-free proton interaction reactions was due essentially to reactions 4 and 5. This can be explained qualitatively by the fact that meson-production processes cause the knock-on nucleons to be slower in the c.m.s. As a result, such a nucleus acquires a large additional momentum, so that the angular distribution is more strongly deformed.

B. Momentum Spectra of the Residual Nuclei. Unlike the situation prevailing in the angular distributions, the kinematic factors play a much smaller role in the momentum spectra of the residual nuclei. As shown by suitable computations, the momentum spectrum of the residual nuclei,

neglecting defects due to the interaction between the knock-on nucleon and nucleus, should duplicate accurately the momentum distribution of the nucleons inside the nucleus. However, an analysis of the angular distributions shows that the interaction between the nucleon and the residual nucleus must be taken into account. This is evidenced also by a certain discrepancy in the momentum spectra of residual nuclei from reactions with protons and pions.

For reasons mentioned earlier, we shall analyze only the spectra of the residual nuclei from reactions 1, 2, and 3. An approximation of the momentum spectrum by means of a Gauss function, carried out by the method of least squares, yields for the residual nuclei from reactions 2 and 3 (with pions) a parameter p_0 of value (130 ± 7) Mev/c, whereas $p_0 = 158 \pm 12$ Mev/c for the spectrum of the nuclei from the reaction (1) with protons (see Figs. 7 and 8, solid lines).

The effect of the bond was taken into account in exactly the same manner as in the preceding section, in the analysis of the angular distributions. Figure 7 shows the corrected experimental points of the spectrum from reactions 2 and 3. A value (150 ± 8) Mev/c is obtained for p_0 in this case (dash-dot line). This value of p_0 was introduced into the initial conditions for the calculation of the spectrum of the H^3 nuclei from the quasi-elastic proton scattering, carried out by the Monte-Carlo method. The resultant value of p_0 was 155 ± 5 Mev/c (dash-dot line in Figure 8). The calculated value of p_0 is close to the experimental value, 158 ± 12 Mev/c, thus indicating that the initial distribution has been correctly chosen.

We see thus that the momentum spectra obtained, with allowance for the bond, for the intranuclear nucleons from reactions with either pions or protons are the same, accurate to experimental errors, and a value 150 Mev/c can be used for p_0. The energy corresponding to this momentum is 12 ± 2 Mev.

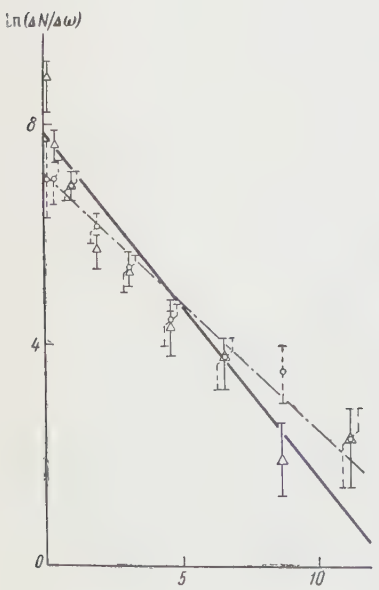

FIG. 7. Momentum spectrum of H^3 nuclei from reactions 2 and 3: Δ – initial spectrum, o – after correction for the influence of the bond.

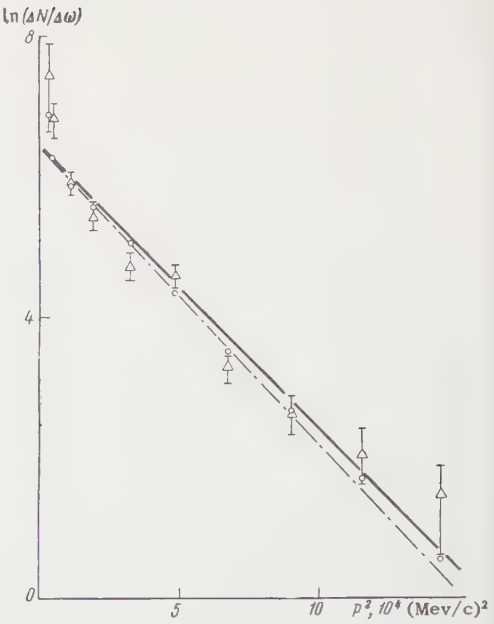

FIG. 8. Momentum spectrum of H^3 nuclei from reactions 2 and 3: Δ – initial distribution, o – distribution obtained in the Monte-Carlo calculation.

The value $E_0 = 12 \pm 2$ Mev as intermediate between the two values for the Gaussian distribution parameter, $E_0 = 5$ Mev and $E_0 = 18$ Mev, analyzed by Hillman et al.[5] The first of these values, obtained previously by Stubbins,[13] is apparently less likely.

Compared with the spectra for the light nuclei, such as carbon or oxygen, the distribution measured in the present work is softer. Thus, according to data by Cladis, Hess, and Moyer,[3] the Gaussian distribution parameter E_0 amounts to 16 ± 3 Mev for carbon. In a later paper by Meshcheryakov et al.[4] a somewhat higher value, $E_0 = 20$ Mev, is given.

It must be noted that the methods used both in the present work and in references 3 — 5 to obtain information on the intranuclear momentum distribution of the nucleons lead to a certain distortion of this distribution in the high-energy region. In the investigation of the momentum spectra of inelastically scattered protons it was impossible to separate the protons which were scattered by groups of nucleons, and consequently the resultant distribution may be "harder" than the actual distribution.

If the momenta of the recoil nuclei are registered and only quasi-elastic scattering events are selected, the momentum distribution of the nucleons may, to the contrary, be too soft, for in such a

selection the cases when the incoming particle interacted with a nucleon which is strongly bound to other nucleons of the nucleus are left out from the distribution. This point of view finds certain confirmation in the results obtained by McEwen, Gibson, and Duke.[14] In these investigations, the quasi-elastic scattering events in emulsion were selected and the residual momentum was estimated from the proton scattering angles. For light nuclei in the emulsion (carbon or oxygen), a Gaussian distribution with $E_0 = 11 \pm 3$ Mev was obtained.

Watanabe,[15] and later on Brueckner, Eden, and Francis[16] have shown that the character of the interaction that takes place between the nucleons of the nucleus influence significantly the shape of the momentum distribution of the nucleons. Calculations carried out on the basis of the pair-interaction model[16] show that in the case of light nuclei the form of the spectrum in the region of large momenta is close to Gaussian for which a parameter $E_0 = 14$ Mev has been obtained in several experiments.[3,17] However, the theory developed does not permit a description of the form of the entire momentum spectrum of the nucleons, which differs in character noticeably from the Fermi distribution in the region of small momenta.

The authors are grateful to I. K. Vzorov and Yu. D. Prokoshkin for discussion of the results of the present investigation. The authors thank I. A. Popova for performing the calculations on an electronic computer, and also E. A. Shvaneva for help in reduction of experimental data.

[1] R. Serber, Phys. Rev. **72**, 1114 (1947).

[2] M. Goldberger, Phys. Rev. **74**, 1269 (1948).

[3] Cladis, Hess, and Moyer, Phys. Rev. **87**, 425 (1952).

[4] Azhgirei, Vzorov, Zrelov, Meshcheryakov, Neganov, Rynding, and Shabudin, JETP **36**, 1631 (1959), Soviet Phys. JETP **9**, 1163 (1959).

[5] Hillman, Johansson, Tibell, Tyren, and Kohler, Nucl. Phys. **12**, 596 (1959).

[6] W. F. Fry, Phys. Rev. **93**, 845 (1954).

[7] G. Takeda, Phys. Rev. **93**, 848 (1954).

[8] Kozodaev, Kulyukin, Sulyaev, Filippov, and Shcherbakov, JETP **38**, 409 (1960), Soviet Phys. JETP **11**, 300 (1960).

[9] Kozodaev, Kulyukin, Sulyaev, Filippov, and Shcherbakov, JETP **38**, 708 (1960), Soviet Phys. JETP **11**, 511 (1960).

[10] W. Selove and J. Teem, Phys. Rev. **112**, 1658 (1958).

[11] P. H. Moulthrop, Phys. Rev. **99**, 1509 (1955).

[12] W. Hess, Revs. Modern Phys. **30**, 368 (1958).

[13] W. F. Stubbins, UCRL-8501 (1958).

[14] McEwen, Gibson, and Duke, Phil. Mag. **2**, 231 (1957).

[15] S. Watanabe, Z. Physik **113**, 482 (1939).

[16] Brueckner, Eden, and Francis, Phys. Rev. **98**, 1445 (1955).

[17] E. Henley, Phys. Rev. **85**, 204 (1952).

Translated by J. G. Adashko
169

INELASTIC INTERACTION OF 7-BEV NEGATIVE PIONS WITH NUCLEONS

V. A. BELYAKOV, WANG SHU-FEN, V. V. GLAGOLEV, N. DALKHAZHAV, R. M. LEBEDEV, N. N. MEL'NIKOVA, V. A. NIKITIN, V. PETRZHILKA, V. A. SVIRIDOV, M. SUK and E. D. TOLSTOV

Joint Institute for Nuclear Research

Submitted to JETP editor May 11, 1960

J. Exptl. Theoret. Phys. (U.S.S.R.) **39**, 937-947 (October, 1960)

A total of 535 π^-N interactions in emulsion are analyzed for ~7-Bev mesons. A large asymmetry is observed in the c.m.s., with the nucleons predominantly emitted in the backward hemisphere. Moreover, the transverse and longitudinal momenta of the emitted nucleons are found to be independent of the number of secondary charged particles. The fast pions are characterized by a considerable anisotropy in the angular distribution, whereas slow mesons are emitted isotropically (in the πN c.m.s.). The average momentum of the fast pions is equal to that of the protons. The total number of pions produced does not depend strongly on the number of concurrently produced charged particles. The multiplicity distribution and the average multiplicity can be made consistent with the statistical theory, but the angular and momentum distributions (particularly for nucleons) contradict the theory. An attempt is made to estimate the upper limit of the radius of the nucleon core.

THE study of the inelastic interaction between pions and nucleons is of great interest from the point of view of the structure of the nucleon.[1] Many experiments have been performed recently with emulsion techniques and with hydrogen-filled chambers, in the energy range from 1 to 5 Bev.[2-6] The results of these investigations are analyzed in the review articles by Veksler[7] and Koba and Takagi.[8] We shall therefore merely summarize here the principal conclusions of these authors.

The results of experiments at 1 — 1.5 Bev were discussed in references 9 and 10. The energy spectra and the angular distributions can be explained by assuming the isobars ($^3/_2$, $^3/_2$) and ($^3/_2$, $^1/_2$) play a significant role in the interaction between a pion and a nucleon. Pions with 4.5 and 5 Bev energy were used in references 5 and 6. An analysis of experimental data given in these papers has led the authors to conclude that neither the statistical theory nor an accounting for the isobars can explain the angular distributions in the c.m.s. Walker[5] introduced also the concept of the knock-out of δ mesons from the nucleon shell, and thereby obtained a qualitative explanation of the experimental data at 4.5 Bev. A similar approach to explain the results of the interaction between pions and nucleons at energies of several Bev was proposed by Barashenkov,[11] who did not, however, consider the knock-out of δ mesons, but applied the statistical theory of multiple production to $\pi\pi$ collisions. The author was able to explain qualitatively the asymmetry in the angular distributions of the generated particles, assuming that peripheral pion-pion collisions amount to approximately 20%, and the remainder of the contribution is made by central collisions between the pions and the core. It must also be noted that in investigations of the inelastic interaction between protons and nucleons, a survey of which was given by V. I. Veksler,[7] indications of the presence of peripheral collisions of nucleon shells were obtained.

In the present work, the preliminary results of which were reported at the Kiev conference,[12] we investigate the inelastic interaction between negative pions and nucleons at ~7 Bev. Of greatest interest here is the study of the angular energy characteristics of the recoil nuclei and the pions.

EXPERIMENTAL PART

A 10 by 20 cm pellicle stack of 240 NIKFI-R emulsions 400 μ thick was irradiated in a negative-pion beam of momentum 6.8 ± 0.6 Bev/c. The fraction of muons in the beam was estimated to be 5 ± 2%.[13] The flux density of the negative pions on the boundary of the emulsion chamber was 6×10^3 cm^{-2}. The collimation of the meson beam was characterized by an angular dispersion ± 20′.

Interactions between the mesons and nucleons were traced by rapid scanning along the track.[14] Any particle from the primary beam with angular

TABLE I

π^-p interactions				π^-n interactions			
Number of prongs	Number of events	%, experiment	%, theory*	Number of prongs	Number of events	%, experiment	%, theory*
0	13	4.4±1.6		1	56	23±3	17.0
2	142	48.5±4.2	46.0	3	143	59±5	57.5
4	122	41.6±3.8	44.0	5	36	14.9±2.5	18.5
6	14	4.8±1.5	6.0	7	7	2.9±1.0	2.0
8	2	0.7±0.7	0.1				
Total	293	100		Total	242	100	

*The results of the calculations were graciously supplied by Barashenkov.[21]

dispersion ± 15′ was tracked. A total of 5300 interactions with emulsion nuclei were found. The average range for the nuclear interaction was found to be 35 ± 3 cm.* The interactions between pions and nucleons were identified by the usual criteria.[4,15] Only inelastic interactions were chosen for the analysis, and were classified by the number of charged particles. A total of 535 inelastic interactions were analyzed.

The charged-particle distribution is shown in Table I.

To analyze the interactions it was necessary to identify the charged particles. The slow particles ($g/g_0 > 1.4$)† were identified by tracing to the end of the range or by the Fowler-Perkins method.[16] The dependence of $p\beta c$ on g/g_0, calculated from the tables of Barkas,[17] was plotted for the fast particles. The multiple scattering and ionization were measured on the tracks of fast particles ($g/g_0 < 1.4$) with dip angles up to 5°, accurate to 2 or 3% for ionization and 10 — 15% for momentum. False scattering was eliminated by using the data we obtained in special measurements (see Table II).

TABLE II

Cell length, μ	Value of $\bar{D}_2$ for false scattering, μ	Upper limit of determination of $p\beta c$ with different microscopes	
		MS2 and KSM	MBI-8M
500	0.12±0.01	2	1.6
1000	0.20±0.02	4	3.6
2000	0.35±0.03	7	6.6

To increase the reliability of the particle identification, the multiple scattering and ionization were measured twice (by independent methods). The results of the repeated measurements were

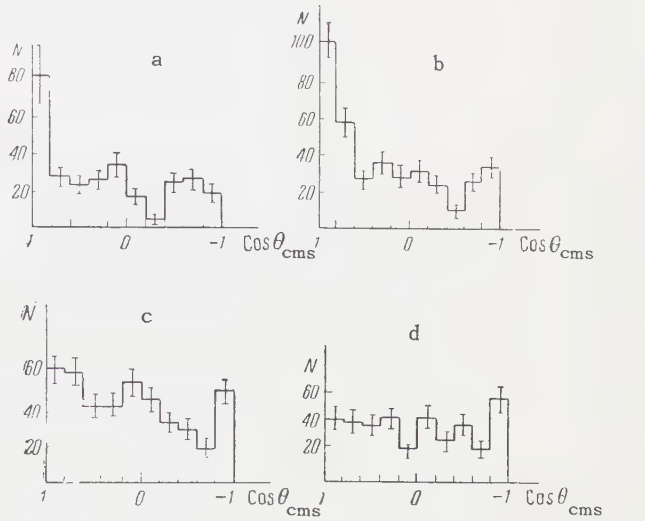

FIG. 1. Angular distributions of the pions in the c.m.s.: a, b, c, and d — distributions for stars with 1–2, 3, 4, and 5–8 prongs, respectively, e — summary angular distribution. The corresponding values of the forward-backward asymmetry coefficient are: a) 2.2 ± 3, b) 1.9 ± 0.2, c) 1.5 ± 0.2, d) 1.0 ± 0.1 and e) 1.6 ± 0.1.

in good agreement. At the attainable accuracy of measuring the scattering and ionization, it was impossible to distinguish pions from protons in the $p\beta$ range from 1.5 to 2.7 Bev/c. However, from the data obtained it can be shown that most particles that fall in the doubtful region are pions (see Appendix). The number of protons falling into this region have been estimated by us to be approximately 10% of the total number of protons.* We identified a total of 459 pions and 134 protons,

*The range was determined for those events, for which reliable control of detection efficiency could be exercised.

†g_0 is the ionization on the track of a pion with momentum 7 Bev/c.

*The K mesons and hyperons have not been identified, but their contribution is small.[18]

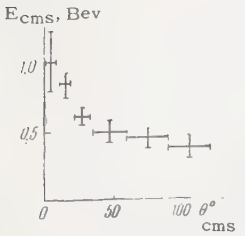

FIG. 2. Dependence of the total pion energy on the angle of emission in c.m.s.

which, allowing for the geometrical corrections, amounts to 1630 ± 70 particles. This is in good agreement with the total number of prongs in all the stars (1590).

The three-dimensional angles of all the tracks were measured accurate to 0.5°, and the accuracy for small angles was better than 0.3°. Figure 1 shows the angular distributions of pions in the meson-nucleon c.m.s. for stars with different number of charged particles, and also the summary distribution for all the stars. The same figure shows the values of the asymmetry η, i.e., the ratio of the number of particles emitted forward and backward relative to the direction of the primary. It is seen that the asymmetry increases rapidly when the number of charged particles in the star is small. It has been noted that the asymmetry is due principally to the pions with large momenta. Figure 2 shows the dependence of the average energy of the secondary mesons on the angle of emission in the c.m.s. An angular dependence is observed here, starting with approximately 0.5 Bev.

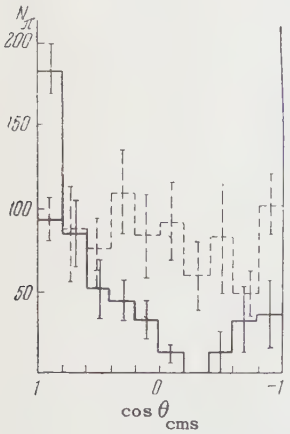

FIG. 3. Angular distributions of pions with momentum $p > 0.5$ Bev/c (solid line) and with $p < 0.5$ Bev/c (dashed line), in the c.m.s.

The angular characteristics of the fast and slow mesons were found to be widely different. Figure 3 shows that the fast mesons conserve so to speak the direction of the momentum of the incoming particle, whereas the small mesons are distributed almost isotropically.*

The number of pions with momentum $p > 0.5$ Bev/c was found to be 522 ± 37, amounting on the average to one fast meson per interaction.

*This conclusion refers to interactions with less than five charged particles.

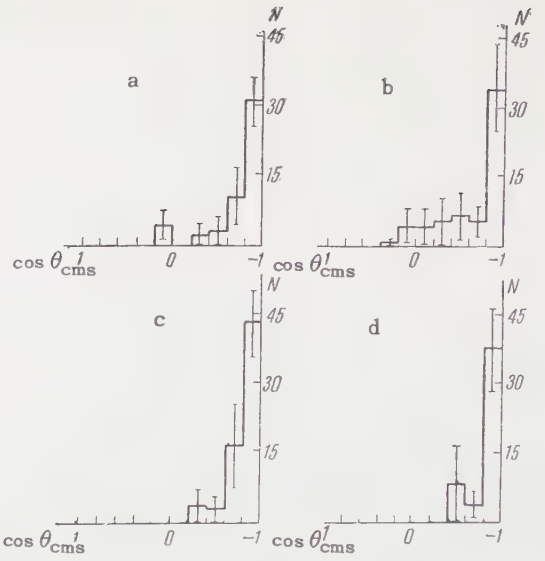

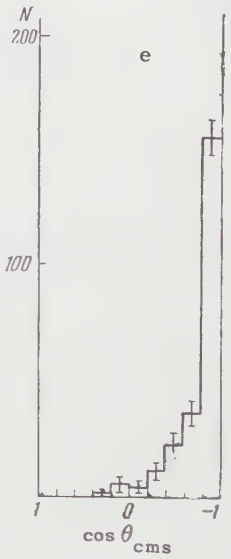

FIG. 4. Angular distributions of protons in the c.m.s. and average values of the angles, in degrees: a – 2-pronged stars, $\overline{\theta} = 136^{+11}_{-9}$, b – 3-prongs, $\overline{\theta} = 133^{+11}_{-8}$, c – 4 prongs, $\overline{\theta} = 143^{+15}_{-11}$, d – 5, 6, 7, and 8 prongs, $\overline{\theta} = 145^{+32}_{-15}$, e – summary angular distribution, $\overline{\theta} = 138^{+19}_{-11}$.

Figure 4 shows the angular distributions of the protons in the c.m.s. for different numbers of charged particles in the star, and also the summary distribution. In all cases the protons are emitted backward and thus retain their initial direction.*

Wherever there is a proton in two-prong stars, the negative pion is as a rule fast. In accordance with this and with the data of Maenchen et al.[6] it can be assumed that most pions with momentum $p > 0.5$ Bev/c are negative.

An examination of the momentum distributions of the pions and nucleons, shown in Figs. 5 and 6, leads us to conclude that the average nuclear momentum, and also the average momentum of the charged pions, does not change, within the limit of statistical errors, with increasing number of

*A similar conclusion was reached in a study[19] of the interaction between the proton and the nucleons.

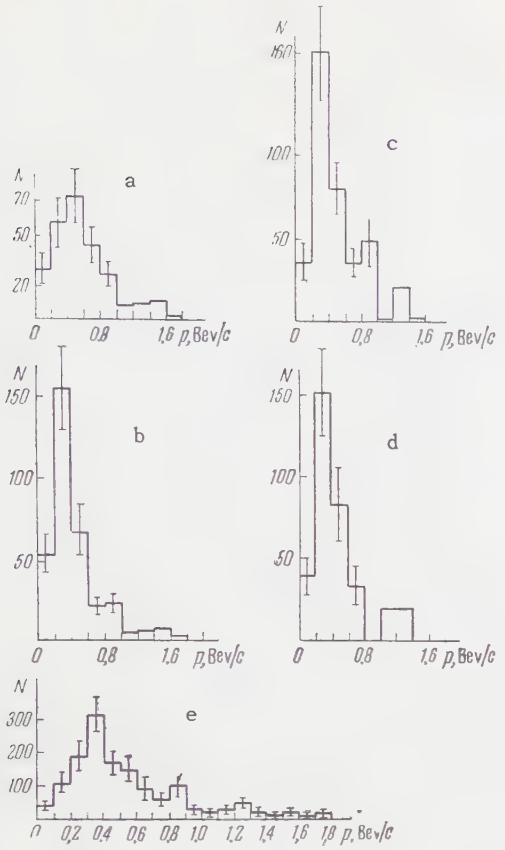

FIG. 5. Pion momentum spectra in the c.m.s. and average values of momenta (in Bev/c): a – 2-pronged stars, $\bar{p} = 0.62 \pm 0.06$, b – 3 prongs, $\bar{p} = 0.44 \pm 0.04$, c – 4 prongs, $\bar{p} = 0.52 \pm 0.05$, d – 5, 6, 7, and 8 prongs, $\bar{p} = 0.46 \pm 0.06$, e – summary momentum spectrum, $\bar{p} = 0.53 \pm 0.03$.

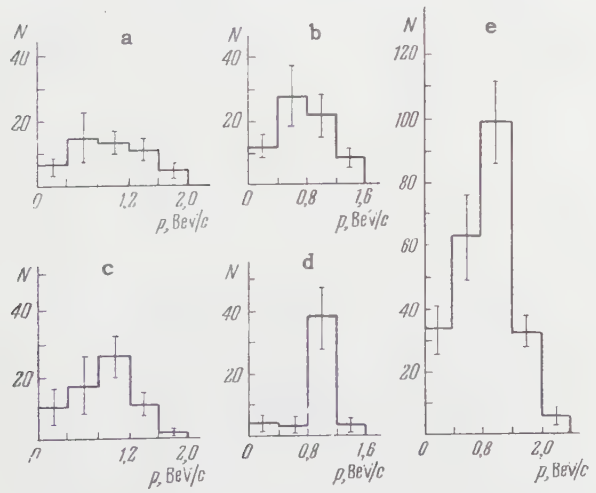

FIG. 6. Momentum spectra of protons in c.m.s. and the average values of momenta: a – 2-pronged stars, $\bar{p} = 0.92 \pm 0.08$, b – 3 prongs, $\bar{p} = 0.79 \pm 0.07$, c – 4 prongs, $\bar{p} = 0.93 \pm 0.06$, d – 5, 6, 7, and 8 prongs, $\bar{p} = 0.92 \pm 0.07$, e – summary momentum spectra, $\bar{p} = 0.89 \pm 0.04$.

TABLE III

n_{ch}	Pions	Protons	Protons*
1—2	0,31±0,04	0.30±0.06	0,38±0.07
3	0,26±0,03	0,37±0.08	0.35±0.07
4	0,36±0.04	0,41±0.08	0,41±0.08
5—8	0,31±0.05	0,40±0.10	0,41±0.10
1—8	0,31±0.02	0,37±0.04	0,39±0.04

*The values of the transverse momenta are given here with suitable allowance for 1/3 of the particles from the doubtful region, which are assumed to be protons, and which are known to exceed the possible number of protons in this region. We see that such a procedure does not change the average transverse momenta, within the limits of errors.

charged particles. It is interesting that the average momentum of fast pions ($p > 0.5$ Bev/c) is 0.87 ± 0.06 Bev/c and is equal to the average nucleon momentum (0.89 ± 0.04 Bev/c).* Starting with the analysis of the angular and momentum characteristics of the secondary protons and pions, it can be assumed that the character of the interaction between the pions and nucleons varies little at 7 Bev with the number of charged particles in the star.

Another interesting characteristic of the interactions at large energies are the transverse momenta of the secondary particles.

We calculated the average transverse momenta $\bar{p}_\perp$ of protons and pions for different multiplicities (relative to the number of charged particles). The values obtained are listed in Table III.

From the data given in Table III we see that, within the limits of statistical accuracy, no significant dependence of $\bar{p}_\perp$ on the number of charged particles in the star is observed for either pions or protons.

ANALYSIS OF EXPERIMENTAL DATA

Attempts were made in many theoretical papers[20-22] to explain the experimental data on the interaction of pions in terms of the statistical theory. Experiments carried out at energies up to 5 Bev, and also the results of the present investigation, have shown that there are many common characteristics which can be explained by this theory, without making any particular assumptions regarding the mechanism of interaction and with-

*It should be noted that our conclusions concerning the behavior of fast pions ($p > 0.5$ Bev/c) and protons are quite reliable for multiplicities $n \leqslant 5$; with $n > 5$, we identified 5 protons in 6-prong stars, 4 protons in 7-prong stars, and 2 protons in 8-prong stars. However, all these protons have in the c.m.s. an angular distribution similar to the angular distributions of the protons in stars with few prongs.

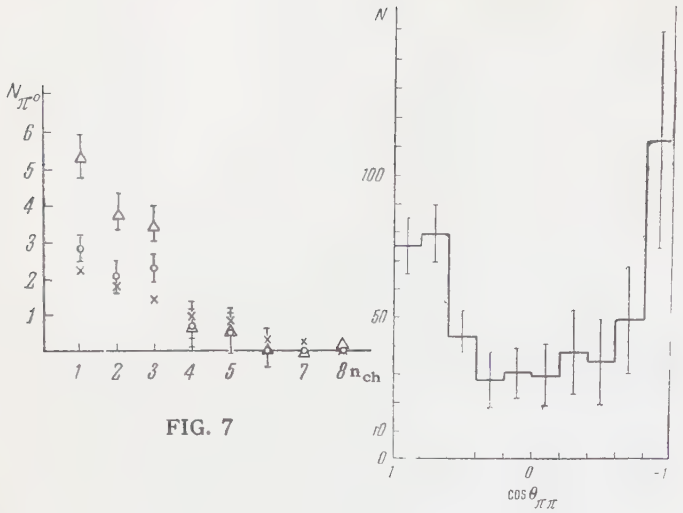

FIG. 7

FIG. 8

FIG. 7. Average number of neutral pions in stars with different numbers of charged particles: o – under the assumption that the neutral-pion spectrum is the same as that of the charged pions (experiment), Δ – under the assumption that all neutral pions belong to the slow part of the spectrum (experiment), x – calculation based on statistical theory.

FIG. 8. Angular distribution of fast pions in the $\pi\pi$ c.m.s.

out introducing any model representations concerning the structure of the nucleon. Characteristics of this kind are, for example, the distribution of the interactions over the number of charged particles, and the relations between the number of charged particles and the neutral mesons. Table I lists data on the distribution of charged particles compared with those calculated by statistical theory. The average number of charged particles in πp collisions is 3 ± 0.01, which agrees with Barashenkov's calculations.[21]

Figure 7 shows the dependence of the number of neutral mesons on the number of charged particles n_{ch}. The experimental points were obtained under two assumptions: a) the charged and neutral mesons have the same average energy for each multiplicity, b) all the neutral pions are slow, $p < 0.5$ Bev/c (isotropic part). The same figure shows the points calculated by statistical theory.[20,22,23] In addition, for 2-pronged stars, for which the momenta of the proton and of the negative pion were measured, a kinematic calculation was made for reactions of the type $\pi^- + p \rightarrow \pi^- + p + k\pi^0$ with $k = 1, 2, \ldots$ In most cases it was found that k should be greater than or equal to 2. The number of charged mesons averaged over all stars is 2.5, while the number of neutral ones is 1.3, if assumption a) is made, or 2.3 if assumption b) is made. It is seen that under assumption a) the fraction of neutral pions is approximately $\frac{1}{3}$ of all the pions.

Other facts, however, cannot be reconciled with statistical theory, unless special model representations are introduced. For example, the asymmetry of the angular distribution of the secondary pions can be explained qualitatively in statistical calculations only by assuming that in some cases a peripheral collision takes place between the pion and a pion of the nucleon shell and using the statistical theory for the $\pi\pi$ collisions, but assuming central collisions for the remaining cases.[11] It seems to us that a more general application of statistics to interactions with the nucleon shell is called for.

As was shown earlier, pions with momenta < 0.5 Bev/c are emitted isotropically in the πp c.m.s., while the faster pions are characterized

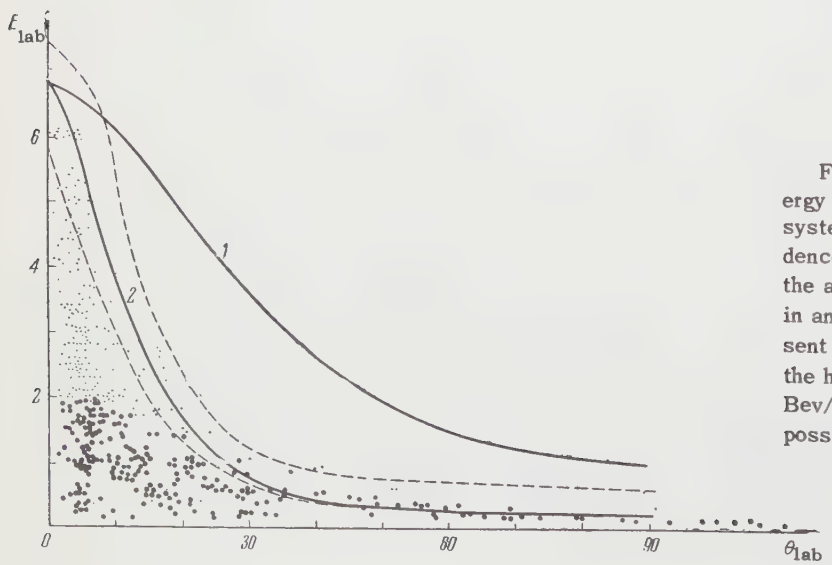

FIG. 9. 1 – dependence of the total pion energy on the angle of emission in the laboratory system in an elastic πN collision; 2 – dependence of the total energy of the π mesons on the angle of emission in the laboratory system in an elastic $\pi\pi$ collision. The light dots represent mesons with momenta $p \geqslant 0.5$ Bev/c, while the heavy dots represent mesons with $p < 0.5$ Bev/c; the dashed lines denote the region of possible deviations in an elastic $\pi\pi$ collision.

by a strong anisotropy. Assuming that a possible connection exists between the anisotropic part and the $\pi\pi$ collision processes, and transforming the fast pions to the $\pi\pi$ c.m.s., we obtain a symmetrical angular distribution with a "forward-backward" ratio 1 ± 0.2 (Fig. 8). It was already noted earlier that on the average there is one such meson per star, and that its average momentum in the πp c.m.s. is 0.87 ± 0.06 Bev/c, which amounts to half the initial momentum (1.7 Bev/c). In Fig. 9 is plotted the dependence of the pion energy on the angle of emission in the laboratory system for elastic πp and elastic $\pi\pi$ scattering. The same figure shows the approximate region of elastic $\pi\pi$ scattering with allowance for the indeterminacy of the momentum of the incident pion and the momentum of the pion in the nucleon shell, ~ 0.3 Bev/c.[24] All the experimental points lie below the curve for elastic $\pi\pi$ scattering, i.e., they do not contradict the assumed inelastic $\pi\pi$ scattering.

If it is assumed that the main process is inelastic $\pi\pi$ interaction and that the secondary mesons are isotropically distributed in the $\pi\pi$ c.m.s., then it is necessary to assume an effective "target" mass $4m_\pi$ to explain the experimental value 1.56 obtained for the asymmetry coefficient of the angular distribution of the mesons in the πp c.m.s. However, since the angular distribution of the secondary mesons can be anisotropic in the $\pi\pi$ c.m.s. (with a maximum at 0 and 180°), the target mass can be less than $4m_\pi$.

It should be noted that a fast negative pion ($p > 0.5$ Bev/c) is present in $\frac{2}{3}$ of the 2-pronged stars with an identified proton. It follows therefore that one negative pion remains for the most part segregated, i.e., its momentum spectrum differs from the spectrum of the other produced mesons.

The most interesting conclusions follow from an analysis of the angular and momentum distributions of the protons (Figs. 4 and 6 and Table III). Much work is done at present in the development of a nucleon model consisting of a dense central part (core) measuring $\sim \hbar/Mc = 0.2 \times 10^{-13}$ cm, surrounded by a meson shell,[1] and on the concepts of central and peripheral collisions associated with this model.[25] An important role in the peripheral interactions could be played by isobars in this case.[7] The peripheral and central interactions could differ from each other in the experiments in having different multiplicity of the produced mesons and different angular and momentum distributions of the recoil nucleons. A higher inelasticity coefficient would be expected in central collisions, owing to the greater opacity of the nucleon; the result would be a greater momentum transfer, and according to statistical theory also a greater multiplicity. The experimental results of the present paper, however, do not confirm the existence of two types of collisions. To the contrary, they indicate that events with different numbers of charged particles have the following like characteristics; 1) angular distribution of the recoil protons (Fig. 4), 2) distribution of the transverse momenta of the recoil nucleons (Table III), 3) total number of produced mesons ($\pi^\pm$ and π^0), which varies little on the average, at most by a factor of two.

Thus, in contrast to the expectation, we observe no central collisions. Owing to methodological peculiarities, we could not identify protons at $p\beta$ values from 1.5 to 2.7 Bev/c. It is easy to see from purely kinematic considerations that such protons (if their angle of emission is $\leq 20°$ in the laboratory system) should travel forward in the πN c.m.s. and can be classified as central collisions. It has been shown earlier that the number of such protons can be on the order of 10% of all the measured protons. Thus, only approximately 10% of all the events could be classified as central collisions.* This yields an estimate of $\sim 4 \times 10^{-14}$ cm for the upper limit of the radius of the core.

An estimate of the dimensions of the region of πN interaction can be made with the aid of the uncertainty relation:†

$$\overline{\Delta p_x^2}\,\overline{\Delta x^2} \geqslant \hbar^2/4.$$

or, in other variables,

$$\overline{\Delta p_\perp^2}\,\overline{\Delta r^2} \geqslant \hbar^2.$$

After substituting the values of $\Delta p_\perp^2$ we get

$$\sqrt{\overline{\Delta r^2}} \geqslant 4 \cdot 10^{-14} \text{ cm}.$$

In conclusion, let us summarize the principal results of the investigation.

1. The angular distributions of the protons have a sharp asymmetry in the πN c.m.s. The average proton momentum is 0.89 ± 0.04 Bev/c; the average transverse momentum is 0.37 ± 0.04 Bev/c. All these characteristics are independent of the number of prongs in the star, within the limits of the indicated errors.

*The authors of reference 19 indicate that a certain possibility remains of assuming all nucleon-nucleon collisions to be central.

†A possibility of such an estimate was pointed out to us by D. I. Blokhintsev.

2. The asymmetry in the angular distribution of all the pions is 1.56 ± 0.10. The pions of momentum $p > 0.5$ Bev/c in the πN c.m.s. have a predominant forward direction. Their average momentum, equal to 0.87 ± 0.06 Bev/c, coincides with the average proton momentum. The remaining pions are distributed almost isotropically in the πN c.m.s. It is shown that the number of pions changes little in stars with different numbers of prongs.

The authors express their gratitude to the proton synchrotron crew for help with the irradiation of the pellicle stack, and to the laboratory group for scanning and measurements.

The authors thank D. I. Blokhintsev and V. I. Veksler for interesting discussions of the results and for useful advice.

APPENDIX

Let us estimate of the fraction of protons in the range of $p\beta$ values from 1.5 to 2.7 Bev/c. In the identification of the particles we found no protons with $p\beta > 2.7$ Bev/c. The energy spectrum of the π mesons in the laboratory system is reasonably interpolated in the momentum range 1.5 — 2.7 Bev/c, if all the particles that enter into this region are assumed to be pions. The angular distribution of these particles is found to be the same as for the identified pions. An estimate of the total number of protons, based on statistical theory, yielded 265 particles, while the experiment produced 238 ± 21. Finally, the unbalanced longitudinal momentum (in the c.m.s.), assuming that it is attributed to the nucleons, is merely 0.10 ± 0.06 Bev/c per nucleon.

Analyzing these facts, we can conclude that all the particles with $p\beta$ ranging from 1.5 to 2.7 Bev/c can be assumed to be pions, while the fraction of protons "lost" thereby amounts in this case to approximately 10% of the total number of protons.

[1] Blohincev, Barashenkov, and Barbasov, Nuovo cimento **12**, 602 (1959).

[2] Walker, Hushfar, and Shephard, Phys. Rev. **104**, 526 (1956).

[3] Eisberg, Fowler, Lea, Shephard, Shutt, Thorndike, and Whittemore, Phys. Rev. **97**, 797 (1955).

[4] W. D. Walker and J. Crussard, Phys. Rev. **98**, 1416 (1955).

[5] W. D. Walker, Phys. Rev. **108**, 872 (1957).

[6] Maenchen, Fowler, Powell, and Wright, Phys. Rev. **108**, 850 (1957).

[7] V. I. Veksler, Proc. Kiev Conf. on High-Energy Physics, 1959 (in press).

[8] Z. Koba and S. Takagi, Fortschr. Physik **7**, 1 (1959).

[9] R. M. Sternheimer and S. J. Lindenbaum, Phys. Rev. **106**, 1107 (1957) **109**, 1723 (1958).

[10] Alles-Borelli, Bergia, Perez Ferriera, and Waloschek, Nuovo cimento **14**, 211 (1959).

[11] V. S. Barashenkov, Nucl. Phys. **15**, 486 (1960).

[12] Belyakov, Wang, Glagolev, Dalkhazhav, Kirillova, Lebedev, Mel'nikova, Nikitin, Sviridov, Suk, and Tolstov, op. cit. ref. 7.

[13] Wang, Wang, Ding, Ivanov, Katyshev, Kladnitskaya, Kulyukina, Nguyen, Nikitin, Otvinovskiĭ, Solov'ev, Sosnovskiĭ, and Shafranov, JETP **38**, 426 (1960), Soviet Phys. JETP **11**, 313 (1960).

[14] B. P. Bannik and M. I. Podgoretskiĭ, Приборы и техника эксперимента (Instrum. and Exptl. Techn.) No. 3, 36 (1960).

[15] N. G. Birger and Yu. A. Smorodin, JETP **36**, 1159 (1959), Soviet Phys. JETP **9**, 823 (1959).

[16] P. H. Fowler and D. H. Perkins, Phil. Mag. **46**, 587 (1955).

[17] W. H. Barkas and D. M. Young, UCRL-2579 (1954).

[18] Wang, Wang, Veksler, Grote, Ding, Ivanov, Kladnitskaya, Nguyen, Nikitin, Otvinovskiĭ, Saitov, and Solov'ev, op. cit. ref. 7.

[19] Wang, Visky, Gramenitskiĭ, Grishin, Dalkhazhav, Lebedev, Nomofilov, Podgoretskiĭ, and Strel'tsov, JETP **39**, 957 (1960), this issue p. 663.

[20] Belen'kiĭ, Maksimenko, Nikishov, and Rozental', Usp. Fiz. Nauk **62**, 1 (1957).

[21] V. S. Barashenkov, Nuovo cimento **14**, 656 (1959).

[22] V. S. Barashenkov and V. M. Maltzev, Acta Phys. Polon. **17**, 177 (1958).

[23] K. Kobayakawa and T. Imamura, Progr. Theor. Phys. **23**, 137 (1960).

[24] Ito, Minami, and Tanaka, Nuovo cimento **9**, 208 (1958).

[25] Barashenkov, Mal'tsev, and Mikhul, JETP **37**, 1484 (1959), Soviet Phys. JETP **10**, 1052 (1960); Nucl. Phys. **13**, 583 (1959).

Translated by J. G. Adashko
170

DETERMINATION OF THE PION-NUCLEON COUPLING CONSTANT FROM DIFFERENTIAL CROSS SECTIONS FOR ELASTIC n-p SCATTERING

N. S. AMAGLOBELI, Yu. M. KAZARINOV, S. N. SOKOLOV, and I. N. SILIN

Submitted to JETP editor May 11, 1960

J. Exptl. Theoret. Phys. (U.S.S.R.) 39, 948-953 (October, 1960)

Experimental data on n-p scattering at 90, 380-400 and 630 Mev have been analyzed for the purpose of determining the pion-nucleon coupling constant, assuming that two poles exist in the real part of the n-p scattering amplitude. It is shown that within experimental error the available data do not disagree with $f^2 = 0.08$.

A method for determining the pion-nucleon coupling constant f has been proposed by Chew.[1] His method is based on the hypothesis that close to the boundaries of the physical region the dependence of the differential cross section $\sigma_{np}(\vartheta)$ on the scattering angle is determined to a considerable extent by those terms of $\sigma_{np}(\vartheta)$ that have second-order poles for $\Delta^2 = -\mu^2$ and $\Delta^2 = 4k^2 + \mu^2$, where Δ is the momentum transferred in a collision, μ is the pion rest mass, and k is the barycentric momentum. Near $\vartheta = 180°$ in this case the function $\sigma_{np}(\vartheta)(4k^2 + \mu^2 - \Delta^2)$, which for the purpose of determining f must be continued analytically into the unphysical region, would vary only slightly, and the analytic continuation might be quite exact even when the experimental errors are relatively large.

In reality, however, the product $\sigma_{np}(\vartheta) \times (4k^2 + \mu^2 - \Delta^2)$ is found to vary strongly in this angular region. f must therefore be determined either by using $\sigma_{np}(\vartheta)$ in a very narrow angular interval close to 180°[2,3] or by using very complicated expressions for the analytic continuation.[4] Rigid requirements are thus set up for the accuracy of the experimental results. It may thus possibly result that when Chew's method is applied to experimental data for $\sigma_{np}(\vartheta)$ in a broad energy interval from 90 to 630 Mev[4,2,3] the result obtained for f^2 will be somewhat smaller than the value 0.08, which is obtained from pion-proton scattering experiments. Yet we know that data on p-p scattering at both high energies (300 Mev)[5] and low energies[6] are in good agreement with $f^2 = 0.08$.

It must also be pointed out that Chew's method[1] will derive considerably different values of f^2 from data on forward scattering ($0 \leq \vartheta \leq 90°$) and backward scattering ($90° \leq \vartheta \leq 180°$), respectively. This can easily be seen when $\sigma_{np}(\vartheta)$ is obtained at 90 Mev.[7] In this case we know that $\sigma_{np}(\vartheta)$ is symmetric with respect to $\vartheta = 90°$ and that the residues in the scattering amplitude at the points $\Delta^2 = -\mu^2$ and $\Delta^2 = 4k^2 + \mu^2$ differ by a factor of 2. It is apparently difficult to explain this difference in the values of f upon the basis of experimental errors alone. Approximately the same situation is observed at 630 Mev.

We have therefore analyzed all known data on n-p scattering at 90, 380—400 and 630 Mev[2,3] for the purpose of determining the pion-nucleon coupling constant while allowing for both poles in the real part of the n-p scattering amplitude (to the right and to the left of the physical-region boundaries).

METHOD OF TREATING EXPERIMENTAL RESULTS

If we assume that the real part of the n-p scattering amplitude contains poles at $\Delta^2 = -\mu^2$ and $\Delta^2 = 4k^2 + \mu^2$[1] the differential cross section $\sigma_{np}(\vartheta)$ in this interval of Δ^2 will be represented by

$$\sigma_{np}(\vartheta) = a_1 b^2 \left[\frac{1}{(x_0 - x)^2} + \frac{4}{(x_0 + x)^2}\right] + \frac{a_2}{x_0 - x} + \frac{a_3}{x_0 + x} + \sum_{n=0}^{n_{max}} a_n x^n,$$

$$x_0 = 1 + \mu^2/2k^2, \qquad x = \cos\vartheta, \qquad b = \mu^2/2k^2, \qquad (1)$$

where α_1, α_2, α_3, αn are undetermined coefficients. The series $\sum_n a_n x^n$ must converge rapidly since the remaining singularities of $\sigma_{np}(\vartheta)$ are quite far from the interval of interest ($-x_0 \leq x \leq x_0$).[8] We note that n_{max} in (1) does not agree with twice the maximum angular momentum ($2l_{max}$). When the first three terms are expanded in powers of x it is easily seen that above 90 Mev the value of $2l_{max}$ is several times larger than that of n_{max}.

Equation (1) is easily derived by expanding $\sigma_{np}(\vartheta)$ in a Laurent series about $x = \pm x_0$. It should also be noted that a similar expression for $\sigma_{np}(\vartheta)$ is obtained by means of dispersion relations.[6,9]

If it is assumed that about the points $x = \pm x_0$ scattering is well represented by a one-meson Feynman diagram[1] (or more precisely by the pole member of this diagram) the coefficient a_1 can be represented in terms of f as follows:

$$a_1 b^2 = m^4 f^4 / 4k^4 (k^2 + m^2),$$

where m is the nucleon mass.

Equation (1) has been used to approximate experimental results at 90, 380 — 400,[7] and 630 Mev.[2] The coefficients a were determined by the method of least squares. We obtained the minimum of

$$\sum_i w_i [y_i - \sigma(x_i)]^2 + [\sigma_{exp} - \sigma_t]^2, \qquad (2)$$

where σ_t is the calculated value of the total cross section, σ_{exp} is the experimental value of the total cross section, y_i represents experimental values of $\sigma_{np}(\vartheta)$, $\sigma(x_i)$ represents renormalized calculated values of $\sigma_{np}(\vartheta)$ [$\sigma(x_i) = N_k \sigma_{np}(\vartheta_i)$, N_k is one of the norms with which data from different experiments are presented].

It was necessary to introduce norms because $\sigma_{np}(\vartheta)$ is measured in relative units. When the norms N_k are treated as auxiliary parameters all expressions for errors in the standard least-squares procedure are automatically derived correctly.*

The coefficient a_1 obtained by minimizing (2) will contain all experimental information regarding the magnitudes of the residues at the poles of the amplitude for $x = \pm x_0$ if no theoretical limitations are placed upon any of the coefficients a. If any such limitations were known they would have to be taken into account, with a corresponding complication of (1).

The following values of the total cross sections were used:

$\sigma_{exp} = (78.3 \pm 2) \cdot 10^{-27}$ cm^2, $E_n = 90$ Mev[7];
$\sigma_{exp} = (33 \pm 1.3) \cdot 10^{-27}$ cm^2, $E_n = 380 - 400$ Mev[7];
$\sigma_{exp} = (26 \pm 4.5) \cdot 10^{-27}$ cm^2, $E_n = 630$ Mev[2].

It was convenient to normalize the cross sections in (2) in a way which made a_1 in (1) equal to f^4. The system of equations for a was solved by successive approximations on an electronic computer. The number of coefficients a_n in (1) was chosen to satisfy the Gaussian criterion in the best manner for positive a_1.

*It is assumed that the relative errors of the norms are small.

The coefficients were also calculated for the fixed value $a_1 = f^4 = 0.0064$ on the basis of considerations that are discussed below.

RESULTS

The values obtained for the coefficients are shown in Table I. The numbers enclosed in parentheses show how strongly the given a coefficient is correlated with all others; the same applies to Table III. These correlation factors indicate by what factor the dispersion of the given a coefficient is reduced if the values of all other coefficients are fixed.* Table II presents the norms of individual measurements.

The values obtained for f^2 from experimental results at 90, 380 — 400 and 630 Mev are 0.06 ± 0.006, 0.065 ± 0.07, and 0.044 ± 0.012, respectively, which agree satisfactorily within experimental error. Unfortunately, appreciable experimental errors (especially in the last case) and the necessity for combining separate relative measurements are a great hindrance to the solution of the problem. Since the a coefficients are strongly correlated among themselves, as the number of coefficients increases their correlations and errors rise sharply. Therefore in view of the existing level of experimental accuracy it is extremely difficult to determine the highest power of x^n in (1); at the same time the number of terms in $\Sigma a_n x^n$ appreciably affects the magnitude of the first coefficient ($a_1 = f^4$). The cause of values of f^2 differing from 0.08 may lie in these circumstances. For the purpose of testing how well the experimental data under consideration satisfy $f^2 = 0.08$, we determined a_2, a_3, and a_n for the fixed value $a_1 = f^4 = 6.4 \times 10^{-3}$. Tables III and IV contain the values thus obtained for the a coefficients together with their correlation factors and norms; the corresponding curves are shown in the figure.

The results show that the presently available experimental data on neutron-proton scattering at 90, 380 — 400 and 630 Mev do not disagree, within the limits of error, with the value $f^2 = 0.08$ for the pion-nucleon coupling constant (for the coefficients, $M/M_{expect} \approx 1$).

When a_1, a_2, and a_3 are compared with the other coefficients it is found that terms having a singularity at $x = \pm x_0$ make a very small contribution to the scattering cross section. Considerable increase of experimental accuracy would therefore

*For example, if there are only two parameters with their correlation coefficient ρ equal to 95% the correlation factor is $K = 1/(1 - \rho^2) \approx 10$.

TABLE I

Energy E, Mev		90 [7]	380—400 [7]	630 [8]
$a_1 \cdot 10^3 = f^4 \cdot 10^3$		3.58±0.74 (1.1·10³)	4.16±0.83 (1.1·10²)	1.94±1.01 (5.0·10²)
$a_2 \cdot 10^3$		0.89±0.60 (3.20·10²)	−0.332±0.16 (6.5·10)	0.05±0.20 (1·10²)
$a_3 \cdot 10^3$		−3.26±1.23 (5.3·10³)	−0.608±0.24 (6.3·10²)	−0.174±0.2 (2.2·10³)
$a_n \cdot 10^3$	$n=0$	6.37±1.3 (1.5·10³)	3.0±0.37 (1.6·10²)	1.58±0.42 (3.2·10²)
	$n=1$	−3.86±0.52 (8.3·10²)	1.29±0.18 (9.0)	1.41±1.26 (6.5·10)
	$n=2$	5.29±1.11 (2.8·10²)	4.01±0.47 (35.0)	3.80±1.26 (3.4·10²)
	$n=3$		−2.43±0.67 (46.0)	−3.80±1.64 (4.5·10²)
	$n=4$		2.16±1.4 (1.6·10²)	−5.07±3.78 (2.0·10³)
	$n=5$			3.77±2.55 (8.2·10³)
	$n=6$			9.39±5.07 (3·10³)
$[M/M_{expect}]^{1/2}$		1.20	1.35	1.15

TABLE II

E, Mev	90 [7]	380—400 [7]	630
N_1	1.008±0.027 (*H*3)*	0.993±0.040 (*H*4)	1.028±0.190[2]
N_2	0.974±0.028 (*S*6)	0.963±0.047 (*D*9)	1.018±0.180[3]
N_3	1.057±0.033 (*W*2)		1.017±0.186[3]
N_4	0.972±0.026 (*S*7)		
N_5	0.950±0.032 (*F*2)		

*The expressions in parentheses correspond to the article by Hess.[7]

TABLE III

Energy E, Mev		90 [7]	380—400 [7]		630 [8]
$a_1 \cdot 10^3 = f^4 \cdot 10^3$		6.4 (fixed)			
$a_2 \cdot 10^3$		−1.05±0.34 (100)	−0.592±0.135 (44)	−0.065±0.345 (296)	−0.37±0.20 (86)
$a_3 \cdot 10^3$		−7.96±0.18 (110)	−1.22±0.06 (27)	−1.36±0.10 (93)	−1.09±0.03 (38)
$a_n \cdot 10^3$	$n=0$	11.23±0.34 (100)	3.89±0.82 (36)	3.46±0.35 (145)	2.96±0.22 (74)
	$n=1$	−5.31±0.31 (30)	1.14±0.17 (7.7)	−0.08±0.52 (76)	1.03±0.37 (42)
	$n=2$	9.28±0.54 (64)	3.98±0.48 (38)	4.33±1.19 (222)	7.53±0.93 (151)
	$n=3$		3.15±0.64 (39)	0.54±1.6 (257)	−3.59±1.72 (405)
	$n=4$		4.82±0.10 (86)	2.71±3.63 (1020)	−16.87±3.14 (1147)
	$n=5$			−6.65±2.85 (487)	2.36±2.76 (783)
	$n=6$			−0.25±4.43 (10^4)	26.79±3.74 (1303)
$[M/M_{expect}]^{1/2}$		1.41	1.54	1.43	1.55

be desirable for the purpose of testing the correctness of (1) for $\sigma_{np}(\vartheta)$ more rigorously.

In order to discover for which angles more precise experimental data are most urgently needed, we compared errors for the cases in which a_1 was, and was not, included among the variable parameters. The angular regions in which the errors for the two cases differ most strongly are most important for the determination of f^2. These regions are represented by the dashed portions of the curves.

It must be noted that the portion of the differential cross section which does not contain singularities at $x = \pm x_0$ is well represented by a rela-

TABLE IV

E, Mev	90 [7]	380—400 [7]	630
N_1	1.000±0.026 (H3)*	0.963±0.036 ** (H4) 0.984±0.040 ***	0.880±0.090 [2]
N_2	0.961±0.027 (S6)	0.935±0.043 ** (D9) 0.950±0.045 ***	0.921±0.064 [2]
N_3	1.016±0.031 (W2)		0.913±0.0476 [3]
N_4	0.961±0.025 (S7)		
N_5	0.930±0.030 (F2)		

*The expressions in parentheses correspond to the article by Hess.[7]
**Expansion to x^4.
***Expansion to x^6.

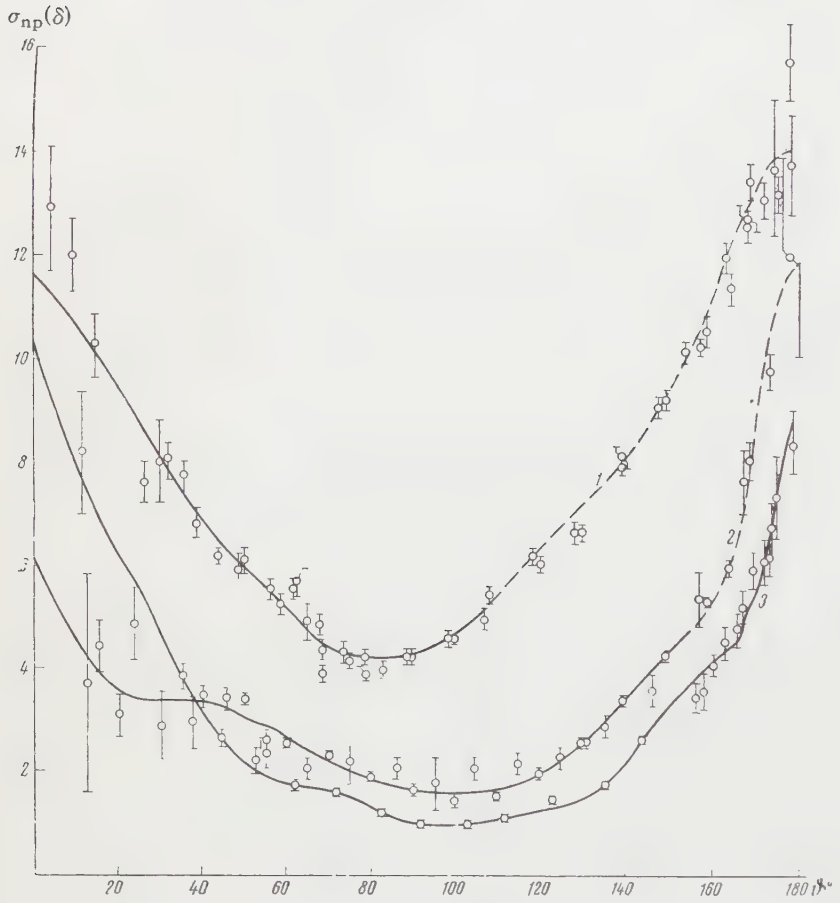

Differential cross sections (in units of 10^{-27} cm²/sr) as a function of the scattering angle. 1 – E_n = 90,[7] 2 – E_n = 380–400,[7] 3 – E_n = 630 Mev.[2] The curves were plotted for $f^2 = 0.08$. The dashed portions represent the angular regions where greater experimental accuracy is desirable before f^2 can be determined more precisely.

tively small number of Legendre polynomials. We believe that this may facilitate the phase analysis of n-p scattering.

The authors are indebted to Prof. Ya. A. Smorodinskiĭ and Prof. B. M. Pontecorvo for an interesting discussion of the results, and to I. N. Kukhtina for assistance.

[1] G. F. Chew, Phys. Rev. **112**, 1380 (1958).
[2] N. S. Amaglobeli and Yu. M. Kazarinov, JETP **37**, 1587 (1959), Soviet Phys. JETP **10**, 1125 (1960).
[3] Amaglobeli, Golovin, Kazarinov, Medved', and Polev, JETP **38**, 660 (1960), Soviet Phys. JETP **11**, 474 (1960).
[4] P. Cziffra and M. I. Moravcsik, Phys. Rev. **116**, 226 (1959).
[5] Cziffra, MacGregor, Moravcsik, and Stapp, Phys. Rev. **114**, 880 (1959).
[6] Cini, Fubini, and Stanghellini, Phys. Rev. **114**, 1633 (1959).
[7] W. H. Hess, Revs. Modern Phys. **30**, 368 (1958).
[8] H. Lehmann, Nuovo cimento **10**, 579 (1958).
[9] Goldberger, Nambu, and Oehme, Ann. Phys. **2**, 226 (1957).

Translated by I. Emin
171

QUADRUPOLE MOMENTS OF ODD BARIUM ISOTOPES

N. I. KALITEEVSKIĬ, É. E. FRADKIN, and M. P. CHAĬKA

Leningrad State University

Submitted to JETP editor May 12, 1960

J. Exptl. Theoret. Phys. (U.S.S.R.) 39, 954-956 (October, 1960)

The quadrupole moments of Ba^{135} and Ba^{137} nuclei are determined on the basis of the deviations from the spacing rule of the hyperfine structure of the Ba^{137} spectrum. The absolute magnitude of the moments cannot be interpreted in terms of the simple shell model.

AN experimental determination of the quadrupole moments of the barium nuclei (Ba^{135} and Ba^{137}) is of interest, in our opinion, in ascertaining the extent to which the properties of these nuclei are accurately described by the simple shell model.

An investigation of the hfs of the BaI spectrum was made using separated highly-enriched barium isotopes (Ba^{135} — 89.2%, Ba^{137} — 78.8%). To determine the quadrupole moments, the deviations from the spacing rule of the hfs were investigated for the term $(6s6p)^3P_1$ of BaI, which, as shown by our preliminary estimates, should display a considerable splitting and a high constant of quadrupole interaction. To determine the structure of the $^3P_1$ term, a photoelectric spectrometer with a Fabry–Perot interferometer[1] was used to investigate the hfs of two spectral line of BaI, $\lambda = 4599.7$ A ($6p^2\,{}^1S_0 - 6^3P_1$) and $\lambda = 4573.9$ A ($6p^2\,{}^3P_0 - 6^3P_1$), whose upper levels are not split. The large aperture ratio of our apparatus[2] enabled us to investigate the hfs of these relatively weak lines, whereas earlier investigations[3,4] concerned the strong resonance lines in the spectra of BaI and BaII, the structures of which do not yield ready data for the determination of the quadrupole moments of Ba^{135} and Ba^{137}.

We know[3,4] that both barium isotopes have a spin $I = 3/2$ and that the structure of the $^3P_1$ term (which coincides with the structure of the investigated spectral lines) is characterized by two independent hfs intervals, the magnitudes of which are directly related to the values of the constants A and B — the spacing factors of the magnetic dipole and electric quadrupole interaction of the nucleus with the electron shell:

$$W_F = W_J + {}^1/_2\,AC + B\,[C\,(C+1) - {}^4/_3\,I\,(I+1)\,J\,(J+1)],$$
$$C = F\,(F+1) - I\,(I+1) - J\,(J+1),\quad F = {}^5/_2,\ {}^3/_2,\ {}^1/_2.$$

The results of the experimental determination of the hfs intervals and of the constants A and B, obtained by averaging 20 measurements of hfs lines BaI $\lambda = 4599.7$ A and $\lambda = 4573.9$ A, are listed in the table.*

Intervals and hfs constants, 10^{-3} cm^{-1}	Ba^{135}	Ba^{137}
$W_{5/2}-W_{3/2}$	83.6±0.6	93.1±0.4
$W_{3/2}-W_{1/2}$	137.4±0.7	151.5±0.7
A	34.0±0.2	37.7±0.2
B	—0.15±0.07	—0.11±0.06

The ratio of the magnetic moments μ^{137}, $\mu^{135} = A^{137}/A^{135} = 1.11$, obtained directly from the experimental data, is in good agreement with the value 1.1187 determined by the paramagnetic resonance method,[5] thus demonstrating the correctness of the spacing factors obtained by us.

To calculate the absolute values of the quadrupole moments of Ba^{135} and Ba^{137}, we used an approximate quantum-mechanical calculation. The state $(6s6p)\,^3P_1$, for an intermediate coupling between the outer electrons, is described by the wave function

$$\Psi = c_1\,\psi_1\,({}^1/_2,\ {}^3/_2)_{J=1} + c_2\,\psi_2\,({}^1/_2,\ {}^1/_2)_{J=1},$$

where $\psi_i\,(j_1, j_2)$, with i = 1 and 2, is the wave function of the (sp) configuration in the case of pure jj coupling. The coupling constants c_1 and c_2 were determined by the Wolfe method[6] ($c_1 = 0.500$, $c_2 = 0.866$). The spacing factor B is determined in this case by the following formula (see reference 7)

$$B = \frac{3Q}{8I\,(2I-1)\,J\,(2J-1)\,\pi a_0^3\,R\alpha}\,\frac{[c_1^2\,R_r'\,(Z_i) - 2c_1c_2\sqrt{2}S_r\,(Z_i)]\,\delta\nu}{15\,Z_i\,H\,(lZ_i)}$$

$$= -0.573\,Q10^{-3}\ \text{cm}$$

*We indicate everywhere the mean arithmetic error of a single spacing measurement.

where a_0 is the Bohr radius, R is Rydberg's constant, α is the fine-structure constant, Q is the electric quadrupole moment of the nucleus in units of 10^{-24} cm^2, Z_i is the effective charge (for the 6p electron in Ba we have $Z_i = 50$); R'_r, S_r and H are the relativistic corrections, and $\delta\nu$ is a part of the fine splitting between 6^3P_0 and 6^3P_2, corresponding to the spin-orbit interaction of the p electron with allowance for the Wolfe correction.

From the values of the constants B listed in the table we obtain the following values for the quadrupole moments of the odd isotopes of barium:

$$Q(Ba^{135}) = (0.25 \pm 0.12)\,10^{-24}\text{cm}^2,$$

$$Q(Ba^{137}) = (0.2 \pm 0.1)\,10^{-24}\text{cm}^2.$$

According to the universally accepted classification of the shell model,[8] the ground state of the Ba^{135} nucleus is $2d_{3/2}$, while that of Ba^{137} is $(2d_{3/2})^3$. The result which we have established ($Q > 0$ for both isotopes) merely indicates that both Ba^{137} and Ba^{135} have a hole at the neutron level $2d_{3/2}$. Consequently, one must assign to the ground state of Ba^{135} either the configuration $(3s_{1/2})^2\ (1h_{11/2})^{10}\ (2d_{3/2})^3$, or the configuration $(3s_{1/2})^0\ (1h_{11/2})^{12}\ (2d_{3/2})^3$. It is interesting to note that Xe^{131}, the ground state of which has a configuration $(3s_{1/2})^2\ (1h_{11/2})^{10}\ 2d_{3/2}$, has a negative quadrupole moment.[9]

The absolute magnitude of the quadrupole moment of the odd isotopes of barium cannot be interpreted in terms of the simple shell model. since according to the estimate that follows from this theory, even an odd proton nucleus with A = 135 and a ground state $d_{3/2}$ would have a lower value of Q than the quadrupole moment which we have obtained for Ba^{135}.

The authors are grateful to V. S. Zolotarev for providing the separated isotopes, to L. K. Peker for discussing the results, and V. A. Strugach for carrying out many calculations.

[1] Kaliteevskiĭ, Malyshev, and Chaĭka, Оптика и спектроскопия (Optics and Spectroscopy) **6**, 820 (1959).

[2] N. I. Kaliteevskiĭ and M. P. Chaĭka, Vestnik, Leningrad State Univ. **16**, 51 (1959).

[3] H. Kallman and H. Schuler, Erg. exakt. Naturwiss. **11**, 134 (1932).

[4] O. H. Arroe, Phys. Rev. **79**, 836 (1950).

[5] Kucheryaev, Szhenov, and Gogichaĭshvili, JETP **37**, 582 (1959), Soviet Phys. JETP **10**, 412 (1960).

[6] H. Wolfe, Phys. Rev. **41**, 474 (1930).

[7] H. Kopferman, Kernmomente, Frankfurt, 1956.

[8] J. P. Elliott and A. M. Lane, Handb. Physik **39**, 1957.

[9] Bohr, Koch, and Rasmussen, Arkiv Fysik **4**, 455 (1952).

Translated by J. G. Adashko
172

INELASTIC INTERACTIONS BETWEEN 9-Bev PROTONS AND NUCLEONS

WANG SHU-FEN, T. VISKY, I. M. GRAMENITSKIĬ, V. G. GRISHIN, N. DALKHAZHAV, R. M. LEBEDEV, A. A. NOMOFILOV, M. I. PODGORETSKIĬ, and V. N. STEL'TSOV

Joint Institute for Nuclear Research

Submitted to JETP editor May 12, 1960

J. Exptl. Theoret. Phys. (U.S.S.R.) **39**, 957-960 (October, 1960)

It is shown that in pp and pn interactions the angular and momentum distributions of secondary protons and pions vary little with the number of charged particles.

A study of inelastic nucleon-nucleon interactions at high energies can apparently yield certain information on the structure of the nucleon. Previously obtained results[1] have indicated a sharp anisotropy of the angular distribution of the secondary nucleons in the c.m.s., and a lower limit has been established for the fraction of the energy consumed in the production of the pions. However, only the slow particles have been identified and their energies measured. We therefore thought it advisable to continue work on the study of pp and pn interactions under conditions in which measurements could be made of the multiple scattering of fast particles.

1. A stack made up of type "R" NIKFI pellicles was exposed to the internal 9-Bev proton beam of the proton synchrotron of the Joint Institute for Nuclear Research. The scanning was along the tracks of the primary protons by two methods, normal and accelerated.[2] A total of 944 m of track was scanned and 2647 nuclear interactions and scatterings by angles $\theta \geq 5°$ were found. The inelastic pp and pn interactions were selected in accordance with the criteria described earlier.[1] We selected 161 pp interactions and 94 pn interactions. The following distribution by the number of charged particles agrees with the earlier data.[1]

	pp interactions:			
Number of prongs	2	4	6	8
Number of interactions, %	46.6 ± 5.4	44.7 ± 5.3	8.1 ± 2.2	0.62 ± 0.62
	pn interactions:			
Number of prongs	1	3	5	7
Number of interactions, %	35.1 ± 6.1	53.2 ± 7.5	9.6 ± 3.2	2.1 ± 1.5

The average number of charged particles in the pp and pn interactions is 3.25 ± 0.10 and 2.58 ± 0.14, respectively.

Table I

	$\bar{E}_{p\ c.m.s.}$ Mev	$\bar{\theta}^{\circ}_{p\ c.m.s.}$	$\bar{E}_{\pi\ c.m.s.}$ Mev	$\bar{\theta}^{\circ}_{\pi\ c.m.s.}$
1	1520±45	22±2	426±30	38±3
2	—	—	442±23	38±2
3	1360±45	37±3	—	—

2. To identify the fast particles, we measured the multiple scattering and the density of the clusters g on secondary tracks with a dip angle $\varphi \leq 3°$. In determining the values of $p\beta$, account was taken of the effect of false scattering, which was calculated from measurements on tracks of primary protons in each layer. The false scattering did not make it possible to measure values of $p\beta$ higher than 6 Bev/c. The particles were identified by curves of g/g_0 vs. $p\beta$ for pions and protons, plotted after Barkas and Young.[3] The data of reference 3 were verified by measuring the density of clusters on tracks of 9- and 3-Bev protons in the same emulsions. The emulsions were exposed to protons of these energies practically simultaneously. The results obtained agree with the data given in reference 3 within approximately 2%.

It must be noted that in the region where the "proton" and "pion" curves intersect ($1.5 \leq p\beta \leq 2.5$ Bev/c), the identification is not unique.* Assuming that the particles corresponding to the intersection region are pions, their angular and energy distributions in the c.m.s. coincide with the same distributions for reliably identified pions. If these particles are assumed to be protons, their angular and energy distributions differ greatly from the distributions of reliably identified protons.

*The dimensions of this region are chosen in accordance with the magnitude of the errors in the determination of $p\beta$ and g/g_0.

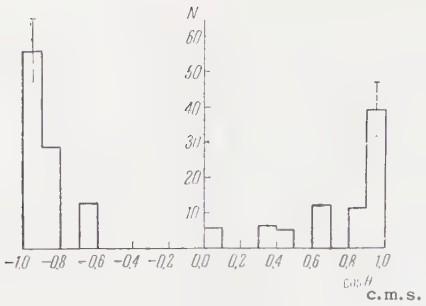

FIG. 1. Angular distribution of the protons in the c.m.s., for pp interactions.

By way of illustration we present Table I, where line 1 shows the average energies and emission angles for reliably identified particles; line 2 includes the particles from the region of intersection of the curves, under the assumption that they are pions; the figures in line 3 are under the assumption that the particles are protons.

In addition, the number of particles that enter into the intersection region increases greatly with the multiplicity. These facts make it quite reasonable to assume that most particles from the intersection region are pions. All further distributions are therefore given under this assumption.

3. An angular distribution was plotted in the c.m.s. (Fig. 1) for the secondary protons from the pp interactions, and was found to be highly anisotropic. The angular distribution of the pions, shown in Fig. 2, is also anisotropic (see also reference 4), but is much broader than the proton distribution.

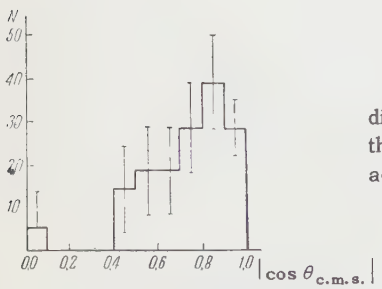

FIG. 2. Angular distribution of pions in the c.m.s., for pp interactions.

The c.m.s. momentum distributions of the protons emitted only in the backward hemisphere is shown in Fig. 3. The point is that the particles emitted in the forward hemisphere include protons, for which only the lower limit of $p\beta$ was determined, owing to the influence of false scattering. The average value of the proton energy in the c.m.s. and the average of the transverse momentum are respectively $\bar{E}_p$ (c.m.s.) = 1520 ± 45 Mev and $\bar{p}_\perp$ = 372 ± 25 Mev/c. The coefficient of inelasticity K and the fraction of the energy going to pion production in the laboratory system (l.s.) are

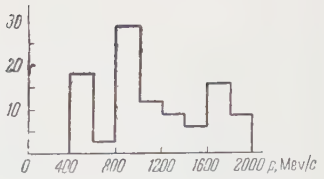

FIG. 3. Momentum distribution of protons emitted in the backward hemisphere, in the c.m.s.

$K = 0.55 \pm 0.03$ and E_π (l.s.)$/E_0 = 0.39 \pm 0.02$. The average number of protons per interaction is $\bar{n}_p = 1.24 \pm 0.28$, and the average number of charged pions $(\bar{n}_\pi)_{ch} = 2.01 \pm 0.31$. Assuming that the number of neutral pions is half the number of charged pions, we can estimate the average number of all the pions per interaction: $\bar{n}_\pi = 1.5\,(\bar{n}_\pi)_{ch} = 3.02 \pm 0.46$. From these data we readily obtain the average energy per meson in the c.m.s., E_π (c.m.s.) = 4.75 ± 78 Mev. The average c.m.s. pion energy measured directly for particles in the backward hemisphere is 432 ± 32 Mev.

Among the particles emitted in the forward hemisphere, there are pions for which only the lower limit of $p\beta$ was determined. Therefore, in calculating the average energy for pions emitted in the forward and backward hemispheres, we determined the lower and upper limits: 442 ± 23 Mev $\leq E_\pi$ (c.m.s.) $\leq$ 490 ± 30 Mev. The upper limit of E_π(c.m.s.) was obtained under the assumption that the pions for which the lower limit of $p\beta$ was determined had the maximum energy possible for the given multiplicity. The transverse momentum of the pions was found to be 232 ± 18 Mev/c $\leq \bar{p}_\perp \leq$ 259 ± 20 Mev/c.

The c.m.s. angular distribution for pn interactions is shown in Fig. 4. The insufficient statistics do not allow us to draw any definite conclusions concerning the asymmetry of the protons. The average proton energy in pn interactions is 1480 ± 100 Mev and does not differ from the average proton energy in pp interactions.

4. A very important question is that of the variation of the angular and energy distribution of the nucleons with the multiplicity. Starting from the existence of two types of collisions — "peripheral" and "central" — one would expect a broader angular distribution at higher multiplicity (see, for ex-

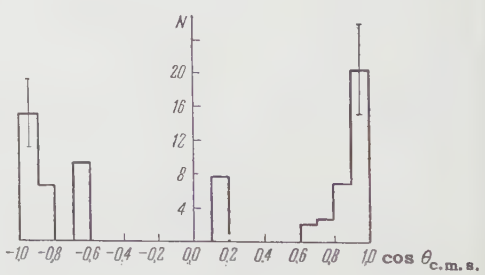

FIG. 4. Angular distribution of protons in the c.m.s., for pn interactions.

Table II

	$\bar{p}_{c.m.s.}$, Mev/c		$\bar{p}_{\perp}$, Mev/c		$\bar{\theta}^{\circ}_{c.m.s.}$	
Multiplicity	2--4	5--7	2--4	5--7	2--4	5--7
Protons	1152±90	1028±80	365±35	349±35	23±2	21±6
Pions	329±30	370±50	244±18	175±20	39±2	46±5

ample, reference 5). To increase the statistical accuracy, we shall consider later on combined data on pp and pn interaction, since the angular and energy characteristics of the nucleons are apparently the same in these interactions. Table II lists the average values of the momentum, the transverse momentum, and c.m.s. angle of emission of protons and pions for low (n = 2, 3, 4) and high (n = 5, 6, 7) multiplicities.

The data given indicate that the angular and momentum distributions vary weakly with the multiplicity. Analogous results were obtained in reference 6, devoted to study of πp and πn interactions.

Table III

	α, Mev/c	
Multiplicity	2--4	5--7
Protons	296	257
Pions	198	140

The quantity $\alpha = \sqrt{\bar{p}_{\perp}^2/2}$ characterizes the transverse dimensions of the interaction
III gives the values of α for protons and pions at different multiplicities. It is seen from this table that α depends little on the multiplicity.

The totality of the given experimental data shows apparently that the character of the interaction changes little with increasing number of secondary charged particles. If we start with the assumed existence of two types of interaction, "peripheral" and "central," then we must conclude that the bulk of the experimental material pertains only to one of these interactions. We can assume, for example, that in "central" collisions the angular distribution of the nucleons should be close to isotropic. In this case we can tentatively associate the 7- and 8-prong stars with "central" collisions, since nothing has been found in the present investigation concerning their properties, owing to the scanty statistics. This enables us to estimate the upper limit of the dimensions of the proposed "core," which does not exceed 0.1 or 0.2 of the radius of the nucleon.

On the other hand, one cannot exclude[7] the possibility the "peripheral" collisions are very rare. In this case the overwhelming majority of the experimentally observed interactions should be classified as "central," but characterized by an anisotropic distribution of the secondary particles.

The authors thank the accelerator crew for help in irradiating the pellicle stack, and to the laboratory staff for scanning and participating in the measurements. The authors are also grateful to D. I. Blokhintsev and V. I. Veksler for participating in discussions.

[1] Bogachev, Bunyatov, Gramenitskiĭ, Lyubimov, Merekov, Podgoretskiĭ, Sidorov, and Tuvdendorzh, JETP **37**, 1225 (1959), Soviet Phys. JETP **10**, 872 (1960).

[2] B. P. Bannik and M. I. Podgoretskiĭ Приборы и техника эксперимента (Instrum. and Exptl. Techniques) No. 3, 36 (1960).

[3] W. H. Barkas and D. M. Young, UCRL-2579, 1954.

[4] Bogachev, Bunyatov, Merekov, Sidorov, and Yarba, JETP **38**, 1346 (1960), Soviet Phys. JETP **11**, 968 (1960).

[5] Barashenkov, Mal'tsev, and Mikhul, JETP **37**, 1484 (1959), Soviet Phys. JETP **10**, 1052 (1960).

[6] Belyakov, Wang, Glagolev, Dalkhazhav, Lebedev, Mel'nikova, Nikitin, Sviridov, Petrzhilka, Suk, and Tolstov, JETP **39**, 937 (1960), this issue, p. 650.

[7] Blokhintsev, Barashenkov, and Barbashov, Usp. Fiz. Nauk **68**, 417 (1959), Soviet Phys.-Uspekhi **2**, 505 (1960).

Translated by J. G. Adashko
173

ANOMALIES IN THE TEMPERATURE DEPENDENCE OF THE COERCIVE FORCE IN RARE EARTH ELEMENT GARNET FERRITES IN THE NEIGHBORHOOD OF THE COMPENSATION POINT

K. P. BELOV and A. V. PED'KO

Moscow State University

Submitted to JETP editor May 16, 1960

J. Exptl. Theoret. Phys. **39**, 961-964 (October, 1960)

Anomalous maxima of the coercive force have been found in the region of the compensation point in rare earth garnet ferrites. In polycrystalline ferrites the height and breadth of these maxima depend on the specimen density and, in addition, a doubling of the peaks is observed. There are also anomalous maxima in single crystal specimens, but they are narrower than in polycrystalline specimens. A qualitative explanation of the observed phenomena is given. It is suggested that the strong broadening of the ferromagnetic resonance absorption lines in ferrites, previously observed, on approaching the compensation point is due to a cause related to that underlying the anomalous increase in coercive force near this point.

1. It was shown by Pauthenet[1] that most rare earth element garnet ferrites ($3M_2O_3 \cdot 5Fe_2O_3$, where M = Gd, Dy, Ho, etc.) have so-called compensation points Θ_k, at which the resultant spontaneous magnetization changes sign. It is of interest to study the magnetic properties of these ferrites in the neighborhood of Θ_k. In this paper we want to discuss further the anomalies in the temperature dependence of the coercive force H_c near Θ_k in garnet ferrites, the discovery of which we communicated earlier.[2]

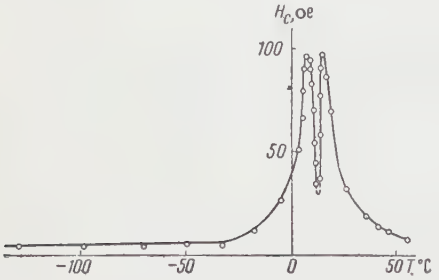

FIG. 1. The temperature dependence of coercive force for the polycrystalline ferrite $3Gd_2O_3 \cdot 5Fe_2O_3$ in the neighborhood of Θ_k = + 12°C (density 5.9 g/cm³).

2. Figure 1 shows the results of measurement of the temperature dependence of H_c for the polycrystalline ferrite $3Gd_2O_3 \cdot 5Fe_2O_3$ in the region of Θ_k. It can be seen that there is a sharp increase in H_c on approaching Θ_k. Although at temperatures far from Θ_k the values of H_c are small, they reach hundreds of oersteds near Θ_k. In the immediate region of Θ_k itself (determined by the change in sign of the remanent magnetization) H_c falls rapidly, resulting in a double maximum in the coercive force on a $H_c(T)$ curve. The sharp decrease in H_c at Θ_k itself can be explained by the fact that at Θ_k the resultant spontaneous magnetization I_s tends to zero, so that all signs of ferromagnetic magnetization must disappear here, in particular magnetic hysteresis phenomena ($H_c \to 0$). There is nearly always incomplete

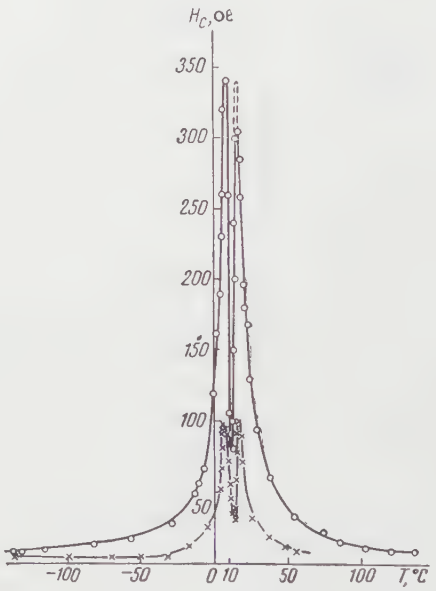

FIG. 2. The temperature dependence of coercive force for polycrystalline gadolinium ferrites with densities: o – 3.15 g/cm³ and × – 5.9 g/cm³.

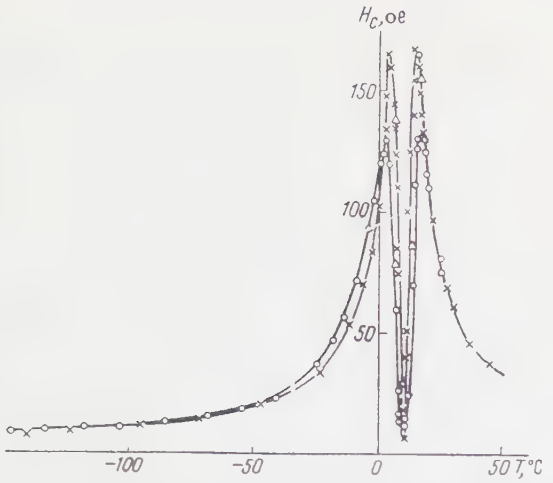

FIG. 3. The effect of quenching on the temperature dependence of coercive force in the ferrite $3Gd_2O_3 \cdot 5Fe_2O_3$. o – original state, × – quenching from 1100°C in a current of air, Δ – heating at 1000°C for 4 hours.

compensation of the magnetic moments of the sublattices[3] because of structural defects, so that there are remains of ferromagnetic magnetization at Θ_k, and H_c does not become exactly zero (see Figs. 1, 2, and 3).

Bol'shova and Elkina[3] did not find a double maximum of H_c in lithium chromite ferrite near Θ_k. This is evidently related to the incomplete compensation, which reaches a considerable magnitude in these ferrites. As a result, magnetic hysteresis phenomena are always great at Θ_k and it is not possible to observe a doubling of the maximum in a $H_c(T)$ plot.

3. In order to determine how the appearance of the anomalous increase in H_c near Θ_k is connected with the crystallinity of the specimens, gadolinium ferrite specimens with garnet structure of different density were prepared from material of identical purity. The $H_c(T)$ curves for two specimens of this ferrite with density 3.15 and 5.9 g/cm^3 are shown in Fig. 2. It can be seen that the form of the anomaly is preserved. The magnitude of the anomaly decreases as the density of the specimen increases, while the temperature interval over which the anomalous growth of H_c is observed narrows considerably. We also examined the effect of heat treatment (quenching from 1100°C in a current of air and heating at 1000°C for 4 hours) on the form of the anomaly in H_c. It can be seen from Fig. 3 that the magnitude of the anomaly is altered, but not as much as by a change in density. We see then that the structural properties of polycrystalline (ceramic) specimens influences the size of the anomaly in H_c near Θ_k.

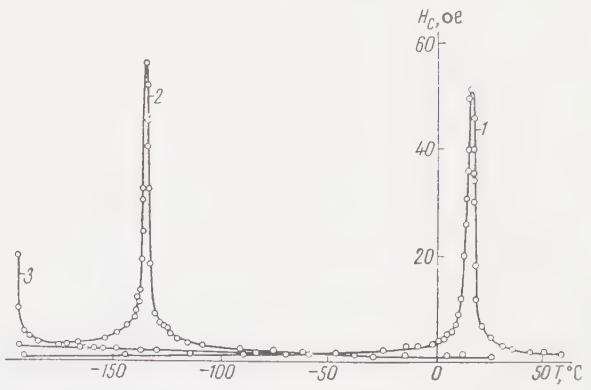

FIG. 4. The temperature dependence of coercive force for single crystal specimens of garnet ferrites: 1 – $3Gd_2O_3 \cdot 5Fe_2O_3$; 2 – $3Ho_2O_3 \cdot 5Fe_2O_3$; 3 – $3Er_2O_3 \cdot 5Fe_2O_3$ (compensation temperatures respectively + 16; – 136; ~ – 195°C).

The question then arises whether the existence of this anomaly is only related to the polycrystalline state of the ferrite. For a direct answer it would be best to measure the temperature dependence of H_c for single crystal specimens of gadolium ferrite. We did not have sufficiently large single crystals of garnet ferrites for measuring H_c. However, we had 10 – 12 small crystals (from one batch) which could be fitted into a tube, thereby increasing the volume of crystalline specimens.* The measured curves of $H_c(T)$ for crystalline specimens of Gd, Ho and Er garnet ferrites are given in Fig. 4. It can be seen that there is a sharp increase in H_c on approaching Θ_k. Due to the specimens being single crystals, the temperature range of the anomalous increase in H_c is greatly narrowed in comparison with that in polycrystalline specimens; in the latter it is always spread over a more or less wide temperature interval. It is probably for this reason that it is difficult to observe a doubling of the maxima of H_c in single crystal specimens.

4. On approaching Θ_k a ferrite takes on more and more the properties of weakly ferromagnetic material. The magnetization curves have a very steep appearance and the magnetic hysteresis loop broadens considerably; technical magnetization is produced mainly by rotation of the spontaneous magnetization vector, whereas far from Θ_k movement of domain boundaries is the main factor. To explain these forms of magnetization curves and hysteresis loops in ferrite crystals near Θ_k, we must either assume that the crystallographic magnetic anisotropy constant rapidly increases near Θ_k or, if this is ruled out, that a ferrite crystal in the region of Θ_k exists as if in a single-domain

*We are grateful to V. A. Timofeeva for providing the garnet ferrite single crystals for our experiments.

condition (i.e., there is no clear-cut domain structure in the crystal since, because of the small resultant spontaneous magnetization, the energy of the internal demagnetizing field is extremely small). Smith, Overmeyer, and Calhoun,[4] have shown, on the basis of measurements of ferromagnetic resonance in gadolinium garnet ferrite crystals, that the magnitude of the magnetic anisotropy constant does not change greatly near Θ_k (according to these authors it even decreases slightly). We must therefore ascribe the increase in the influence of rotation processes near Θ_k to the single-domain state of the ferrite crystal in this temperature region.

We can understand the increase in H_c on approaching Θ_k if we use the relation which applies to a single-domain crystal:

$$H_c \sim K / I_S,$$

where K is the magnetic anisotropy constant and I_S is the resultant spontaneous magnetization. Since K hardly changes on approaching Θ_k while I_S decreases rapidly, we must observe a rapid increase in H_c. All these considerations apply to a ferrite in single crystal form. When we go over to polycrystalline specimens we must take into account the additional influence on the rotation processes of various non-uniformities in the specimen, mechanical stresses, etc. These hinder the remagnetization processes and consequently lead to an increase in H_c, as is found experimentally.

We should note in conclusion that Smith et al.[4] found a sharp rise in magnetic losses at very high frequencies on approaching Θ_k (a broadening of the ferromagnetic resonance absorption line). This occurs both for single crystal and for polycrystalline ferrite specimens. In our view the cause of this phenomenon is related to the anomalous increase in coercive force near the compensation point.

---

[1] R. Pauthenet, Compt. rend. **242**, 1859 (1956); **243**, 1499 (1956); **243**, 1737 (1956).

[2] K. P. Belov and A. V. Ped'ko, Proceedings of Conference on Ferrites, Minsk (1959).

[3] K. M. Bol'shova and T. A. Elkina, Moscow State University Bulletin 4, 85 (1959).

[4] Smith, Overmeyer, and Calhoun, IBM J. Res. Develop. **3**, No. 2 (1955).

Translated by R. Berman
174

INVESTIGATION OF AZIMUTHAL EFFECTS IN MESON SHOWERS PRODUCED BY 9-BEV PROTONS

E. M. FRIEDLÄNDER

Atomic Physics Institute, Rumanian Academy of Sciences

Submitted to JETP editor May 10, 1960

J. Exptl. Theoret. Phys. JETP (U.S.S.R.) 39, 965-969 (October, 1960)

A statistical method is proposed for reducing the data on the azimuthal distribution of particles in low-multiplicity meson showers. It is shown that an azimuthal effect appears in showers produced by cosmic rays, but not in showers produced by 9-Bev protons.

1. The non-uniformity of the azimuth-angle distribution of the particles of meson showers produced by cosmic-ray particles was demonstrated in an earlier experiment carried out in our laboratory.[1,2] Such an effect was predicted already long ago by one of the models of multiple meson production with the participation of excited nucleons.[3,4]

In the present article we describe a statistical method of analysis of a large number of low-multiplicity showers, as well as an attempt to find possible deviations from a uniform azimuthal distribution for meson showers produced in an emulsion stack irradiated by the internal beam of the proton synchrotron of the Joint Institute for Nuclear Research.

2. Let us assume that the secondary particles are concentrated around a certain singled-out plane at least in part of the showers. Statistical fluctuations prevent the detection of such an effect in a single low-multiplicity shower. If we construct a compound shower out of many single ones, then the random distribution of individual planes in the space will lead to a perfectly random distribution of the azimuth angles, and thus will not provide us with the opportunity of detecting the azimuthal effect, even if it exists.

In order to detect such an effect, it is, in principle, necessary to make all the singled-out planes coincide.

The best approximation of such a coincidence can, in practice, be attained if one turns all the "impact diagrams" of the showers in such a way that the average values of $\overline{\psi}$ of the azimuth angles coincide for all showers.

If the initial distribution of the angles ψ is uniform, and if all the showers possesss a high multiplicity, then the average value of $\overline{\psi}$ is well defined, and consequently, the distribution of the azimuth angles of the composite shower will conserve its uniformity. For a low multiplicity, even for a uniform distribution of ψ, the distribution of the angles $\delta = \psi - \overline{\psi}$ will show a tendency to concentrate around $\delta = 0$.

This apparent non-uniformity (which we shall denote in the following by the term "natural") can be calculated in the following manner:

According to our initial assumption, the random variable ψ is distributed uniformly in the angle interval $(0, \pi)$.

Let us now consider the set of N measured values $\psi_1, \psi_2, \ldots \psi_N$ for a given shower. In order to construct the composite shower, it is necessary to collect the deviations of the values ψ_1 from the average value $\overline{\psi}$ in each shower. Thus, we are interested in the distribution of the quantities.

$$\delta_i \equiv \left| \psi_i - \frac{1}{N} \sum_1^N \psi_j \right|. \tag{1}$$

This can be done by means of the generating function

$$G_\delta(s) = \int_0^1 \cdots \int_0^1 \exp\left(s \left| x_i - \frac{1}{N} \sum x_j \right|\right) dx_1 \ldots dx_N, \tag{2}$$

where

$$x_i \equiv \psi_i / \pi.$$

Integrating (2), we obtain

$$G_\delta(s) = \frac{2N}{(N-1)s} \left[\left(\frac{e^{s/N} - 1}{s/N} \right)^{N-1} - 1 \right]. \tag{3}$$

The mathematical expectation of δ is given by the expression

$$\langle \delta \rangle = [(\partial \ln G / \partial s)_{s=0}]^{-1} = \pi (3N-2)/12N \tag{4}$$

for a standard deviation

$$\sigma = \left[(\partial^2 \ln G / \partial s^2)_{s=0} \right]^{-1/2} = \pi \sqrt{3N^2 - 4}/12N. \tag{5}$$

Number	Shower type	Average multiplicity	$\bar{\delta}$	$\langle\delta\rangle$	Number of tracks
1	9 Bev, all showers	5.1	40.0±0.5	39.2	3384
2	H events	~6	41.5±0.8	40.0	1021
3	L events $N \geq 4$	~5	40.1±0.6	39.1	2035
4	" $N=3$	3	37.6±1.3	35.0	348
5	" $N \geq 4$ $\theta > 30°$	~5	39.6±0.9	39.1	797
6	" $N \geq 4$ $\theta \leq 30°$	~5	40.5±0.5	39.1	1238
7	H+L, $N \geq 4$ $\log \cot \theta > 0,4$	~5	41.8±2.9	39.1	283
8	L, $N \geq 4$ $\Sigma \operatorname{cosec} \theta > 30°$	~5	39.6±1.8	39.1	210
9	"Random" showers	5	40.0±2.1	39.1	500
10	Showers produced by charged cosmic-ray particles	~11	34.4±1.6	42.3	230
11	"Random" showers	11	41.3±2.3	42.3	132

For $N \gg 1$, $\langle\delta\rangle$ and σ_δ tend towards the limits

$$\langle\delta\rangle_\infty = \pi/4 = 45°, \quad \sigma_\infty \approx \frac{\sqrt{3}}{12}\pi = 26°. \tag{6}$$

For a small shower, e.g., for N = 3,

$$\langle\delta\rangle_3 = 35°, \quad \sigma_3 \approx 24°. \tag{7}$$

Thus, a comparison of the detected and expected values of $\bar{\delta}$ (or σ) enables us to decide whether, in the given set of showers, there exists any deviation from uniformity greater than the natural one. Of course, similar arguments remain valid even for higher moments, e.g., for $\bar{\delta}^2$.

3. In order to check whether the effect detected by us[1,2] also exists in showers of lower energies, we investigated the azimuthal distribution of 666 meson showers with multiplicity of relativistic traces $N \geq 3$ produced by 9-Bev protons in a stack of 450 μ NIKFI-R emulsions. Details of the irradiation and scanning can be found in an earlier article[5] dealing with the distribution of longitudinal angles θ. Since then, ~400 additional showers on light nuclei were measured, so that the L events* constitute the majority of showers described here.

Both plane angles with respect to the incident proton and the angles with the plane of the emulsion were measured for all the tracks ($J \leq 1.5 \times J_{\text{plateau}}$) of relativistic particles emitted into the forward hemisphere. From these angles, the latitude θ and azimuth ψ with respect to the normal to the emulsion plane were calculated using nomograms with a total accuracy of 1 and 2° respectively.

In order to check the absence of any possible bias in the selection of relativistic tracks, the angles ψ were divided among four quadrants, and the uniformity of their distribution was checked by the Pearson χ^2 test. An agreement with a uniform distribution was obtained at the probability level P ~ 35%.

The average value of $\bar{\psi}$ and deviation δ was calculated for each shower according to Eq. (1). Afterwards, the average $\bar{\delta}$ was calculated and compared with the mathematical expectation $\langle\delta\rangle$ calculated according to Eq. (4), and weighted taking the observed multiplicity distribution into account.

The result is shown in the first row of the table. It can be seen that there is no disagreement with "natural" non-uniformity within the limits of statistical error.

All data were then divided into the following groups: a) H events ($N_h \geq 7$) and L events ($N_h \leq 4$), b) L events with small ($n_s = 3$) and large ($n_s \geq 4$) multiplicity, c) events with small (Σ cosec $\theta > 30°$) and large inelasticity,[5] d) collisions between nucleon and a tunnel, and nucleon-nucleon collisions,[5] e) wide ($\theta \geq 30°$) and narrow ($\theta \leq 30°$) cone.

As can be seen from the table, the results obtained remain unchanged.

Consequently, we must conclude that, at least with the statistics available, it is impossible to detect any azimuthal effect in showers produced by 9-Bev protons.

Using the same method (i.e., by comparing $\bar{\delta}$ and $\langle\delta\rangle$, we analyzed the cosmic-ray showers described in our earlier article.[1] It should be mentioned that, because of the great multiplicity of these showers, the expected natural non-uniformity is smaller than in the case of 9-Bev showers, and it is therefore difficult to detect it. Nevertheless, in cosmic rays, the observed concentration of angles around $\delta = 0$ is markedly greater than the natural concentration. The value of δ in the 10th

*L events were defined in reference 5.

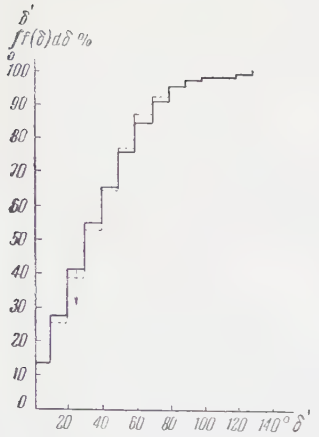

FIG. 1. Comparison of the integral angular distribution for random showers produced by 9-Bev protons (dashed line) with the experiment (solid line).

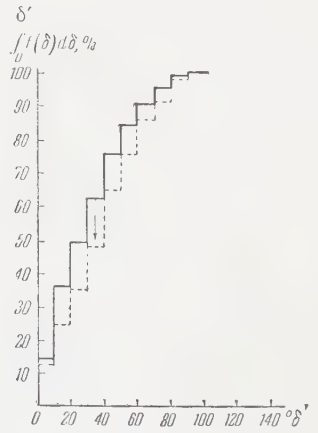

FIG. 2. Same as for Fig. 1 for showers produced by cosmic rays.

row of the table deviates from its mathematical expected value by more than four standard deviations. Thus, our earlier conclusion[1,2] about a considerable non-uniformity in cosmic-ray showers is confirmed.

As is well known, the first moment of ($\bar{\delta}$) provides only limited information on the form of distribution of δ. For a full comparison of the detected and expected distributions, it would still be necessary to compare several moments of higher order, or to carry out an inverse Laplace transformation of Eq. (3) to obtain the distribution function δ in an explicit form.

Instead of these difficult calculations, we have constructed a set of random showers with originally uniform azimuthal distribution, and calculated the fluctuations by the Monte-Carlo method.

A comparison of the integral angular distribution of these random showers with experiment at 9 Bev is shown in Fig. 1. The arrow indicates the one-percent "limit of confidence" according to the Kolmogorov-Smirnov criterion. As can be seen, the corresponding statistical spread is greater than the greatest difference between those two distributions, and, moreover, one can conclude about an agreement at the 95% level.

On the other hand, the same test was applied to cosmic-ray showers studied in reference 1 (Fig. 2). Even for comparatively poor statistics of showers obtained by the Monte-Carlo method (132 tracks), the hypothesis of an agreement with uniform distribution can be contradicted at the 0.07 level.*

*The agreement of the random showers with the natural non-uniformity was tested using the values of δ given in the table.

It is difficult to explain so sharp a difference in behavior between cosmic-ray and 9-Bev proton showers, since their average energies are not very greatly different. Moreover, the various other characteristics of showers (anisotropy of latitude angles in the c.m.s., inelasticity, etc.) in the same energy range vary only little or not at all.

Further investigations of the effect are being carried out in our laboratory.

The author is greatly indebted to the Joint Institute for Nuclear Research for supplying the irradiated plates and expresses his gratitude to Prof. M. I. Danysz for helpful comments, to V. Dumitrescu for help in carrying out the measurements, and to M. Georghiu and M. Ionice for help in reducing the angular data.

[1] Balea, Friedländer, and Potoceanu, Rev. Phys. **4**, 441 (1959).

[2] Balea, Friedländer, Oncescu, Potoceanu, and Sahini, Proceedings of the 1959 Bucharest Conference on Cosmic Rays (in press).

[3] W. Kraushaar and L. Marks, Phys. Rev. **93**, 326 (1954).

[4] Z. Koba and S. Takagi, Nuovo cimento **10**, 755 (1958).

[5] E. M. Friedländer, Nuovo cimento **14**, 796 (1959).

[6] I. V. Dunin-Barkovskiĭ and N. V. Smirnov, Теория вероятностей и математическая статистика в технике (Theory of Probability and Mathematical Statistics in Engineering), Gostekhizdat, 1955.

Translated by H. Kasha
175

PRODUCTION OF MONOENERGETIC POSITRONS IN THE DECAY OF Eu^{152}

S. S. VASILENKO, M. G. KAGANSKIĬ, D. L. KAMINSKIĬ, and S. F. KOKSHAROVA

Leningrad Physico-Technical Institute, Academy of Sciences, U.S.S.R.

Submitted to JETP editor May 21, 1960

J. Exptl. Theoret. Phys. (U.S.S.R.) **39**, 970-972 (October, 1960)

The production of monoenergetic positrons may occur in the de-excitation of the 1531-kev excited state of Sm^{152}, which is formed in the decay of Eu^{152}. Our measurements show that the probability for this process is less than 10^{-8} positron per decay. According to the calculations of L. A. Sliv, this yields for the 1531-kev excited state of Sm^{152} a lifetime exceeding 10^{-14} sec, which points to the collective character of this level.

THE calculations by Sliv[1] have shown that if the nucleus is in a state with excitation energy greater than $2mc^2$ and the electron shell is short one electron, then production of an electron-plus-positron pair is possible upon transition of the nucleus from the excited state to the ground state, wherein the electron occupies the free space in the atomic shell, and the positron is the only particle emitted by the nucleus. Therefore all the positrons produced in such a process are monoenergetic. The equation of such positrons is

$$E_m = E_\gamma - 2mc^2 + E_{sh}, \qquad (1)$$

where $E\gamma$ is the transition energy and E_{sh} is the binding energy of the electron on the shell with the vacancy.

The probability of production of monoenergetic positrons is given by the relation

$$w_m = w_D w_i \Gamma_\gamma / \Gamma_k, \qquad (2)$$

where w_D is the probability of production of a pair with a monoenergetic positron, w_i is the probability of an unfilled level in the electron shell of the excited nucleus, Γ_k is the width of the atomic level, and Γ_γ the width of the excited level of the nucleus.

It is seen from (2) that the lifetimes of nuclei with excitation greater than $2mc^2$ can be determined from the probability of production of monoenergetic positrons.

We have attempted to observe the effect in decay of Eu^{152}. Figure 1 shows the $Eu^{152} \rightarrow Sm^{152}$ decay scheme. It is seen that the 1409-kev E1 transition which accompanies the electron capture in Eu^{152}, has a relatively high intensity. Since the energy of the transition that leads to the excitation of the 1531-kev Sm^{152} level amounts to approximately 330 kev, the probability of K capture is considerably higher than the probability of L capture. According to the calculations of Rose and Jackson,[2] in this case $w_i^K / w_i^L \approx 10$. We have therefore sought monoenergetic positrons produced by an electron filling a level on the K shell. According to (1) the positron energy should be 434 kev.

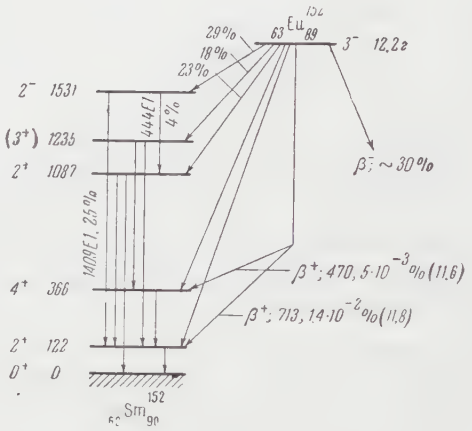

FIG. 1. Eu^{152} – Sm^{152} decay scheme.[3]

The measurements were made with the magnetic spectrometer described in reference 3. The radioactive source was europium oxide of natural isotopic composition, bombarded with thermal neutrons. The half-width of the instrument line was 1.2%.

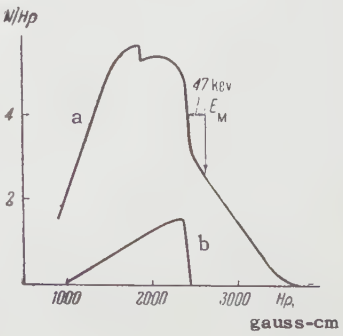

FIG. 2. a – positron spectrum of Eu^{152} (reference 3), b – spectrum of positrons due to internal coversion with pair production in a transition with energy 1409 kev.

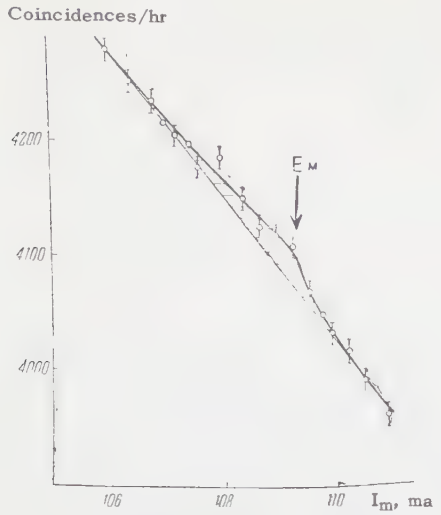

FIG. 3. Spectrum of positrons from Eu^{152} in the region where the line of monoenergetic positrons should be located. I_m – current in the spectrometer magnet.

The positron spectrum used in the decay of $Eu^{152,154}$ is shown in Fig. 2, curve a, and the result of the measurement of this spectrum in the vicinity where the line of monoenergetic K positrons should be located is shown in Fig. 3. As can be seen from Fig. 3, there is no clearly pronounced effect connected with the production of monoenergetic positrons, despite the high statistical accuracy, 0.2 – 0.3%, reached in these measurements. The shaded area on Fig. 3 can be used to estimate the upper limit of the intensity of this effect. A comparison of the intensity I_p of the positrons from internal conversion with pair production (Fig. 2, curve b) and the intensity I_m of monoenergetic positrons yielded

$$I_p / I_m = 3000. \qquad (3)$$

We used here for I_m the value corresponding to the shaded area on Fig. 3, which determines only the upper limits of the probability of production of monoenergetic positrons. Since the coefficient of internal conversion with pair production is known for the 1409-kev transition (it amounts to $1.6 \pm 0.2 \times 10^{-4}$, see reference 3), we can find from (3) that the probability for production of monoenergetic positrons is $w_m \leq 1.3 \times 10^{-8}$ positrons per decay of Eu^{152}. This yields, in accordance with Eq. (2), a value $\Gamma_\gamma \leq 0.1$ ev for the width of the nuclear level or a lifetime $T_\gamma \geq 10^{-14}$ sec. It was assumed in the calculation that $w_D = 3.0 \times 10^{-5}$ (interpolated from Sliv's calculations) and $\Gamma_k \approx 20$ ev (in accordance with Mladjenowich's data.[4])

It is interesting that a calculation of a probability of the single-proton transition, after Weisskopf, gives for the lifetime of the 1409-kev E1 transition a value $T_\gamma = 0.8 \times 10^{-16}$ sec. Thus, according to the data given, the transition investigated here is slowed down by at least 100 times.

The authors are grateful to Professor L. A. Sliv for continuous interest in this work.

[1] L. A. Sliv, Doklady Akad. Nauk SSSR **64**, 521 (1949).

[2] M. E. Rose and J. L. Jackson, Phys. Rev. **76**, 1540 (1949).

[3] Antonova, Vasilenko, Kaganskiĭ, and Kaminskiĭ, JETP **37**, 667 (1959), Soviet Phys. JETP **10**, 477 (1960).

[4] M. Mladjenowich, Ark. Fysik **8**, 27 (1954).

Translated by J. G. Adashko
176

FIVE NEW MILLISECOND ISOMERS PRODUCED BY 19.2-Mev PROTONS

A. M. MOROZOV, V. V. REMAEV and P. A. YAMPOL'SKIĬ

Institute of Physical Chemistry, Academy of Sciences, U.S.S.R. and Physico-Technical Institute, Academy of Sciences, Ukrainian S.S.R.

Submitted to JETP editor May 23, 1960

J. Exptl. Theoret. Phys. (U.S.S.R.) **39**, 973-985 (October, 1960)

Five new short-lived isomers produced by irradiating Sc_2O_3, Nb, La_2O_3, Nd_2O_3 and Os with 19.2-Mev protons have been detected and investigated. The final products of the isomer-yielding nuclear reactions on Sc and La have been identified as Ti^{45m} and Ce^{138m}, respectively. By bombardment of In, the previously known isomer In^{114m} has been produced through a reaction with protons for the first time. More detailed information has been obtained about the properties of In^{114m}, which we previously detected in irradiated Cd. The excitation function and cross section for the reaction at 19.2 Mev were determined for this isomer. The gamma-ray energies, half-lives, and relative yields from thick targets have been determined for all of the short-lived isomers.

1. INTRODUCTION

THE detection and investigation of short-lived isomeric activities resulting from nuclear reactions encounter a number of experimental difficulties. Prior to 1955 no isomers with half-lives in the millisecond range ($10^{-1} - 10^{-4}$ sec) were known. Thereafter a very small number of such isomers were discovered as a result of reactions involving 14-Mev neutrons,[1,2] 32-Mev[3] and 20-Mev[4-6] protons, and 24-Mev and 22-Mev gamma rays.[7,8]

The observation and study of short-lived isomers created by nuclear reactions are of great interest, since some of them cannot be produced in any other way.

By employing data regarding the way in which cross sections for the formation of isomeric and ground states are dependent on incident-particle energies it is possible to observe the transition from a mechanism for compound-nucleus formation to a mechanism of direct interaction.[9,10] It is very important to determine the parts played by various nuclear-reaction mechanisms at different particle energies, since this entire subject is in need of clarification (see reference 11, for example).

The present work continues the study of short-lived isomers produced by fast protons.[4-6]

2. EXPERIMENTAL TECHNIQUE AND APPARATUS

In order to detect and study short-lived isomeric activities with half-lives $T_{1/2} = 10^{-1} - 10^{-4}$ sec produced by fast protons, samples were subjected to pulsed irradiation followed by registration of short-lived gamma emission between accelerator pulses. In the present experiments we improved the method of monitoring the beam intensity employed in our previous work[4-6] and the technique for registering radiation.

1) Monitoring of beam intensity. In the investigation of samples for the purpose of detecting short-lived isomers, as well as in several other measurements, an extracted beam was employed; protons passed through a 40-micron aluminum foil before striking a target in air. Beam intensity in these experiments was monitored by a scintillation monitor (FÉU-19 photomultiplier) which registered flashes from a thin screen covered with willemite (similar to the apparatus described in reference 12). The screen was placed in the beam path prior to the emergence of the protons into air. Each light flash charged a capacitor connected to one of the last photomultiplier dynodes. When a predetermined voltage was reached on the capacitor a cut-off thyratron (TG 3 — 0.1/1.3) was fired; a relay, pulse shaper, and mechanical counter were then triggered. Prior to the experiment the scintillation monitor was calibrated by means of a current integrator, linear in the region from 10^{-6} to 10^{-11} amp[13] which measured the charge of protons that had traversed the willemite screen and entered the Faraday cup located directly behind the screen. The sensitivity of the monitor decreased with time because the protons passing through the screen "aged" the willemite; frequent recalibration of the monitor was therefore required. We therefore used an internal beam in the

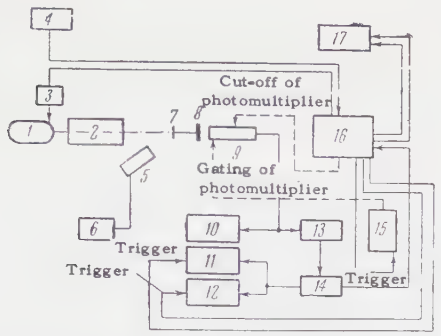

FIG. 1. Block diagram of apparatus. 1 – electrostatic generator; 2 – linear accelerator; 3 – thyratron for phototriggering of electrostatic generator; 4 – master oscillator of accelerator; 5 – scintillation monitor with FEU-19 photomultiplier; 6 – registering circuit of scintillation monitor; 7 – thin aluminum screen covered with willemite; 8 – target; 9 – detector (FEU-11 photomultiplier with NaI(Tl) crystal); 10 – "gray-wedge" analyzer; 11 – single-channel time analyzer; 12 – oscillographic counter; 13 – amplifier; 14 – single-channel pulse-height analyzer; 15 – gating circuit of FEU-11; 16 – control circuit of beam and apparatus; 17 – PS-256 scalers.

experiments requiring knowledge of the number of protons striking the target, the target thus being located in a vacuum. In this case the charge of protons striking the target, which served as the bottom of the Faraday cup, was measured directly by the current integrator.

2) Detection of short-lived isomeric radiation and determination of energy and half-life. Figure 1 is a block diagram of the apparatus. A pulsed linear accelerator (at the Physico-Technical Institute of the Academy of Sciences, Ukrainian S.S.R.) supplied two 19.2-Mev proton pulses per second (each pulse lasting $\sim 300\,\mu$ sec, with $\sim 3 \times 10^9$ maximum number of protons per pulse). Gamma radiation from the target was registered by a FÉU-11 photomultiplier with a NaI(Tl) crystal (diameter 29 mm, thickness 13 mm) in a standard duraluminum container.

Two modes of photomultiplier operation were used to register radiation from the target.[14] The electron current from the photocathode of the photomultiplier was controlled by a modulating grid located between the first dynode and the photocathode. It was shown experimentally that the current through the photomultiplier is cut off when the modulating grid is grounded. In order to prevent charging of the photomultiplier during a proton pulse, in some experiments (see below) the photomultiplier was cut off by the modulating grid during a time $\theta > 300\,\mu$sec following the start of the pulse (photomultiplier cut-off mode). Since the pulse duration θ could vary by an amount of time up to 75 msec, an activity with $T_{1/2} < 15$ msec might possibly not be registered when two short-lived emissions were present. The photomultiplier cut-off mode of operation depended on the delay circuit of the control unit,[15] which was triggered by a pulse from the master oscillator of the accelerator and which fed a pulse of length θ to a tube connected with the modulating grid, which in turn controlled the electron current from the photomultiplier photocathode.

In other experiments when an optimum ratio was required between the number of pulses from short-lived isomeric emission and the background, the photomultiplier functioned only during a time τ of a few tens of milliseconds. At all other times, including the period θ, the photomultiplier was cut off by the same modulating grid (the photomultiplier gating mode). In this case the special circuit used to gate the photomultiplier was triggered by the trailing edge of the pulse of length θ. The output of this circuit fed a pulse of length τ, (which might vary from 0.95 to 390 msec) to another tube connected with the modulating grid.

Resolution of the 1.118-Mev line of Zn^{65} in conjunction with both multiplier modes of operation differs very little (7.5 – 8%) from the resolution in the case of a continuously operating photomultiplier. It must be noted that the sensitivity of a gated photomultiplier decreases somewhat when the width of the gate is reduced. For example, when τ is changed from 280 to 10 msec the 1.118-Mev photopeak is reduced 3%.[14]

When the FÉU-11 was used the detector allowed large loads. Thus when the total count increased from 2×10^3 to 60×10^3 pulses/sec the position of the 1.118-Mev photopeak was practically unchanged and the previous resolution of 7.5 — 8% was retained.

In experiments aimed at detecting short-lived radiation produced by fast protons striking a target we used a gated photomultiplier ($\theta = 1$ msec, $\tau = 82$ msec). An external proton beam was employed, with the target close to the NaI(Tl) crystal. Pulses from the cathode follower of the FÉU-11 were fed to a "gray-wedge" analyzer.[16] A preliminary study of the samples aimed at detecting appreciable activities; radiation from the target was compared with that from a neutral carbon sample. A negligibly small background resulted when carbon was bombarded with 19.2-Mev protons.

After an effect had been observed or when investigating samples which furnished no visual effect the spectrum of the sample and of a neutral target were photographed. The long-lived back-

ground of the target was determined by photographing the spectrum from an irradiated sample in the absence of the proton beam. The gray-wedge analyzer was calibrated by means of monoenergetic gamma-ray sources under the given mode of photomultiplier operation. In these experiments the beam impinged on a neutral target, and the sources were located at such distances that the analyzer load approached the load due to short-lived emission from the investigated target.

Using an external proton beam, we registered the time distribution of pulses by means of a 25-channel time analyzer,[17] which was fed by pulses from the single-channel pulse-height analyzer adjusted to the photopeak under investigation. The employment of a single-channel pulse-height analyzer improved the signal-to-background ratio. For visual observation as well as for photographing the time distribution of pulses we used an oscillographic counting setup with driven sweeps. The time analyzer and the counter were triggered by the trailing edge of the θ pulse. The decay curve was plotted taking into account the neutral-target background that was measured under the given conditions.

3) Identification of the isotope involved in an isomer-producing reaction. In order to determine which isotope of a given element is involved in a reaction that produces an isomer we used enriched mixtures with a different degree of enrichment for each isotope. We measured the yields of isomeric emission from a sample prepared from an enriched mixture along with a sample of the natural mixture. Samples of the same compound with identical densities were prepared in the two cases.

Our experiments were performed with an external beam of protons. Isomeric radiation was measured by a single-channel pulse-height analyzer with channel width sufficient to include almost the entire investigated photopeak. Preliminary experiments showed a difference of less than 7% in photopeak areas measured with a narrow (1 v) or broad (10 v) channel in the case of the 1.118-Mev line of Zn^{65}. For the purpose of reducing the long-lived background the photomultiplier was gated during a time τ equal to a few half-lives of the radiation under investigation. Pulses produced by the long-lived radiation from the target and accelerator which fell within the 10-volt channel width of the analyzer were also registered automatically.

For the purpose of taking the long-lived background into account, we used a control circuit[15] which permitted registration of radiation between two accelerator pulses. A special arrangement[15] was used to switch the accelerator from two pulses to one pulse per second. When the beam struck the target the radiation (including the background) was registered by scaler No. 1. In the absence of a beam the long-lived background was registered by scaler No. 2.

Experiments that were intended for identification of a short-lived isomer were conducted in the following order. After energy calibration of the analyzer the gated photomultiplier was adjusted to the investigated line. An unenriched target was then irradiated. Following the interaction between the beam and the target scaler No. 1 registered, for each reading of the scintillation monitor, ν_1 pulses equaling the sum of pulses from short-lived isomeric emission of the target, long-lived emission of the target, long-lived radiation from the accelerator and the short-lived background which resulted from beam passage through the accelerator. In the absence of a beam scaler No. 2 registered during the same time ν_2 pulses representing long-lived radiation from the target and the long-lived accelerator background. Thus $\Delta\nu'_{un} = \nu_1 - \nu_2$ is the number of pulses produced by short-lived target emission and by the short-lived background of the beam traversing the accelerator, measured for an unenriched target. Under the same conditions an enriched sample yielded $\Delta\nu'_{enr}$. An experiment with a neutral (carbon) target was performed in order to determine the short-lived background. In this case scaler No. 1 registered ν_3 pulses for each scintillation-monitor reading. This number of pulses represents the sum of the long-lived accelerator background and the beam-passage effect. In the absence of a beam, scaler No. 2 registered only the long-lived accelerator background ν_4. Thus $\Delta\nu_{ac} = \nu_3 - \nu_4$ represents the effect resulting from beam passage through the accelerator. Similar experiments performed with all pairs of samples yielded the relations

$$\beta_1 = (\Delta\nu'_{enr} - \Delta\nu_{ac}) / (\Delta\nu'_{un} - \Delta\nu_{ac}),$$

$$\beta_2 = (\Delta\nu''_{enr} - \Delta\nu_{ac}) / (\Delta\nu''_{un} - \Delta\nu_{ac}) \text{ etc.}$$

The isotope involved in a given isomer-producing reaction was determined by comparing these ratios with computations based upon the certified isotopic content of enriched samples.

4) Identification of an isomer-producing reaction. In experiments intended for reaction identification we measured the reaction threshold for a thick target, and compared the result with corresponding values for the thresholds of all energetically possible reactions with protons, as computed from the masses of substances participating

in the reactions. Since isomeric radiation in most instances amounts to only a few tenths of 1 Mev, this can be neglected in a comparison of experimental and calculated results. Since all investigated cases pertain to medium and light nuclei, the correction for Coulomb-barrier penetration may also be neglected because of the closeness of the threshold measurements. In the case of a thin target, the shape of the excitation function was used to determine the type of nuclear reaction.

In these experiments we used an internal beam of protons, which was monitored by a current integrator.[13] The beam energy was varied by means of aluminum filters. Experiments with a neutral target were performed under the same conditions in order to determine the effect produced by beam passage through the accelerator. The experimental sequence is described in item 3).

5) Determination of the isomer-producing reaction cross section. These experiments were performed with an internal beam impinging on a thin sample in which the loss for a 19.2-Mev proton beam amounted to ~0.2 Mev. The sample was backed with a graphite cup (diameter 20 mm and thickness 3 mm), which at the same time served to slow down the protons. Following the experiments with the thin target measurements with the graphite backing were performed under identical conditions. The experimental sequence is described in Item 3). The reaction cross section is represented by

$$\sigma_m(E_p) = \nu / \Pi n \alpha \xi(E_\gamma) \varkappa(\theta, \tau). \quad (1)$$

Here ν is the number of registered pulses resulting from short-lived isomeric radiation (with the background subtracted); Π is the number of protons striking the target and is related to the current-integrator reading M by $\Pi = (2.67 \pm 0.13) \times 10^9$ M; n is the number of nuclei in the natural isotope mixture per cm^2 of the target; α is the relative amount of the isotope on which the isomer-producing reaction takes place; $\xi(E_\gamma)$ is the registration efficiency for radiation with energy E_γ emitted by a thin target with the experimental geometry taken into account. This value also allows for the attenuation of gamma radiation in the material situated between the thin sample and the NaI(Tl) crystal (graphite backing, Plexiglas window of the vacuum attachment; detector cover, crystal packaging). $\varkappa(\theta, \tau)$ is the fraction of gamma radiation with decay constant λ registered in the time τ, with the start of registration shifted by the amount of time θ:

$$\varkappa(\theta, \tau) = \exp(-\lambda\theta) - \exp(-\lambda\theta - \lambda\tau).$$

Since it is very difficult to calculate $\xi(E_\gamma)$ when the sample is located very close to the detector, we used the same experimental arrangement and took into account all materials between the target and crystal while performing experiments in which $\xi(E_\gamma)$ was measured for a few monoenergetic gamma-ray sources of known activity, the sources having the same dimensions as the investigated target. The activities of the following standard sources: Ce^{141} (E_γ = 0.142 Mev), Cr^{51} (E_γ = 0.323 Mev), Cs^{137} (E_γ = 0.662 Mev), Nb^{95} (E_γ = 0.765 Mev), and Zn^{65} (E_γ = 1.118 Mev) were measured by means of a special counter whose sensitivity was only slightly dependent on gamma-ray energy.[18]

6) Estimate of relative isomer yields from thick targets. The yields K_γ from thick targets were normalized by means of a short-lived isomer W^{180m} (E_γ = 0.37 Mev) obtained from tantalum. We had discovered this isomer some time previously.[4] In later experiments we found that the short-lived gamma radiation from bombarded tantalum includes two lines, 0.24 ± 0.01 and 0.37 ± 0.01 Mev, with identical half-lives $T_{1/2}$ = 5.5 ± 0.3 msec.

Since the short-lived isomeric spectrum sometimes contains two or three lines with identical half-lives, for the sake of simplicity K_γ was determined for the gamma radiation of maximum energy.

These measurements were performed with an extracted proton beam and in the experimental order described in Item 3). Since the yields from thick targets differed strongly the measurements were performed for three different target-detector separations. K_γ was calculated by means of a formula similar to (1). ν was computed for a single reading of the scintillation monitor. Since in some instances the thick targets were chemical compounds (oxides or salts), it was necessary to determine the thickness of the target material containing these nuclei in order to compute the number of nuclei which might be involved in a given nuclear reaction. For this purpose we used computed data[19] for the range-energy relations of protons in Al, Cu, Sn and Pb. These data, in conjunction with the measured isomer-producing reaction thresholds and the effective atomic numbers of the compounds, determined the number of nuclei of a given isotope per cm^2. Since the registration efficiency for thick targets with the given experimental geometry was known with insufficient accuracy, the yields of short-lived isomers was determined to within a factor of ~2.

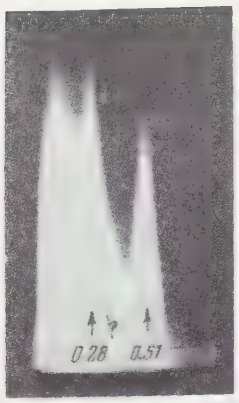

FIG. 2. Spectrum of proton-irradiated Sc_2O_3. The gate $\tau = 82$ msec of the FEU-11 photomultiplier was delayed $\theta = 0.5$ msec following the start of the proton pulse.

3. RESULTS AND DISCUSSION

Accelerator background radiation. Measurements of the gamma-ray spectrum from the accelerator (when the proton beam struck the neutral target) revealed the presence of weak radiation with energy ~0.5 Mev. It was determined by means of the single-channel time analyzer that this radiation is the sum of a short-lived ($T_{1/2} \approx 2$ msec) and a long-lived portion. An analysis of the possible sources of the short-lived portion indicates that this radiation may originate in the interaction of fast protons with iron or copper parts of the accelerator. When a delay $\theta = 10$ msec is introduced only the long-lived radiation is registered.

Remaev has shown that when targets containing oxygen (oxides or salts) are irradiated intense long-lived emission with $E_\gamma = 0.510 \pm 0.005$ Mev is observed, which is annihilation radiation from β^+ activities of N^{13} ($T_{1/2} = 10.6$ min) and O^{15} ($T_{1/2} = 2$ min). These activities result from the reactions $O^{16}(p, \alpha)N^{13}$ and $O^{16}(p, pn)O^{15}$. Experiments also revealed a considerable yield from $O^{16}(p, \alpha)N^{13}$ in oxide films on metals.

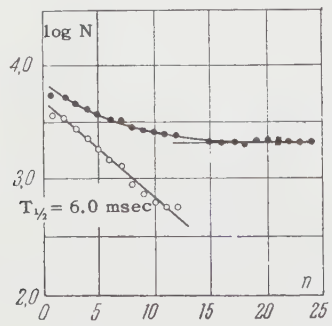

FIG. 3. Decay of 0.28-Mev activity of Sc_2O_3. The horizontal axis represents the channel number of the time discriminator (with 1.8 msec channel width). The vertical axis represents logarithms of differences between counts obtained with the sample and with a neutral target. The lower curve, obtained by subtracting the long-lived background from the sample, represents the decay of Ti^{45m}.

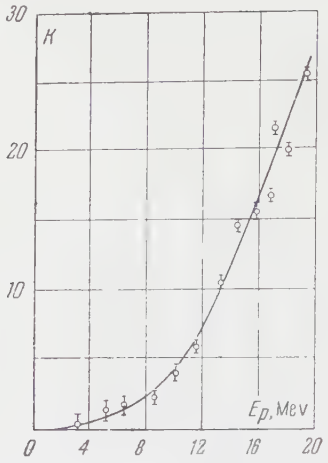

FIG. 4. Yield of short-lived isomer Ti^{45m} ($E_\gamma = 0.28$ Mev, $T_{1/2} = 5.8$ msec) from a thick Sc_2O_3 target, in relative units. Statistical errors are indicated. E_p is the proton energy. The neutral (carbon) target background has been taken into account. $\Delta = 10$ v is the channel width of the pulse-height analyzer. The photomultiplier gate is $\tau = 55$ msec with $\theta = 3.7$ msec delay.

We may assume that long-lived radiation from the accelerator results from both the production of N^{13} and O^{15} and from other positron activities excited by protons and secondary neutrons in various units of the accelerator, especially those made of copper.

Results obtained in our investigations of new short-lived isomers are presented below. The discussion is divided according to the irradiated element.

Scandium. The irradiation of scandium oxide yielded a short-lived isomer with $E_\gamma = 0.28 \pm 0.01$ Mev and $T_{1/2} = 5.8 \pm 0.4$ msec.* Figure 2 is the gamma-ray spectrum produced by 19.2-Mev protons. A 0.28-Mev isomer line is clearly visible, as well as a strong 0.51-Mev line, which represents the annihilation radiation from positron activities, including those of N^{13} and O^{15}. The 0.28-Mev line was not registered when a delay $\theta = 75$ msec was introduced. Figure 3 shows a typical short-lived isomer decay curve. Figure 4 represents the excitation function of an isomer-producing reaction in the case of a thick target. The reaction threshold determined from this curve is ~2 Mev. Scandium has a single isotope, Sc^{45}; the following reactions are possible energetically:

*We present hereinafter averages of several measurements. Errors in energy values are associated with errors in determining the positions of peaks in oscillograms obtained by means of the gray-wedge analyzer. Stated errors of half-lives take into account the accuracy with which the width of the timing channel is measured.

TABLE I Percent contents of Cd in Samples

Sample	Isotopes, %							
	Cd^{106}	Cd^{108}	Cd^{110}	Cd^{111}	Cd^{112}	Cd^{113}	Cd^{114}	Cd^{116}
Natural Cd	1.215	0.875	12.39	12.75	24.07	12.26	28.86	7.58
Cd^{114}	0.1	0.1	0.7	1.9	4.0	14.7	75.2	3.3
Cd^{111}	0.1		11.3	61.5	3.5	18.3	3.0	2.4
Cd^{112}	~0.3	0.3	4.7	37.6	50.7	3.1	2.6	0.7

$Sc^{45}(p, n)Ti^{45}$, $Sc^{45}(p, p')Sc^{45}$, and $Sc^{45}(p, \alpha)K^{42}$. The most probable of these reactions is $Sc^{45}(p, n)Ti^{45}$ with ~2.8 Mev as its calculated threshold. It is therefore suggested that the radiation from Sc which we observed belongs to Ti^{45m}.

The negative results of the attempts to detect short-lived isomers in scandium and titanium irradiated with 14-Mev neutrons[2] and potassium and titanium irradiated with 24-Mev gamma rays[7] do not contradict our identification. Such results may mean that Sc^{45m} and K^{42m} are not produced in reactions with neutrons and gamma rays. Also, an analysis shows that reactions which might produce Ti^{45m} are either energetically impossible or of small probability.

Excited levels of Ti^{45} are unknown; it has a $7/2^-$ ground level.[20] The short-lived 0.28-Mev radiation that we detected may be assigned to a $1/2^+ \rightarrow 7/2^-$ transition (E3). Montalbetti's nomogram for single-particle transitions, which relates lifetime, emitted energy and angular momentum change,[21] can be used to determine the lifetime of a detected short-lived isomer. The lifetime obtained for a E3 transition and $E_\gamma = 0.28$ Mev is $\sim 10^{-2}$ sec, which does not differ markedly from the measured value.

All measurements as well as the short-lived gamma-ray yield from a thick target are given in Table II.

Niobium. Irradiation of metallic niobium yielded two short-lived lines, $E_{\gamma 1} = 0.25 \pm 0.01$ Mev and $E_{\gamma 2} = 0.40 \pm 0.01$ Mev. $E_{\gamma 2}$ has a half-life $T_{1/2} = 5.7 \pm 0.3$ msec. The half-life of $E_{\gamma 1}$ is estimated at ~4.8 msec. We did not identify the final reaction product responsible for the isomeric state.

Cadmium and indium. We have previously[4,5] reported the detection of a short-lived isomer in cadmium irradiated with fast protons ($E_\gamma = 0.28$ Mev, $T_{1/2} = 47 \pm 10$ msec). The present work has yielded improved values for the properties of this radiation and has identified the isomer. Many energy measurements have furnished the result $E_\gamma = 0.32 \pm 0.01$ Mev and the short half-life $T_{1/2} = 42.2 \pm 2.0$ msec.

Natural cadmium has eight isotopes (Table I), two of which (Cd^{106} and Cd^{108}) are present in only small amounts (~2%). We used three samples of cadmium oxide with different enrichments of the isotopes (Table I). Our smallest sample weighed 175 mg ($Cd^{114}O$).

The experiments with cadmium isotopes yielded the following relations between the yields β from the respective samples: $(1 : \beta_{114} : \beta_{111} : \beta_{112})_{exp} = 1 : 2.2 : 0.12 : 0.1$. The calculated yield ratios are closest to the experimental ratio for reactions in Cd^{114} in this case we have $(1 : \beta_{114} : \beta_{111} : \beta_{112})_{calc} = 1 : 2.6 : 0.10 : 0.09$.

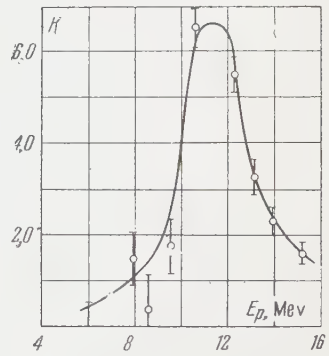

FIG. 5. Excitation function of short-lived isomer In^{114m} ($E_\gamma = 0.32$ Mev, $T_{1/2} = 42.2$ msec) produced in a thin Cd target ($\theta = 4.6$ msec, $\tau = 82$ msec, $\Delta = 4.7$ v).

For identification of the isomer-producing reaction in the case of a thick target we measured the reaction threshold (≤ 4 Mev). Figure 5 shows the excitation function for the isomer produced in a thin Cd target (11.6 mg/cm^2). The shape of the curve indicates the occurrence of a (p, n) reaction. If the isomer resulted from a (p, 2n) or (p, pn) reaction the maximum yield for these reactions would be in the range 16-19 Mev. Therefore the short-lived isomer with $E_\gamma = 0.32 \pm 0.01$ Mev and $T_{1/2} = 42.2 \pm 2.0$ msec is obtained from the reaction $Cd^{114}(p, n)In^{114m}$.

The same thin target was used to measure the cross section σ_m for the production of short-lived In^{114m} by 19.2-Mev protons. $\sigma_m = 53 \pm 5$mb was obtained as a result of many measurements.*

*The error is the average of the rms errors calculated for individual measurements.

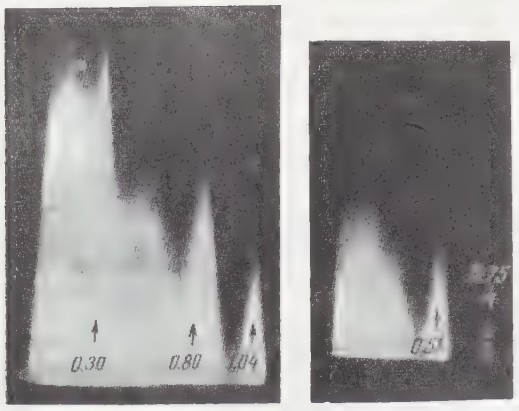

a b

FIG. 6. Gamma-ray spectrum of proton-irradiated La_2O_3. a – θ = 0.5 msec, τ = 82 msec; b – θ = 50 msec, τ = 82 msec.

Since the reaction $In^{115}(p, pn)In^{114m}$ may also take place on indium irradiated with fast protons, we investigated the radiation from indium. Short-lived emission was detected with $E_\gamma = 0.32 \pm 0.01$ Mev and $T_{1/2} = 41.5 \pm 2.0$ msec. The excitation curves obtained with a thick target were used to determine the reaction threshold, which is 10.8 ± 0.8 Mev.

Indium has two isotopes, In^{113} (4.23%) and In^{115} (95.77%); the reaction obviously involes In^{115}. The reaction thresholds for $(p, 2n)Sn^{114}$ and $(p, pn)In^{114}$ which are computed from the masses are ~ 8.2 and ~ 9.4 Mev, respectively. Since Sn^{114} is an even-even nucleus its first excited levels are high, and this nucleus cannot be the final reaction product. This circumstance together with the good agreement of the Cd and In radiation properties suggests that the short-lived indium isomer results from $In^{115}(p, pn)In^{114m}$.

Following the publication of our data in reference 4, a short-lived isomer with similar properties was observed when indium was irradiated in a 22-Mev betatron.[22] Crossover reactions (see references 4 and 22) enabled Glagolev et al.[2] to identify the short-lived gamma radiation, which was detected when indium was bombarded with 14-Mev neutrons ($E_\gamma = 0.32 \pm 0.01$ Mev, $T_{1/2} = 42 \pm 2$ msec), as that of In^{114m} produced in the reaction $In^{115}(n, 2n)In^{114m}$. On the basis of several considerations it was proposed that the observed transition goes from the 8^+ level ($E_\gamma = 0.510$ Mev) to the previously known 5^+ level ($E_\gamma = 0.190$ Mev).[20] This is therefore a magnetic octupole transition (M3). Duffield and Vegors[8] have identified and obtained improved values for the properties of In^{114m}: $E_\gamma = 0.311 \pm 0.005$ Mev, $T_{1/2} = 42 \pm 5$ msec. Since the measured internal conversion coefficient α_c is smaller than 0.13 and is closer to the theoretical value for an E3 transition ($\alpha_c = 0.08$) than for M3 ($\alpha_c = 0.30$), Duffield and Vegors proposed that the 0.501-Mev level is a 8^- state and that the short-lived 0.311-Mev radiation ($T_{1/2} = 42$ msec) is an electric octupole transition (E3). Since precise data for determining the interval conversion coefficient is still unavailable the character of the transition (E3 or M3) cannot be decided.

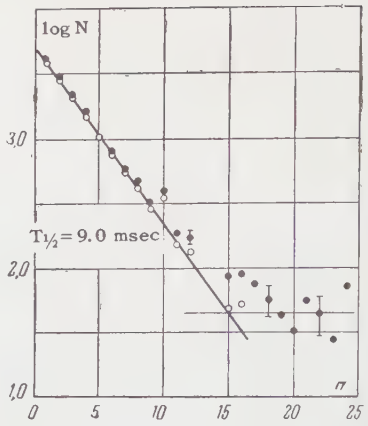

FIG. 7. Decay of activity in La_2O_3 (E_γ = 1.04 Mev). The channel width was 4 msec. The heavy line represents the decay of Ce^{139m}

Lanthanum. When lanthanum was irradiated with fast protons we observed a large yield of short-lived gamma radiation, the spectrum of which is shown in Fig. 6a. Three lines are clearly observed: $E_{\gamma 1} = 0.30 \pm 0.01$ Mev, $E_{\gamma 2} = 0.80 \pm 0.01$ Mev and $E_{\gamma 3} = 1.04 \pm 0.01$ Mev. When the delay θ = 50 msec is introduced none of the three lines is registered (Fig. 6b). In addition to the background line $E_\gamma = 0.51$ Mev, the spectrum then contains a 0.75-Mev line which was shown experimentally to belong to the 55-second isomer Ce^{139m} ($E_\gamma = 0.74$ Mev[20]) produced in the reaction $La^{139}(p, n)Ce^{139m}$.

The measured half-lives of the three lines coincide within experimental error. $T_{1/2} = 9.2 \pm 0.5$ msec is obtained on the basis of numerous measurements. Figure 7 shows the decay curve of the short-lived isomer.

Lanthanum consists practically of only a single isotope (99.91%); identification of the isomer is thus considerably simplified. Figure 8 shows the

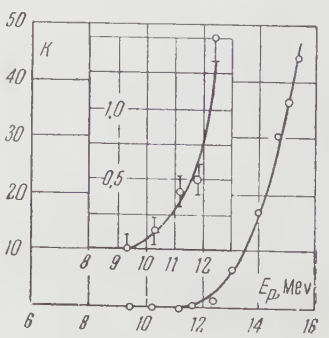

FIG. 8. Yield of short-lived isomer (E_γ = 1.04 Mev, $T_{1/2}$ = 9.2 msec) from thick La_2O_3 target. θ = 4.7 msec, τ = 35 msec, Δ = 4.7 v. The enlargement in the center of the figure represents the yield close to the reaction threshold.

TABLE II

Target	Emitted line, Mev	Half-life, msec	Yield from thick target, K_γ	Reaction which produced isomer
Sc_2O_3	0.28±0.01	5.8±0.4	0.01	Sc^{45} (p, n) Ti^{45m}
Nb	0.25±0.01	~4.8	—	
	0.40±0.01	5.7±0.3	0.005*	—
Cd	0.32±0.01	42.2±2.0	0.2	Cd^{114} $(p, n)In^{114m}$
In	0.32±0.01	41.5±2.0	0.04	In^{115} $(p, pn)In^{114m}$
La_2O_3	0.30±0.01		—	
	0.80±0.01	9.2±0.5	—	La^{139} $(p, 2n)Ce^{138m}$
	1.04±0.01		1	
Nd_2O_3	0.21±0.01	2.2±0.2	—	
	0.43±0.01		0.02**	—
Ta	0.24±0.01	5.5±0.3	—	Ta^{181} $(p, 2n)W^{180m}$
	0.37±0.01		1	
Os	0.32±0.01	10.0±0.6	0.2**	—

experimental excitation curve of the short-lived isomer; the threshold for its formation is ~ 9 Mev. Comparison of the reaction thresholds computed from nuclear masses shows that the thresholds for the (p, pn) and (p, 2n) reactions are closest; these are ~ 8.9 and ~ 9.3 Mev, respectively. It is extremely difficult to distinguish such close thresholds experimentally; it can only be stated that in our case both La^{138m} and Ce^{138m} are energetically possible. It is known from tables in reference 20 that cascade gamma rays (0.80, 1.05 and 0.30 Mev) have been observed in the β^+ decay of Pr^{138} ($T_{1/2}$ = 2 hrs) produced on enriched Ce^{138} by 9.5-Mev protons.[23] The lines $E_{\gamma 1}$ = 0.30 Mev, $E_{\gamma 2}$ = 0.80 Mev, and $E_{\gamma 3}$ = 1.04 Mev that we observed are obviously the same gamma rays that were discovered in connection with the β^+ decay of Pr^{138}.

The short-lived activity that we have detected therefore belongs to the even-even isomer Ce^{138m} that was produced in the reaction La^{139}(p, 2n) Ce^{138m}

No short-lived activities have resulted from the irradiation of La_2O_3 and Ce_2O_3 with 14-Mev neutrons.[2] The short-lived isomer Ce^{188m} could not be observed, since the reaction threshold of Ce^{140}(n, 3n)Ce^{138} is 17 Mev.

When lanthanum was irradiated with 22-Mev gamma rays no short-lived activity was observed.[8] When Ce (~ 88% Ce^{140}) was irradiated with 24-Mev gamma rays Ce^{138m} was also not detected;[7] this is accounted for by the low probability of a $(\gamma, 2n)$ reaction.

The cited failures to produce short-lived activities by bombarding cerium and lanthanum[2,8,7] do not conflict with our identification of the isomer that we detected when lanthanum was irradiated with protons.

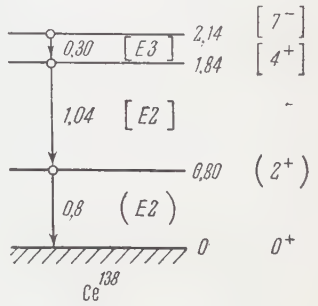

FIG. 9. Proposed decay scheme of Ce^{138m}. The isomeric level is located at 2.14 Mev. All energies and transitions are given in Mev.

Figure 9 shows the possible decay scheme of the short-lived isomer Ce^{138m} which is based on the level scheme of Ce^{138}.[20] The spins, parities and transition types that we have proposed are enclosed in square brackets; data taken from reference 20 are enclosed in round brackets. The transition energies were obtained in the present work. The assignments of spins and parities to the second and third excited states were based on the fact that the 0.8-Mev line belongs to the first excited level 2^+.[24] In this scheme the isomer is located at 2.14-Mev [7⁻]. According to the Montalbetti nomogram the 0.30-Mev E3 transition has a lifetime ~ 2 msec, which is close to the measured value of 9.2 msec. For an M3 transition the lifetime according to the nomogram would be ~ 0.25 sec.

Despite some discrepancy between the experimental threshold (~ 9 Mev) and the expected threshold (9.3 + 2.14 ≈ 11.4 Mev) the proposed decay scheme of Ce^{138m} merits consideration.

Neodymium. Irradiated neodymium oxide yielded two lines, $E_{\gamma 1}$ = 0.21 ± 0.01 Mev and $E_{\gamma 2}$ = 0.43 ± 0.01 Mev. The half-lives of these two lines coincide within the limits of error at 2.2 ± 0.2 msec. Since natural neodymium has seven isotopes and no enriched samples were available, the short-lived radiation was not identified.

Osmium. The bombardment of metallic osmium produced a strong short-lived line ($E_\gamma = 0.32 \pm 0.01$ Mev, $T_{1/2} = 10 \pm 0.6$ msec). Since osmium also has seven isotopes and no enriched samples were available, it was impossible to identify the nuclear reaction involved in the formation of the isomer.

4. BRIEF SUMMARY

Table II summarizes the results obtained in our investigation of short-lived isomers produced by reactions with 19.2-Mev protons.

Since in the case of Nb we did not know the threshold of the reaction which produced the 0.40-Mev level, we assumed $E_{thr} = 10$ Mev and calculated the number of nuclei on which the nuclear reaction might take place within a layer of matter corresponding to the range of protons with energies from 19.2 to 10 Mev. The resulting yield K_γ is marked with an asterisk. In the cases of osmium and neodymium oxide, we knew neither the reaction thresholds nor the isotopes that were involved. In both instances we also assumed $E_{thr} = 10$ Mev and calculated the isomer yield for a natural isotope mixture. These values of K_γ are marked with two asterisks.

The authors are deeply grateful to A. P. Klyucharev for his great interest in the present work, to A. M. Smirnov for uninterrupted operation of the accelerator and to the entire crew of the linear accelerator at the Physico-Technical Institute. The authors also wish to thank technician V. T. Deren'ko for assistance.

[1] Yampol'skiĭ, Leipunskiĭ, Gen, and Tikhomirov, Izv. Akad. Nauk SSSR, Ser. Fiz. **19**, 338 (1955), Columbia Tech. Transl. p. 312.

[2] Glagolev, Kovrizhnykh, Makarov, and Yampol'skiĭ, JETP **36**, 1046 (1959), Soviet Phys. JETP **9**, 742 (1959).

[3] S. D. Softky, Phys. Rev. **98**, 736 (1955).

[4] Leipunskiĭ, Miller, Morozov and Yampol'skiĭ, Doklady Akad. Nauk SSSR **109**, 935 (1956), Soviet Phys.-Doklady **109**, 505 (1956).

[5] Leipunskiĭ, Morozov, Makarov, and Yampol'skiĭ, JETP **32**, 393 (1957), Soviet Phys. JETP **5**, 305 (1957).

[6] A. M. Morozov and P. A. Yampol'skiĭ, JETP **36**, 950 (1959), Soviet Phys. JETP **9**, 671 (1959).

[7] S. H. Vegors and P. Axel, Phys. Rev. **101**, 1067 (1956).

[8] R. B. Duffield and S. H. Vegors, Phys. Rev. **112**, 1958 (1958).

[9] B. Linder and R. A. James, Phys. Rev. **114**, 322 (1959).

[10] Meadows, Diamond, and Sharp, Phys. Rev. **102**, 190 (1956).

[11] V. F. Weisskopf, Physica **22**, 952 (1956).

[12] Yu. V. Makarov and A. P. Morozov, Report, Inst. Chem. Phys., Acad. Sci. U.S.S.R., 1957.

[13] Golovnya, Zalyubovskiĭ and Shilyaev, Приборы и техника эксперимента (Instruments and Exptl. Techniques) (in press).

[14] A. M. Morozov, Report, Inst. Chem. Phys., Acad. Sci. U.S.S.R., 1958.

[15] Morozov, Likin, and Meleshin, Report, Inst. Chem. Phys., Acad. Sci. U.S.S.R., 1958.

[16] O. B. Likin, loc. cit. ref. 13 **2**, 36 (1958).

[17] V. V. Remaev, Report, Inst. Chem. Phys., Acad. Sci. Ukrainian S.S.R., 1960.

[18] V. N. Sakharov, Атомная энергия (Atomic Energy) **3**, 61 (1957), Soviet. J. Atomic Energy p. 807.

[19] H. A. Bethe and J. Ashkin, Experimental Nuclear Physics, E. Segre, Ed., Vol. I, John Wiley, New York, 1955.

[20] B. S. Dzhelepov and L. K. Peker, Схемы распада радиоактивных ядер (Decay Schemes of Radioactive Isotopes), Acad. Sci. Press, 1957.

[21] R. Montalbetti, Can. J. Phys. **30**, 660 (1952).

[22] S. H. Vegors and R. B. Duffield, Bull. Am. Phys. Soc. **1**, 206 (1956).

[23] T. H. Handley and E. L. Oslon, Phys. Rev. **96**, 1003 (1954).

[24] R. N. Glover and D. E. Watt, Phil. Mag. **2**, 49 (1957).

Translated by I. Emin
177

POLARIZATION OF COSMIC-RAY μ^+ MESONS

V. V. BARMIN, V. P. KANAVETS, and B. V. MOROZOV

Submitted to JETP editor May 23, 1960

J. Exptl. Theoret. Phys. (U.S.S.R.) **39**, 986-990 (October, 1960)

Geiger and scintillation counters were used to measure the degree of polarization of cosmic-ray μ^+ mesons of various energies. The μ^+-meson energy was determined from the mean range in a Cu and Pb absorber placed above the array. The measurements were performed at sea level. The cosmic-ray μ^+-meson polarizations obtained for μ^+ mesons with momentum equal to 0.45, 0.9, and 1.7 Bev/c are 0.23 ± 0.10, 0.37 ± 0.11, and 0.31 ± 0.10, respectively.

1. INTRODUCTION

PARITY nonconservation in π-meson decay, and also the character of the momentum spectrum of cosmic-ray π mesons, lead to a considerable polarization of cosmic-ray μ^+ mesons.

Calculations[1-3] carried out under the assumption that all cosmic-ray μ mesons are produced in the decay of the π-meson component showed that the polarization of μ mesons depends on the power exponent γ, if the momentum spectrum of the π mesons is represented by the expression $ap^{-\gamma}$, and amounts to 0.30 for $\gamma \approx 2.7$.[4,5]

The degree of polarization of μ^+ mesons was measured by a number of investigators[3,6-8] from the asymmetry of decay positrons. For μ^+ mesons with momenta 0.35 — 0.55 Bev/c, the results of these experiments are in good agreement with each other, and give polarization values in the range 0.19 — 0.23. Measurements in the high-energy region of the μ^+ mesons carried out by Dolgoshein, Luchkov, and Ushakov[7] indicate a marked increase of the degree of polarization up to 0.44 ± 0.055 for a momentum equal to 1.5 Bev/c.

In the present experiment, the degree of polarization of μ^+ mesons was determined for three various energy ranges. The measurements were carried out at sea level.

2. DESCRIPTION OF THE ARRAY

The experimental array used is shown in Fig. 1, and the block diagram of the electronic equipment in Fig. 2.

Cosmic-ray μ mesons were stopped in a round copper target 220 mm in diameter and 35 mm thick. Four thin scintillation counters (2, 3) and (4, 5) 210 mm in diameter and 7 mm thick were placed in pairs above and below the target for the detection of the μ mesons traversing the array and of the decay positrons. A Geiger-counter tray 1 placed above the array was used for selecting μ mesons within a given solid angle. The array recorded μ mesons inclined by no more than 40° to the vertical.

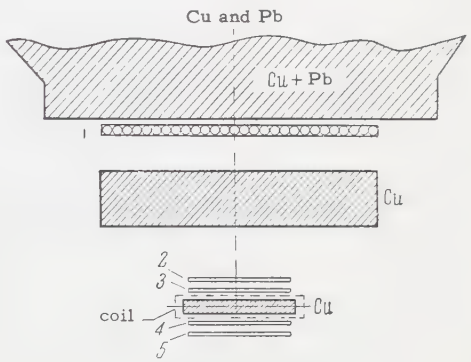

FIG. 1. Diagram of the array: 1 — Geiger-counters; 2, 3, 4, 5 — scintillation counters.

The investigated spectrum interval was selected by means of a copper-lead absorber placed above the array. μ mesons stopping in the target were determined by coincidences (1, 2, 3, $\overline{4}$). Such an event produced a square gating pulse of 4 μsec

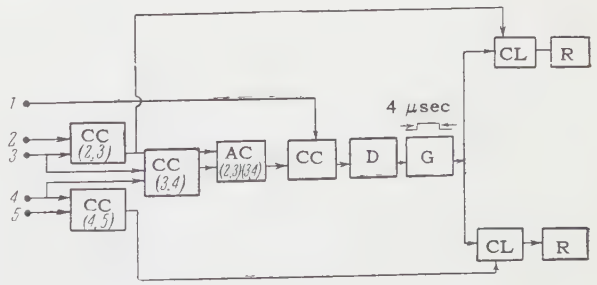

FIG. 2. Circuit diagram of the electronic circuitry: CC — coincidence circuit, AC — anticoincidence circuit, D — delay line, G — gating pulse, CL — clamp, R — recording circuit.

duration with a delay of 0.6 μsec with respect to the time of stopping of the μ meson. Decay positrons were detected by a coincidence of this pulse with a pulse from coincidence circuits (2, 3) or (4, 5). Decay electrons of μ^- mesons were not detected by the array, since the lifetime of μ^- mesons in copper is less than 0.1 μsec.

Since the efficiency of the anticoincidence circuit was not ideal, owing to the geometry of the array, a small background of positrons from μ mesons decaying in the concrete base of the array was present. This background was lowered to 0.5% of the number of decays detected by the array by covering the concrete with a lead layer 10 mm thick. In order to avoid instrumental asymmetry, the target with counters 2, 3, 4, 5 was periodically rotated by 180° around the horizontal axis. Nevertheless, the array was not totally symmetrical, mainly because of μ mesons stopping in counter 3 above the target. The number of decay positrons from these μ mesons was measured and found to be 0.11 ± 0.025 of the total number of positrons detected by the array. The target was placed inside a coil in which a horizontal magnetic field of H = 30 gauss could be produced.

3. RESULTS OF THE EXPERIMENT

To remove the effect of the instrumental asymmetry, a relative method of measurement was used, since even for an ideal geometrical symmetry of the array and an ideal efficiency of the detecting system, an asymmetry of the decay positron emission is possible because of the direction of the μ-meson flux.

In the first and second series of measurements, corresponding to mean momenta of μ^+ meson 0.45 and 0.9 Bev/c respectively, the ratio of the number of decay positrons detected by counters (2, 3) without magnetic field and with magnetic field depolarizing the μ^+ mesons was determined. This ratio was also determined for positrons passing through counters (3, 4). The magnetic field was switched on periodically at two-hour intervals. Such a method of measurement made it possible to exclude completely systematical errors due to instrumental asymmetry. In control experiments, the absence of the influence of the magnetic field on the counting efficiency for decay positrons was established with an accuracy to within 0.5%.

In the third series of measurements, it was attempted to compare the degree of polarization of cosmic-ray μ^+ mesons with momenta 0.45 and 1.7 Bev/c respectively, i.e., to study the possible variation of the polarization with an increase in the energy of the μ^+ meson, irrespective of the theoretical formulas.

The ratio r_1 of the number of decay positrons detected by counters (2, 3) to the number of positrons detected by the counters (4, 5) for 0.45 Bev/c, and the ratio r_2 of the readings of the counters (2, 3) and (4, 5) for 1.7 Bev/c, were measured in the experiment. The difference in the μ^+-meson polarization for these momenta determined by the quantities r_1 and r_2 does not depend strongly on theoretical factors, and is practically independent of instrumental asymmetry, which made it possible to carry out the measurements without using the magnetic field.

The array detected 110 decays of μ^+ mesons per day with momenta of about 0.45 Bev/c. Readings were taken during a two-hour period. The gating pulses were counted continuously in order to check the operation of all the elements in the array. In addition, the efficiency of coincidence circuits (2, 3) and (4, 5) was checked daily by counting cosmic-ray particles passing through the scintillation counters. A periodical check showed that the background of chance counts was not more than 1.5% of the useful count of the array.

For an arbitrary energy and angular selection of the decay positrons, the experimentally observed ratio of the numbers of positrons traveling upwards and downwards can, for a symmetrical array, be expressed by the formula

$$r = (1 + aP)/(1 - aP), \qquad (1)$$

where P is the degree of polarization of the μ^+ mesons. The coefficient a takes the probability that positrons leave the target, and the geometry of the array, into account.

According to the two-component neutrino theory, the degree of asymmetry of decay positrons is a function of the positron energy, and of the angle between the direction of the spin of the decaying μ meson and the momentum of the decay positron. The degree of asymmetry of the decay positrons observed in the experiment therefore depends both on the polarization of the decaying μ mesons and on the bias of the array in the energy- and angular selection of the decay positrons.

The thick flat target used in the experiment was the element defining the angular and energy selection of the decay positrons. In fact, the probability that low-energy positrons leave the target is smaller than for high-energy positrons. In the same way, it is more probable that a positron emitted at a small angle to the vertical will leave the target.

In the case of a semi-infinite target and a uniform distribution of the μ^+ mesons stopping in it, the number of decay positrons emitted at an angle θ to the vertical into a solid angle $d\Omega$ and reaching the target surface is given by the expression

$$N(\theta)\,d\Omega = A\left[\int_0^1\int_0^\infty W(\varepsilon,\, x/\cos\theta)\, N_0(\varepsilon,\, \cos\theta)\, dx\, d\varepsilon\right] d\Omega, \quad (2)$$

where $W(\epsilon, r)$ is the probability that a positron with energy ϵ leaves the surface of the target traversing a path $r = x/\cos\theta$, where x is the distance from the point of decay to the surface of the target, and

$$N_0(\varepsilon, \cos\theta) = 2\varepsilon^2\{(3-2\varepsilon) + \xi P\cos\theta\,(1-2\varepsilon)\}. \quad (3)$$

The probability $W(\epsilon, r)$ was calculated following the procedure of Wilson.[11] In doing this, the mean range of positrons having a given energy was taken into account, and was determined from the ionization and radiation losses, multiple scattering, and fluctuations in the range of positrons due to radiation losses and multiple scattering.

Equation (2) can easily be transformed to

$$N(\theta)\,d\Omega = A(1 + P\eta\cos\theta)\,|\cos\theta|\,d\Omega, \quad (4)$$

where A and η are constants. The factor $|\cos\theta|$ determines the angular selection of positrons. The factor η, which determines the energy selection of positrons by the target, was calculated by numerical integration, and was found to equal 0.412. The value of η corresponding to the absence of energy selection was equal to 0.333.

In the case where all positrons leaving the surface of the target are detected irrespective of the angle of emission, i.e., where there is no geometric angle cut-off, the experimentally observed ratio of the number of positrons travelling upwards and downwards is given by the formula

$$R = \frac{\int_0^1 (1 + \eta P\cos\theta)\,|\cos\theta|\,d\cos\theta}{\int_0^1 (1 - \eta P\cos\theta)\,|\cos\theta|\,d\cos\theta} = \frac{1 + 2P\eta/3}{1 - 2P\eta/3}. \quad (5)$$

From a comparison of Eqs. (1) and (5), it is evident that the factor $a = 2\eta/3 = 0.275$.* In reality, the positrons leaving the target are, in addition, selected according to their angle by the geometry of the array. Therefore, in the calculation, the form of the angular distribution of positrons on the surface of the target was determined taking the multiple scattering in copper into account. Taking the multiple scattering and the angular selection of positrons by counters (2, 3) and (4, 5) into account leads to a = 0.304. A correction was applied to the factor a to account for the selection of μ^+ mesons. Finally, it was assumed that $1/a = 3.65$.

The degree of polarization in the first and second series of measurements was found from the formula

$$P = (R-1)/a(KR+1), \qquad 1/a = 3{,}65, \qquad K = 0{,}21. \quad (6)$$

The coefficient K determines the value of the residual polarization of μ^+ mesons in the presence of the magnetic field, with respect to polarization without field. The value of the residual polarization depends on the applied magnetic field, and on the time moments t_1 and t_2 with respect to the moment at which the μ meson stopped in the target, which define the beginning and end of the operation of the circuit recording the decay positrons. With an increasing magnetic field, the residual polarization decreases to zero, changes sign, attains, maximum, and then, asymptotically, tends towards zero.

The value of the magnetic field H = 30 gauss was chosen for an increase of the measured effect in order to obtain maximum polarization of the opposite sign as compared with polarization without the field.

The value of the residual polarization was determined by the expression

$$K = \int_{t_1}^{t_2} \cos\omega t e^{-t/\tau}\,dt \Big/ \int_{t_1}^{t_2} e^{-t/\tau}\,dt,$$

where τ is the average lifetime of the μ meson, and ω the frequency of Larmor's precession of the spin, proportional to H. Results of all series of measurements, taking corrections for the depolarization of μ mesons in the atmosphere and in the absorbers into account, is as follows:

Momentum, Bev/c	0.45	0.9	1.7
Number of detected decays	4174	4022	5882
P	0.23 ∓ 0.10	0.37 ∓ 0.11	0.31 ∓ 0.10

In the third series of measurements, the difference in the degree of polarization of μ^+ mesons with momentum 1.7 and 0.45 Bev/c was found to be equal to $+0.09 \pm 0.10$. Polarization for momentum p = 1.7 Bev/c was counted relative to the polarization at p = 0.35 — 0.55 Bev/c averaged over all known experimental data[3,6-8] and equal to 0.22 ± 0.03.

Combining the data on the polarization of μ^+ mesons with momentum 0.9 and 1.7 Bev/c, we ob-

*The authors are grateful to B. V. Geshkenbeĭn for comments on a number of problems connected with the calculations.

tain an average value equal to 0.34 ± 0.07, which is markedly greater than the average value 0.22 ± 0.03 obtained by numerous investigators for μ^+ mesons with momenta 0.35 — 0.55 Bev/c. The absolute value of the polarization of μ mesons with momentum 0.9 and 1.7 Bev/c obtained by us is, within the limits of error, in agreement with the theoretical value for the polarization 0.30 obtained under the assumption that polarization of the μ-meson component is due to its origin in the π-meson component. A considerable fraction of μ mesons with momentum of ~ 0.4 Bev/c are produced in the decay of π mesons of relatively low energies, up to 1.5 Bev/c.[9,10] In this energy range, the π-meson spectrum decreases slower than at high energies, which may be one of the reasons for the lower value of polarization in the low-energy region observed in all experiments, as compared with the theory.

In conclusion, the authors express their gratitude to Academician A. I. Alikhanov for his interest in the experiment, and to G. P. Eliseev for help in planning the experiment and discussion of results.

[1] S. Hayakawa, Phys. Rev. **108**, 1533 (1957).

[2] I. I. Gol'dman, JETP **34**, 1017 (1958), Soviet Phys. JETP **7**, 702 (1958).

[3] Fowler, Primakoff, and Sard, Nuovo cimento **9**, 1027 (1958).

[4] G. Puppi, Progress in Cosmic Ray Physics (North-Holland Publishing Co., Amsterdam, 1956), Vol. 3, p. 341.

[5] Pine, Davisson, and Greisen, Nuovo cimento **14**, 1181 (1959).

[6] G. W. Clark and J. Hersil, Phys. Rev. **108**, 1538 (1957).

[7] Dolgoshein, Luchkov, and Ushakov, Proceedings of the 1959 Moscow International Conference on Cosmic Rays (in press).

[8] C. S. Johnson, ibid.

[9] G. M. Garibyan and I. I. Gol'dman, JETP **26**, 257 (1954).

[10] Camerini, Fowler, Lock, and Muirhead, Phil. Mag. **41**, 413 (1950).

[11] R. R. Wilson, Phys. Rev. **84**, 100 (1951).

Translated by H. Kasha
178

PRODUCTION OF THE RADIOACTIVE ISOTOPE Kr^{85} AND MEASUREMENT OF ITS γ RADIATION

I. E. NAKHUTIN, V. V. OVECHKIN, D. V. OCHKIN, A. S. POLYAKOV, and Z. K. KHODULEVA

Submitted to JETP editor May 23, 1960

J. Exptl. Theoret. Phys. (U.S.S.R.) **39**, 991-992 (October, 1960)

The radioactive isotope Kr^{85} was obtained from neutron-irradiated uranium by frontal chromatography of the gases evolved during a solution of the uranium in nitric acid. The Kr^{85} thus obtained was used to determine the γ-ray yield. The γ-ray quantum yield is $(0.41 \pm 0.06)\%$ per decay, which is much smaller than the value given by Zeldes et al.[1]

THE half-life, the maximum β-particle energy and the type of β spectrum of Kr^{85} have been measured in many investigations. A γ radiation of low intensity was also observed and its energy ($E_\gamma = 517$ kev) determined. Zeldes et al.[1] give data on the yield of this γ radiation, amounting to $(0.65 \pm 0.15)\%$ per decay. No other investigations of the absolute yield of gamma rays from Kr^{85} are known at present.

Later on, Snell and Pleasonton[2] raised doubts concerning the reliability of the gamma-radiation yield given in reference 1. They assumed the value $(0.65 \pm 0.15)\%$ to be excessive, since it was still not known in 1950 that the level at which the gamma radiation takes place is metastable (lifetime approximately 1 μsec). In this connection, we obtained a more accurate value for the gamma yield of Kr^{85}.

To obtain the Kr^{85}, the neutron-irradiated uranium was dissolved in nitric acid, and the gases evolved during the solution, which contained the radioactive krypton, were processed by removing the moisture, the oxides of nitrogen, and the radioactive iodine. The remaining gas mixture contained oxygen and nitrogen as the main components. The oxygen and nitrogen were separated by frontal chromatography on activated carbon at 77° K. The mixture was passed through a carbon column, where the krypton was completely absorbed. The concentration of the krypton in the sorbate was approximately 150 times greater than in gases evolved during the solution. The chromatographic enrichment of the krypton was repeated once more, yielding radioactive krypton dissolved in a small amount of carrier gas, fully suitable for our purposes.

In this enrichment method, xenon and its radioactive isotopes are separated together with the krypton, but these decay relatively rapidly.

For the measurements, a gas source of Kr^{85} was produced in a Plexiglas cylinder of 35 mm i.d., 6 mm height and 2 mm wall thickness. Aluminum foil 2.27 mg/cm^2 thick was fastened on the ends of this cylinder. To determine the yield, separate measurements were made of the intensity of the β and γ radiation. The yield was found from the ratio

$$k_\gamma = N_\gamma / N_\beta,$$

where N_γ and N_β are the total numbers of the gamma quanta (of energy 517 kev) and β particles, respectively, emitted by the source per unit time into a solid angle 4π.

The β intensity was measured with an SI-2B end-window β counter. The absorption in aluminum was plotted. Account was taken here of the absorption of β particles in the mica covering the window of the counter, in the aluminum foil of the source itself, and in the layer of air between the source and inlet window of the counter. The geometrical parameters of the experiment were accounted for in accordance with reference 3.

The total intensity of gamma radiation of the same source was determined with a scintillation gamma spectrometer with 10% resolution (relative to Cs^{137}). The scintillator used was a NaI(Tl) crystal 40 mm in diameter and 50 mm high, with an FÉU-13 photomultiplier. The spectra were plotted with an AI-100 100-channel amplitude analyzer. The gamma intensity was calculated from the area of the total-absorption peak. According to our data, the yield of gamma radiation from Kr^{85}, corrected for the gamma-spectrometer efficiency,[4] amounts to $0.41 \pm 0.06\%$ per decay.

To check the reliability of these data, analogous measurements were made with the isotopes I^{131} and Cs^{134}, the gamma quantum yield of which was reliably measured. The maximum energy of the

β particles from these isotopes is close to the maximum energy of the β particles of Kr^{85}, and is 0.61 and 0.66 Mev respectively. In the measurements we determined the yield of the principle gamma lines with energies 0.364 Mev (I^{131}) and 0.797 Mev (Cs^{134}). The deviation from the literature data[5,6] is 3.2% for I^{131} and 7.8% for Cs^{134}, which is within the limit of experimental accuracy.

[1] Zeldes, Ketelle, and Brosi, Phys. Rev. **79**, 901 (1950).

[2] A. Snell and F. Pleasonton, Phys. Rev. **107**, 740 (1957).

[3] N. G. Gusev, Справочник по радиоактивным излучениям и защите (Handbook on Radioactive Radiation and Shielding), Medgiz, 1956, p. 79.

[4] Ovechkin, Ochkin, Polyakov, and Pirkin, Приборы техника и эксперимента (Instrum. and Exptl. Techniques), in press.

[5] R. Bell and R. Graham, Phys. Rev. **86**, 212 (1959).

[6] B. S. Dzhelepov and L. K. Peker, Схемы распада радиоактивных ядер (Decay Schemes of Radioactive Isotopes), U.S.S.R. Acad. Sci. Press, 1958.

Translated by J. G. Adashko
179

INTERACTION OF 5×10^{12} ev *NUCLEONS WITH EMULSION NUCLEI*

N. A. MARUTYAN, K. A. MATEVOSYAN, and R. T. TOSHYAN

Physics Institute, Academy of Sciences, Armenian S.S.R.

Submitted to JETP editor May 27, 1960

J. Exptl. Theoret. Phys. (U.S.S.R.) **39**, 993-996 (October, 1960)

The energy of shower particles produced in a 6 + 31 p interaction is estimated, the primary-particle energy being $\sim 5 \times 10^{12}$ ev. The mean transverse momentum is (0.17 ± 0.02) Bev/c. The fraction of the primary-particle energy spent for the production of secondary particles is greater than 10%. The angular distribution and the transverse momentum distribution measured are compared with Landau's hydrodynamical theory. The best agreement of the transverse momentum distribution has been obtained for $kT = {}^1/_2 \mu_\pi c^2$. The nuclear interaction mean free path is of the order of 30 cm.

AN experimental study of the energy spectrum of secondary particles in high-energy interactions in nuclear emulsion is feasible in rare cases.

We have succeeded in studying the energy spectrum in an interaction of the 6 + 31 p type. The event was found through a systematic search for high-energy interactions in a part of a stack of Ilford G-5 emulsions 600 μ thick, each irradiated for 8 hours at an altitude of 27 — 30 km. The event was interpreted as an interaction of a singly-charged cosmic-ray particle (probably a proton) with an emulsion nucleus, which is indicated by the presence of a large number of evaporated particles, including a Li^8 nucleus with its characteristic decay.

The ratio of the tunnel length which was traversed by the primary particle to the nucleon size was determined according to the formula[1]

$$N_0 = 1.85\, k\, (n - {}^1/_4)^{3/4} E^{1/4}$$

and was found to be 4.4. In the formula, N_0 denotes the total number of particles produced, k is a constant of the order of one, and E is the energy of the primary particle in the laboratory system (l.s.) in the units of the nucleon rest mass.

The Lorenz factor γ was determined, assuming a symmetrical particle distribution in the center-of-mass system (c.m.s.), by the half-angle method[2] and by the Castagnoli method.[3] The values γ obtained by these two methods are in agreement within the limits of statistical error, and are equal to

$$\bar{\gamma} = 23.8 \pm {}^{3.7}_{3.9}.$$

The energy of the primary particle, calculated under the assumption of an interaction between a nucleon and a nuclear tunnel, was found to be equal to $(4.7 \pm 1.0) \times 10^{12}$ ev.

All tracks of secondary particles were followed up to the interaction or up to the place of exit from the stack. In all, 115 cm of shower tracks were followed, and three nuclear interactions of the narrow-cone particles and one interaction of a wide-cone particle were found. The mean free path of the nuclear interaction was found to be of the order of 30 cm.

MEASUREMENT OF ANGLES AND ENERGY

Measurements were carried out using a MBI-8M microscope with a total magnification of $90 \times 2 \times 15$.

The angles of all shower particles with respect to the direction of the primary particle were measured by the coordinate method. The direction of the primary track was taken as the shower axis. Measurements have shown that the distortion of the emulsion has almost no effect on the accuracy of the shower axis determination. Basically, the errors in the shower axis determination were due to the error of the measuring instrument, and were found to be of the order of 1′. The spatial angle θ_i between each shower particle and the direction of the primary particle was determined from the formula

$$\cos\theta_i = \cos\lambda_i \cos\varphi_i \cos\varphi_0 + \sin\varphi_i \sin\varphi_0,$$

where λ_i is the angle between the i-th particle and the primary particle in the plane of the emulsion, and φ_0 and φ_i are the angles of dip of the primary and of the i-th particle respectively. The results of the angle measurements are shown in the second column of the table. The error of

measurement of spatial angles up to 2° was not greater than 2′.

The range of shower particles of the narrow cone reached 6 cm in one emulsion layer, and the primary particle traversed 2.6 cm in the same layer. This made it possible to measure the energy of secondary particles by the multiple-scattering method.

It was found possible to estimate the energy of 28 shower particles. The basic cell length was taken as $t = 500\ \mu$, and a recalculation for 1000, 2000, 4000, and 8000 μ was carried out by the overlapping-cell method. The energy of each shower particle was determined from measurements over two to three cells, under the condition $D/D_n \geq 2$, according to the formula

$$p\beta c = Kt^{3/4} / \bar{D}_k,$$

where p is the particle momentum, K is the scattering constant, $\bar{D}$ is the value of the mean second difference of coordinates ($\bar{D}^2 = \bar{D}_C^2 + \bar{D}_n^2$) measured in the experiment, D_C characterizes the Coulomb scattering, and D_n is the noise due to the noise of the microscope table, minute distortions of the emulsion, and to other factors.

To find the value of D_n, scattering measurements were carried out on the track of the primary particle. Since the energy of the primary particle found from the angular distribution of shower particles is of the order of 5×10^{12} ev, the measured scattering of the primary track D_p is due basically to the table noise and to false scattering.

In the measurement of one of the secondary particles (particle 5 of the table), the measured value of D_5 was found to be close to the value obtained for the primary track, within the limits of statistical error. Consequently, the Coulomb scattering is negligible for this particle also. Since particle 5 passes through the same region as the remaining particles, we can, with small error, accept the value of D_5 for D_n. To reduce the statistical error for D_n, we used the average of D_p and D_5.

Moreover, D_n was determined on several tracks by the multiple-cell method.[4] The values obtained are in good agreement with the mean value $\bar{D}_n$. For cells of 4000 and 8000 μ, the value of $\bar{D}_n$ was found to be equal to 0.3 and 0.6 μ respectively, which corresponds to the Coulomb scattering of particles of 44 and 62 Bev energy. As a result, it was possible to measure the energy of secondary particles up to 25 Bev. Distortion and single scattering were accounted for in the usual way. The values of the energy of secondary particles are shown in column 3 of the table, where statistical errors are also indicated.

For the first three tracks (see table), we succeeded in measuring the relative scattering, which provides one of the best energy measurement methods in the range up to several hundred Bev. These tracks diverged in the emulsion plane by not more than 60 μ over 2.5 cm, and showed almost no divergence with depth. Energy measurements by the relative-scattering method over cells 2000 and 4000 μ were found to be in good agreement with the energy values found from measurements on individual tracks. If we take into account the high energies of the particles, then the good agreement between the data obtained confirms once more the accuracy of our measurements.

Particle No.	θ_i	E, Bev	$p_\perp/\mu_\pi c^2$	Particle No.	θ_i	E, Bev	$p_\perp/\mu_\pi c^2$
1	16′	28±6.5**	0.94	17	2°25′	5.2±0.7	1.56
2	18′	27±6.5**	1.00	18	2°28′	2.3±0.5	0.72
3*	21′	20±4.2**	0.87	19	2°40′	4.9±0.8	0.93
4	26′	20±4.3	1.08	20	2°45′	2.4±0.4	0.82
5	43′	>75	>9	21	2°59′	4.5±1.1	1.67
6*	48′	20.5±6.3	2.06	22	3°32′	4.3±2.3	1.90
7	50′	12.1±3.2	1.25	23	4°24′	1.1±0.3	0.60
8*	1° 5′	>10	>2	24*	4°39′	4.0±1.3	2.32
9	1° 7′	4.0±0.8	0.56	25	7° 6′	0.5±0.2	0.40
10	1° 8′	6.5±2.4	0.94	26	8° 3′	1.0±0.3	1.00
11	1°20′	4.3±1.9	0.71	27	12°24′	1.3±0.2	2.00
12	1°23′	5.2±1.4	0.89	28	16° 6′	0.6±0.2	1.19
13	1°34′	7.8±1.9	1.51	29	19°31′	—	—
14	1°45′	5.7±2.0	1.24	30	30°56′	—	—
15	2°24′	5.8±1.5	1.73	31	77°57′	—	—
16	2°24′	4 7±1.0	1.4				

*Particles 3, 6, 8, and 24 produced nuclear interactions of types 2 + 5p, 9 + 2p, 2 + ?p, and 5 + 6p respectively.

**From relative scattering measurements over a 4000-μ cell, an energy of (29 ± 8) Bev was obtained for particles 1 – 3, and (25 ± 8) Bev for particles 2 and 3.

ANGULAR AND ENERGY DISTRIBUTIONS

As has been mentioned, the event studied was interpreted as an interaction of a nucleon with an emulsion nucleus with a tunnel length n = 4.4.

A further development of the hydrodynamical theory of Landau for the nucleon-nucleon and nucleon-tunnel interaction was given by Milekhin and Rozental'.[5,6] The angular distribution of secondary particles for nucleon-nuclear tunnel interactions was calculated only for cases with $n \leq 3.7$. It can, however, be assumed that, for $n > 3.7$, the angular distributions will not be greatly different from the distributions obtained for small values of n. The experimentally obtained angular distribution of shower particles in the system of equal velocities is shown in Fig. 1.

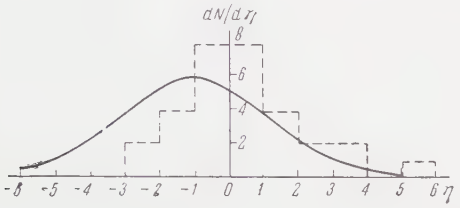

FIG. 1. Angular distribution of secondary particles in the system of equal velocities (histogram – experiment, solid line – theory. [5])

In the same figure, the theoretical curve of the angular distribution for n = 3.7 is shown, as calculated according to the formula

$$\frac{dN}{d\eta} = \frac{N_0}{\sqrt{2\pi L}} \exp(-\eta^2/2L),$$

$$L = 0.56 \ln E + 1.6 \ln\left(\frac{2}{n+1}\right) + 1.6,$$

where $\eta = \ln \tan(\theta_c/2)$, and θ_c is the angle of particle emission in the c.m.s. The transformation to the angles θ_c from the angles in the l.s. is based on the assumption that all particles produced are relativistic. As can be seen from Fig. 1, the observed experimental distribution is shifted towards large angles as compared with the theory (in the l.s.). It cannot be excluded that such a shift is due to secondary effects in the target nucleus.

The goodness of fit of the angular distribution with the symmetrical one was tested using the χ^2 criterion, and it was found that $P(\chi^2) = 90\%$.

The transverse momenta $p_\perp$, as determined from the energies of the particles and their angles of emissions with respect to the primary track, are shown in column 4 of the table (in units of $\mu_\pi c^2$). The mean transverse momentum, without taking particle 5 into account, was found to be equal to (0.17 ± 0.02) Bev/c. The lower limit of transverse momentum of particle 5, equal to 1.2 Bev/c, is considerably higher than the mean value, and is in good agreement with the mean value of the transverse momentum obtained for nucleons by Edwards et al.[7] Thus, it follows from the data obtained that the charged particle carrying away the maximum energy is heavier than a π meson, and is most probably a nucleon. The probability that this particle is the primary particle conserving a considerable part of its energy is small, since it is emitted at an angle of 43′ to the shower axis.

A histogram of the observed transverse momenta distribution is shown in Fig. 2. The corresponding theoretical curves are taken from the article of Milekhin and Rozental'.[6] The maximum of the curves is expected in the region $(1-2)\,\mu_\pi c^2$,

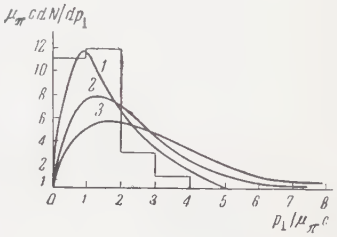

FIG. 2. Tranverse momentum distribution. Curves 1, 2, 3, correspond to temperatures $kT = \frac{1}{2}\mu_\pi c^2$; $\mu_\pi c^2$; $\frac{3}{2}\mu_\pi c^2$.

which is in good agreement with our experimental distribution. Best fit with the experimental histogram is observed for the curve 1, i.e., for $kT = \frac{1}{2}\mu_\pi c^2$. Thus, the experimentally-found spectrum of the secondary particles is softer than the one predicted by the Milekhin variant of the hydrodynamical theory for $kT = \mu_\pi c^2$. This is evidently due to the fact that the hydrodynamical theory gives a very anisotropic (in the c.m.s.) angular distribution of secondary particles; experimentally, as a rule, the angular distribution is more isotropic. The inelasticity factor was estimated from the ratio of the total energy of all secondary particles, taking neutral ones into account, to the primary energy. The value obtained for the inelasticity factor was found to be greater than 0.1.

[1] S. E. Belen'kiĭ and G. A. Milekhin, JETP **29**, 20 (1955), Soviet Phys. JETP **2**, 14 (1956).

[2] Dilworth, Goldsack, Hoang, and Scarsi, Nuovo cimento **10**, 1261 (1953).

[3] Castagnoli, Cortini, Franzinetti, Manfredini, and Moreno, Nuovo cimento **10**, 1539 (1953).

[4] Chasnikov, Takibaev, and Boos, Приборы техника и эксперимента (Instruments and Exptl. Technique) No. 1, 54 (1959).

[5] G. A. Milekhin, JETP **35**, 1185 (1958), Soviet Phys. JETP **8**, 829 (1959).

[6] G. A. Milekhin and I. L. Rozental', JETP **33**, 197 (1957), Soviet Phys. JETP **6**, 154 (1958).

[7] Edwards, Losty, Perkins, Pinkau, and Reynolds, Phil. Mag. **3**, 237 (1958).

Translated by H. Kasha
180

A HIGH CURRENT MICROTRON

S. P. KAPITZA, V. P. BYKOV, and V. N. MELEKHIN

Institute for Physical Problems, Academy of Sciences, U.S.S.R.

Submitted to JETP editor June 15, 1960

J. Exptl. Theoret. Phys. (U.S.S.R.) 39, 997-1000 (October, 1960)

Preliminary data are presented on a new, efficient electron accelerator in the 5 — 15 Mev energy range. The accelerator is of the electron cyclotron type. The efficiency of electron capture into resonance orbits and also the general efficiency of the accelerator are appreciably increased by injecting the electrons from a hot cathode located directly in the cavity. The accelerated electrons are well defined in energy and momentum.

THIS paper presents some preliminary data on a new, efficient cyclic accelerator for electrons in the energy range 5 — 15 Mev. The efficiency and current of the accelerator have been significantly increased by making fundamental changes in the geometry of the accelerating field and in the method used to inject the electrons.

In 1944, Veksler discussed the acceleration of fast particles in a machine with a constant magnetic field.[1] However, the low efficiency of the first microtrons[2,3] and the rapid development of linear accelerators led to a lack of interest in this field.

Two fundamental characteristics of electron cyclotrons — a monoenergetic beam and phase stability over a narrow interval only — aroused our interest in connection with the problem of obtaining bunches of electrons. We built a microtron with magnet pole faces 700 mm in diameter spaced 110 mm apart. The radio-frequency field was supplied by a pulsed magnetron operating in the 10-cm band.

The energy ΔE gained by a charge during one circuit of the accelerator is related to the constant magnetic field H through

$$\Delta E / E_0 = H / H_0,$$

where $E_0 = mc^2$ is the rest mass and $H_0 = E_0\omega/ec$ is the nominal magnetic field corresponding to an accelerating field of frequency ω. The total energy of the particle after n circuits is given by

$$E_n = E_0 + E_i + n\Delta E = k\Delta E,$$

where k is the time for one revolution of the particle, this time being measured in periods of the accelerating field, while E_i is the injection energy, determined by putting n = 0, i.e.,

$$E_i = k\Delta E - E_0 \qquad (k = 1,2\ldots).$$

In our first experiments we used a toroidal cavity, and obtained a beam of 6 Mev electrons on the 12-th orbit. The current in each pulse was 7 ma and the length of the pulse 2 μsec. This intensity was about 5 times greater than any that had been reported earlier. The rf power was 300 kw and the duty cycle was one in 1000. The attenuation of the beam during acceleration was negligible.

The source of these accelerated electrons was apparently emission from the walls of the accelerating chamber, the field in which was as high as 1.5×10^6 v/cm.

The toroidal cavity with cold emission suffers from the drawbacks that it is hard to increase the intensity further, that the emission cannot be controlled, and, consequently, that the results are not reproducible.

We modified the microtron by installing a cylindrical cavity operating in the E_{010} mode. The accelerator is shown schematically in Fig. 1.

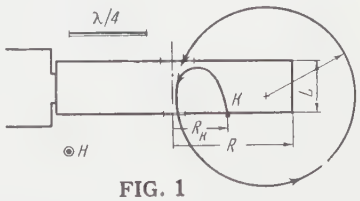

FIG. 1

Electrons are emitted from the cathode K, located at a definite distance R_K from the axis. Acted upon by electric and magnetic fields, the electrons follow some trajectory and leave the cavity through a hole in its wall, the hole being located close to the axis. The electrons are subsequently accelerated by conventional microtron action, an electron gaining an energy ΔE = (1 to 1.2) E_0 every time it passes through the cavity. It should be noted that Aitken[4] has proposed locating the cathode inside the microtron cavity.

The initial motion of the electrons was studied with the analog computer described by Prudkovskiĭ.[5] Prudkovskiĭ's new machine plots the trajectories of relativistic electrons acted on by time-dependent electromagnetic fields. The capture into a resonant orbit, the phase oscillations, the orbit positions, and other parameters of the accelerator were studied in detail by numerical integration with an electronic digital computer of the full relativistic equations of motion of the electrons.

The beam could be kept monoenergetic over a fairly wide range of magnetic field and rf field strengths. This implies that the accelerated electrons can have arbitrary energy, not limited to integral multiples of the electron rest energy.

An accelerator with the following parameters was built, the choice of parameters being based on the results of the computations: R = 3.83 cm, R_K = 1.75 cm, L = 1.63 cm (R is the radius of the cavity and L is its height). The magnetic field strength was somewhat greater than the nominal value H_0 ($H/H_0 = 1.1$). The beam current at the 12-th orbit was 15 ma, and the beam energy was 7 Mev. The power input to the cavity was 600 kw, of which 400 kw went into ohmic heating of the cavity walls, 100 kw into accelerating background electrons in the cavity, and 100kw into the resonant electrons.

The electrons captured were those emitted near zero phase of the rf oscillation, i.e. those emitted when the electric field was maximum. About $1/30$ of the total emission current was captured, in agreement with calculations. It should be noted that for a thermionic cathode this is not the most advantageous phase for capture to take place.

The cathode was one face (1 to 2 mm^2) of a lanthanum boride cube heated to 1600°C. At a field strength of 350 kv/cm in the cavity, the emission current density was 200 amp/cm^2. The diameter of the beam at the 12-th orbit was about 5 mm. At the 12-th orbit, 80% of the electrons were magnetically deflected out of the chamber.

The accelerator operated stably. The beam current could easily be controlled by varying the cathode temperature.

One of the disadvantages of the microtron as usually operated is that a small magnetic field is required (H_0 = 1070 oe at λ = 10 cm). With the method described above for injecting the electrons into the resonant orbit, it is impossible to increase the magnetic field and thus increase the energy of the accelerated electrons without changing the orbit radius. For this reason, we considered another set of electron trajectories in a cylindrical cavity. In this design, the cathode is placed near the axis and the electron beam first leaves the cavity at point A in Fig. 2.

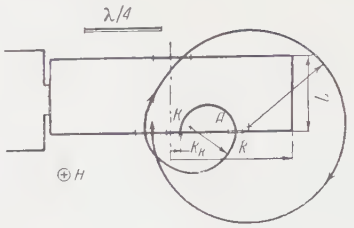

FIG. 2

For such trajectories, the magnetic field can be 2 or 2.5 times greater than the nominal value; in passing through the cavity, an electron gains energy $\Delta E = (2 \text{ to } 2.5)\, E_0$. A cavity with dimensions R = 3.83 cm, R_K = 0.32 cm, L = 2.32 cm gave a beam of 5 ma and 13 Mev at the 12-th orbit with a magnetic field of 1950 oe. The capture efficiency was 5%, and 10% of the captured electrons were accelerated.

We also considered the motion of electrons in a rectangular cavity. With such a cavity, the spacing between magnet pole faces can be decreased, while the electron energy at a particular orbit can be increased because the rf field is spread over a large region.

We note some new possibilities suggested by work with this type of cavity.

Increasing the thickness of the accelerating gap would allow the field strength inside the cavity to be decreased, which in turn might lead to less rf power and so to continuous instead of pulsed operation of the microtron.

Moroz has discussed the use of such cavities in an azimuth-dependent magnetic field with edge focusing.[6]

The method described above for injecting electrons into accelerating orbits might prove useful in circular strong-focusing accelerators whose magnetic field is constant in time.

We believe the new microtron will be competitive with linear accelerators and betatrons in the energy range up to 50 or 100 Mev. The microtron may be useful as an injector for big accelerators because the microtron beam is well collimated and monoenergetic.

The high efficiency of the accelerator is due not only to the new trajectories, but also to the complete and detailed calculations, to the decreased electric field strength, and the use of a controllable cathode.

A more detailed report on the machine and on the trajectory calculations will be published in the near future. The construction of a high-energy accelerator has been started.

In conclusion, it is our pleasant duty to thank Academician P. L. Kapitza for his support and interest. We are also grateful to L. A. Vaĭnshteĭn for useful discussions, to G. P. Prudkovskiĭ for his valuable help with the trajectory calculations, to I. G. Krutikova for numerical calculations on the "Strela" computer, and finally to A. A. Kolosov, S. V. Melekhin and L. Zykin for their help with this research.

[1] V. I. Veksler, Dokl. Akad. Nauk SSSR **43**, 346 (1944); J. Phys. (U.S.S.R.) **9**, 153 (1945).

[2] Redhead, LeCaine, and Henderson, Can. J. Research **A28**, 73 (1950).

[3] Henderson, Heymann, and Jennings, Proc. Phys. Soc. (London) **B66**, 654 (1953).

[4] D. K. Aitken, Proc. Phys. Soc. (London) **A70**, 550 (1957).

[5] G. P. Prudkovskii, Некоторые вопросы инженерной физики (Some Problems in Engineering Physics), No. 2, Moscow Eng. Phys. Inst., 1957, page 36.

[6] E. M. Moroz, Dokl. Akad. Nauk SSSR **115**, 78 (1957), Soviet Phys.-Doklady **2**, 311 (1958).

Translated by R. Krotkov
181

FAST PHOTONEUTRONS FROM SOME ELEMENTS

L. A. KUL'CHITSKIĬ and V. PRESPERIN

Leningrad Physico-Technical Institute, Academy of Sciences, U.S.S.R.

Submitted to JETP editor June 23, 1960

J. Exptl. Theoret. Phys. (U.S.S.R.) **39**, 1001-1004 (October, 1960)

We investigated the angular distributions of photoneutrons of energy $\gtrsim 10$ Mev produced by irradiating lithium and iodine with bremsstrahlung of 90 Mev peak energy. The distribution was found to be highly asymmetric with respect to the angle 90°, most of the neutrons being emitted at small angles. The energy distributions of the neutrons and protons, measured with the same apparatus, were compared. The yields of fast photoneutrons from some elements were measured.

THE present investigation is a continuation of our earlier work[1] on the investigation of fast photoneutrons. The experimental apparatus and the data-reduction procedure were described earlier. The modifications pertain essentially to the data reduction. We have estimated the difference in the energy distributions of the neutrons emitted forward and backward relative to the direction of the gamma-quantum beam. We used for this purpose a data-reduction method analogous to that described earlier[1] for the "telescopes" used to measure the energy distributions. The paraffin converters previously employed were replaced by polyethylene converters to improve the accuracy. In the measurements of the angular distributions we used a converter 5 mm thick, directly glued to the forward crystal of the "telescope," and in the measurements of the energy distributions we used a 3 mm converter located 97 mm away from the rear crystal. "Telescopes" with thicker converters were used also to measure the yields. The targets were made of elements of natural isotopic composition, and the yield from the oxygen was measured by irradiating ordinary water. All the investigations were carried out at a bremsstrahlung spectrum with $E_{\gamma\ max} = 90$ Mev.

Figure 1 shows the angular distribution in the laboratory system of coordinates (l.s.), for neutrons with energy $\gtrsim 10$ Mev and a lithium target. The form of the angular distribution does not differ in its main outlines from the angular distributions measured earlier.[1] An asymmetry is observed relative to the angle 90°, with a considerable shift of the maximum of the angular distribution towards the smaller angles. The solid curve represents the angular distribution of the neutrons, obtained from the experimental data on photodisintegration of the deuteron[2] by the method described in reference 1. The curve was normalized for best agreement with the experimental results. The position of the maximum on the curve agrees sufficiently well with the observations, but the experimental results decrease less steeply at large angles.

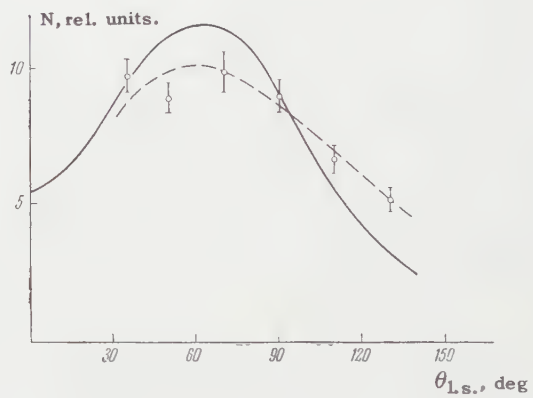

FIG. 1. Angular distribution of l.s. of neutrons of energy $\geqslant$ 10 Mev from Li. Solid curve – calculated from the data of reference 2, dashed curve – interpolation of the experimental data.

In order to explain the dependence of the angular distribution of the neutrons on their energy, we plotted also the angular distribution of neutrons of energy $\gtrsim 18$ Mev (Fig. 2). In this case, unfortunately, the statistical accuracy is greatly reduced, but the curve drawn through the experimental points shows that the isotropic part of the angular distribution is in this case much smaller than for neutrons with lower threshold energy (dashed curve of Fig. 1).

When we measured the angular distributions of the neutrons from lithium, we undertook simultaneously to ascertain whether the measured shift

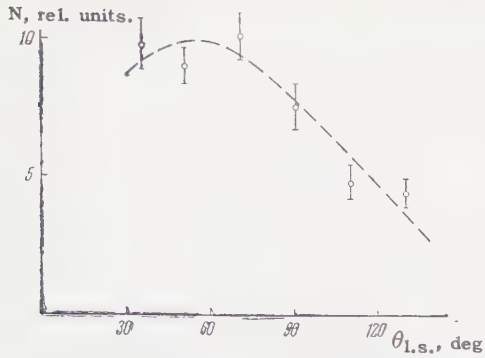

FIG. 2. Angular distribution of $\geqslant$ 18-Mev neutrons from Li. Dashed curve – interpolation of experimental data.

of the maximum of the angular distribution is real or merely due to the apparatus. As noted earlier,[1] the measured angular distribution can differ from the actual distribution if the neutrons have different energy distributions at different angles. To answer this question, we made the measurements for 35° and 130° with greater statistical accuracy than for the remaining angles.

The solid curves of Fig. 3 show the energy distribution of the recoil protons in the rear crystal of the "telescope" under the assumption that the energy spectrum of the neutrons from the target falls off as E^{-n}, with n = 1, 2, 3, 4. It is seen that within the limits of statistical accuracy no differences can be observed in the energy distributions for different angles. The initial parts of

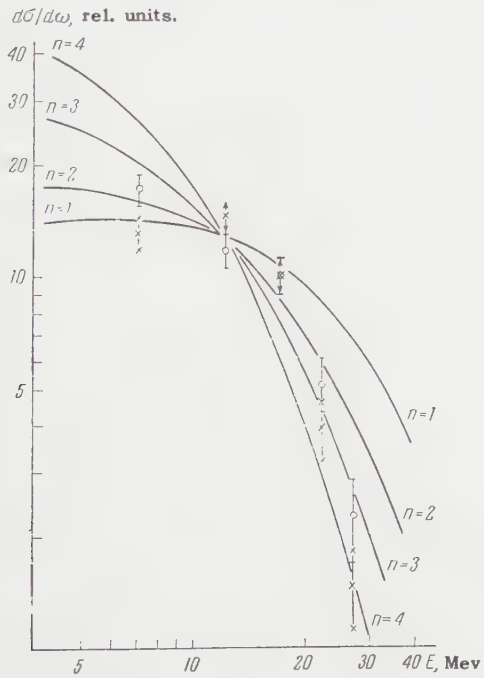

FIG. 3. Energy distribution of recoil protons in the rear crystal of "telescope" in the case of neutrons from lithium: o – for 35°, × – for 130°. The solid curves have been calculated under the assumption that the neutral spectrum has a form $\sim E^{-n}$.

FIG. 4. Energy distribution from Li($\theta_{l.s.}$ = 75°); × – of neutrons, o – of protons.

both energy distributions can be described by means of a decreasing power-law function with exponent n between 2 and 3 (in agreement with the measurement of the energy distribution of the neutrons from Li with "telescopes" having thinner converters, the results of which are shown in Fig. 4). In any case, it can be stated within the limits of statistical accuracy that the exponents n of the two energy distributions differ by less than 2 in the initial parts (which make the main contribution to the total number of neutrons). We have calculated the extent to which an angular distribution of the form $A + B \sin^2 \vartheta$ will be distorted by the dependence of the "telescope" efficiency on the neutron energy, if the energy distribution at 130° can be described by a power-law function falling off with an exponent n = 3, while the exponent for 35° is equal to 2. It was found that the maximum actually does shift towards the smaller angles, but only by about 6°. An analogous calculation for n = 2 and n = 4 produces a shift of approximately 12° in the maximum. It is seen that even if n differs by 2, we still cannot obtain in this case the experimentally-observed shift towards the smaller angles. Consequently, the measured strong shift of the maximum of the angular distribution of fast photoneutrons towards the smaller angles is not an apparatus effect. The existence of a shift of this kind in the angular distribution of the neutrons was noted by Ferrero et al.[3] at a low bremsstrahlung energy (31 Mev) and a lower neutron registration threshold (~5 Mev). According to data by others[4-6] the angular distribution of the photoneutrons is of the form $A + B \sin^2 \vartheta$. The asymmetry in the angular distribution can be explained qualitatively by the quasi-deuteron mechanism of interaction between the gamma quanta and the nuclei. Calculations by Shklyarevskiĭ,[7]

who uses the direct-photoeffect model, do not lead to a shift of the maximum towards the smaller angles.

We have measured also the angular distribution of neutrons of energy $\gtrsim 10$ Mev from iodine (Fig. 5). The measurement could not be performed for 35° because of the strong background of light particles. Here, too, a strong asymmetry is observed in the angular distribution, with the number of neutrons emitted at small angles predominating.

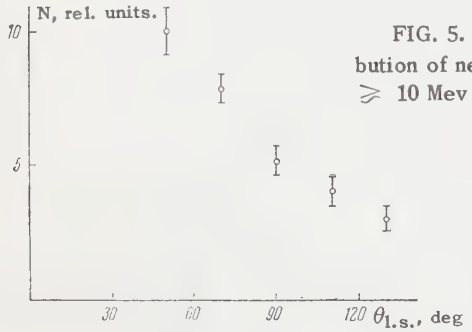

FIG. 5. Angular distribution of neutrons of energy $\geqslant$ 10 Mev from iodine.

The energy distributions of the neutrons from lithium at 75° is shown in Fig. 4. The same figure shows the results of the measurements of the energy distribution of protons (also at 75°) with the same apparatus with the converters removed. Both energy distributions are given in absolute units. No significant difference is observed in energy distribution of the protons and neutrons. The number of neutrons coincides with the number of protons within the limits of the experimental errors (~30%).

The yields of fast neutrons of energy $\gtrsim 10$ Mev were measured with four "telescopes," two of which were set at 80° (relative to the gamma-quantum beam) and two at 125°. We measured the yields from the following elements: lithium, beryllium, oxygen, aluminum, calcium, copper, cadmium, iodine, and bismuth. A correction was introduced for the attenuation of the gamma-quantum beam in the target. The results of the measurements are listed in the table. The yields were recalculated for one nuclear neutron, the yield from the lithium target being taken as unity. For the heavier nuclei, starting approximately with calcium, the yields are approximately proportional to the number of neutrons in the nucleus. The yields from the light elements are, on the average, noticeably greater. The possible irregularities in the yields from the light elements call for measurements on a large number of elements.

Element	Relative neutron yield	Element	Relative neutron yield
Li	1.00±0.05	Cu	0.37±0.02
Be	1.22±0.09	Cd	0.35±0.02
O	0.74±0.05	I	0.39±0.02
Al	0.49±0.03	Bi	0.41±0.03
Ca	0.33±0.02		

[1] L. A. Kul'chitskiĭ and V. Presperin, JETP **37**, 1524 (1959), Soviet Phys. JETP **10**, 1082 (1960).

[2] L. Allen, Phys. Rev. **98**, 705 (1955).

[3] Ferrero, Gonella, Malvano, Tribuno, and Hanson, Nuovo cimento **5**, 242 (1957).

[4] G. A. Price, Phys. Rev. **93**, 1279 (1954).

[5] S. A. E. Johansson, Phys. Rev. **97**, 434 (1955).

[6] W. R. Dixon, Canad. J. Phys. **33**, 785 (1955).

[7] G. M. Shklyarevskiĭ, JETP **36**, 1492 (1959), Soviet Phys. JETP **9**, 1057 (1959).

Translated by J. G. Adashko
182

THE MOTION OF SHOCK WAVES ALONG A MAGNETIC FIELD

R. V. POLOVIN

Physico-Technical Institute, Academy of Sciences, Ukrainian S.S.R.

Submitted to JETP editor March 23, 1960

J. Exptl. Theoret. Phys. (U.S.S.R.) 39, 1005-1007 (October, 1960)

A shock wave is considered that is excited in a magnetohydrodynamic medium by a conducting piston moving along the magnetic field. The conditions are found under which the shock wave becomes nonevolutionary and splits into two magnetohydrodynamic waves. The supposition is put forward that such a disintegration is one of the ways of forming filamentary nebulae.

In contrast with ordinary hydrodynamics, two shock waves (fast and slow[1]), which do not overtake one another, can be propagated in one direction in magnetohydrodynamics. Therefore, the study of the discontinuities of magnetohydrodynamic quantities on two successive shocks presents some interest. Such waves are formed, for example, by moving a piston in a magnetohydrodynamic medium.[2]

Let an infinite half-space $x > 0$ be filled with an ideally conducting medium and located in a magnetic field H_x ($H_y = H_z = 0$). Further, let the medium be at rest at the time $t = 0$. The state of the system is characterized by the density ρ_0 and the pressure p_0. The medium is described by the equation of state of an ideal gas with a Poisson adiabatic exponent $\gamma = 5/3$. At the time $t = 0$, the piston begins to move with a constant velocity u parallel to the x axis. Three qualitatively different modes of motion of the medium are possible, depending on the value of the velocity of the piston.

Case 1:

$$0 < u < u_-, \qquad u_- = 3(U_{0x}^2 - c_0^2)/4U_{0x},$$

$$U_{0x} = H_x/\sqrt{4\pi\rho_0}.$$

Here the fast shock wave will have an infinitesimally small amplitude, while the slow shock will be the same as in the absence of a magnetic field. The velocity of the slow shock D_-, and also the discontinuities of the density, pressure and velocity, are determined by the relations

$$D_- = 2u/3 + \sqrt{4u^2/9 + c_0^2}, \qquad \rho_2/\rho_0 = D_-/(D_- - u),$$

$$p_2 = p_0(1 + 5uD_-/3c_0^2), \quad \Delta_- v_x = u$$

(the index 2 refers to the region in front of the slow shock).

Case 2:

$$u_- < u < u_+; \qquad u_+ = 3(U_{0x}^2 - c_0^2)/\sqrt{4U_{0x}^2 - 3c_0^2}\,.$$

In this case, the same shock wave is formally possible as in the absence of a magnetic field. However, this wave will be nonevolutionary, i.e., it will be unstable relative to disintegration.[1] Two magnetohydrodynamic shock waves are produced in the disintegration of the initial shock, with velocities that are infinitely close together:

$$D_+ = D_- = 2u/3 + \sqrt{4u^2/9 + c_0^2}\,.$$

In the region between the two waves, a transverse magnetic field is developed, parallel to, say, the y axis. The magnitude of this field is determined by the formula

$$H_{1y}^2/4\pi\rho_1 = 2(D_+^2 - U_{0x}^2)(4U_{0x}^2 - D_+^2 - 3c_0^2)/3D_+^2$$

(the index 1 refers to the region between the two shock waves). The discontinuities of the remaining magnetohydrodynamic quantities in these waves are determined by the relations

$$\rho_1/\rho_0 = D_+^2/U_{0x}^2,$$

$$p_1 = p_0 + \rho_0(D_+^2 - U_{0x}^2)(3c_0^2 + D_+^2 - U_{0x}^2)/3U_{0x}^2,$$

$$\rho_2/\rho_1 = U_{0x}^2/D_+(D_+ - u), \qquad p_2 = p_0(1 + 5uD_+/3c_0^2),$$

$$\Delta_+ v_x = (D_+^2 - U_{0x}^2)/D_+, \qquad \Delta_- v_x = u - \Delta_+ v_x$$

(the plus index refers to the fast wave, the minus to the slow; see Figs. 1 and 2).

Case 3:

$$u_+ < u.$$

Here the fast wave will be the same as in the absence of the magnetic field:

$$D_+ = 2u/3 + \sqrt{4u^2/9 + c_0^2}, \qquad \rho_1/\rho_0 = D_+(D_+ - u),$$

$$p_1 = p_0(1 + 5uD_+/3c_0^2), \qquad \Delta_+ v_x = u,$$

while the slow wave will have an infinitesimally small amplitude.

The disintegration of the shock that we mentioned can easily be observed experimentally,

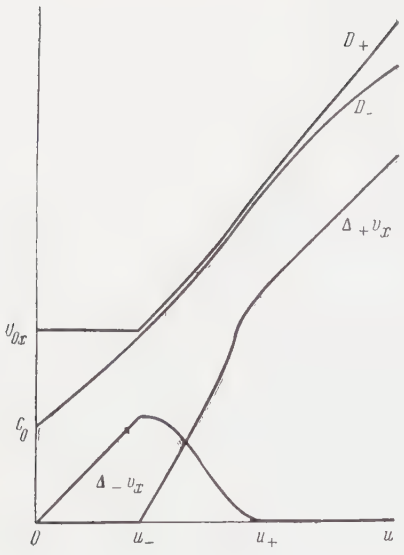

FIG. 1

since the motion of the shock wave in the second case is accompanied by an electromagnetic pulse, which is absent in the first and third cases.

It is possible that the filamentary nebulae observed in galaxies are instantaneous photographs of a set of disintegrating magnetohydrodynamic shock waves. Such a disintegration sets in if the amplitude of the shock changes in the collision of two shocks or of a shock with a contact discontinuity, and the shock wave falls into the nonevolutionary region.

The author expresses his gratitude to A. I. Akhiezer, G. Ya. Lyubarskiĭ and K. D. Sinel'nikov for valuable discussions.

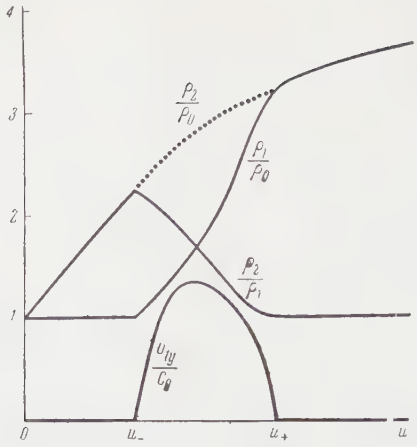

FIG. 2

[1] Akhiezer, Lyubarskiĭ, and Polovin, JETP **35**, 731 (1958), Soviet Phys. JETP **8**, 507 (1959).

[2] G. Ya. Lyubarskiĭ and R. V. Polovin, Dokl. Akad. Nauk SSSR **128**, 684 (1959), Soviet Phys.-Doklady **4**, 977 (1960).

[3] S. I. Syrovat-skiĭ, JETP **35**, 1466 (1958), Soviet Phys. JETP **8**, 1024 (1959).

[4] S. A. Kaplan, Астрономический журнал (Astron. J.) **31**, 358 (1954).

[5] S. B. Pikel'ner, Изв. Крымск. астрофиз. обсерв. (News, Crimean Astrophys. Obs.) **12**, 93 (1954).

Translated by R. T. Beyer
183

POLARIZATION OF DEUTERONS ELASTICALLY SCATTERED ON HELIUM

L. S. DUL'KOVA

P. N. Lebedev Physics Institute, Academy of Sciences, U.S.S.R.

Submitted to JETP editor April 6, 1960

J. Exptl. Theoret. Phys. (U.S.S.R.) **39**, 1008-1010 (October, 1960)

Results are given of numerical computation of the components of the polarization tensor for deuterons from elastic scattering on helium. The calculations were made for angles 40, 50, 60, 70, and 90° in the c.m.s., over the energy range 1 — 3 Mev. The computations were based on the phase-shift analysis of available experimental data.

INVESTIGATION of the scattering of polarized particles gives additional information concerning the spin dependence of nuclear forces. In addition to polarized nucleons, one can also obtain polarized deuterons by scattering on nuclei.

As an analyzer for determining the magnitude of the deuteron polarization at low energies, it is convenient to use helium since, in the scattering of deuterons on helium, one should expect a high value of the polarization in the region of the deuteron resonance energy E = 1.07 Mev, which corresponds to the single-particle level in Li^6 with $J = 3^+$ and $T = 0$,[1-3] as a result of interference between resonance scattering and potential and Coulomb scattering.

The experiments available at present on scattering of deuterons by helium and the phase shift analysis[3] enable one to compute the magnitude of the polarization.

If we select a right-handed system of coordinates, in which the z axis is along the wave vector of the scattered particle, and the y axis along the normal to the scattering plane, the polarization of the deuteron beam will be characterized by the four average values of the components of the tensors of first and second rank formed from the three-dimensional matrix components of the spin operator[4] S

$$\langle T_{11}\rangle = -(i\sqrt{3}/2)\langle S_y\rangle, \qquad \langle T_{20}\rangle = \left(\tfrac{1}{2}\right)^{1/2}\langle 3S_z^2 - 2\rangle,$$
$$\langle T_{21}\rangle = -(\sqrt{3}/2)\langle iS_y S_z + iS_z S_y\rangle,$$
$$\langle T_{22}\rangle = -(\sqrt{3}/2)\langle S_y^2\rangle. \qquad (1)$$

The quantity $i\langle T_{11}\rangle$ is the polarization vector. All the quantities (1) are functions of the deuteron energy and the angle of scattering, and are expressed in terms of the phase shifts. The computations made in various papers[5-7] do not give the complete energy dependence of the polarization, and also are in contradiction with one another in the region of the resonance energy.[5,6]

We have carried out a numerical computation of the quantities (1) over the interval of deuteron energies from 1 to 3 Mev for angles of 40, 50, 60, 70, and 90° in the c.m.s., in which we have used the relation between the tensor components and the phases which is given in the papers of O. D. Cheĭshvili and G. R. Khutsishvili.[8,9] Since the available data concerning the phase shift analysis[3] do not give the necessary accuracy for determining the resonance phase in the region of the resonance, we carried out a phase analysis of the available experimental data using the one-level formula of Wigner and Eisenbud.[10] The phase δ_2^+ satisfies the relation

$$\tan\delta_2^+ = \Gamma_\lambda/2(E_\lambda + \Delta_\lambda - E), \qquad \Gamma_\lambda = 2ka\gamma_\lambda{}^2 \cdot F + G_l^2)_a,$$

$$\Delta_\lambda = -\gamma_\lambda\left[\frac{d\ln(F_l^2+G_l^2)^{1/2}}{d(\ln kr)} + l\right]_a$$

for the following values of the parameters: γ_λ = 1.90 Mev, E_λ = 0.769 Mev in the c.m.s., a = 3.5×10^{-13} cm. Here E_λ is the characteristic energy of the state of the compound nucleus, (in the present case Li^6), γ_λ is the reduced width, a is the radius of interaction, k is the wave number of the deuteron, Fl and Gl are Coulomb wave functions, and l is the orbital angular momentum.

In Fig. 1 is shown the energy dependence of the vector $i\langle T_{11}\rangle$ for angles θ = 40, 50, 60, 70°. For θ = 90° the coefficient of polarization always goes to zero. In addition to the maximum at E = 1.06 Mev, which had already been noted earlier,[6] the curve has a second maximum at E = 1.09 — 1.10 Mev and θ = 60 — 70°. The angular dependence of the polarization coefficient changes slowly with energy: $i\langle T_{11}\rangle$ takes on its largest value for θ = 60 — 70°.

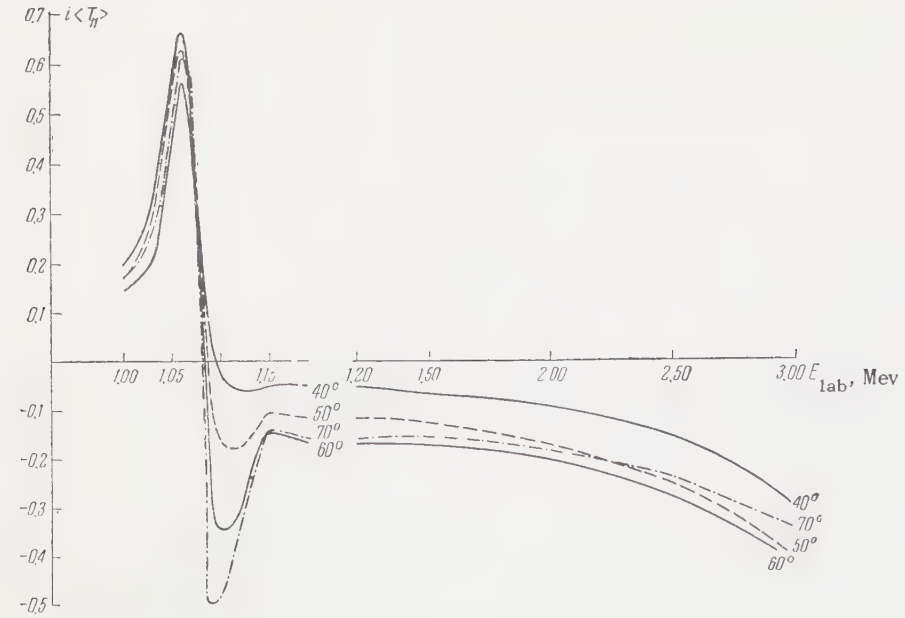

FIG. 1. Dependence of polarization coefficient $i\langle T_{11}\rangle$ on deuteron energy.

FIG. 2. Dependence of components of polarization tensor on deuteron energy: a $-\langle T_{21}\rangle$ for $\theta = 50°$, b $-\langle T_{20}\rangle$ for $\theta = 70°$, c $-\langle T_{22}\rangle$ for $\theta = 70°$.

In Fig. 2 we show the energy dependence of the components of the polarization tensor of second rank, for those angles at which it reaches its maximum values. The components of the tensor are much smaller than the polarization vector, and are significant only over the region of the resonance. The results obtained are in good agreement with the data of Goldfarb and Rook[5] and Phillips,[7] but differ essentially in the value of the components of the tensor and the angular dependence of the polarization coefficient from the data of Pondrom.[6]

The author thanks I. Ya. Barit for directing the work, M. V. Kazarnovskiĭ and V. A. Sergeev for valuable discussions, and I. V. Surkova for help in the computations.

[1] Lauritsen, Huus, and Nilsson, Phys. Rev. **92**, 1501 (1953).

[2] Galonsky, Douglas, Haeberli, McEllistrem, and Richards, Phys. Rev. **98**, 586 (1955).

[3] A. Galonsky and M. T. McEllistrem, Phys. Rev. **98**, 590 (1955).

[4] W. Lakin, Phys. Rev. **98**, 139 (1955).

[5] L. J. B. Goldfarb and J. R. Rook, Nucl. Phys. **12**, 494 (1959).

[6] L. G. Pondrom, Phys. Rev. Lett. **2**, 346 (1959).

[7] R. J. N. Phillips, Phys. Rev. Lett. **3**, 101 (1959).

[8] O. D. Cheĭshvili, JETP **30**, 1147 (1956), Soviet Phys. JETP **3**, 974 (1956-57).

[9] O. D. Cheĭshvili and G. R. Khutsishvili, Nuovo cimento **11**, 334 (1959).

[10] E. P. Wigner and L. Eisenbud, Phys. Rev. **72**, 29 (1947).

Translated by M. Hamermesh
184

TRANSITION RADIATION IN THE CASE OF A DIFFUSE BOUNDARY BETWEEN TWO MEDIA

A. Ts. AMATUNI and N. A. KORKHMAZYAN

Physics Institute, Academy of Sciences, Armenian S.S.R. and Erevan State University

Submitted to JETP editor April 15, 1960

J. Exptl. Theoret. Phys. (U.S.S.R.) **39**, 1011-1019 (October, 1960)

We consider the transition radiation of a charged relativistic particle in the case of a diffuse boundary between two media. General formulas are obtained for the main part of the radiation, and a detailed study is made of the case when the dimension of the diffusion zone z_0 is much smaller than that of the zone where the transition radiation is produced in either medium, R_0 or R_m, and also the cases when $z_0 \gg R_0 > R_m$ and $R_m \ll z_0 \ll R_0$.

1. We consider a medium whose dielectric properties vary in the z direction and remain constant in the planes perpendicular to this direction. We assume, furthermore, that the medium is nonmagnetic, i.e., $\mu = 1$.

Let a point particle of charge e move with a constant velocity **v** along the z axis. Maxwell's equations for this case are

$$\begin{aligned} \operatorname{curl}\mathbf{H} &= \frac{1}{c}\frac{\partial \mathbf{D}}{\partial t} + \frac{4\pi}{c}\mathbf{v}\delta(x)\,\delta(y)\,\delta(z-vt), \\ \operatorname{curl}\mathbf{E} &= -\frac{1}{c}\frac{\partial \mathbf{H}}{\partial t}, \qquad \operatorname{div}\mathbf{H} = 0, \\ \operatorname{div}\mathbf{D} &= 4\pi e\delta(x)\,\delta(y)\,\delta(z-vt). \end{aligned} \tag{1}$$

It is convenient to replace **E** etc. by Fourier components obtained by taking Fourier transforms in t, x, and y:

$$\mathbf{E}(\mathbf{r}, t) = \int \mathbf{E}(\varkappa, \omega, z)\, e^{i(\varkappa\rho - \omega t)} d\varkappa d\omega. \tag{2}$$

Analogous transformations are carried out for the other field, charge-density, and current vectors.

Noting now that $\mathbf{D}(\kappa, \omega, z) = \epsilon(z, \omega)\mathbf{E}(\kappa, \omega, z)$, we can rewrite Maxwell's equations (1) for the Fourier components in the form

$$\begin{aligned} &\frac{\partial}{\partial z}[\mathbf{n}\times\mathbf{H}_\rho] - iH_z[\mathbf{n}\times\varkappa] + i[\varkappa\times\mathbf{H}_\rho] = -\frac{i\omega}{c}\varepsilon\mathbf{E} + \frac{en}{2\pi^2 c}e^{i\omega z/v}, \\ &\frac{\partial}{\partial z}[\mathbf{n}\times\mathbf{E}_\rho] - iE_z[\mathbf{n}\times\varkappa] + i[\varkappa\times\mathbf{E}_\rho] = \frac{i\omega}{c}\mathbf{H}, \\ &\frac{\partial H_z}{\partial z} + i\varkappa\mathbf{H}_\rho = 0, \qquad \frac{\partial}{\partial z}(\varepsilon E_z) + i\varepsilon\varkappa\mathbf{E}_\rho = \frac{e}{2\pi^2 v}e^{i\omega z/v}. \end{aligned} \tag{3}$$

Here $\mathbf{n} = \mathbf{v}/v$; **E** and **H** have components $\mathbf{E}_\rho$ and $\mathbf{H}_\rho$ perpendicular to the z axis and components E_z and H_z along this axis.

It can be shown with the aid of the first and second equations of the system (3) that in our case $\mathbf{E}_\rho$ is parallel to κ and therefore $H_z = 0$. This leads in turn to a simpler equation (compared with the equation for **E**) for the determination of $\mathbf{H}_\rho = \mathbf{H}$, obtained by eliminating **E** from the two first equations of (3)

$$\frac{d}{dz}\left(\frac{1}{\varepsilon}\frac{d}{dz}\mathbf{H}_\rho\right) + \left(\frac{\omega^2}{c^2} - \frac{\varkappa^2}{\varepsilon}\right)\mathbf{H}_\rho = \frac{ie[\mathbf{n}\times\varkappa]}{2\pi^2 c\varepsilon}e^{i\omega z/v}. \tag{4}$$

Having determined $\mathbf{H}_\rho$ as a solution of (4), we can obtain also **E** from the first equation of (3). Introducing instead of $\mathbf{H}_\rho$ a new function $u(\kappa, \omega, z)$, defined by

$$\mathbf{H}_\rho = [\mathbf{n}\times\varkappa]\sqrt{\varepsilon}\; u(\varkappa, \omega, z), \tag{5}$$

we obtain the following equation for u

$$u'' + \left[-\sqrt{\varepsilon}\left(\frac{1}{\sqrt{\varepsilon}}\right)'' + \frac{\omega^2}{c^2}\varepsilon - \varkappa^2\right]u = \frac{ie}{2\pi^2 c\sqrt{\varepsilon}}e^{i\omega z/v}. \tag{6}$$

Equation (6) can be solved in the approximation of geometric optics (a solution of a corresponding homogeneous equation, obtained in the same approximation, is found in the book by Landau and Lifshitz[1]).

2. We consider now a certain $\epsilon(\omega, z)$, which we choose in the form

$$\varepsilon(\omega, z) = 1 + \frac{\alpha(\omega)}{1 + e^{-az}}, \qquad a > 0. \tag{7}$$

$\epsilon \to \epsilon_0 = 1 + \alpha(\omega)$ as $z \to +\infty$ and $\epsilon \to 1$ as $z \to -\infty$, i.e., this choice of ϵ corresponds to the case of a diffuse boundary between the vacuum and the medium with $\epsilon = \epsilon_0$. The diffuse zone extends over a distance on the order of $z_0 = 1/a$. At $a \to \infty$, the dielectric constant is $\epsilon = \epsilon_0$ for $z > 0$ and $\epsilon = 1$ for $z < 0$, i.e., in this case we deal with a sharp boundary between the vacuum and the medium. As $a \to 0$, all of space is filled with a homogeneous dielectric with $\epsilon = (\epsilon_0 + 1)/2$.

We shall be interested henceforth in the transition radiation, which occurs when a charged particle passes from one medium into another, with a diffuse boundary between the media and ϵ given in the form of (7). In the case of a sharp boundary, the transition radiation was first considered by Ginzburg and Frank,[2] and later on by many others.

Let a charged particle move with relativistic velocity; then its transition radiation is characterized by frequencies higher than optical, and the radiation at these frequencies is concentrated essentially in a narrow cone about the direction of motion.[3] We can then assume

$$\alpha = -\omega_0^2/\omega^2, \qquad \omega_0 = 4\pi e^2 N/m,$$
$$|\alpha| \ll 1, \qquad \omega^2\varepsilon - c^2\varkappa^2 \sim \omega^2. \tag{8}$$

The solution of (6) without the right half will be sought in the zeroth approximation of perturbation theory, the perturbation being the quantity $-\sqrt{\epsilon} \times (1/\sqrt{\epsilon})''$. It can be shown (see, for example, reference 4), by taking account of the fact that the perturbing term differs noticeably from zero near $z \sim 1/a$, that the condition for the applicability of the zeroth approximation of perturbation theory is $z_0 = 1/a \gg \lambda |\alpha|$. It is evident that a can be quite large for the considered interval of high-frequencies. Thus, for example, if we consider the case of ordinary media, for which $\omega \sim 10^{16}$, and choose $\omega \gtrsim 10^{17}$, then $z_0 \gg 10^{-9}$ cm = 0.1 A. Such a "diffusion" takes place also in the case of a real "sharp" boundary.

In our approximation, we can write Eq. (6) in the form

$$u'' + \left[\frac{\omega^2}{c^2}\varepsilon - \varkappa^2\right] u = \frac{ie}{2\pi^2 c\sqrt{\varepsilon}} e^{i\omega z/v}, \tag{9}$$

where ϵ is given by (7). Let us find a solution of (9) without the right half. It is advantageous to introduce a new variable $x = -e^{-az}$ and a new function $u = x^{\nu} v(x)$. We then obtain for v the hypergeometric equation

$$x(1-x)v'' + [2\nu + 1 - (2\nu+1)x]v' - (\nu^2 - \mu^2)v = 0, \tag{10}$$

$$\nu = i\lambda_2/a, \qquad \mu = i\lambda_1/a,$$
$$\lambda_2 = \pm\sqrt{\omega^2\varepsilon_0/c^2 - \varkappa^2}, \qquad \lambda_1 = \pm\sqrt{\omega^2/c^2 - \varkappa^2}; \tag{10'}$$

The plus sign in front of the radical is chosen when $\omega > 0$, and the minus sign when $\omega < 0$.

The suitably chosen independent solutions of the homogeneous part of (9) assume the form

$$u_1 = e^{i\lambda_1 z} F(-\nu+\mu, -\nu-\mu, 1-2\nu, -e^{-az}),$$
$$u_2 = e^{-i\lambda_1 z} F(-\nu-\mu, -\mu+\nu, 1-2\mu, -e^{az}). \tag{11}$$

As $z \to \infty$, the solution u_1 represents a plane wave propagating along the z axis, while as $z \to -\infty$ the solution u_2 is a plane wave propagating in the negative z direction. This indeed determines the convenience of the choice of u_1 and u_2 as two independent solutions of the homogeneous part of (9).

Using a property of hypergeometric functions, u_1 and u_2 can also be written

$$u_1 = e^{i\lambda_1 z}\Gamma_1^1 F(-\nu+\mu, \mu+\nu, 1+2\mu, -e^{az}) + e^{-i\lambda_1 z}\Gamma_1^2 F(-\nu-\mu, -\mu+\nu, 1-2\mu, -e^{az}), \tag{12}$$

$$u_2 = e^{i\lambda_2 z}\Gamma_2^1 F(-\nu-\mu, \mu-\nu, 1-2\nu, -e^{-az}) + e^{-i\lambda_2 z}\Gamma_2^2 F(\nu-\mu, \mu+\nu, 1+2\nu, -e^{-az}),$$

where

$$\Gamma_1^1 = \frac{\Gamma(1-2\nu)\Gamma(-2\mu)}{\Gamma(-\nu-\mu)\Gamma(1-\nu-\mu)}, \quad \Gamma_1^2 = \frac{\Gamma(1-2\nu)\Gamma(2\mu)}{\Gamma(-\nu+\mu)\Gamma(1-\nu+\mu)},$$
$$\Gamma_2^1 = \frac{\Gamma(1-2\mu)\Gamma(2\nu)}{\Gamma(\nu-\mu)\Gamma(1+\nu-\mu)}, \quad \Gamma_2^2 = \frac{\Gamma(1-2\mu)\Gamma(-2\nu)}{\Gamma(-\nu-\mu)\Gamma(1-\nu-\mu)}. \tag{13}$$

Solutions in the form (12) have simple asymptotic values as $z \to -\infty$ (u_1) and $z \to +\infty$ (u_2).

The solution of the inhomogeneous equation (9) is written in the form

$$\frac{W}{b}u = u_1\int^z \frac{u_2}{\sqrt{\varepsilon}} e^{i\omega z/v}dz - u_2\int^z \frac{u_1}{\sqrt{\varepsilon}} e^{i\omega z/v}dz + c_1u_1 + c_2u_2, \tag{14}$$

where $W = u_1u_2' - u_1'u_2$ is the Wronskian, which in our case is independent of z; $b = -ie/2\pi^2c$. The value of W can be obtained by using asymptotic expressions for u_1 and u_2, using (11) and (12):

$$W = -2i\lambda_1\Gamma_1^1 = -2i\lambda_2\Gamma_2^2 = -i(\lambda_1\Gamma_1^1 + \lambda_2\Gamma_2^2). \tag{15}$$

Recognizing that we are interested only in the region of high frequencies, where $|\alpha| \ll 1$, we can approximate the value of $\sqrt{\epsilon}$ in the integrals of (14) by unity. The resultant integrals can be determined by using the Barnes integral representation for hypergeometric functions (see, for example, reference 5):

$$F(\alpha, \beta, \gamma, t) = \frac{1}{2\pi i}\frac{\Gamma(\gamma)}{\Gamma(\alpha)\Gamma(\beta)}\int_{-i\infty}^{+i\infty}\frac{\Gamma(\alpha+s)\Gamma(\beta+s)\Gamma(-s)}{\Gamma(\gamma+s)}(-t)^s ds. \tag{16}$$

In (16), $|\arg(-t)| < \pi$ and the integration path in the plane of the complex variable s is chosen such that the poles of the functions $\Gamma(\alpha+s)$ and $\Gamma(\beta+s)$ lie to the left of the path, while the poles of the function $\Gamma(-s)$ lie to the right of the path.

Let $z > 0$. We consider the first integral in the expression (14); substituting u_2 from (12) and using the representation (16), we first integrate with respect to z. We have

$$I_1 = \int u_2 e^{i\omega z/v} dz = -\widetilde{\Gamma}_2^1 e^{i(\omega/v+\lambda_2)z} \frac{1}{2\pi i a}$$

$$\times \int_{-i\infty}^{+i\infty} \frac{\Gamma(-\nu-\mu+s)\,\Gamma(\mu-\nu+s)\,\Gamma(-s)}{\Gamma(1+2\nu+s)\,[s-(\sigma+\nu)]}$$

$$\times e^{-azs} ds - \widetilde{\Gamma}_2^2 e^{i(\omega/v-\lambda_2)z} \frac{1}{2\pi i a}$$

$$\times \int_{-i\infty}^{+i\infty} \frac{\Gamma(\nu-\mu+s)\,\Gamma(\mu+\nu+s)\,\Gamma(-s)}{\Gamma(1+2\nu+s)\,[s-(\sigma-\nu)]} e^{-a\,s} ds. \qquad (17)$$

Here $\sigma = i\omega/av$,

$$\widetilde{\Gamma}_2^1 = \Gamma_2^1 \frac{\Gamma(1-2\nu)}{\Gamma(-\nu-\mu)\,\Gamma(\mu-\nu)}, \qquad \widetilde{\Gamma}_2^2 = \Gamma_2^2 \frac{\Gamma(1+2\nu)}{\Gamma(\nu-\mu)\,\Gamma(\mu+\nu)}. \qquad (17')$$

We now integrate with respect to s in (17). Noting that $|-e^{-az}| < 1$ when $z > 0$, we close the contour of integration by means of a large semicircle with center at the origin, located in the half plane $\mathrm{Re}\, s > 0$; the integral over this semicircle vanishes as $|s| \to \infty$.[5] Only the poles of the function $\Gamma(-s)$ lie inside this contour, and the additional poles at the points $s_1 = \sigma + \nu$ and $s_2 = \sigma - \nu$ are located on the straight-line portion of the contour (in the case of a transparent medium they are pure imaginary). The values of the considered integrals are therefore $-2\pi i$ times the sum of the residues at the poles $\Gamma(-s)$ and of the half-residues at the points s_1 in the first integral and s_2 in the second one:

$$I_1 = -\frac{1}{a} \widetilde{\Gamma}_2^1 e^{i(\omega/v+\lambda_2)z} \sum_{n=0}^{\infty} \frac{(-1)^n}{n!} \frac{\Gamma(-\nu-\mu+n)\,\Gamma(\mu-\nu+n)}{\Gamma(1-2\nu+n)\,[n-(\sigma+\nu)]}$$

$$\times e^{-azn} - \frac{1}{a} \widetilde{\Gamma}_2^2 e^{i(\omega/v-\lambda_2)z}$$

$$\times \sum_{n=0}^{\infty} \frac{(-1)^n}{n!} \frac{\Gamma(\nu-\mu+n)\,\Gamma(\mu+\nu+n)}{\Gamma(1+2\nu+n)\,[n-(\sigma-\nu)]} e^{-azn}$$

$$+ \frac{1}{2a} \left\{ \widetilde{\Gamma}_2^1 \frac{\Gamma(\sigma-\mu)\,\Gamma(\sigma+\mu)\,\Gamma(-\sigma-\nu)}{\Gamma(1-\nu+\sigma)} \right.$$

$$\left. + \widetilde{\Gamma}_2^2 \frac{\Gamma(\sigma-\mu)\,\Gamma(\sigma+\mu)\,\Gamma(-\sigma+\mu)}{\Gamma(1+\nu+\sigma)} \right\}. \qquad (18)$$

Analogously we calculate the second integral in (14), and in this case we use the expression (11) for u_1. As a result we obtain from (14), at $z > 0$,

$$\frac{W}{b} u = \frac{1}{a} e^{i\omega z/v} \Gamma_2^2 \{v(-\nu, \mu, \sigma, e^{-az}) - v(\nu, \mu, \sigma, e^{-az})\} \qquad (19)$$

$$+ \frac{u_1}{2a} \Gamma(-\sigma, \nu, -\mu) - \frac{u_2}{2a} \Gamma(\sigma, \mu, -\nu) + c_1 u_1 + c_2 u_2.$$

In (19) we have introduced the following notation:

$$\Gamma(\sigma, \mu, \nu) = \frac{\Gamma(1+2\nu)\,\Gamma(\sigma-\mu)\,\Gamma(\mu+\sigma)\,\Gamma(-\sigma+\nu)}{\Gamma(\nu-\mu)\,\Gamma(\mu+\nu)\,\Gamma(1+\nu+\sigma)}, \qquad (19')$$

$$v(\nu, \mu, \sigma, e^{-az}) = F(-\nu+\mu, -\nu-\mu; 1-2\nu; -e^{-az})$$

$$\times \frac{\Gamma(1+2\nu)}{\Gamma(\nu-\mu)\,\Gamma(\nu+\mu)} \sum_{n=0}^{\infty} \frac{(-1)^n}{n!} \frac{\Gamma(\nu-\mu+n)\,\Gamma(\nu+\mu+n)}{\Gamma(1+2\nu+n)\,[n-(\sigma-\nu)]} e^{-azn}. \qquad (19'')$$

In addition, we have used in the derivation of (19), the identity

$$\Gamma_2^1 \Gamma(\sigma, \mu, -\nu) + \Gamma_2^2 \Gamma(\sigma, \mu, \nu) = \Gamma(-\sigma, \nu, -\mu), \qquad (19''')$$

which is easy to prove by using the property of the gamma function

$$\Gamma(1-z)\,\Gamma(z) = \pi / \sin \pi z.$$

Let us consider now the region $z < 0$. In the calculation of the integrals in (14) we have used u_1 from (12) and u_2 from (11). In this case, inasmuch as the argument $|-e^{az}|$ of the hypergeometric functions is less than unity when $z < 0$, the contours of integration must also be closed by an infinity semicircle in the half plane $\mathrm{Re}\, s > 0$. The poles of $\Gamma(-s)$ again lie inside the contour, and the additional poles at the points $s_3 = -\sigma + \mu$ and $s_4 = -\sigma - \mu$ lie on the linear portion of the contour. As a result of taking the residues at the poles of $\Gamma(-s)$ and the half-residues of the point s_3 and s_4, we obtain for $z < 0$

$$\frac{W}{b} u = \frac{1}{a} e^{i\omega z/v} \Gamma_1^1 \{v(-\mu, -\nu, -\sigma, e^{az})$$

$$- v(\mu, -\nu, -\sigma, e^{az})\} - \frac{u_1}{2a} \Gamma(-\sigma, \nu, -\mu)$$

$$+ \frac{u_2}{2a} \Gamma(\sigma, \mu, -\nu) + c_1 u_1 + c_2 u_2. \qquad (20)$$

The term proportional to $e^{i\omega z/v}$ in (19) and (20) is the result of taking the residues at the poles of the function $\Gamma(-s)$; the next two terms, proportional to the solutions u_1 and u_2 of the homogeneous equation, occur when the half-residues are taken at the points s_1 and s_2 (19) and s_3 and s_4 in (20).

The first terms in the braces in (19) and (20) correspond to the field of the particle. This can be readily verified by going to the limit of large a in both formulas, corresponding, as already mentioned, to a "sharp" boundary between the vacuum ($z < 0$) and the medium with $\epsilon = \epsilon_0$ ($z > 0$). In this transition to the limit, the first terms of (19) and (20) yield

$$\mathbf{H}_{p\,1,2} = [\mathbf{n}\times\mathbf{x}] \sqrt{\varepsilon} u_p \approx [\mathbf{n}\times\mathbf{x}]\, u_p = -\frac{ie\,[\mathbf{n}\times\mathbf{x}]}{2\pi^2 c} \frac{e^{i\omega z/v}}{\omega^2/v^2 - \lambda_{1,2}^2}, \qquad (21)$$

i.e., the field of the particle in vacuum (subscript 1) and in the medium (subscript 2), something that can be readily verified directly [compare also with formula (3) of the paper by Garibyan[6]].

The remaining terms in (19) and (20) describe the radiation field. The constants c_1 and c_2 in (19) and (20) can be determined from the condition that as $z \to \infty$ the radiation field in (19) should consist only of waves propagating in the positive

z direction, while as $z \to -\infty$ the radiation field in (20) should be described by a wave going towards minus infinity. From these conditions, using the asymptotic values of u_1 and u_2 obtained with the aid of (11) and (12), we get

$$c_1 = \tfrac{1}{2} a^{-1} \Gamma(-\sigma, \nu, -\mu), \qquad c_2 = \tfrac{1}{2} a^{-1} \Gamma(\sigma, \mu, -\nu). \quad (22)$$

Thus, the radiation field is written for $z > 0$ in the form

$$\frac{W}{b} u_{\text{rad}} = \frac{u_1}{a} \Gamma(-\sigma, \nu, -\mu), \quad (23)$$

and for $z < 0$ in the form

$$\frac{W}{b} u_{\text{rad}} = \frac{u_2}{a} \Gamma(\sigma, \mu, -\nu). \quad (24)$$

The radiation determined by (23) and (24) is the transition radiation in the case of a diffuse boundary, "forward" ($z > 0$) and "backward" ($z < 0$) respectively at high frequencies $\omega \gg \omega_0$. This can be verified by putting $\mu = \nu$, that is, by going to the case of a homogeneous medium with $\epsilon = \epsilon_0 = 1 + \alpha$. In this case the radiation field vanishes in (23) and (24). We notice also that expressions analogous to (23) and (24) can be obtained for transition radiation also in the more general case, by choosing instead of (7) another expression for the dielectric constant:

$$\varepsilon = \varepsilon_1 + 1 + \frac{\alpha}{1 + e^{-az}}, \quad (7')$$

which corresponds to a medium with $\epsilon = \epsilon_1 + \epsilon_0$ as $z \to +\infty$, and to a medium with $\epsilon = \epsilon_1 + 1$ as $z \to -\infty$. With such a choice of ϵ, only the definition of λ_1 and λ_2 in (10′) would change in the given results, for we would have:

$$\lambda_1 = \pm \sqrt{\omega^2 (\varepsilon_1 + 1)/c^2 - \varkappa^2},$$

$$\lambda_2 = \pm \sqrt{\omega^2 (\varepsilon_0 + \varepsilon_1)/c^2 - \varkappa^2}. \quad (10'')$$

Formulas (23) and (24) could be obtained also in a somewhat different manner, by assuming the presence of small imaginary parts of ϵ_1 and ϵ_0. In this case the additional poles [for example, at the points $s_1 = \sigma + \nu$ and $s_2 = \sigma - \nu$ in the calculation of the integral I_1 in (17)] would shift to opposite sides of the path of integration, and for $z > 0$, using (16) for u_2, we would have to take the total residue of only one of the poles. When $z < 0$, the integration contour [again using (16) for u_2] would have to be closed by a large semicircle in the left half plane $\operatorname{Re} s < 0$, and the additional residue would be then due to the presence of the second pole. Proceeding similarly in the calculation of the second integral in (14), and again determining the constants c_1 and c_2 from the radiation conditions, we arrive once more at (23) and (24).

3. Let us consider now the intensity of the radiation "forward," the main part of which, in the case of a relativistic particle, is known[3,6] to be concentrated in the frequency region $\omega \gg \omega_0$. For this purpose we consider the flux of the Poynting vector through a sufficiently remote point perpendicular to the z axis. The electric vector of the radiation field will be obtained from the homogeneous part of the first equation of the system (3):

$$\mathbf{E}_\rho = \mathbf{E}_t(\varkappa, \omega, z) = -\frac{c}{\omega} \lambda_2 [\mathbf{n} \times \mathbf{H}_\rho]. \quad (25)$$

We have

$$S = \frac{c}{4\pi} \int [\mathbf{E}(\mathbf{r}, t) \times \mathbf{H}_\rho(\mathbf{r}, t)]_z dx dy dt$$

$$= -2\pi^2 c^2 \int \frac{\lambda_2}{\omega} [[\mathbf{n} \times \mathbf{H}_\rho(\varkappa, \omega, z)] \times \mathbf{H}_\rho(-\varkappa, -\omega, z)] d\varkappa d\omega$$

$$= -2\pi^2 c^2 \int \frac{\lambda_2 \varkappa^2}{\omega} u(\varkappa, \omega, z)\, u(-\varkappa, -\omega, z)\, d\varkappa d\omega. \quad (26)$$

The quantity $u(\kappa, \omega, z)\, u(-\kappa, -\omega, z)$, which enters under the integral sign in (26), can be written by using (23), (19′), and the formula

$$\Gamma(t)\Gamma(-t) = -\pi / t \sin \pi t \quad (27)$$

in the following form:

$$u(\varkappa, \omega, z)\, u(-\varkappa, -\omega, z) = \frac{e^2 (\nu^2 - \mu^2)\, \nu}{8\pi^3 c^2 a^2 \lambda_2^2 (\sigma^2 - \nu^2)(\sigma^2 - \mu^2)} \times \frac{\sin \pi(\nu - \mu) \sin \pi(\mu + \sigma) \sin 2\pi\nu}{\sin \pi(\sigma - \nu) \sin \pi(\sigma - \mu) \sin \pi(\sigma + \nu) \sin \pi(\nu + \mu)}. \quad (28)$$

a) Let us analyze now in greater detail the particular case of the general formula (26), when

$$|\mu - \nu| \ll 1, \qquad |\sigma - \mu| \ll 1, \qquad |\sigma - \nu| \ll 1 \quad (29)$$

for all significant values of the angles and frequencies. We can then readily see (we recall that σ, μ, and ν are pure imaginary) that

$$\frac{\sin \pi(\mu + \sigma) \sin 2\pi\nu}{\sin \pi(\sigma + \nu) \sin \pi(\nu + \mu)} = \frac{\cos \pi(\mu + \sigma + 2\nu) - \cos \pi[(\mu - \nu) + (\sigma - \nu)]}{\cos \pi(\mu + \sigma + 2\nu) - \cos \pi[(\mu - \nu) - (\sigma - \nu)]}$$

$$\approx 1 + \frac{2\pi^2 (\mu - \nu)(\sigma - \nu)}{\cos \pi(\mu + \sigma + 2\nu) - 1}, \quad (30)$$

$$\frac{\sin \pi(\mu - \nu)}{\sin \pi(\sigma - \nu) \sin \pi(\sigma - \mu)} \approx \frac{1}{\pi} \frac{(\mu - \nu)}{(\sigma - \nu)(\sigma - \mu)} \left[1 + \frac{\pi^2}{3} (\sigma - \nu)(\sigma - \mu)\right]. \quad (30')$$

Neglecting the squares of small quantities compared with unity, we obtain the flux S_0 in the zeroth approximation by substituting (29) and (28) in (26). Putting in (26) $\kappa = (\omega/c)\sqrt{\epsilon_0} \sin\theta$, where

θ is the radiation angle, and replacing ν, μ, and σ by their expressions in (10′) and (17′), we carry out the integration in (26) with respect to $\varphi\,(d\kappa = \kappa\, d\kappa\, d\varphi)$ and write down the integral with respect to ω from minus to plus infinity as twice the integral from zero to infinity (the integrand is an even function of ω). We can then readily note that the main contribution to the radiation is made by small angles $\theta \approx \sqrt{1-\beta^2}$ and high frequencies, which do not exceed, however, the limiting frequency $\omega_{\lim} = \omega_0/2\sqrt{1-\beta^2}$. Making use of this, we integrate in (26) first over the frequencies and then over the angles. We thus obtain for S_0 the well-known[3] expression

$$S_0 = e^2\omega_0/3c\sqrt{1-\beta^2}. \qquad (31)$$

Calculation of the next terms of the expansion in (30) and (31) in the region of small angles and at frequencies not exceeding the limiting frequency (terms which are essential for the calculation of the principal term and for which the assumed smallness of the differences $\mu-\nu$ and $\sigma-\mu$ is valid) leads to a correction to (31), by which (31) is multiplied by $1-b^2\,(z_0/R_0^{\lim})^2$. Here b^2 is some numerical factor on the order of unity and $R_0^{\lim}$ is the formation zone for the limiting frequency, $R_0^{\lim} = c/\omega\sqrt{1-\beta^2} \gg z_0$ [by virtue of (29)].

The conditions for the applicability of the obtained result have the following form [see (29)]

$$z_0 \ll R_0(\omega, \theta), \qquad z_0 \ll R_m(\omega, \theta), \quad \omega_{cr}/\omega \ll 1. \qquad (29')$$

Here (see references 3 and 6)

$$R_0(\omega, \theta) = \frac{c}{\omega\,(1-\beta+\theta^2/2)}$$

is the formation zone for the frequency ω in the vacuum,

$$R_m(\omega, \theta) = \frac{c}{\omega\,(1-\beta+\omega_0^2/2\omega^2+\theta^2/2)}$$

is the formation zone for the frequency ω in the medium ($R_m < R_0$, and $\omega_{cr} = \omega_0^2/ac$ is some critical frequency, with $\omega_{cr} \ll \omega_{\lim}$ by virtue of the first condition of (29′), written out for the limiting frequency; $\omega_{cr} > \omega_0$ if $z_0 > \lambda\!\!\!^{-}_0 = c/\omega_0$, and $\omega_{cr} < \omega_0$ if $z_0 < \lambda\!\!\!^{-}$, and consequently the result obtained is true for the frequencies in the following intervals:

$$\omega_0 \lesssim \omega_{cr} \ll \omega \lesssim \omega_{\lim}, \quad \text{if} \quad z_0 > \lambda\!\!\!^{-}_0,$$
$$\omega_0 \ll \omega \lesssim \omega_{\lim}, \quad \text{if} \quad z_0 < \lambda\!\!\!^{-}_0.$$

b) Let us consider the opposite case, when the diffusion is much greater than the formation zone in vacuum (and hence in the medium),

$$z_0 \gg R_0(\omega, \theta), \qquad z_0 \gg R_m(\omega, \theta). \qquad (32)$$

Unlike the preceding case, the intensity of the transition radiation is expected to diminish sharply here. Inasmuch as $|\mu+\sigma| \gg |\sigma-\mu| \gg 1$ and $|\sigma+\nu| \gg |\sigma-\mu| \gg 1$, the ratio of the sines of the sums in (30) is exponentially close to unity, and

$$\frac{\sin\pi(\mu-\nu)}{\sin\pi(\sigma-\mu)\sin\pi(\sigma-\nu)} = \pm\frac{i}{2}\{e^{-2\pi|\sigma-\nu|} - e^{-2\pi|\sigma-\mu|}\}, \qquad (33)$$

where the plus sign in (33) pertains to $\omega > 0$ and the minus sign to $\omega < 0$.

Writing down the expression for the intensity, we find now

$$S = \frac{e^2}{2ac^2}\int_{\omega_1 > \omega_0}^{\infty} d\omega \int \frac{\sin^3\theta\cos\theta\, d\theta\,\omega\,(1-\varepsilon_0)}{[1-\beta^2(1-\varepsilon_0\sin^2\theta)][1-\beta^2\varepsilon_0\cos^2\theta]}$$
$$\times\left[\exp\left\{-\frac{2\pi\omega}{av}(1-\beta\sqrt{1-\varepsilon_0\sin^2\theta})\right\}\right.$$
$$\left. - \exp\left\{-\frac{2\pi\omega}{av}[1-\beta\sqrt{\varepsilon_0}\cos\theta]\right\}\right]. \qquad (34)$$

We see from (34) that the region of small angles $\theta \sim \sqrt{1-\beta^2}$ is essential to the integral.

Considering that the radiation in (34) is small, as can be readily noted, we need merely estimate it. Since the angles θ are small, we can rewrite (34) approximately as

$$S = \frac{e^2}{4ac^2}\int_0^{\infty}\frac{\theta^3\, d\theta}{(1-\beta+\theta^2/2)}$$
$$\times\int_{\omega_1}^{\infty}\frac{\omega\exp\left[-\frac{2\pi\omega}{av}\left(1-\beta+\frac{\theta^2}{2}\right)\right]}{(1+b\omega^2)}[1-e^{-\pi\omega_{cr}/\omega}]\,d\omega, \qquad (35)$$

where $b = \omega_0^{-2}(1-\beta^2+\theta^2)$. Taking the largest values of the functions $\omega/(1+b\omega^2)$ and $1-e^{-\pi\omega_{cr}/\omega}$ outside the integral with respect to ω [$\omega_{cr} \gg \omega_0$ by virtue of (32)] in the considered frequency interval, and estimating then the integrals with respect to θ, we get

$$S < \frac{e^2\omega_0}{16\pi c}\sqrt{1-\beta^2}\exp\left[-\frac{2\pi\omega_1}{ac}(1-\beta^2)\right], \qquad (36)$$

i.e., the radiation is negligibly small in this case, as expected.

c) Finally, we consider still another particular case of the general formula (25), when

$$R_m(\omega, \theta) \ll z_0 \ll R_0(\omega, \theta) \qquad (37)$$

for the frequency interval under consideration. We see from the expressions for R_0 and R_m that the condition (37) holds for small radiation angles, provided

$$1-\beta^2 \ll \omega_0^2/\omega^2. \qquad (37')$$

The conditions (37) denote that $|\sigma-\mu| \ll 1$ and $|\sigma-\nu| \gg 1$, and therefore $|\mu-\nu| = |(\sigma-\nu) - (\sigma-\mu)| \gg 1$. At small radiation angles, which

are significant in this case, too, the last condition can be rewritten also in the form $\omega \ll \omega_{cr}$. According to conditions (37) and (37′), $\omega_{cr} = \omega_0^2/ac$ can be both greater and smaller than the limiting frequency, and remains in the latter case much greater than ω_0.

In our case the ratio (30) is again exponentially close to unity, and

$$\frac{\sin \pi(\mu - \nu)}{\sin \pi(\sigma - \nu) \sin \pi(\sigma - \mu)}$$

$$\approx \frac{e^{-\pi|\sigma-\mu|}}{\pi(\sigma-\mu)}\left[1 + \frac{\pi^2}{6}(\sigma-\mu)^2 + \ldots\right] \approx \frac{1}{\pi(\sigma-\mu)}. \quad (38)$$

In this case the calculation of the intensity, with allowance for (37′), leads to

$$S_0 \approx \frac{2e^2}{\pi c} \Delta\omega \ln \frac{E}{m_0 c^2}. \quad (39)$$

The spectrum is independent here of the frequency, as can be seen from (38), and the radiation is contained in the interval $\Delta\omega = \omega_2 - \omega_1$, $\omega_0 \ll \omega_1 < \omega_2 \ll \min(\omega_{cr}, \omega_{lim})$. The limitations on the upper boundary of the interval follow from the requirement $\omega \ll \omega_{cr}$ and (37′). When estimating the corrections to formula (39), which arise when the next terms of the expansion in (38) are taken into account, it is found that (39) is multiplied by a factor $1 - b^2 z_0/R_0(\omega_2)$, where b^2 is a constant on the order of unity.

The authors are grateful to G. M. Garibyan and I. I. Gol'dman for useful advice, and also to all the participants of the Theoretical Seminar of the Physics Institute of the Armenian S.S.R. Academy of Sciences, who took part in the discussion of this work.

[1] L. D. Landau and E. M. Lifshitz, Электродинамика сплошных сред (Electrodynamics of Continuous Media), Gostekhizdat 1957, Sec. 68, p. 361.

[2] V. L. Ginzburg and I. M. Frank, JETP **18**, 15 (1946).

[3] G. M. Garibyan, JETP **37**, 527 (1959), Soviet Phys. JETP **10**, 372 (1960).

[4] L. D. Landau and E. M. Lifshitz, Квантовая механика (Quantum Mechanics), Gostekhizdat, 1948, Sec. 45, p. 183 [Engl. Transl., Addison-Wesley, 1958].

[5] E. T. Whittaker and G. N. Watson, A Course in Modern Analysis (Russ. Transl.) Gostekhizdat, 1934, Part II, p. 71 [Cambridge].

[6] G. M. Garibyan, JETP **33**, 1403 (1957), Soviet Phys. JETP **6**, 1079 (1958).

Translated by J. G. Adashko
185

THE INFLUENCE OF INELASTIC PROCESSES ON ELASTIC SCATTERING IN THE VICINITY OF THRESHOLDS FOR INELASTIC REACTION MODES

L. A. KHALFIN

Submitted to JETP editor April 16, 1960

J. Exptl. Theoret. Phys. (U.S.S.R.) 39, 1020-1022 (October, 1960)

It is shown that the specific effects that occur in the vicinity of thresholds for inelastic reactions can be treated in the general case by using dispersion relations.

In a series of recent papers,[1-4] attention has been called to the specific effects of inelastic processes on the characteristics of elastic scattering in the vicinity of thresholds for the inelastic processes. The specific effects which have been pointed out in references 1 — 4 consist in the occurrence of discontinuities in the properties of elastic scattering in the vicinities of thresholds for inelastic processes. The basis of these papers is the use of the unitarity condition (relating the amplitudes for elastic and inelastic scattering) and the treatment (on the basis of the quantum-mechanical Schrödinger equation) of the asymptotic behavior of inelastic processes in the vicinity of the energy threshold.

In the present paper it is pointed out that the investigation of specific threshold effects can be carried out in general on the basis of dispersion relations.

1. The mathematical basis of the present investigation is the set of theorems of Muskhelishvili,[5] concerning the behavior of integrals of the Cauchy type near their limits:* Suppose that $g(E) \equiv \operatorname{Im} f(E)$ satisfies the Hoelder condition in the interval $E \in [E_1, \infty)$ with an exponent $\mu \leq 1$ and $g(E_1) = \operatorname{Im} f(E_1) = 0$.† Then the Cauchy integral

$$h(E) \equiv \frac{1}{\pi} P \int_{E_1}^{\infty} \frac{g(E')}{E' - E} dE' . \qquad (1)$$

defines a function $h(E) = \operatorname{Re} f(E)$ which, for $E \in [E_1, \infty)$ also satisfies the Hoelder condition with exponent μ if $\mu < 1$, and with exponent $\mu' = 1 - \epsilon$ where $\epsilon > 0$ is an arbitrarily small number, if $\mu = 1$. The expression $h(E)$ is an analytic function for $E < E_1$, tending to a definite limit when $E \to E_1 - 0$. We remind the reader[5] that the function $g(E)$ is said to satisfy a Hoelder condition with Hoelder exponent $\mu > 0$ for $E \in [E_1, \infty)$ if for arbitrary E_k, E_m of $[E_1, \infty)$ the relation

$$|g(E_k) - g(E_m)| \leqslant A |E_k - E_m|^{\mu},$$

holds, where $A > 0$.

We now call attention to the following natural extension of the result given above.

Theorem. Let $\mu < 1$ be the maximum value of the Hoelder exponent* for the function $g(E) = \operatorname{Im} f(E)$ on the interval $E \in [E_1, \infty)$, where $g(E_1) = 0$. Then the Cauchy integral (1) defines a function $h(E) \equiv \operatorname{Re} f(E)$ which, for $E \in [E_1, \infty)$ also satisfies the Hoelder condition with maximum value of the exponent $\mu < 1$.

The proof of the theorem is almost obvious. In fact, let us assume the contrary, namely that $h(E)$ for $E \in [E_1, \infty)$ satisfies a Hoelder condition with exponent μ_1, where $1 > \mu_1 > \mu$. Defining the function $\tilde{g}(E)$

$$\tilde{g}(E) \equiv \begin{cases} 0, & E < E_1 \\ g(E), & E \in [E_1, \infty), \end{cases} \qquad (2)$$

we obtain, in place of (1), the expression

$$h(E) = \operatorname{Re} f(E) = \frac{1}{\pi} P \int_{-\infty}^{\infty} \frac{\tilde{g}(E')}{E' - E} dE', \qquad (3)$$

where, on the basis of the theorem of Muskhelishvili which was stated above, the function $h(E)$ for $E \in (-\infty, \infty)$ satisfies the Hoelder condition with exponent $\mu_1 > \mu$. Then making use of the uniqueness of the Hilbert transformation (cf. reference 5) (under the natural assumption that $|f(E)| = |h(E) + i\tilde{g}(E)|$ falls off for $|E| \to \infty$), we obtain

$$g(E) = \operatorname{Im} f(E) = -\frac{1}{\pi} P \int_{-\infty}^{\infty} \frac{h(E')}{E' - E} dE', \quad E \in [E_1, \infty). \qquad (4)$$

On the basis of the theorem of Plemelj and

*We state only that part of the theorem of Muskhelishvili which is necessary for the following presentation.

†This condition is known to be satisfied in the physical applications treated here.

*The maximum value of the Hoelder exponent is actually determined by its value for $E = E_1$.

Privalov (cf. reference 5) $g(E) = \mathrm{Im}\, f(E)$ for $E \in [E_1, \infty)$ satisfies the Hoelder condition with exponent $\mu_1 > \mu$, which contradicts the starting condition of the theorem.

Starting from the theorem which has been formulated and proven above, we obtain the following consequence which is basic to the remainder of the presentation: If $g(E) = \mathrm{Im}\, f(E)$ does not have a finite derivative for $E = E_1$ and satisfies the Hoelder condition with maximum exponent $\mu < 1$, then $h(E) = \mathrm{Re}\, f(E)$ also does not have a finite derivative for $E = E_1$ and satisfies a Hoelder condition with the same maximum exponent $\mu < 1$.

To prove this result it is sufficient to recall that functions having finite derivatives necessarily satisfy a Hoelder condition with exponent equal to unity.

2. Let $f(E)$ be the amplitude for elastic scattering, analytic in the upper half plane $\mathrm{Im}\, E > 0$. On the basis of the "optical" theorem, i.e., on the basis of the unitarity condition,[6]* we obtain

$$\mathrm{Im}\, f(E) = \frac{E}{4\pi}\sigma(E) = \frac{E}{4\pi}\sigma_{\mathrm{el}}(E) + \frac{E}{4\pi}\sigma_{\mathrm{inel}}(E), \qquad (5)$$

where $\sigma(E)$ is the total cross section, $\sigma_{\mathrm{el}}(E)$ is the total elastic scattering cross section, and $\sigma_{\mathrm{inel}}(E)$ is the total cross section for inelastic scattering.

Under the usual assumptions regarding $|f(E)|$ for $|E| \to \infty$ (actually the results obtained are also valid under wider assumptions concerning $|f(E)|$ for $|E| \to \infty$), from the analyticity of $f(E)$ there follows the dispersion relation

$$\mathrm{Re}\, f(E) = \mathrm{Re}\, f(0) + \frac{E}{\pi} P \int_{-\infty}^{\infty} \frac{\mathrm{Im}\, f(E')}{E'(E' - E)}\, dE'. \qquad (6)$$

$\mathrm{Im}\, f(E')$ for $E' < 0$ is determined on the basis of a condition of the type of "crossing symmetry."[6] Let E_1 be the threshold energy for the inelastic process. Then

$$\mathrm{Re}\, f(E) = \mathrm{Re}\, f(0) + \frac{E}{4\pi^2} P \int_{E_1}^{\infty} \frac{\sigma_{\mathrm{inel}}(E')}{E' - E}\, dE' + \frac{E}{4\pi^2} P \int_{0}^{\infty} \frac{\sigma_{\mathrm{el}}(E')}{E' - E}\, dE' + \frac{E}{\pi} P \int_{-\infty}^{0} \frac{\mathrm{Im}\, f(E')}{E'(E' - E)}\, dE' \qquad (7)$$

The first integral in (7) is just the type which was investigated in Sec. 1. The last integral in (7) is an analytic function of E for $E \sim E_1$.

On the basis of the results of the preceding paragraph we arrive at the following description of the specific threshold effects. If the total cross section for inelastic scattering at the threshold $E = E_1$ has a discontinuity, i.e., does not have a finite derivative for $E = E_1$, then $\mathrm{Re}\, f(E)$ — the real part of the elastic scattering amplitude which characterizes the phase-shift analysis — also does not have a finite derivative for $E = E_1$. Moreover, the maximum value of the Hoelder exponents for $E = E_1$ for $\sigma_{\mathrm{inel}}(E)$ and $\mathrm{Re}\, f(E)$ coincide. In particular, if E_1 is the threshold for an inelastic process of the first order,[2] i.e., $\sigma_{\mathrm{inel}}(E) \sim \sqrt{E - E_1}$ for $E \sim E_1$, then the singularity of $\mathrm{Re}\, f(E)$ at the threshold $E = E_1$ is also of this same order. If the threshold for the inelastic process is of higher order, then one must apply a similar treatment investigating, in place of the dispersion relations for $f(E)$, the dispersion relations for the derivatives of $f(E)$ of the appropriate order.

Note (Added May 9, 1960). After the present paper was sent to press, I was informed of the paper prepared for press by L. I. Lapidus and Chou Kuang-Chao, in which they investigated threshold effects, within the framework of the dispersion relations, for the specific process of scattering of γ quanta by nuclei. I am grateful to L. I. Lapidus for informing me of his work.

*To simplify the expression we use, without limiting our generality, the "optical" theorem for particles with zero rest mass.

[1] E. P. Wigner, Phys. Rev. **73**, 1002 (1948).

[2] A. I. Baz', JETP **33**, 923 (1957), Soviet Phys. JETP **6**, 709 (1958).

[3] G. Breit, Phys. Rev. **107**, 1612 (1957).

[4] R. Newton, Ann. of Phys. **4**, 29 (1958).

[5] N. I. Muskhelishvili, Сингулярные интегральные уравнения (Singular Integral Equations), Gostekhizdat, 1946; translation, P. Noordhoff, Groningen, 1953.

[6] N. N. Bogolyubov and D. V. Shirkov, Введение в теорию квантовых полей (Introduction to the Theory of Quantized Fields), Gostekhizdat, 1957; translation, Interscience, New York, 1959.

Translated by M. Hamermesh
186

THE EFFECT OF EXTERNAL FIELDS ON THE ANGULAR CORRELATIONS AND RESONANCE PROCESSES DURING QUANTUM TRANSITIONS

L. G. ZASTAVENKO and M. I. PODGORETSKIĬ

Joint Institute for Nuclear Research

Submitted to JETP editor April 19, 1960

J. Exptl. Theoret. Phys. (U.S.S.R.) 39, 1023-1026 (October, 1960)

The scattering of light and γ rays on isolated and overlapping magnetic sublevels is considered. A new method is discussed for the experimental determination of the Stark constant and the gyromagnetic ratio.

RECENTLY, in connection with the development of the Mössbauer method[1-3] and the first experiments on the nuclear Zeeman effect,[4] the study of the resonance scattering of γ rays on isolated nonoverlapping magnetic sublevels has taken on a definite meaning, as has the case in which several of the sublevels overlap. Similar questions arise in the consideration of processes of the emission of light and γ quanta during various excitation mechanisms. One of the authors[5] has shown that sufficiently general methods can be suggested along these lines for the measurement of the splitting and displacement of quantum levels.

In the present paper we treat as an example the method suggested in reference 5 for the determination of the Stark constant of an excited atom by means of the observation of the resonance scattering of light in parallel electric and magnetic fields (Sec. 1).

In Sec. 2, a partial analysis is carried out of the effect of a magnetic field on the resonance scattering of γ rays under the conditions of application of the Mössbauer method.[3,4]

1. DETERMINATION OF THE STARK SPLITTING OF THE EXCITED LEVELS OF AN ATOM

We consider the resonance scattering of light on atoms by means of some excited intermediate state.* We shall introduce the following notation: τ is the lifetime of the excited atom, j is its angular momentum, m is the projection of the angular momentum on the z axis, E_m is the energy of the level with projection m, A_m is the amplitude of resonance scattering, corresponding to this level.

In the absence of external fields, all the E_m are identical; therefore, the amplitudes A_m add, so that the differential cross section of resonance scattering is

$$W = \left| \sum_{m=-j}^{j} A_m \right|^2. \tag{1}$$

We further superpose a strong magnetic field on the scatterer in the direction of the z axis (the field is considered strong if the separation of levels with different m produced by it is much greater than the natural width of the excited level):

$$\tau |E_{m_1} - E_{m_2}| \gg \hbar, \qquad m_1 \neq m_2. \tag{2}$$

We shall assume that the intensity of the radiation incident on the scatterer undergoes little change in the energy region of interest to us.

In this case the contributions of the states of the excited atom with different m add without interference, so that the resonance scattering cross section is

$$W = \sum_{m=-j}^{j} |A_m|^2. \tag{3}$$

We now superpose an electric field on the scatterer in the direction of the z axis. The energy levels in this case (i.e., in the presence of both fields) are given by the formula

$$E_m = A + Bm + Cm^2,$$

from which it is seen that the values of the field can be so chosen that some of the levels with different m will coincide: $E_{m_1} = E_{m_2}$ for $m_1 \neq m_2$. The contributions of these states to the resonance scattering will interfere with one another, and we get for the scattering cross section

$$W = |A_{m_1} + A_{m_2}|^2 - |A_{m_1}|^2 - |A_{m_2}|^2 + \sum_{m=-j}^{j} |A_m|^2. \tag{4}$$

*The considerations given here apply also to other means of excitation of the atom, for example, to electron excitation.

The coincidence of levels will be broken up upon change of either of the fields; when this "disordering" reaches such a magnitude that the condition (2) is satisfied for all m_1 and m_2 ($m_1 \neq m_2$), the scattering cross section again takes the form (3).

Thus the dependence of the resonance scattering on the magnetic field for a fixed electric field is a curve which is constant everywhere, except for regions in which a partial overlapping of levels with different m takes place, and where the curve has narrow extrema; the location of these extrema can be accurately determined and used for the experimental evaluation of the Stark constants.

It is significant that the motion of the atoms and the Doppler frequency shift of the photons associated with that motion do not affect the picture given above; therefore, an electric field that is sufficient for its observation is one that separates the levels of the excited atom by an amount which is large or comparable with the natural, but not with the "Doppler" width of these levels. We note that for the existence of the effect described above it is necessary that reorientation of the angular momentum of the atom as a result of collisions not take place within the lifetime of the excited state.

To be specific, we assume that the ground state of the atoms of the scatterer have zero angular momentum, while the excited state, by means of which the resonance scattering takes place, has the angular momentum 1.

In the absence of external fields, the differential scattering cross section is equal to

$$W \equiv W_0 = 1 + (\mathbf{n}_1 \mathbf{n}_2)^2$$

(here and below $\mathbf{n}_1$ and $\mathbf{n}_2$ are the directions of the photon before and after scattering; $\mathbf{n}_0$ is the direction of the external field).

In a strong magnetic field we have

$$W \equiv W_1 = {}^3/_2 [1 + (\mathbf{n}_1 \mathbf{n}_0)^2 (\mathbf{n}_2 \mathbf{n}_0)^2] - {}^1/_2 [(\mathbf{n}_1 \mathbf{n}_0)^2 + (\mathbf{n}_2 \mathbf{n}_0)^2].$$

Finally, Eq. (4) corresponds to the expression

$$W \equiv W_2 = W_1 + (\mathbf{n}_1 \mathbf{n}_0)(\mathbf{n}_2 \mathbf{n}_0)[(\mathbf{n}_1 \mathbf{n}_2) - (\mathbf{n}_1 \mathbf{n}_0)(\mathbf{n}_2 \mathbf{n}_0)].$$

The ratio W_2/W_1 varies (for different $\mathbf{n}_1$ and $\mathbf{n}_2$) from 0.82 to 1.18, which is quite sufficient for observation of the effect and for the experimental determination of the Stark constant.

In similar fashion we can measure the value of the nuclear quadrupole splitting, investigating the nonmonotonicity in the dependence of correlations on the magnetic field intensity directed parallel to the gradient of the electric field of the crystal. This effect was observed experimentally in the work of Albers-Schönberg, Alder et al.,[6] but it is impossible to consider the explanation given there and in reference 7 as sufficiently clear.

The dependence of $\gamma - \gamma$ correlation on the magnetic field, in the case when the interaction of the spin of the intermediate nucleus with the electron shell of the atom creates a hyperfine splitting of the atomic energy levels, has a character similar to the foregoing. For certain values of the applied magnetic field some of the levels of the hyperfine structure overlap, which leads to an extremum in the correlation which is associated with interference.

Such an experiment can serve for the determination of the gyromagnetic ratio of the intermediate state of the nucleus. It is of interest that the shift in levels which is made use of is almost completely determined by the large gyromagnetic ratio of the electron shell; therefore, only a small field is necessary for observation of the effect. In conclusion, we point out that the experiment is very close in its nature to the experiment on the observation of the external magnetic field dependence of the resonance scattering of light from atoms possessing a fine structure.[8]

2. RESONANCE SCATTERING OF γ RAYS IN A MAGNETIC FIELD

We denote the spin of the ground state of a nucleus by J and the spin of the excited state by j; the excited state undergoes a transition to the ground state with the emission of a γ quantum. We shall assume that the states in the radiator with different projections of the spin of the excited nucleus are equally probable. The radiation accompanying the transition of these nuclei to the ground state undergoes resonance scattering by the scatterer, which consists of the same nuclei as the radiator.

We shall consider how the resonance scattering changes in the case of integral j when a strong magnetic field (the definition of a "strong" magnetic field was given above) is applied to the scatterer. The resonance scattering in this case will take place only on states of the scattering nucleus with a projection of the angular momentum in the direction of the field equal to zero.

If the transition of the excited state to the ground state is dipole, then the scattering at J = j will not occur (this follows from the fact that the matrix element $\langle j100 | j1j0 \rangle = 0$ for integral j. For J = j + 1, the angular distribution of the resonance scattering W_{j+1} and the ratio X_{j+1} of the total resonance scattering cross section in the

field to the total resonance scattering cross section without the field are given by the formulas

$$W_{j+1} = 1 - (\mathbf{n}_0\mathbf{n}_2)^2\, j/(3j+4),$$
$$X_{j+1} = {}^3/_2\,[1-(\mathbf{n}_0\mathbf{n}_1)^2]\,(j+1)/(2j+1)(2j+3).$$

For $J = j - 1$, the corresponding formulas are obtained by the substitution $j \to -1-j$.

If the transition between the excited and ground states of the nucleus is quadrupole, then the scattering in the field will take place only for $J = j$ and $j \pm 2$. Similarly, we have:

$$W_{j+2} = \{(j+3)(5j+8) + 6j(j+1)(\mathbf{n}_0\mathbf{n}_2)^2 - 3j(j-1)(\mathbf{n}_0\mathbf{n}_2)^4\}/(j+3)(5j+8),$$

$$W_j = \{j^2+j-1+(2j^2+2j-3)(\mathbf{n}_0\mathbf{n}_2)^2 - 3(j-1)(j+2)(\mathbf{n}_0\mathbf{n}_2)^4\}/(j^2+j-1),$$

$$X_{j+2} = \frac{45(j+1)(j+2)}{4(2j+1)(2j+3)(2j+5)}(\mathbf{n}_0\mathbf{n}_1)^2[1-(\mathbf{n}_0\mathbf{n}_1)^2],$$

$$X_j = \frac{15j(j+1)}{2(2j-1)(2j+1)(2j+3)}(\mathbf{n}_0\mathbf{n}_1)^2[1-(\mathbf{n}_0\mathbf{n}_1)^2].$$

W_{j-2} and X_{j-2} are obtained from W_{j+2} and X_{j+2} by the substitution $j \to -1-j$.

For half-integral j we take as an example the case in which $J = {}^1/_2$, $j = {}^3/_2$, and the transition is magnetic dipole, while strong magnetic fields, identical in magnitude and direction, are applied to the source and to the scatterer. The angular distributions of resonance scattering in the absence of a field and in a strong field are given by the formulas

$$W_0 = 28 + 21(\mathbf{n}_1\mathbf{n}_2)^2,$$

$$W_1 = 14 - 12(\mathbf{n}_1\mathbf{n}_0)^2 + 14(\mathbf{n}_1\mathbf{n}_0)^4 - 3(\mathbf{n}_2\mathbf{n}_0)^2[1-6(\mathbf{n}_1\mathbf{n}_0)^2+(\mathbf{n}_1\mathbf{n}_0)^4].$$

Here the numerical factors are so chosen that these formulas give the correct relation for total cross sections.

The authors thank Professor M. A. Markov and Professor I. Ya. Pomeranchuk for discussion of the research.

[1] R. L. Mössbauer, Z. Physik **151**, 124 (1958).

[2] R. L. Mössbauer, Z. Naturforsch. **14a**, 211 (1959).

[3] A. A. Hanna, J. Heberle et al., Phys. Rev. Lett. **4**, 28 (1960).

[4] De Pasquali, Frauenfelder, Margulis, and Reacock, Phys. Rev. Lett. **4**, 71 (1960).

[5] M. I. Podgoretskiĭ, Preprint, Joint Institute for Nuclear Research (in Russian).

[6] Albers-Schönberg, Alder, Heer, Novey, and Scherrer, Proc. Phys. Soc. (London) **A66**, 952 (1953).

[7] Alder, Albers-Schönberg, Heer, and Novey, Helv. Phys. Acta **26**, 761 (1953).

[8] Colegrove, Franken, Lewis, and Sands, Phys. Rev. Lett. **3**, 420 (1959).

Translated by R. T. Beyer
187

INELASTIC MAGNETIC SCATTERING OF SLOW NEUTRONS BY PHONONS

B. M. KHABIBULLIN

Physico-Technical Institute, Kazan' Branch, Academy of Sciences, U.S.S.R.

Submitted to JETP editor April 27, 1960; resubmitted June 21, 1960

J. Exptl. Theoret. Phys. (U.S.S.R.) 39, 1027-1030 (October, 1960)

An estimate is made of the differential cross section for inelastic scattering of neutrons by phonons due to magnetic interaction of the neutrons with the spin system of a paramagnet. A value $d\sigma/d\Omega = 10^{-27}$ cm^2 is obtained for the cross section.

1. The theoretical treatment of the scattering of slow neutrons due to magnetic interaction of the neutron with the spins of the atoms of a para- or ferromagnet was given in the papers of Bloch, Schwinger and, in more detail including polarization effects, by Halpern and Johnson.[1] The effects of the orbital part of the magnetic moment of the atom were included by Migdal and Trammell.[2] The analysis of the effect of slight changes in neutron energy in passing through the paramagnet, because of inelastic collisions with transition of atoms between quasi-stationary levels formed in the field of the exchange forces, was given by Van Vleck.[3] However, in addition to the inelastic scattering treated by Van Vleck, one can also have scattering with transition of the atoms of the paramagnet between Stark levels formed in the crystalline field.

In the manganese compounds used by Bendt and Brockhouse,[4] the magnetically-active shell of which is in an S state, such inelastic scattering could not be observed since, in these compounds, the exchange energy considerably exceeds the splittings produced by the Jahn-Teller effect in the crystalline field.

Here we shall look at the problem of inelastic scattering of neutrons on Stark levels. The estimates show that the differential cross section for such scattering will be of the order of tens of barns.

In this paper we consider the problem of inelastic magnetic scattering of neutrons due to dynamical processes which give rise to a transfer of energy between the spin-system and the lattice vibrations. The thermal vibrations of the lattice cause a change in the energy of interaction between the atoms of the paramagnet. As a consequence of these perturbations, there occur transitions between the levels which are formed in the electric or magnetic field of the crystal (the latter resulting from exchange interaction), with absorption of radiation of phonons of the corresponding energies. The various mechanisms for spin-lattice coupling have been treated in detail in the theory of paramagnetic relaxation.[5-7] This coupling may be the result of modulation of the magnetic dipole interaction[5] or of the electric field of the crystal[6] by elastic vibrations of the lattice. In certain paramagnets the anisotropic exchange forces[7] may play an important part in the relaxation mechanism.

We shall limit ourselves to the case most convenient for computation, in which the spin-system is an aggregate of paramagnetic atoms located in the electric field of a crystal, while the coupling between the spin-system and the lattice is achieved by modulation of the electric field by the lattice oscillations. Under the influence of thermal oscillations the atom continually carries out radiationless transitions between Stark levels. In a transition from one Stark level to another the effective magnetic moment of the atom changes. The magnetic interaction of the atom and the neutron will thus be an oscillating quantity.

In the scattering of neutrons by a paramagnet, there is a certain probability for exchange of energy between neutrons and phonons via the spin system through magnetic interaction — magnetic inelastic scattering by phonons. The classical analog of this process is the effect of change of energy of particles passing through a potential barrier whose height varies with time as $V = A \times \cos x \sin\omega t$, for $|x| \leq \pi/2$.

2. The scattering is described by the equation

$$(H_0 + H_L + H_n)\,\psi = i\hbar\frac{\partial\psi}{\partial t}, \qquad (1)$$

H_0 is the Hamiltonian for the stationary state of the atom and free motion of the neutron, H_L is the spin-lattice interaction, H_n is the magnetic interaction between atom and neutron.

To estimate the order of magnitude of the cross section we use the Van Vleck expression for the operator for H_L:[6]

$$H_L = \sum_m V^{(m)} Q_m;$$
$$Q_m = \sum_i a_{mi} q_i, \qquad V^{(m)} = \sum_i \frac{\partial V^{(m)}}{\partial q_i} \frac{\partial q_i}{\partial Q_m}, \tag{2}$$

where q_i is the normal coordinate of the lattice; Q_m is a linear combination of normal coordinates q_i which depends on the symmetry type of the crystal; a_{mi} is a coefficient depending on the direction of propagation and polarization of the vibrations. On the other hand

$$H_n = -e\mu \sum_l \frac{[\alpha_l \times (\mathbf{r}_n - \mathbf{r}_l)]}{|\mathbf{r}_n - \mathbf{r}_l|^3}, \tag{3}$$

where α_l is the operator for the current density of the l'th electron of the magnetically active shell of the atoms, $\mathbf{r}_n$, $\mathbf{r}_l$ are the radius vectors of the neutron and the l'th electron respectively, $\mu = (e^2\gamma/mc^2)\hat{\mathbf{S}}$ is the magnetic moment of the neutron.

Substituting (2) and (3) in the formula for the transition probability (cf. reference 8), we obtain for collision with absorption of a phonon,

$$W^{n_s-1,\,p}_{n_s,\,p_0} = \frac{2\pi}{\hbar} \left| \sum_{n_s \beta'} \frac{\langle \mathbf{p}_0, n_s - 1, \beta' | H_L | \mathbf{p}_0, n_s, \beta\rangle \langle \mathbf{p}, n_s - 1, \beta'' | H_n | \mathbf{p}_0, n_s - 1, \beta'\rangle}{\Delta E_{\beta\beta'} + \hbar\omega_s} + \frac{\langle \mathbf{p}, n_s \beta' | H_n | \mathbf{p}_0, n_s, \beta''\rangle \langle n_s - 1, \beta, \mathbf{p} | H_L | n_s, \beta', \mathbf{p}\rangle}{\Delta E_{\beta''\beta'} + (p_0^2 - p^2)/2M} \right|^2$$
$$\times \delta\left(\frac{p_0^2 - p^2}{2M} + \hbar\omega_s + \Delta E_{\beta\beta''}\right) d\mathbf{p},$$

where $\mathbf{p}$ is the neutron momentum, n_s the number of phonons of frequency ω_s with polarization and propagation direction s[9], and β denotes the state of the atom.

Let us restrict ourselves to the case $\beta'' = \beta$. The cross section for this scattering is obtained after integration over the momentum space $\mathbf{p}$ and averaging over all directions of polarization and propagation s of the lattice vibrations.[10]

The matrix elements of the operators H_L and H_n are independent of one another, so that the averaging can be done separately. In particular the expression

$$\frac{2\pi}{\hbar} \int |\langle \mathbf{p}, \beta' | H_n | \mathbf{p}_0, \beta''\rangle|^2 \delta\left(\frac{p_0^2 - p^2}{2M} + \hbar\omega\right) d\mathbf{p} \approx \frac{p}{p_0} \left(\frac{e^2\gamma}{mc^2}\right)^2$$

coincides with the cross section for magnetic inelastic scattering with transition of the atom from one Stark level to another, in the Born approximation.[1,2]

The matrix element of the operator H_L splits into a product of two factors, one of which depends only on the lattice variables, and the other only on the coordinates of the magnetic electrons of the atom:

$$\frac{8\pi}{\hbar} \left| \sum_{\beta',\, s,\, m} \frac{\langle a_{mi}\rangle \langle n_s - 1 | q_i | n_s\rangle \langle \beta' | V^{(m)} | \beta\rangle}{\Delta E_{\beta\beta'} + \hbar\omega_s} \right|^2.$$

After averaging, we obtain[10]

$$\{|\langle n_s - 1 | q_i | n_s\rangle|^2\}_{\mathbf{av}} = \frac{\hbar}{2\omega_s} [1 - e^{-\hbar\omega_s/kT}]^{-1}.$$

In the case of isotropy of the velocity of propagation of sound in the paramagnet,[10]

$$\langle a_{mi}^2\rangle_{\mathbf{av}} = 15\pi^2 R^2 \omega_s^2 / v_s^2,$$

where R is the interatomic spacing, v_s is the velocity of propagation of sound in the paramagnet. The matrix element $\langle \beta' | V^{(m)} | \beta\rangle$ for this mechanism of relaxation is a quantity of order e^2/R^2.

As will be shown in the following, the scattering has resonance character. The interference terms which appear in the summation over β' will not give a significant contribution to the scattering, so that the summation over β' can be omitted.

For the matrix element of the operator H_L we obtain

$$|\langle n_s - 1, \beta' | H_L | n_s, \beta\rangle|^2 \approx \frac{60\pi^2 e^4}{v_s^2 R^2} \frac{\hbar\omega}{1 - e^{-\hbar\omega/kT}}.$$

The dependence of the scattering cross section on the energy of the absorbed phonon is essentially determined by the factor $(\Delta E_{\beta\beta'} + \hbar\omega)^{-2} = \xi^{-2}$, which diverges for $\xi \to 0$. In the regions $\xi \to 0$ it becomes important to take account of the width of the levels E_β and $E_{\beta'}$ (cf., for example, reference 8, page 196). The effect of interaction of the atom with the neutron which is scattered also results in a certain distortion of the relaxation process in the neighborhood of resonance.

The interaction energies H_L and H_n are quantities of the order of 0.01 cm^{-1}. We shall restrict ourselves to values $|\xi| \gg |V_{pert}|$. In paramagnetic salts of the rare earth elements, the energy of Stark splittings is $\Delta E = 100 - 10$ cm^{-1}, $v_s \approx 10^5$ cm/sec. Taking a value $\xi = 0.1$ cm^{-1}, we obtain an order of magnitude of the cross section for one-phonon scattering in the resonance region equal to $d\sigma/d\Omega \approx 10^{-33}$ cm^2.

Modulation of the electric field by lattice vibrations with frequencies ω_s and ω_q can be represented as a modulation by the frequencies ω_s

$+ \omega_q$ and $\omega_s - \omega_q$. Thus, the change in electric field by lattice vibrations with frequencies close to the resonance ω can be caused by any two frequencies which are related by $\omega_s - \omega_q = \omega$. Therefore almost the entire spectrum of lattice vibrations participates in the two-phonon process.

For the same values of ξ, the order of magnitude of the cross section for two-phonon scattering with absorption of energy $\hbar(\omega_s - \omega_q) = \hbar q$ is given by the following expression:

$$\frac{d\sigma}{d\Omega} \approx \frac{p}{p_0}\left(\frac{e^2\gamma}{mc^2}\right)^2 \frac{215\,\pi^5 e^8 \hbar^2}{v_{зв}^7 R^4} \int \frac{\omega_s^2 - q\omega_s}{(\Delta E + \hbar\omega_s)^4} \rho_{\omega_s} d\omega_s,$$

ρ_{ω_s} is the density of oscillators of frequency ω_s. Integration over the domains of q, $\omega_{\beta\beta'} - \xi$ and $\omega_{\beta\beta'} + \xi$, ω_{max} gives the value $d\sigma/d\Omega \approx 10^{-27}$ cm^2.

The mechanism for inelastic scattering of neutrons which we have considered here is caused by dynamical processes which are studied in the theory of paramagnetic relaxation. Contributions resulting from three-or-more-phonon processes[11] have not been treated in detail in computing relaxation times.

For temperatures of the order of 300° K the values of relaxation times computed including two-phonon processes are in satisfactory agreement with experiment.

[1] F. Bloch, Phys. Rev. **50**, 259 (1936); J. Schwinger, Phys. Rev. **51**, 544 (1937); O. Halpern and M. H. Johnson, Phys. Rev. **55**, 898 (1939).

[2] A. B. Migdal, JETP **10**, 5 (1940). G. T. Trammell, Phys. Rev. **92**, 1387 (1953).

[3] J. H. Van Vleck, Phys. Rev. **55**, 924 (1939).

[4] P. J. Bendt, Phys. Rev. **89**, 561 (1953). B. N. Brockhouse, Phys. Rev. **99**, 601 (1955).

[5] I. Waller, Z. Physik **79**, 370 (1932). W. Heitler and E. Teller, Proc. Roy. Soc. **A155**, 629 (1936).

[6] J. H. Van Vleck, Phys. Rev. **57**, 426 (1940). R. de L. Kronig, Physica **6**, 33 (1939).

[7] W. Opechowski, Physica **14**, 237 (1948).

[8] W. Heitler, The Quantum Theory of Radiation, Oxford, Clarendon Press, 1954.

[9] R. E. Peierls, Quantum Theory of Solids, Oxford, Clarendon Press, 1955.

[10] Max Born and Huang-Kun, Dynamical Theory of Crystal Lattices, London, Oxford University Press, 1954.

[11] S. A. Al'tshuler, JETP **24**, 681 (1953).

Translated by M. Hamermesh
188

THEORY OF PHOTONUCLEAR REACTION ON LIGHT NUCLEI WITH EMISSION OF DEUTERONS

G. M. SHKLYAREVSKIĬ

Leningrad Physico-Technical Institute, Academy of Sciences, U.S.S.R.

Submitted to JETP editor April 30, 1960

J. Exptl. Theoret. Phys. (U.S.S.R.) 39, 1031-1038 (October, 1960)

A theory of the γd reaction on light nuclei is developed within the framework of the independent-pair model in the small correlator approximation. The mechanism of excitation of the product nucleus through rapid variation of the self-consistent field of the nucleus in the emission of a pair of nucleons is considered, and the probability of excitation in the region of the continuous spectrum is calculated for the case of independent particles. Correct values for the γd cross sections on light nuclei and the shapes of the energy spectra and angular distributions can be obtained by using the literature values of the parameters involved in the theory.

1. Several experiments on a detailed investigation of the γd reaction on several light nuclei have been recently reported.[1-3] The most interesting results are the large ratios of the cross sections, $\sigma_{\gamma d}/\sigma_{\gamma p}$, and the indication that transitions with excitation of the product nucleus of the reaction make a considerable contribution.

We thought it interesting to investigate the characteristic features of the γd reaction on light nuclei, using existing ideas concerning the structure of atomic nuclei. In the present paper we use the independent-pair model[4,5] to formulate a theory of the γd reaction for light nuclei. In this model we consider, in addition to the general self-consistent field, also the pair interaction that lead to correlations of the nucleon motion. The wave function of the nucleus can be written in the independent-pair model in the form*

$$\Psi = |\psi_{\alpha_1}(1)\psi_{\alpha_2}(2)\ldots\psi_{\alpha_n}(n)|(1+\Sigma\chi_{ij}), \qquad (1)$$

where ψ_{α_i} (i = 1, 2, ...n) are the single-particle wave functions, and χ_{ij} are the correlators. The small-correlator approximation is used: $\chi_{ij} \ll 1$ at distances on the order of the mean distance between the nucleons of the nucleus.

The theory proposed is based on the assumption that the deuteron is produced in the γd reaction as a result of the interaction between a proton which has absorbed a γ quantum, and a neutron which is in the s state relative to the proton. Since the interaction is accounted for exactly in the independent-pair model (at least in principle), this interaction, which is responsible for the emission of the deuterons, is considered in the theory of the γd reaction with sufficient accuracy even in the wave function of the nucleus.

The transition of the product nucleus of the reaction to the excited state is investigated in the approximation of the model of independent particles, and the results of this part of the investigation are preliminary.

2. We write down the Hamiltonian of the initial nucleus in the form

$$H(1, 2, \xi) = H_f + V_c = H_c(\xi) + H(1, 2) + V_c(1, 2, \xi). \qquad (2)$$

Here $H(1, 2) = T_1 + T_2 + V_{12}$, where $T_{1,2}$ are the kinetic energies of the two separated nucleons, V_{12} is their interaction, H_C is the Hamiltonian of the remaining A − 2 nucleons of the nucleus, ξ are the coordinates and other variables of the remaining A − 2 nucleons, and V_C is the interaction between the separated nucleon pair and the remaining ones. The operator of interaction between the gamma quantum and the nucleus is denoted H_ζ. We introduce $\Psi_0 = \Psi^A|1\zeta)$, where Ψ^A is the wave function of the ground state of the initial nucleus and $|1\zeta)$ is the state of the electromagnetic field with one photon of energy $\hbar\omega$ and polarization ζ. In the final state there is a deuteron and residual nucleus, but no photons. The assembly of eigenfunctions of the free Hamiltonian H_f will be denoted $\Phi_f \equiv \Phi^{E*}\Phi^d$, where Φ^{E*} is the wave function of the final nucleus (E* is its excitation energy) and Φ^d is the wave function of the deuteron.

*In formulas (1), (11), and (12) the vertical lines denote normalization and antisymmetrization, i.e., the operation $(N!)^{-1/2}$ Det |...|, where N is the number of particles in the system.

We introduce also the state vector $\chi^{(-)}$ in accordance with the equation $\chi^{(-)} = \Phi_f + (E - H - i\epsilon)^{-1} \times V_c \Phi_f$. Then, as was shown by Gell-Mann and Goldberger,[6] the cross section of the reaction, is given in first order in H_ζ by

$$d\sigma = 2\pi\hbar^{-1}\, \mathfrak{S}\, |(\chi^{(-)}|\, H_\zeta |\, \Psi_0)|^2 \rho\, (E_d, E^*), \qquad (3)$$

where ρ is the density of the final states of the system and $\mathfrak{S}$ denotes averaging over the initial states and summation over the final ones.

Stapp has shown[7] that the non-diagonal matrix elements of the interaction $V_c(1, 2, \xi)$ are small; neglecting these, we obtain $\chi^{(-)} = \Phi^{E^*}\, \Phi^{d(-)}$, where $\Phi^{d(-)}$ is the deuteron wave, distorted by the potential V_c. Further, separating the state of the pair of nucleons of the initial nucleus (see Sec. 3), we can represent Ψ^A in a form $\Sigma M_q \Psi^{A-2}_q \Psi^2_q$ [q is the totality of the parameters $\alpha' \alpha_0\, J' J_0$ that enter in formula (4)]. In view of the fact of H_ζ is a single-particle operator, i.e., $H_\zeta = \Sigma_i H_{\zeta i}$, we obtain

$$(\chi^{(-)}|\, H_\zeta |\, \Psi_0) = \sum_{qi} M_q\, (\Phi^{E^*}|\, \Psi^{A-2}_q)\, (\Phi^{d(-)}|\, H_{\zeta i}|\, \psi^2_q),$$

i.e., the transition matrix elements for the nucleon pair are separated from those for the residual nucleus.

Several remarks are in order regarding the mechanism of excitation of the final nucleus. It is clear that in any nuclear model in which the individuality of the nucleons is retained* a direct interaction with a γ quantum does not lead to excitation of the final nucleus, in view of the single-particle form of the operator H_ζ; the excitation is due to the interaction between the residual nucleus and the emitted particle. We have neglected above the non-diagonal elements of the interaction V_c, and it may appear therefore that an investigation of the excitation process is impossible. This is not so, however. It is important that the self-consistent fields in the initial and in the final states are different from each other (for example, the radius of the potential changes). A sufficiently rapid change in the field of the nucleus upon emission of a pair of nucleons leads to the possibility of excitation of the residual nucleus of the reaction.

The matrix element $(\Phi^{E^*}|\, \Psi^{A-2})$ has a form corresponding to the sudden-perturbation approximation; the condition for the applicability of this approximation is that the time of variation of the potential be small compared with the characteristic nuclear period $\tau_0 \sim 10^{-21}$ sec. It is apparently reasonable to assume that the time τ of the variation of the potential is close to the time of transition of the nucleon pair to the excited state. Then $\tau \sim \hbar/\Delta E$, where ΔE is the change in the energy of the nucleon pair. In the cases of interest to us, $\Delta E \gtrsim 40$ Mev, therefore $\tau \sim 10^{-23}$ sec, i.e., the condition indicated above is sufficiently well satisfied.

3. The wave function of the target nucleus can be constructed by the method outlined in the review of Elliot and Lane.[8] Using the parentage-coefficient technique and carrying out the necessary reshuffling of the momenta, we obtain for the configuration $s^{n_1}[\lambda_1]\, p^{n_2}[\lambda_2]$ the following expression (see reference 8 for the notation):

$$\Psi^A_{jm\, TM_T} = \sum_{\alpha'\alpha_0} R_{\alpha'\alpha_0} \sum_{J'J_0} \begin{pmatrix} L' & L_0 & L \\ S' & S_0 & S \\ J' & J_0 & j \end{pmatrix} \{\Psi^{A-2}_{\alpha' J'},\ \psi^{l_1 l_2 \alpha_0}_{J_0 M_0}\}_{jm\, TM_T}. \qquad (4)$$

Here $\psi^{l_1 l_2 \alpha_0}_{J_0 M_0}$ is the wave function of the separated pair:

$$\psi^{l_1 l_2 \alpha_0}_{J_0 M_0} = \sum C^{J_0 M_0}_{L_0 \Lambda_0 S_0 \Sigma}\, |\, n_1 l_1 n_2 l_2;\ L_0 \Lambda_0)\, \chi_{S_0 \Sigma} \omega_{T_0 \tau},$$

$$|\, n_1 l_1 n_2 l_2;\ L_0 \Lambda_0) = \sum C^{L_0 \Lambda_0}_{l_1 m_1 l_2 m_2}\, |\, n_1 l_1 m_1)\, |\, n_2 l_2 m_2)\, f_{12};$$

$l_{1,2}$ are the orbital momenta of the separated nucleons. Formula (4) does not contain the correlators χ_{1j} and χ_{2j} ($j = 3, \ldots$); it is shown in the Appendix that their contribution to the reaction cross section can be neglected.

We know[9] that the wave functions of relative motion and of the motion of the center of gravity of the pair of nucleons are separated, if $|n l m)$ are oscillator functions:*

$$n_1 l_1 n_2 l_2;\ L_0 \Lambda_0) = \sum_{nlNL} (n_1 l_1 n_2 l_2;\ L_0\, |\, nlNL;\ L_0)\, |\, nlm;\ \mathbf{r})\, f_{12}\, |\, NL\Lambda;\ \mathbf{R}). \qquad (5)$$

We assume the correlation function in the same form as given by Dabrowski:[10]

$$f(r) = 0, \qquad r < r_c;$$

$$f(r) = 1 - \exp\{-\beta[(r/r_c)^2 - 1]\}, \qquad r \geqslant r_c, \qquad (6)$$

where r_c is the radius of the "hard core" of the nucleon and β is a numerical parameter, which determines the correlation radius. According to reference 10, $\beta = 0.75$ to 2.00. Numerical calculations show that our final results are not very sensitive to the choice of the parameter β.

The motion of the center of gravity of the pair is determined in the assumed approximation only by the self-consistent field of the nucleus, and is described by the wave functions $|NL_0\Lambda_0;\ \mathbf{R})$.

*Unlike Migdal's or Goldberger and Teller's model of dipole oscillations, for example.

*We note that the Bethe-Goldstone equation actually admits of this separation only approximately, even in the oscillator potential.

Choosing the deuteron wave function φ_d according to Hulthen and Sugawara,[11] and assuming, as customary, that the interaction V_c depends only on the coordinate $\mathbf{R}$, of the center of gravity of the deuteron, we obtain

$$\Phi^{d(-)} = \Phi^d_{1\mu}\Phi^{(-)}_{K_0}, \qquad \Phi^d_{1\mu} = \varphi_d(\mathbf{r})\,\chi_{1\mu}\omega_{00},$$

where $\Phi^{(-)}_{K_0}$ is the wave function of the motion of the center of gravity of the deuteron (we neglect the D state of the deuteron).

The states of the final nucleus will be denoted by the quantum numbers $X'' \equiv J'', M'', T'', L'', S'', \lambda_1'', \lambda_2''$. See Sec. 4 concerning the total assembly of final states.

Neglecting in H_ζ the terms containing the magnetic moments of the nucleons, we have

$$H_\zeta = \mathbf{B}\sum_{i=1}^{A} e^{i\varkappa\mathbf{r}_i}\nabla_i O_+, \qquad \mathbf{B} = \frac{i\hbar e}{m}\sqrt{\frac{2\pi\hbar}{c\omega}}\,\zeta, \tag{7}$$

where m and $\mathbf{r}_i$ are the mass and coordinate of the nucleon, $\varkappa$ is the wave vector of the photon, and O_+ is the projection operator for the proton. We shall not carry out any further deviations here, but merely note that the contributions of the terms with different L_0 in Eq. (4) to the cross section of the reaction are incoherent.

As a final result we obtain (writing out only the term that makes the main contribution)

$$\begin{aligned}\mathfrak{S}\,|(\chi^{(-)}\,|\,H_\zeta\,|\,\Psi_0)|^2 &= \frac{1}{16}n_2(n_2-1)\sum_{J_0}\begin{pmatrix} L'' & 2 & L \\ S'' & 1 & S \\ J'' & J_0 & j\end{pmatrix}^2 \\ &\times\Big|\sum_{\widetilde{\alpha}_2} U(L_1\widetilde{L}_2L2;L''L_2)\,U(S_1\widetilde{S}_2S1;\,S''S_2)\,U(T_1\widetilde{T}_2T0;T''T_2) \\ &\times(p^{n_2-2}\,|\,\}\,p^{n_2})\,\delta_{L_02}\,(\Phi^{E^*}_{X''}|\,\Psi^{A-2})^2\Big|\frac{1}{2L_0+1}\sum_{\Lambda_0}|\,G_{02\Lambda_0}|^2\,g^2(\varkappa) \\ &+\ldots\ldots\end{aligned} \tag{8}$$

Here

$$g(\varkappa) = (\varphi_d\,|\exp i\varkappa\mathbf{r}/2\,|\,000;\,\mathbf{r}),$$

$$C_{NL_0\Lambda_0} = (\Phi^{(-)}_{K_0}\,|\exp(i\varkappa\mathbf{R})\,\mathbf{B}\nabla|\,NL_0\Lambda_0;\,\mathbf{R}), \qquad \widetilde{\alpha}_2 \equiv \widetilde{L}_2\widetilde{S}_2\widetilde{T}_2.$$

Substituting (8) in (3) we obtain the reaction cross section for the case when a photon of energy E_γ is absorbed, a deuteron of energy E_d is emitted, and the nucleus remains in one of the states of the complete assembly [see formula (12)] with excitation energy E*. In fact, the target is exposed to a bremsstrahlung spectrum having an end-point energy $E_{\gamma\,max}$ and a gamma-quantum distribution N_γ over the spectrum; the state of the final nucleus is not fixed. It is therefore necessary to integrate the cross section over the spectrum N_γ, to sum over all possible states of the final nucleus with given excitation energy, and to integrate over all the distributions of this energy between the excited particles and over the emission angles. Finally, bearing in mind experiments with the accelerator bremsstrahlung spectrum, it is also necessary to normalize the cross section for the "effective quantum." Only after performing all these operations do we obtain a quantity comparable with experiment.

4. We denote all the operations indicated at the end of the last section (with the exception of integration over the spectrum of the gamma quanta) by the symbol $\mathfrak{S}_f$ and calculate the quantity

$$\mathfrak{S}_f\,|(\Phi^{E^*}_{X''}|\,\Psi^{A-2})|^2\,\rho(E^*).$$

We consider first the excitation of one particle in an abruptly-changing potential. We denote by ψ_{nlm} the initial (bound) state and by $\varphi_{El'm'}$ the total assembly of the states of the particle in the changed potential.* We carry out the expansion†

$$\psi_{nlm} = \sum c^{nlm}_{n'l'm'}\varphi_{n'l'm'} + \sum\int c^{nlm}_{El'm'}\varphi_{El'm'}\,dE \tag{9}$$

$$\sum\Big|c^{nlm}_{n'l'm'}\Big|^2 + \sum\int\Big|c^{nlm}_{El'm'}\Big|^2\,dE = 1. \tag{10}$$

Then

$$(\varphi_{El'm'}\,|\,\psi_{nlm}) = c^{nlm}_{El'm'}\delta_{ll'}\delta_{mm'} \equiv c_{nl}(E),$$

i.e., the orbital momentum and its projection remain unchanged in the transition. Since the dimensions of the potential well in a light nucleus are such that the unoccupied states with the same values of l as the occupied ones but with greater principal quantum numbers lie in the region of the continuous spectrum, the first sum in (10) actually contains only one term with $n' = n$.

We now consider a system of h independent particles, in individual states nlm_i ($\equiv ns_i$), $i = 1, 2, \ldots h$. The wave function of this system has the form‡

$$\Psi = |\,\psi_{ns_1}(1)\,\psi_{ns_2}(2)\ldots\psi_{ns_h}(h)\,|. \tag{11}$$

The complete system of final states $\Phi^{E^*}_{X''}$ in the new potential, as can be readily verified, has the form

$$\begin{aligned}&\Phi_0 = |\,\varphi_{ns_1}(1)\,\varphi_{ns_2}(2)\ldots\varphi_{ns_h}(h)\,|, \\ &\Phi_{E_1s_1} = |\,\varphi_{E_1s_1}(1)\,\varphi_{ns_2}(2)\ldots\varphi_{ns_h}(h)\,|, \\ &\Phi_{E_2s_2} = |\,\varphi_{ns_1}(1)\,\varphi_{E_2s_2}(2)\ldots\varphi_{ns_h}(h)\,|,\ \ldots, \\ &\Phi_{E_1s_1E_2s_2} = |\,\varphi_{E_1s_1}(1)\,\varphi_{E_2s_2}(2)\,\varphi_{ns_3}(3)\ldots\varphi_{ns_h}(h)\,|, \\ &\Phi_{E_1s_1E_3s_3} = |\,\varphi_{E_1s_1}(1)\,\varphi_{ns_2}(2)\,\varphi_{E_3s_3}(3)\ldots\varphi_{ns_h}(h)\,|\ldots.\end{aligned} \tag{12}$$

*For a discrete spectrum, E will be replaced by n'.

†The φ_{Elm} are normalized here to $\delta(E-E')$.

‡Formulas (11) and (12) contain certain linear combinations of the determinants corresponding to a definite J', L", etc. This, however, does not change the results.

Using formulas (10)—(12), we obtain

$$\mathfrak{S}_f |(\Phi^{E^*} | \Psi^{A-2})|^2 \rho(E^*) = |c_{nl}|^{2h} \delta_{E^*0} + 4\pi \binom{h}{1} |c_{nl}|^{2(h-1)} |c_{nl}(E^*)|^2 \times (4\pi)^2 \binom{h}{2} |c_{nl}|^{2(h-2)} \int |c_{nl}(E_1) c_{nl}(E_2)|^2 \delta(E^* - E_1 - E_2) dE_1 dE_2 + \ldots \quad (13)$$

For a real nucleus with a ground-state configuration $s^{n_1'} p^{n_2'}$ ($n_1' + n_2' = A - 2$) we readily obtain a somewhat more complicated, but clearly analogous expression. The estimate obtained here for the probability of the product-nucleus excitation is approximate; we hope to consider in the future the effect of the correlation of the nucleon and the probability of excitation of the nucleus due to a sudden change in the potential.

We have used oscillator functions to calculate c_{nl}, while perturbation theory (since the change in potential $V = V^A - V^{A-2}$ is sufficiently small) with a rectangular potential well of finite depth has been used to calculate $c_{nl}(E^*)$. These expressions are reconciled by the normalization condition (10). As a result we obtain the following formulas

$$|c_{0l}|^2 = (1 - \delta^2)^{3/2+l} \qquad (\delta = (\omega_{01} - \omega_{02}) / (\omega_{01} + \omega_{02})), \quad (14)$$

$$|c_{0l}(E^*)|^2 \approx \tfrac{3}{2} E_0^{3/2} (1 - |c_{0l}|^2) / E^{*3/2}, \quad (15)$$

where $\omega_{01,02}$ are the parameters of the wave functions of the nucleons in the initial and final nuclei, respectively, and E_0 is the energy of particle detachment in the nucleus.

5. Let us consider in somewhat greater detail the calculation of the matrix elements $G_{NL_0\Lambda_0}$ in formula (8). We describe the interaction between the deuteron and the residual nucleus by means of an optical potential $U_d(R)$:[12]

$$U_d(R) = 0, \quad R > R_0; \quad U_d(R) = -V_0 - iW_0, \; R \leqslant R_0. \quad (16)$$

Unfortunately, our knowledge of the potential U_d is quite limited. Following Greider,[12] we assume the value of V_0 to be the same as for nucleons of corresponding energy. Comparison with experiment can indicate the necessary values of the imaginary part of the potential W_0.

It is desirable to take account in (8) of the electric dipole transitions with sufficient accuracy (since they make the main contribution to the cross section) and to determine simultaneously the remaining multipoles in the Born approximation. For this purpose we retain in the expansion in partial waves

$$\Phi_{\mathbf{K}_0}^{(-)} = (2\pi)^{-3/2} \left\{ e^{i\mathbf{KR}} + \sum_{l'} \sqrt{4\pi(2l'+1)} [e^{-i\delta_{l'}} A_{l'} - 1] j_{l'}(KR) i^{l'} Y_{l'0}(\cos\theta) \right\}$$

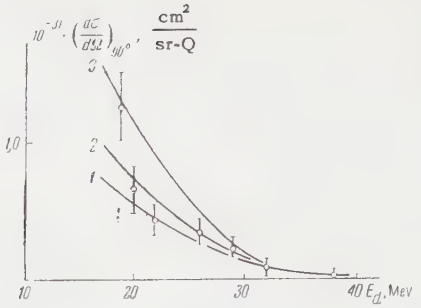

FIG. 1. Results of the calculation for C^{12}. Curve 1 – transitions without change in the configuration of the nucleus; curve 2 – transitions with allowance for single-particle excitations, curve 3 – with allowance for two-particle excitations. The parameters $\hbar\omega$ were calculated from the rms radii of the corresponding nuclei:[16] $\hbar\omega(C^{12}) = 15.2$ Mev, $\hbar\omega(B^{10}) = 17.0$ Mev, $E_{\gamma\,max} = 80$ Mev.

only the terms with $l' = L_0 \pm 1$. The phase shifts $\delta_{l'}$ were calculated from the approximate formulas of Pargamanik and Ul'yanov,[13] which are sufficiently accurate when $E_d \gtrsim 15$ Mev.

6. Comparison with experiment has been made for the nuclei C^{12} and Be^9. Chizhov and Kul'chitskiĭ[1,2] give the ratio $\sigma_{\gamma d}/\sigma_{\gamma p}$. The value of $\sigma_{\gamma d}$ was determined from the known cross section of the reaction $C^{12}(\gamma p)$ at the corresponding values of $E_{\gamma\,max}$,[14] as well as from the experimental fact[2] that the cross section of the γp reaction is proportional to Z at low values of Z.

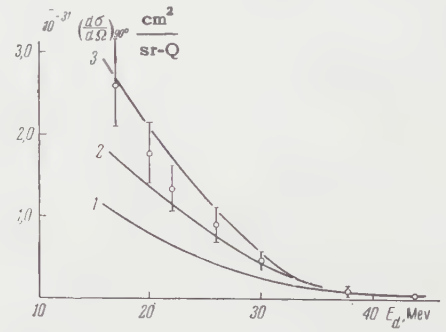

FIG. 2. Results of the calculation for Be^9. The notation is the same as in Figure 1. $\hbar\omega(Be^9) = 16.2$ Mev, $\hbar\omega(Li^7) = 18.9$ Mev, $E_{\gamma\,max} = 90$ Mev.

The following values were assumed for the potential (16): $U_d = (-40 - 20i)$ Mev and $R = 1.5A^{1/3} \times 10^{-13}$ cm. The results of the calculations and the experimental data are shown in Figs. 1—3. Only single- and two-particle excitations of the final nuclei were considered.

It is seen first that transitions with excitations of the final nucleus actually make a large contribution in the region of the continuous spectrum: this contribution is approximately equal, in the case of C^{12}, to the contribution due to transitions to the ground state and weakly-excited (discrete)

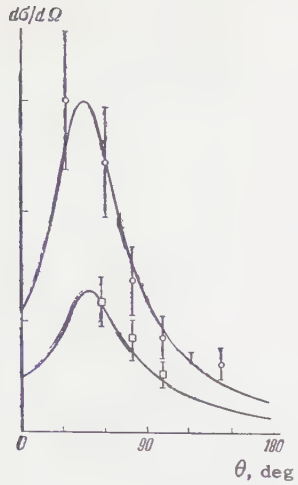

FIG. 3. Angular distributions of the reactions $C^{12}(\gamma\, d)$ and $Be^{9}(\gamma\, d)$. Normalized for $\theta = 60°$ ○ – Be^{9}, □ – C^{12} (the ordinates are arbitrary).

states; it is even greater for Be^{9}. The reason is that while the threshold of the reaction $Be^{9}(\gamma d)$ is approximately 9 Mev lower than that of C^{12}, the experiment was carried out at values of $E_{\gamma\,max}$ which were 10 Mev higher. One might think that experiments on the behavior of $\sigma_{\gamma d}$ as a function of $E_{\gamma\,max}$, or on the deuteron spectrum in the irradiation of nuclei by monochromatic gamma quanta, can be useful in the study of the mechanism of excitation of final nuclei in direct reactions.

The imaginary part of the potential U_d is assumed to be quite large (this agrees with other data[12,15]). In this connection, the contribution to the cross section $\sigma_{\gamma d}$ of the reaction comes essentially only from the pairs whose center of gravity has an orbital momentum $L_0 = 2$; the contribution of the remaining pairs is one order of magnitude less.

It remains also to note that the cross section $\sigma_{\gamma d}$ is little sensitive to changes in the parameters of the correlation function; consequently photoreactions with emission of deuterons cannot, unfortunately, be used to investigate the correlations of nucleons in atomic nuclei. However, the very presence of the correlator χ_{12} is significant; if neglected, the computed cross section is changed by 15 – 30% in the energy range of interest to us.

In conclusion, I am grateful to S. V. Maleev, A. D. Piliya and Professor L. A. Sliv for discussing the work and for critical remarks, and also to V. P. Chizhov for evaluating the experimental data.

APPENDIX

We consider the matrix element* of the transition to the ground state

$$M_{12}=\Big(\varphi_d(1,2)\,\psi_{\alpha_3}(3)\ldots\psi_{\alpha_n}(n)\Big(1+\sum_{i,j\geqslant 3}\chi_{ij}\Big)\Big|\,H_{12}\,\Big|\,\psi_{\alpha_1}\times(1)\ldots\psi_{\alpha_n}(n)\Big(1+\sum\chi_{ij}\Big)\Big).$$

We leave out here the correlators between nucleons 1 or 2 and the remaining nucleons in the final state, since it is assumed that the interaction is described by the potential U_d. It is readily seen that in view of the property[5] $(\psi_{\alpha i}\,\psi_{\alpha j}|\,\chi_{ij}|\,\psi_{\alpha_i}\,\psi_{\alpha_j})\equiv 0$ and the assumed smallness of the correlators, under which the terms containing products of two or more correlators are omitted, the terms with $i, j \geq 3$ make no contribution. Using the expansion

$$\psi_{\alpha_i}\psi_{\alpha_j}\chi_{ij}=\sum_{mn}c_{mn}^{ij}\psi_{\alpha_m}\psi_{\alpha_n}\qquad (c_{mn}^{ij}\equiv 0 \quad \text{for} \quad i,j=m,n),$$

we obtain

$$M_{12}=(\varphi_d(1,2)\,|\,H_{12}\,|\,\psi_{\alpha_1}(1)\,\psi_{\alpha_2}(2)\,(1+\chi_{12}))+\sum_{i\geqslant 3}\sum_{mn}c_{mn}^{1i}\,(\varphi_d(1,2)\,|\,H_{12}\,|\,\psi_{\alpha_m}(1)\,\psi_{\alpha_2}(2))\,\delta_{n\alpha_i}+\sum_{j\geqslant 3}\sum_{mn}c_{mn}^{2j}\,(\varphi_d(1,2)\,|\,H_{12}\,|\,\psi_{\alpha_1}(1)\,\psi_{\alpha_m}(2))\,\delta_{n\alpha_j}.$$

An estimate with aid of (6) yields $\Sigma_{mn}|\,c_{mn}^{ij}\,|^2 \lesssim 0.04$. Since a contribution to M_{12} is made only by a few of the coefficients c_{mn}^{1i} (or c_{mn}^{2j}), and, on the other hand, since the probability of finding nucleons 1 and 2 in the s state of relative motion diminishes rapidly with increasing quantum number α_m, the contribution of the correlators χ_{1m} and χ_{2n} to the cross section, as can be seen from a numerical estimate, does not exceed 1 or 2%; the same pertains to transitions to excited states.

*We disregard here effects connected with the change of the potential of the nucleus upon emission of a deuteron.

[1] V. P. Chizhov and L. A. Kul'chinskiĭ, JETP **36**, 345 (1959), Soviet Phys. JETP **9**, 239 (1959).
[2] V. P. Chizhov, JETP **38**, 809 (1960), Soviet Phys. JETP **11**, 587 (1960).
[3] de Wire, Silberman, and Wolfe, Phys. Rev. **92**, 519 (1953).
[4] A. de-Shalit and V. Weisskopf, Ann. Physik, **5**, 266 (1958).
[5] R. Eden and V. Emery, Proc. Roy. Soc. **248**, 266 (1958).
[6] M. Gell-Mann and M. Goldberger, Phys. Rev. **91**, 398 (1953).
[7] H. Stapp, Phys. Rev. **107**, 607 (1957).
[8] T. Elliot and A. Lane, Handbuch der Physik, Springer-Verlag, Berlin, **39**, (1957).
[9] I. Talmi, Helv. Phys. Acta **25**, 185 (1952).
[10] J. Dabrowski, Proc. Phys. Soc. **A71**, 658 (1958).
[11] L. Hulthen and M. Sugawara, Handbuch der Physik, Springer-Verlag, Berlin, **39**, (1957).
[12] K. Greider, Phys. Rev. **114**, 786 (1959).

[13] L. E. Pargamanik and V. V. Ul'yanov, JETP **35**, 258 (1958), Soviet Phys. JETP **8**, 177 (1959).
[14] E. B. Bazhanov, JETP **37**, 374 (1959), Soviet Phys. JETP **10**, 267 (1960).
[15] I. Slaus and W. Alford, Phys. Rev. **114**, 1054 (1959).
[16] R. Hofstadter, Ann. Rev. Nucl. Sc. **7**, 231 (1957), Meyer-Berkhout, Ford, and Green. Ann. Phys. **8**, 119 (1959).

Translated by J. G. Adashko
189

ELASTIC RESONANCE SCATTERING OF SLOW NEUTRONS IN CRYSTALS

M. V. KAZARNOVSKIĬ and A. V. STEPANOV

P. N. Lebedev Physics Institute, Academy of Sciences, U.S.S.R.

Submitted to JETP editor May 3, 1960; resubmitted July 28, 1960

J. Exptl. Theoret. Phys. (U.S.S.R.) **39**, 1039-1041 (October, 1960)

Formulas are derived for the differential cross section for elastic resonance scattering of slow neutrons in crystals. The expressions obtained are evaluated in the Debye approximation.

THE resonance interaction of slow neutrons in crystals was first treated theoretically by Lamb[1], who computed the shape of the resonance absorption line for neutrons. (A presentation of this work[1] is also given in the book by Akhiezer and Pomeranchuk.[2])

In an analogous way Mössbauer[3] treated resonance scattering of γ quanta in crystals. In these papers it was shown in particular that experiments of this sort can serve as a method for analyzing the dynamical properties of a crystal. In this connection it may also be important to investigate elastic scattering (without change of the quantum state of the crystal lattice) of neutrons by nuclei (such as Xe^{135}, Yb^{168}, Tm^{169}, Hf^{177}, Re^{185}, Au^{197}, Pu^{240}) which have levels with resonance energies less than or of the order of a few ev and relatively large ratio of neutron width to total width of the level ($\gtrsim 0.1$).

The expression for the probability of elastic resonance scattering of neutrons in a crystal, following Lamb and neglecting the dependence of the total width of the resonance level Γ on the quantum state of the lattice, and also neglecting potential scattering,* can be written, except for a trivial constant factor, in the form

$$W=\overline{\left[\left|\sum_{\{n_s\}}\sum_{l}\frac{\langle \mathbf{p}\{n_s^0\}A_l|H_l|\{n_s\}C_l\rangle\langle\{n_s\}C_l|H_l|\mathbf{p}_0\{n_s^0\}A_l\rangle}{p^2/2m-E_0-\sum_s\hbar\omega_s(n_s-n_s^0)+i\Gamma/2}\right|^2\right]}. \tag{1}$$

Here $\mathbf{p}_0$ and $\mathbf{p}$ are the momenta of the neutron before and after scattering, m is the neutron mass, $\{n_s^0\}$ and $\{n_s\}$ are respectively the occupation numbers for the phonons in the initial (or final) and intermediate state, where ω_s and $\mathbf{e}_s$ are respectively the frequency and polarization of the phonon of type s, H_l is the operator for the interaction of the l'th nucleus with the neutron, the symbols A and C denote respectively the initial and compound nucleus, E_0 and Γ are the energy and width of the resonance. A bar over a symbol denotes averaging with respect to the initial state of the crystal.

Writing the denominator of (1) as an integral

$$-i\int_0^\infty dt\exp\left\{-it\left[\sum_s\hbar\omega_s(n_s-n_s^0)+E_0-\frac{p^2}{2m}-i\frac{\Gamma}{2}\right]\right\}$$

and using Lamb's result, we can by simple computations reduce the expression for W to the form

$$W=|M_{\mathbf{f}}|^2\,\overline{|P|^2}\,\Big|\sum_l\exp[i\mathbf{r}_l^0\times(\mathbf{p}_0-\mathbf{p})]\Big|^2e^{-2W_T}, \tag{2}$$

$$P=\int_0^\infty dt\exp\left\{it\left(\frac{p^2}{2m}-E_0\right)-\tfrac{1}{2}\Gamma t+g(t)\right\}, \tag{3}$$

$$g(t)=\sum_s\frac{(\mathbf{p}\mathbf{e}_s)(\mathbf{p}_0\mathbf{e}_s)}{2MN\hbar\omega_s}\left[(n_s^0+1)e^{-i\hbar\omega_st}+n_s^0e^{i\hbar\omega_st}-2n_s^0-1\right], \tag{4}$$

where M_f is the matrix element corresponding to scattering of the neutron by the free nucleus, M is the mass of the nucleus, N is the number of nuclei per unit volume of the crystal, and

$$W_T=\tfrac{1}{2}\sum_s|(\mathbf{p}_0-\mathbf{p})\mathbf{e}_s|^2\left[\bar{n}(\omega_s)+\tfrac{1}{2}\right]/MN\hbar\omega_s,$$

$$\bar{n}(\omega_s)=[\exp(\hbar\omega_s/kT)-1]^{-1} \tag{5}$$

is the temperature exponent and T is the temperature of the crystal.

We note that the imaginary part of the forward scattering amplitude (which is proportional to Re P for $\mathbf{p}=\mathbf{p}_0$), in accordance with the optical theorem, coincides with the total cross section.[1] It is easy to verify that, averaging $|P^2|$ over the initial state of the crystal reduces to replacing n_s^0 in g(t) by $\bar{n}(\omega_s)$. [We denote the corresponding g(t) by $\bar{g}(t)$.]

Thus, while a measurement of total cross section (or absorption cross section) gives us a de-

*Including potential scattering reduces to simply adding the amplitudes for resonant and potential scattering.

termination of $\mathrm{Re}\,\bar{P}$ for $\mathbf{p} = \mathbf{p}_0$, the investigation of elastic scattering enables us to determine $\overline{|P|^2}$ for any angles between $\mathbf{p}$ and $\mathbf{p}_0$.

Let us evaluate $\overline{|P|^2}$ in the Debye approximation. Then

$$\bar{g}(t) = \frac{3}{2}\frac{\hbar^2 p_0^2}{Mk^3\Theta^3}\cos\varphi \int_0^{k\Theta/\hbar} \{[1+\bar{n}(\omega)]e^{-it\hbar\omega} + \bar{n}(\omega)e^{it\hbar\omega} - 2\bar{n}(\omega) - 1\}\,\omega\,d\omega, \tag{6}$$

where Θ is the Debye temperature and φ is the scattering angle. An analogous expression for $\varphi = 0$ determines the cross section for absorption of neutrons; it was considered by Lamb.[1] Lamb's results can be used completely if $\cos\varphi > 0$. The case of $\cos\varphi < 0$ requires special treatment, since the formal expansion of $\bar{g}(t)$ in powers of t used by Lamb leads to diverging integrals.

If $|\bar{g}(t)| \lesssim 1$, the value of W depends essentially on the parameter $\gamma = \sqrt{[(E_0 - p^2/2m)^2 + \Gamma^2/4]}/k\Theta$. For $\gamma \gg 1$, the important region in (3) is at small values of t, $\bar{g}(t)$ can be expanded in powers of t, and we can limit ourselves to the first term in the expansion. Then

$$P = [\Gamma/2 + i(E_0 - p^2/2m + \cos\varphi\, p^2/2M)]^{-1}. \tag{7}$$

Thus W depends exponentially on $(\mathbf{p}_0 - \mathbf{p})^2$. If $\gamma \ll 1$, then the quantities which are important in (3) are large values of t, and we can in the expression (6) for $\bar{g}(t)$ neglect the rapidly oscillating terms under the integral sign. Then

$$P = [\Gamma/2 + i(E_0 - p^2/2m)]^{-1} \exp\left\{-\frac{3}{2}\frac{\hbar^2 p_0^2}{Mk^3\Theta^3}\cos\varphi \int_0^{k\Theta/\hbar} [2\bar{n}(\omega)+1]\,\omega d\omega\right\}. \tag{8}$$

Substituting (8) in (2) and using the fact that in the Debye approximation

$$W_T = \frac{3}{4}(\mathbf{p}_0 - \mathbf{p})^2 \frac{\hbar^2}{Mk^3\Theta^3}\int_0^{k\Theta/\hbar} [2\bar{n}(\omega)+1]\,\omega d\omega,$$

[cf. Eq. (5)], we obtain

$$W = |M_f|^2 [\Gamma^2/4 + (p^2/2m - E_0)^2]^{-1} \times \exp\left\{-\frac{3}{2}\frac{p^2}{M}\frac{\hbar^2}{k^2\Theta^3}\int_0^{k\Theta/\hbar} [2\bar{n}(\omega)+1]\,\omega d\omega\right\},$$

i.e., W depends only on the energy of the incident neutron. Such a result is a consequence of the fact that in the last case the nucleus stays in the excited state for a long time, during which it "forgets" the direction of the momentum of the incident neutron.

Now let us consider the more complicated case when g_0 — the maximum value of $\bar{g}(t)$ — is much greater than unity. Then $\overline{|P|^2}$ depends essentially on the ratio of the quantities γ and g_0. Namely, if $\gamma \gg g_0$, we again easily obtain formula (7). If, however, $\gamma \ll g_0$, then P can be computed by the saddle-point method. The result is

$$\overline{|P|^2} = 2\pi a^{-2}\exp\{2\mathrm{Re}\, f(t_0)\}, \qquad a^2 = |d^2 g(t)/dt^2|_{t=t_0},$$

where t_0 is the value of t corresponding to the maximum of the function

$$f(t) = g(t) + it(p^2/2m - E_0) - \Gamma t/2.$$

Since it does not appear possible to compute the integral (3) in general form, we shall limit ourselves in the calculation of $f(t_0)$, t_0 and a^2 to the limiting cases $T \gg \Theta$, for which

$$\bar{g}(t) \approx -3\cos\varphi\,(p^2 T/Mk\Theta^2)[1 - (k\Theta t)^{-1}\sin(k\Theta t)],$$

and $T = 0$, for which

$$\bar{g}(t) = -\frac{3}{4}\cos\varphi\,\frac{p^2}{Mk\Theta}\left[1 + 2\frac{\exp(-ik\Theta t)}{ik\Theta t} + 2\frac{1-\exp(-ik\Theta t)}{(k\Theta t)^2}\right].$$

In the first case

$$f(t_0) = it_0\left(\frac{p^2}{2m} - E_0\right) - \frac{\Gamma t_0}{2} - 3{,}65\,T p_0^2\frac{\cos\varphi}{Mk\Theta^2} + \frac{1}{2}\left[-\frac{\Gamma}{2} + i\left(\frac{p_0^2}{2m} - E_0\right)\right]^2 a^{-2},$$

$$t = 4.49/k\Theta, \qquad a^2 = -0{,}65 p_0^2 kT\cos\varphi/M.$$

In the second case

$$f(t_0) = B/2 - \Gamma t_0/2 + {}^1\!/_2(2B\gamma^2)^{1/3}e^{-2i\psi}, \quad t_0 = (k\Theta)^{-1}(2B/\gamma)^{1/3}e^{i\psi},$$

$$a^2 = 3(\gamma^4/2B)^{1/3}, \qquad B = -(3p^2/2Mk\Theta)\cos\varphi,$$

$$\psi = \tfrac{1}{3}\tan^{-1}[2(p^2/2m - E_0)/\Gamma].$$

In conclusion the authors express their sincere appreciation to F. L. Shapiro for valuable discussions.

[1] W. Lamb, Phys. Rev. **55**, 190 (1939).

[2] A. Akhiezer and I. Pomeranchuk, Некоторые вопросы теории ядра (Some Problems of Nuclear Theory), second edition, Gostekhizdat, 1950.

[33] R. L. Mössbauer, Z. Physik **151**, 124 (1958); Naturwiss. **45**, 538 (1958); Z. f. Naturf. **14a**, 211 (1959).

Translated by M. Hamermesh
190

SHOCK WAVES IN RELATIVISTIC MAGNETOHYDRODYNAMICS

L. M. KOVRIZHNYKH

P. N. Lebedev Physics Institute, Academy of Sciences, U.S.S.R.

Submitted to JETP editor April 30, 1960

J. Exptl. Theoret. Phys. (U.S.S.R.) **39**, 1042-1045 (October, 1960)

The properties of a shock adiabat in relativistic magnetohydrodynamics are investigated for the case of perpendicular waves. In a number of limiting cases some simple expressions have been derived which relate the thermodynamic quantities on both sides of a discontinuity. The possibility of accelerating charged particles by means of shock waves is briefly considered. It is shown that in the ultrarelativistic case of perpendicular waves such acceleration is impossible.

A paper by Hoffman and Teller[1] was devoted to problems of relativistic magnetohydrodynamics. They obtained for the shock adiabat an equation which is valid in the relativistic case. In the present paper we shall investigate in more detail the properties of this adiabat and find the relation between the various thermodynamic quantities on both sides of the discontinuity for the case of a shock wave which is perpendicular to the direction of the field.*

We denote by the indices 1 and 2 the values of corresponding quantities in front of and behind the shock wave. Assuming that the vector of the magnetic field lies in a plane parallel to the plane of discontinuity, and making use of the conditions of continuity of the flux densities of the energy, momentum, and particles, and also the tangential component of the electric field, we obtain

$$w_1^* v_1/(1-v_1^2/c^2) = w_2^* v_2/(1-v_2^2/c^2), \tag{1}$$

$$p_1^* + w_1^* v_1^2/c^2(1-v_1^2/c^2) = p_2^* + w_2^* v_2^2/c^2(1-v_2^2/c^2), \tag{2}$$

$$n_1 v_1/(1-v_1^2/c^2)^{1/2} = n_2 v_2/(1-v_2^2/c^2)^{1/2}, \qquad H_1/n_1 = H_2/n_2,$$
$$w^* = e^* + p^*, \qquad p^* = p + H^2/8\pi,$$
$$e^* = e + H^2/8\pi, \qquad e = w - p. \tag{3}$$

Here e is the internal energy per unit volume, w is the heat function, p is the pressure, n is the particle number density, v is the velocity of the front, H is the magnetic field intensity, and c is the velocity of light. We emphasize that for all quantities we mean their values in a system of coordinates in which the corresponding medium is at rest.

*The conditions under which the existence of ultrarelativistic perpendicular shock waves is possible have been considered by Stanyukovich.[2]

After simple transformations, we get from (1), (2),

$$v_1 = c\left[\frac{(p_2^*-p_1^*)(e_2^*+p_1^*)}{(e_2^*-e_1^*)(e_1^*+p_2^*)}\right]^{1/2}, \qquad v_2 = c\left[\frac{(p_2^*-p_1^*)(e_1^*+p_2^*)}{(e_2^*-e_1^*)(e_2^*+p_1^*)}\right]^{1/2},$$
$$v_{12} = \frac{v_1-v_2}{1-v_1v_2/c^2} = c\left[\frac{(p_2^*-p_1^*)(e_2^*-e_1^*)}{(e_1^*+p_2^*)(e_2^*+p_1^*)}\right]^{1/2}. \tag{4}$$

Eliminating v_1 and v_2 from (1) – (3), we obtain the equation for the shock adiabat:

$$w_1^*/n_1^2 - w_2^{*2}/n_2^2 + (p_2^*-p_1^*)[w_1^*/n_1^2 + w_2^*/n_2^2] = 0. \tag{5}$$

We note that Eqs. (4) and (5) coincide completely with similar expressions obtained in the usual relativistic hydrodynamics by Taub,[3] if we replace w* by w, e* by e and p* by p.

We now investigate the relation (4), (5) in a number of limiting cases, and shall assume that the gas is ideal.

1. The equation of state is nonrelativistic, i.e., $p \ll m_0nc^2$, but $H^2/8\pi \gg m_0nc^2$ (m_0 is the rest mass of the particle). In this case, expanding (4), (5) in powers of $8\pi m_0nc^2/H^2$ and p/m_0nc^2, and assuming that $e = m_0nc^2 + p/(\gamma-1)$, we obtain

$$v_1 \approx v_2 = c[1 - 4\pi m_0 n_1 c^2/H_1^2]^{1/2}, \qquad v_{12} = c(y-1),$$
$$(y-1)^3 = \frac{4}{\gamma-1}\frac{p_2-p_1}{m_0n_1c^2} \qquad \left(\frac{p_2}{m_0n_2c^2} \ll 1\right), \tag{6}$$

where $\gamma = c_p/c_v$ is the ratio of specific heats, and $y = n_2/n_1 = H_2/H_1$.

Thus, at nonrelativistic temperatures and in strong magnetic fields, the velocity of the shock is close to the velocity of light, the relative velocity v_{12} is very small ($1 - y \ll 1$), the density jump and the jump in the field are also small.

The equation of state is ultrarelativistic, but the magnetic energy is much smaller than the kinetic energy of the particles, i.e.,

$$p_1 = \tfrac{1}{3} e_1 \gg H_1^2/8\pi.$$

In this case, with accuracy to small quantities of order $H_1^2/8\pi p_1$, we find

$$v_1 = c\,[(p_2 + p_1/3)/(p_2 + 3p_1)]^{1/2},$$

$$v_2 = \tfrac{1}{3} c\,[(p_2 + 3p_1)/(p_2 + p_1/3)]^{1/2},$$

$$v_{12} = c\,[3(p_2 - p_1)^2/(3p_2 + p_1)(p_2 + 3p_1)]^{1/2},$$

$$y^2 = n_2^2/n_1^2 = H_2^2/H_1^2 = p_2(3p_2 + p_1)/p_1(p_2 + 3p_1), \qquad (7)$$

that is, the velocity and magnetic field discontinuities are positive and increase in strong shocks ($p_2/p_1 \gg 1$) is proportional to the square root of the square of the pressure ratio.

3. Finally, for very powerful fields and high temperatures, when $H_1^2/8\pi \gg p_1 = \frac{1}{3} e_1$, we shall have*

$$v_1 = c\left[1 - \frac{16\pi(p_2 - p_1)}{H_1^2(y^4 - 1)}\right]^{1/2}, \qquad v_2 = c\left[1 - \frac{16\pi y^2(p_2 - p_1)}{H_1^2(y^4 - 1)}\right]^{1/2},$$

$$v_{12} = c\,\frac{y^2 - 1}{y^2 + 1}\left[1 - \frac{32\pi p_1}{H_1^2}\,\frac{y^2 - p_2/p_1}{y^4 - 1}\right]^{1/2},$$

$$y^2 = n_2^2/n_1^2 = H_2^2/H_1^2 = [p_2 - p_1 + (p_2^2 - p_2 p_1 + p_1^2)^{1/2}]/p_1. \qquad (8)$$

It follows therefore that the values of the velocities v_1 and v_2 are close to the velocity of light, while the dependence of the magnitude of the field intensity discontinuities on the behavior of the pressure for strong shock waves is similar to what is given above.

In conclusion, we shall consider briefly the question of the possibility of the reflection of charged particles from a shock front.† This can be of interest in connection with the possibility of accelerating particles by means of shock waves. Actually, if such a reflection takes place, then the particle which lands on the wave front, being reflected, will obtain an additional energy similar to what happens in reflection from "magnetic clouds."[4]

For simplicity, we shall consider the case in which medium 1 is at rest and a particle with charge Ze, mass M and velocity v_0 enters medium 2 normal to the shock front (the velocity of which is v_1). Since our purpose here is only to obtain the necessary condition for reflection, we shall neglect energy losses of the particle which take place as a result of interaction with the medium. We transform to a system of coordinates in which medium 2 is at rest and, consequently, there is only a magnetic field $\mathbf{H}_2$. In this system of coordinates, the velocity of the particle will obviously be

$$v_0' = (v_0 - v_{12})/(1 - v_0 v_{12}/c^2) \qquad (v_0' \leqslant 0),$$

while the velocity of motion of the front is v_2.

In order that reflection take place, it is clearly necessary that the particle again cross the shock front which, as is easy to show, leads to the condition

$$v_2 < v_0'/\sqrt{1 + x^2} \approx v_0'/4.6, \qquad (9)$$

where $0 < x < 3\pi/2$ is the first non-trivial root of the equation

$$x = \tan x \qquad (x \approx 4.49).$$

Physically, (9) is equivalent to the condition that the front is displaced a distance less than the Larmor radius of the particle after a time of the order of $\frac{3}{4}$ of a period.

If condition (9) is satisfied, then the particle can be reflected from the front. In this case the relative increase in its energy (in the laboratory system of coordinates) $\Delta W/W$ will be equal to

$$\Delta W/W = \{(1 - v_0 v_{12}/c^2)(1 + v_x v_{12}/c^2)/(1 - v_{12}^2/c^2) - 1\}. \qquad (10)$$

Here

$$v_x = v_0' \cos \omega t_0, \qquad \omega = (ZeH_2/Mc)\sqrt{1 - v_0'^2/c^2},$$

and $t_0 < x/\omega$ is the time interval between the first and second crossings of the front by the particle, determined from the equation

$$v_0' \sin \omega t_0 - v_2 \omega t_0 = 0.$$

We emphasize that, according to (10), the increase in energy is determined principally by the velocity of the second medium v_{12} and not by the velocity of the front v_1. This is due to the fact that the electric field differs from zero in a system of coordinates connected with the shock front.

Thus, with the satisfaction of condition (9), it is apparently possible to use the shock front for accelerating charged particles. This method would be especially interesting in the case of relativistic shocks where the velocity v_{12} is close to the velocity of light, inasmuch as the relative increase of energy in this case can be very great. Unfortunately, in the case of the perpendicular shock waves that we have considered here, the condition $1 - v_{12}^2/c^2 \ll 1$ is incompatible with the reflection condition (9). Actually, for (9) to be fulfilled it is necessary in any case that the velocity not exceed the value $c/\sqrt{1 + x^2} \approx c/4.6$, which in accord with (4), cannot take place [see also Eqs. (6) — (8)], i.e.,

*We note that it follows from the conditions $p_1 \gg H_1^2/8\pi$ (in case 2) and $p_1 \ll H_1^2/8\pi$ (in case 3) that $p_2 \gg H_2^2/8\pi$ and $p_2 \ll H_2^2/8\pi$, respectively.

†V. I. Veksler has drawn our attention to this question.

no particle passing through the shock front can cross it a second time.

We note that the considerations given above obviously correspond to the case in which the Larmor radius of the particle exceeds the thickness of the shock front. In the opposite case, solution of the problem of the possibility of acceleration requires a knowledge of the structure of the transition layer and generally falls outside the framework of phenomenological hydrodynamics and outside of the present paper.

The author acknowledges V. I. Veksler for fruitful discussions.

[1] F. Hoffman and E. Teller, Phys. Rev. **80**, 692 (1950).

[2] K. P. Stanyukovich, JETP **35**, 520 (1958), Soviet Phys. JETP **8**, 358 (1959).

[3] A. Taub, Phys. Rev. **74**, 328 (1948).

[4] E. Fermi, Phys. Rev. **75**, 469 (1949).

Translated by R. T. Beyer
191

ON THE DETERMINATION OF THE RELATIVE PARITY OF Σ^0 AND Λ PARTICLES FROM THE REACTION $\Sigma^0 \to \Lambda + e^+ + e^-$

B. N. VALUEV and B. V. GESHKENBEĬN

Submitted to JETP editor May 11, 1960

J. Exptl. Theoret. Phys. (U.S.S.R.) 39, 1046-1048 (October, 1960)

The problem considered is that of the correlation of the polarizations of the Σ^0 and Λ particles and the electron-positron pair in the reaction $\Sigma^0 \to \Lambda + e^+ + e^-$, in its dependence on the relative parity of Σ^0 and Λ. The correlations are very different for positive and negative relative parity. When there is a polarization of the Σ^0 particles arising in their production, the measurement of the correlation in question can be a comparatively convenient method for determining the relative parity of Σ^0 and Λ.

IN papers by Feinberg[1] and by Feldman and Fulton[2] it has been pointed out that the reactions $\Sigma^0 \to \Lambda + \gamma$ and $\Sigma^0 \to \Lambda + e^+ + e^-$ can serve for the determination of the relative parity of the Σ^0 and Λ particles. Namely, the conversion coefficients were calculated for the cases of positive (+) and negative (−) parity. They differ by 13 percent. The calculated spectrum of the Λ particles was found to be sensitive to the parity in the domain of small momenta, but unfortunately small momenta are improbable. The determination of the correlation of the linear polarization of the photon with the polarizations of the Σ^0 and Λ, which was proposed by Feldman and Fulton,[2] is based on the requirement of measuring the polarization of the photon, which is evidently difficult to do (see, for example, the analysis made by Karlson[3]).

In the present paper we calculate the correlation of the electron-positron pair and the polarizations of the Σ^0 and Λ particles in the reaction $\Sigma^0 \to \Lambda + e^+ + e^-$. As has been shown in a paper by Kroll and Wada,[4] an internal-conversion pair has a good "memory" of the direction of polarization of the γ-ray quantum. Therefore we can expect a sizable correlation between the polarizations of Σ^0 and Λ and the orientation of the pair.

We shall calculate the density matrix for the Λ particles produced in the reaction as a function of the variables that characterize the orientation of the pair.

The matrix element for the process in question can be written in the form

$$\mathfrak{M}_\pm = \Gamma_\mu^{(\pm)} \Omega_\mu \delta^4 (p - q - r - s),$$

$$\Gamma_\mu^{(\pm)} = f^{(+)}(k^2) \sqrt{M_\Sigma M_\Lambda / p_0 q_0}\, \bar{\Lambda}(q)\, \sigma_{\mu\nu} k_\nu M^{-1} \Sigma(p),$$

$$\Gamma_\mu^{(-)} = f^{(-)}(k^2) \sqrt{M_\Sigma M_\Lambda / p_0 q_0}\, \bar{\Lambda}(q)\, \gamma_5 \sigma_{\mu\nu} k_\nu M^{-1} \Sigma(p),$$

$$\Omega_\mu = e \sqrt{m^2 / s_0 r_0}\, \bar{u}(r)\, \gamma_\mu v(s), \qquad k = p - q, \qquad k^2 = \mathbf{k}^2 - k_0^2.$$

Here p and q are the four-momenta of the Σ^0 and Λ^0 particles, and M_Σ and M_Λ are their masses; $M = {}^1/_2 (M_\Sigma + M_\Lambda)$; r and s are the four-momenta of the electron and positron; m is the mass of the electron; $\sigma_{\mu\nu} = (2i)^{-1}(\gamma_\mu \gamma_\nu - \gamma_\nu \gamma_\mu)$, and $\gamma_5 = \gamma_1 \gamma_2 \gamma_3 \gamma_4$, γ_μ being the Dirac matrices; $\Sigma(p)$, $\Lambda(p)$, $u(r)$, $v(s)$ are bispinors describing the Σ^0, Λ^0, e^- and e^+ particles; the signs ± distinguish the cases of like and unlike parities of the Σ^0 and Λ^0 particles.

In the expressions for $\Gamma_\mu^{(\pm)}$ the terms proportional to k_μ are omitted, since they make no contribution owing to gauge invariance ($k_\mu \Omega_\mu = 0$). Terms $\sim k^2$, which make a small contribution, are also omitted. The resulting error can be estimated, and is $\lesssim 1$ percent. Therefore we set the functions $f^{(\pm)}(k^2)$ equal to $f^{(\pm)}(0)$.

In the rest system of the Σ^0 particle its state of polarization is described by the density matrix

$$\rho_\Sigma = {}^1/_2 (1 + (\sigma \mathbf{P}_\Sigma)).$$

The state of the Λ particle that is produced will be described by the density matrix

$$\rho_\Lambda = \mathfrak{M} \rho_\Sigma \mathfrak{M}^+,$$

where $\mathfrak{M}$ is taken in the rest system of the Σ^0 particle. By simple calculations in which terms

$\sim \Delta^2 / M_\Lambda^2$ are neglected, we get the expressions for $\rho_\Lambda^\pm$ (apart from a common factor):

$$\rho_\Lambda^{(+)} = \frac{|f^{(+)}|^2}{r_0 s_0} \frac{M_\Sigma}{M_\Lambda} [-2[\mathbf{rs}]^2 - k^2\mathbf{k}^2 + \{2[\mathbf{r}\times\mathbf{s}]^2(\mathbf{P}_\Sigma - 2\mathbf{n}(\mathbf{nP}_\Sigma)) + k^2(\mathbf{kP}_\Sigma)\mathbf{k} + \frac{k^2}{M_\Lambda}(r_0 - s_0)[\mathbf{P}_\Sigma \times [\mathbf{s}\times\mathbf{r}]]\}\sigma] \frac{\delta^4(r+s-k)}{k^4},$$

$$\rho_\Lambda^{(-)} = \frac{|f^{(-)}|^2}{r_0 s_0} \left[\frac{M_\Sigma}{M_\Lambda}\frac{k^2\mathbf{k}^2}{2} - \frac{3}{2}\Delta^2 k^2 - 2\mathbf{a}^2 + \left\{\frac{M_\Sigma}{M_\Lambda} k^2(\mathbf{kP}_\Sigma)\mathbf{k} - 4(\mathbf{aP}_\Sigma)\mathbf{a} + \left(2\mathbf{a}^2 - \frac{1}{2}\frac{M_\Sigma}{M_\Lambda}k^2\mathbf{k}^2 \cdot \pm \frac{k^2\Delta^2}{2}\right)\mathbf{P}_\Sigma\right\}\sigma\right] \frac{\delta^4(r+s-k)}{k^4}.$$

Here

$$\mathbf{n} = [\mathbf{r}\times\mathbf{s}]/|[\mathbf{r}\times\mathbf{s}]|, \quad \mathbf{a} = \left[r_0 + \frac{(\mathbf{rk})}{2M_\Lambda}\right]\mathbf{k} - \Delta\mathbf{r},$$

and σ_i are the Pauli matrices. Let us introduce the unit vectors $\boldsymbol{\kappa} = \mathbf{k}/|\mathbf{k}|$, $\mathbf{N} \perp \boldsymbol{\kappa}$ and in the plane of the pair, and $\mathbf{n} = \boldsymbol{\kappa} \times \mathbf{N}$. Then, averaging over the other variables, we get the following expressions:

$$\overline{\rho_\Lambda^{(+)}} \sim 2.55\,|f^{(+)}|^2\{1 - 1.41(\mathbf{P}_\Sigma\boldsymbol{\kappa})(\sigma\boldsymbol{\kappa}) - 0.41[2(\mathbf{nP}_\Sigma)(\sigma\mathbf{n}) - (\sigma\mathbf{P}_\Sigma)]\},$$

$$\overline{\rho_\Lambda^{(-)}} \sim 2.88\,|f^{(-)}|^2\{1 - 0.64[2(\mathbf{P}_\Sigma\boldsymbol{\kappa})(\sigma\boldsymbol{\kappa}) - (\sigma\mathbf{P}_\Sigma)] - 0.68(\sigma\mathbf{P}_\Sigma) - 0.40[2(\mathbf{P}_\Sigma\mathbf{N})(\sigma\mathbf{N}) - (\sigma\mathbf{P}_\Sigma)]\}.$$

It is found that the ratio of the conversion coefficients for the cases of negative and positive parity is 1.13, which agrees with the calculations in references 1 and 2.

Now let us set

$$P_{\Lambda N} = \langle \sigma\mathbf{N} \rangle_{av}$$

and so on. We have:
in the case of positive parity

$$P_{\Lambda N} = 0.41\,P_{\Sigma N}, \qquad P_{\Lambda n} = -0.41\,P_{\Sigma n}, \qquad P_{\Lambda\kappa} = -P_{\Sigma\kappa};$$

in the case of negative parity

$$P_{\Lambda N} = -0.44 P_{\Sigma N}, \qquad P_{\Lambda n} = 0.36 P_{\Sigma n}, \quad P_{\Lambda\kappa} = -0.92 P_{\Sigma\kappa}.$$

Here $P_{\Lambda N}$, $P_{\Sigma N}$, and so on are the components of the polarization vector in the directions of $\mathbf{N}$ and so on. As can be seen from the data given, there is a considerable difference between the cases of positive and negative parity, which may make it possible to distinguish these cases experimentally.

As is well known,[2,5] the polarization of the Σ^0 can be determined from the polarization of the Λ particle in the decay $\Sigma^0 \to \Lambda + \gamma[P_{\Lambda av} = -(1/3)P_\Sigma]$, and the polarization of the Λ can be found from the asymmetry in its decay. A weak point in the proposed method for determining the relative parity of Σ^0 and Λ is the necessity of having Σ^0 particles with sufficiently large polarization. (A fairly large polarization of Σ^0 is necessary for the method to be favorable from the point of view of statistics.) The possibility is not excluded, however, that Σ^0 particles with considerable polarization can be obtained by production in the reaction $\pi^- + p \to \Sigma^0 + K^0$ (for $E_\pi \sim$ Bev), as is the case for Σ^+ particles produced in the reaction $\pi^+ + p \to K^+ + \Sigma^+$.

Thus the proposed method for determining the relative parity of Σ^0 and Λ may be practically convenient.

We are extremely grateful to V. I. Ogievetskiĭ and L. B. Okun' for a discussion and for comments.

[1] G. Feinberg, Phys. Rev. **109**, 1019 (L) (1958).
[2] G. Feldman and T. Fulton, Nuclear Phys. **8**, 106 (1958).
[3] E. Karlson, Arkiv Fysik **13**, 1 (1958).
[4] N. Kroll and W. Wada, Phys. Rev. **98**, 1355 (1955).
[5] R. Gatto, Phys. Rev. **109**, 610 (L) (1958).

Translated by W. H. Furry
192

ON RESONANCE PHOTON-PHOTON SCATTERING

V. N. ORAEVSKIĬ

Novosibirsk State University

Submitted to JETP editor May 11, 1960

J. Exotl. Theoret. Phys. (U.S.S.R.) **39**, 1049-1050 (October, 1960)

The effective cross section for resonance photon-photon scattering due to the existence of a π^0 meson decaying into two photons is estimated.

As is well known, the charged-particles vacuum leads to the existence of a nonlinear effect — photon-photon scattering. We shall consider photon-photon scattering associated with the account of the vacuum of π^0 mesons.

We write down the interaction of the electromagnetic field with the field of the π^0 mesons *

$$L = \eta\varphi\mathbf{E}\mathbf{H}f(q^2),$$

where η is the effective coupling constant; φ, $\mathbf{E}$, $\mathbf{H}$ are the operators of the meson and electromagnetic fields; q is the 4-momentum of the π^0 meson. The interaction (1) differs from the interaction introduced by Dalitz[1] by the form factor $f(q^2)$ which takes into account phenomenologically the effects of "smearing out" of the π^0 mesons [where $f(-m^2) = 1$].

By making use of (1), we write down the matrix element of photon-photon scattering in terms of the π^0 meson with account of damping of the π^0 meson:

$$S = \eta^2 f^2(q^2)(2\pi)^4(\mathbf{E}\mathbf{H})\frac{a(q^2)}{q^2+(m-i\Gamma/2)^2}(\mathbf{E}'\mathbf{H}')\delta(q_1+q_2 - q_1'-q_2'), \quad (2)$$

where $a(q^2)/[q^2 + (m - i\Gamma/2)^2]$ is the renormalized Green's function of the π^0 meson; $\Gamma = t^{-1}$, t is the lifetime of the π^0 meson; q_1, q_2, $\mathbf{E}$, $\mathbf{H}$, q_1', q_2', $\mathbf{E}'$, $\mathbf{H}'$ are the 4-momenta, the electric and the magnetic fields of the colliding and scattered photons, respectively.

By means of (2) and the expression for the lifetime of the π^0 meson ($t^{-1} = \eta^2 m^3/16\pi$), it is easy to obtain the scattering cross section of unpolarized photons by unpolarized photons (in the reference frame in which $\mathbf{q}_1 + \mathbf{q}_2 = 0$):

$$\sigma = \frac{32\Gamma^2 f^4(-4\omega^2)a^2(-4\omega^2)}{(m-2\omega)^2+\Gamma^2/4}\left(\frac{\omega}{m}\right)^6\frac{1}{(m+2\omega)^2}\int d\Omega, \quad (3)$$

where ω is the photon frequency. As expected, the cross section has a resonance in the region $\omega_1 = m/2$.

From (3), we get the cross section averaged over the width of the "level" (taking it into account that $a(-m^2) \approx f(-m^2) = 1$):

$$\bar{\sigma}_1 = \frac{\pi}{4\omega_1^2}\tan^{-1}2. \quad (4)$$

If we substitute the numerical value of the resonance frequency, we get

$$\bar{\sigma}_1 \approx 0{,}75\cdot 10^{-25}\ \text{cm}^2. \quad (5)$$

Since the "level" has a small width ($\Gamma \approx 5$ ev), we get the value of the cross section averaged over a large ($10^2\Gamma$, i.e., 0.5 kev) range of energies close to resonance:

$$\bar{\sigma}_2 \approx 1\cdot 10^{-27}\ \text{cm}^2. \quad (6)$$

The experimental proof of the given effect is of course difficult, although the results obtained for the cross sections (5) and (6) appreciably exceed the photon-photon scattering cross sections usually observed, which are associated with the polarization of the vacuum of charged particles.

The author is deeply grateful to D. V. Volkov for discussion of the results of the research and for advice.

*We use the system of units in which $\hbar = c = 1$.

[1] R. H. Dalitz, Proc. Roy. Soc. (London) **A64**, 667 (1951).

Translated by R. T. Beyer
193

ENERGIES OF ROTATIONAL STATES OF NON-AXIAL NUCLEI WITH J = 10 *AND* J = 12

V. K. LUK'YANOV

Saratov State University

Submitted to JETP editor May 11, 1960

J. Exptl. Theoret. Phys. (U.S.S.R.) 39, 1051-1052 (October, 1960)

The energy levels of the lower rotational band in non-axial nuclei have been derived for J = 10 and J = 12. A comparison with the experimental data for U^{238} and Th^{232} is made.

DAVYDOV et al.[1,2] have developed a theory of non-axial nuclei and obtained the energies of the rotational levels with angular momentum up to J = 8. It is of interest to compute the rotational levels of fairly high energies with J = 10 and J = 12, since the comparison with experiment can in this case serve as a means of testing the adiabatic assumption, which was used in constructing the theory.

The calculations were done numerically. As in the paper of Davydov and Rostovskiĭ,[2] we substituted in the Schrödinger equation $(\hat{H} - \epsilon)\psi = 0$ wave functions of the form

$$\psi_{JM} = \sum_{K \geqslant 0} |JK\rangle A_K.$$

Here $\hat{H}$ is the operator of the rotational energy of the non-axial nucleus; it depends on the parameter γ which determines the deviation of the shape of the nucleus from axial symmetry. Since the matrix elements $\langle JK|\hat{H}|JK\rangle$ and $\langle JK+2|\hat{H}|JK\rangle$ are known, we obtain a system of homogeneous algebraic equations for a given J. The requirement that this system have a nontrivial solution (vanishing of the determinant) allows us to determine the rotational energy levels. For J = 10 the determinant was expanded explicitly, and the resulting equation of the sixth degree was solved numerically for different values of γ. For J = 12 the determinant was evaluated numerically. In both cases we required those solutions which coincide with the solutions for the axially symmetric nucleus in the limit $\gamma = 0$. The rotational energies $\epsilon(10)$ and $\epsilon(12)$ obtained in this way belong to the basic rotational band of the non-axial nucleus. These values (in the units $\hbar^2/4B\beta^2$) are given in the table for different values of γ. To facilitate the comparison with experiment we exhibit in the figure the ratios $\epsilon(10)/\epsilon(2)$ and $\epsilon(12)/\epsilon(2)$ of the basic rotational band as functions of γ. The figure also shows the curves for the other levels of the rotational band, taken from reference 2.

γ°	0	10	15	20	25	30
$\epsilon(10)$	73.33	76.14	75.28	72.51	70.62	70
$\epsilon(12)$	104	106,9	103,8	99.52	97.11	96

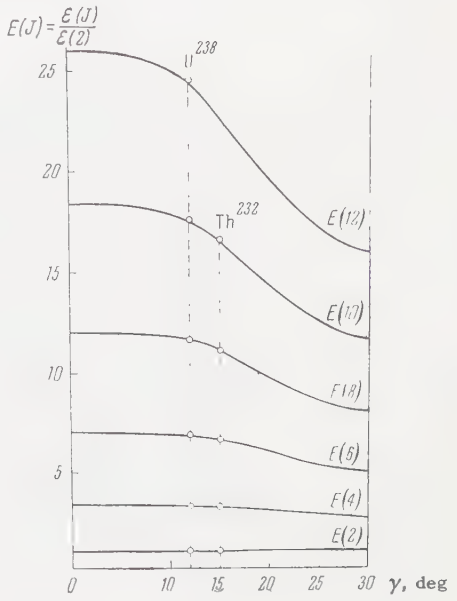

The transition energies between the rotational states up to J = 10 for Th^{232} and J = 12 for U^{238} were recently measured by Stephens, Diamond, and Perlman,[3] using the method of multiple Coulomb excitation. To obtain agreement between the experimental data and the theory of axially symmetric nuclei, these authors were forced to supplement the formula $\epsilon = AJ(J+1)$ with the correction terms $-BJ^2(J+1)^2$ for U^{238} and $-BJ^2(J+1)^2 + CJ^3(J+1)^3$ for Th^{232}, where B and C are parameters which are determined by comparison with experiment. The model of non-axial nuclei enables us to fit the level schemes of these nuclei without introducing sizable corrections for non-adiabaticity. The two ratios $\epsilon(4)/\epsilon(2)$ and $\epsilon(6)/\epsilon(2)$ were used for the determination of γ. The figure shows that the resulting values $\gamma = 12^\circ$ (U^{238}) and $\gamma = 15^\circ$ (Th^{232}) lead to rather good agreement with the experimental ratios indi-

cated by the circles. The small discrepancies for the higher levels may be due to non-adiabaticity.

In conclusion I express my gratitude to Prof. A. S. Davydov and V. S. Rostovskiĭ for advice and comments.

[1] A. S. Davydov and G. F. Filippov, JETP **35**, 440 (1958), Soviet Phys. JETP **8**, 303 (1959).

[2] A. S. Davydov and V. S. Rostovskiĭ, JETP **36**, 1788 (1958), Soviet Phys. JETP **9**, 1275 (1959).

[3] Stephens, Diamond, and Perlman, Phys. Rev. Lett. **3**, 435 (1959).

Translated by R. Lipperheide
194

ON THE DIAMAGNETISM OF A SYSTEM OF INTERACTING PARTICLES

I. G. KAPLAN

Institute for Chemical Physics, Academy of Sciences, U.S.S.R.

Submitted to JETP editor May 13, 1960

J. Exptl. Theoret. Phys. (U.S.S.R.) 39, 1053-1055 (October, 1960)

It is shown that the diamagnetic susceptibility of a system of interacting particles is independent of their interaction up to terms of the order h^2.

IT is well known that in classical mechanics the diamagnetic moment of a substance is equal to zero. It can only arise because of quantum effects in the particle motion. Landau[1] gave in 1930 a rigorous quantum-mechanical solution of the problem of diamagnetism of free electrons in a uniform magnetic field, but it is not possible to solve in general form the problem of finding the diamagnetic susceptibility of a system of interacting particles. It is of interest to find its expansion in powers of h, restricting oneself to terms of the order h^2. To take the next terms of the expansion into account, quantum statistics must be employed; this will not be considered in the present paper. We shall not impose any restrictions on the potential energy of the system. A completely ionized plasma heated to a temperature on the order of 10^6 to 10^7° is an example of a system for which our expansion is valid.

We shall find, however, that the final answer will not contain the potential energy, i.e., we shall show that up to terms in h^2 the interaction between particles does not affect their magnetic properties. We note that the plasma is almost ideal, because Boltzmann statistics can be applied and because the plasma is completely ionized. A rigorous absence of non-ideal corrections in the diamagnetic terms of order h^2 is, however, by no means obvious.

When we neglect relativistic interactions, the Hamiltonian of a system of N particles can be written in the form

$$\hat{\mathcal{H}} = \sum_{\alpha=1}^{N} \frac{1}{2m_\alpha}\left[-h^2\nabla_\alpha^2 + 2\frac{ihe_\alpha}{c}\mathbf{A}(\mathbf{r}_\alpha)\nabla_\alpha + \frac{e_\alpha^2}{c^2}A^2(\mathbf{r}_\alpha)\right] + U(\mathbf{r}_\alpha).$$

By a suitable choice of gauge we can always put $\operatorname{div}\mathbf{A}_\alpha = 0$. We do not consider the paramagnetic terms in the Hamiltonian since they do not affect the diamagnetism in the given approximation. The paramagnetic part of the susceptibility itself is known to be unchanged by the interaction in the nonrelativistic approximation and is given by the normal expression for a perfect gas.

To obtain the characteristics of the magnetic properties of the system, we find the expansion of its free energy in terms of h. We use the method due to Wigner[2] and Uhlenbeck and Gropper[3] (in the form given by Landau and Lifshitz[4]) to evaluate the partition function $Z = \operatorname{Tr}\{\exp(-\lambda\hat{\mathcal{H}})\}$

We take for our complete orthonormal set of functions ψ_i the wave functions of free particles enclosed in some finite though large volume. Z has then the form of an integral over phase space

$$Z = \int I d\Gamma, \qquad I = V^N \psi_i^* \exp(-\lambda\hat{H})\,\psi_i.$$

The problem is reduced to finding I, which can easily be shown to satisfy the differential equation

$$\frac{\partial I}{\partial\lambda} = \sum_\alpha \frac{1}{2m_\alpha}\{h^2\nabla_\alpha^2 I + 2ih(\mathbf{t}_\alpha\nabla_\alpha)I\} - E(\mathbf{p}_\alpha, \mathbf{r}_\alpha)I,$$

where $\mathbf{t}_\alpha = \mathbf{p}_\alpha - e_\alpha c^{-1}\mathbf{A}_\alpha$ is the generalized momentum [$\mathbf{A}_\alpha \equiv \mathbf{A}(\mathbf{r}_\alpha)$] and $E(\mathbf{p}_\alpha, \mathbf{r}_\alpha)$ is the classical energy of the system. If we write I in the form $I = e^{-\lambda E}\chi$ we get an equation for χ, which we solve by the method of successive approximations restricting ourselves to terms of the order h^2,

$$\chi = 1 + h\chi_1 + h^2\chi_2.$$

The result is*

*We do not give the expression for χ_1 the average of which vanishes. It is understood that one sums from 1 to 3 over repeated Latin indices i, k, l, and m, and that the summation over the Greek indices α and β which number the particles is from 1 to N.

$$\chi_2 = \frac{\lambda^2}{4}\sum_\alpha \frac{1}{m_\alpha}\left\{\frac{e_\alpha}{cm_\alpha}\, t_{\alpha k}\frac{\partial^2 A_{\alpha k}}{\partial q_{\alpha i}^2} - \frac{e_\alpha^2}{c^2 m_\alpha^2}\left(\frac{\partial A_{\alpha k}}{\partial q_{\alpha i}}\right)^2 - \frac{\partial^2 U}{\partial q_{\alpha i}^2}\right\}$$
$$+ \frac{\lambda^3}{6}\sum_\alpha \frac{1}{m_\alpha}\left\{\frac{e_\alpha^2}{c^2 m_\alpha^2}\, t_{\alpha k}^2\left(\frac{\partial A_{\alpha l}}{\partial q_{\alpha i}}\right)^2 - \frac{2e_\alpha}{cm_\alpha}\, t_{\alpha k}\frac{\partial A_{\alpha k}}{\partial q_{\alpha i}}\frac{\partial U}{\partial q_{\alpha l}}\right.$$
$$\left. + \left(\frac{\partial U}{\partial q_{\alpha i}}\right)^2\right\} - \frac{\lambda^3}{6}\sum_\alpha \frac{1}{m_\alpha^2}\left\{\frac{e_\alpha}{cm_\alpha}\, t_{\alpha i}t_{\alpha k}t_{\alpha l}\frac{\partial^2 A_{\alpha k}}{\partial q_{\alpha l}\partial q_{\alpha i}}\right.$$
$$- \frac{e_\alpha^2}{c^2 m_\alpha^2}\, t_{\alpha i}t_{\alpha l}\frac{\partial A_{\alpha k}}{\partial q_{\alpha i}}\frac{\partial A_{\alpha k}}{\partial q_{\alpha l}} - \frac{e_\alpha^2}{c^2 m_\alpha^2}\, t_{\alpha i}t_{\alpha k}\frac{\partial A_{\alpha l}}{\partial q_{\alpha i}}\frac{\partial A_{\alpha k}}{\partial q_{\alpha l}}$$
$$\left. + \frac{e_\alpha}{cm_\alpha}\, t_{\alpha i}\frac{\partial A_{\alpha l}}{\partial q_{\alpha i}}\frac{\partial U}{\partial q_{\alpha l}}\right\} + \frac{\lambda^3}{6}\sum_\alpha\sum_\beta \frac{1}{m_\alpha m_\beta}\, t_{\alpha i}t_{\beta l}\frac{\partial^2 U}{\partial q_{\alpha i}\partial q_{\beta l}}$$
$$- \frac{\lambda^4}{8}\sum_\alpha\sum_\beta \frac{1}{m_\alpha m_\beta}\, t_{\alpha i}t_{\beta l}\left(\frac{e_\alpha}{cm_\alpha}\, t_{\alpha k}\frac{\partial A_{\alpha k}}{\partial q_{\alpha i}}\right.$$
$$\left. - \frac{\partial U}{\partial q_{\alpha i}}\right)\left(\frac{e_\beta}{cm_\beta}\, t_{\beta m}\frac{\partial A_{\beta m}}{\partial q_{\beta l}} - \frac{\partial U}{\partial q_{\beta l}}\right). \qquad (2)$$

The partition function and at the same time the free energy of the system can be expressed in terms of the average value of χ_2

$$Z = (1 + h^2\overline{\chi}_2)\int e^{-\lambda E}\, d\Gamma, \qquad F = -kT\ln Z = F_{cl} - \frac{h^2}{\lambda}\overline{\chi}_2.$$

When averaging over the momenta we take into account that

$$\overline{t_{\alpha i}t_{\beta k}} = (m_\alpha/\lambda)\,\delta_{\alpha\beta}\delta_{ik},$$
$$\overline{t_{\alpha i}t_{\alpha k}t_{\alpha l}t_{\alpha m}} = (m_\alpha^2/\lambda^2)\,(\delta_{ik}\delta_{lm} + \delta_{il}\delta_{km} + \delta_{im}\delta_{kl}).$$

The average of the product of any odd number of momentum components is equal to zero. As a result all terms in (2) containing simultaneously the vector potential and the potential energy drop out. Averaging and expressing the vector potential in terms of the field we get the following expression for the free energy

$$F = F_{cl} + \frac{h^2}{24\,(kT)^2}\sum_\alpha \frac{1}{m_\alpha}\overline{\left(\frac{\partial U}{\partial q_{\alpha i}}\right)^2} + \frac{h^2}{24kT}\sum_\alpha \frac{e_\alpha^2}{c^2 m_\alpha^2}\,\overline{H^2(\mathbf{r})}. \qquad (3)$$

By changing the integration variables one shows easily that the statistical average of $H^2(\mathbf{r})$ is equal to an average over the volume. The first two terms in the free energy are independent of the magnetic field and we denote them by F_0.

We have finally

$$F = F_0 + \frac{h^2}{24kT}\frac{n}{c^2}\overline{\left(\frac{e}{m}\right)^2}\int H^2(\mathbf{r})\, dV, \qquad (4)$$

where

$$n = \frac{N}{V}, \qquad \overline{\frac{e^2}{m^2}} = \frac{1}{N}\sum_\alpha \frac{e_\alpha^2}{m_\alpha^2}.$$

The magnetic term in the free energy is in the given approximation thus independent of the particle interaction. It is thus obvious that the diamagnetic susceptibility obtained from our formulae for an electron gas is the same as the corresponding expression of Landau's for free electrons taken in the same approximation (see reference 5). Indeed,

$$\varkappa = -\frac{\partial^2 F}{\partial H^2} = -\frac{n}{12kT}\frac{h^2e^2}{m^2c^2} = -\frac{n\mu_0^2}{3kT}, \qquad (5)$$

where μ_0 is the Bohr magneton.

I am grateful to L. P. Pitaevskiĭ for advice and helpful discussions.

[1] L. Landau, Z. Physik **64**, 629 (1930).
[2] E. Wigner, Phys. Rev. **40**, 749 (1932).
[3] G. E. Uhlenbeck and L. Gropper, Phys. Rev. **41**, 79 (1932).
[4] L. D. Landau and E. M. Lifshitz, Статистическая физика (Statistical Physics) Gostekhizdat, 1951 (Engl. Translation Pergamon Press, 1958) § 33.
[5] F. Bloch, Molecular Theory of Magnetism (Russ. Transl.) ONTI, 1936.

Translated by D. ter Haar
195

ELASTIC SCATTERING OF GAMMA QUANTA BY NUCLEI

L. I. LAPIDUS and CHOU KUANG-CHAO

Joint Institute of Nuclear Research

Submitted to JETP editor May 12, 1960

J. Exptl. Theoret. Phys. (U.S.S.R.) 39, 1056-1058 (October, 1960)

The energy dependence of the cross section for elastic scattering of γ quanta near the photonuclear threshold is investigated with the help of the dispersion relation for forward scattering. The first peak in the scattering cross section is attributed to dispersion effects. Experiments required for a more detailed analysis are discussed.

1. A recent investigation of the scattering of γ quanta by deuterons below the threshold for pion production with the help of dispersion relations[1] shows that photonuclear processes have a very strong effect on the elastic scattering of γ quanta in a wide region of energies (up to ~ 100 Mev). In the present paper we discuss the scattering of low-energy γ quanta by nuclei.

Fuller and Hayward,[2] as well as Penfold and Garwin,[3] have already used dispersion relations for the analysis of the elastic scattering of γ quanta by nuclei. However, they considered only the scattering above the threshold for the (γN) reaction. Taking the formation of particles in the S state into account leads to the known non-monotonic behavior near the threshold for the (γn) reaction. The dispersion relations not only allow us to discuss the Wigner-Baz' effect, but also to take account of the general effect of inelastic processes on the energy dependence of the elastic scattering amplitude in a wide region of energies. It appears to us that, within the framework of the dispersion relations, the first peak in the scattering cross section of γ quanta[2] is related to the near-threshold effects in a natural way.

We restrict the discussion to forward scattering. In the dipole approximation, which, apparently, does not contradict the experimental data on the absorption of γ quanta by nuclei up to ~ 30 Mev,[3] our results are also valid for other scattering angles and for the total elastic scattering cross section $\sigma_S(\nu)$.

2. The scattering amplitude for γ quanta has the form

$$T = R_1(\mathbf{e'e}) + R_2([\mathbf{k}\times\mathbf{e}]\times[\mathbf{k'}\times\mathbf{e'}]) + (\mathbf{e'e})[R_1 + (\mathbf{kk'})R_2] - R_2(\mathbf{ke'})(\mathbf{k'e}) \quad (1)$$

for a spinless nucleus and

$$T = R_1(\mathbf{e'e}) + R_2([\mathbf{k}\times\mathbf{e}][\mathbf{k'}\times\mathbf{e'}]) + iR_3(\sigma[\mathbf{e}_\times\mathbf{e}]) + iR_4(\sigma[[\mathbf{k'}\times\mathbf{e'}]\times[\mathbf{k}\times\mathbf{e}]]) + iR_5[(\sigma\mathbf{k})(\mathbf{e}[\mathbf{k'}\times\mathbf{e'}]) - (\sigma\mathbf{k'})([\mathbf{k}\times\mathbf{e}]\mathbf{e'})] + iR_6[(\sigma\mathbf{k'})([\mathbf{k'}\times\mathbf{e'}]\mathbf{e}) - (\sigma\mathbf{k})(\mathbf{e'}[\mathbf{k}\times\mathbf{e}])] \quad (2)$$

for the scattering from a nucleus with spin $\frac{1}{2}$. The corresponding expressions for nuclei with larger spins are more complicated.

In the dipole approximation only R_1 is different from zero. Dispersion relations can be written down for all scalar functions R_i. The imaginary parts of the amplitudes are related to the cross sections for absorption of γ quanta in different states by the unitarity condition. The scattering amplitude for γ quanta at low energies is known, so that the real and imaginary parts of all R_i can be calculated from the data on the absorption of γ quanta in different states with the help of the dispersion relations and the unitarity condition. However, up to the present time no detailed analysis of the absorption of γ quanta by nuclei has been carried out. Therefore we restrict ourselves to the dispersion relation for $R_1 + R_2$, which has the usual form

$$\mathrm{Re}[R_1(\nu, \theta = 0^\circ) + R_2(\nu, \theta = 0^\circ)] = -\frac{Z^2e^2}{M_A} + \frac{\nu_0}{2\pi^2}\mathrm{P}\int_{\nu_t}^{\infty}\frac{\sigma_t(\nu)\,d\nu}{\nu^2 - \nu_0^2} \quad (3)$$

In the literature accessible to us (see the new review article of Wilkinson[4]) we did not find detailed information on the energy dependence of the cross section for absorption of γ quanta by nuclei. Only in the case of He_2^4 (and the deuteron) is the photodisintegration cross section known in a wide region of energies.[5] Experimental data on $\sigma_t(\nu)$ for aluminum up to ~ 30 Mev were obtained recently by Mihailović et al.[6] These authors found evidence of a fine structure in the dependence of

the cross section in the region of the giant resonance. Data for the region near threshold are not available. By smoothing out these experimental data, we obtained with the help of relation (3) the energy dependence of the scattering amplitude shown schematically in Fig. 1. This behavior of the scattering amplitude is apparently characteristic for a whole group of nuclei with large $\sigma_t(\nu)$.

The photodisintegration of the deuteron leads to a decrease in the cross section for γd scattering near the threshold, as compared to the Thomson cross section. However, for other nuclei with a large absorption cross section the picture is different. Since the dispersive part of the amplitude below and slightly above the threshold is positive, the total amplitude vanishes at some energy below ν_t and then becomes positive (in the case of the deuteron[1] the amplitude does not change its sign). Above the threshold the real part of the amplitude decreases rapidly, goes through zero, and becomes negative, increasing in absolute value with increasing energy. Above the threshold, the amplitude has, of course, both a real and an imaginary part.

All this leads to an energy dependence of the scattering cross section which is shown in Fig. 2.

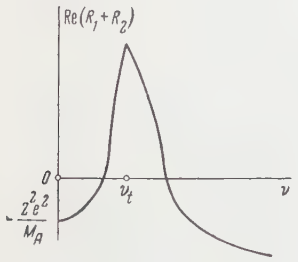

FIG. 1

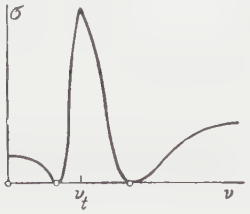

FIG. 2

In its general behavior, it agrees with the experimental data.[2] For the aluminum nucleus the scattering cross section reaches the value $\sigma_S(\nu) \approx 2 \times 10^{-28}$ cm^2 in the region of the first maximum, which is close to the experimental value. It is clear that, if the dispersion effects are not so large as to change the sign of the scattering amplitude in the threshold region, the first maximum will not appear.

The ratios between the cross sections at the maxima for different nuclei are connected with the relative role of the absorption of γ quanta in the region near threshold and in the region of the giant resonance. The fact that not only the region near threshold, but also the giant resonance, gives a contribution to the first maximum leads to an appreciable widening of this peak. The half-width for aluminum exceeds 2 Mev.

In the evaluation of the data on the absorption of γ quanta by aluminum we did not consider the effects connected with the difference in the thresholds for the (γp) and (γn) reactions, and we also neglected the resolving power of the apparatus. It seems to us that a more detailed analysis would lead to little change in the basic result.

3. The interpretation of the energy dependence of the cross section for scattering of γ quanta by nuclei proposed earlier[7] is thus apparently confirmed. Owing to the relatively poor accuracy of the experimental data on the absorption cross sections and to the absence of data on the absorption cross sections for a whole series of nuclei, it is not possible now to conduct a reliable analysis for all nuclei whose scattering properties are known.

The fruitfulness of using the dispersion relations in the analysis of the scattering of γ quanta by nuclei makes it feasible to conduct a whole series of investigations with γ quanta. First of all, it appears necessary to obtain information on the energy dependence of the absorption cross sections of γ quanta in the region near threshold as well as in the region of high energies. The consideration of the cross sections for photoproduction of pions in the calculation of $\sigma_t(\nu)$ may become necessary in the energy region of ~ 120 to 150 Mev and above. Knowing the absorption cross sections in a wide region of energies, one can obtain information on the polarizability of nuclei. For Al the polarizability

$$\alpha \equiv \left[\frac{d}{d\nu^2}\mathrm{Re}(R_1+R_2)\right]_{\nu=0} = \frac{\hbar c}{2\pi^2}\,\mathrm{P}\int_{\nu_t}^{\infty}\frac{\sigma_t(\nu)\,d\nu}{\nu^2}$$

turns out to equal $\sim 2 \times 10^{-39}$ cm^3 (the error may be as large as 50%). For He_2^4 the value is $\alpha = (0.70 \pm 0.05) \times 10^{-40}$ cm^3.

A more detailed phenomenological analysis of the absorption of γ quanta in a wide region of energies becomes inevitable if one wants to obtain information on the spin dependence of the dispersive parts of the scattering amplitudes for the γ quanta. On the other hand, the dispersion relations and the unitarity of the S matrix can be used to obtain information on the absorption cross section from the experimental data on the scattering of γ quanta by nuclei. For this purpose the inverse dispersion relations may prove to be convenient.

The authors are grateful to Ya. A. Smorodinskiĭ for useful comments.

[1] L. I. Lapidus and Chou Kuang-Chao, JETP (in press).

[2] E. G. Fuller and E. Hayward, Phys. Rev. **101**, 692 (1956).

[3] A. S. Penfold and E. L. Garwin, Phys. Rev. **116**, 120 (1959).

[4] D. H. Wilkinson, Ann. Rev. Nucl. Sci. **9**, 1 (1959).

[5] A. N. Gorbunov, Tr. FIAN (Proceedings of the Physics Institute, Academy of Sciences) **13**, 145 (1960).

[6] Mihailović, Prege, Kernel, and Kregar, Phys. Rev. **114**, 1621 (1959).

[7] L. I. Lapidus and Chou Kuang-Chao, JETP **39**, 112 (1960), Soviet Phys. JETP **12**, 82 (1961).

Translated by R. Lipperheide
196

ANNIHILATION OF AN ANTIPROTON-PROTON SYSTEM

É. O. OKONOV

Joint Institute of Nuclear Research

Submitted to JETP editor May 12, 1960

J. Exptl. Theoret. Phys. (U.S.S.R.) **39**, 1059-1061 (October, 1960)

A strong dependence of the annihilation transition matrix on the isotopic and spin states of the antiproton-proton system may significantly affect the annihilation process. In particular, a predominance of the $^1_1S_0$ state during annihilation may lead to an increase of the multiplicity of the π mesons, and annihilation occurring mainly in the singlet state may inhibit two-meson annihilation. Experiments are suggested to ascertain whether such a dependence occurs in reality. It is also pointed out that an experiment can be performed to determine whether the capture of stopped antiprotons takes place from the S orbit in accordance with the estimates[5] made for K^- mesons.

M. I. Shirokov and myself[1] have shown that the study of the annihilation of an antiproton-proton system into two π mesons may yield information about the internal space and charge parities of this system. It appeared, in particular, that the two-meson annihilation is generally forbidden if the charge parity of the $(\bar{p}p)$ system is opposite to that prescribed by the Dirac equation. Until now more than 300 cases of antiproton annihilation on a proton have been registered, but no annihilations into π^+ and π^- have been detected among them.[1] Considering the small statistical weight of the two-meson annihilation,* it is premature to draw any conclusions on the basis of this experimental evidence. Nevertheless, it does merit attention, as was also noted by Segrè.[2]

It should be noted in this connection that this experimental situation can also be interpreted with the help of less fundamental assumptions, which do not go beyond the consequences of the Dirac equation. As was already mentioned in the discussion of the available experimental data, the suppression of the reaction $\bar{p} + p \rightarrow \pi^- + \pi^+$ can be due to the fact that the annihilation occurs mainly in the singlet state of the $(\bar{p}p)$ system.[4] In this case the emission of two π mesons is forbidden for the lowest orbital states of the $(\bar{p}p)$ system by the conservation laws for the space and charge parities. This was first noted by Amati and Vitale.[7]

There is nothing unnatural about the above assumption. It is entirely possible that the annihilation transition matrix has a strong dependence on the isotopic and spin states of the $(\bar{p}p)$ system.* From this point of view it is of definite interest to investigate the relative probability for annihilation from different states of the $(\bar{p}p)$ system, especially from the S state (the simplest case), where this dependence should have its most explicit form. This investigation is greatly facilitated if the estimates of Day et al.,[5] which show that the stopped K^- meson (or antiproton) is captured by the proton mainly from the S orbit, are correct. The validity of this assertion can be confirmed experimentally in the case of the antiproton, by considering the annihilation into two π^0 mesons. According to the existing selection rules, the annihilation into two π^0 mesons is forbidden if the antiproton is captured from an S state. The emission of two π^0 mesons during the annihilation can therefore serve as evidence for the admixture of higher orbital states.

The crosses in the Table indicate forbidden annihilation transitions for the $(\bar{p}p)$ system in an S state, in accordance with the well-known selection rules (see, for example, reference 6).

It is seen from the table that the $(\bar{p}p)$ system can go into $\pi^+ + \pi^-$ only from the state $^3_3S_1$, so that the absence of such transitions in the annihi-

*According to the different versions of the statistical theory which lead to satisfactory agreement with the experimental value of the average multiplicity of the π mesons, the share of the two-meson annihilation should amount to 3 to 5% (see, for example, reference 3).

*Thus, for example, the existence of the π meson in the framework of the Fermi-Yang model points to a strong attraction between the nucleon and the antinucleon in the singlet state with isospin I = 1. On the other hand, the analogous bound states with spin $\sigma = 1$ and the state with I = 0, $\sigma = 0$ (the so-called π^0_0 meson) do not seem to exist.

State of the $(\bar{p}p)$ system	$^1S_0$	$^3S_0$	$^3S_1$	$^3S_1$
Spin	0	0	1	1
Isospin	0	1	0	1
Parity	−	−	−	−
Charge parity	+	+	−	−
$2\pi^0$	+	+	+	−
$\pi^+\pi^-$	±	±	±	
$3\pi^0$	+		+	−
$\pi^+\pi^-\pi^0$	±		±	∓
$4\pi^0$			+	+
$\pi^+\pi^-2\pi^0$		+	±	
$2\pi^+2\pi^-$		+	±	

lation of stopped antiprotons can indicate a suppression of this channel. The study of the annihilation into three π mesons permits us to determine the ratio between the probabilities for annihilation from the states $^1S_0$ and $^3S_1$, which have different ordinary and isotopic spins (for the other two S states the three-meson annihilation is forbidden). If the annihilation went predominantly through the channel with I = 1 (i.e., from the state $^1S_0$), we would obtain the definite isotopic ratio

$$w(\bar{p}+p\to\pi^-+\pi^++\pi^0)/w(\bar{p}+p\to 3\pi^0)=\tfrac{2}{3}. \qquad (1)$$

Since a transition from the state $^3S_1$ into three π^0 mesons is forbidden by the conservation law for charge parity, the contribution to the annihilation from this state should lead to an increase of the ratio (1). A measurement of this increase will enable us to make some quantitative estimates. The isotopic functions describing the system $(\pi^+\pi^-\pi^0)$ resulting from the annihilation from the states $^1S_0$ and $^3S_1$ will, respectively, be symmetric and antisymmetric under charge conjugation. This imposes some definite restrictions on the type of space symmetry, since the total wave function, expressed in terms of bilinear combinations of isotopic and coordinate functions, must, of course, be symmetric, because it describes a system of Bose particles. As a result, the system $(\pi^+\pi^-\pi^0)$ is symmetric under the interchange $\pi^+ \rightleftarrows \pi^-$ in the state with I = 1, and antisymmetric in the state with I = 0. This provides us with another criterion for distinguishing the case where the annihilation proceeds predominantly from the state $^1S_0$ ($^3S_1$), so that we can dispense with the registration of the difficult to observe annihilation into three π^0 mesons.

In this case the momentum of the π^+ (π^-) mesons should exceed the momentum of the π^- (π^+) mesons in half of all annihilation events. A violation of this "symmetry" should indicate the admixture of annihilations from the state $^3S_1$ ($^1S_0$).

The different behavior of the various states of the $(\bar{p}p)$ system with regard to its "decay" into π mesons can seriously affect the value of the average multiplicity of the π mesons in the annihilation process (N_π). Thus, for example, a predominant annihilation from the state $^1S_0$ leads to an increase of N_π, since from this state the $(\bar{p}p)$ system must decay into at least four π mesons. It is possible (although rather improbable) that this is precisely the reason for the high multiplicity of the π mesons in the annihilation process. If this is actually the case, then N_π should decrease for higher orbital states of the $(\bar{p}p)$ system (annihilation at higher energies of $\bar{p}$).

The study of the annihilation at higher energies also allows us to determine whether the prohibition of two-meson annihilation (if it really exists) has absolute character, or whether this type of reaction for S (and, perhaps, P) states is simply suppressed for reasons which do not go beyond the framework of the Dirac theory.

I take this opportunity to express my gratitude to V. S. Barashenkov, S. M. Bilen'kiĭ, and V. I. Ogievetskiĭ for a discussion and critical comments.

[1] M. I. Shirokov and É. O. Okonov, JETP, in press.

[2] E. Segrè, Report at the Kiev Conference on High Energy Physics, 1959.

[3] E. Eberle, Nuovo cimento 8, 610 (1958).

[4] E. O. Okonov, Note on the Report of E. Segrè at the Kiev Conference on High Energy Physics, 1959 (in press).

[5] Day, Snow, and Sucher, Phys. Rev. Lett. 3, 61 (1959).

[6] T. D. Lee and C. N. Yang, Nuovo cimento 3, 749 (1956).

[7] D. Amati and B. Vitale, Nuovo cimento 2, 719 (1955).

Translated by R. Lipperheide
197

MAGNETIC MIRRORS, CHANNELS AND BOTTLES FOR COLD NEUTRONS

V. V. VLADIMIRSKIĬ

Submitted to JETP editor, May 13, 1960

J. Exptl. Theoret. Phys. (U.S.S.R.) **39**, 1062-1070 (October, 1960)

It is well known that neutrons with spins oriented along a magnetic field are repelled from regions of strong field. This makes it possible to use magnetic mirrors and channels for obtaining focused beams of polarized neutrons. By surrounding an evacuated region by magnetic mirrors one can accomplish the confinement of cold neutrons. In the paper we consider conditions of adiabaticity necessary for maintaining the orientation of the spin relative to the field, we give some possible configurations for the magnetic field, and make estimates of the intensities of polarized beams and neutron densities in a magnetic bottle.

1. INTRODUCTION

THE energy of the magnetic moment of a neutron in a magnetic field is usually small compared to the kinetic energy of a thermal neutron. The magnetic moment of the neutron (-1.913 nuclear magnetons) is equal to

$$\mu = -6.03 \cdot 10^{-12}\ \text{ev/oe}. \tag{1}$$

The magnetic field in not too complex magnetic structures reaches values of the order of several thousands of oersteds. The corresponding energy is consequently of the order of $10^{-7} - 10^{-8}$ ev. Neutrons with such small energies can alter their motion drastically under the action of magnetic forces and, in particular with a suitable orientation of their spin, will be reflected from regions with high values of magnetic field. Neutrons with higher energy ϵ can be reflected from a magnetic mirror only for sufficiently small grazing angles

$$\sin\alpha \leqslant \sqrt{\mu H/\varepsilon}. \tag{2}$$

Despite the relatively small size of magnetic forces, there is a possibility of using a magnetic field in vacuum for obtaining beams of polarized neutrons. The choice of a suitable configuration of magnetic field gives a possibility for focussing beams and obtaining intensities somewhat greater than for the case of a magnetized cobalt mirror. Finally, when various conditions are satisfied, one can achieve an apparatus for confining super-cold neutrons which would make it possible to measure the lifetime of the neutron independently of an absolute calibration of the intensity of the neutron beam.

The magnetic energy of a neutron in an external field is equal to $\pm|\mu H|$ for a neutron with spin projection $s_H = \pm \frac{1}{2}$ on the direction of the magnetic field. The quantity s_H is an adiabatic invariant. This means that for sufficiently slow change in direction of the magnetic field the spin turns with the field and no depolarization results. The angular velocity of rotation of the field vector ν must be small compared with the frequency of precession of the magnetic moment in the field:

$$\nu \ll 2\mu H/\hbar. \tag{3}$$

When the adiabatic condition (3) is satisfied sufficiently closely, one can solve the problem of the motion of neutrons purely classically by treating $\pm|\mu H(\mathbf{x})|$ as a potential energy for two types of particles (neutron with spin along the field, and neutron with spin opposite to the field), which do not change into one another. Before considering various applications, it is worthwhile to investigate in more detail cases of possible breakdown of the adiabatic condition and to estimate the probability of a flipping of the neutron spin in passing through such dangerous regions.

2. ADIABATIC CONDITION

A characteristic case of breakdown of adiabaticity is the passage of the neutron near a point where $\mathbf{H} = 0$, or a region of rapid rotation of the field. To investigate changes in orientation of the spin we may give the field as a function of time. Over a sufficiently small interval we may regard the field $\mathbf{H}$ as a linear function of time. Obviously then $|\mathbf{H}|$ reaches a minimum at that moment when $\mathbf{H} \perp \dot{\mathbf{H}}$. Choosing this point as the reference origin for the time, and choosing the x and z axes along $\mathbf{H}_{min}$ and $\dot{\mathbf{H}}$, respectively, we obtain

$$H_x = \text{const}, \qquad H_y = 0, \qquad H_z = t\dot{H}, \qquad \dot{H} = \text{const}. \tag{4}$$

The spin wave function $\psi = \binom{\varphi}{\chi}$ satisfies the equation

$$i\hbar\dot{\psi} + \mu H_x\sigma_x\psi + \mu t\dot{H}\sigma_z\psi = 0. \quad (5)$$

Introducing the notation

$$\omega = \mu H_x/\hbar, \qquad a = \mu\dot{H}/\hbar, \quad (6)$$

we rewrite the equation in explicit expanded form

$$i\dot{\varphi} + \omega\chi + at\varphi = 0, \qquad i\dot{\chi} + \omega\varphi - at\chi = 0, \quad (7)$$

where ω is one-half the precession rate of the spin. Eliminating χ, we get

$$\ddot{\varphi} + (\omega^2 - ia + a^2t^2)\varphi = 0 \quad (8)$$

The substitution

$$\varphi = e^{-z/2}u, \qquad z = -iat^2 \quad (9)$$

reduces this equation to the confluent hypergeometric equation

$$z\frac{d^2u}{dz^2} + \left(\frac{1}{2} - z\right)\frac{du}{dz} - \frac{\omega^2}{4ia}u = 0. \quad (10)$$

The two solutions of the confluent hypergeometric equation give the function $\varphi(t)$ which is regular for $t = 0$:

$$\varphi = e^{iat^2/2}\{c_1F(\alpha, {}^1/_2, -iat^2) + c_2i\omega tF(\alpha + {}^1/_2, {}^3/_2, -iat^2)\}, \quad (11)$$

where $\alpha = \omega^2/4ia$. Expressing the second amplitude in terms of these same constants we get

$$\chi = e^{iat^2/2}\{c_1i\omega tF(\alpha + 1, {}^3/_2, -iat^2) + c_2F(\alpha + {}^1/_2, {}^1/_2, -iat^2)\}. \quad (12)$$

In view of the identity $F(\alpha, \gamma, z) \equiv e^zF(\gamma-\alpha, \gamma, -z)$ these formulas are symmetric with respect to the interchange $\varphi \rightleftarrows \chi$, $z \to -z$. Using the asymptotic expressions for the confluent hypergeometric functions, it is easy to set up the expressions for the amplitudes, valid for $t \to \pm\infty$:

$$\varphi(t) = \sqrt{\pi}e^{-\pi\omega^2/8a}\left[\frac{c_1}{\Gamma({}^1/_2 - \alpha)} + \frac{i\omega}{2\sqrt{ia}}\frac{c_2}{\Gamma(1-\alpha)}\frac{t}{|t|}\right](at^2)^{-\alpha}e^{iat^2/2},$$

$$\chi(t) = \sqrt{\pi}e^{-\pi\omega^2/8a}\left[\frac{i\omega}{2\sqrt{-ia}}\frac{c_1}{\Gamma(1+\alpha)}\frac{t}{|t|} + \frac{c_2}{\Gamma({}^1/_2 + \alpha)}\right](at^2)^{\alpha}e^{-iat^2/2}. \quad (13)$$

Here t is assumed to be real, the factors to the right of the square brackets have a modulus equal to unity, and the normalization of the functions is the usual one:

$$|\psi|^2 = |\varphi|^2 + |\chi|^2 = |c_1|^2 + |c_2|^2. \quad (14)$$

In the asymptotic expressions only the leading terms have been kept.

It is now easy to obtain the probability for a reorientation of the spin. Taking for $t \to -\infty$,

$$|\varphi|^2 = 1, \quad |\chi|^2 = 0, \quad (15)$$

we find a solution for $t \to +\infty$,

$$|\varphi|^2 = e^{-\pi\omega^2/a}, \quad |\chi|^2 = 1 - e^{-\pi\omega^2/a}. \quad (16)$$

If we consider that the magnetic field has reversed its direction, then for complete adiabaticity we should expect the values $|\varphi|^2 = 0$, $|\chi|^2 = 1$ for $t \to +\infty$. The factor $e^{-\pi\omega^2/a}$ is equal to the probability of non-adiabatic re-orientation of the spin with respect to the field direction. Introducing the effective time for re-orientation of the field

$$\tau = \nu^{-1} = H_x/\dot{H} = \omega/a, \quad (17)$$

we can write the probability for re-orientation of the spin in the form

$$w = e^{-\pi\omega\tau}. \quad (18)$$

If the neutron undergoes a large number N_p of passages near danger points, the necessary condition for preserving adiabaticity is $N_p\omega \ll 1$. For the minimum value of the magnetic field we obtain the estimate

$$\pi\mu H^2_{min}/\hbar|\dot{H}| > \ln N_p. \quad (19)$$

The important thing is that the probability of reorientation of the spin falls off exponentially with increase of the dimensionless factor $\omega\tau$. This makes it possible for each particular case to choose such a value of H_{min} that the non-adiabatic reorientation of the spin can be neglected.

3. MAGNETIC FIELD CONFIGURATION

Let us first consider a plane magnetic mirror. A period structure of conductors placed in the

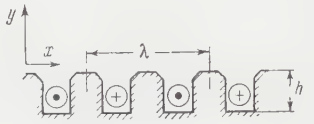

FIG. 1

grooves of an iron magnet support (Fig. 1) gives a magnetic field which, even at relatively small distances, is described very well by the formula

$$H_x = H_0e^{-ky}\sin kx, \quad H_y = H_0e^{-ky}\cos kx, \quad k = 2\pi/\lambda, \quad (20)$$

where λ is the period of the structure. For $H = |\mathbf{H}|$ we get

$$H = H_0e^{-ky}. \quad (21)$$

Such a structure of magnetic field is convenient for obtaining a potential barrier near the walls

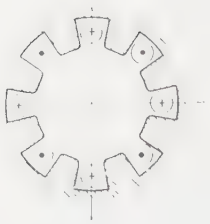

FIG. 2

and can serve as the prototype for constructing magnetic focussing channels and closed regions. We give some data for rough engineering computations. The power supply (in W/cm^2) for a good filling of the groove with copper is

$$P \approx H_0^2 h^{-1}, \qquad (22)$$

where H_0 is in kilooersted, and the depth of the groove h in centimeters. If the depth of the groove is approximately equal to the step in the structure, $h \sim \lambda$, the induction in the lower part of the groove will be approximately four times H_0. In this connection, the value $H_0 \approx 5{,}000$ oe should be regarded as a reasonable economic limit for the value of the mirror field. For smaller depth of groove, because of a somewhat increased power, one can achieve a field up to 7 — 8 koe.

For magnetic focussing channels (neutron pipes for cold neutrons) one can use different variants of arrangement of such structures on a cylindrical surface. Placing the poles along the generator of a cylinder (Fig. 2), we obtain a multipole lens (an octupole lens in the figure) with a field lying in the plane perpendicular to the axis of the lens:

$$H_r = (r/r_0)^{m-1} \sin m\varphi, \qquad H_\varphi = (r/r_0)^{m-1} \cos m\varphi, \qquad (23)$$

where m is the number of pairs of poles. In particular, for m = 3 one gets the well-known case of a sextupole lens, which is used for focusing molecular beams.

A second variant corresponds to arrangement of the poles along equidistant circles (Fig. 3). The field is then given by the formulas

$$H_r = I_0'(kr) \sin kz, \qquad H_z = I_0(kr) \cos kz, \qquad (24)$$

where I_0 is the Bessel function of imaginary argument.

Finally, a mixed variant is possible with an arrangement of the poles along a helix (Fig. 4).

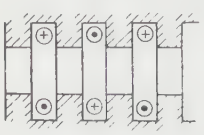

FIG. 3.

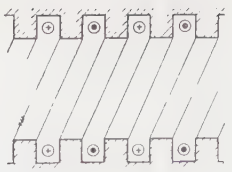

FIG. 4

The field in this case has a somewhat more complicated structure:

$$H_r = I_m'(kr) \cos(m\varphi - kz),$$

$$H_\varphi = -(m/kr) I_m(kr) \sin(m\varphi - kz),$$

$$H_z = I_m(kr) \sin(m\varphi - kz). \qquad (25)$$

Each of these variants has its advantages, and no one of them is universal. The variant with the multipole lens (Fig. 2) is relatively simple in construction. The danger associated with breakdown of adiabaticity at the field nodes can be easily eliminated if we place along the cylindrical surface a small auxiliary winding giving a weak constant longitudinal field H_z. Some construction difficulties can arise because of the necessity of changing the diameter of the pipe along its length and for bends in the channel.

The variant with disc-shaped poles (Fig. 3) does not have these disadvantages, since the magnetic circuit can consist of individual discs with their own windings. By smoothly varying the diameter and number of ampere turns in the lenses, one can achieve a widening of the channel and even a change in the period of the structure. By placing the disc lenses at small angles to one another, one can change the direction of the channel. We must regard as a defect of this variant a certain difficulty in satisfactorily eliminating possible breakdowns of adiabaticity at the field nodes: in this case the field vanishes not on nodal lines, but at isolated nodal points on the axis. The probability of passage through a node is small, but nevertheless it is not equal to zero. At the nodal points, all three Cartesian components of the field have a finite longitudinal derivative, so that the addition of a small constant field can only shift the nodal point, but not eliminate it. When nodal lines were present in the case of a plane field, it was sufficient to add a small component of field along the nodal line.

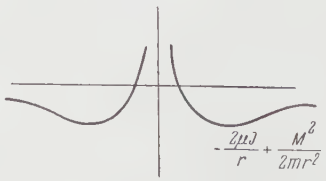

FIG. 5

A channel with disc lenses can be used apparently only in those cases where the total number of passages in the neighborhood of nodal points is small: for example, for single passage of neutrons through a relatively short channel.

The helical structure of the channel for m = 1 (two-pole helix) gives a magnetic field which has no nodal lines or nodal points. Therefore, the magnetic channel shown in Fig. 4 can be used without any auxiliary windings. Construction difficulties arise for turns of the channel and changes in cross section. The transition to another cross section does not require changing the ampere turns in the winding, as in the case of multipole lenses, but one need only preserve sufficiently well the constancy of the width of the pole and the groove. However, the shape of the poles and windings in these transitions will be quite complex.

All the configurations enumerated for magnetic mirrors and channels are computed on the basis of repulsion of neutrons with spin parallel to the field from regions with high field value. One can, of course, also use the attraction of neutrons of opposite polarization. However, neutrons with anti-parallel spin will necessarily be attracted to the magnetic poles or conductors carrying current and will be lost.

An exception might be the following lone case: a rectangular conductor with field $H = 2J/r$. In the neighborhood of the conductor, for neutrons with anti-parallel spin, there will be an attraction with potential $-2\mu J/r$. In combination with the centrifugal potential $M^2/2mr^2$ this gives a certain region of stable helical motion (Fig. 5) for neutrons which have a suitable value of their initial angular momentum $M < 2\sqrt{m\mu r_0 J}$ around the axis of the conductor. Here it is essential that the region accessible for motion of the neutrons be doubly connected, and any supports of the conductor will result in a partial loss in beam.

4. POLARIZED BEAMS

One possible application of mirrors with periodic magnetic structure may be the obtaining of beams of polarized neutrons. It is easy to see that the plane mirrors of the type shown in Fig. 1 do not have any advantages compared to the cobalt mirrors used at present, since the maximum grazing angle for a cobalt mirror is 2 — 3 times greater than for the period structure and correspondingly one has a higher intensity for the same size of mirror.

In the case of magnetic channels of cylindrical shape, certain advantages appear, associated with

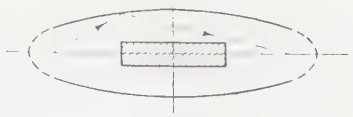

FIG. 6

focussing of the beam. The beam intensity in a long magnetic channel is equal to

$$N = \frac{\overline{n\upsilon}}{2}\frac{\pi\alpha^2}{4\pi}S, \qquad (26)$$

where $\overline{nv}$ is the flux of thermal neutrons at the wall of the reactor, α is an angle given by formula (2), S is the cross section area of the channel. The factor associated with solid angle is smaller than in the case of the cobalt mirror. However, the beam cross section in this case may be considerably greater. As a result, by using a sufficiently large magnetic channel with periodic structure, one can apparently obtain in practice a beam intensity several times (3 — 5) greater than with a good cobalt mirror. Of course, one should keep in mind that the magnetic channel is an extremely complicated gadget compared with a cobalt mirror. Thus, for example, for neutrons with energy $\sim 3 \times 10^{-2}$ ev emerging from the reactor, the limiting angle for a field of 5000 oe is $\alpha = 10^{-3}$. The length of channel must be no less than $2r/\alpha$, i.e. several tens of meters even for a beam only a few centimeters in diameter.

It is possible that the use of magnetic channels will turn out to be useful for obtaining beams of cold polarized neutrons with energies of the order of $10^{-4} - 10^{-3}$ ev. In this case, the glancing angle is somewhat larger, and the focussing properties of the channel can be used at smaller sizes. For purposes of reducing background one can use in place of a simple cylindrical mirror a periodic structure arranged on the surface of a highly prolate ellipsoid of revolution (Fig. 6) similar to the electrostatic mirror proposed by Grigor'ev.[1] In this case one can place a fast neutron shield along the axis of the channel.

5. CONFINEMENT OF COLD NEUTRONS

By applying the principle of reflection of neutrons from regions with high values of magnetic field, one can realize confinement of neutrons in vacuum by two methods: by bending the magnetically focusing channel into a ring, or making a simple, singly-connected region surrounded by a strong magnetic field. In the first case, there is a possibility for keeping neutrons with energies considerably exceeding the height of the magnetic potential barrier, and even to increase consider-

ably the phase volume of the neutron beam which can be captured in such an apparatus. However, motion of the neutron beam with small solid angle in such a ring channel would be based on an approximate independence of the transverse and longitudinal degrees of freedom, i.e., on the existence of approximate integrals of the motion. Over a long period of time even slight inaccuracies in the magnetic field configuration would lead to exchange of energy between these degrees of freedom and to loss of the neutrons as a result of their going beyond the admissible boundaries in solid angle.

In this connection, the estimates of possible neutron densities in "magnetic bottle" which follow refer to such a filling of the phase volume for which the moving of neutrons away from the walls is associated not with approximate integrals of the motion, but only with their total energy in the magnetic and gravitational fields, which for a field constant in time is an exact integral of the motion:

$$p^2/2m + |\mu H| + mgz = \text{const}. \qquad (27)$$

Here at each point inside the magnetic bottle motion of the neutrons is permitted in any direction, but the velocities are extremely small - of the order of 2 — 3 m/sec. Complicated regions similar to a torus have no advantages in this case, and magnetic channels are conveniently used only for initial filling of the volume with neutrons. Such a method for confining cold neutrons is very similar to that proposed by Zel'dovich[2] for preserving cold neutrons in vacuum by means of a potential barrier at the surface of a material with a positive coherent scattering amplitude.

If we take the magnetic channel from the reactor wall to some vacuum region surrounded by a magnetic field of periodic structure, it can be filled with super-cold neutrons with energy less than the value of the potential barrier $\mu H \approx 3 \times 10^{-8}$ ev (for H = 5000 oe). Moreover, one can carry out an isolation of the magnetic channel from the volume intended for storage by using a magnetic plug. After this the magnetic field in the channel can be switched off, or one can even disconnect the channel mechanically to eliminate background.

The time during which cold neutrons will remain in a magnetic bottle should be determined only by the half-life if the experimental arrangement is properly done. The number of neutrons remaining after a definite time of storage can be measured by a counter which during the storage time is either switched off the bottle by a magnetic field, or simply fed in and removed from the volume of the bottle.

To estimate the density of cold neutrons in the bottle we can use the formula

$$n = (2n_\Theta / 3\sqrt{\pi})\,(\mu H/\Theta)^{3/2}, \qquad (28)$$

where n is the neutron density in the bottle, n_Θ is the density of thermal neutrons at the boundary of the reactor, Θ is the neutron temperature. Here it is assumed that the cold part of the neutrons at the surface of the reactor is described by the usual thermal spectrum. Actually, the number of cold neutrons will be somewhat smaller because of absorption. The correction factor is approximately equal to

$$\sigma_0/(\sigma_0 + \sigma_a), \qquad (29)$$

where σ_a is the absorption cross section, σ_0 is the cross section for the process of energy exchange of the neutron with the moderator. In crystalline bodies, the cross section for inelastic scattering (collision with phonons) increases for cold neutrons proportional to v^{-1}, as does the absorption cross section. Because of this, there is no reason to expect any essential reduction in the factor (29) for super-cold neutrons. For good moderators (graphite, beryllium) it is close to unity. Heavy water in both liquid and solid state also satisfies the condition $\sigma_a \ll \sigma_0$ for extremely cold neutrons, and can be used as a source in such an experiment. The feasibility of using ice made from ordinary water and other cooling agents of solid hydrogenous materials requires more detailed investigation, since the absorption cross section of hydrogen is comparatively large, while the experimental data concerning inelastic cross sections for supercooled neutrons are not known in sufficient detail. Butterworth, Egelstaff, et al.[3] have used liquid hydrogen inside a reactor as moderator and obtained an increase in yield of cold neutrons compared with the beam from a graphite scatterer by a factor of 20 — 25.

The interaction of cold neutrons with vibrational degrees of freedom for chemically bound hydrogen in solids at low temperatures is relatively small.[4,5] The cross section for exchange of energy at low temperatures is of the same order as the absorption cross section, which limits the efficiency of cold coolants of hydrogen-containing moderator. It is possible that, despite the technical difficulties of working with liquid hydrogen inside a reactor, this method for obtaining an intense beam of cold neutrons is the most efficient.

For a reactor with a thermal neutron density of 10^8 cm^{-3}, the estimate (28) gives a value of the density in the magnetic bottle of the order of 10^4 m^{-3}. The use of cryogenic techniques inside a

reactor may increase this quantity by at least an order of magnitude.

In connection with the small value of the magnetic potential barrier, it is necessary to consider various secondary phenomena which may affect the collection and storage of cold neutrons in a magnetic bottle. Among such effects are: the influence of gravitation; the influence of a surface potential barrier on the boundary of the body, which serves as a source of cold neutrons, and also in possible thin shells along the path of the beam; heating and absorption of neutrons in collisions with residual gas and heating associated with mechanical vibrations of the magnetic bottle and noise in the magnetic field.

The force of gravity produces a potential energy varying with height approximately by 10^{-9} ev/cm. Consequently, neutrons with an energy of 3×10^{-8} ev can rise above the surface of the mirror to a height no greater than 30 cm. In this connection, the magnetic bottle need not necessarily be closed, but can be constructed in the form of a cup or a plate with the heavy neutron gas poured into it. The gravitational potential has an essential influence on the possible arrangement of the magnetic bottle near the reactor. Obviously, one can not place the storage region for cold neutrons lower than the point where the magnetic channel meets the reactor. In this case, even the slowest neutrons would be accelerated by the gravitational field, and the potential barrier of the magnetic field could not retain them. If the magnetic channel is arranged horizontally between the reactor and the storage region, the gravitational field will have practically no effect on the process of filling the magnetic bottle with neutrons.

There is also the possibility of arranging the magnetic bottle above the reactor and connecting it with the neutron source by a vertical channel. In this case, those neutrons will reach the storage region which when they were below had a velocity sufficient for overcoming the gravitational barrier. For a sufficiently exact arrangement of the magnetic channel, the degrees of freedom corresponding to the vertical and horizontal motion in it will be separated. In motion along the channel, the vertical component will change in accordance with the increase in gravitational potential, while the distribution of horizontal velocities will not depend on height. In the lower region, neutrons which are able to reach the bottle will move within a comparatively small solid angle. In the upper portion of the channel there will be all directions of motion. Since we are considering a single passage through the channel, the effect of inaccuracies on the separation of the degrees of freedom will not be too critical.

At the boundary of a material with a coherent scattering amplitude a and an atom density N, there is a potential barrier

$$u = 2\pi\hbar^2 Na/m, \tag{30}$$

where m is the neutron mass. For most light materials this potential is of the order of 10^{-7} ev. Obviously, in the neutron spectrum emerging from a material with positive scattering amplitude there will be very few neutrons with energy below the height of the barrier, since such neutrons can be produced only in the immediate surface layer of the material. (They must have negative kinetic energy inside the body.) If along the path of the neutrons from the source, located at the surface of the reactor, there is no change in the velocity of the neutrons until they reach the bottle region, then one can use as a source of cold neutrons with energy below 10^{-7} ev only materials with negative scattering amplitude. Of the light elements only hydrogen has a negative coherent scattering amplitude.

By making use of the gravitational potential one can, as was described above, transform the neutron spectrum leaving the reactor and obtain neutrons with kinetic energy of the order 10^{-8} ev even from a source with positive scattering amplitude. So, for example, in the case of a graphite source, which has a positive potential $\sim 1.5 \times 10^{-7}$ ev, one can obtain very cold neutrons with a length of vertical magnetic channel of the order of 1.5 m and more.

The repulsive action of nuclei with positive scattering amplitude eliminates the use of even the very thinnest films of such materials in cold neutron counters. For these purposes one can use only materials with negative scattering amplitude.

Let us consider the estimates of heating of neutrons associated with vibrations of the walls of the bottle. The number of collisions of the neutron with the walls, N_{coll}, during the time of observation t is equal to

$$N_{coll} \approx vt/l, \tag{31}$$

where l is the linear dimension of the bottle, v is the velocity of the neutrons. The change in kinetic energy of the neutron is given by

$$2m^{-1}\Delta\varepsilon = \Delta\overline{v^2} = 2N_{coll}\overline{v_w^2}, \tag{32}$$

where v_w is the effective velocity of the reflecting wall which is made up of mechanical vibrations and the fluctuations in the magnetic field

$$v_{ст} = v_{vib} + k\dot{H}/H. \tag{33}$$

The important vibrations are those with periods at least as great as the collision time of the neutron with the wall

$$\tau_{coll} \approx (kv)^{-1}, \quad (34)$$

i.e., in practice noise and vibrations with frequencies no higher than several hundred cycles per second. These estimates lead to requirements on mechanical vibrations which are easily fulfilled. The admissible modulation depth for the magnetic field at standard frequencies is found to be of the order of 10^{-4}, which is completely achievable technically if we consider the filtering action of the magnetic system itself. In fact, the depth of modulation of the field is $R/L\Omega$ times less than the depth of modulation of the voltage. Even for a time constant L/R of the order of 0.3 sec and a modulation depth for the voltage of 3×10^3, which is usual for rectifying equipment, the depth of modulation of a field of frequency 50 cps will be of the order of 3×10^{-5}.

Field fluctuations with higher frequencies $\Omega > \tau_{coll}^{-1}$ will also give some contribution to the heating of the neutrons, but they are easily filtered out by the conducting walls of the vacuum chamber and can in practice be completely eliminated.

These estimates show that the losses of cold neutrons due to heating upon reflection from the walls can be made sufficiently small. An elementary computation shows that losses of neutrons because of heating and absorption in collisions with residual gas is small compared with the natural decay even for pressures of the order of 10^{-5} mm Hg. Thus apparently there is nothing to prevent a direct determination of the neutron lifetime by using magnetic bottles, except for the relatively small density $10^4 - 10^5$ m^{-3} and the difficulties associated with background in the neighborhood of the reactor.

[1] V. K. Grigor'ev, Приборы техника и эксперимента (Instrum. and Exptl. Techniques) 5, (1960).

[2] Ya. B. Zel'dovich, JETP **36**, 1952 (1959), Soviet Phys. JETP **9**, 1389 (1959).

[3] Butterworth, Egelstaff, London, and Webb, Phil. Mag. **2**, 917 (1957).

[4] McReynolds, Nelkin, Rosenbluth, and Whittemore, Report of Second United Nations International Conference on the Peaceful Uses of Atomic Energy, Geneva, 1958, Volume **16**, page 279.

[5] Andresen, McReynolds, Nelkin, Rosenbluth, and Whittemore, Phys. Rev. **108**, 1092 (1957).

Translated by M. Hamermesh
198

THEORY OF ABSORPTION OF ULTRASOUND BY METALS IN A STRONG MAGNETIC FIELD. II

É. A. KANER

Institute of Radiophysics and Electronics, Academy of Sciences, Ukrainian S.S.R.

Submitted to JETP editor May 13, 1960

J. Exptl. Theoret. Phys. (U.S.S.R.) 39, 1071-1077 (October, 1960)

The asymptotic absorption of ultrasound by open Fermi surface metals located in a strong magnetic field is investigated. It is shown that the deformation absorption coefficient becomes saturated irrespective of the presence of open trajectories. A pronounced anisotropy of the saturation exists, depending on the position of the sound wave vector relative to the magnetic field and the direction of the open trajectory. Peculiarities of inductive absorption of ultrasound are studied in the case of open Fermi surfaces. The asymptotic value of the conductivity tensor in a magnetic field is computed by taking into account space dispersion.

1. INTRODUCTION

In a previous paper,[1] and also in the papers of V. Gurevich,[2,3] a theory of the magnetic absorption of ultrasound in metals at low temperatures has been constructed. In the works of Galkin and Gurevich,[2,4] the effect of the non-monotonic dependence of the absorption coefficient α on the magnetic field is investigated in the region of fields in which $\lambda\!\!\!^{-} \lesssim r \ll l$ ($2\pi\lambda\!\!\!^{-}$ is the length and k is the wave vector of the sound wave, r and l are the characteristic dimensions of the orbit and the length of the mean free path of the electron, respectively). The absorption has been studied[1,3] in strong fields, where $r \ll \lambda\!\!\!^{-}$. However, only closed energy surfaces have been considered as a basis. At the same time, it is well known that for most metals the presence of open Fermi surfaces passing through the entire reciprocal lattice is characteristic. Therefore, consideration of the peculiarities of ultrasonic absorption in metals with open Fermi surfaces is of interest, the more so that it has been generally impossible to interpret a series of experimental data[4,5] in terms of closed surfaces.

In the present communication, which is a continuation of a previous research,[1] results are given of a calculation of the asymptotic ultrasonic absorption in a strong magnetic field for metals with open Fermi surfaces. Mainly a surface of the type "spatial grid"[6] is considered, on which there are open trajectories of a different kind, together with closed and extremely elongated trajectories. In this regard, the "spatial grid" is very rich in different types of electron trajectories.

2. GENERAL FORMULAS FOR THE ABSORPTION COEFFICIENTS

The ultrasonic absorption coefficient has the form

$$\alpha = \hbar^{-3} W^{-1} \int d\tau_{\mathbf{p}} v \,|\, \chi^2 \,|\, \delta(\varepsilon - \mu), \tag{2.1}$$

where

$$\chi = \int_{-\infty}^{t} dt_1 (\Lambda - e\mathbf{E}'\mathbf{v}) \exp\left[\int_{t}^{t_1} (\nu - i\mathbf{k}\mathbf{v})\, dt'\right], \tag{2.2}$$

$$\Lambda = \dot{\delta\varepsilon} - \langle \dot{\delta\varepsilon} \rangle, \qquad \delta\varepsilon = \lambda_{ik}(\mathbf{p})\, u_{ik},$$

$$e\mathbf{E}' = e\mathbf{E} + c^{-1}[\dot{\mathbf{u}} \times \mathbf{H}] - \nabla \langle \delta\varepsilon \rangle; \qquad W = \tfrac{1}{2}\rho\omega^2 \,|\, \mathbf{u} \,|^2. \tag{2.3}$$

The rest of the notation here and below is the same as in reference 1. It is assumed that the collision integral can be replaced by the relaxation time $t_0(\mathbf{p}) = \nu^{-1}(\mathbf{p})$.

After integration by parts in Eq. (2.1), it is not difficult to show that the absorption is determined by the sum of three components:

$$\alpha = \alpha_\Lambda + \alpha_\sigma + \alpha_j, \tag{2.4}$$

α_Λ is the coefficient of deformation absorption:

$$\alpha_\Lambda = \hbar^{-3} W^{-1} \operatorname{Re} \int d\tau_{\mathbf{p}} \delta(\varepsilon - \mu)\, \Lambda^*(\mathbf{p}) \times \int_{-\infty}^{t} dt_1 \Lambda(t_1) \exp\left[\int_{t}^{t_1} dt' (\nu - i\mathbf{k}\mathbf{v})\right]; \tag{2.5}$$

α_σ is the coefficient of inductive absorption:

$$\alpha_\sigma = (2W)^{-1} \operatorname{Re} \sigma^s_{ik} E'_i E'^*_k; \tag{2.6}$$

α_j is the interference term:

$$\alpha_j = (2W)^{-1} \operatorname{Re}(\mathbf{j}_\Lambda(-\mathbf{H}) - \mathbf{j}_\Lambda(\mathbf{H}))\mathbf{E}'^*. \quad (2.7)$$

The quantities $\sigma^S_{ik} = \frac{1}{2}(\sigma_{ik} + \sigma_{ki})$ are the components of the symmetric part of the electrical conductivity tensor with account of spatial dispersion and magnetic field dependence:

$$\sigma_{ik}(\mathbf{k}, \mathbf{H}) = 2e^2h^{-3}\int d\tau_p \delta(\varepsilon - \mu) v_i(\mathbf{p}) \times \int_{-\infty}^{t} dt_1 v_k \exp\left[\int_t^{t_1} (\nu - i\mathbf{kv})\, dt'\right]; \quad (2.8)$$

$$\sigma_{ik}(\mathbf{k}, \mathbf{H}) = \sigma_{ik}(-\mathbf{k}, \mathbf{H}) = \sigma_{ki}(\mathbf{k}, -\mathbf{H}). \quad (2.9)$$

The deformation current is equal to

$$\mathbf{j}_\Lambda(\mathbf{k}, \mathbf{H}) = 2eh^{-3}\int d\tau_p \delta(\varepsilon - \mu)\mathbf{v} \times \int_{-\infty}^{t} dt_1 \Lambda(t_1) \exp\left[\int_t^{t_1} (\nu - i\mathbf{kv})\, dt'\right], \quad (2.10)$$

$$\mathbf{j}_\Lambda(\mathbf{k}, \mathbf{H}) = -\mathbf{j}_\Lambda(-\mathbf{k}, \mathbf{H}). \quad (2.11)$$

It follows from the symmetry properties (2.9) and (2.11) that the σ_{ik} are real and even quantities, while the components of the deformation current $\mathbf{j}_\Lambda$ are odd functions of the wave vector $\mathbf{k}$.

Thus our problem is the calculation of the deformation absorption α_Λ, the tensor $\sigma_{ik}(\mathbf{k}, \mathbf{H})$, the deformation current $\mathbf{j}_\Lambda$ and the electric field $\mathbf{E}$. To determine the latter, it is necessary to solve the Maxwell equation:

$$\frac{c^2}{4\pi i\omega}(k_i k_k - k^2\delta_{ik})E_k = \sigma_{ik}E'_k - j_{\Lambda i}. \quad (2.12)$$

This same equation, written in terms of E'_k, has the form

$$\left\{\sigma_{ik} - \frac{p^2}{4\pi i\omega}(k_i k_k - k^2\delta_{ik})\right\} E'_k = j_{\Lambda i} + \frac{c^2}{4\pi i\omega}(k^2\delta_{ik} - k_i k_k) G_k \equiv j'_i, \quad (2.13)$$

where

$$\mathbf{G} = c^{-1}[\dot{\mathbf{u}} \times \mathbf{H}].$$

The solution of the latter equation can be written down with the aid of the effective electric resistance tensor ρ'_{ik}:

$$E'_i = \rho'_{ik} j'_k, \qquad \rho'_{ik} = \left\{\sigma_{ik} + \frac{c^2}{4\pi i\omega}(k^2\delta_{ik} - k_i k_k)\right\}^{-1}. \quad (2.14)$$

These general formulas are employed below for the investigation of absorption in strong fields when the quantities $\gamma_0 = \nu T_0$ and $q_0 = kv_0 T_0$ are small (v_0 and T_0 are the characteristic velocity and period of motion of the electron in the magnetic field) and when one can expand σ_{ik} and $\mathbf{j}_\Lambda$ in series of these small parameters.

3. ASYMPTOTIC BEHAVIOR OF THE DEFORMATION ABSORPTION IN STRONG FIELDS

It is simplest to investigate the asymptotic behavior of the deformation absorption α_Λ in strong fields. We have

$$\alpha_\Lambda = h^{-3}W^{-1}eHc^{-1}\operatorname{Re}\int dp_z T(p_z)|\bar{\Lambda}|^2(\bar{\nu} - i\mathbf{k}\bar{\mathbf{v}})^{-1} = h^{-3}W^{-1}\int d\tau_p \delta(\varepsilon - \mu)|\bar{\Lambda}|^2\bar{\nu}[\bar{\nu}^2 + (\mathbf{k}\bar{\mathbf{v}})^2]^{-1}. \quad (3.1)$$

It is seen from this equation that if $\bar{\Lambda}$ does not vanish identically, then the deformation absorption does not depend on the magnetic field. Equation (3.1) coincides in form with the absorption in the absence of a magnetic field,[7] in which, however, all quantities are replaced by their average values over the trajectory $\epsilon(\mathbf{p}) = \mu$, $p_z = \text{const}$. If the trajectory is periodic, then the bar denotes simply the average over a period. In the case of a nonperiodic open trajectory, it is necessary to interpret the mean as

$$\bar{f} = \lim_{T\to\infty} T^{-1}\int_0^T f dt.$$

Physically, this circumstance is quite obvious if we consider that the rapid rotation of an electron with small radius leads to the averaging of all its characteristics over this rotational motion.

The frequency and temperature dependence of α_Λ depend essentially on the mutual orientation of the vectors $\mathbf{k}$ and $\mathbf{H}$ and the topology of the Fermi surface $\epsilon(\mathbf{p}) = \mu$.

Let us consider different possible cases.

a) $\mathbf{k}\cdot\bar{\mathbf{v}} \equiv 0$. This case is realized on closed trajectories for perpendicular vectors $\mathbf{k}$ and $\mathbf{H}$, and on open trajectories if $\mathbf{k}$ is parallel to the mean direction of the open trajectory.

Actually, for $\mathbf{k} \perp \mathbf{H}$ ($\mathbf{k} \parallel Ox$, $\mathbf{H} \parallel Oz$), we have $\mathbf{k}\cdot\bar{\mathbf{v}}_x = (kc/eH)\overline{dp_y/dt} \equiv 0$, if $p_y(t)$ changes within finite limits. On closed trajectories, the motion of the electron in the xy plane is always finite. On open trajectories, the motion of the electron in momentum space is finite only along the p_y axis, that is, when the wave vector is parallel to the Ox direction of the open trajectory. The absorption in this case is proportional to the square of the frequency and depends on the relaxation time (temperature):

$$\alpha_\Lambda = h^{-3}W^{-1}\int d\tau_p \delta(\varepsilon - \mu)|\bar{\Lambda}|^2\bar{\nu}^{-1} \sim N\mu\omega^2/\rho s^2\bar{\nu}. \quad (3.2)$$

b) The value of $\mathbf{k}\cdot\bar{\mathbf{v}}$ differs from zero but can vanish at certain p_z. Then $\bar{\nu}/[\bar{\nu}^2 + (\mathbf{k}\cdot\bar{\mathbf{v}})^2] = \pi\delta(\mathbf{k}\cdot\bar{\mathbf{v}})$, by definition of the δ function, and the

absorption increases linearly with frequency but does not depend on the relaxation time:

$$\alpha_\Lambda = \pi\hbar^{-3}W^{-1}\int d\tau_p |\bar{\Lambda}|^2 \delta(\mathbf{k}\bar{\mathbf{v}})\,\delta(\varepsilon-\mu) \sim N\mu\omega/\rho s v. \quad (3.3)$$

The identical situation takes place for perpendicular $\mathbf{k}$ and $\mathbf{H}$ both on closed and on open trajectories.

c) Finally, the value of $\mathbf{k}\cdot\bar{\mathbf{v}}$ never vanishes. This is possible only on open trajectories, when the wave vector $\mathbf{k}$ has a non-vanishing projection k_y in the direction perpendicular to the magnetic field and to the mean direction of the open trajectory Ox.

The absorption α_Λ in this case does not depend on the frequency:

$$\alpha_\Lambda = \hbar^{-3}W^{-1}\int d\tau_p |\bar{\Lambda}|^2 \bar{v}\,(\mathbf{k}\bar{\mathbf{v}})^{-2}\delta(\varepsilon-\mu) \sim N\mu\bar{v}/\rho v^2. \quad (3.4)$$

4. ASYMPTOTIC VALUE OF THE ELECTRICAL CONDUCTIVITY TENSOR AND OF THE DEFORMATION CURRENT

The dependence of the components of the tensor σ_{ik} and the current density j_{ik} on the magnetic field and the frequency, as also the asymptotic value of the deformation absorption, are essentially connected with the presence of open surfaces and orientations of the sound wave vector relative to the mean direction of the open trajectories. The latter as a rule exist along with closed trajectories, and therefore the total contribution to the absorption of these and the others depends on their relative "weight." The results given below are valid under the assumption that the "weights" of open and closed trajectories are identical.

a) The vector $\mathbf{k}$ is parallel to Ox (more precisely, $\vartheta \ll \varkappa/l$, ϑ is the angle between $\mathbf{k}$ and the Ox axis). In this case,

$$\sigma_{ik} = \begin{pmatrix} \gamma_0^2 A_{xx} & \gamma_0 A_{xy} & \gamma_0 A_{xz} \\ \gamma_0 A_{yx} & \alpha_{yy} & \alpha_{yz} \\ \gamma_0 A_{zx} & \alpha_{zy} & A_{zz} \end{pmatrix}, \qquad j_\Lambda \sim \frac{\sigma\Lambda_0}{ev_0}\begin{pmatrix} \gamma_0 q_0 \\ \gamma_0 \\ q_0 \end{pmatrix}, \quad (4.1)$$

where $A_{ik} = a_{ik} + \alpha_{ik}$; the tensor a_{ik} determines the contribution from closed, α_{ik} from open orbits. Inasmuch as the "weights" of both types of trajectories are identical, then $a_{ik} \sim \alpha_{ik} \sim \sigma$, where σ is the static electrical conductivity of the metal. $\Lambda_0 \sim \mu\omega ku$ is the characteristic value of the deformation potential.

b) For rotation of the wave vector in the plane perpendicular to $\mathbf{H}$ by an angle larger than $\varkappa/l$, the asymptotic values of σ_{ik} and j_Λ are essentially different:

$$\sigma_{ik} = \begin{pmatrix} q_0^2 a_{xx} & \gamma_0 a_{xy} & \gamma_0 A_{xz} \\ \gamma_0 a_{yx} & \gamma_0^2 q_0^{-2}\alpha_{yy} & \gamma_0^2 q_0^{-2}\alpha_{yz} \\ \gamma_0 A_{zx} & \gamma_0^2 q_0^{-2}\alpha_{zy} & a_{zz} \end{pmatrix}, \qquad j_\Lambda \sim \frac{\sigma\Lambda_0}{ev_0}\begin{pmatrix} q_0 \\ \gamma_0 q_0^{-1} \\ \gamma_0 q_0^{-1} \end{pmatrix} \quad (4.2)$$

We do not write down the precise expressions for the components of j_Λ, since they are expressed by integrals of the deformation potential Λ which in turn is known only in order of magnitude.

c) The vector $\mathbf{k}$ is deflected in the xz plane, where $k_z l \gg 1$ ($k_y = 0$). In this case,

$$\sigma_{ik} = \begin{pmatrix} \gamma_0 q_0 A_{xx} & \gamma_0 A_{xy} & \gamma_0^2 q_0^{-1} A_{xz} \\ \gamma_0 A_{yx} & \gamma_0 q_0^{-1}\alpha_{yy} & \gamma_0^2 q_0^{-2}\alpha_{yz} \\ \gamma_0^2 q_0^{-1} A_{zx} & \gamma_0^2 q_0^{-2}\alpha_{zy} & \gamma_0^2 q_0^{-2} A_{zz} \end{pmatrix}, \qquad j_\Lambda \sim \frac{\sigma\Lambda_0}{ev_0}\begin{pmatrix} \gamma_0 \\ \gamma_0 q_0^{-1} \\ \gamma_0^2 q_0^{-2} \end{pmatrix} \quad (4.3)$$

In all the formulas terms of higher degrees in the inverse field are kept. In particular, it is assumed that $q_0^2 \ll \gamma_0$.

d) Finally, for $k_y l \gg 1$, $k_z l \gg 1$,

$$\sigma_{ik} = \begin{pmatrix} \gamma_0 q_0 a_{xx} & \gamma_0 A_{xy} & k_y k_z^{-1}\gamma_0 A_{yx} \\ \gamma_0 A_{yx} & \gamma_0^2 q_0^{-2}\alpha_{yy} & \gamma_0^2 q_0^{-2}\alpha_{yz} \\ k_y k_z^{-1}\gamma_0 A_{xy} & \gamma_0^2 q_0^{-2}\alpha_{zy} & \gamma_0^2 q_0^{-2} A_{zz} \end{pmatrix},$$

$$j_\Lambda \sim \frac{\sigma\Lambda_0}{ev_0}\begin{pmatrix} \gamma_0 \\ \gamma_0 q_0^{-1} \\ \gamma_0 q_0^{-1} \end{pmatrix} \quad (4.4)$$

It is obvious from the results that have been given that the asymptotic value of the current density $j_i = \sigma_{ik}E'_k - j_{\Lambda i}$ is anisotropic and changes rapidly upon approach of the vector $\mathbf{k}$ to the direction of the open trajectory.

With the asymptotic expressions (4.1) — (4.4), it is not difficult to compute the tensor ρ'_{ik}, whose components determine the electric field $\mathbf{E}'$. However, the corresponding general formulas are extremely complicated and therefore we shall not write them out. In the next section the final results are given for the computation of the total absorption coefficient in the different limiting cases.

5. THE ANISOTROPY OF THE ABSORPTION IN A STRONG FIELD

a) The wave vector is parallel to the direction of the open trajectory. In the case in which $\delta < (r\varkappa)^{1/2}$ ($\delta = c(4\pi\omega\sigma)^{-1/2}$) is the characteristic thickness of the skin layer in the absence of a magnetic field), the deformation absorption plays the principal role and one can neglect the inductive and interference components in (2.4):

$$\alpha = \alpha_\Lambda = \hbar^{-3}W^{-1}\int d\tau_p \delta(\varepsilon-\mu)\,\bar{v}^{-1}|\bar{\Lambda}|^2 \sim N\mu\omega^2/\rho s^2 v. \quad (5.1)$$

Integration in this formula is carried out over

the entire surface $\epsilon(\mathbf{p}) = \mu$, on which there are both closed and open trajectories. The absorption α_Λ in a strong field is generally $l/\lambda\!\!\!^{-}$ times the absorption in the absence of the field α_0, equal to[7]

$$\alpha_0 = \pi h^{-3} W^{-1} \int d\tau_p \delta(\varepsilon - \mu) |\Lambda|^2 \delta(\mathbf{kv}) \sim N\mu\omega/\rho s v. \quad (5.2)$$

Upon subsequent increase of the magnetic field, where $(r\lambda\!\!\!^{-})^{1/2} < \delta$, the inductive absorption α_σ begins to play a principal role, and the deformation and interference terms can be neglected. We obtain:

$$\alpha = (2W)^{-1}\left(\frac{k^2c^2}{4\pi\omega}\right)^2 \rho_{yy} |G_y|^2 \sim \frac{N\mu\omega^2}{\rho s^2 \nu}\left(\frac{\delta^2}{r\lambda\!\!\!^{-}}\right)^2 \sim \omega^2 H^2 \nu u_x^2, \quad (5.3)$$

$$\rho_{yy} = (\sigma_{xx}\sigma_{zz} - \sigma_{xz}\sigma_{zx}) / \mathrm{Det}\,\sigma_{ik},$$

u_x is the projection of the sound polarization vector on the direction of the open trajectory. If $\mathbf{u} \perp Ox$, then the absorption is determined by Eq. (5.1) in the entire region of strong fields.

The inductive absorption α_σ, as Gurevich has shown,[3] is connected with the Joule losses from the electric field $\mathbf{G}$ which arises in the cutting of the magnetic lines of force by the conductor moving with velocity $\dot{\mathbf{u}}$.

b) The vector $\mathbf{k}$ is perpendicular to $\mathbf{H}$, $k_u l \gg 1$. In this case, deformation absorption takes place for $\delta < r$:

$$\alpha \sim N\mu\omega^2/\rho s^2 \nu \sim \alpha_0 (l/\lambda\!\!\!^{-}). \quad (5.4)$$

The exact formula is too cumbersome to write out. We only note that although the order estimate (5.4) for the absorption is the same as for $\mathbf{k} \parallel Ox$ [see (5.1)], a small change in the angle between $\mathbf{k}$ and the direction of the open trajectory in the interval $\vartheta \sim \lambda\!\!\!^{-}/l$ leads to a sharp change of α by a quantity of the order of magnitude of α itself. This change should be observed both for rotation of $\mathbf{k}$ relative to $\mathbf{H}$ and also for rotation of the magnetic field in the plane $\mathbf{H} \perp \mathbf{k}$, and can have any sign depending on the relative contribution of the open and closed trajectories.

Upon further increase of the magnetic field in the region where $r \lesssim \delta$, the estimate (5.4) remains in force, but the absorption can increase by a quantity of the same order as α.

c) The vector $\mathbf{k}$ lies in the plane xz ($k_y = 0$, $k_x l \gg 1$). Deformation absorption takes place for $\delta < r(\lambda\!\!\!^{-}/l)^{1/2}$:

$$\alpha \sim N\mu\omega/\rho s v \sim \alpha_0. \quad (5.5)$$

It is seen from a comparison of Eqs. (5.5) and (5.1) that the deflection of the vector $\mathbf{k}$ in the xz plane by a small angle $\vartheta \sim \lambda\!\!\!^{-}/l$ leads to a sharp decrease in the deformation of the absorption in a strong field (by a factor of kl). Upon further increase of the magnetic field, in the region where $r(\lambda\!\!\!^{-}/l)^{1/2} < \delta < \lambda\!\!\!^{-}(\lambda\!\!\!^{-}/r)^{1/2}$, the absorption increases by a quantity of the order of α_0, since the inductive field begins to play a role. In still greater fields, when $r \ll \delta^2 l/\lambda\!\!\!^{-2}$, while $\delta^2 l \ll \lambda\!\!\!^{-3}$, the inductive absorption dominates:

$$\alpha = \frac{1}{2W}\left(\frac{k^2c^2}{4\pi\omega}\right)^2 \frac{|G_y|^2}{\sigma_{yy}} \sim \alpha_0 \left(\frac{\delta^2 l}{r\lambda\!\!\!^{-2}}\right)^2 \sim \omega^3 H^2 u_x^2. \quad (5.6)$$

If $r \ll \delta^2 l/\lambda\!\!\!^{-2}$, $\delta^2 l \gg \lambda\!\!\!^{-3}$, then

$$\alpha = \sigma_{yy} |G_y|^2 / 2W \sim \alpha_0 q_0^{-2} \sim \omega^{-1} H^2 u_x^2. \quad (5.7)$$

d) The direction of the vector $\mathbf{k}$ is arbitrary, $k_y l \gg 1$, $k_z l \gg 1$. We shall not write down the general formula because of its unwieldy character, but will limit ourselves to qualitative discussion of the results. The order estimate (5.5) in the region where the deformation absorption plays the principal role is valid; however, the analytic expression for α has another form than in case c). In other words, for a small deviation of the vector $\mathbf{k}$ from the plane xz, a sharp change takes place in the absorption, of order of magnitude α_0.

In the region of inductive absorption,

$$\alpha = (\sigma_{xy}^2 \rho_{xx}/2W)|G_y|^2 \sim \alpha_0 \gamma_0 q_0^{-3} \sim H^2 \omega^{-2} \nu^{-1} u_x^2. \quad (5.8)$$

For arbitrary orientation of the vector $\mathbf{k}$ an unusual "resonance" effect ought to take place on the boundary between the regions of inductive and deformation absorptions. The maximum absorption is realized for $|kk_z c^2/4\pi\omega\sigma_{xy}| = 1$, and at the maximum, $\alpha_{max} \sim \alpha_0 kl \gg \alpha_0$. However, we note that this maximum is broad and smeared out, and that for "good" metals ($\sigma \sim 10^{20}$ sec^{-1}) it should be observed at a frequency $\omega/2\pi \sim 10^8 - 10^9$ cps, in very large fields of the order of several hundred kilooersteds. Generally inductive absorption takes place only in very strong magnetic fields. However, it is possible that in bismuth, where the conductivity is several orders smaller than in the case of other metals, this phenomenon can be observed, the more so that in the case of closed surfaces for $N_1 \neq N_2$, the "resonance" maximum is already sharper than in the presence of open trajectories. At the maximum $\alpha_{max} \sim \alpha_0 q_0^{-2}$, and far from it in both directions of deformation and inductive absorptions, $\alpha \sim \alpha_0 \ll \alpha_{max}$.*

Thus the calculations of the asymptotic value of the ultrasonic absorption in a strong magnetic field shows that the absorption coefficient reaches

*Evidently in the arrangement of similar experiments on Bi, it is necessary to take special precautions for violation of the equality $N_1 = N_2$ (for example, by introducing impurities).

saturation, the value of which depends essentially on the topology of the Fermi surface and the mutual orientation of the wave vector of the sound and the magnetic field. Experimental study of the anisotropy of the saturation makes it possible to draw certain conclusions on the presence of open trajectories, although it does not permit one to determine their direction uniquely. Upon further increase of the magnetic field, the inductive absorption begins to play a role. This absorption increases quadratically with the field. However, observation of inductive absorption at low temperatures is made difficult by the large value of the magnetic field.

A separate paper will be devoted to the comparison of the results of the theory developed here with experimental data.

[1] É. A. Kaner, JETP **38**, 212 (1960), Soviet Phys. JETP **11**, 154 (1960).

[2] V. L. Gurevich, JETP **37**, 71 (1959), Soviet Phys. JETP **10**, 51 (1960).

[3] V. L. Gurevich, JETP **37**, 1680 (1959), Soviet Phys. JETP **10**, 1190 (1960).

[4] Galkin, Kaner, and Korolyuk, Dokl. Akad. Nauk SSSR (1960) (in press).

[5] A. A. Galkin and A. P. Korolyuk, JETP **36**, 1307 (1958) and **37**, 310 (1959), Soviet Phys. JETP **9**, 925 (1959) and **10**, 219 (1960).

[6] I. M. Lifshitz and V. G. Peschanskiĭ, JETP **35**, 1251 (1958) and **38**, 188 (1960), Soviet Phys. JETP **8**, 875 (1959) and **11**, 137 (1960).

[7] Akhiezer, Kaganov, and Lyubarskiĭ, JETP **32**, 837 (1957), Soviet Phys. JETP **5**, 685 (1957).

Translated by R. T. Beyer
199

ASYMPTOTIC BEHAVIOR OF CROSS SECTIONS AT HIGH ENERGIES

V. B. BERESTETSKIĬ and I. Ya. POMERANCHUK

Submitted to JETP editor May 25, 1960

J. Exptl. Theoret. Phys. (U.S.S.R.) 39, 1078-1086 (October, 1960)

The transformation of two particles into three or four particles at high energies is treated in the pole approximation. In the energy region, in which the total elastic scattering cross section is independent of the energy, the cross section for the transformation of two particles into three does not decrease with increasing energy. The cross section for the transformation of two particles into four increases logarithmically with the energy. This result seems to indicate that at very high energies the elastic scattering cross section tends to zero.

1. The presently available data on the collisions of high energy particles make it plausible to suppose that the total effective cross section tends with increasing energy to a constant limit. This limit is of the order of $1/\mu^2$, where $1/\mu$ is the pion Compton wave length. Simultaneously with the total cross section also the diffraction elastic scattering cross section tends to a constant limit. It is then natural to assume in regard to the cross sections of individual inelastic processes (the formation of showers with a given number of particles), that each of these tends to zero with increasing energy. This is because the possible number of produced particles increases without bound with increasing energy and therefore the constant total cross section must be distributed among an ever increasing number of competing processes.

This simple picture may, however, be unwarranted. We shall give approximate calculations of effective cross sections of inelastic processes. These calculations result in a substantially different asymptotic behavior of the cross sections. The approximations made are not justified rigorously and therefore we do not claim that the results are fully convincing. These results however do indicate that the situation at high energies may be substantially more complex than expected.

2. Let us consider the transformation of two particles into three: $p_1 + q_1 \rightarrow p_2 + q_2 + k_2$, for example pion production in meson-nucleon or nucleon-nucleon collisions. The amplitude A for this process can be written as follows:

$$A = g\bar{u}(p_2)\gamma_5 u(p_1)\frac{A_1}{t-\mu^2} + A', \qquad t = (p_1 - p_2)^2. \quad (1)$$

Here the first term represents the pole term corresponding to the diagram of Fig. 1, A′ represents the remainder of the amplitude, g is the pion-nucleon coupling constant, and A_1 is the amplitude for scattering of pions by the particle q_1 (pion or nucleon).

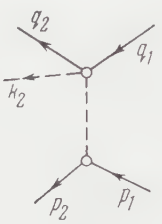

FIG. 1

We calculate the cross section for the process under study for small momentum transfers (of the order of μ), keeping the pole term only.[1] It seems natural to believe that, since A′ is determined by singularities for $t > 4\mu^2$, the discarded terms cannot fully compensate the contribution to the cross section from the pole term. Therefore the contribution from the pole term should give the correct order of magnitude for the cross section for small t. A more rigorous approach to the problem might consist of an investigation of the transition amplitude for large values of the orbital angular momentum $l > p/\mu$ (where p is the momentum of the incident particles in the barycentric frame). It seems plausible that for such cases the interaction would be dominated by the one meson exchange term (which corresponds to the pole term). In other words the partial cross sections for large values of l will be determined by only the pole diagram here considered.[2]

Let us emphasize that the partial cross sections so obtained are expressed in terms of real elastic scattering cross sections, determined by the amplitude A_1, and represent intrinsically positive quantities. If the partial cross sections are summed over l from p/μ to ∞, then the part of the cross section obtained in this manner will coincide in

order of magnitude with the cross section calculated by keeping only the pole term in the amplitude and integrating it over t between limits up to μ^2.

Let us remark that this approach does not coincide literally with the Chew and Low "pology,"[1] which results in a negative cross section and is connected with an extrapolation of the cross section into the unphysical region $t = \mu^2$. In contrast, we remain within the limits of the physical region $t < 0$. Since, however, we depart from the mass shell of the virtual meson by a quantity $< 2\mu^2$, and the mass singularities of the meson Green's function lie at values in excess of $9\mu^2$, there is reason to believe that the ignored terms will not affect the order of magnitude of the effect.

By keeping only the first term in Eq. (1) we obtain the following expression for the differential effective cross section:

$$d\sigma = \frac{f^2}{\pi}\,\frac{2M^2}{\mu^2}\,\frac{[s_1^2 - 2(m^2+\mu^2)s_1 + (m^2-\mu^2)^2]^{1/2}}{s^2 - 2(M^2+m^2)s + (M^2-m^2)^2}\,\sigma_1(s_1)\,ds_1, \tag{2}$$

$$s = (p_1+q_1)^2, \qquad s_1 = (q_2+k_2)^2, \qquad t = (p_1-p_2)^2,$$
$$f^2 = (g^2/4\pi)(\mu/2M)^2 = 0.08,$$

where M is the nucleon mass, μ is the pion mass, and σ_1 is the elastic scattering cross section of the meson by the particle q_1 ($q_1^2 = m^2$).

For high energies of the colliding particles ($s \gg M^2$) a small momentum transfer $|t| \lesssim \mu^2$ is possible provided that s_1 is within the limits

$$M^2 < s_1 < s\mu/M. \tag{3}$$

Indeed, t can be expressed in terms of s, s_1 and the angle ϑ between p_1 and p_2 in the barycentric frame as

$$\begin{aligned} t = {} & m^2 + s_1 - 2\left[\tfrac{1}{4}s + \tfrac{1}{2}(s_1 - M^2) + \tfrac{1}{4}s^{-1}(s_1-M^2)^2\right]^{1/2} \\ & \times\left[\tfrac{1}{4}s + \tfrac{1}{2}(m^2-M^2) + \tfrac{1}{4}s^{-1}(m^2-M^2)^2\right]^{1/2} \\ & + 2\cos\vartheta\left[\tfrac{1}{4}s - \tfrac{1}{2}(s_1+M^2) + \tfrac{1}{4}s^{-1}(s_1-M^2)^2\right]^{1/2} \\ & \times\left[\tfrac{1}{4}s - \tfrac{1}{2}(M^2+m^2) + \tfrac{1}{4}s^{-1}(M^2-m^2)^2\right]^{1/2}. \end{aligned} \tag{4}$$

For $s \gg M^2$ the requirement that t be small ($|t| \lesssim \mu^2$) can be satisfied only if $s_1 \ll s$. If at the same time $s_1 \gg M^2$ then the expression (4) becomes

$$t = -M^2 s_1^2/s^2 - s\vartheta^2/4, \tag{5}$$

from which Eq. (3) follows.

Formula (3) determines the region within which our pole approximation can be considered to be justified. For $s_1 \gg M^2$ the differential cross section (2) may be written as

$$d\sigma = \frac{f^2}{\pi}\,\frac{2M^2}{\mu^2}\,\sigma_1(s_1)\,\frac{s_1 ds_1}{s^2}. \tag{6}$$

Assuming σ_1 to be constant and integrating between the limits determined by the inequality (3) we obtain for the cross section of the process under study

$$\sigma = \frac{f^2}{\pi}\,\sigma_1. \tag{7}$$

Formula (7) is valid for the emission of a π^0 meson, as well as for the emission of a π^+ meson.

Chew and Low[1] obtained an analogous result but with a coefficient larger in comparison with Eq. (5) by a factor of M^2/μ^2 (see also Bonsignori and Selleri[3]). This is due to the fact that they integrated over s_1 up to values of order s, which corresponds to limits on the momentum transfer $|t|$ of about M^2. It seems to us that such an enlargement of the region requires additional justifications, since the discarded (non-pole) terms in the amplitude may turn out to play an important role.

We see that the cross section for the inelastic process of shower formation amounts to about 1 mb, does not decrease with energy, and represents a sizable fraction of the elastic scattering cross section.

3. Let us discuss now the energy spectrum and the angular distribution of the produced pion. To this end we assume that the process n + n → n + n + π has been reduced to elastic pion-nucleon scattering. At high energies of the π + n system the elastic scattering process is characterized by the dominant role played by small angle scattering events, to which correspond momentum transfers $t' = (q_1 - q_2)^2$ of the order of μ^2 or less:

$$|t'| = |(q_1-q_2)^2| \lesssim \mu^2.$$

On the other hand, in the integration of Eq. (2) over s_1 large values of s_1 dominate. Let us clarify what are the consequences of the conditions

$$|(q_1-q_2)^2| \lesssim \mu^2, \qquad s_1 = (q_2+k_2)^2 \gg m^2. \tag{8}$$

In the laboratory coordinate system, where $p_1 = 0$, we have

$$\begin{aligned} t' &= 2m^2 - 2q_1q_2 = 2m^2 - 2(E_1E_2 - \mathbf{q}_1\mathbf{q}_2) \\ &\approx 2m^2 - 2\left[E_1E_2 - \sqrt{E_1^2-m^2}\sqrt{E_2^2-m^2} + \tfrac{1}{2}E_1E_2\theta_{12}^2\right] \\ &\approx -m^2(E_1-E_2)^2/E_1E_2 - \theta_{12}^2E_1E_2. \end{aligned} \tag{9}$$

In the derivation of this relation the angle θ_{12} between $\mathbf{q}_1$ and $\mathbf{q}_2$ was assumed to be small since otherwise the condition that t' be small would be violated.

It follows from Eqs. (8) and (9) that

$$\theta_{12}^2E_1E_2 \lesssim \mu^2, \qquad m^2(E_1-E_2)^2/E_1E_2 \lesssim \mu^2. \tag{10}$$

As a consequence of the smallness of the recoil nucleon energy ($|t| \sim \mu^2$) the difference $E_1 - E_2$ is practically equal to the energy ω_2 of the produced pion. Therefore the second part of Eq. (10) can be replaced by

$$m^2\omega_2^2 / E_1(E_1 - \omega_2) \lesssim \mu^2. \tag{11}$$

This means, in effect, that ω_2 is limited from above as follows:

$$\omega_2 < \mu E_1 / m$$

[this result can also be seen from Eq. (3)].

Let us consider now the second of the conditions (8):

$$s_1 = m^2 + \mu^2 + 2q_2k_2 = m^2 + \mu^2 + 2(E_2\omega_2 - \mathbf{q}_2\mathbf{k}_2) \gg m^2. \tag{12}$$

From the inequality $|t| = |(p_1 - p_2)^2| \lesssim \mu^2$ it follows that in the laboratory system $|\mathbf{p}_2| \lesssim \mu$ [since $(p_{10} - p_{20})^2 \lesssim (\mu^2/2M)^2 \ll \mu^2$]. This is the momentum of the intermediate meson. Thus, the transverse momentum of the "incident" intermediate meson is of the order of or less than μ. As a result of the characteristics of elastic scattering the transverse momentum of the "scattered", i.e. produced, pion $\mathbf{k}_2$ must be of the same order of magnitude. Consequently the meson $\mathbf{k}_2$ must be emitted practically in the direction of $\mathbf{q}_1$, if its energy is high compared to μ. Taking this into account we obtain

$$\begin{aligned} s_1 &\approx \mu^2 + m^2 + 2\left[E_2\omega_2 \right. \\ &\quad \left. - \sqrt{E_2^2 - m^2}\sqrt{\omega_2^2 - \mu^2}\left(1 - \tfrac{1}{2}\theta^2_{k_2q_2}\right)\right] \\ &\approx m^2 + \mu^2 E_1/\omega_1 + E_2\omega_2\theta^2_{k_2q_2}. \end{aligned}$$

Here $\theta_{\mathbf{k}_2\mathbf{q}_2}$ is the angle between $\mathbf{k}_2$ and $\mathbf{q}_2$. Introducing the angles $\theta_{\mathbf{q}_1\mathbf{k}_2}$ and $\theta_{\mathbf{q}_1\mathbf{q}_2}$ by

$$\begin{aligned} \mathbf{q}_1\mathbf{q}_2 &= |\mathbf{q}_1||\mathbf{q}_2|\left(1 - \tfrac{1}{2}\theta^2_{q_1q_2}\right), \\ \mathbf{k}_2\mathbf{q}_1 &= |\mathbf{k}_2||\mathbf{q}_1|\left(1 - \tfrac{1}{2}\theta^2_{k_2q_1}\right), \end{aligned}$$

we see that as a consequence of the first inequality (10) we have $\theta_{\mathbf{q}_1\mathbf{q}_2} \lesssim \mu/\sqrt{E_1E_2} \approx \mu/E_1$, whereas $\theta_{\mathbf{k}_2\mathbf{q}_1}|\mathbf{k}_2|$, being the transverse momentum of the produced meson, satisfies the condition $|\mathbf{k}_2|\theta_{\mathbf{k}_2\mathbf{q}_1} \lesssim \mu$.

The angle $\theta_{\mathbf{k}_2\mathbf{q}_2}$ is determined in the usual manner:

$$\theta_{k_2q_2} = \theta_{k_2q_1} + \theta_{q_1q_2}.$$

We now rewrite Eq. (12) as follows:

$$s_1 \approx m^2 + \mu^2 E_1/\omega_2 + E_1\omega_2[\theta^2_{k_2q_1} + \theta^2_{q_1q_2} + 2\theta_{k_2q_1}\theta_{q_1q_2}], \tag{12a}$$
$$\theta_{k_2q_1} \lesssim \mu/\omega_2, \qquad \theta_{q_1q_2} \lesssim \mu/E_1, \qquad \omega_2 < \mu E_1/m.$$

The only way in which s_1 can be made large is to have

$$\omega_2 \ll E_1,$$

because the terms involving the angles contribute at most $E_1\omega_2\theta^2_{\mathbf{k}_2\mathbf{q}_1} \lesssim \mu^2E_1/\omega_2$, which is of the same order of magnitude as the term μ^2E_1/ω_2. Consequently, $s_1 \sim \mu^2E_1/\omega_2$. From here and from Eq. (4) it follows that the energy distribution of the produced pions is given in the region $\sigma(s_1) = \text{const}$ by:

$$As_1ds_1 = Bd\omega_2/\omega_2^3. \tag{13}$$

In summary, we arrive at the following characteristics of the part of the process $n + n \to n + n + \pi$ under discussion:

1. The transverse momenta of all particles at the end of the process are of order of μ.

2. The energy of the produced pion is low in comparison with the energy of the incident particle. The energy distribution is given by Eq. (13).

It is obvious that all these properties are independent of the nature of the incident particle, i.e. they are equally true for the processes

$$\pi + n \to \pi + \pi + n, \quad K + n \to K + \pi + n,$$

$$Y + n \to Y + \pi + n.$$

In principle, a possible experimental method for the studying of the above discussed processes would be to separate those events, in which the angular and energy distributions of the produced particles correspond to those obtained in elastic scattering of the incident particle by a particle with a mass of the order of the pion mass.

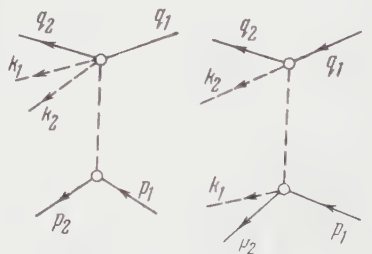

FIG. 2

FIG. 3

4. We discuss next the two particles into four particles transition process: $p_1 + q_1 \to p_2 + k_1 + q_2 + k_2$. Under the same assumptions, that were stated above in the discussion of the two particles into three particles transition, we may separate out a definite part of the cross section, determined by the pole term in the amplitude. There will be two types of such "pole" processes. First, the "single-stream" process depicted in the diagram of Fig. 2. Here the upper vertex is determined by the amplitude of the inelastic process corresponding to the two particles into three particles transition. And, second, the "double-stream" process depicted in the diagram of Fig. 3.

The amplitude for the double-stream process becomes in the pole approximation:

$$A = A_1 A_2 / (t - \mu^2), \tag{14}$$

where A_1 and A_2 are the amplitudes of the corresponding elastic scattering processes. For t $= (p_1 - p_2 - k_1)^2$ small ($|t| \lesssim \mu^2$) we may, as before, assume that the cross section is determined by the amplitude (14). In this manner we obtain the following expression for the differential cross section:

$$d\sigma = \frac{1}{16\pi^3} \frac{[s_1^2 - 2(m^2+\mu^2)s_1 + (m^2-\mu^2)^2]^{1/2}[s_2^2 - 2(M^2+\mu^2)s_2 + (M^2-\mu^2)^2]^{1/2}}{s^2 - 2(M^2+m^2)s + (M^2-\mu^2)^2} \sigma_1(s_1)\sigma_2(s_2)\, ds_1 ds_2 \int dt/(t-\mu^2)^2, \tag{15}$$

where $s_1 = (q_2 + k_2)^2$ and $s_2 = (p_2 + k_1)^2$. As before we are justified in extending the integration over t in the region $|t| \lesssim \mu^2$. At that the values of s_1 and s_2 must be restricted by

$$s_1 s_2 < \mu^2 s. \tag{16}$$

Equation (16) is easily derivable, just like Eq. (3). One need only in calculating t replace p_2 by $p_2 + k_1$, i.e. replace in Eq. (4) $s_1 \pm M^2$ by $s_1 \pm s_2$ ($s_1 \gg M^2$, $s_2 \gg M^2$). Equation (15) becomes

$$d\sigma = \frac{1}{16\pi^3} \frac{1}{\mu^2} \sigma_1(s_1)\sigma_2(s_2) \frac{s_1 s_2 ds_1 ds_2}{s^2}. \tag{17}$$

Let us discuss the energy and angular distributions of the produced particles. We shall characterize the process by the following invariants:

$$t_1 = (q_1 - q_2)^2; \quad s_1 = (k_2 + q_2)^2; \quad t_2 = (p_1 - p_2)^2,$$
$$s_2 = (k_1 + p_2)^2, \quad t = (q_1 - q_2 - k_2)^2.$$

As a consequence of the properties of the matrix elements of A_1 and A_2 we have

$$|t_1| \lesssim \mu^2, \qquad |t_2| \lesssim \mu^2.$$

The condition $|t_2| \leq \mu^2$ gives (in the coordinate system in which $p_1 = 0$)

$$|t_2| = 2p_1p_2 - 2m^2 = 2m(\sqrt{m^2 + \mathbf{p}_2^2} - m) \approx \mathbf{p}_2^2 \leqslant \mu^2,$$
$$|\mathbf{p}_2| \lesssim \mu. \tag{18}$$

For t_1 we obtain an expression analogous to Eq. (9):

$$|t_1| \approx m^2(E_1 - E_2)^2 / E_1E_2 + E_1E_2\theta_{q_1q_2}^2 \leqslant \mu^2, \quad E_1E_2\theta_{q_1q_2}^2 \leqslant \mu^2;$$
$$\frac{(E_1-E_2)^2}{E_1E_2} m^2 \approx \frac{(\omega_1+\omega_2)^2 m^2}{E_1(E_1-\omega_1-\omega_2)} \lesssim \mu^2, \qquad \omega_1 + \omega_2 < \frac{\mu}{m} E_1. \tag{19}$$

It is seen that E_2 is close to E_1 and therefore Eq. (18) gives the following estimate for $q_{2\perp}$ ($q_{2\perp}$ is perpendicular to q_1)

$$q_{2\perp} \approx E_1\theta_{q_1q_2} \lesssim \mu. \tag{20}$$

The pole approximation imposes on t the restriction: $t \lesssim \mu^2$. Introducing the vector $R = k_2 + q_2$, $R^2 = s_1$, we obtain

$$t = (q_1 - R)^2 = m^2 + s_1 - 2q_1R = m^2 + s_1 - 2E_1R_0$$
$$+ 2\mathbf{q}_1\mathbf{R} = m^2 + s_1 - 2E_1R_0 + 2\sqrt{E_1^2 - m^2}\sqrt{R_0^2 - R_\perp^2 - s_1}$$
$$= m^2 + s_1 - 2E_1^2 + 2\sqrt{E_1^2 - m^2}\sqrt{E_1^2 - s_1}$$
$$+ 2\left\{E_1(E_1 - R_0) + \sqrt{E_1^2 - m^2}\left[\sqrt{R_0^2 - s_1 - R_\perp^2}\right.\right.$$
$$\left.\left. - \sqrt{R_0^2 - s_1}\right] + \sqrt{E_1^2 - m^2}\left[\sqrt{R_0^2 - s_1} - \sqrt{E_1^2 - s_1}\right]\right\}$$
$$= -\Delta^2 - \left(\sqrt{E_1^2 - m^2} - \sqrt{E_1^2 - s_1}\right)^2$$
$$- 2[\Phi(E_1, E_1) - \Phi(E_1, R_0)], \tag{21}$$

$$\Delta^2 = \sqrt{E_1^2 - m^2}\left[\sqrt{R_0^2 - s_1} - \sqrt{R_0^2 - s_1 - R_\perp^2}\right] > 0,$$

$$\Phi(E_1, R_0) = \sqrt{E_1^2 - m^2}\sqrt{R_0^2 - s_1} - E_1R_0.$$

Let us determine the derivative of Φ with respect to R_0:

$$\frac{\partial\Phi}{\partial R_0} = \frac{R_0}{\sqrt{R_0^2 - s_1}}\sqrt{E_1^2 - m^2} - E_1$$
$$= E_1\left[\frac{\sqrt{1 - m^2/E_1^2}}{\sqrt{1 - s_1/R_0^2}} - 1\right] > 0,$$

since $s_1 > m$, and $R_0 < E_1$. Thus $\Phi(E_1, E_1)$ is larger than $\Phi(E_1, R_0)$ for $R_0 < E_1$. Consequently all three terms entering into Eq. (21) have the same sign. Hence from the condition $|t| \lesssim \mu^2$ we obtain a restriction on Δ^2 and, consequently, on $R_\perp$:

$$\Delta^2 \lesssim \mu^2, \; R_\perp^2 \lesssim \mu^2, \qquad |\mathbf{k}_{2\perp} + \mathbf{q}_{2\perp}| \lesssim \mu. \tag{22}$$

Together with Eq. (19) this yields

$$|\mathbf{k}_{2\perp}| \sim \omega_2\theta_{k_2q_1} \lesssim \mu. \tag{23}$$

Thus the virtual meson k_2 has a transverse momentum of the order of μ. And from here it, finally, follows (on the basis of Eqs. (18) and (22)) that the transverse momentum of the meson k_1 is also of order of μ:

$$k_{1\perp} = \omega_1\theta_{k_1q_1} \lesssim \mu. \tag{24}$$

Equations (20), (23), and (24) give the effective angular region within which most of the produced particles are emitted. The transverse momentum

of each particle is of the order of μ. All particles (except for the recoil nucleon p_2) are emitted at a small angle with respect to the direction of the incident particle. The energy distribution of the produced mesons k_1 and k_2, integrated over their angles, is determined by the distribution in s_1 and s_2 (for constant σ_1 and σ_2):

$$s_1 s_2 \, ds_1 \, ds_2. \tag{25}$$

The relation between s_2 and the frequency ω_2 is as follows:

$$s_2 = (p_2 + k_1)^2 = M^2 + \mu^2 + 2\varepsilon_2\omega_1 - \mathbf{p}_2\mathbf{k}_1.$$

On the basis of Eq. (18) we find $|\mathbf{p}_2| \lesssim \mu \ll \epsilon_2 \approx m$ and therefore s_2 takes on the simple form: $s_2 \approx 2m\omega_1$ (when $s_2 \gg m^2$).

In analogy with Eq. (12a) $s_1 = (k_2 + q_1)^2$ can be expressed as follows:

$$s_1 \sim \mu^2 E_1 / \omega_2 \approx \mu^2 s / 2m\omega_2.$$

The condition $s_1 s_2 < \mu^2 s$ gives $\omega_1 < \omega_2$. Using Eq. (25) we get for the energy distribution of the produced mesons:

$$\omega_1 d\omega_1 \cdot \omega_2^{-3} d\omega_2; \qquad \mu < \omega_1 < \omega_2, \qquad \mu < \omega_2 < \mu E_1 / m$$

[the last condition is a consequence of Eq. (16)].

In evaluating Eq. (17) we did not take into account the contribution of the crossed diagram obtained from Fig. 3 by interchanging the meson lines k_1 and k_2. The results obtained above indicate that we may neglect the interference terms arising from the pole terms in the diagram of Fig. 3 and its crossed diagram. Indeed, the quantities s_1 and s_2, entering into the amplitude A corresponding to the diagram of Fig. 3, are of the order of $\mu^2 E_1/\omega_1$ and $2m\omega_2$. The corresponding quantities s_1' and s_2' entering into the amplitude $A^{(c)}$ corresponding to the crossed diagram are equal to $\mu^2 E_1/\omega_2$ and $2m\omega_1$. At high energies, each of the elastic scattering amplitudes appearing in A and $A^{(c)}$ is proportional to its s parameter [the elastic pion-nucleon scattering amplitude in the most important diffraction region is, for σ = const, of the form $s_1 f(t_1)$ and $s_2 f(t_2)$ respectively]. Therefore A is proportional to $s_1 s_2 \sim \omega_2/\omega_1$, whereas $A^{(c)}$ is proportional to $s_1' s_2' \sim \omega_1/\omega_2$. Since $\omega_1 \neq \omega_2$, the neglect of the interference terms cannot affect the order of magnitude of the cross section.

Let us integrate Eq. (17) over the region (16) treating σ_1 and σ_2 as constant. When the crossed diagram and the isotopic states of the produced mesons are taken into account this yields for the cross section

$$\sigma \approx \frac{3\mu^2}{8\pi^3} \sigma_1 \sigma_2 \ln \frac{s}{M^2}. \tag{26}$$

The result, Eq. (26), exhibits the internal inconsistency of the hypothesis of constant total and elastic cross sections at high energies. Starting from the assumption of constant elastic and total cross sections we have arrived at a logarithmically increasing cross section for two-pion production. Gribov[4] has independently and by a different method arrived at the conclusion that there could be a contradiction in the assumption of a constant elastic scattering cross section.

5. In an analogous manner we can crudely estimate production processes of arbitrary multiplicity. The amplitudes for such processes contain pole

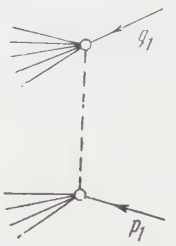

FIG. 4

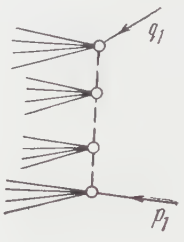

FIG. 5

diagrams, of the type shown in Fig. 4, with an arbitrary number of particles at each knot.* To the diagram of Fig. 4 corresponds the amplitude

$$A = A_1 A_2 / (t - \mu^2),$$

where A_1 and A_2 are the amplitudes for the inelastic processes resulting from the collision of the intermediate meson with the particles q_1 and p_1. Summing the cross sections corresponding to various inelastic processes we arrive at the expression:

$$d\sigma(s) \sim \sigma(s_1)\,\sigma(s_2)\, s_1 s_2 s^{-2} \, ds_1 \, ds_2, \tag{27}$$

where σ is the total cross section. Equation (27) exhibits the same internal inconsistency as Eq. (17). The assumption of a constant cross section σ leads after its integration to a proportionality of the cross section to the logarithm of s. Let us note, however, that Eq. (27) is less reliable than Eq. (17) because in addition to the diagram of Fig. 5 a large number of crossed diagrams should have been taken into account, and it is difficult to estimate the corresponding interference terms and to calculate the value of the coefficient in Eq. (27). An investigation of the "many-stream" processes of the type pictured in Fig. 5 leads to analogous

*Such a process, for an energy of 9 Bev, was discussed by Dremin and Chernavskiĭ.[5]

contradictions $\sigma \sim (\ln s)^N$, where N is the number of "streams".

If the assumption of constant cross sections is given up, then Eqs. (17) and (27) may be viewed as integral equations which must be satisfied by the cross sections $\sigma(s)$. They are satisfied if the cross sections fall off with energy, and it turns out that a rather slow fall off is sufficient [just barely faster than $(\ln s)^{-1}$]. The considerations of Gribov[4] lead to the same conclusions. Let us note here that under these conditions the resultant showers are characterized by a specific distribution in s_1 and s_2. Namely their main part has one of the masses ($\sqrt{s_1}$ or $\sqrt{s_2}$) always small and s-independent, and the other mass is of the order of s. Such a distribution is substantially different from that given by the statistical-thermodynamical theory of Fermi and Landau, in which each mass is (on the average) proportional to $s^{1/4}$.

6. It is not quite clear what conclusions may be drawn from the above obtained results. It may be that they are simply an indication that our approximation, consisting of neglecting of all contributions other than those arising from pole terms, is unjustifiable although at this time we see no serious basis for such a conclusion. If, however, our approximation is reasonable and if it can be assumed that nuclear interactions continue also at high energies to fall off exponentially at distances in excess of $1/\mu$, then it seems to us that the only possible conclusion is that the total and elastic cross sections for the interaction tend to zero as the energy is indefinitely increased.

The existing experimental data seem to indicate that the cross sections are constant in a large interval of high energies. This, however, is not in contradiction with the conclusion on the asymptotic fall off of cross sections. The point is that the expression (17) for the cross section contains a small numerical coefficient.* Therefore the possibility cannot be excluded that the effects due to the discussed by us processes only begin to be significant at ultra high energies. [As was noted above, we were not able to determine the coefficient in Eq. (27).] The authors cannot hide the feelings of surprise experienced by them at the thought that coefficients consisting purely of numbers can result in the appearance of new asymptotic regions. In order to understand the physics connected with the falling off of the cross sections at high energies it would be most desirable to see directly (for example, by means of diagrams) the mechanism responsible for this phenomenon, provided of course that it is really there.

In conclusion we wish to express our gratitude to V. N. Gribov, L. D. Landau, V. N. Mel'nikov, L. B. Okun' and I. M. Shmushkevich for interesting discussions related to this work.

*It should be once more emphasized that the smallness of this coefficient is due to the restriction of the region of integration by $|t| < \mu^2$. One cannot a priori exclude the possibility that the value of the coefficient might be changed by contributions from the region $|t| > \mu^2$.

[1] G. F. Chew and F. E. Low, Phys. Rev. **113**, 1640 (1959).

[2] L. B. Okun' and I. Ya. Pomeranchuk, JETP **36**, 300 (1959), Soviet Phys. JETP **9**, 207 (1959).

[3] B. Bonsignori and F. Selleri, Nuovo cimento **15**, 464 (1960).

[4] V. N. Gribov, Nucl. Phys. (in press).

[5] I. M. Dremin and D. S. Chernavskiĭ, JETP **38**, 229 (1960), Soviet Phys. JETP **11**, 167 (1960).

Translated by A. M. Bincer
200

ENERGY FLUCTUATIONS IN PARTICLE INTERACTIONS AT HIGH ENERGIES

N. M. GERASIMOVA

P. N. Lebedev Physics Institute Academy of Sciences, U.S.S.R.

Submitted to JETP editor May 28, 1960

J. Exptl. Theoret. Phys. (U.S.S.R.) **39**, 1087-1090 (October, 1960)

We consider fluctuations in the energy given to particles of a particular kind in an elementary interaction at high energy. The calculations are carried out on the basis of the hydrodynamical theory of multiple particle production.

At the present time, many experiments on multiple particle production are concerned with fluctuations in various characteristics of the interaction between high energy particles. It is interesting to consider this question from the point of view of Landau's hydrodynamic theory.[1]

There are several reasons why it is difficult to obtain the magnitude of the fluctuations predicted by this theory. The theory itself is applicable only at sufficiently high energies, where the fluctuations are small. Experimentally attainable energies are just at the lower limit of the theory's range of validity. Moreover, fluctuations in the various quantities of interest must be distinguished from fluctuations in the temperature T_k at which the system decays, this temperature being a parameter in the theory. For these reasons, the calculations described below should be considered as giving estimates only.

Bearing the above considerations in mind, let us examine the fluctuations in the energy given to a particular kind of particles as these particles are produced in high energy interactions.

Podgoretskiĭ et al.[2] have calculated the magnitudes of the fluctuations in the total energy and the total number of particles. For simplicity, we assume that only π mesons and nucleons are produced in the interaction of particles at high energies. At the moment when the element of fluid decays, its temperature in its rest frame is T_k; the mesons and nucleons are distributed according to the Bose and Fermi equilibrium distributions respectively.

The motion of the expanding liquid is isentropic; each element of volume is thermally insulated. The existence of two kinds of particles in each volume element can be taken into account by considering two sub-systems in each volume element, the sub-systems being able to exchange energy with each other. Then for each kind of particle, the fluctuations in the number of particles N_i and in their energy E'_i can be calculated from the usual formulas for an isothermal process:[3]

$$\overline{(\Delta N_i)^2} = T_k \frac{\partial N_i}{\partial \mu_i}; \qquad \overline{(\Delta E')^2} = T_k \int_{m_i}^{\infty} \varepsilon_i'^2 \frac{\partial}{\partial \mu_i} dN_i. \tag{1}$$

In (1), μ_i is the chemical potential and m_i is the mass of particles of type i*; the prime denotes quantities in the laboratory frame of reference.

The relation between the energy fluctuations in the laboratory frame of reference and the distribution function $\rho(\epsilon) = dN(\epsilon)/2\pi d\epsilon$ in the rest frame is given by the following equation (see reference 1):

$$\overline{(\Delta E_i')^2} = \frac{g_i T_k}{4\pi^2} \frac{\partial}{\partial \mu_i} \int dV' \int_{m_i}^{\infty} \varepsilon_i' d\varepsilon_i' \int_{\varepsilon_i'/2\gamma'}^{\infty} \frac{\rho(\varepsilon_i)\, d\varepsilon_i}{(\varepsilon_i^2 - m_i^2)^{1/2}}, \tag{2}$$

where $\gamma' = (1 - v'^2)^{-1/2}$ and v' is the speed of the particle in the laboratory frame of reference.

We substitute the expression for $\rho(\epsilon)$ into (2) and differentiate with respect to μ_i. We then set μ_i equal to zero, and carry out the following calculations for π mesons only. Integration with respect to $d\epsilon_i$ and $d\epsilon'_i$ leads to the expression

$$\overline{(\Delta E')^2} = \frac{gm^3}{4\pi} T_k^2 \int dV' \sum_{n=0}^{\infty} \frac{(-1)^n}{n+1} \exp\left[-\frac{(n+1)m}{2\gamma' T_k}\right] \times \left[1 + 8\frac{T_k \gamma'}{m(n+1)} + 16\left(\frac{T_k}{m}\right)^2 \left(\frac{\gamma'}{n+1}\right)^2 + 32\left(\frac{T_k}{m}\right)^3 \left(\frac{\gamma'}{n+1}\right)^3\right]. \tag{3}$$

The next step is to integrate with respect to dV'. It should be noted that each element of the system decays at its own time t_k, determined by the equation $T(x, t_k) = T_k$. Hence we must be careful to state what we mean by integrating over

*The units are such that $\hbar = c = k = 1$, where k is Boltzmann's constant.

the whole system, i.e., by the integration over dV′ in (2) and (3). (Each dV′ must be taken at its own moment of time t_k.)

To do this we make use of the fact that the entropy of each element is conserved as it decays. Hence, in order to sum over all the volume elements, each decaying into discrete particles when its own time comes, it is convenient to integrate over the entropy of these elements, the entropy being given by

$$dV' = \frac{dV'}{dS}\, dS, \tag{4}$$

dV′/dS and dS are taken at the critical time. The integration over dS can in its turn be replaced by an integration over dγ′ ("velocities"), since the integrand in (3) depends on x′ only through γ′.

If the condition $T(x, t_k) = T_k$ is satisfied, the relation between entropy and momentum can be taken to be that obtained from a one-dimensional solution of the problem. As shown by Milekhin,[4] this is given to a good approximation by

$$dS \simeq \frac{S_0}{\sqrt{2\pi L}} \exp\left[-\frac{\eta_0^2}{2L}\right] \frac{d\eta_0}{d\gamma'}\, d\gamma' \tag{5}$$

where the index 0 denotes quantities in the center-of-mass frame, and $\gamma_c = (1 - v_c^2)^{-1/2}$, v_c being the velocity in the center-of-mass system. The quantity $S_0 = s_0 x_0$, where s_0 is the initial entropy density and $x_0 = V_0/\sigma$. $V_0 = 2\pi/3m^3\gamma_c$ is the initial volume of the system and σ is the cross section. Furthermore,

$$\eta_0 = \ln 2\gamma_0, \quad \eta' = \ln 2\gamma', \quad \eta_c = \ln 2\gamma_c, \quad \eta' = \eta_0 + \eta_c, \tag{6}$$

where $\gamma_0 = (1 - v_0^2)^{-1/2}$, v_0 being the particle velocity in the center-of-mass frame. (This notation agrees with that of Milekhin[4].)

On the other hand, the entropy in a thickness dx_0 is given by $dS_0 \approx s u_0 dx_0$, so that

$$dV'/ds \approx \sigma/\gamma_c\gamma_0 s \qquad (u_0 \equiv \gamma_0). \tag{7}$$

Finally, we have the equations

$$dV'/d\gamma' = 2V_0 (T_0/T_\kappa)^3 \exp\left\{\frac{-(\ln 2\gamma' - \ln 2\gamma_c)^2}{2L}\right\}/\gamma'^2\sqrt{2\pi L},$$

$$T_0 \approx mc^2 (E'/Mc^2)^{1/4}, \qquad L = \tfrac{1}{2}\ln(E'/M) = \eta_c - \ln 2. \tag{8}$$

The derivation of formula (8) uses Landau's expression[1] for dS_0 in the non-trivial solution of the hydrodynamic problem. Hence, upon substituting (8) in (3), the limits of integration should be γ_1' and γ_2', which define the region of validity of the non-trivial solution with running waves,[5] i.e.,

$$\gamma_1' = \gamma_c (T_k/T_0)^{\sqrt{3}}, \qquad \gamma_2' = \gamma_c (T_0/T_k)^{\sqrt{3}}. \tag{9}$$

In evaluating the integral (3) for energies E′ $\gtrsim 10^{12}$ ev, so that the hydrodynamic theory is valid, we can take $\gamma' \gg 1$, so that all terms except the last can be neglected. Similarly, all terms in the sum over n except the zeroth one can be neglected without introducing an error greater than ~10%. Then

$$\overline{(\Delta E')^2_{min}} \approx \frac{32}{3\pi\gamma_c} g T_k^2 \left(\frac{T_0}{m}\right)^3 \frac{1}{\sqrt{2\pi L}} \times \int_{\gamma_1'}^{\gamma_2'} \exp\left[-\frac{m}{2T_k\gamma'} - \frac{(\ln 2\gamma' - \eta_c)^2}{2L}\right] \gamma' d\gamma'. \tag{10}$$

Upon putting g = 1 in (10) we obtain the order of magnitude of the lower limit to the size of the fluctuations in the energy given to π^0 or $\pi^\pm$ mesons in high-energy interactions.

We can estimate qualitatively the contribution to the energy fluctuation given by the fastest particle not taken into account in formula (10). To do this, we put in (3) $\gamma' = \gamma_2'$, which corresponds to a traveling wave, and integrate (3) over the volume occupied by the traveling wave when the condition $T(x, t) = T_k$ is satisfied. The result is

$$(\Delta E')^2 \approx (32/3\pi)\, g T_k^2 (T_k/m)^3 (T_0/T_k)^{3\sqrt{3}} \gamma_c^2. \tag{11}$$

Similarly we can make a very rough estimate of the probability that the fastest particle carries away a definite fraction of the energy possessed by the primary particle. To do this we substitute γ_2' in the differential equation obtained by Podgoretskiĭ et al.[2] for the distribution in energy of the particles in a given volume element in the laboratory frame. Carrying out the appropriate integrations, we obtain

$$\frac{dW}{dE} = D \sum_{n=0}^{\infty} \frac{(-1)^n}{\gamma' m} \exp\left[-\frac{(n+1)}{2\gamma'}\frac{\delta E'}{m}\alpha\right]\left(\frac{\delta E'}{2\gamma' m} + \frac{\alpha}{n+1}\right),$$

$$D = \sum_{n=0}^{\infty} \frac{(-1)^n}{n+1} K_2[(n+1)\alpha], \tag{12}$$

where $\alpha = T_k/m$, and K_2 is the modified second-order Bessel function.[6]

From an analysis of interactions in certain materials, Grigorov, Murzin, and Rapoport[7] have found how much of the primary particle energy was carried away by π^0 mesons and how much was carried away by one charged particle. According to preliminary data privately communicated to the author by V. S. Murzin, for cosmic rays having energy ~ 10^{12} ev and interacting with iron nuclei, $\overline{(\Delta E')^2}/(E')^2 \approx 0.03$ for π^0 mesons. Values of $\overline{(\Delta E')^2}/(E')^2$ calculated from (10) for about the same energy are of about the same magnitude [(10) and (11) contribute about equally for E′ ~ 10^{12} ev and together amount to ~ 0.05].

Similarly, there is fairly close agreement between the experimental curve for the distribution in energy of the fastest charged particles and formula (12). However, as mentioned above, such an agreement probably has no quantitative significance.

In conclusion, comparison with experiment shows that the fluctuations in the energy given to π mesons in interactions at high energy can be qualitatively described by the hydrodynamic theory of multiple particle production.

The author would like to thank I. L. Rozental', G. A. Milekhin, and V. S. Murzin for useful discussions.

[1] L. D. Landau, Izv. Akad. Nauk SSSR, Ser. Fiz. **17**, 51 (1953); S. Z. Belenkiĭ and L. D. Landau, Usp. Fiz. Nauk **56**, 309 (1955).

[2] Podgoretskiĭ, Rozental', and Chernavskiĭ, JETP **29**, 296 (1955), Soviet Phys. JETP **2**, 211 (1956).

[3] L. D. Landau and E. M. Lifshitz, Статистическая физика (Statistical Physics), Gostekhizdat (1951); Engl. Transl. Addison-Wesley, Reading, Mass. (1958).

[4] G. A. Milekhin, JETP **35**, 978, 1185 (1958), Soviet Phys. JETP **8**, 682, 829 (1959).

[5] N. M. Gerasimova and D. S. Chernavskiĭ, JETP **29**, 372 (1955), Soviet Phys. JETP **2**, 344 (1956).

[6] G. N. Watson, Theory of Bessel Functions (Russ. Transl.), II L, Vol. 2, 1949, p. 89.

[7] Grigorov, Murzin, and Rapoport, JETP **36**, 1068 (1959), Soviet Phys. JETP **9**, 759 (1959).

Translated by R. Krotkov
201

A METHOD FOR THE CALCULATION OF THE STATISTICAL WEIGHTS AND DISTRIBUTIONS IN THEORIES OF MULTIPLE PRODUCTION

G. I. KOPYLOV

Joint Institute for Nuclear Research

Submitted to JETP editor May 11, 1960

J. Exptl. Theoret. Phys. (U.S.S.R.) 39, 1091-1098 (October, 1960)

An effective method for obtaining the distributions and correlations in arbitrary models of multiple production has been developed. The formulas for the covariant model are especially simple. It is shown how a study of this model may facilitate the calculations for more complicated models.

THE success of Fermi's statistical theory in predicting the yield of antiprotons at 25 Bev received much attention. However, there was compelling evidence that the final states in multiple production do not have equal probability.[1] This implies that one must take account of the dependence of the square of the transition matrix element

$$|H_{if}|^2 = F(\mathbf{p}_1, \ldots, \mathbf{p}_n) \equiv F(\mathbf{p})$$

on the characteristics of the states in the general expression for the transition probability. The calculation of the statistical weights and spectra in the new theories of multiple production, therefore, involves integrals of the type

$$S_n(E, \mathbf{P}) = \int F(\mathbf{p})\, \delta(\Sigma \mathbf{p}_k - \mathbf{P})\, \delta(\Sigma e_k - E)\, d\mathbf{p}_1 \ldots d\mathbf{p}_n \quad (1)$$

An example of this is the covariant model of Srivastava and Sudarshan,[2] where

$$F = (2^n e_1 \ldots e_n)^{-1}. \quad (1')$$

The usual methods for calculating statistical weights,[3] including the very effective Monte Carlo methods,[4] apply to the case $F(\mathbf{p}) = \text{const}$ and cannot be used for arbitrary functions F. We are thus confronted with the task of finding a general method for the determination of the characteristics of the interaction, i.e., the momentum and angular distributions, the correlations, the weights of the reactions, etc, for an arbitrary model of multiple production characterized by some function $F(\mathbf{p})$ (called the model F in the following). It was shown by the author[5] that this problem is solved by the construction of a table of random stars corresponding to the given model.

However, two circumstances impair the efficiency of the procedure for picking the random stars proposed earlier:[5] 1) the difficulty of "hitting" the physical region of momentum transfers, i.e., the necessity of discarding impossible choices of momentum, and 2) the complications in reproducing the distribution of physically possible momenta required by the model, i.e., the necessity of discarding a large number of less probable choices of momentum.

In Sec. 1 of the present paper the first of the above-mentioned problems is solved completely by two methods. This can be done in a general form, since the physical region of momentum variation is determined by the conservation laws alone. The second difficulty depends on the model. It can be alleviated, however, in the case of factorable models. Convenient formulas are obtained, in particular, for the Fermi model and especially for the covariant model (see Sec. 2). The covariant model yields distributions and weights with even better accuracy than more complicated models (see Sec. 3). This is due to the fact that the efficiency of the Monte Carlo method must increase with the improvement of the approximate models (if the accumulated information is used correctly).

It seems to us that our formulas are simple enough to allow us to compute the distributions and weights in systems of some 10 to 50 particles with the covariant model, and in systems of 8 to 10 particles with other, more complicated models.

1. Let us assume that the distribution over $\mathbf{p}_1, \ldots, \mathbf{p}_n$ of a system of particles with masses m_k and energies e_k is given by the square of the matrix element $F(\mathbf{p})$. The region D of allowed values of momentum is determined by the conservation laws. Owing to the complicated form of D it is very difficult to pick a $\mathbf{p}_k$ from D, and, furthermore, to make this selection uniformly. Both of these difficulties disappear if we can find the

transformation which transforms D into a $(3n-4)$ dimensional cube. One such transformation has been found, in essence, by Yu. N. Blagoveshchenskiĭ and the author.[6]

Let us consider another variant, which is in closer correspondence with the physics of the problem. We introduce the notation[5]

$$E_k = E_{k-1} - e_{k-1}, \quad \mathbf{P}_k = \mathbf{P}_{k-1} + \mathbf{p}_{k-1},$$

$$M_k^2 = E_k^2 - \mathbf{P}_k^2, \quad \mu_k = \sum_{k+1}^{n} m_i,$$

$$e_{k\max} = (M_k^2 + m_k^2 - \mu_k^2)/2M_k, \quad p_{k\max}^2 = e_{k\max}^2 - m_k^2. \quad (2)$$

We then write (1) in the form

$$S_n(E_1, \mathbf{P}_1) = \int_{d_1} d^3\mathbf{p}_1 \ldots \int_{d_k} d^3\mathbf{p}_k \ldots \int_{(\infty)} d^3\mathbf{p}_{n-1} \int_{(\infty)} d^3\mathbf{p}_n F(\mathbf{p})$$

$$\times \delta(\mathbf{p}_{n-1} + \mathbf{p}_n + \mathbf{P}_{n-1})\, \delta(e_{n-1} + e_n - E_{n-1}). \quad (3)$$

Here d_k denotes the region of integration for $\mathbf{p}_k$ with fixed $\mathbf{p}_1, \ldots, \mathbf{p}_{k-1}$. We shall use spherical coordinate systems (p_k, η_k, φ_k) with polar axes along the $\mathbf{P}_k$.[5] For each $k < n$ we make successively the transformation of variables $\mathbf{p}_k = T_k^{-1}\bar{\mathbf{p}}_k$, where $T_k(\mathbf{p}_1, \ldots, \mathbf{p}_{k-1})$ is the Lorentz transformation matrix in the rest system of the particles $k, k+1, \ldots, n$:

$$p_k\eta_k = \gamma_k(\bar{p}_k\bar{\eta}_k + v_k\bar{e}_k), \quad \gamma_k = E_k/M_k,$$

$$p_k(1-\eta_k^2)^{1/2} = \bar{p}_k(1-\bar{\eta}_k^2)^{1/2}, \quad \gamma_k v_k = -P_k/M_k,$$

$$e_k = \gamma_k(\bar{e}_k + v_k\bar{p}_k\bar{\eta}_k), \quad \gamma_1 v_1 = P_1/M_1. \quad (4)$$

Then the ellipsoids d_k go into spheres ω_k of radius $p_{k\max}$. Their radius does not depend on $\bar{\eta}_1, \ldots, \bar{\eta}_{k-1}, \bar{\varphi}_1, \ldots, \bar{\varphi}_{k-1}$, since

$$M_k^2 = M_{k-1}^2 + m_{k-1}^2 - 2M_{k-1}\bar{e}_{k-1}. \quad (5)$$

We have now $(\bar{\mathbf{p}}_n = T_{n-1}\mathbf{p}_n)$

$$S_n = \int_{\omega_1} d^3\bar{\mathbf{p}}_1 \ldots \int_{\omega_k} d^3\bar{\mathbf{p}}_k \ldots \int_{(\infty)} d^3\bar{\mathbf{p}}_{n-1} \int_{(\infty)} d^3\bar{\mathbf{p}}_n F\, \delta(\bar{\mathbf{p}}_{n-1} + \bar{\mathbf{p}}_n)$$

$$\times \delta(\bar{e}_{n-1} + \bar{e}_n - M_{n-1}) \prod_1^n (e_k/\bar{e}_k), \quad (6)$$

or, after integrating the δ functions,

$$S_n = \int_{\omega_1} d^3\mathbf{p}_1 \ldots \int_{\omega_k} d^3\mathbf{p}_k \ldots \int_{\omega_{n-2}} d^3\mathbf{p}_{n-2}$$

$$\times \int_{\bar{p}_{n-1}=1} d\Omega_{n-1} F \frac{e_{n-1}e_n\bar{p}_{n-1}}{M_{n-1}} \prod_1^{n-2} \frac{e_k}{\bar{e}_k} \quad (7)$$

Here $p_{n-1} = (p_{n-1})_{\max}$, and the region ω_k is determined by the inequalities

$$0 \leqslant p_k \leqslant (p_k)_{\max}, \quad -1 \leqslant \eta_k \leqslant 1, \quad 0 \leqslant \varphi_k \leqslant 2\pi. \quad (8)$$

The momentum $\bar{\mathbf{p}}_k$ can also be given by the numbers

$$\bar{\tau}_{k+1} = M_{k+1} - \mu_k;\ \bar{\eta}_k,\ \bar{\varphi}_k \quad (9)$$

instead of the components $\bar{p}_k$, $\bar{\eta}_k$, $\bar{\varphi}_k$.

From (5) and (1) we easily find the form of the region D in terms of the variables $\bar{\tau}_k$:

$$\bar{\tau}_1 \geqslant \ldots \geqslant \bar{\tau}_k \geqslant \bar{\tau}_{k+1} \geqslant \ldots \geqslant \bar{\tau}_{n-1} \geqslant 0. \quad (10)$$

Formula (7) goes over into

$$S_n(E_1, \mathbf{P}_1)$$

$$= M_1^{-1} \int_0^{\bar{\tau}_1} d\bar{\tau}_2 \iint d\bar{\Omega}_1 \ldots \int_0^{\bar{\tau}_{n-2}} d\bar{\tau}_{n-1} \iint d\bar{\Omega}_{n-2} \iint d\bar{\Omega}_{n-1}\Phi, \quad (11)$$

where

$$\Phi = F \prod_1^{n-1} \bar{p}_k \prod_1^n e_k. \quad (12)$$

In order to stay within D in picking the random stars, we must choose a sequence of n-2 random numbers in decreasing order and take them to be equal to $\bar{\tau}_2/\bar{\tau}_1, \ldots, \bar{\tau}_{n-1}/\bar{\tau}_1$. In carrying out the summation, Φ must be multiplied by $(4\pi)^{n-1}/(n-2)!$ A more general method consists in extending D to a cube according to the formulas of reference 6 and multiplying Φ by the product of the differences of the limits of integration. Each star, i.e., each choice of the $3n-4$ random values of the integration variables in (11) will have the "weight" $\Phi(\mathbf{p})$ [formula (12)] if the values of $\mathbf{p}$ are evenly distributed over the cube, or the weight $\Phi(\mathbf{p})/\Phi^*(\mathbf{p})$ if they are distributed with the density $\Phi^*(\mathbf{p})$. The average value of $\Phi(\mathbf{p})/\Phi^*(\mathbf{p})$ goes over into the statistical weight as the number of stars is increased. To obtain histograms [distributions of the stars with respect to an arbitrary characteristic of the interaction $q(\mathbf{p})$] we must also compute the average value of $\Phi(\mathbf{p})/\Phi^*(\mathbf{p})$ over all values of $\mathbf{p}$ for which $q(\mathbf{p})$ lies between q and $q + dq$. A table of random stars (in the proper meaning of the word) is obtained by casting out[5,7] part of the number of stars in such a way that the number of the remaining stars with momenta between $\mathbf{p}$ and $\mathbf{p} + d\mathbf{p}$ is proportional to $\Phi(\mathbf{p})/\Phi^*(\mathbf{p})$. Then we can assign the weight 1 to each of the remaining stars. This set of stars corresponds in all its statistical aspects exactly to the model F.

It should be recalled that each momentum $\bar{\mathbf{p}}_k$ is measured in its own reference system (except the momenta $\bar{\mathbf{p}}_{n-1}$ and $\bar{\mathbf{p}}_n$, which are obtained in a common rest system). For the transformation to

a single system we must use (4) and (2), and then (2.5) to (2.7) of reference 5.

Let us now turn to special cases of formula (11). In the case of the Fermi model we can carry out the integration over $\overline{\varphi}_1, \ldots, \overline{\varphi}_{n-1}, \overline{\eta}_{n-1}$ in (11). We then find an expression which is similar to expression (2.15) of reference 5, with the difference that the drawing of the remaining 2n-4 variables is now simpler. In the case of the covariant model, substitution of (1′) in (6) leads to an expression which depends neither on $\overline{\varphi}_k$ nor on $\overline{\eta}_k$, so that the weight is given by the $(n-2)$-fold integral

$$S_n(E_1, P_1) \equiv S_n(M_1, 0) = (2\pi)^{n-1} \int \ldots \int \prod_1^{n-2} \overline{p}_k \, d\overline{e}_k \, (\overline{p}_{n-1} / 2M_{n-1}), \tag{13}$$

where the limits of the integration over $\overline{e}_k$ are m and $(e_k)_{max}$, and

$$\overline{p}_{n-1} / M_{n-1} = R(M_{n-1}, m_{n-1}, m_n) / 2M_{n-1}^2,$$

$$R^2(a, b, c) = \prod_{\varepsilon=\pm 1} [a^2 - (b - \varepsilon c)^2]. \tag{14}$$

Then formula (11) leads to the expression

$$S_n(M_1) = \frac{\pi^{n-1}}{2M_1^2} \int_0^{\overline{\tau}_1} d\overline{\tau}_2 \ldots \int_0^{\overline{\tau}_{n-2}} d\overline{\tau}_{n-1} \, M_n \prod_{k=2}^{n} \frac{R(M_{k-1}, m_{k-1}, M_k)}{M_k}, \tag{15}$$

where

$$M_k = \overline{\tau}_k + \mu_{k-1}, \qquad M_n = m_n \tag{16}$$

The function under the integral sign vanishes at the surface of the hypercube. The number theoretical method of Korobov,[8] which under these conditions achieves an accuracy not attained by the Monte Carlo method, is therefore very efficient in this case. But even apart from this, formula (15) for the weight is simpler than the corresponding formula of reference 4, which has been used for the calculation of the production of 15 particles. Formula (15) enables us to go further.

Since the density distribution depends only on the n-2 values of the energy of the particles [the remaining $2n-2$ quantities $\overline{\eta}_1, \ldots, \overline{\varphi}_{n-1}$ are always chosen at random from the intervals $(-1, 1)$ and $(0, 2\pi)$], the efficiency of drawing "covariant stars" is much higher than usual.

2. Let us now consider factorable models, i.e., models in which $F(p)$ can be split up into at least two independent factors (describing the production of non-interacting subsystems). In this case the efficiency of the drawing is further increased by the method of grouping.

Let us divide the system of N particles into n independent groups: $F(p) = \prod_{i=1}^{n} F_i(p_{ij})$; the mass, energy, and momentum of the particle j of group i are now denoted by m_{ij}, e_{ij}, and p_{ij}, while m_i, e_i, and p_i refer to the whole group i:

$$\sum_j e_{ij} = e_i, \qquad \sum_j p_{ij} = p_i; \qquad m_i^2 = e_i^2 - p_i^2.$$

Instead of (1) we can now write

$$S_N(E, P) = \int \prod_i^n d^4 p_i S_i(p_i) \, \delta^4 \left(\sum_i^n p_i - P \right), \tag{17}$$

where

$$S_i(p_i) = \int \prod_j^{n_i} d^3 p_{ij} \delta^4 \left(\sum_j^{n_i} p_{ij} - p_i \right) F_i(p_{ij}). \tag{18}$$

The grouping formula (17) expresses the weight of the system in terms of the weights of the non-interacting subsystems through a natural generalization of the formulas of references 9 and 4. If the analytic expressions for S_i are known, the drawing of p_i, e_i according to (19) and then of p_{ij} according to (18) (by the rejection method) is more efficient than the direct drawing of p_{ij} according to (11) by the same method, since the multiplicity of the integrals (17) is lower than in (11).

For the drawing of e_i, p_i we again go over to the rest system of the groups i, ..., n in which all directions of p_i have the same probability. The region δ_i of allowed values of e_i, p_i is shown in the figure. Its equation was given by the author in reference 10. As before, it does not depend on $\overline{\eta}_1$, ..., $\overline{\eta}_{i-1}$, $\overline{\varphi}_1, \ldots, \overline{\varphi}_{i-1}$. We obtain [$(\overline{S}_i(\overline{e}_i, \overline{p}_i)$

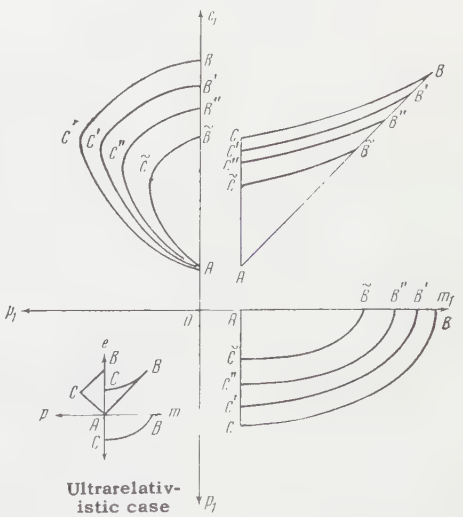

Projection of the physical region of variation of the characteristics of a particle with variable mass m_i on the planes (m_i, e_i), (e_i, p_i), and (p_i, m_i): ABC if the masses $m_2, \ldots, m_n$ of all other particles of the system are also variable; AB′C′ if m_2 = const, $m_3, \ldots, m_n$ variable; AB″C″ if m_2, m_3 = const; $\tilde{A}\tilde{B}\tilde{C}$ if all masses $m_2, \ldots, m_n$ = const.

$\equiv S_i(e_i, p_i)]$:

$$S_N = \int_{\delta_1} d^4\bar{p}_1 \bar{S}_1(\bar{e}_1, \bar{p}_1) \ldots \int_{\delta_{n-1}} d^4\bar{p}_{n-1} \bar{S}_{n-1}(\bar{e}_{n-1}, \bar{p}_{n-1}) \times \bar{S}_n(M_{n-1} - \bar{e}_{n-1}, -\bar{p}_{n-1}). \quad (19)$$

The bigger the groups, the higher is the efficiency of the grouping. However, there are practically no simple general formulas for the calculation of (18) for $n_i > 2$. But even the grouping into a pair should have an appreciable effect (for example, for the Fermi model[10]).

Let us again consider the covariant model as an example. In this case general expressions exist for the weight of two arbitrary particles,

$$S^{(2)}(M, m_1, m_2) = (\pi/2M^2) R(M, m_1, m_2) \quad (20)$$

and of three particles with equal mass (with an accuracy of better than 1.6%),

$$S^{(3)}(M, m, m, m) = \tfrac{1}{8} \pi^2 M^2 (1 + 0.997\alpha^2)(1 - \alpha)^{3/2} (1 - 9\alpha^2)^2,$$

$$\alpha = m/M. \quad (21)$$

Furthermore, by covariance we can replace $\bar{S}_i(\bar{e}_i, \bar{p}_i)$ by $S_i(\bar{e}_i, \bar{p}_i)$ in (19) and integrate over the directions ($\tilde{m}_i = \sum_j^{n_i} m_{ij}$, $\mu_k = \sum_{i>k}^{n} \tilde{m}_i$):

$$S_N(M_1) = (4\pi)^{n-1} \int \ldots \int_{\tilde{m}_k}^{M_k - \mu_k} S_k(m_k)\, m_k dm_k \int_{m_k}^{(e_k)_{max}} \bar{p}_k d\bar{e}_k \ldots \times \int_{\tilde{m}_{n-1}}^{M_{n-1} - \mu_{n-1}} S_{n-1}(m_{n-1})\, m_{n-1}\, dm_{n-1} \times \int_{m_{n-1}}^{(e_{n-1})_{max}} \bar{p}_{n-1} S_n(M_n)\, d\bar{e}_{n-1}. \quad (22)$$

Thus the weight of the system of N particles is expressed in terms of $2(n-1)$-fold integrals (n is the number of groups into which the total number of N particles is divided up). In computing the weight of 9 particles [using (21)] we thus only have to calculate a quadruple integral.

A special case of formula (22) is the doubling formula. Let the index of S denote the number of particles in the group and not the number of the group. We divide the number of N particles into two groups whose weights have a known energy dependence. Then (22) yields ($\bar{t}_i = m_i - \tilde{m}_i$, $\bar{e}_i = (M_i^2 + m_i^2 - m_2^2)/2M_1$)

$$S_n(M_1) = (4\pi/M_1) \int_0^{\bar{\tau}_1} d\bar{t}_1 \int_0^{\bar{\tau}_1 - \bar{t}_1} d\bar{t}_2 m_1 S_\nu(m_1) \bar{p}_1 m_2 S_{N-\nu}(m_2). \quad (23)$$

The doubling of the index is then achieved by setting $N = 2\nu$. If both groups have identical structure, we only have to know the single function $S_{N/2}(m_1)$ for the calculation of S_N. In the particularly convenient case when all particles are identical and $N = 3 \times 2^{n-1}$ or 2^n, we only have to calculate the $n-1$ functions $S_6, S_{12}, \ldots$ or $S_4, S_8, \ldots$, starting with $\nu = 3$ or 2 [formulas (21) and (20)]. This implies the calculation of $n-1$ triple integrals. Thus the computational difficulties grow very slowly (logarithmically) with increasing number of particles. The calculation of the production probabilities and the spectra of some 10 to 50 particles appears to be within the capabilities of modern computing machines.*

We note that the construction of the table of random stars for a system with large N can be considerably simplified in the covariant model, if each type of particles is described by only one representative in the table. The table for the system N, $(n+1)\pi$ can then be obtained from the expression

$$S_{N(n+1)\pi}(M) = 4\pi^2 \int \bar{p}_N d\bar{e}_N \int \bar{p}_\pi d\bar{e}_\pi S_{n\pi}(M_{n\pi}),$$
$$M_{n\pi}^2 = M_{(n+1)\pi}^2 + m_\pi^2 - 2M_{(n+1)\pi}\bar{e}_\pi,$$
$$M_{(n+1)\pi}^2 = M^2 + m_N^2 - 2M\bar{e}_N, \quad (24)$$

if we first determine the function $S_{n\pi}$ and then use the usual method of picking random stars.

3. The convergence of the process of calculation of the integral (12) or of obtaining histograms by the Monte Carlo method can, in principle, be made as rapid as we please by augmenting the amount of information about the function under the integral sign. Thus, the closer $\Phi^*(p)$ is to $\Phi(p)$ [see formula (12) and the following discussion], the more accurately is $S(E, P)$ determined in a given computing time. The use of a density $\Phi^*(p)$ close to $\Phi(p)$ is called essential sampling.[7]

This characteristic feature of probability methods of calculation leads to interesting results in the problem of establishing a model for multiple production. Let us assume that a table of random stars has been obtained for the model F_1. In this model the frequency of different states p is proportional to their weights $\Phi_1(p)$ [formula (12)]. The calculation with the help of models Φ_j $(j > 1)$ which are closer to reality can be carried out with increased accuracy if one uses essential sampling with the density $\Phi^*(p) = \Phi_1(p)$, i.e., if the computer successively extracts from its memory

*However, a specific difficulty appears, namely the fact that for large N the functions to be calculated increase extremely rapidly with the energy.

choices of p and their weights $\Phi_1(p)$, calculates $\Phi_j(p)$, and takes the average of Φ_j/Φ_1. The closer the model F_1 is to reality, the simpler are the calculations for the models F_j which improve on F_1.*

For such a "basic" model one can probably already take the covariant model, because it is simple and its predictions are in sufficient agreement with the experimental data.[2,11] In going over to the model F_j, the "covariant stars" will have to be assigned the weight $2^n e_1 \ldots e_n F_j$. In the case of extremely relativistic particles the table of "covariant stars" can be easily set up by the machine itself. It can be shown[10] that in this case

$$\bar{\tau}_{n-\nu+1} = \bar{\tau}_1 (t_\nu \ldots t_{n-1})^{1/2}, \qquad (25)$$

where t_ν are the roots of the equations

$$(\nu - 1)\, t_\nu^\nu - \nu t_\nu^{\nu-1} + \alpha_\nu = 0,$$

and α_ν are random numbers. Since the form of the region D is independent of $m_1, \ldots, m_n$, and E, the essential sampling (25) may turn out to be useful even for $m_k \neq 0$.

CONCLUSIONS

In the description of a system of n particles, the momentum of the particle $k\,(k < n)$ is conveniently given in the rest system of the particles $k, k+1, \ldots, n$. This imposes no restriction on the direction of the momentum, while the magnitude of the momentum is restricted only by the requirement of energy conservation. This facilitates the calculation of the statistical weights and the determination of the physically allowed momenta in establishing a model of multiple production (point 1).

If one group of particles is assumed to have no interaction with the remaining group of particles in the model of multiple production under consideration, the preliminary calculation of the statistical weights of the independent groups facilitates the establishment of a model for the whole system (point 2).

The table of random stars constructed for a given model F_1 can also be used for the investigation of other models F_j. In setting up the histograms it is here only necessary to assign the weight Φ_j/Φ_1 instead of 1 to each star in the table. The best efficiency in constructing the table is achieved with the covariant model (extremely relativistic case) (point 3).

*It is appropriate here to make an analogy with perturbation theory, which is a method of investigating complicated systems by using the information obtained from the study of simple unperturbed systems.

Since the Monte Carlo method yields histograms of experimental interest for arbitrary models, with exact account of the motion of the target nucleon, the presence of bound states, the decay of secondary particles, etc., it must be regarded to be in closer correspondence with the problems of multiple production than the usual analytic methods. In particular, the proposed method can be used in a natural way in the calculation of cascades inside the nucleus,[12] thus allowing us to compute the multiple production on nuclei.[10]

The results of this paper are treated in more detail in reference 10. In particular, some analytic expressions for the covariant weight are given and the equations for the region δ_i are considered (see the figure).

The author takes this opportunity to thank B. N. Valuev, L. G. Zastavenko, and I. V. Polubarinov for valuable advice.

[1] Bogachev, Bunyatov, Gramenitskiĭ, Lyubimov, Merekov, Podgoretskiĭ, Sidorov, and Tuvdendorzh, JETP **37**, 1225 (1959), Soviet Phys. JETP **10**, 872 (1960). Kalbach, Lord, and Tsao, Phys. Rev. **113**, 330 (1959).

[2] P. P. Srivastava and G. Sudarshan, Phys. Rev. **110**, 765 (1958).

[3] R. H. Milburn, Revs. Modern Phys. **27**, 1 (1955). V. M. Maksimenko and I. L. Rozental', JETP **32**, 658 (1957), Soviet Phys. JETP **5**, 546 (1957). G. E. Fialho, Phys. Rev. **105**, 328 (1957). L. G. Zastavenko, JETP **37**, 1319 (1959), Soviet Phys. JETP **10**, 939 (1960).

[4] F. Cerulus and R. Hagedorn, Nuovo cimento Suppl. **9**, 646 and 659 (1958).

[5] G. I. Kopylov, JETP **35**, 1426 (1958), Soviet Phys. JETP **8**, 996 (1959).

[6] Yu. N. Blagoveshchenskiĭ and G. I. Kopylov, preprint P 213, Joint Institute for Nuclear Research.

[7] J. W. Butler, see H. A. Meyer, Symposium on Monte Carlo Methods, N. Y. (1956).

[8] N. M. Korobov, Dokl. Akad. Nauk SSSR **128**, 235 (1959) and **124**, 1207 (1959); Vestnik, Moscow State University **4**, 19 (1959).

[9] Belen'kiĭ, Maksimenko, Nikishov, and Rozental', Usp. Fiz. Nauk **62**, No. 2, 1 (1957).

[10] G. I. Kopylov, preprint E 528, Joint Institute for Nuclear Research.

[11] Goldhaber, Fowler, Goldhaber, Hoang, Kalogeropoulos, and Powell, Phys. Rev. Lett. **3**, 181 (1959).

[12] Metropolis, Bivins, Storm, Miller, Friedlander, and Turkevich, Phys. Rev. **110**, 204 (1958).

Translated by R. Lipperheide
202

PION-NUCLEON SCATTERING AT LOW ENERGIES, II

A. V. EFREMOV, V. A. MESHCHERYAKOV, and D. V. SHIRKOV

Joint Institute for Nuclear Research

Submitted to JETP editor May 31, 1960

J. Exptl. Theoret. Phys. (U.S.S.R.) **39**, 1099-1105 (October, 1960)

On the basis of results given in a previous article,[1] an integral equation for the α_{33} phase shift is obtained along with expressions for the other phase shifts, which involve the π-π scattering phase shifts δ_0 and δ_1. The important role of the dispersion relations for backward pion-nucleon scattering is established. It is shown that the δ_0 phase shift greatly influences the π-N scattering. The scattering length for the δ_0 phase shift is determined by an analysis of small p phase shifts near the π-N scattering threshold.

1. THE TRANSFORMATION TO PARTIAL WAVES

IN a previous article[1]* we reported on an investigation of the analytic properties of the scalar amplitudes for pion-nucleon scattering in the complex q^2 plane for fixed cos $\theta = c$ (in the center-of-mass system).

The contribution from the cut specified by reaction III ($\pi + \pi \rightarrow N + \bar{N}$) was approximately reduced there to two functions

$$F_0(q^2, c) = e^{u_0(q^2, c)}, \qquad F_1(q^2, c) = e^{u_1(q^2, c)}. \qquad (1.1)$$

The functions u_0 and u_1 occurring in (1.1) are expressed by Eq. (I.5.5)† in terms of the π-π scattering phase shifts δ_0 and δ_1.

When $c = -1$, the function F_1 is an electromagnetic pion form factor.[2] Therefore, for the sake of brevity, we shall call F_0 and F_1 respectively s and p form factors (even though for F_0 such a designation is merely formal).

These form factors F_i enter in the kernels of the final system of integral relations (I.5.4), (I.5.6), and (I.5.10), which determine the pion-nucleon scattering amplitude. The integral terms of these relations are explicitly expressed by the partial scattering amplitudes. To deduce integral equations for the individual partial waves it is necessary to transform to partial waves in the left-hand terms of the equations.

Ordinarily this transformation is accomplished by integration with the proper weighting function over the interval $-1 \leq c \leq 1$. This is not the only method; for instance, as was done by Chew et al.,[3] the transformation to partial waves can be effected by a Taylor expansion in c at $c = 1$.

*Henceforth referred to as I.

†i.e., Eq. (5.5) in I.

To select a method of expansion in partial waves we shall examine more closely the analytic properties of the Φ functions in the non-physical region of reaction I. In our derivation of the integral relations we used an expansion of the functions Φ in the angles of reaction III, which are in the non-physical region. The regions of convergence of such expansions are determined by the singularities of the Mandelstam representation. The nearest singularities, disregarding the poles, that limit the expansion of Re Φ are the asymptotes $s = (M + \mu)^2$ and $\bar{s} = (M + \mu)^2$. The region of convergence for Im Φ is broader and is determined by the boundaries of the spectral functions (the curves C_{13} and C_{23} in Mandelstam's notation[4]).

Using Heine's theorem,[5] we can construct the ellipses of analyticity in the cos θ_3 complex plane. Using then formulae (I.5.1) to transform to the variables q^2 and c, we obtain the curves plotted in the figure. The C_R curve defines the analytical region of the function Re Φ, while C_I does the same for Im Φ.

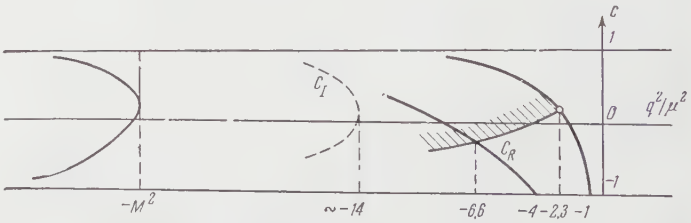

As can be seen from the figure, the conventional procedure for transforming to partial waves by averaging the functions with the Legendre polynomials allows us to account for the nearest singularity from reaction III only as far as $q^2 = -2.35$. In practice we confine ourselves to s and p waves for reaction III. This approximation causes a large error in a certain region below the C_R

curve, where $\cos\theta_3$ assumes a large complex value. We therefore transform to partial waves by means of a Taylor expansion of our functions at $c = -1$ (see in this connection also the article by Efremov et al.[6]).

There are several advantages to this method. First, the nearest part of the non-physical contribution by reaction III is included with considerable accuracy. Second, since the integrand contains the amplitude of reaction III for the physical value $\cos\theta_3 = -1$, we shall not in fact be using an analytical continuation into the non-physical region of $\cos\theta_3$ and shall always be in the region of convergence. We can expect our formulae to be correct in some region below $q^2 = -4\mu^2$ where the inelastic contribution is still small.

Further, when $c = -1$, there are no non-physical cuts due to the crossing reaction II ($\pi' + N \to \pi + N'$), and the only non-physical cut is from reaction III, which we allowed for. Finally, when $c = -1$, our formulae are very simple, since the relation (I.4.7) is greatly simplified.

2. EQUATIONS FOR PARTIAL WAVES

Having in mind the application at low energies, we confine ourselves to s and p waves. In this approximation we have

$$f_s^{(+)}(q^2) = f_1^{(\pm)}(q^2, -1) + f_1^{(\pm)\prime}(q^2, -1),$$

$$f_{p^3/_2}^{(\pm)}(q^2) = \tfrac{1}{3} f_1^{(\pm)\prime}(q^2, -1), \qquad (2.1)$$

$$f_{p^1/_2}^{(\pm)}(q^2) = f_2^{(\pm)}(q^2, -1) + \tfrac{1}{3} f_1^{(\pm)\prime}(q^2, -1). \qquad (2.2)$$

According to (I.2.3) $f_{1,2}^{(\pm)}(q^2, -1)$ is expressed through $A^{(+)}$, $\alpha = A^{(-)}/(s - \bar{s})$, $\beta = B^{(+)}/(s - \bar{s})$, and $B^{(-)}$ as follows:

$$f_1^{(+)}(q^2, -1) = \frac{p_0 + M}{8\pi W}[A^{(+)}(q^2) + 4p_0\omega(W - M)\beta(q^2)],$$

$$f_1^{(-)}(q^2, -1) = \frac{p_0 + M}{8\pi W}[4p_0\omega\alpha(q^2) + (W - M)B^{(-)}(q^2)],$$

$$f_2^{(+)}(q^2, -1) = \frac{p_0 - M}{8\pi W}[-A^{(+)}(q^2) + 4p_0\omega(W + M)\beta(q^2)],$$

$$f_2^{(-)}(q^2, -1) = \frac{p_0 - M}{8\pi W}[-4p_0\omega\alpha(q^2) + (W + M)B^{(-)}(q^2)],$$

$$f_1^{(+)\prime}(q^2, -1) = \frac{p_0 + M}{8\pi W}[A^{(+)\prime}(q^2) + (W - M)(2q^2\beta(q^2) + 4p_0\omega\beta'(q^2)],$$

$$f_1^{(-)\prime}(q^2, -1) = \frac{p_0 + M}{8\pi W}[2q^2\alpha(q^2) + 4p_0\omega\alpha'(q^2) + (W - M)B^{(-)\prime}(q^2)]. \qquad (2.3)$$

Here $\omega = q_0$, while $\Phi(q^2)$ and $\Phi'(q^2)$ denote $\Phi(q^2, c)$ and $d\Phi/dc$ when $c = -1$ after a subtraction at the point $q^2 = 0$.

The rest of the designations are identical with their counterparts in I.

Let us consider the subtraction procedure. Assuming as usual a linear increase of the amplitude at infinity and allowing for the properties of crossing symmetry, one can easily show that one subtraction suffices for the functions $A^{(+)}$, α, and $B^{(-)}$, while none is required for β. As subtraction parameters it is convenient to select the experimental scattering lengths a_1 and a_3, as well as

$$a_{33} = \lim_{q \to 0} \alpha_{33} q^{-3}.$$

In order to ensure that the $\Phi'(q^2)$ functions vanish as $q^2 \to 0$, we also perform a subtraction in these, without introducing any new constants.

Let us introduce the following notation:

$$\Phi = \Phi_0 + \Phi_p + \Phi_{\pi N} + \Phi_{\pi\pi}, \quad \Phi' = \Phi_p' + \Phi_{\pi N}' + \Phi_{\pi\pi}'. \qquad (2.4)$$

Here Φ_p denotes the contribution by the pole; $\Phi_{\pi N}$ designates that part of the integral which does not contain form factors, while $\Phi_{\pi\pi}$ is the part containing them and which is zero when $F_0 = F_1 = 1$, and Φ_0 is the subtraction constant.

All the terms in the right side of (2.4) vanish when $q^2 = 0$, except for the subtraction constant Φ_0. These, except β_0, can be expressed through the experimental values

$$a_- = \tfrac{1}{3}(a_1 - a_3), \qquad a_+ = \tfrac{1}{3}(a_1 + 2a_3), \quad a_{33}, \qquad (2.5)$$

We shall make one more approximation. Because of the relative values of the phase shifts, we shall restrict ourselves in the integrand to the α_{33} phase shift only. Consequently, the integrals in the right side of (2.4) will depend only on $\operatorname{Im} f_{33} = \psi(q^2)$ and the form factors. The result is that we obtain an integral equation for f_{33}, while the other phase shifts will be determined by integral relations in terms of ψ. This approximation corresponds to the first iteration when the entire system of equations for partial waves is solved, with the zero approximation containing only the experimental value of α_{33}.

The subtraction constants are ($\mu = 1$)

$$A^{(+)}(0)/4\pi = (1 + 1/M)a_+ - M\beta(0)/\pi,$$

$$B^{(-)}(0)/4\pi = (1 + 1/M)a_- - M\alpha(0)/\pi,$$

$$\frac{\beta(0)}{\pi} = -\frac{4f^2}{1 - 1/4M^2} + \frac{1}{\pi^2}\int_{\infty} \frac{\operatorname{Im}\beta(x)}{x}dx,$$

$$\frac{\alpha(0)}{\pi} = \frac{\beta(0)}{\pi} - 6\left(1 + \frac{1}{M}\right)a_{33} + \lim_{q^2 \to 0} \frac{A^{(+)\prime}(q^2) - B^{(-)\prime}(q^2) + 4M\beta'(q^2) - 4M\alpha'(q^2)}{q^2}, \qquad (2.6)$$

while the pole terms are

$$\beta_p = \frac{4\pi f^2 q^2}{(1-1/4M^2)(1+q^2-1/4M^2)},$$

$$\beta'_p = \frac{8\pi f^2 q^2}{(1+q^2-1/4M^2)(2p_0\omega-1-2q^2)}$$

$$B_p^{(-)} = \frac{8\pi f^2 q^2 (1-1/2M^2)}{(1+q^2-1/4M^2)(1-1/4M^2)}$$
$$- 16\pi M f^2 \left[q^2 (p^0\omega)^{-1} \left(\frac{p_0}{\omega+1} - \frac{1}{M+p_0} \right) \ln \frac{p_0+\omega}{p_0-\omega} + \frac{M-1}{p_0-\omega} \ln \frac{p_0+\omega}{M+1} \right],$$

$$B_p^{(-)'} = -32\pi M^2 f^2 \frac{q^2}{(2p_0\omega-1-2q^2)^2}$$
$$+ 4\pi M^2 f^2 \frac{q^2}{p_0^2\omega^2} \left[2 - \frac{M^2+1+2q^2}{p_0\omega} \ln \frac{W}{p_0-\omega} \right]. \qquad (2.7)$$

Now let us proceed to the integral terms. Assuming $c = -1$ in (I.5.4), (I.5.6) and (I.5.10) and taking (I.6.3) into account, we obtain

$$\Phi_{\pi N} = \frac{q^2}{\pi} \int \frac{\operatorname{Im} \Phi(x)}{x(x-q^2)} dx, \qquad (2.8)$$

$$\Phi_{\pi\pi} = -\frac{q^2}{\pi} \int \frac{\operatorname{Im} \Phi(x)}{x-q^2} G_i(x, q^2)\, dx,$$

$$G_i(x, q^2) = (E_i(x) - E_i(q^2)) / F_i(x), \quad F_i(x) = 1 - xE_i(x). \qquad (2.9)$$

Then, differentiating the aforementioned formulae in I with respect to c at $c = -1$, we find

$$\Phi'_{\pi N} = \frac{q^2}{\pi} \int \frac{\operatorname{Im} \Phi'(x)}{x(x-q^2)} [1 - 2(x-q^2)\varphi(x, q^2)]\, dx$$
$$+ \frac{q^2}{\pi} \int \operatorname{Im} \Phi(x)\, d\varphi(x, q^2),$$

$$\varphi(x, q^2) = \frac{\frac{x}{q^2}[K(q)-M] - [K(x)-M]}{x-q^2} \frac{1}{W^2(x)}, \qquad (2.10)$$

$$\frac{1}{q^2} \Phi'_{\pi\pi} = -\frac{1}{\pi} \int \frac{\operatorname{Im} \Phi'(x)}{x-q^2} G_i(x, q^2) \frac{p_0^2(x)+\omega^2(x)}{W^2(x)} dx$$
$$- \frac{1}{2\pi} \int \frac{\operatorname{Im} \Phi(x)}{x-q^2} \Delta_i(x, q^2)\, dx$$
$$- \frac{1}{\pi} \int \operatorname{Im} \Phi(x)\, d\left(xK(x) \frac{G_i(x, q^2)}{W^2(x)(x-q^2)} \right),$$

$$\Delta_i(x, q^2) = \frac{F'_i(x)(xE_i(q^2)-1) + F'_i(q^2) F_i(x)}{F_i^2(x)}. \qquad (2.11)$$

In Eqs. (2.9) and (2.11) we put i = 0 for A^+, i = 1 for α and $\beta^{(-)}$, and $\beta_{\pi\pi} = 0$. The sign of Δ_i and G_i is selected so as to make $G_i(x, q^2)$ and $\Delta_i \geq 0$ when the π-π scattering lengths are positive.

The imaginary parts of $\Phi(x)$ and $\Phi'(x)$ which occur in Eq. (2.8)–(2.11) are expressed through ψ by the formulae

$$\operatorname{Im} A^{(+)}(x) = -\frac{16\pi}{3} \frac{\psi(x)}{x} [p_0(x)\omega(x) + x - 2M\omega(x)],$$

$$\operatorname{Im} A^{(+)'}(x) = 8\pi \frac{\psi}{x} [(p_0 - M)\omega + x],$$

$$\operatorname{Im} B^{(-)} = \frac{8\pi}{3} \frac{\psi}{x} (2p_0 - M), \qquad \operatorname{Im} B^{(-)'} = -4\pi \frac{\psi}{x} (p_0 - M),$$

$$\operatorname{Im} \alpha = \frac{3\pi}{2} \frac{\psi}{x} \frac{p_0\omega + x - 2\omega M}{\omega p_0},$$

$$\operatorname{Im} \alpha' = -\frac{\pi}{3} \frac{\psi}{x} \frac{3\omega p_0 [(p_0 - M)\omega + x] + (p_0\omega + x - 2M\omega)x}{(\omega p_0)^2},$$

$$\operatorname{Im} \beta = -\frac{4\pi}{3} \frac{\psi}{x} \frac{2p_0 - M}{p_0\omega},$$

$$\operatorname{Im} \beta' = 2\pi \frac{\psi}{x} \left(\frac{(2p_0 - M)x}{3(p_0\omega)^2} + \frac{p_0 - M}{p_0\omega} \right). \qquad (2.12)$$

Thus we have for f_{33} an integral equation that contains the pion form factors, and for the rest of the partial waves we have expressions dependent on ψ and on known constants and form factors.

3. EXPANSION IN 1/M AND EVALUATION OF SMALL p WAVES

Let us examine the properties of the derived equations. After an expansion in 1/M, the principal terms of the π-N part will coincide with the principal terms of the equations deduced by Chew et al.,[3] provided that subtractions like ours are made in the latter. However, our equations contain in addition π-π terms. We note that our equations differ from those of Chew et al. in that a formal transition to the static limit ($M \to \infty$) is impossible even in the p waves, shift contributions of the $\Phi_{\pi\pi}$ terms, which contain the s phase shift, are proportional to M.

When $q^2 \to 0$, the small p phase shifts have the form $\alpha_{ik} \approx a_{ik} q^3$ and are determined by subtraction constants a_+, a_-, and a_{33}, as well as by the integrals containing $\psi(x)$ and the form factors. Performing the calculations, we obtain with accuracy to 1/M,

$$a_{31} = -0{,}141 + 2M\Psi_0,$$
$$a_{13} = -0.164 + 2M\Psi_0 - \Psi_1,$$
$$a_{11} = 0.075 - 2M\Psi_0 + 2\Psi_1. \qquad (3.1)$$

Here

$$\Psi_0 = \int_0^\infty \frac{\omega(x)\psi(x)}{x^2} \Delta_0(x, 0)\, dx,$$

$$\Psi_1 = \int_0^\infty \frac{dx\, \psi(x)}{x\omega(x)} [2G_1(x, 0) + \Delta_1(x, 0)]. \qquad (3.2)$$

The values $f = 0.08$, $a_+ = -0.016$, $a_- = -0.094$, $a_{33} = 0.232$ have been used.

The integrals containing f_{33} were computed in the interval from 0 to $q^2 = 6$. The values for f_{33}

in this interval were taken from Pontecorvo's review.[7,8] The accuracy of these calculations, taking into account the effect of neglecting the integrals from 6 to ∞, was estimated to be 5%, which corresponds in (3.1) to approximately a few thousandths.

By comparing the right side of (3.1) with the experimental data, we can estimate the integrals Ψ_0 and Ψ_1. A reasonable fit can be obtained only for Ψ_0. The table lists the experimental data[8] and the values of the right sides of (3.1) for $2M\Psi_0 = 0.12$

Experiment	-0.039 ± 0.022	-0.044 ± 0.005	-0.038 ± 0.038
Theory	-0.02	$-0.04-\Psi_1$	$-0.045+2\Psi_1$

It is evident that the large experimental errors make it impossible to draw any conclusion about the integral Ψ_1, which depends on the p phase of π-π scattering. However, the sign and order of magnitude of Ψ_0 can be considered reliable.

Our results are in agreement with the conclusions reached by Ishida et al.[9] If we take for the s phase shift of π-π scattering, δ_0, the "scattering length approximation" [9]

$$\tan\delta_0(q) = \alpha_s q,$$

which gives us

$$\Psi_0 \approx 0.01\,\frac{\alpha_s}{1+\alpha_s}\left(1+\frac{2\alpha_s}{1+\alpha_s}\right),$$

then we obtain $\alpha_S = 0.9/\mu$ from the condition $2M\Psi_0 = 0.12$. This value is also in agreement with the results of Ishida et al.,[9] who obtained $\alpha_S = 1/\mu$.

We must stress that the numbers in the right size of (3.1) are not reliable. The trouble is that a difference of large terms occurs, and "small terms" of the order of 1/M become important. However, these terms cannot be computed with the necessary accuracy because the terms which arise in the expansion of denominators like $1 + 2\omega(x)/M$ are expressed by slowly converging integrals. Therefore, a reliable calculation of the small p waves should be computed without an expansion in 1/M. This computation, together with the calculation of the energy dependence of the s and p phase shifts and the solution of the integral equation for f_{33}, is now in progress.

4. DISCUSSION OF THE RESULTS

1. From the Mandelstam's double spectral representation, we have derived a system of integral equations for the partial waves for pion-nucleon scattering. In this connection, the especially important role of the dispersion relations for π-N backward scattering was ascertained. These relations alone are in fact sufficient for obtaining a system of integral equations. Because there is little hope for the strict proof of Mandelstam's representation, the proof of the dispersion relations for backward scattering becomes of great interest.

2. The s phase shift of π-π scattering, δ_0, is shown to enter in the expressions for the π-N partial waves with a large factor M. Consequently, despite the approximate nature of our numerical calculations and the large degree of experimental error, one can reliably determine the sign and order of magnitude of the scattering length for the phase shift δ_0 merely from an examination of the small p waves of π-N scattering near the threshold. We hope that a more accurate computation of the s and p waves in the energy interval 100 — 200 Mev will enable us to obtain some information about the p wave of π-π scattering.

3. These results are in agreement with those of Ishida et al.[9] and contradict those of Bowcock et al.[10] Setting aside the question of the different methods of obtaining the equations for the partial waves (in this connection, see reference 6), we make the following comments about the paper of Bowcock et al.:[10] a) the authors, concerning themselves with the problem of obtaining information about the resonance behavior of the p wave of π-π scattering, have neglected the s wave, which by itself gives the main contribution to π-N scattering; b) they have also failed to perform a subtraction the necessity of which was emphasized by Chew et al.;[3] as a result, for instance, δ_1 contributes to a_{13}. Moreover, they have estimated the integrals which depend on Im f_{33} very roughly. If our method is used to compute the magnitude of a_{33} as defined by their Eq. (5.3), we obtain 0.176 instead of 0.213.

The authors wish to express their gratitude to Prof. Chou Hung-Yüan for his very valuable comments.

[1] Efremov, Meshcheryakov, and Shirkov, JETP **39**, 438 (1960), Soviet Phys. JETP **12**, 000 (1961).

[2] W. Frazer and J. Fulco, Phys. Rev. Lett. **2**, 365 (1959).

[3] Chew, Goldberger, Low, and Nambu, Phys. Rev. **106**, 1335 (1957).

[4] S. Mandelstam, Phys. Rev. **112**, 1344 (1958).

[5] E. T. Whittaker and G. N. Watson, A Course of Modern Analysis, Cambridge (1945).

[6] Efremov, Mescheryakov, Chou Hung-Yüan, and Shirkov, On the Derivation of Equations from Mandelstam's Representation, (submitted to Nuclear Physics).

[7] B. M. Pontecorvo, Three Lectures on High-energy Physics, Kiev Conference on High Energy Physics (1959) (in press); CERN, Symposium **11**, pp. 225, 230 (1956).

[8] CERN, Symposium on High-Energy Accelerators and Pion Physics, **2**, 195 (1956).

[9] Ishida, Takahashi, and Ueda, Progr. Theoret. Phys. **23**, 731 (1960).

[10] Bowcock, Cottingham, and Lurie, Effect of a Pion-pion Scattering Resonance at Low-energy Pion-nucleon Scattering, (submitted to Nuovo cimento).

Translated by A. Skumanich
203

ON THE POSSIBILITY OF PROTON DECAY OF NUCLEI*

V. A. KARNAUKHOV and N. I. TARANTIN

Submitted to JETP editor June 15, 1960

J. Exptl. Theoret. Phys. (U.S.S.R.) **39**, 1106-1111 (October, 1960)

The possible existence of proton radioactivity is considered. The region of nuclei in which it seems most feasible to search for proton radioactive isotopes is determined. The expected lifetimes of p-active nuclei are estimated and the role of competing processes (α and β^+ decay, K capture) is discussed. Possible reactions leading to the formation of p-active isotopes are indicated and their cross sections are estimated.

1. In all presently known nuclei the last proton has positive binding energy, i.e., these nuclei are stable against proton decay. However, if the number of neutrons in the nucleus is lowered, the binding energy of the last proton decreases and can become negative. In this case an unexcited nucleus may emit a proton.

The decrease of the binding energy of the proton is due to the fact that the number of unpaired nucleons in the nucleus increases if there are fewer neutrons. This leads to a weakening of the nuclear interaction and to a relative strengthening of the Coulomb repulsion. This behavior is characteristic of all nuclei; only the quantitative aspects of this dependence change: as Z increases, the change of the binding energy of the proton with changing A becomes slower. To illustrate this situation, we show in Fig. 1 the binding energy of the last proton as a function of the mass number for the isotopes of Sc and Bi.[2,3]

An analytic expression for this behavior is easily obtained by using the semi-empirical Weizsäcker formula (see, for example, Fermi's book[4]). According to this formula the binding energy of the last proton (E_p) in Mev is given by

$$E_p \approx 931.14\left\{a_1 - a_2\frac{2}{3A^{1/3}} + a_3\frac{1}{A-1}\left[\left(\frac{A}{2}-Z\right)+\frac{1}{4}\right] - a_4\frac{2Z-1}{A^{1/3}} + \delta\right\}, \quad (1)$$

where

$$a_1 = 0.015, \quad a_2 = 0.014, \quad a_3 = 0.083, \quad a_4 = 0.00063,$$

$$\delta = \begin{cases} -0.036\,A^{-3/4} & \text{for nuclei with odd Z,} \\ +0.036\,A^{-3/4} & \text{for nuclei with even Z.} \end{cases}$$

The term most sensitive to changes of A is the third term, which is related to the isotopic number. It essentially determines the change of the binding energy with changing mass number. As the nuclei become heavier, this term becomes less important, and the removal of a single neutron has a weaker effect on the binding energy of the last proton.

The extent of the region of nuclei which are stable against proton emission can be estimated with the help of Eq. (1), setting $E_p = 0$, or by extrapolating the experimental binding energies of the last proton.[2,3,5] The results of these estimates are given in Fig. 2*. The following can be concluded from Fig. 2. First, proton instability occurs sooner, i.e., in relatively heavier isotopes, for nuclei with odd Z. This can also be seen immediately from Eq. (1) by considering the contribution of the last term connected with the parity of the number of nucleons in the nucleus to the binding energy of the proton.

Second, the boundary of p stability recedes from the region of stable isotopes as Z increases. For nuclei with $Z > 60$, more than 10 neutrons must be removed from the nucleus in order to obtain a p-active isotope. It is very difficult to obtain such nuclei experimentally. The determination of the boundary of p stability for nuclei with $Z > 60$ is therefore of no practical significance as yet.

It should be noted that Alvarez[6,7] called attention to the fact that the light nuclei ($Z < 20$) of the series $Z = 2n + 1$, $A = 4n$ are close to p instability. Experiments[6-8] showed, however, that,

*The basic results of this paper were presented in the report of Karnaukhov.[1]

*In the Appendix of the paper of Cameron,[11] kindly given to us by V. I. Gol'danskiĭ, E_p was estimated for the light isotopes with the help of a revised semi-empirical formula for the mass of the nucleus. According to these data the boundary of p stability agrees, within the limits of a displacement of one unit in N, with that shown in Fig. 2 for $20 \leqslant Z \leqslant 50$. For Sb and I the data of Cameron are close to our extrapolated values.

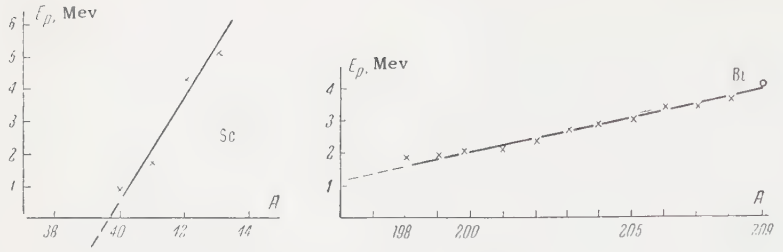

FIG. 1. Proton binding energy as a function of the mass number for the isotopes of scandium and bismuth (according to the data of references 2 and 3). o – stable isotopes, x – radioactive isotopes.

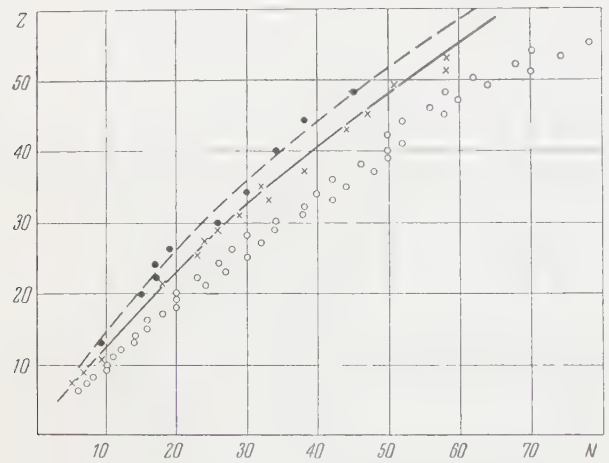

FIG. 2. Boundary of the region of stable nuclei with respect to proton emission: o – lightest stable isotope of a given element, x – stability boundary for nuclei with odd Z, obtained by extrapolation of the experimental data, • – similarly for even Z. The solid curve indicates the boundary for p stability for nuclei with odd Z, obtained from the Weizsäcker formula; the stability boundary obtained from the same formula for even Z is indicated by the dashed curve.

with the exclusion of F^{16}, these nuclei are p stable. In the case of F^{16} indirect evidence indicates that it is unstable against proton decay.

2. The instability of a nucleus against proton emission shows up only if the probability of other decay modes is smaller than the probability of proton emission, or is at most comparable to it. Processes competing with p decay are K capture and β^+ decay for light and intermediate nuclei and α decay for the heaviest among them.

In the case of the first p-active isotopes the energy of the K and β^+ transformations can be estimated with the help of the Weizsäcker formula or by extrapolation of the experimental data. These estimates show that this energy is 10 to 15 Mev for the nuclei under consideration. The half-life for an allowed β^+ transition is in this case 0.1 to 0.01 sec. The lifetime with respect to K capture is considerably greater. We see from this that in the region of light and intermediate nuclei the proton decay is noticeable if the lifetime of the nucleus with respect to proton emission is smaller than or comparable to the value 0.1 to 0.01 sec.

It can be shown with the help of the Weizsäcker formula that α decay becomes energetically possible for nuclei with $Z > 40$ on the boundary of p stability. Since the accuracy of calculations based on the Weizsäcker formula is poor, while the lifetime of the nucleus with respect to α decay depends strongly on the energy of the decay, it is not possible to estimate the half-life with sufficient reliability in this case. The only thing one can say is that the lifetime with respect to α decay will not exceed 10^{-6} sec for the first p active isotopes of elements with $Z > 55$. This means that for nuclei with $Z < 50$ the most important process competing with p decay is apparently β^+ decay, whereas α decay is the strongest competitor for $Z > 50$.

3. The lifetime of a nucleus with respect to proton emission can be estimated by regarding the p decay as the result of the passage of a proton through the Coulomb barrier. According to Bethe,[9] the disintegration constant for proton emission, λ, is given by the relation

$$\lambda = 1/\tau = (v/2R)\exp(-G_0);$$
$$G_0 = 2g\,[x^{-1/2}\arccos x^{1/2} - (1-x)^{1/2}],$$
$$g = \hbar^{-1}\sqrt{2mZe^2R}, \qquad x = E_p/V_p, \qquad V_p = Ze^2/R. \qquad (2)$$

Here v is the velocity of the proton in the nucleus, m is the mass of the proton, E_p is the energy of the proton decay, R is the radius, and Ze, the charge of the daughter nucleus.

Since it is impossible to predict with sufficient reliability the disintegration energy of the first p active isotopes, one cannot compute the lifetime of these nuclei with satisfactory accuracy. It is therefore more feasible to determine the proton energy corresponding to a prescribed lifetime of the nucleus. We restrict ourselves to the values $\tau' = 10^{-12}$ sec, $\tau'' = 10^{-8}$ sec, and $\tau''' = 10^{-1}$ sec. τ' and τ'' were chosen such as to accommodate a certain group of experiments; τ''' represents the maximal lifetime of the nucleus with respect to p decay, when the competition from allowed β^+ decay is still insignificant. The results of the calculations for several nuclei are given in Table I.

It is seen from Table I that the intervals $E_{p1} - E_{p3}$ within which the energy of the proton must

TABLE I

Nucleus	E_{p1}, Mev $\tau=10^{-13}$ sec	E_{p2}, Mev $\tau=10^{-8}$ sec	E_{p3}, Mev, $\tau=10^{-1}$ sec	$E_{p1}-E_{p3}$
Sc^{39}	0.38	0.2	0.12	0.26
As^{63}	0.75	0.45	0.25	0.50
Sb^{160}	1.5	1.0	0.5	1.0

lie in order that the p decay can be observed experimentally are small (especially for small Z). Observation of a p-active nucleus with $Z < 20$ is therefore rather improbable. As Z increases, the range of admissible values of the proton energy is widened; however, it becomes narrower again for nuclei with $Z > 50$ due to the growing competition from α decay.

It should be noted that the range of admissible energy values of the proton can be extended somewhat into the region of high energies if a proton with non-vanishing angular momentum is emitted or if the parities of the state of the daughter nucleus and of the core remaining after emission of the proton are different.

The effect of the angular momentum of the proton on the probability for its emission can be determined by replacing G_0 in Eq. (2) by G_l (see Bethe[9]), which characterizes the penetrability of the barrier for particles emitted with an angular momentum equal to $\hbar\sqrt{l(l+1)}$. The effect of the angular momentum is more pronounced in proton decay than in α decay, since in the first case the height of the centrifugal barrier is four times greater for the same l, while the Coulomb barrier is lower by the factor $\frac{1}{2}$. In Table II we give the retardation factor $f_l = \lambda_0/\lambda l = \tau_l/\tau_0$ for different values of l, calculated for a proton energy corresponding to $\tau_0 = 10^{-8}$ sec. As was to be expected, the effect of the angular momentum is more pronounced for the lighter nuclei.

4. Together with p decay from nuclei in the ground state, a proton can also be emitted through the barrier by an excited nucleus formed, for example, as a result of β^+ decay. This phenomenon is analogous to the emission of delayed neutrons from fission fragments. In this case the proton decay may be accompanied by a competing radiative transition. Estimates show, however, that for p active isotopes of intermediate nuclei this competition becomes unimportant already for excitation energies of 1 to 2 Mev.

TABLE II

Nucleus	f_1	f_2	f_3
Sc^{39}	3	70	1400
As^{63}	2	20	300
Sb^{106}	1	10	100

As examples of this case we take the nuclei Sc^{41} and As^{67}, in which the binding energy of the proton is 1.8 and ~1 Mev, respectively. If these nuclei are excited to an energy $\gtrsim 4$ Mev as a result of the preceding β^+ decay of Ti^{41} and Se^{67} (the β^+ disintegration energy for Ti^{41} and Se^{67} is 8 to 9 Mev), there is a high probability that the excitation energy of Sc^{41} and As^{67} is removed by emitting a proton through the barrier.

The observation of delayed protons has been attempted by a number of authors.[6-8,10] The failure of these attempts is apparently connected with the fact that the binding energy of the proton is large in the nuclei investigated, which means that practically the entire β^+ disintegration energy had to remain in the form of excitation energy of the daughter nucleus in order to make the emission of the proton possible.

5. As was shown above, p activity should also be expected in very light isotopes. These isotopes may be obtained with the help of nuclear reactions involving neutron emission. Most convenient for the production of p active isotopes are reactions initiated by charged particles. Here it is better to use particles with odd Z, while the target should consist of elements with even Z which have relatively lighter isotopes. This permits one to obtain p active nuclei with odd Z as a result of a reaction with emission of a minimal number of neutrons. In Table III we list some of the presumed p active nuclei which can be obtained in reactions initiated by protons or ions of N^{14}. We also give the approximate values of the threshold energies E_{thresh} and of the maximal cross sections σ_{max} for these reactions.

TABLE III

p-active nucleus	Reaction for production	E_{thresh}, Mev	σ_{max}, cm²
Sc^{39}	Ca^{40} $(p, 2n)$	25	$5\cdot10^{-27}$
	Si^{28} $(N^{14}, 3n)$	35	$1\cdot10^{-27}$
Mn^{47}	Cr^{50} $(p, 4n)$	50	$1\cdot10^{-28}$
	A^{36} $(N^{14}, 3n)$	35	$1\cdot10^{-27}$
As^{63}	Ge^{70} $(p, 8n)$	85	$<5\cdot10^{-30}$
	Fe^{54} $(N^{14}, 5n)$	70	$1\cdot10^{-28}$
Rb^{78}	Kr^{78} $(p, 6n)$	65	$<1\cdot10^{-28}$
	Zn^{64} $(N^{14}, 5n)$	65	$1\cdot10^{-27}$
Sb^{106}	Sn^{112} $(p, 7n)$	70	$<5\cdot10^{-28}$
	Ru^{96} $(N^{14}, 4n)$	60	$1\cdot10^{-26}$

The reaction cross sections quoted in Table III were computed with the help of the relation

$$\sigma_{max} \approx \sigma_c \prod_{i=1}^{x} \left(\frac{\Gamma_n}{\Gamma_n+\Gamma_p+\Gamma_\alpha}\right)_i, \qquad (3)$$

where x is the number of neutrons emitted in the reaction; σ_c is the cross section for compound nucleus formation, Γ_n, Γ_p, and Γ_α are the partial level widths of the nucleus corresponding to the emission of a neutron, proton, or α particle; i = 1 refers to the compound nucleus, i = 2, 3, . . . , x refers to the intermediate nuclei formed after emission of 1, 2, etc., neutrons from the compound nucleus.

The value of $\Gamma_n/(\Gamma_n + \Gamma_p + \Gamma_\alpha)$ was estimated with the help of the statistical model for the evaporation of nucleons from an excited nucleus. According to this model

$$\frac{\Gamma_p}{\Gamma_n} \approx \frac{Z}{N} \exp\left\{\frac{B_n - B_p - 0.9V_p}{T}\right\},$$

$$\frac{\Gamma_\alpha}{\Gamma_n} \approx \frac{Z}{2N} \exp\left\{\frac{B_n - B_\alpha - 0.9V_\alpha}{T}\right\}.$$

In these formulas B_n, B_p, and B_α are the binding energies of the neutron, proton, and α particle in the nucleus; V_p and V_α are the heights of the Coulomb barrier corresponding to proton and α emission from the nucleus; T is the nuclear temperature.

For the cross section of the reaction (p, 6 − 8n) we give an upper limit in the table, since calculations based on formula (3) do not take account of the cascade knock-out of nucleons, which occurs when the nuclei are bombarded by energetic (> 50 Mev) protons.

It is seen from the table that the cross sections for the reactions leading to the formation of p active nuclei are small and amount to less than 10^{-2} times the cross section for compound nucleus formation ($\sigma_c \approx 10^{-24}$ cm^2). This is due to the fact that the probability for the evaporation of a neutron from a nucleus sufficiently close to a p unstable nucleus is considerably smaller than the probability for the emission of a proton or in some cases even of an α particle (the binding energy of the neutron in these nuclei is considerably larger then the binding energy of the proton or the α particle).

The considerations of this paper are based on estimates with no pretense to quantitative accuracy. It seems to us, however, that our results must be considered in the planning of experiments on the production of p active nuclei.

In conclusion the authors express their gratitude to Prof. G. N. Flerov for proposing the problem and discussion of the results.

[1] V. A. Karnaukhov, Collection of Papers Presented at the Conference on Nuclear Reactions with Multiply Charged Ions, March 1958, Dubna, 1959, p. 71.

[2] V. A. Kravtsov, Usp. Fiz. Nauk **54**, 3 (1954).

[3] V. A. Kravtsov, Usp. Fiz. Nauk **47**, 341 (1952).

[4] E. Fermi, Nuclear Physics (Russ. Transl.) IIL (1951).

[5] W. Barkas, Phys. Rev. **55**, 691 (1939).

[6] L. W. Alvarez, Phys. Rev. **75**, 1815 (1949).

[7] L. W. Alvarez, Phys. Rev. **80**, 519 (1950).

[8] Breckon, Henrikson, Martin, and Foster, Canad. J. Phys. **32**, 223 (1954).

[9] H. A. Bethe, Nuclear Physics (Russ. Transl.) pt. II, IIL (1948).

[10] A. C. Birge, Phys. Rev. **85**, 753 (1952).

[11] A. G. W. Cameron, Canad. J. Phys. **35**, 1021 (1957).

Translated by R. Lipperheide
204

CAPTURE OF μ^- MESONS BY THE O^{16} NUCLEUS

I. S. SHAPIRO and L. D. BLOKHINTSEV

Submitted to JETP editor June 15, 1960

J. Exptl. Theoret. Phys. (U.S.S.R.) 39, 1112-1114 (October, 1960)

The ratio of the probabilities for μ^- capture by the O^{16} nucleus with formation of N^{16} in the 0^- and 1^- states is calculated. It is found to be strongly dependent on the effective pseudoscalar constant and can be used for its measurement.

1. INTRODUCTION

BECAUSE of the strong interaction of pions and nucleons, the constants of weak four fermion interaction $C_V(q^2)$ and $C_A(q^2)$ are functions of the transferred momentum $q = p_p - p_n$ (p_p and p_n are the momenta of the proton and the neutron). In this case the matrix elements are shown to be dependent on two other quantities: the weak magnetism constant

$$D(q^2) = \frac{\mu_p - \mu_n}{2M} C_V(q^2), \qquad (1)$$

where μ_p and μ_n are the anomalous magnetic moments of the proton and neutron (in nuclear magnetons), M is the mass of the nucleon ($\hbar = c = 1$), and the effective pseudoscalar interaction constant $C_p(q^2)$. $C_p(q^2)$ cannot be calculated theoretically — there exist only estimates based on unreliable postulates. According to these estimates, the following relations hold for the capture of μ^- mesons by free protons ($q^2/m_\pi^2 = 0.5$, m_π is the pion mass):[1,2]

$$C_P^\mu = +8C_A, \qquad C_P^\mu \equiv C_P(0,\ 5), \qquad C_A \equiv C_A(0). \qquad (2)$$

By using isotopic invariance and data on the electric form factor of the proton, the quantity $C_V(0.5) \equiv C_V^\mu$ can be expressed in terms of the vector constant of β decay:[3]

$$C_V^\mu = 0.972C_V, \qquad C_V \equiv C_V(0). \qquad (3)$$

From the estimate of Goldberger and Treiman,[1]

$$C_A^\mu = 0.999C_A, \qquad C_A^\mu \equiv C_A(0.5). \qquad (4)$$

The relations (1) and (3) are indubitable in the scheme of universal interaction (with accuracy up to electromagnetic corrections), and the closeness of the constants C_A^μ and C_A [as expressed by Eq. (4)] is very probable if we keep in mind the relation (3) for the vector constants.

The least trivial is Eq. (2), which demonstrates the large value of the effective pseudoscalar constant in processes of muon interaction with nucleons.

At the present time, the most definite information on the constants of weak muon-nucleon interaction is obtained from a comparison of experimental data on the probability of the reaction

$$\mu^- + C^{12} \to B^{12} + \nu \qquad (5)$$

with theoretical calculations.[3-5] These results do not contradict the relations (1) — (4), but they are shown to be little sensitive to the absolute value and sign of C_P^μ: upon change in C_P^μ from $-8C_A$ to $+8C_A$, the probability of process (5) changes in all by a factor of 1.6 to 1.7 [the pseudoscalar term gives approximately 30 per cent contribution to the probability of reaction (5)]. Inasmuch as the experimental data of various authors differ in some cases by as much as a factor of 1.5 (accurate to 5 — 25 percent, as given by the authors themselves, see references 3 — 5), the information currently available on the value of C_P^μ is insufficient for verification of the relation (2).

It is shown in this research that the measurement of the relative probability of capture of μ^- mesons by the O^{16} nucleus with the formation of N^{16} in the 0^- and 1^- states can be employed for the determination of C_P^μ. It is demonstrated that the ratio of the capture probabilities for these levels changes by a factor of about six in the change of the constant C_P^μ from $-8C_A$ to $+8C_A$. Such a large change in this ratio is due to the important role of the pseudoscalar interaction in the transition $0^+(O^{16}) \to 0^-(N^{16})$.

The ratio of the capture probabilities for the 0^- and 1^- levels can be determined experimentally by measurement of the relative intensities of γ radiation corresponding to the radiative transition $1^- \to 0^-$ (272 kev) of the N^{16} nucleus, or the transitions $1^- \to 2^-$ (392 kev) and $0^- \to 2^-$ (120 kev) of the same nucleus.

2. EXCITED STATES OF THE N^{16} NUCLEUS

The structure of the ground state of the N^{16} nucleus, which has spin and parity 2^-, is charac-

terized by one unfilled place in the proton shell $1p_{1/2}$ and by one neutron in the state $1d_{5/2}$. This same configuration $(1p_{1/2})_p^{-1}(1d_{5/2})_n^1$ exists in the excited state 3^- (with excitation energy 285 kev). The excited states 0^- and 1^- are characterized by the configurations $(1p_{1/2})_p^{-1}(2s_{1/2})_n^1$. Evidently the so-called intermediate coupling in the addition of angular momenta exists in light nuclei.

In our case, however, the wave functions of the 0^- and 1^- states are close to the wave functions in the jj coupling scheme (for the 0^- state, this agreement is exact):

$$\left\langle 0^- \right|_{N^{16}} = \frac{1}{\sqrt{2}}\left(\left\langle 1p_{1/2}^{-1}, +\frac{1}{2}\right|_p \left\langle 2s_{1/2}^1, -\frac{1}{2}\right|_n - \left\langle 1p_{1/2}^{-1}, -\frac{1}{2}\right|_p \left\langle 2s_{1/2}^1, +\frac{1}{2}\right|_n\right), \quad (6)$$

$$\left\langle 1^-, m\right|_{N^{16}} = \sum_{m_1, m_2}\left(\frac{1}{2}, \frac{1}{2}, m_1, m_2\middle|\frac{1}{2}, \frac{1}{2}, 1, m\right) \times \left\langle 1p_{1/2}^{-1}, m_1\right|_p \left\langle 2s_{1/2}^1, m_2\right|_n. \quad (7)$$

The wave function of the ground state of O^{16} can be taken in the form

$$\left\langle 0^+\right|_{O^{16}} = \frac{1}{\sqrt{2}}\left(\left\langle 1p_{1/2}^{-1}, +\frac{1}{2}\right|_p \left\langle 1p_{1/2}^1, -\frac{1}{2}\right|_p - \left\langle 1p_{1/2}^{-1}\frac{1}{2}\right|_p \left\langle 1p_{1/2}^1, +\frac{1}{2}\right|_p\right). \quad (8)$$

The radial parts of the wave functions (6) and (7) should differ little from one another because of the small difference in the energies of the 0^- and 1^- levels (in the absence of interaction between the neutron and the hole, the 0^- and 1^- levels would be degenerate). This circumstance also makes it possible to compute the ratio of probabilities of capture to the levels 0^- and 1^- without having recourse to the details of the potential of the single particle model, since the radial parts of the matrix elements of the transitions 0^+ (O^{16}) $\rightarrow 0^-$ (N^{16}) and 0^+ (O^{16}) $\rightarrow 1^-$ (N^{16}) are identical and do not enter into the final result.

3. RESULTS OF THE CALCULATION

The formulas given below were obtained in an approximation in which the relativistic corrections to the wave functions of the nucleons were taken to be first order in V/M (V = 94.5 Mev is the energy of the neutron emitted in the process) the same as in the work of Fujii and Primakoff.[3] The probability of μ^- meson capture from the K orbit of the μ mesonic nucleus i with formation of the nucleus f is given by the formula:

$$W_{if} = \frac{C_A^{\mu^2}}{2\pi^2}\frac{V^2}{a_\mu^3}M_{if}, \quad (9)$$

where a_μ is the radius of the K orbit of the μ-mesic atom and M_{if} has the following form for transitions to the final states 0^- and 1^- of the N^{16} nucleus:

$$M_{0^+0^-} = 2[1 + x(1-\rho)]^2 I^2, \quad (10)$$

$$M_{0^+1^-} = [R^2(1+x)^2 + 2(1 - R\mu x)^2] I^2. \quad (11)$$

Here

$$R = -C_V^\mu/C_A^\mu = 0.78 \cdot 0.02, \qquad \rho = C_P^\mu/C_A^\mu,$$

$$x = V/2M = 5.03\cdot 10^{-2}, \qquad \mu = 1 + \mu_p - \mu_n = 5{,}7,$$

$$I = \int_0^\infty r^2 dr j_1(vr) R_{1s_{1/2}}(r) R_{1p_{1/2}}(r).$$

Thus we get for the ratio $\alpha = W_{0^+0^-}/W_{0^+1^-}$

$$\alpha = 0.29(1.05 - 0.05\rho)^2. \quad (12)$$

For $\rho = +8$, -8 and 0, the value of α is equal, respectively, to 0.12, 0.59 and 0.32. Such a dependence of α on ρ makes it possible to determine the sign and order of magnitude of ρ from the proposed experiment even if the true α differs from (12), because of the inaccuracy of the model (jj coupling, single particle approximation, etc), by a factor of 1.5 – 2, which is of slight probability.

One can estimate the absolute probability of capture by using calculations of the radial matrix elements.[6] A value of the order of 5×10^3/sec is obtained for the total absolute probability of capture with excitation of the 1^- and 0^- levels, which agrees approximately with the probability of the well-observed process (5). We note that the formation of the N^{16} nucleus in the 2^- state will take place with a probability of the same order as for the excitation of the 0^- and 1^- levels. Capture with excitation of the 3^- level is virtually excluded.

The authors express their debt to A. I. Alikhanov, M. Ya. Balats, and L. G. Landsberg for interesting discussions of possible experiments.

[1] M. L. Goldberger and S. B. Treiman, Phys. Rev. **111**, 355 (1958).

[2] L. Wolfenstein, Nuovo cimento **8**, 882 (1958).

[3] A. Fujii and H. Primakoff, Nuovo cimento **12**, 327 (1959).

[4] B. L. Ioffe, JETP **37**, 159 (1959), Soviet Phys. JETP **10**, 113 (1960).

[5] A. I. Alikhanov, Paper at the International Conference on the Physics of High-Energy Particles, Kiev, July, 1959.

[6] E. G. Beltrametti and L. A. Radicati, Nuovo cimento **11**, 793 (1959).

Translated by R. T. Beyer
205

THE EFFECT OF WEAK INTERACTION ON THE ELECTROMAGNETIC PROPERTIES OF PARTICLES

Ya. B. ZEL'DOVICH and A. M. PERELOMOV

Submitted to JETP editor March 23, 1960

J. Exptl. Theoret. Phys. (U.S.S.R.) **39**, 1115-1125 (October, 1960)

The contribution to the electromagnetic interaction caused by the weak interaction of particles is examined. In some cases the order of this contribution in the weak-interaction constant is different in the theory of the direct four-fermion interaction and in the theory with an intermediate vector boson. Estimates are given for the magnetic-moment correction and for the parity nonconservation of the "anapole" interaction of particles with the electromagnetic field. Expressions are given for the scattering of neutrinos in the Coulomb field of a nucleus, and the polarization of recoil protons from the scattering of electrons is examined. The possibility of the existence of weak neutral currents is considered, and the influence of such currents on the scattering of electrons by protons and on atomic effects is discussed.

1. INTRODUCTION

THE effects indicated in the abstract are undoubtedly small in absolute magnitude. It seems justified, however, to examine them now, since the recent discovery of parity nonconservation and the establishment of the universal V-A interaction[1,2] provide a firm basis for the discussion.

On the experimental side the study of the contribution of the weak interaction to electromagnetic properties (EMP) is not hopeless, despite the smallness of the effects. In the case of the neutrino all the EMP depend entirely on the weak interaction,* and the scattering of neutrinos by nuclei with large Z (with cross section of the order of 10^{-42} cm^2) is entirely caused by the EMP of the neutrino. In the cases of the electron and the μ meson the EMP that do not depend on the weak interaction can in principle be calculated with great precision in local electrodynamics.† Therefore diviations of the EMP from those calculated for e and μ can arise from two causes: from violations of the laws of electrodynamics at small distances and from the weak interaction.[3,4] In studying the problem of the limits of applicability of electrodynamics it is necessary to include possible effects of EMP arising from the weak interactions.

For strongly interacting particles, in particular for baryons, a quantitative theory does not exist, so that there is no problem of corrections. In the case of e and μ, however, just as in the case of the baryons, owing to parity nonconservation the weak interactions give specific EMP, which can be detected against the background of the interactions that are strong but conserve parity. In the nonrelativistic limit one such EMP of particles with spin is the anapole moment,[5] which gives an effective interaction energy σ curl $\mathbf{H} = \sigma \cdot \mathbf{j}$, where σ is the spin of the particle, $\mathbf{H}$ is the magnetic field, and $\mathbf{j}$ is the external current that produces the magnetic field.

In Sec. 2 of the present paper we examine the diagrams that contribute to the EMP and determine their orders in the weak-interaction constant in the various cases. Two types of theory are considered: that with a four-fermion interaction, and that with an intermediate heavy charged X boson; in some cases the introduction of the X boson lowers the order in g, i.e., increases the effect.

In Sec. 3 we consider the general features of the EMP that result from the Lorentz and gauge invariances of the theory, from Ward's identity, and also from the theory of the universal weak interaction and the two-component neutrino.

In Sec. 4 we examine the order of divergence of the integrals involved and give numerical estimates of the quantities that characterize the EMP of particles. Here for baryons we can assume that the strong interactions cut off the weak interactions already at momenta of the order of M_n, the mass of the nucleon.

*The problem of the EMP of the neutrino in the two-component theory was first considered by L. B. Okun'; for completeness, this problem is included in the present paper.

†The limit of accuracy here is not due to the divergence of the perturbation-theory series of electrodynamics, but appears much earlier – when the strongly interacting particles participate in the vacuum polarization.

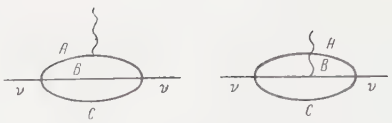

FIG. 1

In Sec. 5 we consider the experimentally observable effects in the scattering of particles, in particular the polarization of particles in the plane of the scattering, which depends on parity nonconservation. We discuss the scattering of neutrinos by nuclei, and also the effects of the new EMP in atomic physics.

Finally, in Sec. 6 we consider the question of a possible change of the initial assumptions about the weak interactions through the addition of a product of neutral currents to the usual product of charged currents. We examine the conditions under which the added term does not lead to decays that are not observed experimentally, and also the effects that are produced in the scattering of electrons by protons and in atomic physics.

2. THE DIAGRAMS

The neutrino. Introducing in the Lagrangian only those four-fermion terms that are necessary for the description of the experimentally observed processes of μ decay, μ capture, and β processes, we find that the only diagrams are those of the types shown in Fig. 1. In such a diagram two particles (say A and B) out of three (A, B, C) are charged, and the line for an electromagnetic quantum can be joined to either of the two lines. The particles A, B, C can be μ, e, ν or p, e, n. The diagram is of the order eg^2.

FIG. 2

If, however, we write the interaction as the product of two weak currents, then the theory predicts the scattering of a neutrino by an electron in first order in g. Corresponding to this there is a diagram of order eg in the electromagnetic interaction (Fig. 2).

The introduction of the X boson does not change the order of the diagram. The diagrams with the X boson are shown in Fig. 3, a, b. They are of the order eg_X^2, but $g_X^2/M_X^2 \approx g$, so that the diagrams of Figs. 2 and 3 are of the same order.

The leptons e and μ. The essential point for e and μ is that even in the formulation as a product of currents the four-fermion interaction gives the diagrams of Fig. 4, of order eg^2. Here the introduction of the X boson radically changes the situation, and gives diagrams of the type of Fig. 5, of order $eg_X^2/M_X^2 \approx eg$.

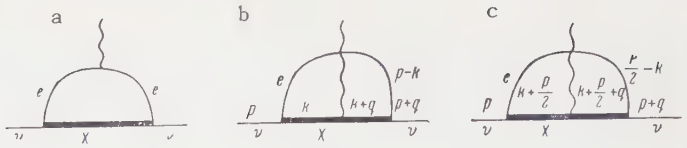

FIG. 3

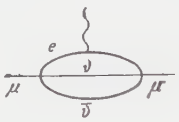

FIG. 4

FIG. 5

The baryons. The situation for the neutron would be the same as that for the neutrino, and that for the proton the same as for the electron and the μ meson, if it were not for the strong interaction. The difference between the two cases is that owing to the strong interactions the neutron can interact with the electromagnetic field, whereas the neutrino cannot (see the diagram of Fig. 6).

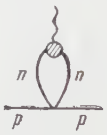

FIG. 6

3. THE GENERAL EMP DEPENDING ON THE WEAK INTERACTION

For brevity we shall denote the projection operators that convert four-component wave functions into two-component functions by the following symbols:

$$(1+\gamma_5)/2=\pi, \quad (1-\gamma_5)/2=\lambda, \quad \pi^2=\pi, \quad \lambda^2=\lambda, \quad \pi\lambda=\lambda\pi=0. \tag{3.1}$$

According to the hypothesis of Gell-Mann and Feynman, which has had excellent experimental confirmation, the weak interaction for a given type of particle always involves the same two-component wave function, for example $\pi\psi$. Therefore in all diagrams of the types of Figs. 1 — 5, in which the external lines are those of the quantum and of the same particle present initially and finally, the matrix element contains $\pi\psi$ and $\bar{\psi}\lambda$.

Diagrams of the types of Figs. 1 — 5 give matrix elements of the form

$$2e\bar{\psi}_1\lambda a_\mu \Gamma_\mu (p_1, p_2; q)\,\pi\psi_2, \tag{3.2}$$

where in addition to the momenta indicated the quantity $\Gamma\mu$ contains also Dirac matrices. Owing to the relations $p_1^2 = p_2^2 = -m^2$, $p_1 - p_2 = q$, the only independent scalar quantity is $q^2 = -2(m^2 + p_1p_2)$. Let us introduce the notation $p = p_1 + p_2$.

It follows from Lorentz and CP invariance that

$$a_\mu\Gamma_\mu = \hat{a}f(q^2) - (aq)\hat{q}g(q^2) - (ap)\hat{p}h(q^2) - (\hat{a}\hat{q}\hat{p} - \hat{p}\hat{q}\hat{a})k(q^2); \tag{3.3}$$

in particular, CP invariance excludes terms of the forms $(ap)\hat{q}$ and $(aq)\hat{p}$, the first of which would give an electric dipole moment. The anomalous magnetic moment is usually taken to be the coefficient of $(\hat{a}\hat{q} - \hat{q}\hat{a})$.

Since terms of the types $a_\mu q_\mu$ or $a_\mu q_\nu \gamma_\mu \gamma_\nu$ with an even number of factors γ_α placed between the projection operators give zero, it seems[7] at first glance that the anomalous magnetic moment arising from the weak interaction is zero. Because of the terms of types $(ap)\hat{p}$ and $(\hat{a}\hat{p}\hat{q} - \hat{q}\hat{p}\hat{a})$, however, even the simplest diagrams of the types of Figs. 1 — 5 contribute to the anomalous magnetic moment.

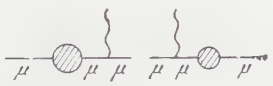

FIG. 7

There remain to be considered diagrams of the types shown in Fig. 7, where the shaded circle is a self-energy part (contribution Σ), which is obtained from a diagram of the type of Figs. 1 — 5 by omitting the photon line. It is obvious that as a whole a diagram of the type of Fig. 7 gives a contribution of the form

$$e[\bar{\psi}_1\lambda\Sigma(p_1)\,\pi(i\hat{p}_1 + m)^{-1}\hat{a}\psi_2 + \bar{\psi}_1\hat{a}(i\hat{p}_2 + m)^{-1}\lambda\Sigma(p_2)\,\pi\psi_2]. \tag{3.4}$$

Let us write

$$\lambda\Sigma(p_1)\,\pi(i\hat{p}_1 + m)^{-1} = F_1(p_1),$$
$$(i\hat{p}_2 + m)^{-1}\lambda\Sigma(p_2)\,\pi = F_2(p_2).$$

Since $F_1(p_1)$ does not depend on the momentum p_2, when acting on $\bar{\psi}_1$ from the right the operator F_1 can give only a quantity $F_{10} - \gamma_5 F'_{10}$, which is independent of the momentum. When the operator $F_2(p_2)$ acts from the left on ψ_2 we get a quantity $F_{20} + \gamma_5 F'_{20}$.

We finally get the contribution of the "ends" in the form

$$e[\bar{\psi}_1\hat{a}(F_{10} + \gamma_5 F'_{10})\psi_2 + \bar{\psi}_1\hat{a}(F_{20} + \gamma_5 F'_{20})\psi_2]. \tag{3.5}$$

Combining this with the main diagram and using the Dirac equation, we bring the expression into the form

$$M = [F_{10} + F_{20} + f(q^2) + 4m^2h(q^2) - 2q^2k(q^2)]\,\bar{\psi}_1\hat{a}\psi_2 + [h(q^2) + 2k(q^2)]\,im\hat{\psi}_1(\hat{q}\hat{a} - \hat{a}\hat{q})\psi_2 + [F'_{10} + F'_{20} + f(q^2) - 2q^2k(q^2)]\bar{\psi}_1\hat{a}\gamma_5\psi_2 - [g(q^2) - 2k(q^2)](aq)\bar{\psi}_1\hat{q}\gamma_5\psi_2. \tag{3.6}$$

According to Ward's theorem virtual processes of the type under consideration do not lead to a charge renormalization. Therefore the coefficient of $\bar{\psi}_1\hat{a}\psi_2$ must vanish for the value $q = 0$. Consequently the expansion of this coefficient in powers of q^2 must begin with a term proportional to q^2,

$$[F_{10} + F_{20} + f(q^2) + 4m^2h(q^2) - 2q^2k(q^2)] = q^2b(q^2),$$

$b(0) \neq \infty$.

The second term in Eq. (3.6) diverges logarithmically and gives the contribution from the weak interaction to the anomalous magnetic moments of the electron and μ meson. If we assume that the logarithmically divergent integral is of the order of unity, then the correction to the anomalous magnetic moment is $\sim 10^{-5}m^2\mu/M_n^2$ (in the theory with the X meson), whereas the correction to the magnetic moment from the electromagnetic interaction* is $\alpha m^2\mu/\Lambda^2$ if we break off at momenta $\sim\Lambda$; here μ is the Dirac magnetic moment of the particle.

Thus if in determining the limits of applicability of quantum electrodynamics by measuring the magnetic moments of the electron[3] and meson[4] one should find a discrepancy between theory and experiment of the order of $10^{-5}m^2\mu/M_n^2$, this difference can come from the weak interaction (if there is an X meson), and consequently is not a proof of a change of the electromagnetic interaction at momenta exceeding $\Lambda = (\alpha/10^{-5})^{1/2}M_n \approx 30\,M_n$.

The third and fourth terms of the matrix element M, which contain γ_5, are characteristic of a theory with parity nonconservation; by the condition of gauge invariance they must combine into an expression

$$c(q^2)\,\bar{\psi}_1(\hat{a}q^2 - (aq)\hat{q})\gamma_5\psi_2. \tag{3.7}$$

From this it follows that

$$[F'_{10} + F'_{20} + f(q^2) - 2q^2k(q^2)] = q^2c(q^2), \quad c(0) \neq \infty.$$

Substituting $q = p_1 - p_2$, we can write the expression (3.7) in the form

$$c(q^2)\,\bar{\psi}_1(q^2\hat{a} - (aq)\,2im)\gamma_5\psi_2. \tag{3.8}$$

*An error in the formula for $\delta\mu$ in reference 3 is corrected in a later paper.[4]

It is easy to verify that the term (3.7) does not give any interaction with free photons, for which $q^2 = 0$, and that we can choose a gauge with $(aq) = 0$.

The combination of terms (3.7) can be rewritten in the form

$$c(q^2)\,\bar{\psi}_1\gamma_\mu\gamma_5\psi_2\,[q^2 a_\mu - a_\nu q_\nu q_\mu]$$
$$= -c(q^2)\,\bar{\psi}_1\gamma_\mu\gamma_5\psi_2\left(\frac{\partial^2 a_\mu}{\partial x_\nu^2} - \frac{\partial^2 a_\nu}{\partial x_\mu \partial x_\nu}\right)$$
$$= c(q^2)\,\bar{\psi}_1\gamma_\mu\gamma_5\psi_2\,\partial F_{\mu\nu}/\partial x_\nu. \qquad (3.9)$$

From the equations of electrodynamics we have $\partial F_{\mu\nu}/\partial x_\nu = j_\mu$, where j_μ is the external current that produces the field $F_{\mu\nu}$. If the external current is that of a fermion with charge e and wave function ξ, then in a transition of this fermion to a state 1 from a state 2 we have $j_\mu = ie\xi_1\gamma_\mu\xi_2$, so that

$$M = iec(q^2)\,\bar{\psi}_1\gamma_\mu\gamma_5\psi_2\,\bar{\xi}_1\gamma_\mu\xi_2, \qquad (3.10)$$

where all the wave functions are taken at the same space-time point (a subsequent integration over d^4x is understood, to get the transition probability).

For small momentum transfer in a coordinate system in which our particle (with the wave function ψ) is at rest,

$$\bar{\psi}_1\gamma_4\gamma_5\psi_2 \to 0, \qquad \bar{\psi}_1\gamma\gamma_5\psi_2 \to \bar{\psi}_1\sigma\psi_2,$$

and in the limit the interaction becomes

$$iec(0)\,\bar{\psi}_1\sigma\psi_2 j = iec(0)\bar{\psi}_1\sigma\psi_2\,\mathrm{curl}\,\mathbf{H}.$$

Thus the EMP that does not conserve parity is indeed an anapole interaction.[5] The name pseudocharge (see the paper by Bander and Feinberg) seems less appropriate.

4. PERTURBATION-THEORY CALCULATION OF THE INTERACTION

For a neutral particle (neutrino) the diagram of Fig. 2 gives a contribution of the order eg even if there is no X boson.* Writing the interaction

$$(g/\sqrt{2})\,\bar{\psi}_e\gamma_\mu(1+\gamma_5)\,\psi_\nu\bar{\psi}_\nu\gamma_\mu(1+\gamma_5)\,\psi_e \qquad (4.1)$$

in the form

$$(g/\sqrt{2})\,\bar{\psi}_e\gamma_\mu(1+\gamma_5)\,\psi_e\;\bar{\psi}_\nu\gamma_\mu(1+\gamma_5)\,\psi_\nu, \qquad (4.2)$$

we get the matrix element

$$M_2 = \frac{g}{\sqrt{2}}\,\bar{\psi}_\nu\gamma_\mu(1+\gamma_5)\psi_\nu$$
$$\times \int \mathrm{Sp}\left[\gamma_\mu(1+\gamma_5)\,\frac{1}{i(\hat{q}/2-\hat{k})+m}\,\hat{a}\,\frac{1}{i(\hat{q}/2+\hat{k})+m}\right]d^4k. \qquad (4.3)$$

In the square brackets in the integrand the matrix $(1+\gamma_5)$ can be replaced by unity, since after the integration over d^4k the number of matrices γ_μ remaining in the brackets is less than four, and

$$\mathrm{Sp}\,\gamma_5 = \mathrm{Sp}\,\gamma_\mu\gamma_5 = \mathrm{Sp}\,\gamma_\mu\gamma_\nu\gamma_5 = \mathrm{Sp}\,\gamma_\mu\gamma_\nu\gamma_\lambda\gamma_5 = 0.$$

The part that is left is $K_{\mu\nu}a_\nu$, where $K_{\mu\nu}$ is the well known vacuum-polarization tensor (cf. e. g., reference 8):

$$K_{\mu\nu} = K_0\delta_{\mu\nu} + (q^2\delta_{\mu\nu} - q_\mu q_\nu)\,c(q^2).$$

Since the neutrino has no charge, we drop the quadratically diverging integral K_0, which is independent of q. The remaining part is gauge invariant and diverges logarithmically. We get

$$M_2 = egc(q^2)\,(q^2\delta_{\mu\nu} - q_\mu q_\nu)\,\bar{\psi}_\nu\gamma_\mu(1+\gamma_5)\,\psi_\nu a_\nu;$$
$$c_2(q^2) = \frac{1}{3\pi}\left(\ln\frac{m_e^2}{L^2} - \frac{1}{6}\right) + \frac{1}{15\pi}\,\frac{q^2}{m_e^2},$$
$$\frac{q^2}{m_e^2} \ll 1, \quad c_2(0) \sim 2, \qquad c_2(q^2) = \frac{1}{3\pi}\left(\ln\frac{q^2}{L^2} + \frac{1}{6}\right),$$
$$\frac{q^2}{m_e^2} \gg 1, \quad c_2(q^2) \sim 0.7. \qquad (4.4)$$

Here the numerical estimates are given for $L \sim 30\,M_n$; in the second case, $q^2 \gg m_e^2$, we have taken $q \approx M_n$.

In the case in which there is an X boson we must calculate the two diagrams of Fig. 3a and 3b. For the same reasons as before we drop the quadratically diverging integrals, which leaves logarithmic divergences. The calculation gives

$$M_{3a} = 7\,\frac{g_X^2}{M_X^2}\,\frac{1}{3\pi}\ln\frac{m_e^2}{M_X^2}\,\bar{\psi}_\nu\gamma_\mu(1+\gamma_5)\,\psi_\nu(q^2\delta_{\mu\nu} - q_\mu q_\nu)\,a_\nu,$$
$$c_{3a}(0) \sim 14;$$
$$M_{3b} = 13\,\frac{g_X^2}{M_X^2}\,\frac{1}{4\pi}\ln\frac{M_X^2}{L^2}\,\bar{\psi}_\nu\gamma_\mu(1+\gamma_5)\,\psi_\nu(q^2\delta_{\mu\nu} - q_\mu q_\nu),$$
$$c_{3b}(0) \sim 1 \qquad (4.5)$$

for

$$q^2/m_e^2 \ll 1, \qquad \ln(L^2/M_X^2) \sim 1, \qquad L \sim 30\,M_n.$$

We note that these expressions are only estimates, for the following reason. Because of the strong (quadratic) divergence of the diagrams in the theory with the vector meson we get a logarithmically divergent result which depends on the designations of the momenta in the diagram. For example, diagram 3c can be obtained from diagram

*A. M. Brodskiĭ has kindly made available to us a manuscript of a paper[7] which deals with the EMP of the neutrino that correspond to the diagram of Fig. 2.

3b by replacing the momentum k over which one integrates by $k + p/2$, and when this is done and we cut off with respect to k we get additional terms $\sim \ln(L^2/M_X^2)$. For the same reason the usual proof of the Ward identity and the gauge invariance does not go through. (In the theory with logarithmic divergences when we replace the momentum variable of integration k by $k + p/2$ we get* an error $\sim M_X^2/L^2$.) We note further that such diagrams do not reduce to local diagrams for $M_X \to \infty$, since one takes the integration over the momentum of the virtual meson to values L that must be much larger than M_X, in order for the value obtained to have only a weak dependence on the cut-off momentum. In view of all that has been said, we do not give expressions for the c's as functions of q^2. We have

$$g_X^2 / M_X^2 \sim g = 10^{-5} M_n^{-2}.$$

If the particles are charged, the effects will be of first order in g only if there is a charged vector meson, when they are given by the diagram of Fig. 5. The calculation from this diagram gives the coefficient $c_{3b} = 1$ in the formula (4.5).

5. THE EXPERIMENTAL EFFECTS

We have established that a particle can have an anapole moment. In the case in which a charged vector meson exists, when charged particles are scattered by protons there can be interference between the Coulomb and anapole interactions, owing to which there are effects of first order in g.[9] In this case $g = g_X^2/M_X^2$, that is, g must be a positive quantity. A negative value of g obtained experimentally will mean that the hypothesis of the intermediate vector meson is untrue. For the case of interference of scatterings from nuclear and weak interference this idea has been put forward by Smorodinskiĭ and Fradkin (cf. reference 10) (measurement of the longitudinal polarization from scattering at angle 0°).

Let us consider the scattering of an electron with an anapole moment by a proton. (The scattering of electrons by protons that have an anapole moment is of less interest, since protons and neutrons must have relatively small anapole moments.†) The matrix element for the scattering is of the form

$$M = \bar{\psi}_p \left[A\gamma_\mu + i \frac{B}{4M_p} (\gamma_\mu \hat{q} - \hat{q}\gamma_\mu) \right] \times \psi_p \bar{\psi}_e \left[-\frac{e^2}{q^2} \gamma_\mu + c(q^2)\gamma_\mu (1 + \gamma_5) \right] \psi_e. \quad (5.1)$$

Here we have omitted the radiative corrections to the electron current, which, though indeed larger than the anapole effects, conserve parity.

The calculations of the cross section and the polarization are analogous to the calculations in the paper by Akhiezer, Rozentsveĭg, and Shmushkevich.[11] The electron is treated relativistically. It turns out that the cross section does not depend on the polarization of the electrons,* and thus there is no polarization of the electrons in the final state. Therefore we might be able to observe the following effects:

1) When an unpolarized electron beam is scattered by unpolarized protons there is a polarization of the recoil protons.

2) The cross section depends on the polarization of the target protons.

Experimentally one can measure the scattering cross sections for protons polarized parallel and antiparallel to the momentum of the incident electrons. These cross sections should be different. With transverse polarization of the protons the probability of scattering in the plane that contains the momentum **k** of the incident electron and the polarization of the target proton is different for scattering angles θ and $-\theta$ relative to the momentum **k**. When an unpolarized electron beam acts on unpolarized protons one gets different probabilities for scattering of the recoil protons, in the plane containing the momentum **p′** of the recoil proton and the vector $\mathbf{k} \times \mathbf{k}'$, through the angles ϑ and $-\vartheta$ relative to the vector **p′**. An interaction that conserves parity does not give such effects.

We present the formula for the cross section for scattering of electrons with an anapole moment by polarized protons:

$$\sigma = \sigma_0 (1 + \alpha\zeta_\parallel + \beta\zeta_\perp),$$

$$\alpha = gc \frac{16p^2 \sin^2(\theta/2) \tan^2(\theta/2)}{(p+E)^2} \frac{A+B}{e^2} \times \frac{A(p^2 + pE\cos^2(\theta/2)) + Bp^2 \sin^2(\theta/2)}{A^2 + B^2 p^2 \sin^2(\theta/2) + 2(A+B)^2 p^2 (p+E)^{-2} \sin^2(\theta/2) \tan^2(\theta/2)},$$

$$\beta = gc \frac{16p^2 \sin^2(\theta/2) \tan^2(\theta/2)}{(p+E)^2} \frac{A+B}{2e^2} \times \frac{[A - Bp(p+E)]\, p \sin\theta}{A^2 + B^2 p^2 \sin^2(\theta/2) + 2(A+B)^2 p^2 (p+E)^{-2} \sin^2(\theta/2) \tan^2(\theta/2)}; \quad (5.2)$$

*Similar unpleasantnesses are encountered in the calculation of other effects associated with the existence of the X meson, for example in the decay $\mu \to e + \gamma$. One does not see how one can get an unambiguous value of the quantity we need.

†Just as this paper was finished there appeared a preprint by Bander and Feinberg, in which detailed formulas are obtained for the scattering of electrons by protons with anapole and dipole moments.

*We are referring throughout to the polarization in the plane of the scattering, which is specific for the case of parity nonconservation.

since $c \sim 0.01$, for $p \sim M_n$ and $\theta \sim \pi/2$ we have $\alpha \sim 10^{-5}$ and $\beta \sim 10^{-5}$. Here A is the form factor of the charge, B is the form factor of the magnetic moment, p and E are the momentum and energy of the proton in the center-of-mass system, θ is the scattering angle, $\zeta_{\parallel}$ is the component of the polarization parallel to the momentum of the incident proton, and $\zeta_{\perp}$ is the component of the polarization perpendicular to the momentum of the incident proton and in the plane of the scattering.

For the neutrino there are no interference effects, but on account of the electromagnetic interaction a neutrino can be scattered by a proton or by a heavy nucleus.* The matrix element for this case can be written in the form

$$M = f\bar{\psi}_p \left[A\gamma_\mu + \tfrac{1}{4} iBM^{-1}(\gamma_\mu \hat{q} - \hat{q}\gamma_\mu)\right] \psi_p \bar{\psi}_\nu \gamma_\mu (1+\gamma_5)\psi_\nu. \tag{5.3}$$

The scattering cross section in the center-of-mass system is of the form

$$\frac{d\sigma}{d\Omega} = \frac{f^2}{\pi} p^2 \left\{ [A^2 + B^2 p^2 x](1-x) + 2(A+B)^2 \left(\frac{p}{p+E}\right)^2 x^2 \right\}. \tag{5.4}$$

Here the energy is in units M_n, $q^2 = 4p^2x$ is the momentum transferred, p is the momentum of the proton, and E is the energy of the proton.

To find the total cross section we must integrate the differential cross section, taking the form factors into account. Choosing the form factors in the form $\exp[-r_0^2 q^2/6]$,[12] we get*

$$\sigma = \frac{3}{2}\frac{f^2}{\pi}\frac{1}{r_0^2}\left\{\left[A^2 h_1(y) + \frac{3}{2}B^2 \frac{1}{r_0^2} h_2(y)\right] + 2(A+B)^2 \left(\frac{p}{p+E}\right)^2 h_3(y)\right\};$$

$$h_1(y) = 1 - y^{-1}(1-e^{-y}),$$

$$h_2(y) = (1+e^{-y}) - 2y^{-1}(1-e^{-y}),$$

$$h_3(y) = y^{-2}[2 - (2+2y+y^2)e^{-y}], \tag{5.5}$$

where $y = 2p^2 r_0^2/3$, and $r_0 = 0.8 \times 10^{-13}$ cm; for $p \sim 300$ Mev, $f = \alpha g c_2$, $c_2 \sim 1$ we have $\sigma \sim 10^{-13}$ cm^2.

For the scattering of neutrinos by heavy nuclei the cross section is proportional to Z^2, but for this the wavelength of the neutrino must be smaller than the nuclear radius $R = bA^{1/3}$, $b \approx 1.2 \times 10^{-13}$ cm. The maximum momentum transfer is $\sim 1/R \approx (M_n/6)A^{-1/3}$, and the kinetic energy is $\sim (M_n/72)A^{-5/3}$. If ϵ is the minimum kinetic energy at which a recoil nucleus can be observed, then we can take a nucleus of atomic number $A = (72\epsilon/M_n)^{-3/5}$. For $A = 1$ the maximum recoil energy at which the recoil nucleus interacts as a whole with the neutrino is $E \approx 13$ Mev; for $A = 10$ we get $E \approx 0.25$ Mev, and for $A = 100$, $E = 6.4$ kev.

Effects of parity nonconservation in an atom are very small. Just as in references 13—15, which were concerned with a dipole moment, on our assumptions also the matrix element for the transition $2S_{1/2} - 2P_{1/2}$ on account of the anomalous interaction is

$$V_{2S2P} \approx 10^{-7}\alpha^2 (m_e/M_n)^2 \text{ atom. units}$$

The shifts of the $2S_{1/2}$ and $2P_{1/2}$ levels are negligible. The admixture of the $2P_{1/2}$ state in the $2S_{1/2}$ state is $\beta \approx 10^{-9}$. The lifetime of the $2S_{1/2}$ state is decreased by a fraction $\beta^2(\tau_{2S-1S}/\tau_{2P-1S}) \approx 10^{-9}$ of its value, and it is impossible to measure such a change experimentally.

We note, however, that the transition $2S_{1/2} \to 1S_{1/2}$ with lifetime 1/7 sec is a two-quantum transition, whereas $2S_{1/2} + \beta P_{1/2} \to 1S_{1/2}$ is a one-quantum transition. Therefore the lifetime corresponding to this transition, equal to about 10^{-9} sec, is to be compared not with the lifetime of the two-quantum transition, but with that of the one-quantum magnetic-dipole transition, which is 2×10^5 sec (cf., e. g., reference 16).

6. NEUTRAL CURRENTS

The effects arising from neutral currents have been briefly considered in reference 9. In the theory of the universal weak interaction the interaction Hamiltonian is written in the form

$$H_{int} = gJ_\mu J_\mu^+,$$

$$J_\mu = L_\mu + B_\mu + S_\mu,$$

$$L_\mu = \bar{e}\gamma_\mu(1+\gamma_5)\nu + \bar{\mu}\gamma_\mu(1+\gamma_5)\nu, \tag{6.1}$$

where L_μ is the lepton current, B_μ is the current of strongly interacting particles that conserves strangeness, and S_μ is the current of strongly interacting particles with equal changes of charge and strangeness $\Delta Q = \Delta S$.

Let us consider the part B_μ of the current. From B_μ and B_μ^+ we can construct the quantities

$$B_\mu^1 = (B_\mu^+ + B_\mu)/\sqrt{2}, \qquad B_\mu^2 = (B_\mu^+ - B_\mu)/i\sqrt{2},$$

$$B_\mu^+ B_\mu = B_\mu^1 B_\mu^1 + B_\mu^2 B_\mu^2.$$

B_μ^1 and B_μ^2 transform like projections along the first and second axes in the isotopic space. Such an interaction is not isotopically invariant, and becomes invariant when one adds the product of the

*As was already mentioned in the Introduction, the scattering of neutrinos has been considered by L. B. Okun'.

*We note that the distribution of the recoil nuclei differs from the distribution for the scattering of electrons by nuclei only by the factor q^4.

neutral currents. The question arises, can we supplement each of the currents with a neutral component? On doing so, we get new terms of the forms

$$L^0L^0,\ B^0B^0,\ S^0S^0,\ L^0S^0,\ B^0S^0,\ L^0B^0,$$

and furthermore we introduce two isotopic doublets

$$l_1 = \begin{pmatrix} \nu_e \\ e^- \end{pmatrix}, \quad l_2 = \begin{pmatrix} \nu_\mu \\ \mu^- \end{pmatrix}$$

with different neutrinos.[17,18,21]

The terms L^0L^0 then give an interaction that causes parity nonconservation in positronium and muonium, and also some other less interesting effects. Furthermore processes of the types

$$\mu^\pm \to e^\pm + \gamma, \qquad \mu^\pm \to e^\pm + e^+ + e^-$$

will be forbidden in arbitrary order in g.

The terms of types B^0B^0 and S^0S^0 in the interaction also do not lead to any new effects that would be in contradiction with the experimental data known at present. L^0S^0 gives decays of the type $K^0 \to e^+ + e^-$ in first order in g, which have not been observed, and we require that $L^0S^0 = 0$, from which we have either $L^0 = 0$ or $S^0 = 0$. The case $S^0 = 0$ has been considered by one of the writers,[9] and the case $L^0 = 0$, by Treiman.[19] In this case S^0 is constructed in such a way that the rules $\Delta Q = \Delta S$ and $|\Delta T| = 1/2$ will hold in nonleptonic decays of strange particles given by the terms B^0S^0.

The interaction B^0L^0 leads to mixing of the $2S_{1/2}$ and $2P_{1/2}$ levels owing to parity-nonconserving interactions between electron and proton and between electron and neutron.* Since such an interaction is 137 times as strong as that considered in the preceding section, the probabilities of the one-quantum transition $2S_{1/2} \to 1S_{1/2}$ on account of the magnetic-dipole interaction and on account of the parity-nonconserving weak interaction are comparable, and therefore the experimental probability of the one-quantum transition should be appreciably larger than the theoretical probability obtained by taking into account only the magnetic interaction.

This same interaction term gives the decays $\pi^0 \to e^+ + e^-$ and $\Sigma^0 \to \Lambda^0 + e^+ + e^-$, but these same decays can occur through the strong and electromagnetic interactions with larger probabilities than through the weak interaction L^0B^0.

We present the formulas for the scattering of electrons by protons in the case of the existence of neutral currents. Taking into account the form factors of the heavy particles that exist on account of the strong interactions,[20] we have

$$\begin{aligned} M = &-\frac{e^2}{q^2}\bar{\psi}_p\left[A\gamma_\mu + i\frac{B}{4M_p}(\gamma_\mu\hat{q} - \hat{q}\gamma_\mu)\right]\psi_p\bar{\psi}_e\gamma_\mu\psi_e \\ &+ \frac{g}{2\sqrt{2}}\bar{\psi}_p[a\gamma_\mu + ib(\gamma_\mu\hat{q} - \hat{q}\gamma_\mu) + c\gamma_\mu\gamma_5 \\ &+ dq_\mu\gamma_5]\psi_p\cdot\bar{\psi}_e\gamma_\mu(1+\gamma_5)\psi_e, \end{aligned} \tag{6.2}$$

where A and B are the usual form factors of Hofstadter[12] and a, b, c, d are the formfactors of Goldberger and Treiman.[20]

The scattering cross sections for longitudinally polarized (right and left handed) electrons are different:

$$d\sigma/d\Omega = (d\sigma/d\Omega)_0 \quad \text{for right-handed electrons}$$

$$d\sigma/d\Omega = (1+\lambda)(d\sigma/d\Omega)_0 \quad \text{for left-handed electrons} \tag{6.3}$$

where $(d\sigma/d\Omega)_0$ is the cross section for the scattering of unpolarized electrons and

$$\lambda = -\frac{gq^2}{\sqrt{2}e^2} \times \frac{aA + 1/4\, q^2\{2(a+b) + (A+B)\tan^2(\theta/2) + 2c(A+B)[1/\varepsilon + (1+1/\varepsilon)\tan^2(\theta/2)] + bB\}}{A^2 + 1/4\, q^2[2(A+B)^2\tan^2(\theta/2) + B^2]};$$

$\lambda \approx 10^{-3}$ for $\theta = \pi/2$, $\epsilon = M_n$.

Here $q^2 = 4\epsilon^2 \sin^2(\theta/2)/[1 + 2\epsilon \sin^2(\theta/2)]$, and ϵ is the energy of the electron in units M_n. All quantities are taken in the laboratory system.

The polarization of the recoil protons in the plane of the scattering and perpendicular to the recoil momentum is given by

$$P_\perp = -\frac{g}{\sqrt{2}e^2}\frac{8\cot^2\vartheta\sin\vartheta}{(\varepsilon+1)^2} \times \frac{cA\varepsilon + 1/4\, q^2\{a(A+B) + (a+b-c)A - cB\varepsilon - [b(A+B) + (a+b-c)B]\, q^2/4\}}{A^2 + 1/4\, q^2[2(A+B)^2(\varepsilon+1)^{-2}\cot^2\vartheta + B^2]} \tag{6.4}$$

For $\vartheta = \pi/4$, $\epsilon = M_n$ we have $P_\perp \approx 10^{-3}$.

The longitudinal polarization of the recoil protons is given by

$$P_\parallel = -\frac{g}{\sqrt{2}e^2}\frac{8\cot^2\vartheta\cos\vartheta}{(q^2+2)(\varepsilon+1)^2} \times \frac{(a+b)(A+B)\{1/2 q^2[r(2\varepsilon+1) - 1/2 q^2] - 2\varepsilon\} + c(A+B)\{-r[\varepsilon(2\varepsilon+1) - \varepsilon q^2 + q^4/4] + \varepsilon(2\varepsilon - q^2/2)\}}{A^2 + 1/4\, q^2[2(A+B)^2(\varepsilon+1)^{-2}\cot^2\vartheta + B^2]}; \tag{6.5}$$

For $\vartheta = 0$, $\epsilon \approx M_n$ we have $P_\parallel \approx 10^{-3}$.

We take occasion to express our gratitude to A. M. Brodskii, G. M. Gandel'man, B. L. Ioffe, L. B. Okun', and K. A. Ter-Martirosyan for helpful discussions.

*The signs of the interactions with proton and neutron are opposite; the effect should exist in hydrogen and not in deuterium.

[1] R. Feynman and M. Gell-Mann, Phys. Rev. **109**, 193 (1958).

[2] E. C. G. Sudarshan and R. E. Marshak, Phys. Rev. **109**, 1860 (1958).

[3] G. M. Gandel'man and Ya. B. Zel'dovich, Doklady Akad. Nauk SSSR **105**, 445 (1955).

[4] Berestetskiĭ, Krokhin, Khlebnikov, JETP **30**, 788 (1956), Soviet Phys. JETP **3**, 761 (1956).

[5] Ya. B. Zel'dovich, JETP **33**, 1531 (1957), Soviet Phys. JETP **6**, 1184 (1958).

[6] M. Bander and G. Feinberg, Preprint, Columbia (1959).

[7] A. M. Brodskiĭ, JETP **39**, 322 (1960), Soviet Phys. JETP **12**, 229 (1961); A. M. Brodski and D. Ivanenko, Nuovo cimento **16**, 556 (1960).

[8] A. I. Akhiezer and V. B. Berestetskiĭ, Квантовая электродинамика (Quantum Electrodynamics), 2nd ed., Moscow, 1959.

[9] Ya. B. Zel'dovich, JETP **36**, 964 (1959), Soviet Phys. JETP **9**, 682 (1959).

[10] Ya. A. Smorodinskiĭ, Usp. Fiz. Nauk **68**, 653 (1959), Soviet Phys.-Uspekhi **2**, 557 (1960).

[11] Akhiezer, Rozentsveĭg, and Shmushkevich, JETP **33**, 765 (1957), Soviet Phys. JETP **6**, 588 (1958).

[12] R. Hofstadter, Revs. Modern Phys. **28**, 214 (1956).

[13] G. Feinberg, Phys. Rev. **112**, 1637 (1958).

[14] E. E. Salpeter, Phys. Rev. **112**, 1642 (1958).

[15] R. M. Sternheimer, Phys. Rev. **113**, 828 (1959).

[16] H. A. Bethe and E. E. Salpeter, Quantum Mechanics of One- and Two-Electron Atoms, Springer Verlag, 1957.

[17] É. M. Lipmanov, JETP **37**, 1054 (1959), Soviet Phys. JETP **10**, 750 (1960).

[18] B. Pontekorvo, JETP **37**, 1751 (1959), Soviet Phys. JETP **10**, 1236 (1960).

[19] S. B. Treiman, Nuovo cimento **15**, 916 (1959).

[20] M. L. Goldberger and S. B. Treiman, Phys. Rev. **111**, 354 (1959).

[21] T. D. Lee and C. N. Yang, Phys. Rev. Letters **4**, 307 (1960).

Translated by W. H. Furry
206

SPIN-LATTICE RELAXATION OF LOCAL ELECTRON CENTERS IN NON-METALLIC CRYSTALS

M. F. DEĬGEN and V. Ya. ZEVIN

Institute of Physics of the Academy of Sciences of the Ukrainian S.S.R. and Brest Pedagogical Institute

Submitted to JETP editor April 29, 1960

J. Exptl. Theoret. Phys. (U.S.S.R.) 39, 1126-1137 (October, 1960)

A theory is developed for spin-lattice relaxation of local electron centers in non-metallic crystals in strong magnetic fields. Hyperfine contact interaction between the localized electron and the nuclei on the lattice is considered as the relaxation mechanism. The general theory is developed in greater detail for crystals in which the wave function of the localized electron may be written in the atomic-orbital approximation. As an example, the F center in a KCl-type crystal is discussed. A numerical calculation carried out for a KCl crystal yields a paramagnetic relaxation time of the order of several minutes at $T = 4°K$ and $H \approx 3000$ oersteds.

1. INTRODUCTION

It was considered in the fundamental paper of Waller[1] that spin-lattice relaxation in strong magnetic fields is due to the change in the interatomic distances resulting from the thermal lattice vibrations. These vibrations modulate the dipole-dipole interaction of the magnetic moments located at the lattice points. Thus, processes of reorientation of the magnetic moment of a particle become possible, being accompanied by a simultaneous change in the occupation numbers of the lattice oscillators. At sufficiently low temperatures, the direct process plays the fundamental role; here the change in orientation of the spin in the external magnetic field is accompanied by the emission (or absorption) of a single phonon of frequency $\nu = g\mu H/h$. Here, g is the Landé factor, μ is the magnetic moment, and H is the intensity of the external magnetic field. At high temperatures, the fundamental role is played by Raman scattering of phonons. In this process, upon reorientation of the magnetic moment, the number of phonons of frequency ν_1 is increased (or decreased) by unity, while the number of phonons of frequency ν_2 is correspondingly decreased (or increased) by unity. Then we must have: $\nu_1 - \nu_2 = \pm g\mu H/h$. At a sufficiently high temperature, the Raman scattering may play a more essential role than the direct effect.

However, while the mechanism discussed by Waller reveals many characteristic features of spin-lattice relaxation, it is often not effective (see, e.g., reference 2). This refers, in particular, to the paramagnetic relaxation of local electron centers (LEC) in non-metallic crystals. The concentrations of the LEC ordinarily have values such that the dipole-dipole interaction between the spins of the localized electrons are small in comparison with the hyperfine interaction of the electron with the magnetic moments of the nearest nuclei.

In turn, the hyperfine interaction of the electron with the magnetic moment of the nucleus may be written as the sum of the Fermi (contact) and dipole-dipole interactions. Experiments on paramagnetic and double spin resonance[3] have shown that in many LEC (e.g., F centers), the contact interaction is considerably greater than the dipole interaction. For these same LEC, it is reasonable to consider the dipole-dipole interaction of the nuclei with the electrons to be the cause of the relaxation process. Nevertheless, we may not apply Waller's results[1] directly, since he assumes that the magnetic moments are fixed at the lattice points. This would mean, in essence, that the wave function of the localized electron must be a δ function.

We shall discuss below the spin-lattice relaxation caused by the change in the contact-interaction energy of the spins of the localized electron and the nuclei due to the thermal lattice vibrations. Such a relaxation mechanism always results in the so-called relaxation time τ_X.[4] This relaxation time corresponds to a process in which a reorientation of the nuclear spin takes place simultaneously, compensating for the change in the angular momentum of the electron. There are other mech-

anisms of relaxation which bring about the reorientation of the electron spin without a corresponding reorientation of the spins of those nuclei which fundamentally give rise to the hyperfine structure of the paramagnetic absorption lines of the LEC (these mechanisms correspond to the relaxation time τ_S). Such a classification of the relaxation mechanisms, and correspondingly, such a consideration of two relaxation times, τ_X and τ_S, is reasonable in relation to experiments on the orientation of the nuclei in non-metals (e.g., the Overhauser effect).[4]

Among other mechanisms, Pines, Bardeen, and Slichter[4] have studied the paramagnetic relaxation of donor atoms in silicon, taking place by means of the contact hyperfine interaction of the spins of the localized electron and the donor nucleus. The treatment of this relaxation mechanism in reference 4 is not completely correct from the theoretical standpoint.

First, it is dubious to apply the theory of the deformation potential[5] to such a singular function as the operator for the contact hyperfine interaction (the Dirac δ function). Second, the calculation of the value of the relaxation time by use of the wave function from the effective-mass method is also incorrect, as the authors themselves note, since the effective-mass method is invalid in the vicinity of the donor. Finally, the application of the deformation-potential theory seems somewhat illusory, since the authors introduce in the second stage of the solution the operator of the hyperfine interaction, by means of which the spin functions of the lower and upper states are "mixed." The latter operation is necessary since otherwise the paramagnetic relaxation time turns out to be zero.

It seems possible to obtain the qualitative results of Pines, Bardeen, and Slichter[4] for this relaxation mechanism without resorting to the theory of the deformation potential. However, we shall make use below of another method of calculating the time τ_X, rejecting the macroscopic approach.

In the adiabatic approximation (the instantaneous positions of the nuclei being fixed) in a strong magnetic field, the wave function of the LEC may be written as follows:

$$\Psi = \psi(\mathbf{r}, q)\,\chi \prod_{n_{\varkappa\alpha}} \Phi_{n_{\varkappa\alpha}}(q_{\varkappa\alpha} - q^0_{\varkappa\alpha}), \tag{1.1}$$

where $\psi(\mathbf{r}, q)$ is the wave function of the subsystem of electrons, and the product $\Pi\Phi$ is the wave function of the subsystem of nuclei, $n_{\kappa\alpha}$ are the occupation numbers of the oxcillators, κ is the wave vector of the phonon, α is the number denoting the branch of oscillations, the $q_{\kappa\alpha}$ are the normal coordinates of the subsystem of nuclei, and the $q^0_{\kappa\alpha}$ are the equilibrium values of the normal coordinates, as determined from the condition of minimum potential energy of the nuclear subsystem (see, e.g., reference 6), and χ is the spin wave function. In a strong magnetic field, the latter is the product of the spin functions of the electron and of the nuclei surrounding the center of localization, i.e.,

$$\chi = \chi_{1/2}(M_S) \prod_k \chi_{I_k}(M_k). \tag{1.2}$$

In Eq. (1.2) M_S and M_k are the projections of the electron spin and that of the k-th nuclus on the direction of the field $\mathbf{H}$. The quantity I_k is the spin of the k-th nucleus.

The wave function of the electronic subsystem in the micro-approximation* can be written, for example, by making use of the atomic-orbital method.[7] In this case

$$\psi(\mathbf{r}, q) = \sum_{m=1}^{r} A_m \psi_m(\mathbf{r} - \mathbf{R}_m), \tag{1.3}$$

where ψ_m are the "orbital" functions, $\mathbf{R}_m$ is the radius vector of the mth nucleus, displaced from its equilibrium position. We shall assume below that $\mathbf{R}_m = \mathbf{R}^0_m + \mathbf{u}_m$, where $\mathbf{R}^0_m$ is the equilibrium radius vector of the nucleus, and $\mathbf{u}_m$ is the displacement vector of the nucleus from its equilibrium position. The values of the superposition coefficients A_m, of course, do not agree with their equilibrium values, and are functions of the displacements of the nuclei.

Such a way of expressing the wave function of the electronic subsystem is appropriate in those crystals for which the strong-binding approximation of the "extra" electron with the ions (or atoms) is valid. An example of such crystals is that of the alkali halide crystals and many other ionic crystals.

The expression of the wave function of the subsystem of electrons in the form (1.3) is also justified by the fact that the Hamiltonian of the contact hyperfine interaction of the electron with the kth nucleus has the form

$$\mathcal{H}_S = \tfrac{8}{3}\pi(\mu\mu_k/SI_k)\,\hat{\mathbf{I}}_k\hat{\mathbf{S}}\delta(\mathbf{r} - \mathbf{R}_k), \tag{1.4}$$

where μ, μ_k, S, and I_k are, respectively, the magnetic moments and the spins of the electron and the k-th nucleus, and δ is the Dirac function.

We see from Eq. (1.4) that the slope of the wave function is quite marked in the vicinity of the k-th nucleus. Function (1.3) is a good description of

*The authors wish to thank L. V. Keldysh for a discussion of this problem.

the behavior of the electron in the vicinity of the k-th nucleus.

In numerous papers concerned with the properties of the LEC, successful use has been made of the macroscopic approximation and the adiabatic perturbation theory.[8] The calculations have usually been limited to the zero-order approximation of the adiabatic method, in which the wave function has the form

$$\Psi = \psi(\mathbf{r}, q_{\varkappa}^{0}) \prod_{n_{\varkappa\alpha}} \Phi_{n_{\varkappa\alpha}}(q_{\varkappa\alpha} - q_{\varkappa\alpha}^{0}). \tag{1.5}$$

The wave function of the subsystem of electrons in Eq. (1.5) does not give a detailed description of the behavior of the electron in the vicinity of the nuclei. Hence, it is not suitable to use such a function in the calculation of the paramagnetic relaxation time. In this case, the paramagnetic relaxation time turns out to be $\sim \mathrm{grad}_{\mathbf{u}_k} |\psi(\mathbf{R}_k)|^2)_{\mathbf{u}=0}^{-2}$, independently of the intensity of the static magnetic field.

2. THE PROBABILITY OF REORIENTATION OF THE SPIN OF THE LOCALIZED ELECTRON IN A ONE-PHONON PROCESS

We shall write the Hamiltonian of the contact magnetic hyperfine interaction of the spin of the localized electron with the surrounding nuclei in the following form:

$$\hat{\mathcal{H}}_S = \sum_{l=1}^{r} a_l \hat{\mathbf{S}}\hat{\mathbf{I}}_l \, \delta(\mathbf{r} - \mathbf{R}_l), \qquad a_l = \frac{8\pi}{3} \frac{\mu\mu_l}{SI_l}, \tag{2.1}$$

summing over the nearest neighboring nuclei.

The quantum numbers describing the spin system in a strong magnetic field are the projections of the electron spin M_S and the nuclear spins M_k on the direction of the external magnetic field $\mathbf{H}$. We shall denote the state of the spin system having $M_S = +1/2$ and the given set of numbers M_k by the symbol +, and the state having $M_S = -1/2$ and the same set of M_k by the symbol −. We shall denote the probability of transition from the + state to the − state by P_{+-}.

As follows from the general formulas for the transition probability in a continuous spectrum,[9,2] the value of P_{+-} is given by the following expression:

$$P_{+-} = \frac{4\pi^2}{h^2} \sum_{\alpha} \rho_{\nu\alpha} \langle | \langle -;\ n_{\nu\alpha} + 1 | \hat{\mathcal{H}}_{S1} | +;\ n_{\nu\alpha} \rangle |^2 \rangle_{\mathrm{av}}. \tag{2.2}$$

Here $\rho_{\nu\alpha}$ is the density of frequencies of lattice vibrations, $\nu = g\mu H/h$, and $\langle \rangle_{\mathrm{av}}$ indicates the averaging of the square of the modulus of the matrix element over the directions of propagation and polarization of the phonons, and over their occupation numbers $n_{\nu\alpha}$.

For values of the field H such as are used in paramagnetic relaxation and resonance experiments, the frequencies $\nu = g\mu H/h$ do not fall within the optical branch of the lattice vibrations. Thus, $\rho_{\nu\alpha}$ is the density of frequencies of the acoustic branch, and may be written in the form

$$\rho_{\nu\alpha} = 4\pi L^3 \nu^2 v_{\alpha}^{-3} G_{\alpha}, \tag{2.3}$$

$G_\alpha = 1$ or 2, respectively, for longitudinal and transverse waves, L^3 is the volume of the unit cell of the crystal, and v_α is the velocity of sound.

In Eq. (2.2), the matrix element of the operator $\hat{\mathcal{H}}_{S_1}$ may be calculated from the spin and oscillator functions of the system. This operator is associated with operator (2.1), averaged over the wave functions of the electronic subsystem:

$$\hat{\mathcal{H}}_S = \int \psi^* \hat{\mathcal{H}}_S \psi \, d\mathbf{r}. \tag{2.4}$$

The operator (2.4) depends in a complex manner on the nuclear coordinates $\mathbf{R}_l$, or in other words on the small quantities $\mathbf{u}_l$. The subscript 1 in $\hat{\mathcal{H}}_S$ denotes that only the terms linear with respect to the displacements of the nuclei from the equilibrium positions are retained in the operator (2.4).

Substituting expression (2.1) in Eq. (2.4), we obtain

$$\hat{\mathcal{H}}_S = \sum_{l=1}^{r} a_l \hat{\mathbf{S}}\hat{\mathbf{I}}_l \, |\psi(\mathbf{R}_l)|^2. \tag{2.5}$$

This operator takes the following form for the wave function (1.3):

$$\hat{\mathcal{H}}_S = \sum_{l=1}^{r} a_l \hat{\mathbf{S}}\hat{\mathbf{I}}_l \sum_{m,n} A_m^* A_n \psi_{lm}^* \psi_{ln} \tag{2.5a}$$

Here and below, for brevity ψ_{l_n} will denote $\psi_n(\mathbf{R}_{l_n})$, and hence, ψ_{ll} will be equal to the value of ψ_l at the origin, $\psi_{ll} = \psi_l(0)$.

We may derive a simple expression for $\hat{\mathcal{H}}_{S_1}$ by taking into account the fact that ψ_{l_n} depends on the difference of the nuclear displacement vectors $\mathbf{u}_l - \mathbf{u}_n = \mathbf{u}_{l_n}$. It turns out (see Sec. 3) that the coefficients A_m depend on the differences of the vectors of the displacements of the nuclei from their equilibrium positions:

$$\mathbf{u}_{ij} = \mathbf{u}_i - \mathbf{u}_j \quad (i, j = 1, 2, \ldots, r).$$

The number of such vector differences is equal to $r(r-1)/2$ (taking into account only values $i > j$). Not all of these differences will be independent (the number of independent vector differences is $r - 1$). However, if we limit ourselves to the linear terms, the operator H_S may be expanded in a series over all the $\mathbf{u}_{ij}$ $(i > j)$.

Then we have

$$|\psi(\mathbf{R}_l)|^2 = |\psi(\mathbf{R}_l^0)|^2 + \sum_{i>j} (\mathrm{grad}_{ij}|\psi(\mathbf{R}_l)|^2)_0\, \mathbf{u}_{ij} + \ldots;$$

$$\mathrm{grad}_{ij} \equiv \mathrm{grad}_{\mathbf{u}_{ij}}. \qquad (2.6)$$

Substituting (2.6) into Eq. (2.5), we obtain

$$\hat{\mathcal{H}}_{S1} = 2\sum_{l=1}^{r} a_l \hat{\mathbf{S}}\hat{\mathbf{I}}_l \,\mathrm{Re}\Big[\psi^*(\mathbf{R}_l^0)\sum_{i>j}\mathbf{u}_{ij}(\mathrm{grad}_{ij}\psi(\mathbf{R}_l))_0\Big]. \qquad (2.7)$$

For the orbital wave function (1.3)

$$(\mathrm{grad}_{ij}\psi(\mathbf{R}_l))_0 = \sum_{m=1}^{r} (\mathrm{grad}_{ij} A_m\, \psi_{lm})_0$$

$$= \sum_{m=1}^{r} [A_m^0 (\mathrm{grad}_{ij}\psi_{lm})_0 + \psi_{lm}^0 (\mathrm{grad}_{ij} A_m)_0]. \qquad (2.8)$$

Thus, the relaxation process in this case is due to two causes: the change in the superposition coefficients A_m of the orbital wave functions and the change in ψ_{lm}.

We shall introduce the normal coordinates $q_{\kappa\alpha}$ as follows:

$$\mathbf{u}_i = \sqrt{2/L^3}\sum_{\kappa\alpha} q_{\kappa\alpha}\mathbf{e}_{\kappa\alpha} a_{\kappa\alpha} \sin\Big(\boldsymbol{\varkappa}_\alpha \mathbf{R}_i^0 + \frac{\pi}{4}\Big). \qquad (2.9)$$

Here, the wave vector $\boldsymbol{\kappa}_\alpha = \kappa_\alpha \boldsymbol{\lambda}_{\kappa\alpha}$, $\mathbf{e}_{\kappa\alpha}$ is the unit polarization vector, $a_\kappa = \sqrt{\hbar/4\pi^2\nu d}$, and d is the density of the crystal.

In order to calculate the probability (2.2), taking Eqs. (2.9) and (2.7) into account, use was made of the fact that only resonance phonons with a wave number $\kappa_\alpha = 2\pi\nu/v_\alpha$ contribute to (2.2). Hence, in the expression for $\mathbf{u}_{ij}$ we have

$$\sin(\boldsymbol{\varkappa}_\alpha \mathbf{R}_i^0 + \pi/4) - \sin(\boldsymbol{\varkappa}_\alpha \mathbf{R}_j^0 + \pi/4) \approx \boldsymbol{\varkappa}_\alpha R_{ij}^0 (\boldsymbol{\lambda}_{\kappa\alpha}\mathbf{n}_{ij})/\sqrt{2}.$$

Here, $\mathbf{n}_{ij}$ is the unit vector of $\mathbf{R}_{ij}^0$. Besides, in Eq. (2.2), the matrix elements for the spin and the oscillator wave functions are calculated independently. The oscillator matrix element is equal to

$$\langle n_\nu + 1 | q_{\kappa\alpha} a_{\kappa\alpha} | n_\nu \rangle = [\hbar(n_\nu + 1)/8\pi^2\nu d]^{1/2}. \qquad (2.10)$$

The spin matrix element differs from zero if

$$M_j' = M_j, \quad j \neq k; \qquad M_k' = M_k + 1. \qquad (2.11)$$

In other words, the change in the orientation of the electron spin is accompanied by a change in the orientation of the spin of only one nucleus, for example, the kth. Here, $\Delta(M_S + M_k) = 0$, and in the summation in Eq. (2.7) only the kth term remains, containing the factor

$$\langle - | \hat{\mathbf{S}}\hat{\mathbf{I}}_k | + \rangle = \tfrac{1}{2}[(I_k + M_k + 1)(I_k - M_k)]^{1/2}. \qquad (2.12)$$

Taking all of this into account, we have

$$P_{+-}^{(k)} = \frac{8\pi^3}{d}(\mathbf{v}_1\mathbf{v})^2 \hbar\nu(\bar{n}_\nu + 1)(I_k + M_k + 1)(I_k - M_k)\sum_\alpha \frac{G_\alpha}{v_\alpha^2}$$
$$\times \Big\langle \Big\{ \mathrm{Re}\,\psi^*(\mathbf{R}_k^0)\sum_{i>j} R_{ij}^0 (\boldsymbol{\lambda}_{\kappa\alpha}\mathbf{n}_{ij})$$
$$\times (\mathbf{e}_{\kappa\alpha}\,\mathrm{grad}_{ij}\psi(\mathbf{R}_k))_0 |\psi(\mathbf{R}_k^0)|^{-2}\Big\}^2 \Big\rangle_{\mathrm{av}}. \qquad (2.13)$$

In Eq. (2.13) we assume the validity of the Planck distribution

$$\bar{n}_\nu + 1 = (1 - e^{-h\nu/kT})^{-1}.$$

The factor within the curly brackets is a dimensionless quantity; the averaging is carried out over the propagation and polarization directions of the phonons,

$$h\nu_1 = a_k |\psi(\mathbf{R}_k^0)|^2 = \frac{8\pi}{3}\frac{\mu\mu_k}{SI_k}|\psi(\mathbf{R}_k^0)|^2. \qquad (2.14)$$

The maximum value of $P_{+-}^{(k)}$, determines the minimum relaxation time. Hence, in estimating (2.13) we must substitute in the maximum value of the spin factor [for half-integral nuclear spins, this is $(I_k + \frac{1}{2})^2$, while for integral spins, it is $I_k(I_k + 1)$].

Without finding a more accurate value for the expression in curly brackets, we may see that

$$P_{+-} \sim H^2 T, \quad kT \gg g\mu H; \qquad P_{+-} \sim H^3, \quad kT \ll g\mu H. \qquad (2.15)$$

For intermediate values of the temperature T (for fields $\approx$ 3000 oe, $T \lesssim 1°K$), we may expect a more complex dependence on the magnetic field, given by the factor

$$\nu^3/(1 - e^{-h\nu/kT}), \quad \nu = g\mu H/h.$$

Equation (2.13) is a general expression for the probability of spin reorientation in a one-phonon process. In deriving P_{+-}, we have not assumed a concrete model of the center nor a definite approximation in the choice of the wave function of the subsystem of electrons. We have relied only on the fact that the value of the wave function of the electronic subsystem at the point of the instantaneous position of the lattice nucleus depends only on the difference of the nuclear displacements $\mathbf{u}_{ij}$.

If we assume that $h\nu \ll kT$, the spin-lattice relaxation time may be written as follows:

$$\tau = 1/2P_{+-} \qquad (2.16)$$

At a temperature at which we can still use Eq. (2.2) to calculate the relaxation time, we can determine the upper limit by calculating the probability of Raman scattering of phonons accompanied by reorientation of the electron spin.

We may determine a value of τ by assigning a definite model for the LEC, and adopting an approximation permitting a choice of the wave function of the LEC. If we select the wave function of the electronic subsystem in the form (1.3), we must, as follows from Eq. (2.8), determine $(\mathrm{grad}_{ij} A_m)_{\mathbf{u}=0}$.

In the next section we shall show that we need not solve the complex problem of determining A_m

with the nuclei displaced in order to determine these derivatives. It is sufficient to solve the corresponding problem for the equilibrium positions of the nuclei.

3. DETERMINATION OF THE PARAMETERS $(\partial A_m/\partial u_{ijp})_0$

We shall represent the wave function of the electronic subsystem in the form (1.3). Making use of the adiabatic method, we find the coefficients A_m for any arbitrary configuration of the nuclei. We shall consider the A_m to be variational parameters, and shall select them by means of the condition of minimum value of the function

$$J = \int \psi^* (\hat{\mathcal{H}} - \lambda)\, \psi\, d\mathbf{r}, \tag{3.1}$$

where $\hat{\mathcal{H}}$ is the Hamiltonian of the localized electron (in the absence of the magnetic field **H**), and λ is a Lagrangian multiplier.

Substituting (1.3) into (3.1), we have

$$J = \sum_{mm'} (F_{mm'} - \lambda f_{mm'})\, A_m^* A_{m'} \tag{3.2a}$$

where

$$\sum_{mm'} f_{mm'} A_m^* A_{m'} = 1, \tag{3.2b}$$

in which

$$f_{mm'} = \int \psi_m^* \psi_{m'}\, d\mathbf{r}, \quad F_{mm'} = \int \psi_m^* \hat{\mathcal{H}} \psi_{m'}\, d\mathbf{r}. \tag{3.3}$$

We introduce the symbols

$$c_{mm'} = F_{mm'} - \lambda f_{mm'} \qquad (c_{mm'} = c_{m'm}) \tag{3.4}$$

and derive in the usual manner the following system of linear homogeneous equations

$$\sum_{m=1}^{r} c_{mm'} A_m = 0, \quad m' = 1.2, \ldots, r. \tag{3.5}$$

The characteristic equation for λ has the well-known form

$$\| c_{mm'} \| = 0. \tag{3.6}$$

In finding the roots of Eq. (3.6), we must select that root λ_{min} for which the solution of the system (3.5) gives the lowest value of the energy of the LEC, with the additional condition of normalization (3.2b).

We shall assume that A_m and λ in (3.5) correspond to such a solution. Then the system (3.5) becomes an identity. We shall differentiate it with respect to the u_{ijp} ($p = x, y, z$) and set all u_i equal to zero. We obtain as a result

$$\sum_m c^0_{mm'} A^m_{ijp} = -\sum_m A^0_m c^{mm'}_{ijp}. \tag{3.7}$$

Here and below we shall make use of the symbol

$$(\partial f_{mm'}/\partial u_{ijp})_0 = f^{mm'}_{ijp}.$$

The $c^0_{mm'}$ are the coefficients in (3.4) when all of the ions are located at the points of the undeformed lattice, the A^0_m are the superposition coefficients of (1.3) for the equilibrium positions of the nuclei. Here λ_{min} goes over into the Lagrangian multiplier λ_0. All quantities with the subscript zero will correspond hereinafter to the equilibrium positions of the nuclei.

The determinant of the system (3.7) is zero; however, the system (3.7) is consistent. It may be shown that any r-th order determinant obtained from the determinant of the system by replacement of the i-th column by the right-hand side of (3.7) is equal to zero. Hence, in order to determine the A^m_{ijp}, we require one more equation independent of (3.7). We can derive this equation by differentiating the normalization condition (3.2b) with respect to u_{ijp}. As a result, we obtain the following system of equations for determining the A^m_{ijp}.

$$\sum_{m=1}^{r} c^0_{m'm} A^m_{ijp} = -\sum_{m=1}^{r} A^0_m c^{m'm}_{ijp}, \qquad m' = 1, 2, \ldots, r-1. \tag{3.8a}$$

$$\sum_{m=1}^{r} \Big(\sum_{m'=1}^{r} A^0_{m'} f^0_{mm'} \Big) A^m_{ijp} = -\tfrac{1}{2} \sum_{m,m'} A^0_m A^0_{m'} f^{mm'}_{ijp}. \tag{3.8b}$$

Since $f_{mm'} = f_{mm'}(R_{mm'})$, the right-hand side of (3.8b) may be written in the form

$$-A^0_i A^0_j \frac{df_{ij}(R^0_{ij})}{dR^0_{ij}}\, n_{ijp}.$$

As follows from (3.4),

$$c^{mm'}_{ijp} = F^{mm'}_{ijp} - \lambda_0 f^{mm'}_{ijp} - f^0_{mm'} \lambda^{min}_{ijp}.$$

We must know $F_{mm'}$ in order to calculate the values of the $F^{mm'}_{ijp}$. The quantities $F_{mm'}$ contain as terms two- and three-center integrals; the $F_{mm'}$ are functions of the differences u_{ijp}. The derivatives of the overlap integrals are calculated as was indicated above. Hence, we must find the derivatives $(\partial\lambda_{min}/\partial u_{ijp})_0$, which may be calculated as follows.

The quantity λ_{min} is a root of the characteristic equation (3.6). We assume that this root has been found. If we substitute it in (3.6), the characteristic equation becomes an identity. By differentiating this identity with respect to u_{ijp}, and setting $u_i = 0$ in the result obtained, we obtain an equation linear in the desired derivative. We shall not give this equation here because of its unwieldiness.

Naturally, the solution of Eqs. (3.8) and the calculation of the derivatives on the right-hand side of the system are greatly simplified when the electron center has high symmetry, or in the case in which we may limit the treatment to a small num-

ber of ions r. The latter case occurs, for example, in the case of the F center in alkali halide crystals. We shall not present the solution of this problem, but shall give only the final results.

It is convenient to introduce here the following symbols. The index $-m$ denotes an ion located on the same [100]-type axis as the ion m. The index $\perp m$ denotes ions located on [100]-type axes perpendicular to the axis on which the m-th ion is located. We shall denote $F^0_{mm'}$, $f^0_{mm'}$, and $c^0_{mm'}$ by F, f, c; F_1, f_1, c_1; F_2, f_2, c_2, respectively, for the cases $m' = m$, $m' = -m$, and $m' = \perp m$.

We note that Eq. (3.8b) is greatly simplified in the case of the F center. Since here all of the A^0_m are identical, we obtain

$$\sum_{m=1}^{r} A^m_{ijp} = -6A_0^3 n_{ijp} df_{ij}(R^0_{ij})/dR^0_{ij}. \qquad (3.9)$$

By means of the procedure indicated above, we have found for an F center in a KCl-type structure, for the first coordination sphere:

$$A^m_{ijp} = -A_0^3 n_{ijp} \frac{df_{ij}(R^0_{ij})}{dR^0_{ij}} + \frac{(5c+c_1)\,b_m^{(ijp)} - (5c_1+c)\,b_{-m}^{(ijp)}}{6(c^2-c_1^2)}; \qquad (3.10)$$

$$b_m^{(ijp)} = A_0 n_{ijp}(\delta_{mi}+\delta_{mj}-\tfrac{1}{3})\left\{\lambda_0 \frac{df_{ij}(R^0_{ij})}{dR^0_{ij}} - \frac{d}{dR^0_{ij}}[T(R^0_{ij}) + 2V_1(R^0_{ij}) + V_2(R^0_{ij})]\right\} + A_0 \frac{\partial}{\partial R^0_{ijp}}\left[(\tfrac{1}{3}-\delta_{mi}-\delta_{mj})V_3' + (\tfrac{1}{3}-\delta_{mi})V_3'' + (\tfrac{1}{3}-\delta_{mj})V_3''' - (1-\delta_{mi}-\delta_{mj})(V_{mij}+V_{mji})\right]; \qquad (3.11)$$

$$A_0 = [6(1+f_1+4f_2)]^{-1/2}; \qquad \lambda_0 = \frac{F+F_1+4F_2}{1+f_1+4f_2}. \qquad (3.12)$$

In the calculation of the coefficients of (3.11), the Hamiltonian of the F center was written in the form

$$\hat{\mathcal{H}}_0 = -\frac{\hbar^2}{2m}\Delta_r + \sum_{k=1}^{6} V_k(\mathbf{r}-\mathbf{R}^0_k), \qquad (3.13)$$

where V_k is the potential energy of the localized electron in the field of the k-th ion;

$$T(R^0_{ij}) = \int \psi_i(\mathbf{r}-\mathbf{R}^0_i)\left(-\frac{\hbar^2}{2m}\Delta_r\right)\psi_j(\mathbf{r}-\mathbf{R}^0_j)\,d\mathbf{r},$$

$$V_1(R^0_{ij}) = \int \psi_i(\mathbf{r}-\mathbf{R}^0_i)\,V_i(\mathbf{r}-\mathbf{R}^0_i)\,\psi_j(\mathbf{r}-\mathbf{R}^0_j)\,d\mathbf{r},$$

$$V_2(R^0_{ij}) = \int |\psi_i(\mathbf{r}-\mathbf{R}^0_i)|^2 V_j(\mathbf{r}-\mathbf{R}^0_j)\,d\mathbf{r},$$

$$V_{klm} = \int \psi_k(\mathbf{r}-\mathbf{R}^0_k)\,\psi_l(\mathbf{r}-\mathbf{R}^0_l)\,V_m(\mathbf{r}-\mathbf{R}^0_m)\,d\mathbf{r},$$

$k \neq l \neq m \neq k$,

$$V_3' = \sum_{\substack{k=1\\k\neq i,j}}^{4} V_{ijk}, \qquad V_3'' = \sum_{\substack{k=1\\k\neq i,l}}^{4} V_{kij}, \qquad V_3''' = \sum_{\substack{k=1\\k\neq i,j}}^{4} V_{kji}. \qquad (3.14)$$

In estimating the three-center integrals and their derivatives, the fact was taken into account that at the actual distances (6 — 12 atomic units), an integral of the type V_{klm} is approximately equal to f_{kl}/R_q, where R_q is the distance from the lattice point m to the midpoint of the line segment joining lattice points k and l. Obviously, q may take on three values: $R_I = a^0$, $R_{II} = (3/2)^{1/2}a^0$, and $R_{III} = (5/2)^{1/2}a^0$, where a^0 is the lattice parameter. Estimates show that the error in such an approximation is $\sim 15\%$.

From the calculations, the contribution $b_m^{(ijp)'}$ of the three-center integrals in Eq. (3.11) is the following:

$$b_m^{(ijp)'} = (A_0/R^0_{ij})\,n_{ijp}\{-4(\tfrac{1}{3}-\delta_{mi} - \delta_{mj})(R^0_{ij}/R_I)\,df(R^0_{ij})/dR^0_{ij} + [1-3(\delta_{mi}+\delta_{mj})]\,2f_2/5R_{III}\} \quad (i=-j); \qquad (3.15a)$$

$$b_m^{(ijp)'} \approx \left(\frac{A_0}{R^0_{ij}}\right) n_{ijp}\left\{-2(\tfrac{1}{3}-\delta_{mi}-\delta_{mj})(1/R_{II} + 1/R_{III})\,R^0_{ij}\frac{df(R^0_{ij})}{dR^0_{ij}} + \tfrac{1}{3}\sqrt{2}\,(f_1/2R_I + f_2/3R_{II} + f_2/5R_{III}) + (\tfrac{2}{3}-\delta_{mi}-\delta_{mj})(2f_2/3R_{II}+f_2/5R_{III})\right\}$$

$(i = \perp j)$. (3.15b)

The first formula takes into account the contribution of all of the existing derivatives of V_{klm}, while the second formula is approximate, since it omits certain small terms which make the value of $b_m^{(ijp)'}$ $(i = \perp j)$, depend weakly on which index m takes on. Within the accuracy of our estimate of V_{klm}, it is not expedient to take these small terms into account.

Formulas (3.10) and (3.15) complete the solution of the assigned problem for the F center in an alkali halide crystal, the first coordination sphere being taken into account.

We see from (3.5) and (3.2b) that the coefficients A_m are determined by the values of $c_{mm'}$. The latter quantities, as follows from their definition, are functions of the differences $\mathbf{u}_i - \mathbf{u}_j$. This justifies the assumption made in the previous section that the coefficients A_m depend on the differences of the vectors of displacement of the nuclei from their equilibrium positions.

In concluding this section, we note that a knowledge of the quantities $(\partial A_m/\partial u_{ijp})_0$, whose method of calculation was presented above, permits us to solve a number of other problems, in which the determining factor is the interaction of the localized electron with the lattice vibrations (the form of the optical absorption and luminescence bands, radiationless transitions, etc.)

4. THE SPIN-LATTICE RELAXATION TIME OF F CENTERS IN A KCl-TYPE LATTICE

We shall write the wave function of an F center for arbitrary, but small displacements of the nuclei from their equilibrium positions in the form (1.3). At equilibrium, all of the $A_m = A_0$, A_0 being determined by the normalization condition (3.12). In the case of alkali-halide crystals, the ψ_m are s functions, to within a sufficient degree of accuracy.

We shall denote by the symbol K_α the dimensionless factor included within the curly brackets in (2.13). In order to estimate the effectiveness of a given relaxation mechanism, we first calculate the magnitude of K_α from dimensional considerations. Such an estimate gives

$$K_\alpha \approx 4 \sum_{i<j}^{15} \sum_{i'<j'}^{15} \langle L_{ij} L_{i'j'} \rangle_{\text{av}}, \qquad L_{ij} = (\mathfrak{n}_{ij} \boldsymbol{\lambda}_{\varkappa\alpha})(\mathfrak{n}_{ij} \mathbf{e}_{\varkappa\alpha}). \quad (4.1)$$

Averaging over the directions of propagation and polarization of the phonons is facilitated by the following useful relations:

$$\langle L_{ij} L_{i'j'} \rangle_{\text{av}} = \begin{cases} \frac{1}{15}(1 + 2\cos^2(\widehat{n_{ij} n_{i'j'}})) - \text{longitudinal phonons,} \\ \frac{1}{10}\left(-\frac{1}{3} + \cos^2(\widehat{n_{ij} n_{i'j'}})\right) - \text{transverse phonons.} \end{cases} \quad (4.2)$$

The mean value of the square of the cosine in (4.2) is equal, as may be shown, to $1/3$. Hence, expression (4.1) is equal to 100 for longitudinal phonons and zero for transverse phonons.

We shall carry out the numerical calculations for an F center in KCl. By using (2.16) and (2.13) for the paramagnetic relaxation time, we obtain

$$\tau_{min} = 0.845 \cdot 10^2 / T \text{ min}, \quad \tau_{max} = 4.87 \cdot 10^2 / T \text{ min}.$$

For T = 4°K, $\tau \approx (21 - 122)$ min. In Eq. (2.13), the Zeeman frequency ν = 9000 Mc/sec (H ≈ 3000 oe), ν_1 = 21.6 Mc/sec (reference 3).

$$(I_k + M_k + 1)(I_k - M_k)_{max} = 4, \qquad I_k = \tfrac{3}{2}, \qquad d = 2\ e/cm^3.$$

The two values of the time τ are obtained by using the minimum and the maximum values of the speed of sound. The two values of the speed of sound (both for longitudinal waves v_l and for transverse waves v_t) are the result of a certain arbitrariness existing in the determination of v_l and v_t in an anisotropic crystal. For KCl, v_l = $(4.47 - 3.05) \times 10^5$ cm/sec, and v_t = $(1.76 - 2.90) \times 10^5$ cm/sec.

We shall now calculate τ, using the formulas of the previous section. With the aid of Eqs. (3.10), (3.11), and (3.15) for K_α respectively, for the cases of longitudinal and transverse waves, we obtain

$$K_l = [D_1 + 4D_2 + \tfrac{1}{3}(C_1 + 4C_2)]^2 + \tfrac{4}{45}[3(1 - 6A_0 \psi_k(R_2)/\psi(R_k^0)) \times (E_1 + E_2) - (C_1 + C_2)]^2;$$

$$K_t = \tfrac{1}{15}[3(1 - 6A_0 \psi_k(R_2)/\psi(R_k^0))(E_1 + E_2) - (C_1 + C_2)]^2. \quad (4.3)$$

Here we have used the notation

$$C = A_0 R \frac{d\psi_k(R)}{dR} \frac{1}{\psi(R_k^0)}, \qquad D = A_0^2 R \frac{df(R)}{dR},$$

$$E_1 = \frac{2R_1}{9(c + c_1)} \left\{ \left(-\lambda_0 - \frac{4}{R_1} \right) \frac{df_1}{dR_1} + \frac{6f_2}{5R_{III}} + \frac{d}{dR_1}[T(R_1) + 2V_1(R_1) + V_2(R_1)] \right\},$$

$$E_2 = \frac{2R_2}{9(c + c_1)} \left\{ [-\lambda_0 - 2(1/R_{II} + 1/R_{III})] \frac{df_2}{dR_2} + \frac{d}{dR_2}[T(R_2) + 2V_1(R_2) + V_2(R_2)] \right\}. \quad (4.4)$$

The subscripts 1 and 2 in Eqs. (4.4) indicate, respectively, that R is equal to $2a^0$ or $\sqrt{2}\ a^0$. Only the first term of Eq. (3.15b) has been taken into account in the expression for E_2, since the contribution of the other terms is within the limits of accuracy of the calculation (we must remember that these terms only decrease τ).

A calculation of the values of C, D, and E with the aid of the wave function of the 4s state of potassium[10] and the approximation to it taken from the paper of Dykman[11] show that the contributions of C and D are not important.

By substituting (4.3) into (2.13), we obtain

$$\tau_{min} = 7.6 / T \text{ min}, \quad \tau_{max} = 87 / T \text{ min}. \quad (4.5a)$$

At T = 4°K and H = 3000 oe, we have

$$\tau_{min} = 1.9 \text{ min}, \quad \tau_{max} = 22 \text{ min}. \quad (4.5b)$$

It is stated in a paper by Feher[12] that the paramagnetic relaxation time of color centers in alkali-halide crystals is shorter that the corresponding time τ_X for donor impurities in silicon (at a temperature of 4°K, the latter ≈ 10 hours). The value of the time which we have derived in (4.5) agrees with this conclusion.

[1] I. Waller, Z. Physik **79**, 370 (1932).

[2] J. H. Van Vleck, Phys. Rev. **57**, 426 (1940).

[3] Kip, Kittel, Levy, and Portis, Phys. Rev. **91**, 1066 (1955); G. Feher, Phys. Rev. **105**, 1122 (1957).

[4] Pines, Bardeen, and Slichter, Phys. Rev. **106**, 489 (1957).

[5] W. Shockley, Electrons and Holes in Semiconductors, Van Nostrand, 1950; J. Bardeen and W. Shockley, Phys. Rev. **80**, 72 (1950).

[6] S. I. Pekar, JETP **22**, 641 (1952).

[7] T. Muto, Prog. Theoret. Phys. 4, 243 (1949); T. Inui and J. Uemura, ibid. 5, 252, 395 (1950).

[8] S. I. Pekar, Исследования по электронной теории кристаллов (Studies on the Electronic Theory of Crystals), Gostekhizdat (1951); M. F. Deĭgen, Doctoral dissertaion, Physico-Technical Institute, Academy of Sciences U.S.S.R., 1959.

[9] L. D. Landau and E. M. Lifshitz, Квантовая механика (Quantum Mechanics), Chap. 1, [Transl: Addison-Wesley 1958].

[10] D. R. Hartree and W. Hartree, Proc. Cambridge Phil. Soc. 34, 550 (1938).

[11] I. M. Dykman, Тр. ИФАН УССР (Proceedings of the Institute of Physics of the Academy of Sciences of the Ukrainian SSR) No. 5, 48 (1954).

[12] G. Feher, Phys. Rev. 114, 1219 (1959).

Translated by M. V. King
207

ON THE POSSIBILITY OF DETERMINING THE CORRELATION FUNCTION FOR A FERMI LIQUID IN METALS

M. Ya. AZBEL'

Institute for Technical Physics, Academy of Sciences, Ukrainian S.S.R.

Submitted to JETP editor April 9, 1960

J. Exptl. Theoret. Phys. (U.S.S.R.) 39, 1138-1147 (October, 1960)

We give the set of equations for the general case of the electron Fermi liquid in an electromagnetic field in a form which is more convenient than the one normally used. (The simplicity of the proposed form is conserved also for an electron gas.) We show that the liquid properties at high frequencies manifest themselves always in the same way as the presence of an electrical field normal to the metal surface. We find that the only case where the Fermi liquid effects turn out to be important is that of cyclotron resonance at very high frequencies, appreciably higher than those considered before. The Fermi liquid leads then in particular to an additional broadening of the resonance curve. We discuss the possibility of determining the correlation function in metals in this case.

1. THE POSSIBILITY OF DETERMINING LANDAU'S CORRELATION FUNCTION

LANDAU[1,2] devised in 1956 a Fermi liquid theory which was very important for understanding the properties of liquid He^3 and of the electronic properties of metals.

The basic equation in this theory was the relation between the energy of the quasi-particles and the distribution function, which was determined by the correlation function $\Phi(p, p')$ (p is the momentum of the quasi-particle). The correlation function turned thus out to be a basic characteristic of a Fermi liquid together with the "bare electron" dispersion law $\epsilon_0 = \epsilon_0(p)$ (ϵ is the energy) corresponding to the equilibrium distribution function. [$\epsilon_0(p)$ and $\Phi(p, p')$ are, of course, generally speaking independent only in the case of a non-uniform medium where there is an additional "background" which does not take into account the interaction of the quasi-particles under consideration, and which is created in a metal, for instance, by the ions.] In the homogeneous case $\Phi(p, p')$ determines $\epsilon(p)$, apart from a constant term. The connection between $\epsilon_0(p)$ and $\Phi(p, p')$ is given by the relativity principle.

The theoretical determination of $\Phi(p, p')$ for the general case of an arbitrary crystalline lattice is, apparently, an almost hopeless problem. The experimental determination of $\Phi(p, p')$ turns, however, also out to be very complicated.

Indeed, let us consider all frequency regions. When $\omega\tau \ll 1$ (τ is a time of the order of the mean free flight time of an electron in the metal) we get immediately, by writing down the transport equation and the current density for the Fermi liquid, that the difference between the Fermi liquid and the Fermi gas is small and appears only in the second approximation in $1/\omega\tau$, and that the corresponding terms depend on the collision integral and $\epsilon_0(p)$.

When $\omega\tau \gtrsim 1$, the skin depth $\delta_0 \sim c/\omega_0 \sim 10^{-5}$ cm (ω_0 is the plasma frequency) is of the same order of magnitude as or smaller than the mean free path l in the metal. The case $\delta_0 \sim l$ is clearly not a convenient one to analyze, and when $\delta_0 \ll l$ there are two possibilities.

If $\delta_0 \ll v/\omega$ (v is the electron velocity, $v/\omega \lesssim v\tau = l$) the so-called anomalous skin-effect occurs, in which only the electrons move for a long period in the skin-layer, i.e., move almost parallel to the surface ($\delta_0 \ll v/\omega \lesssim l$), are important. This leads to a steep maximum in the distribution function, which is averaged out in the "liquid" terms, and the latter give again a small effect (see, for instance, an earlier paper by the present author[3]) which depends on the collision integral, just as when $\omega\tau \lesssim 1$.

Finally, the case $v/\omega \ll \delta_0 \ll l$ corresponds to the infrared region. The "volume" effect was in that case calculated for an arbitrary dispersion law by Pitaevskiĭ.[4] The complex dielectric constant tensor ϵ_{ik} depends in an essential way on Φ, as should have been expected. This gives, however, only a few (at most six) numbers connected with Φ and $\epsilon_0(p)$ and this does not enable us, of

course, to obtain any detailed information about $\Phi(p, p')$.

The "surface" terms in the infrared region turn out to depend also in an essential way on Φ (as was shown by Gurzhi and the present author; this will be the subject of a separate paper) and give now the function $Z_{ik}(n)$ (Z_{ik} is the surface impedance tensor, and n the normal to the metal surface, which characterizes the orientation of the latter with respect to the crystallographic axes). The integral connection between Z_{ik} and Φ is, however, so complicated that it is doubtful whether it can be used effectively to find $\Phi(p, p')$ even when one knows the value of $\epsilon_0(p)$ (from other experiment which do not involve Φ). (We are here, of course, interested all the time in functions at the Fermi surface $\epsilon_0(p) = \epsilon_0$, which is the only important quantity.)

The Fermi liquid will thus always lead to small terms in the equation, except in the infrared region where it is practically impossible to determine $\Phi(p, p')$. There remains therefore for us to look for a case where a small correction in the equation leads to a large difference in the final results. This is, of course, possible only near an eigenvalue of the equation, i.e., physically near a resonance (for more details see Sec. 4) at very high frequencies, which are appreciably higher than the ones considered before.[5,6]

We must thus study cyclotron resonance, which will be shown in the present paper to be very convenient for finding the correlation function. This particular convenience is connected with the fact that at resonance the distribution function has a steep maximum only near isolated points where the electrons move almost parallel to the surface and take part in the resonance, i.e., have a mass which is nearly an extremum. Thanks to this only the values of the correlation function at these points are important, and this makes the analysis appreciably easier. To solve the equations it turns out to be more convenient to write them down in a form somewhat different from the usual one, and we shall consider this in Sec. 2.

2. FORM OF THE COMPLETE SET OF EQUATIONS

For the sake of simplicity we consider a one-dimensional case when the set of equations of our problem for a monochromatic wave is of the form (we neglect, of course, the displacement current)

$$E_\alpha''(y) = 4\pi i\omega c^{-2} j_\alpha, \tag{2.1}$$

$$j_y(y) = 0 \quad \text{or} \quad \rho' = 0 \ * \tag{2.2}$$

*The equivalence of these equations follows from the equation of continuity.

Here $\mathbf{E}$ is the electrical field strength, j the current density, and ρ' the charge density:

$$j = \frac{2e}{(2\pi\hbar)^3}\int v\, n\, dp, \quad d\mathbf{p} = dp_x dp_y dp_z;$$

$$\rho' = \frac{2e}{(2\pi\hbar)^3}\int \{n - n_0(\varepsilon_0)\}\, d\mathbf{p}, \tag{2.3}$$

$$\left(\frac{dn}{dt_1}\right)_{\text{field}} \equiv \frac{\partial n}{\partial t_1} + \frac{\partial n}{\partial r}\frac{\partial \varepsilon}{\partial p} - \frac{\partial n}{\partial p}\frac{\partial \varepsilon}{\partial r} = I\{n\}, \tag{2.4}$$

where ϵ and $\mathbf{p}$ are the energy and quasi-momentum and $v = \partial\epsilon/\partial\mathbf{p}$ the electron velocity; $I\{n\}$ is the collision integral.

In order that the set of equations be complete it is necessary to write down the connection between the difference $\delta\epsilon$ of the energy ϵ of an elementary excitation in the Fermi liquid and the energy ϵ_0 in the Fermi gas and the deviation of the distribution function n from the equilibrium one n_0 (ϵ_0)

$$n = n_0(\varepsilon_0) - ev\,\partial n_0/\partial\varepsilon.$$

According to Landau[1] this connection is given by the correlation function $\Phi(\mathbf{p}, \mathbf{p}')$

$$\varepsilon = \varepsilon_0 + \delta\varepsilon; \qquad \delta\varepsilon = -e\int \Phi(\mathbf{p}, \mathbf{p}')\frac{\partial n_0}{\partial\varepsilon_0} v(p')\, dp' \equiv e\hat{\Phi}v. \tag{2.5}$$

If we put

$$v = (1 + \hat{\Phi})^{-1} n_1, \quad \hat{\Phi}(1 + \hat{\Phi})^{-1} = \hat{G},$$

so that

$$\delta\varepsilon = \int G(\mathbf{p}, \mathbf{p}')(n - n_0(\varepsilon))\, d\mathbf{p}',$$

we get the complete set of equations for our problem

$$E_\alpha'' = 4\pi i\omega c^{-2} j_\alpha; \tag{2.6}$$

$$j_y = 0, \qquad \rho' = 0; \tag{2.7}$$

$$j = \frac{2e^2}{(2\pi\hbar)^3}\frac{eH}{c}\overline{\mathbf{v}n_1}; \quad \rho' = \frac{2e^2}{(2\pi\hbar)^3}\frac{eH}{c}\overline{(1 - \hat{G})\, n_1}; \tag{2.8}$$

$$i\omega(1 - \hat{G})\, n_1 + v_y\frac{\partial n_1}{\partial y} + \frac{\partial n_1}{\partial t} + \left(\frac{\partial n_1}{\partial t}\right)_{\text{coll}} = \mathbf{vE} = v_\beta E_\beta + v_y E_y. \tag{2.9}$$

The averages are defined by the equation

$$\bar{f} = -\frac{c}{eH}\int f\frac{\partial n_0}{\partial\varepsilon}\, dp = -\int f\frac{\partial n_0}{\partial\varepsilon}\, d\varepsilon\, dp_z\, dt. \tag{2.10}$$

We shall show that one can at once satisfy (2.7) in the general case, without making any approximations (this possibility was mentioned in an earlier paper by the present author[5]). To do this it is convenient not to use the condition $j_y = 0$, but to use the condition of electrical neutrality $\rho' = 0$ which is equivalent to it [because of (2.9)]. We put

$$n_1 = \nu_1 - \varphi = \nu_1 - \int_y^\infty E_y dy, \qquad E_y = -\varphi'(y) \tag{2.11}$$

This corresponds physically to choosing as the zeroth approximation not

$$n_0(\varepsilon - \zeta_0) = n_0(\varepsilon^{\text{tot}} - \zeta^{\text{tot}})$$

[ϵ^{tot} is the total (kinetic and potential) energy of the electron in the field; $\zeta^{\text{tot}} = \zeta_0 + e\varphi$ is the chemical potential in the field] but the quantity $n_0(\epsilon^{\text{tot}} - \zeta_0)$ which is the natural thing to do when the field changes rapidly and when the chemical potential in the field does not have time to get established.

Since $(\partial\varphi/\partial t)_{\text{coll}} = 0$, the transport equation (2.9) has the form

$$i\omega(1-\hat{G})\nu_1 + \{v_y\partial/\partial y + \partial/\partial t + (\partial/\partial t)_{\text{coll}}\}\nu_1 = v_\alpha E_\alpha + i\omega\varphi(1-\hat{G}),$$

and (2.7) enables us to determine at once the function φ (and thus also E_y)

$$\overline{(1-\hat{G})\nu_1} - \varphi\overline{(1-\hat{G})} = 0, \qquad \varphi = \overline{(1-\hat{G})\nu_1}/\overline{(1-\hat{G})}, \tag{2.11a}$$

and to write down the transport equation in the form

$$i\omega(1-\hat{G})\nu_1 + \left\{v_y\frac{\partial}{\partial y} + \frac{\partial}{\partial t} + \left(\frac{\partial}{\partial t}\right)_{\text{coll}}\right\}\nu_1 = -v_\beta E_\beta + i\omega\frac{\overline{(1-\hat{G})\nu_1}}{\overline{1-\hat{G}}}(1-\hat{G}). \tag{2.12}$$

Equation (2.12) together with (2.6) and (2.8), which can be put in the form

$$E_\alpha'' = \frac{4\pi i\omega}{c^2}\frac{2e^2}{(2\pi\hbar)^3}\frac{eH}{c}\overline{v_\alpha\nu_1}, \tag{2.13}$$

give the complete set of equations for the problem. (We see easily that by averaging Eq. (2.12) and taking the relation $\overline{(\partial\nu_1/\partial t)_{\text{coll}}} = 0$ into account, we get $j_y = 0$, i.e., this equation is satisfied automatically as expected.)

The proposed transformation enables us thus indeed to find Ey from (2.11) and (2.11a) while automatically satisfying (2.2). This is, of course, also valid in the usual case of a Fermi gas, when $\hat{G} = 0$.

One realizes easily when such a transformation is convenient. The transformation (2.11) introduces an inhomogeneity in the equation and one must in (2.12) always (even in the static case*) retain the term with the derivative with respect to the coordinate. In the case of the normal skin effect this turns out to be inconvenient, but for the anomalous skin effect, when the derivative $v_y\partial\nu_1/\partial y$ is different from zero, Eq. (2.12) is very convenient.

An additional advantage of Eq. (2.12) in the case of the anomalous skin effect, when the smallest length is the skin depth, is that ν_1 has a steep maximum as a function of the angles (near $v_y = 0$ and in the case of resonance near $p_z = p_z^{\text{ext}}$, $v_y = 0$) which makes it possible to simplify (2.12) considerably (vide infra). It is clear that n_1, which contains φ, which in turn is isotropic in the angles, does not possess this property.

It is already clear from the form of Eq. (2.12) that the Fermi-liquid plays on the whole the same role as a field E_y normal to the metal surface (to check this it is sufficient to put $\hat{G} = 0$), and does so at the same time, i.e., at sufficiently high frequencies (vide infra), in particular at frequencies appreciably higher than the ones studied in references 5 and 6.

It remains now to derive the boundary conditions for Eq. (2.12). The condition in t is obvious: periodicity with a period $\Omega = eH/m^*c$ for closed orbits and boundedness as $t \to \infty$ for open orbits. At infinity (where $\varphi = 0$), we have

$$n|_{y=\infty,\, v_y<0} = n_0(\varepsilon_0 - \zeta_0), \qquad \nu_1|_{y=\infty,\, v_y<0} = 0. \tag{2.14}$$

Since the conditions $\rho' = 0$ and $j_y = 0$ are automatically satisfied everywhere (and in particular on the surface y = 0), it is natural that we have

$$n|_{y=0,\, v_y>0} = n_0(\varepsilon_0 - \zeta_0). \tag{2.15}$$

when the reflection from the surface is diffuse. (The equilibrium function is chosen here to depend on ϵ_0 and ζ_0, since the surface manifests itself at interatomic distances while the field, which leads to a change in the chemical potential and to the liquid effects, manifests itself at appreciably larger distances on the order of the skin-depth; ϵ_0 is a function of the kinematic momentum.) It follows from (2.15) that

$$(1-\hat{G})\left(\nu_1 - \overline{(1-\hat{G})\nu_1}/\overline{(1-\hat{G})}\right)\Big|_{y=0,\, v_y>0} = 0. \tag{2.16}$$

We average (2.16) over the region $v_y > 0$. This averaging is defined by Eq. (2.10), where the integral over v_y is taken over the region $v_y > 0$. Such an averaging will be denoted by the symbol $\overline{f}^+$. We denote the analogous averaging over the region $v_y < 0$ by the symbol $\overline{f}^-$.

It is easy to verify the validity of the relation

$$\overline{1-\hat{G}} = 2\overline{(1-\hat{G}^+)}, \quad \overline{f} = \overline{f}^+ + \overline{f}^-,$$

from which it follows at once that

$$\overline{(1-\hat{G})\nu_1}^+ = \overline{(1-\hat{G})\nu_1}^-.$$

(2.16) can thus be rewritten as

$$(1-\hat{G})\nu_1|_{y=0,\, v_y>0} = \frac{\overline{(1-\hat{G})\nu_1}^-}{\overline{1-\hat{G}}^-}(1-\hat{G}). \tag{2.17}$$

(2.17) is the equation for $\nu_1|_{y=0,\, v_y>0}$ in terms

*In the static case one must, of course, choose a finite upper limit in (2.11), for instance zero; the choice of the value ∞ is convenient when E_y decreases at infinity, as will be the case for a variable field in the half-space outside the metal.

of the value $\nu_1|_{y=0,\ v_y<0}$, for which (2.14) gives the boundary condition. (For $\hat{G} = \text{const}$ we have thus

$$\nu_1|_{y=0,\ v_y>0} = \bar{\nu}_1|_{y=0}.)$$

Conditions (2.14) and (2.17) are the boundary conditions for Eq. (2.12).

The complete set is thus defined by Eqs. (2.12) to (2.14) and (2.17).

3. THE SET OF EQUATIONS NEAR RESONANCE

We have stated in Sec. 1 that we are only interested in the region near resonance. By using this fact we can first simplify greatly the consideration of the boundary conditions. Since only electrons that do not collide with the surface can take part in the resonance, we can assume ν_1 to be different from zero only for those electrons and replace in Eq. (2.13) for the current density the quantity ν_1 by

$$\nu_1 s_1(y - r_1(t)); \quad s_1(\omega) = \begin{cases} 1, & \omega > 0 \\ 0, & \omega < 0 \end{cases}; \tag{3.1}$$

$r_1(t)$ is the orbit traversed by an electron from the vertex of the trajectory after a time t (for details see reference 5).

We take it also into account that in the case of resonance and a non-quadratic dispersion law only the "upper" ($p_x > 0$) and the "lower" ($p_x < 0$) points of the orbit, i.e., the points $p = \pm p_0$, where $\epsilon = \epsilon_0$, $p_z = 0$, and $v_y = 0$, are important. (We shall for the sake of simplicity consider only the case of resonance on the central cross section.) We note that for the case of an anomalous skin effect and resonance on the central cross section, ν_1 [which is defined by Eq. (2.12)] has a steep maximum in momentum space for $p \approx p_0$ or $-p_0$ (it was pointed out in Sec. 2 that this is one of the advantages of this set of equations). Because of this we have for $r\sqrt{\omega\tau}/\delta \gg \Theta/T$ (Θ is the Debye temperature):

$$(\partial\nu_1/\partial t)_{\text{coll}} \approx \nu_1/\tau(p), \quad \tau^{-1}(p) = \int W(p, p')\,dp', \tag{3.2}$$

where $W(p, p')$ is the probability for a transition from p to p' during a collision.

Since

$$W(-p, -p') = W(p, p'),$$

$$\varepsilon(-p) = \varepsilon(p), \quad \tau(-p) = \tau(p),$$

we can also perform the substitution (arguing in analogy with reference 6)

$$(\partial\nu_1/\partial t)_{\text{coll}} \to \nu_1/\tau_0, \quad \tau_0 = T_0^{-1}\int_0^{T_0} \tau^{-1}(p)\,dt|_{p=p_0}. \tag{3.3}$$

For the same reason (because of the steep maximum of ν_1 at $\pm p_0$) the following substitutions are valid:

$$\hat{G}\cdot 1 = -\int \frac{\partial n_0}{\partial \varepsilon_0} G(p, p')\,dp' = g(p) = g(-p) \to g(p_0) = g_0 \tag{3.4}$$

[we recall that $G(-p, -p') = G(p, p')$ because of spherical symmetry],

$$\frac{eH}{c}\overline{\hat{G}\nu_1} = \iint G(p, p')\frac{\partial n_0}{\partial \varepsilon_0}\frac{\partial n_0}{\partial \varepsilon_0'}\nu_1(p')\,dp\,dp'$$

$$= \int \nu_1(p')\frac{\partial n_0}{\partial \varepsilon_0'}dp' \int \frac{\partial n_0}{\partial \varepsilon_0} G(p, p')\,dp$$

$$= g_0\frac{eH}{c}\bar{\nu}_1; \quad \overline{\hat{G}\nu_1} \to g_0\bar{\nu}_1;$$

$$\hat{G}\nu_1 = -\int \frac{\partial n_0}{\partial \varepsilon_0} G(p, p')\nu_1(p')\,dp' = G(p, p_0)\,\bar{\nu}_1^{+}$$

$$+ G(p, -p_0)\,\bar{\nu}_1^{-} = \tfrac{1}{2}G(p, p_0)(\bar{\nu}_1 + \bar{s\nu}_1)$$

$$+ \tfrac{1}{2}G(p, -p_0)(\bar{\nu}_1 - \bar{s\nu}_1) = \bar{\nu}_1 g_{10} + \bar{s\nu}_1 sb;$$

$$g_{10} = \tfrac{1}{2}[G(p_0, p_0) + G(p_0, -p_0)],$$

$$b = \tfrac{1}{2}[G(p_0, p_0) - G(p_0, -p_0)], \tag{3.5}$$

where a bar with a plus or a minus sign indicates averaging over the "upper" (where $s = 1$) and the "lower" (where $s = -1$) parts of the trajectory, respectively. The parameter s, the value of which is important only near $\pm p_0$, can be set equal to

$$s \equiv \operatorname{sign} v_x, \tag{3.6}$$

$$v_\alpha = v_\alpha(p_0)\,s = v_\alpha^0 s. \tag{3.7}$$

We now write (2.12) and (2.13) in the form

$$\left(i\omega + v_y\frac{\partial}{\partial y} + \frac{\partial}{\partial t} + \frac{1}{\tau_0}\right)n_\beta'$$

$$= sE_\beta + i\omega\left\{\left[\frac{(1-g_0)^2}{1-g} + g_{10}\right]\bar{n}_\beta' + sb\overline{sn}_\beta'\right\},$$

$$E_\alpha'' = \frac{4\pi i\omega}{c^2}\frac{2e^2}{(2\pi\hbar)^3}\frac{eH}{c}v_\alpha^0 v_\beta^0\,\overline{sn_\beta' s_1(y - r_1(t))} \quad (v_1 = v_\beta^0 n_\beta').$$

We now choose the α axis in the direction of v in the point p_0 and thus diagonalize the equations. Since we are interested only in the component $Z_{\alpha\alpha}$ (Z is the impedance), which show a resonant behavior, we get, dropping for the sake of simplicity the index α,

$$E'' = \frac{4\pi i\omega}{c^2}\frac{2e^2}{(2\pi\hbar)^3}\frac{eH}{c}v_0^2\overline{sn'} = i\omega N\overline{sn'}, \tag{3.8}$$

$$(i\omega + v_y\partial/\partial y + \partial/\partial t + 1/\tau_0)\,n' = sE + i\omega(an' + sb\overline{sn'}), \tag{3.9}$$

$$a = \frac{(1-g_0)^2}{1-g} + g_{10}, \quad N = \frac{8\pi e^3 H v_0^2}{c^3(2\pi\hbar)^3} = \frac{8\pi m^* v_0^2 e^2\Omega_0}{c^2(2\pi\hbar)^3}. \tag{3.10}$$

In (3.8) we have dropped a term with $1 - s(y - r_1(t))$, which takes the boundary conditions into account. This simplifies the solution considerably, as it contributes only an unimportant factor

of the order of unity[5] to the impedance (in the general case the solution is similar to the one given in reference 6).

We now recognize easily when the difference between a Fermi liquid and a Fermi gas turns out to be important. First of all it is clear that when $\tau_0 = \infty$ and a = b = 0 there exists a periodic solution of the homogeneous equation (3.9) [and also of (2.12)], which corresponds to an eigenvalue of Eq. (3.9) [or respectively (2.12)]. The two small terms n'/τ_0 and $\omega(a\overline{an'} + sb\overline{sn'})$ ensure that the value of the resonance n′ is finite and are thus very important. We shall estimate the ratio of these terms. One sees easily that

$$\overline{an'} \sim b\overline{sn'} \sim n'(\delta_0/r)(\omega\tau)^{-1/2},$$

so that their ratio is of the order of magnitude

$$\gamma = \delta_0/r\sqrt{\omega\tau}. \tag{3.11}$$

From an earlier paper by the present author[5] it is clear that we have always $\gamma \lesssim 1$, while $|\gamma| \sim 1$ (and the Fermi-liquid character of the spectrum is important), when

$$\hbar\omega \gtrsim kT, \quad l \sim l_{eff} \sim (\hbar v/k\Theta)(k\Theta/\hbar\omega)^3 \tag{3.12}$$

(l_{eff} is the effective electron-phonon mean free path).

If the dispersion law is quadratic (when the Fermi surface is an ellipsoid) the Fermi-liquid effects manifest themselves appreciably earlier, when

$$\omega\tau\delta_0/r \gtrsim 1. \tag{3.13}$$

All values of p_z are then, of course, important (since the frequencies for the circulation of all electrons are the same) and Eq. (3.9) is only qualitatively valid.

4. THE SOLUTION OF THE EQUATIONS

To solve Eqs. (3.8) and (3.9) we note that they can easily be continued on the negative semi-axis y < 0, if we put

$$E(-y) = E(y), \quad n'(-y, -\mathbf{p}) = -n'(y, \mathbf{p}). \tag{4.1}$$

Changing in (3.8) and (3.9) to Fourier components and finding the solution of the corresponding equations, which is periodic in t, we get near resonance ($\omega\tau \gg 1$, $\omega \approx q\Omega_0 = q\Omega|_{p_z=0}$)

$$-k^2\varepsilon(k) - 2E'(0) = i\omega N\overline{sn'}; \tag{4.2}$$

$$n'(k) = \left[1 - \exp\left(-2\pi i\frac{\omega}{\Omega} - \frac{2\pi}{\Omega\tau}\right)\right]^{-1} \int_{t-T}^{t} \exp\left\{-(t-t')\left(i\omega + \frac{1}{\tau}\right) + ik(r_1(t) - r_1(t'))\right\} dt' [s(t')E + i\omega(\overline{an'} + bs(t')\overline{sn'})]$$

$$\approx \exp\{-iq\Omega_0 t + ikr_1(t)\}\left[1 - \exp\left(-2\pi i\frac{\omega}{\Omega} - \frac{2\pi}{\Omega\tau}\right)\right]^{-1} \int_0^{T_0} \exp\{iq\Omega_0 t' - ikr_1(t')\}[s(t')E + i\omega(\overline{an'} + bs(t')\overline{sn'})]\,dt', \tag{4.3}$$

$$\varepsilon(k) = \int_{-\infty}^{\infty} E(y)e^{iky}dy, \quad n'(k) = \int_{-\infty}^{\infty} n'(y)e^{iky}dy. \tag{4.4}$$

Calculating from (4.3) the average values $\overline{n'}$ and $\overline{sn'}$ and solving the resultant set of algebraic equations we find for the value of $\overline{sn'}$, which occurs in (4.2), the expression

$$\overline{sn'} = E\begin{vmatrix} 1 - i\omega a\langle R|\widetilde{A}|^2\rangle & \langle R\widetilde{A}s\widetilde{A}^*\rangle \\ -i\omega a\langle R\widetilde{A}_s^*\widetilde{A}\rangle & \langle R|\widetilde{A}s|^2\rangle \end{vmatrix} \times \begin{vmatrix} 1 - i\omega a\langle R|\widetilde{A}|^2\rangle & -i\omega b\langle R\widetilde{A}s\widetilde{A}^*\rangle \\ -i\omega a\langle R\widetilde{A}_s^*\widetilde{A}\rangle & 1 - i\omega b\langle R|\widetilde{A}s|^2\rangle \end{vmatrix}^{-1}.$$

Here we have used the notation

$$\langle f\rangle = \int f dp_z, \quad \widetilde{f} = \int_0^{T_0} f dt, \quad A = \exp\{iq\Omega_0 t - ikr_1(t)\},$$
$$R = \left[1 - \exp\left(-2\pi i\frac{\omega}{\Omega} - \frac{2\pi}{\Omega\tau_0}\right)\right]^{-1}. \tag{4.5}$$

We use now the condition

$$\omega\tau_0 \sim (r/\delta_0)^2 \gg r/\delta_0 \gg 1,$$

so that only $p_z \approx 0$ and $v_y \approx 0$ are important. We have then (dots indicate differentiation with respect to t, $\dot{r}_1 = v_y$; dashes indicate differentiation with respect to p_z)

$$\langle R\varphi(p_z)\rangle = \langle R\rangle\varphi(0); \quad \widetilde{A} \approx 2i\sqrt{\pi/|\ddot{r}_{10}k|}\sin(kd_0/2 - \pi/4);$$
$$\widetilde{As} \approx 2\sqrt{\pi/|\ddot{r}_{10}k|}\cos(kd_0/2 - \pi/4);$$
$$d_0 = (2cp_x^{max}/eH)|_{p_z=0}; \qquad \varkappa = (\omega - q\Omega_0)/\omega = |\varkappa|s,$$
$$\sigma = \operatorname{sign}(\Omega_0/\Omega_0''); \quad p_0 = \sqrt{2|\Omega_0''/\Omega_0|^{-1}},$$
$$i\omega\overline{sn'} = E(k)\frac{2\pi i\omega R_0|\ddot{r}_{10}k|^{-1}(1 + \sin kd_0)}{1 + 2\pi i\omega R_0|\ddot{r}_{10}k|^{-1}[(a+b) + (b-a)\sin kd_0]};$$
$$R_0 = \int\frac{dp_z}{R} \approx \frac{p_0}{2q(\varkappa^2 + \xi^2)^{1/4}}\exp\left\{i\frac{\pi}{4}(s+\sigma) + \frac{1}{2}is\tan^{-1}\frac{\xi}{|\varkappa|}\right\},$$
$$\xi = \frac{1}{\omega\tau_0}. \tag{4.6}$$

Using (4.6) we can show that the behavior of the field in the metal is the same as that found in reference 5: the magnitude of the field has steep maxima for y = 0, d_0, $2d_0$, ... We find now from (4.2) and (4.6)

$$Z = -\frac{4\pi i\omega}{c^2}\frac{E(0)}{E'(0)} = \frac{8i\omega d_0}{c^2}\int_0^{\infty}\left[x^3 + Nd_0^2\frac{2\pi i\omega R_0 d_0}{|\ddot{r}_{10}|} \times \frac{(1+\sin x)}{1 + (2\pi i\omega R_0 d_0/|\ddot{r}_{10}|x)[(b+a) + (b-a)\sin x]}\right]^{-1} x\,dx.$$

Transforming the integral obtained here in a way similar to that used in reference 5 we find

$$Z = \frac{8i\omega}{c^2 A}\left[1 + \frac{b+a}{b-a}\frac{1}{f}\right]^{-1}\int_0^\infty \left\{1 - \frac{(\alpha+\beta)u_1}{1+\beta u_1}\right\} z\,dz; \quad (4.7)$$

$$A = (2\pi\omega R_0 N/|\dot{v}_y^0|)^{1/3}, \quad u_1^2 + 2\beta u_1 - 1 = 0, \quad |u_1| < 1,$$

$$\beta = \frac{z^3 + i(f+1)}{1 + f(b-a)/(b+a)}, \qquad \alpha = \frac{a+b}{b-a}\frac{1+if}{f},$$

$$f = (2\pi\omega R_0/|\dot{v}_y^0|)^{2/3} N^{-1/3}(b+a) \sim (\delta_0^2/d_0^2\sqrt{\varkappa^2+\xi^2})^{1/3}. \quad (4.8)$$

We must bear in mind that the quantity f depends in an essential way on the actual values of the quantities occurring in (4.8), and that a change in f greatly influences the impedance.

As was stated in the foregoing the Fermi liquid properties are important when

$$\omega\tau \sim d_0^2/\delta_0^2, \quad (4.9)$$

i.e., when Eqs. (3.12) are satisfied. The resonance curve is then broadened corresponding to an effective τ of the order of

$$\tau_{eff} \sim \omega_1^{-1}(\omega_1/\omega)^3, \quad \hbar\omega_1 \sim \varepsilon_0 v/c,$$

so that $X \neq 0$ when $\tau = \infty$.*

5. CONSTRUCTION OF THE CORRELATION FUNCTION

Equations (4.9) and (3.12) show that under our conditions (resonance at very high frequencies) we can effectively construct the correlation function from Eqs. (4.7) and (4.8).

The function Z(H, ω, T) contains five independent parameters: κ corresponding to the effective mass on the central cross section (m_0^*); two parameters that determine the value of $\xi = 1/\omega\tau_0$

$$1/\tau_0 = 1/\tau_{imp} + \omega^3/\tau', \quad (5.1)$$

where τ_{imp} and τ'/ω^3 are respectively the times between collision with impurities and phonons (when the skin effect is anomalous these times are introduced in sequence); the parameter $Np_0|v_{0y}|^{-1}$, which is easily determined from the value of the impedance outside the resonance; and the parameters f and $f(b-a)/(b+a)$.

One can, of course, determine from the experimental behavior of Z(H, ω, T) all these parameters (it is, for instance, sufficient to perform measurements for only two values of ω). To do this one must, finally, use beforehand numerical integration to plot the function (4.7) for different values of these parameters.

*The equations are obtained for resonance on the central cross section only for the sake of simplicity. (We note that when (3.12) is satisfied in the base points the resonance is in general impossible; see also reference 5.)

The measurement of Z(H, T) is already sufficient to determine the quantity

$$\frac{a-b}{a+b} = \left[\frac{(1-g_0)^2}{1-g} + G(\mathbf{p}_0, -\mathbf{p}_0)\right] \Big/ \left[\frac{(1-g_0)^2}{1-g} + G(\mathbf{p}_0, \mathbf{p}_0)\right], \quad (5.2)$$

which completely characterizes the correlation function. If, moreover, we determine (by independent measurements in a region where the Fermi-liquid effects are unimportant) both (for instance, by studying the vanishing of the resonance harmonics in plates; see reference 5) and v_0 (from the resonance frequencies by the Lifshitz-Pogorelov method[7]) we can determine b + a and b − a independently. As a result one can find the values

$$G(\mathbf{p}_0, \mathbf{p}_0) - G(\mathbf{p}_0, -\mathbf{p}_0) = \varphi(\mathbf{p}_0),$$

$$(1-g_0)^2/\overline{(1-g)} + G(\mathbf{p}_0, \mathbf{p}_0) = \psi(\mathbf{p}_0).$$

The functions $\varphi(p_0)$ and $\psi(p_0)$ give very complete information about the correlation function.

Note added in proof (September 7, 1960): Resonance "splashes" of the field[5] can occur: 1) when **H** rotates in a plane, leading to $\sim a = D/d$ extremal resonance values of the impedance; 2) when ω and **H**/H are fixed and when $\omega\tau \gtrsim (d/\delta)^{4/3}$ and $M^{3/2} \gtrsim a \gtrsim (d/\delta)^{4/3}$ (the notation is that of reference 5). In the latter case a change in the number of maxima in the high-frequency field in a plate while **H** is varied in the resonance region leads to the splitting up of one resonance peak into several ones, i.e., to the appearance of additional extrema in the resonance curve.

[1] L. D. Landau, JETP **30**, 1058 (1956), Soviet Phys. JETP **3**, 920 (1957).

[2] L. D. Landau, JETP **35**, 97 (1958), Soviet Phys. JETP **8**, 70 (1959).

[3] M. Ya. Azbel', JETP **34**, 766 (1958), Soviet Phys. JETP **7**, 527 (1958).

[4] L. P. Pitaevskiĭ, JETP **34**, 942 (1958), Soviet Phys. JETP **7**, 652 (1958).

[5] M. Ya. Azbel', JETP **39**, 400 (1960), Soviet Phys. JETP **12**, 283 (1961).

[6] M. Ya. Azbel' and É. A. Kaner, JETP **32**, 896 (1957), Soviet Phys. JETP **5**, 730 (1957).

[7] I. M. Lifshitz and A. V. Pogorelov, Dokl. Akad. Nauk SSSR **96**, 1143 (1954).

Translated by D. Ter Haar
208

Letters to the Editor

MAGNETIC PROPERTIES OF ORTHOFERRITES OF LANTHANUM AND PRASEODYMIUM WITH PARTIAL REPLACEMENT OF Fe^{3+} IONS BY Al^{3+} IONS

K. P. BELOV, M. A. ZAĬTSEVA, and A. M. KADOMTSEVA

Moscow State University

Submitted to JETP editor July 6, 1960

J. Exptl. Theoret. Phys. (U.S.S.R.) **39**, 1148-1150 (October, 1960)

ORTHOFERRITES of the rare-earth elements (the general formula is $M_2O_3 \cdot Fe_2O_3$, where M is an ion of a rare-earth element) are antiferromagnetic but exhibit a weak ferromagnetism. A theoretical explanation of the presence of weak ferromagnetism in various antiferromagnetic materials has been given by a number of authors.[1] Earlier[2] we investigated unusual hysteretic phenomena in $Pr_2O_3 \cdot Fe_2O_3$ and $La_2O_3 \cdot Fe_2O_3$; the unusual feature was that hysteresis loops taken after cooling in a magnetic field from the Curie point to room temperature were displaced upward along the magnetization axis. A magnetic field of approximately 8000 oe did not reduce the thermoremanent magnetization to zero, a fact indicative of the presence of a large coercive force.

Bozorth,[3] in investigations of monocrystals of similar orthoferrites, showed that in these compounds the magnetic moment is directed along the c axis of the orthorhombic crystal. This should lead to a large magnetic anisotropy of these crystals, and consequently to an increase of the coercive force. The orthorhombic distortion in the crystals should decrease[4] upon replacement of the iron ions in the perovskite structure by ions of smaller radius. Accordingly, we have carried out a partial replacement of Fe^{3+} ions (ionic radius 0.67 A) by nonmagnetic Al^{3+} ions (ionic radius 0.57 A) in the compounds $La_2O_3 \cdot Fe_2O_3$ and $Pr_2O_3 \cdot Fe_2O_3$. The polycrystalline specimens were prepared by the same method that was described earlier.[2]

Figure 1b shows a hysteresis loop for the orthoferrite $La_2O_3 \cdot 0.9Fe_2O_3 \cdot 0.1Al_2O_3$, taken by the ponderomotive method after cooling from the Curie point in a magnetic field H = 4000 oe. Shown also for comparison (Fig. 1a) is a hysteresis loop obtained under similar conditions for $La_2O_3 \cdot Fe_2O_3$. In $La_2O_3 \cdot Fe_2O_3$; clearly, the thermoremanent magnetization is not destroyed even in fields ~ 20000 oe. The hysteresis loop in the substituted compound has become much more symmetric. The thermoremanent magnetization is already reduced to zero at fields of order 3000 oe, an indication of a decrease of coercive force. The decrease of coercive force is also observed in the compound $Pr_2O_3 \cdot 0.9Fe_2O_3 \cdot 0.1Al_2O_3$ (Fig. 2).*

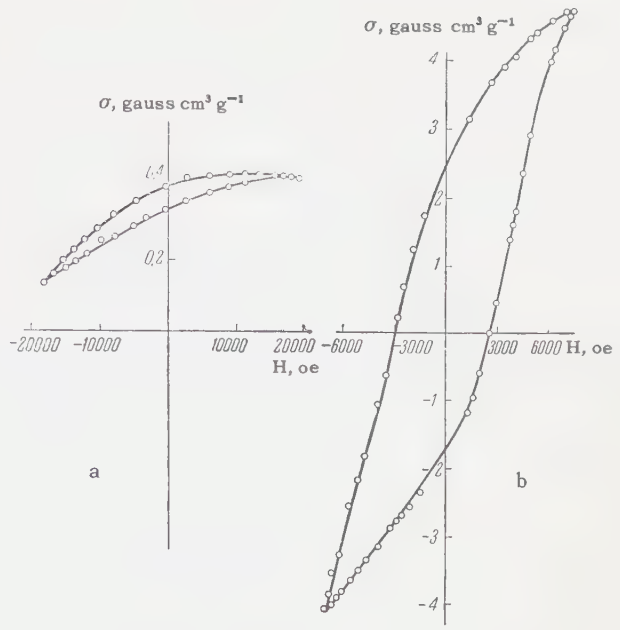

FIG. 1. Magnetic hysteresis loops at 20°C after cooling in a magnetic field H = 4000 oe from the Curie point: a – for the ferrite $La_2O_3 \cdot Fe_2O_3$; b – for the ferrite $La_2O_3 \cdot 0.9Fe_2O_3 \cdot 0.1Al_2O_3$.

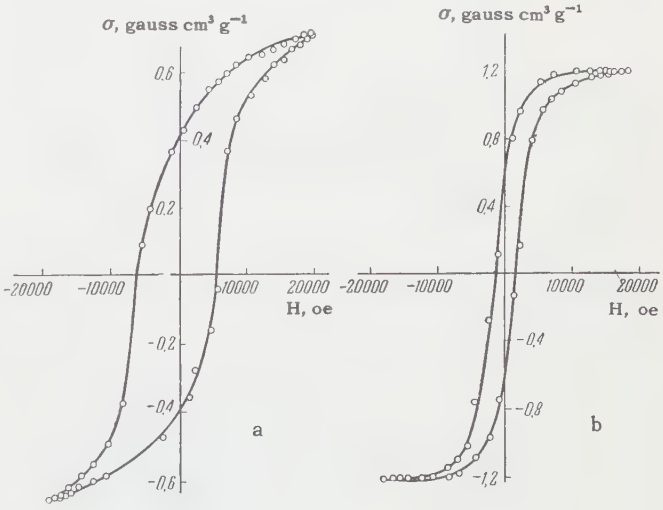

FIG. 2. Magnetic hysteresis loops at 20°C, taken without cooling in a magnetic field: a – for the ferrite $Pr_2O_3 \cdot Fe_2O_3$; b – for the ferrite $Pr_2O_3 \cdot 0.9Fe_2O_3 \cdot 0.1Al_2O_3$.

As was mentioned above, this decrease may be connected with a decrease of the orthorhombic distortion of the crystal lattice. In the substituted compounds there was also observed a change of several other magnetic properties. Figure 3 shows the variation of magnetization with temperature in the original and in the substituted compounds. As is clear from the figure, the Curie points for the compositions $La_2O_3 \cdot 0.9Fe_2O_3 \cdot 0.1Al_2O_3$ and $Pr_2O_3 \cdot 0.9Fe_2O_3 \cdot 0.1Al_2O_3$ are slightly decreased in comparison with the stoichiometric; this is evidently connected with a decrease in the number of $Fe^{3+} - O^{2-} - Fe^{3+}$ super-exchange interactions.

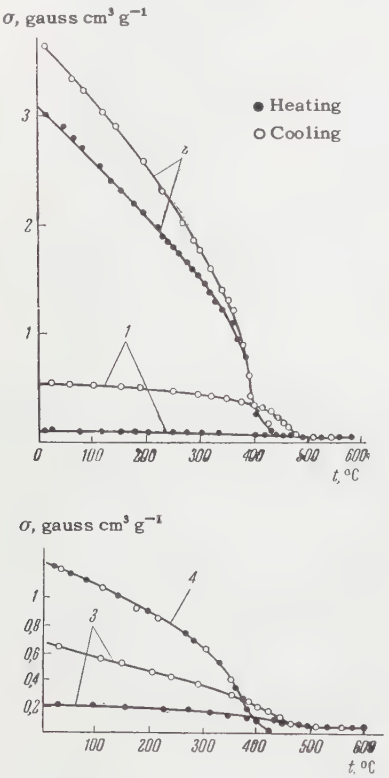

FIG. 3. Temperature dependence of the specific magnetization, taken in a field of 4000 oe: 1 – for the ferrite $La_2O_3 \cdot Fe_2O_3$; 2 – for the ferrite $La_2O_3 \cdot 0.9Fe_2O_3 \cdot 0.1Al_2O_3$; 3 – for the ferrite $Pr_2O_3 \cdot Fe_2O_3$; 4 – for the ferrite $Pr_2O_3 \cdot 0.9Fe_2O_3 \cdot 0.1Al_2O_3$.

From Fig. 3 it is also evident that if the thermoremanent magnetization (cooling curve) at the stoichiometric compositions is two to three times larger than the initial magnetization (heating curve), upon substitution of ions in the lanthanum compounds the thermoremanent magnetization exceeds the initial by 15%, and in the praseodymium compounds it is quite unobservable at the field used.

It is also interesting to note that in the orthoferrites we have studied, partial replacement of Fe^{3+} ions by Al^{3+} ions, possessing zero magnetic moment, led to a marked increase of magnetization (Fig. 3); this is perhaps connected with an increase of the difference between the magnetizations of the two sublattices of Fe^{3+} ions in the structure when some of the Fe^{3+} ions are replaced by nonmagnetic Al^{3+} ions.

*For comparison of the magnitudes of the coercive force, the hysteresis loops shown in Fig. 2 are those taken without cooling in a magnetic field, since they are more symmetric with respect to the coordinate axes.

[1] I. E. Dzyaloshinskiĭ, JETP **32**, 1547 (1957), Soviet Phys. JETP **5**, 1259 (1957); A. S. Borovik-Romanov, JETP **36**, 766 (1959), Soviet Phys. JETP **9**, 539 (1959); E. A. Turov and V. E. Naish, Физика металлов и металловедение (Phys. of Metals and Metallography) **9**, 10 (1960).

[2] Belov, Zaĭtseva, and Kadomtseva, JETP **37**, 1159 (1959), Soviet Phys JETP **10**, 825 (1960).

[3] R. M. Bozorth, Phys. Rev. Letters **1**, 362 (1958).

[4] F. Bertaut and F. Forrat, Compt. rend. **243**, 1219 (1956).

Translated by W. F. Brown, Jr.
209

ON THE ROLE OF THE NONPHYSICAL REGION IN THE DISPERSION RELATIONS FOR THE PHOTOPRODUCTION OF π MESONS

A. M. BALDIN

P. N. Lebedev Physics Institute, Academy of Sciences, U.S.S.R.

Submitted to JETP editor July 12, 1960

J. Exptl. Theoret. Phys. (U.S.S.R.) **39**, 1151-1153 (October, 1960)

In a paper by Govorkov and the writer[1] it has been shown that the amplitudes for the photoproduction of π mesons in the region near the threshold that were obtained by Chew, Goldberger, Low, and Nambu (referred to hereafter as CGLN)[2] are clearly in contradiction with experiment.

There have previously been studies[1,3] of the initial assumptions of CGLN, which were made on the basis of a direct comparison of the dispersion relations for photoproduction with the experimental data. The observed disagreement with the disper-

sion relations is illustrated in Fig. 1, where A and C are the coefficients of the angular distribution $d\sigma/d\Omega = A + B \cos\theta + C \cos^2\theta$ in the reaction $\gamma + p \rightarrow p + \pi^0$. Here A′ is equal to A after the subtraction of the S-wave contribution, q is the momentum of the meson, $\hbar = c = \mu = 1$, and $\omega = (q^2 + 1)^{1/2}$. The solid curve is the result of calculations on the basis of the dispersion relations (concerning the calculation of the dispersion integrals see references 1 and 3). Experiment agrees with the resonance model in giving a constant value for the quantity $(A' + C)/\omega q^3$ (dashed curve). As has already pointed out,[3] this value is in good agreement with the experimental data over a wide range of energies.

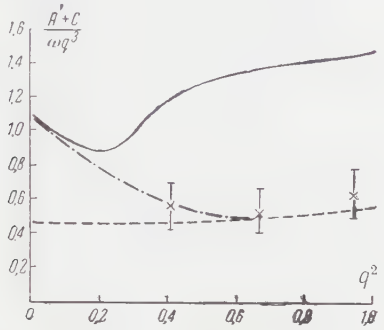

FIG. 1

The conclusions drawn from an examination of this discrepancy were as follows:

a) CGLN's original equations are in contradiction with experiment, and it is not possible to get complete agreement with experiment by an improvement of their solution.[4-6]

b) The possibility of removing the difficulty in the direct comparison of the dispersion relations with experiment must be sought in the calculation of the dispersion integrals.

We have taken this last conclusion to mean[1,3] that it is necessary to take into account the contribution of the energy range above 1 Bev and to give more careful consideration to small partial amplitudes.* It must be remarked, however, (and this is the main purpose of the present note), that in calculations of the dispersion integrals there is the possibility of a much more serious error, which is due to the analytic continuation into the nonphysical region of an amplitude expanded in partial waves. In spite of the fact that the possibility of analytic continuation of the amplitude in this energy region has been proved by Longunov,[9] the question of the rapidity of convergence of the series of Legendre polynomials for $\cos\theta \gg 1$ remains an open one.

We have made a detailed analysis of the possibility of explaining the difficulties that have been indicated in terms of a large contribution of the nonphysical region, which was not taken into account in the equations of CGLN, and have found that the disagreement with experiment occurs only for those values of the angles and energies for which the size of the nonphysical region exceeds $\Delta\omega \sim 0.1$. At values of the angles and energies for which the nonphysical region is absent ($k\omega - kq\cos\theta = k_{thresh}$, where k is the energy of the photon), there is good agreement with experiment.

We give as an example Fig. 2, which shows the calculated cross section $d\sigma/d\Omega$ of the reaction $\gamma + p \rightarrow p + \pi^0$ for $\cos\theta = 3^{-1/2}$ (solid curve).

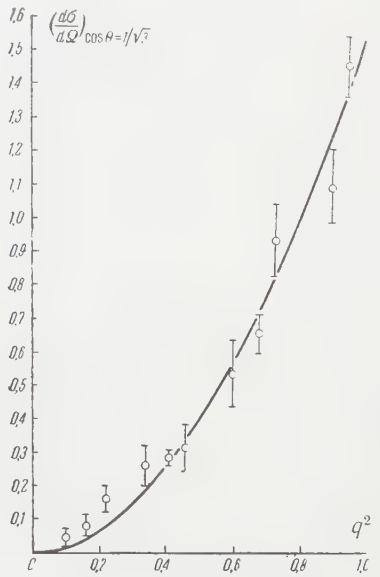

FIG. 2

The experimental points are obtained from the detailed measurements of the total cross section of this reaction.[10,11] For $\cos\theta = 3^{-1/2}$ the quantity $d\sigma/d\Omega$ lies in the neighborhood of the line $k\omega - kq\cos\theta = k_{thresh}$. The solution of the difficulty indicated above is as follows. The nonphysical region vanishes for $q^2 \rightarrow 0$. As can be seen from Fig. 1, for the neighborhood of $q^2 = 0$ the calculation on the basis of the dispersion relations gives a curve that clearly has a tendency to go through the experimental values. The difference between the functions represented by the dash-dot line and the solid line must be ascribed to the contribution of the nonphysical region. In this connection it must be emphasized that the value of the resonance amplitude M_{1+}/q for $q \rightarrow 0$ is found to be 0.63 ± 0.03, in complete agreement with the entire set

of data on the reaction $\gamma + p \rightarrow p + \pi^0$ in the region $0.4 < q^2 < 4$, which gives $M_{1+}q^{-1}|_{q\rightarrow 0} = 0.66 \pm 0.02$. The difference between the functions represented by the dashed curve (with only the amplitude M_{1+} included) and the dash-dot curve is due to the amplitude M_{1-}, which has not yet been observed experimentally. As can be seen, near the threshold the contribution of this amplitude is very large. It decidedly decreases the coefficient C, and can even change its sign for $q \rightarrow 0$. An experimental test of this conclusion is extremely desirable. Another sensitive test for the point of view stated here would be a study of the angular distributions in the reaction $\gamma + p \rightarrow n + \pi^+$ for γ-ray energies of 180 — 200 Mev.

A complete analysis of the consequences that follow from our assertion about the role of the nonphysical region, other arguments in favor of this assertion, and suggestions for experiments will be published separately.

The correctness of our assertion would mean (besides the removal of a difficulty) that in the small region of energies and angles defined by the inequalities

$$(k\omega - 1.6)/kq \leqslant \cos\theta \leqslant (k\omega - 0.7)/kq, \qquad (1)$$

there does exist a theory of the photoproduction of mesons. By a theory we mean a prediction of the amplitude for photoproduction in this region, with the imaginary part of the resonance part of the amplitude being taken from experiment.† (The real part of this amplitude is calculated and, as has been noted, agrees well with experiment.) This theory will enable us to calculate threshold values of cross sections without risky extrapolations, and thus to clarify the values of the basic parameters of π-meson physics in the low-energy region (cf., e. g., reference 12).

The writer is grateful to A. A. Logunov, D. V. Shirkov, and L. D. Solov'ev for a discussion of some questions in the theory of dispersion relations, and to I. A. Egorova for invaluable help with cumbersome numerical calculations.

*Solov'ev and Tentyukova[7] have eliminated the divergence for the coefficient C by the introduction of a pole at $\omega = 98$ and an assumption about the phase a_{11} that is in contradiction with experiment,[8] but no complete comparison of their theory with experiment was carried out.

†We remark that this sort of theory is not the same as the theory of CGLN if the latter is restricted to the region where Eq. (1) holds, because we are singling out just a narrow range of angles; on the other hand, the expansion in multipoles (used by CGLN) presupposes integration over all angles. According to the point of view expressed here, equations obtained from one-dimensional dispersion relations with only the low partial waves included are invalid.

[1] A. M. Baldin and B. B. Govorkov, Nuclear Phys. **13**, 193 (1959).
[2] Chew, Goldberger, Low, and Nambu, Phys. Rev. **106**, 1345 (1957).
[3] A. M. Baldin, JETP **38**, 579 (1960), Soviet Phys. JETP **11**, 416 (1960).
[4] G. Höhler and A. Müllensiefen, Z. Physik **157**, 30 (1959).
[5] G. Jona-Lasinio and H. Munczek, Phys. Rev. **117**, 585 (1960).
[6] S. Gartenhaus and R. Blankenbecler, Phys. Rev. **116**, 1305 (1959).
[7] L. D. Solov'ev and G. N. Tentyukova, JETP **37**, 889 (1959), Soviet Phys. JETP **10**, 634 (1960).
[8] B. Pontekorvo, Report at the Ninth Conference on High-energy Physics, Kiev, July, 1959.
[9] A. A. Logunov, Doctoral Dissertation, Joint Institute of Nuclear Studies, 1959.
[10] R. G. Vasil'kov and B. B. Govorkov, JETP **37**, 317 (1959), Soviet Phys. JETP **10**, 224 (1960).
[11] Vasil'kov, Govorkov, and Gol'danskiĭ, JETP **37**, 11 (1959), Soviet Phys. JETP **10**, 7 (1960).
[12] A. Baldin, Nuovo cimento **8**, 569 (1958).

Translated by W. H. Furry
210

NOTE ON THE OPTICAL THEOREM

D. BLOKHINTSEV

Joint Institute for Nuclear Research

Submitted to JETP editor June 27, 1960

J. Exptl. Theoret. Phys. (U.S.S.R.) **39**, 1153-1154 (October, 1960)

A case encountered frequently is that in which the initial state of the primary beam and the target consists of a combination of incoherent states ("mixed state"). For example, the state of the target or that of the beam particles can be a mixture of different states with respect to the ordinary or the isotopic spin, with respect to the strangeness of the particles, etc.

In this case the primary beam J is a sum of beams J_s ($s = 1, 2, \ldots, n$), for the different states of the beam particles or of the target. The fractional amounts of these states are $P_s = J_s/J$. For each individual state we have the optical theorem

$$\mathrm{Im}\, f_s(0) = (k_s/4\pi)\,\sigma_{s,\,tot}, \qquad (1)$$

where, as usual, $f_s(0)$ is the scattering amplitude at zero angle, $\sigma_{s,\,tot}$ is the total cross section for the s-th beam, and k_s is the wave vector for particles of the s-th beam. We note that even if all of the k_s^0 in the beam are the same, the relative momenta k_s of particle and beam can still be different. For example, this will be so if one takes account of the motion of the nucleons in the target nucleus and assigns a certain probability to each momentum of a nucleon in the nucleus. The total number of transitions into a certain final state r is $dN(r) = \sum J_s d\sigma_s(r)$, where $d\sigma_s(r)$ is the cross section for the transition $s \to r$. Consequently, the total cross section for processes $s \to r$ is

$$d\sigma(r) = dN(r)/J = \sum P_s d\sigma_s(r).$$

In particular, the elastic differential cross section at angle 0 is

$$\left(\frac{d\sigma_{el}}{d\Omega}\right)_0 = \sum_{s=1}^{h} P_s \left(\frac{d\sigma_{el}}{d\Omega}\right)_0 = \sum_{s=1}^{n} P_s \{[\operatorname{Im} f_s(0)]^2 + [\operatorname{Re} f_s(0)]^2\}$$

$$= \sum_{s=1}^{n} P_s \left\{\left(\frac{k_s}{4\pi}\sigma_{s,\,tot}\right)^2 + [\operatorname{Re} f_s(0)]^2\right\},$$

or

$$\left(\frac{d\sigma_{el}}{d\Omega}\right)_0 = \overline{\left(\frac{k_s}{4\pi}\sigma_{s,\,tot}\right)^2} + [\operatorname{Re} f_s(0)]^2, \qquad (2)$$

where the bar denotes the average over the incoherent states s = 1, 2, . . . , n. On the other hand the total cross section for all processes is given by

$$\sigma_{tot} = \overline{\sigma_{s,\,tot}}. \qquad (3)$$

The relation (2) is the most general expression of the optical theorem. In particular, if all of the k_s are equal, then by using Eq. (3) and the general relation $(\overline{\sigma})^2 \leq \overline{\sigma^2}$ we get

$$\left(\frac{d\sigma_{el}}{d\Omega}\right)_0 \geqslant \left(\frac{k}{4\pi}\sigma_{tot}\right)^2 + \overline{[\operatorname{Re} f_s(0)]^2}. \qquad (4)$$

It can be seen from this that even if $\operatorname{Re} f_s(0) = 0$, $(d\sigma_{el}/d\Omega)_0$ can still be larger than $(k\sigma_{tot}/4\pi)^2$. These considerations can be useful in the analysis of collisions both in the high energy domain and also in "classical" nuclear physics.

Translated by W. H. Furry
211

HIGH-ENERGY BEHAVIOR OF THE TOTAL CROSS SECTION FOR π-p SCATTERING

Yu. M. LOMSADZE, V. I. LEND'EL, and B. M. ERNST

Uzhgorod State University

Submitted to JETP editor June 29, 1960

J. Exptl. Theoret. Phys. (U.S.S.R.) **39**, 1154-1155 (October, 1960)

IT is of considerable theoretical interest to investigate the asymptotic behavior (at energy $\omega \to \infty$) of the total cross section for different processes (see, particularly, reference 1). Dispersion relations are at the present time the main source of information about the asymptotic behavior of cross sections.

I. Ya. Pomeranchuk[2] studied the asymptotic form of the dispersion relation for N-N scattering, under the assumption that $\sigma_+(\omega)$ and $\sigma_-(\omega)$ tend toward the constants $\sigma_+(\infty)$ and $\sigma_-(\infty)$ as $\omega \to \infty$. He found that $\sigma_+(\infty) = \sigma_-(\infty)$, since the asymptotic form of $D_+(\infty)$ must not contain the term $[\sigma_+(\omega) - \sigma_-(\omega)]\omega \ln \omega$. (Completely analogous results hold for π-p scattering.) This really means[3] that the difference $\sigma_+(\omega) - \sigma_-(\omega)$ must decrease at least as $1/\ln \omega$ as $\omega \to \infty$.

In the present note we analyze the dispersion relation for the square of the π^+-p foreward scattering amplitude to show that this assertion can be considerably strengthened (for N-N scattering one obtains analogous results).

The dispersion relation for the square of the π^+-p foreward scattering amplitude can be obtained in two ways. One can either follow the ideas set forth in reference 4 and apply the Cauchy integral theorem to the function

$$\mathfrak{S}\,[D(\omega) + iA(\omega)]^2/\omega(\omega - \omega_0)^2$$

($\mathfrak{S}$ denotes the symmetric part of the function). Alternatively, one can adopt the general form of the functions $D(\omega)$ and $A(\omega)$, introduced by Goldberger.[5] Using the analyticity of the amplitude in the complex plane, and integrating over ω', we can then verify that the relation below is an identity. This dispersion relation has the form

$$D_1(\omega)D_2(\omega) - A_1(\omega)A_2(\omega) - \frac{\omega}{\mu}D_1(\mu)D_2(\mu)$$

$$= \frac{2k^2}{\pi}\int_0^\infty d\omega' \frac{A_1(\omega')D_2(\omega') + A_2(\omega')D_1(\omega')}{k'^2(\omega'^2 - \omega^2)}. \qquad (1)$$

In (1) we introduce $D_\pm(\omega)$ and $A_\pm(\omega)$ and exclude the unphysical region of energy $0 < \omega < \mu$ by

means of the usual expansion of $A(\omega)$ in a complete orthonormal system of eigenfunctions of the energy-momentum operator. We thus obtain the final "physical" dispersion relation

$$D_-^2(\omega) - D_+^2(\omega) = \left(\frac{k}{4\pi}\right)^2 [\sigma_-^2(\omega) - \sigma_+^2(\omega)] + \frac{\omega}{\mu}[D_-^2(\mu) - D_+^2(\mu)] + \frac{\omega k^2}{\pi^2}\int_\mu^\infty d\omega' \frac{D_-(\omega')\sigma_-(\omega') - D_+(\omega')\sigma_+(\omega')}{k'(\omega'^2 - \omega^2)} + 8f^2 D_+\left(\frac{\mu^2}{2M}\right)\frac{\omega k^2}{\mu^2[(\mu^2/2M)^2 - \omega^2]}. \quad (2)$$

Consider the asymptotic form of (2). As usual[2] we split up the dispersion integral into two parts, one with limits from μ to a sufficiently large ϵ, the other from ϵ to ∞. In the second integral we can then replace $D_\pm(\omega)$ and $\sigma_\pm(\omega)$ by their asymptotic forms, namely

$$D_\pm(\omega) \to \pm a\omega + b, \quad \sigma_\pm(\omega) \to \sigma_\pm(\infty), \quad (3)$$

where a and b are certain constants. The dispersion relation (2) then assumes the following asymptotic form:

$$\left(\frac{\omega}{4\pi}\right)^2 [\sigma_-^2(\omega) - \sigma_+^2(\omega)] + A\omega + B + \ldots = 0. \quad (4)$$

This leads to the stronger result

$$\sigma_-(\omega) - \sigma_+(\omega) \to \text{const}/\omega, \text{ and } \omega \to \infty.$$

Since the dispersion relation (2) is mathematically equivalent to the usual dispersion relation, the same result can also be obtained from the usual dispersion relations, in particular, in the Blank-Shirkov form,[6] but at the cost of some more cumbersome calculations.

The authors are extremely grateful to Yu. A. Gol'fand and V. Ya. Faĭnberg for a very stimulating discussion, and to F. M. Kuni for valuable remarks.

[1] V. C. Barashenkov, Preprint P-509, Joint Inst. Nuc. Res. (1960).

[2] N. Ya. Pomeranchuk, JETP **34**, 725 (1958), Soviet Phys. JETP **7**, 499 (1958).

[3] Amati, Fierz, and Glaser, Phys. Rev. Letters **4**, 89 (1960).

[4] N. N. Bogolyubov and D. B. Shirkov, Введение в теорию квантованных полей (Introduction to the Theory of Quantized Fields), Gostekhizdat 1957.

[5] M. L. Goldberger, Phys. Rev. **99**, 979 (1955).

[6] V. Z. Blank and D. B. Shirkov, JETP **33**, 1251 (1957), Soviet Phys. JETP **6**, 962 (1958).

Translated by D. Brill
212

INTERPRETATION OF EXPERIMENTAL DATA ON THE SPECTRUM OF ELECTRON-PHOTON CASCADES WITH ENERGY $> 10^{12}$ ev IN THE UPPER LAYERS OF THE ATMOSPHERE

S. I. NIKOL'SKIĬ and Yu. A. SMORODIN

Physics Institute, Academy of Sciences, U.S.S.R.

Submitted to JETP editor July 7, 1960

J. Exptl. Theoret. Phys. (U.S.S.R.) **39**, 1156-1157 (October, 1960)

RESULTS of a study of the energy spectrum of electron-photon cascades at an altitude of 10 — 12 km were reported at the 1959 International Cosmic-Ray Conference in Moscow.[1] A considerable difference between the energy spectrum of electron-photon cascades ($\sim E^{-4}dE$) and the energy spectrum of the primary cosmic radiation in the corresponding energy range ($\sim E^{-2.7}dE$) was observed.

It should be mentioned that the assumption made at the conference,[1] that the energy fraction transferred to the electron-photon component decreases with increasing energy of interacting particles, apparently meets with unsurmountable difficulties in the analysis of the data on extensive air showers.[2]

It seems to us that the above results can be explained by a hypothesis concerning the change in the character of the elementary act of interaction of particles at $10^{14} - 3 \times 10^{14}$ ev which has been proposed in connection with data analysis on extensive air showers.[3] The applicability of such an explanation lies in the fact that it is not necessary to assume that the direct experimental data on the energy spectrum of electron-photon showers in the energy range $10^{11} - 10^{13}$ ev at 10 — 12 km altitude obtained by various methods[1,4] are in error.

Let us calculate the total energy flux carried by electrons and photons with energy $> 10^{12}$ ev at the above altitude. Experimental data concerning the energy spectrum of electron-photon cascades obtained in emulsion[1] and by means of ionization chambers[4] are shown in the figure by circles and squares respectively.* All electrons and photons with energy $> 10^{12}$ ev observed in the emulsion should certainly also be detected by ionization chambers. In addition, ionization chambers can detect electrons and photons of lower energies if they are incident upon the chamber in groups. Therefore, the total energy flux detected by means

of ionization chambers should be greater than the energy flux carried by electrons and photons with energy $> 10^{12}$ ev observed in the emulsion. In order to find the total energy flux of the electron-photon cascades, the experimentally observed energy spectrum should be extrapolated towards higher energies. It is found that if, in doing such an extrapolation, we assume that the energy spectrum is constant, then the energy flux measured by the emulsion method is, contrary to expectation, greater than the energy measured by means of ionization chambers.

If we rely on both series of measurements, then the only way to make the experimental data agree is to assume that the majority of electrons and photons with energy $> 10^{12}$ ev observed in the emulsion come in large groups. The energy spectrum of such groups, when detected by ionization chambers, should not be a monotonic power function roughly similar to the energy spectrum of primary cosmic radiation, but should contain a certain flat region starting with an energy of $10^{13} - 5 \times 10^{13}$ ev. That flat region should spread over a three- to five-fold energy interval, after which the energy spectrum of photon showers should become similar to the spectrum of the primary cosmic radiation. So far, no more than a tendency towards such variation of the spectrum measured by means of ionization chambers has been observed in experiments. It is easy to see that a similar variation in the spectrum corresponds to the assumption concerning the increase of the energy fraction carried away by the electron-photon component in the interaction of particles with energy $\gtrsim 10^{14}$ ev.

One should also note that a large number of electron and photon groups with energy $>10^{12}$ ev was observed in emulsions with an angular spread of $\sim 10^{-5}$ radian.

In conclusion, we can make a few comments about possible models of interaction processes at energies $> 10^{14}$ ev. According to our opinion, an attempt to describe the above-mentioned change of the elementary act by means of a statistical model of nuclear interaction will meet with a series of difficulties: 1) the transverse momentum obtained by particles in the emission is $\lesssim 10^8$ ev/c; 2) the ratio between the number of $\pi^{\pm}$ mesons and the number of π^0 mesons apparently does not correspond to a statistical distribution; and 3) the soft component is monochromatic. As one of the models, one can mention the possibility of the appearance at energies $> 10^{14}$ ev of excited nucleons,[4] "super hyperons," which undergo a great number of consecutive decays with time $\lesssim 10^{-12}$ sec and decay energy $\lesssim 10^8$ ev.

*The authors express their gratitude to L. T. Baradzeĭ, V. I. Rubtsov, M. V. Solov'ev, and B. V. Tolkachev for permitting us to use the preliminary data on the intensity in the range of the highest energies.

[1] Duthie, Fisher, Fowler, Kaddoura, Perkins, and Pinkau, Proceedings of the Moscow International Conference on Cosmic Rays, U.S.S.R. Acad. Sci., Vol I, 1960.

[2] E. V. Gedalin, JETP, in press.

[3] S. I. Nikol'skiĭ and A. A. Pomanskiĭ, Proceedings of the 1959 Moscow International Conference on Cosmic Rays, in press.

[4] Baradzeĭ, Rubtsov, Smorodin, Solov'ev, and Tolkachev, ibid.

[5] M. A. Markov, Гипероны и К-мезоны (Hyperons and K Mesons), Fizmatgiz, 1958.

Translated by H. Kasha
213

ON THE PROBLEM OF PAIRING WITH NON-ZERO ANGULAR MOMENTA

V. M. GALITSKIĬ

Moscow Institute for Engineering Physics

Submitted to JETP editor July 16, 1960

J. Exptl. Theoret. Phys. (U.S.S.R.) **39**, 1157-1159 (October, 1960)

A number of authors (Brueckner et al.,[1] and also a private communication from L. D. Landau and I. Ya. Pomeranchuk) have shown that there can exist bound pairs of particles near the Fermi surface with non-vanishing angular momenta. This possibility is realized in the case where the potential $V(\mathbf{p}-\mathbf{p}')$ contains negative spherical harmonics in its expansion in the angle between the vectors $\mathbf{p}$ and $\mathbf{p}'$. If the binding energy of these pairs is less than the binding energy in the s state, the ground state of the system is, as before, the Bose-condensate of pairs with zero angular momenta. There are then excited states corresponding to the transition of a pair into a state with non-vanishing orbital angular momentum. There may, however, exist systems where the interaction is only attractive for states with an angular momentum l which is not zero. He^3 is apparently such a system. The ground state of the system is in that case built up of pairs with angular momentum l. The present paper is devoted to the study of the possible properties of such systems.

We restrict ourselves henceforth to the case where the interaction is non-vanishing only in the l state and where the total momentum of the pair is equal to zero. The Hamiltonian of the system can in that case be written in the form

$$H=\sum_k(\varepsilon_k-\lambda)a_k^+a_k-\frac{1}{2\Omega}\sum_{kk'}V(k,k')P_l\left(\frac{\mathbf{kk}'}{kk'}\right)a_{\mathbf{k}}^+a_{-\mathbf{k}}^+a_{-\mathbf{k}'}a_{\mathbf{k}'}. \quad (1)$$

One can solve this problem using the Bogolyubov transformation with complex functions u and v or using the Bardeen-Cooper-Schrieffer (BCS) method with a similar improvement; as a result we obtain states with energies below the ground state energy of the non-interacting particles. The energies of the one-particle excitations near these states are of the form

$$E_k=\left[(\varepsilon_k-\lambda)^2+\left|\sum_\mu\Delta_\mu Y_{l\mu}(\mathbf{k}/k)\right|^2\right]^{1/2}, \quad (2)$$

where the Δ_μ are determined by the set of equations

$$\Delta_\mu=\frac{2\pi}{2l+1}\int dk'\,\frac{V(k,k')}{E_{k'}}Y_{l\mu}\left(\frac{\mathbf{k}'}{k'}\right)\sum_{\mu'}\Delta_{\mu'}Y_{l\mu'}\left(\frac{\mathbf{k}'}{k'}\right). \quad (3)$$

One sees easily that the set (3) does not determine the quantities Δ_μ uniquely. Indeed, it follows from the axial symmetry of the E_k and the orthogonality of the functions $Y_{l\mu}$ with respect to the angle φ that (3) has a set of solutions for which only one of the Δ_μ does not vanish. The energies of the system corresponding to these solutions depend on $|\mu|$ and the lowest energy always corresponds to $\mu=\pm1$ (this result was obtained independently by Anderson[2]). This means that the most favorable state will be the one where the angular momenta of all pairs are in the same direction. In other words, such a system must have the property which can be called orbital ferromagnetism.

One can, however, not assume that this result is sufficiently convincing, because of the limitation in the class of wave functions in the methods used. Indeed, the BCS-Bogolyubov theory assumes that all pairs are in the same state, and it is assumed in the present problem in particular that all pairs have the same angular momentum component along the z axis of some selected system of coordinates. It is clear that such states do not possess a well defined value of the total orbital angular momentum of the system and thus violate the spherical symmetry of the initial Hamiltonian (1). One can obtain states with a well defined value of the total orbital angular momentum of the system by taking a superposition of the functions of the BCS-Bogolyubov theory in the form

$$\Phi_{LM}=C_{LM}\int d\mathbf{n}\,Y_{LM}(\mathbf{n})\exp\left\{\sum_k h(\mathbf{nk})\,a_{\mathbf{k}}^+a_{-\mathbf{k}}^+\right\}|0\rangle, \quad (4)$$

where C_{LM} is a normalization factor.

One verifies easily that under rotations the functions Φ_{LM} transform into one another in the same way as the spherical harmonics Y_{LM}. Averaging the Hamiltonian (1) over the functions (4) and taking the variation with respect to the coefficients h we get the energy of the system in the state L, M. We performed the calculations for a model in which the pairing occurred in a p state; the particles are on the surface with a given absolute magnitude of the momentum $|\mathbf{k}|=k_0$; the spins of all the particles are in the same direction. This model is similar to Mottelson's model for an isolated level of a spherical nucleus, and can be solved exactly in the case where the pairing is in an s state. In the case of small angular momenta (L much less than the number of particles) we get as a result of our calculations for the energy W of the system an expression of the form

$$W=W_0+L(L+1)/2J \quad (5)$$

with a negative value for the moment of inertia J In the case of small occupation numbers the problem can be solved for any value of L and the lowest energy value corresponds to a state for which L is equal to the number of pairs.

The functions (4) considered here remind us very much of the wave functions of a rotating nucleus in the form used in the papers by Peierls and Yoccoz.[3] It is well known that the value of the moment of inertia obtained in those papers is incorrect so that our result for the pairing with non-vanishing angular momenta can also not be considered to be a final one.

The results obtained here do not enable us to reach unambiguous conclusions about the superfluid properties of such systems. First of all, it is clear from Eq. (2) that for some directions of the momentum of the quasi-particles the gap tends to zero. From the point of view of the single-particle excitations the system must therefore possess the properties of an "asymmetric" superfluidity. On the other hand, it is necessary for superfluidity that all forms of excitations satisfy the appropriate criterion. The resemblance between the state of orbital ferromagnetism and an ordinary spin ferromagnet enables us to expect a dispersion law $\omega \sim k^2$ for the two-particle excitations connected with the reorientation of the angular momentum of a pair. This result is confirmed also by a consideration of the simplest model of a Bose gas of particles with a spin which is different from zero.

In conclusion I express my gratitude to S. T. Belyaev and A. B. Migdal for interesting discussions.

[1] Brueckner, Soda, Anderson, and Morel, Phys. Rev., in press.

[2] P. W. Anderson and P. Morel, Physica, in press.

[3] R. E. Peierls and J. Yoccoz, Proc. Phys. Soc. (London) **A 70,** 381, 388 (1957).

Translated by D. ter Haar
214

A NEW METHOD TO IDENTIFY GAMMA RADIATION FROM (p, p′ γ), (p, γ) *AND* (p, n γ) *REACTIONS*

A. K. VAL'TER, I. I. ZALYUBOVSKIĬ, A. P. KLYUCHAREV, and V. A. LUTSIK

Physico-Technical Institute, Academy of Sciences, Ukrainian S.S.R.

Submitted to JETP editor July 18, 1960

J. Exptl. Theoret. Phys. (U.S.S.R.) **39,** 1159-1161 (October, 1960)

THE study of nuclear level structure by means of the γ radiation from a target bombarded with low-energy protons is difficult because γ radiation from several reactions, (p, p′ γ), (p, γ), and (p, n γ), may occur simultaneously. Before the γ radiation can be investigated it is necessary to determine the possible reaction with which it is connected. There is a threshold for the (p, n γ) reaction, and γ radiation from it can occur only above a certain proton energy. However, if some level of the nucleus is exited weakly in this reaction, then γ radiation is discovered only considerably above the threshold, because of the high level of γ background from other reactions in the target and from the accelerator. Besides, for weakly exited levels in (p, n γ) reactions, the dependence of the γ-ray yield on the proton energy is almost the same as in the (p, γ) and (p, p′ γ) reactions, and it is often very difficult to determine reliably which reaction produced the observed γ radiation. In investigations on the origin of γ radiation from the (p, p′ γ), (p, γ), and (p, n γ) reactions it is therefore very useful to exploit the competition between these reactions.

It is well known that emission of a nucleon from a strongly exited nucleus, if energetically feasible, is a more probable process than the decay of this state by emission of one or several γ quanta. The existence of a potential barrier for protons appreciably decreases the probability of their emission from the nucleus as compared to emission of neutrons, for which there is no potential barrier. If neutron emission from the nuclear state, which appears after the capture of a proton, is energetically possible, then this process will be preferred. Since the probability of neutron emission near the (p, n) threshold increases very quickly with increasing energy of the emitted neutrons, a sharp decrease is observed in the yield of the (p, p′ γ) and (p, γ) reactions for some interval of proton

energy above the threshold of the (p, n) reaction.

By examining the dependence on proton energy of the yield of γ quanta for every observed γ line separately in the region of the (p, n) threshold, one can distinguish the γ radiation produced by (p, p' γ) and (p, γ) reactions on the investigated isotope from the γ radiation produced by impurities, since it is unlikely that the (p, n)-reaction thresholds of the isotope and of the impurities lie very close. With further increase in the proton energy above the threshold of the (p, n) reaction, higher nuclear levels will be successively excited by (p, n γ) reactions, and a decrease of γ intensity from the (p, p' γ) and (p, γ) reactions in the isotope under investigation will be observed after every excitation threshold. The thresholds of the (p, n) reaction (except the very high ones) are well known for almost all stable isotopes; for the isotopes of one and the same element they usually differ considerably from each other. By increasing the proton energy we can therefore successively investigate several isotopes contained in the target and distinguish the γ radiation from each isotope.

It is well known that capture of protons into a level of the compound nucleus (and, consequently, the yield of the reactions) has a resonant behavior. One should exclude variations in the yield of γ radiation which arise from different probabilities of proton capture into different levels of the compound nucleus. Therefore the target must be thick enough that protons can be simultaneously captured into a number of levels, in which case individual characteristics of the separate resonance levels cannot show up. For nuclei of average atomic weight, targets about one micron thick can be used.

To study the structure of nuclear energy levels in (p, n γ) reactions, the analysis of the γ radiation is carried out in inverse order. By measuring the dependence of the γ yield from the (p, p' γ) or (p, γ) reactions for the isotope under investigation over a wide range of proton energies above the threshold of the (p, n) reaction one determines the excitation thresholds of the nuclear levels in the latter reaction. Then one measures the threshold for the appearance of the γ rays from the (p, n γ) reaction. The two threshold values obtained in this way must coincide if the γ radiation under study is really due to the (p, n γ) reaction, and corresponds to the transition from the level under investigation to the ground state. It is not necessary in this method to determine the excitation threshold with high accuracy, since the energy of the level is determined not from the excitation threshold, but more accurately by measurement of the γ-ray energy.

The accuracy of the measurement of the level energy does not depend in the present method on the thickness of the target and the non-monoenergeticity of the proton beam, whereas these factors are essential for all other methods used to study the nuclear energy level structure in (p, n γ) reactions. The most accurate values of level energies can be obtained by measuring the γ-ray energy with a magnetic β spectrometer, but because of insufficient γ-ray intensity such measurements have seldom been performed.

As an example of the successful application of the described method, we give some results of an investigation of γ radiation in the reactions Co^{59} (p, n γ) Ni^{59} and Cu^{65} (p, n γ) Zn^{65}. In Fig. 1 we show the exitation function for several γ lines

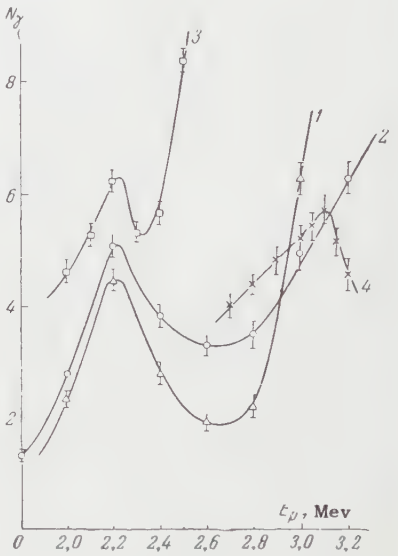

Excitation function for γ radiation of 770 kev (curve 1) and 1015 kev (curve 2) for Cu^{65} target and 465 kev (curve 3) and 1330 kev (curve 4) for Co^{59} target.

which were observed during proton bombardment of a Co^{59} target 1 μ thick and of copper enriched to 98% by the isotope Cu^{65}, 5 μ thick. The 770-kev (curve 1) and 1015-kev (curve 2) γ radiation reaches the maximum yield at a proton energy E_p = 2.2 Mev (which corresponds to the (p, n) threshold for Cu^{65}). It then shows a sharp drop of intensity upon further increase of the proton energy. This indicates that the 770- and 1015-kev γ radiation is the result of the (p, p γ) or (p, γ) reaction in the Cu^{65} target, but not in the impurities. γ radiation of 465 and 1330 kev (curves 3 and 4) occurs as a result of the Co^{59} (p, γ) Ni^{60} reaction. The γ yield at 465 kev experiences a sharp decrease at E_p = 2.24 Mev, which corresponds to the excitation threshold of the 342-kev level of Ni^{59} in the reaction Co^{59} (p, n γ) Ni^{59}.

For γ radiation of 1330 kev (curve 4), an analogous behavior is observed at E_p = 3.125 Mev, which corresponds to the exitation threshold of the 1206-kev level in the reaction $Co^{59}(p, n\gamma)Ni^{59}$. A sharp increase of the yield of 465-kev γ's at $E_p > 2.4$ Mev and of 770 kev γ's at $E_p > 2.8$ Mev indicates that the $(p, n\gamma)$ reactions in Cu^{65} and Co^{59} cause excitation of the 465 and 770 kev levels, respectively. It is impossible to use a scintillation γ spectrometer to separate this γ radiation from the γ radiation exited in these same targets as a result of the $(p, p'\gamma)$ and (p, γ) reaction, since the γ-ray energies probably differ by at most a few kev.

[1] Elwyn, Landon, Oleska, and Glascoe, Phys. Rev. **112**, 1200 (1958).

[2] Val'ter, Zalyubovskiĭ, Klyucharev, and Lutsik, Ядерные реакции при малых и средних энергиях (Nuclear Reactions at Low and Intermediate Energies), U.S.S.R. Acad. Sci., 1958, p. 279.

Translated by D. R. Brill
215

THE HYDROSTATIC EFFECT NEAR THE CRITICAL POINT OF A LIQUID

A. V. VORONEL' and M. Sh. GITERMAN

Institute for Physico-Technical and Radiotechnical Measurements

Submitted to JETP editor July 26, 1960

J. Exptl. Theoret. Phys. (U.S.S.R.) **39**, 1162-1163 (October, 1960)

THE compressibility of a pure substance increases without limit near the critical point. Even the small change in pressure due to the pressure of the upper layers of a liquid on the lower may, therefore, prove important.

The change of pressure in a liquid with height is determined by the relation

$$dp = (\mu g / V)\, dh, \tag{1}$$

where V is the specific volume of the liquid at height h and μ is the molecular weight. If we consider the deviation of p and V from the critical values p_c and V_c to be small throughout the system, which will be true under all real experimental conditions, and using the relation (cf. reference 1)

$$-\left(\frac{\partial p}{\partial V}\right)_T = A(T - T_c) + \frac{B}{2}(V - V_c)^2 + \ldots,$$

where $B = (\partial^3 p / \partial V^3)_{T_c}$, we obtain from Eq. (1) for a thermostated system ($T = T_c$)

$$-dh/dV = (B/2\mu g)\, V (V - V_c)^2. \tag{2}$$

According to Eq. (2) the dependence of the specific volume of the liquid on height is of the following form:

$$V = V_c - \alpha (h - h_0)^{1/3}, \quad \alpha = (6\mu g / BV_c)^{1/3}, \tag{3}$$

where h_0 is the constant of integration determining the level at which the critical conditions are realized.

Experimentally one measures the mean specific volume over the whole vessel and the pressure at some fixed level. We shall assume that the pressure p_0 is measured, for example, at the bottom of the vessel ($h = 0$). Expressing p_0 as a series near $p_c = p(V_c)$, we obtain

$$p_0 = p(V_c + \alpha h_0^{1/3}) = p_c + B\alpha^3 h_0 / 6 + \ldots = p_c + \mu g h_0 / V_c. \tag{4}$$

The mean specific volume is

$$V_{mean} = \frac{1}{H}\int_0^H V(h)\, dh = V_c - \frac{3\alpha}{4H}[(H - h_0)^{1/3} - h_0^{1/3}]. \tag{5}$$

A numerical calculation shows that for all substances, if $0 < h_0 < H$ (the critical state occurs within the vessel), and $H \sim 10$ cm, $(p_0 - p_c)/p_c \sim 10^{-4} - 10^{-5}$, i.e. $p_0 = p_c$ with considerable accuracy. Since B is apparently very small[2,3] we can expect that for $p_0 \approx p_c$, V_{mean} will differ considerably from V_c and $V_{mean} - V_c$ will be a maximum for the values $h_0 = 0$ and $h_0 = H$.

This means that the curve showing the co-existence of liquid and vapor in p, V (or, analogously, T, V) coordinates will have a practically straight-line portion of width

$$\Delta = \tfrac{3}{2}(6\mu g H / BV_c)^{1/3}. \tag{6}$$

The shape of curve determined by the conditions discussed above is shown in Fig. 1 (the dashed curve is the usual form). This form of curve (in the variables T and V) has actually been found for xenon,[4,5] ethane, and ethylene.[5] We can compare Eq. (6) with experiment for not too small vessel heights. The experimental error is then not more than 10%.

According to references 4 and 5 the ratio of heights in two experiments on xenon was H_1/H_2 = 19 cm/13 cm and the corresponding lengths of the straight line portions $(\Delta_1/\Delta_2)^3 = 1.57$. For ethylene H_1/H_2 = 15 cm/6 cm = 2.50 and $(\Delta_1/\Delta_2)^3$

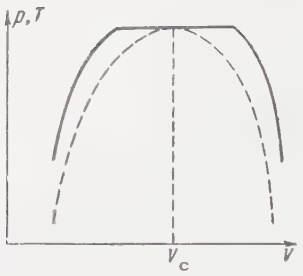

= 2.56. These results can be seen to be in good agreement with Eq. (6).

We can also deduce the value of B from the experimental results and Eq. (6). For H = 19 cm, $\Delta = 0.20$ g cm^{-3},[4] which gives $B \approx -4 \times 10^{-5}$ atm/cm^9 for xenon. This result does not disagree with data from other work[2,3].

An experimental study of this effect can be important in studying the actual form of the singularity in thermodynamic potential at the critical point.* If B = 0 the relation $\Delta(H)$ will be different.

It would therefore be interesting to study the form of the dependence of Δ on H in specially designed experiments of sufficient accuracy and to calculate $(\partial^3 p/\partial V^3)_{T_c}$ at the critical point, which is of considerable theoretical interest.

The authors thank M. Ya. Azbel' for a discussion of the questions raised here.

*We should point out that the existence of the straight-line portion is connected with the condition $(\delta^2 P/\delta V^2)_T = 0$, which holds not only at the critical point but at all limiting states of the supercooled vapor and superheated liquid. In these cases, however, $(\delta^2 p/\delta V^2)_T \neq 0$ and as a result $\Delta \sim H^{1/3}$.

[1] L. D. Landau and E. M. Lifshitz, Gostekhizdat, Статистическая физика (Statistical Physics), 1951.

[2] I. R. Krichevskiĭ and N. E. Khazanova, J. Phys. Chem. (U.S.S.R.) **29**, 1087 (1955).

[3] H. W. Habgood and W. G. Schneider, Canad. J. Chem. **32**, 98, 164 (1954).

[4] M. A. Weinberger and W. G. Schneider, Canad. J. Chem. **30**, 422 (1952).

[5] S. G. Whiteway and S. G. Mason, Canad. J. Chem. **31**, 569 (1953).

Translated by R. Berman
216

THE ANISOTROPY OF THE ENERGY GAP IN TIN IN THE BASAL PLANE OF THE CRYSTAL

P. A. BEZUGLYĬ and A. A. GALKIN

Submitted to JETP editor, July 30, 1960

J. Exptl. Theoret. Phys. (U.S.S.R.) **39**, 1163-1164 (October, 1960)

THE study of the temperature dependence of the absorption coefficient of 70 Mc/sec longitudinal ultrasonic waves propagating in a super-conducting single crystal of tin along the [001] and [100] directions[1,2] has shown that the temperature variations of α_s/α_n are different in these directions (α_s and α_n are the electronic parts of the absorption coefficient of the ultrasonic wave in the superconducting and normal states). From this data it was concluded that the energy gap in tin is anisotropic, and the width of the gap for the [001] and [100] directions was evaluated at the absolute zero of temperature.

In the present note data are presented concerning the anisotropy of the energy gap in the plane containing the twofold axes (i.e., the basal plane) in a single crystal of tin. This data was obtained from measurements of the temperature dependence of α_s/α_n from T_c to 1° K at an ultrasonic frequency of 70 Mc/sec on tin specimens of the same purity as the tin used in the previous investigations.[1,2] The procedure followed during the investigation was as before.[2] The experimental data was treated to determine the width of the energy gap at the absolute zero of temperature in a way which has been already described.[2,3]

The width of the energy gap $2\epsilon_0$ in tin, expressed in units of kT_c at T = 0° K for various angles φ between the wave vector of the ultrasonic wave and the [100] direction, has the following values:

$\varphi^\circ = 0$	6	12	18	24	30	45
$2\epsilon_0 = 3{,}5^*$	3.7	4.0	4.3*	4.1	4.0	3.8*

(the error in the values of $2\epsilon_0$ is everywhere $\pm 0.2\, kT_c$).

We see that in the basal plane the maximum difference in the width of the gap amounts to 25%, the width of the gap being smallest for the directions [100] and [110]. It is curious that the minimum values of the gap width in the basal plane of tin are found for just those directions for which the existence of open electronic trajectories[6] has been established by galvanomagnetic studies,[4] and

by measurements of the absorption coefficient of ultrasonic waves in a magnetic field.[5]

Of interest in this connection is the study of the anisotropy of the energy gap in indium, which, according to the galvanomagnetic measurements of Borovik and Volotskaya,[7] is a metal with a closed Fermi surface.[6]

It should be mentioned, in conclusion, that the gap widths in the basal plane of single crystal tin obtained by other investigators[3,8] (indicated in the table above by asterisks), agree well with the values given in the present note.

[1] Bezuglyĭ, Galkin, and Korolyuk, JETP **36**, 1951 (1959), Soviet Phys. JETP **9**, 1388 (1959).

[2] Bezuglyĭ, Galkin, and Korolyuk, JETP **39**, 7 (1960), Soviet Phys. JETP **12**, 4 (1961).

[3] Morse, Olsen, and Gavenda, Phys. Rev. Letters **3**, 15 (1959).

[4] N. E. Alekseevskiĭ and Yu. P. Gaĭdukov, JETP **36**, 447 (1959), Soviet Phys. JETP **9**, 311 (1959).

[5] Galkin, Kaner, and Korolyuk, Doklady Akad. Nauk SSSR **134**, 74 (1960), Soviet Phys.-Doklady, in press.

[6] Lifshits, Azbel', and Kaganov, JETP **31**, 63 (1956), Soviet Phys. JETP **4**, 41 (1957).

[7] E. S. Borovik and V. G. Volotskaya, JETP **38**, 261 (1960), Soviet Phys. JETP **11**, 189 (1960).

[8] Morse, Olsen, and Gavenda, Phys. Rev. Letters **3**, 193 (1959).

Translated by K. F. Hulme
217

POLYMORPHIC TRANSFORMATIONS OF LITHIUM, SODIUM, AND POTASSIUM IN FILMS CONDENSED ON A COLD SUBSTRATE

B. G. LAZAREV, E. E. SEMENENKO, and A. I. SUDOVTSOV

Khar'kov Physico-Technical Institute, Academy of Sciences, U.S.S.R.

Submitted to JETP editor August 10, 1960

J. Exptl. Theoret. Phys. (U.S.S.R.) **39**, 1165-1166 (October, 1960)

As is known, low-temperature polymorphism is found in the alkali metal group. Thus, according to the data existing in the literature, lithium and sodium exist in three modifications. Here, for lithium the temperature of one of the transitions is 143 — 167° K,[1,2] and of the other, 70 — 74° K.[3,4] The corresponding transformations occur in sodium at temperatures of 73 — 88° K,[2] and at 40° K.[4]

One of the effective methods of study of these transformations has been the method of low-temperature deformation of the metal in a strongly supercooled state. Plastic deformation of lithium and sodium at liquid-helium temperature leads to practically complete transformation to the stable modification; in the deformation diagram this transformation is manifested as a sharp break in the stress-strain curve. Certain irregularities in this curve have led the authors of the cited papers[1,2] to a discussion of the possibility of similar transformations in the other alkali metals. However, according to the data of Barrett,[4] potassium exists in only one modification throughout the entire temperature range.

Another method sensitive to structural transformations is also used to detect low-temperature polymorphism in metals. This is the study of the peculiarities of the temperature-dependence of the electrical resistance R of metallic films obtained by condensation on a surface chilled to very low temperatures. The existence has been shown by this method, for example, of two modifications of bismuth[5,6] and of iron,* and three modifications of beryllium (according to our latest data) and of gallium.[6] The same method has been applied in the present study to the low-temperature polymorphism of the alkali metals, lithium, sodium, and potassium. The films were deposited by condensation at 4.2° K on a glass substrate, and their electrical resistance was measured as a function of temperature on warming to 200 — 300° K.

Breaks in the R(T) curve are observed, apparently giving evidence of the existence of three modifications in each of these alkali metals. One of the curves of this temperature-dependence is given in the figure for potassium. In fact, there is a sharp break in the curve for the temperature-dependence of the electrical resistance of lithium films at 160 — 170° K. The data on the transition in lithium (143 — 167° K) obtained by plastic deformation[1,2] are very close to these values. For sodium, the break in the curve occurs at ~80° K, corresponding to the transformation temperature in the mechanical experiments.[2] For potassium, the polymorphic transformation is manifested as a sharp break in the electrical resistance in the heating curve of the films at ~ 55 — 78° K.†

We observe further breaks in the heating curves R(T) at lower temperatures, at 80° K and 40° K

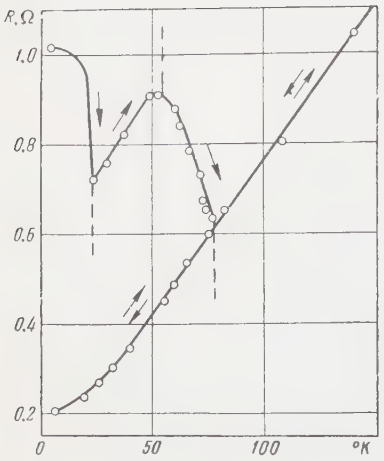

Curve of the temperature-dependence of the electrical resistance of a potassium film (the dotted lines indicate the polymorphic transformations).

for lithium and sodium, respectively. These values are close to the observed transformation temperatures of these metals: lithium at 74° K,[3] and sodium at 40° K.[4] The low-temperature transition for potassium may be seen on the R(T) curve for the films at ~20° K.

However, we may note that the low-temperature breaks in the curves may reflect to a considerable degree the readjustment of the crystal structures, which are initially formed under highly non-equilibrium conditions, since plastic deformation of metals at very low temperatures sharply lowers the temperature for structural readjustment.[8,9]

Thus the existence of polymorphic transitions in lithium and sodium has been confirmed, and a low-temperature transition in potassium has been discovered. As was proposed previously,[2] the polymorphic-transition temperatures of the studied metals have turned out to decrease with decreasing Debye temperature.

*There are other data also on the polymorphism of iron in the literature.[7]

†An anomaly in the plastic properties of potassium is observed in the range 64–20°K.[3]

[1] Gindin, Lazarev, Starodubov, and Khotkevich, JETP **35**, 802 (1958), Soviet Phys. JETP **8**, 556 (1959).

[2] Gindin, Lazarev, Starodubov, and Khotkevich, Collected Volume of Articles for the Jubilee of N. N. Davidenkov, "Некоторые проблемы прочности твердого тела" (Certain Problems of the Strength of Solids), U.S.S.R. Academy of Sciences, 1959.

[3] Gindin, Lazarev, and Starodubov, Физика металлов и металловедение (Physics of Metals and Metallography) (1960), in press.

[4] C. S. Barrett, Acta Cryst. 9, 671 (1956).

[5] H. V. Zavaritskiĭ, Dokl. Akad. Nauk SSSR **86**, 687 (1952).

[6] W. Buckel and R. Hilsch, Z. Physik **138**, 109 (1954); W. Buckel, ibid. 136 (1954).

[7] Mikhaĭlov, Nikulin, Reĭnov, and Smirnov, J. Tech. Phys. (U.S.S.R.) **29**, 931 (1959), Soviet Phys.-Tech. Phys. **4**, 844 (1960).

[8] Garber, Gindin, Kogan, and Lazarev, Dokl. Akad. Nauk SSSR **110**, 64 (1956).

[9] Garber, Gindin, Lazarev, and Starodubov, Физика твердого тела **6**, 1096 (1960), Soviet Phys.-Solid State **2**, 991 (1960).

Translated by M. V. King
218

EXPERIMENTS WITH NEUTRINOS EMITTED BY MESONS

B. PONTECORVO

Joint Institute for Nuclear Research

Submitted to JETP editor August 13, 1960

J. Exptl. Theoret. Phys. (U.S.S.R.) **39**, 1166-1167 (October, 1960)

THE possible use of high-energy neutrino beams emitted by mesons has widely been considered recently for obtaining information about the weak interactions.[1-5] Lee and Yang[3] and Cabbibo and Gatto[4] have shown that the formfactors induced by the presence of strongly interacting particles prevent further increase of the cross section with energy for reactions of the type $\bar{\nu} + p \rightarrow e^+ + n$ when the neutrino energy reaches the 1-Bev region.

The problem of the existence of an intermediate meson (B) in the weak interactions has a special place in discussions of high-energy ($\gtrsim 1$ Bev) neutrino experiments. Such experiments may turn out to be feasible at the present time. In fact, R. M. Ryndin and the author[6] and also Lee and Yang[3] have shown that an intermediate boson with mass equal to a few nucleon masses can be detected in the reaction

$$\nu + Z \rightarrow B + Z + \begin{cases} \mu \\ e \end{cases}.$$

The cross section of this reaction exceeds by several orders the typical cross section of reactions induced by neutrinos in the case of strictly localized interaction.

To check the identity of the neutrinos emitted in π-μ decay (ν_μ) and those emitted in β decay (ν_e) it was proposed in reference 1 to use $\bar{\nu}_\mu$ radiation with relatively low energy from stopped μ^+ mesons. Below we consider, in addition, neutrinos of intermediate energies (< 300 Mev) for

the solution of some questions of neutrino physics. These considerations may be useful in planning neutrino experiments, and in designing accelerators to perform such experiments.

Apart from the problem of the B meson and of the energy-dependence of cross sections for weak processes, for the solution of which very high-energy neutrinos are evidently necessary, the fundamental qualitative questions of neutrino physics are the following: (1) are the ν_e and ν_μ identical particles? (2) does neutrino scattering by electrons occur as a first-order process in the weak interaction constant?

For experimental solution of these problems, neutrinos with intermediate energies present definite advantages. Not only can their intensity (for a number of reasons) appreciably exceed the intensity of high-energy neutrinos, but they can also be easily obtained with very well-defined energy, so that one can interpret the induced events kinematically.

Sources of monoenergetic neutrinos may be obtained by stopping π^+, K^+, and μ^- in matter:*

Neutrino source	Neutrino energy (Mev)
$\pi^+ \to \mu^+ + \nu_\mu$	29.8
$K^+ \to \mu^+ + \nu_\mu$	235.7
$\mu^- + Z \to \nu_\mu + \ldots$	~ 100

One should note that monoenergetic ν_μ, rather than $\bar{\nu}_\mu$, are obtained when protons with energy $\gtrsim 1$ Bev are stopped in a block of heavy matter. Stopping of secondary particles in the same block provides, according to the table above, neutrinos with known energy in a rather well localized region. These monoenergetic neutrinos are, of course, accompanied by a continuous-background spectrum, particularly of ν_e and $\bar{\nu}_\mu$ from μ^+ meson decay.[1]

For example, to test the identity of ν_e and ν_μ one can measure the cross section of the reaction $\nu_\mu + C^{12} \to e^- + N^{12}$. The energy of the electrons emitted by the incident monoenergetic ν_μ's is known; the time of emission of the electrons must coincide with the time of absorption of the neutrino (modern electronic circuitry permits use of the time characteristics of the accelerator, including the cyclotron with a spatial variation of the magnetic field); it is necessary here to record the delayed positrons from N^{12} decay. Such an experiment can be performed with a large propane "magnetic" bubble chamber, or with electronic particle-counting methods. The counting rate in experiments of this type is comparable to that expected for the experiments proposed in reference 1.

*The possibility of using a K-capture radioelement as a strong source of monoenergetic ν_e(E ~ 1 Mev) is beyond the scope of this note. This possibility is attractive for experiments on ν_e–e scattering, under conditions in which the scattering events can be kinematically analyzed. Here we wish to mention also the possibility that astrophysical effects which are connected with ν_e–e scattering may help to solve the problem of the existence of these processes.

[1] B. Pontecorvo, JETP 37, 1751 (1959), Soviet Phys. JETP **10**, 1236 (1960), and Ninth International Conference of High-Energy Physics, Kiev, 1959.

[2] M. Schwartz, Phys. Rev. Letters **4**, 306, (1960).

[3] T. D. Lee and C. N. Yang, Phys. Rev. Letters **4**, 307 (1960).

[4] N. Cabibbo and R. Gatto, Nuovo cimento **15**, 304 (1960).

[5] M. A. Markow, Hyperonen und K-Mesonen, Verlag der Wissenschaften, Berlin, 1960.

[6] B. Pontecorvo and R. Ryndin, Ninth International Conference of High-Energy Physics, Kiev, 1959. Discussion of the report of A. I. Alikhanov. See also the report of R. Marshak.

[7] B. Pontecorvo, JETP **36**, 1615 (1959), Soviet Phys. JETP **9**, 1148 (1959). G. M. Gandel'man and V. S. Pinaev, JETP **37**, 1072 (1959), Soviet Phys. JETP **10**, 764 (1960). Hong Yee Chin, Preprint, Institute for Advanced Study, Princeton, 1960.

Translated by D. Brill
219

INTENSITY OF NONRADIATIVE TRANSITIONS IN MU-MESIC ATOMS

M. Ya. BALATS, L. N. KONDRAT'EV, L. G. LANDSBERG, P. I. LEBEDEV, B. V. OBUKHOV, and B. PONTECORVO

Joint Institute for Nuclear Research; Institute of Theoretical and Experimental Physics, Academy of Sciences, U.S.S.R.

Submitted to JETP editor August 13, 1960

J. Exptl. Theoret. Phys. (U.S.S.R.) **39**, 1168-1170 (October, 1960)

WE have observed earlier[1] that the intensity of the 2P — 1S mesic x radiation in U^{238}, normalized for one stopped muon, is considerably smaller in U^{238} than in lead. This indicates the existence in heavy mesic atoms of "nonradiative transitions,"

at which the energy of the 2P — 1S transition is not released in the form of one x-ray photon. Assuming that the probability of the nonradiative transition (W_n) in mesic lead is negligibly small compared with the probability ($W_{h\nu}$) of emitting a single photon [$(W_{h\nu})_{Pb} = 1$], we found that

$$1 > (W_n)_{U^{238}}/(W_{h\nu})_{U^{238}} > 0.1.$$

In the present note we report our systematic investigations of the intensities of the 2P — 1S transitions in mesic atoms of lead, bismuth, sodium, U^{235} and U^{238}. The principal scheme of the experiment is analogous to that already used: a scintillation spectrometer, triggered by the negative muons stopped in the investigated sample, is used to measure the spectrum of the x rays in the energy range corresponding to the given transition.

Compared with the preceding investigation, particular attention was paid to a determination of the background level, i.e., the count of the NaI gamma detector of amplitude close to that due to the 2P — 1S transitions, but not actually caused by these transitions. The intensity of this background was greatly reduced by means of a Cerenkov gas-filled threshold counter, which eliminated almost all the electrons in the meson beam. The number of pions in the beam was also reduced by a factor of several times relative to the number of muons. In addition, the background due to other transitions (essentially 3D — 2P) of the investigated mesic atom in the region of the pulse amplitudes corresponding to the transitions 2P — 1S, was measured in special experiments, in which samples of molybdenum and cadmium were used. These were used essentially to measure the shape of the line of the 3D — 2P transitions of the investigated mesic atoms.

Examples of the plotted spectra are shown in Figs. 1 and 2. The table lists the intensities of the 2P — 1S mesic x radiation normalized to a single stopped negative muon, in relative units. Account is taken here of different corrections for the fact

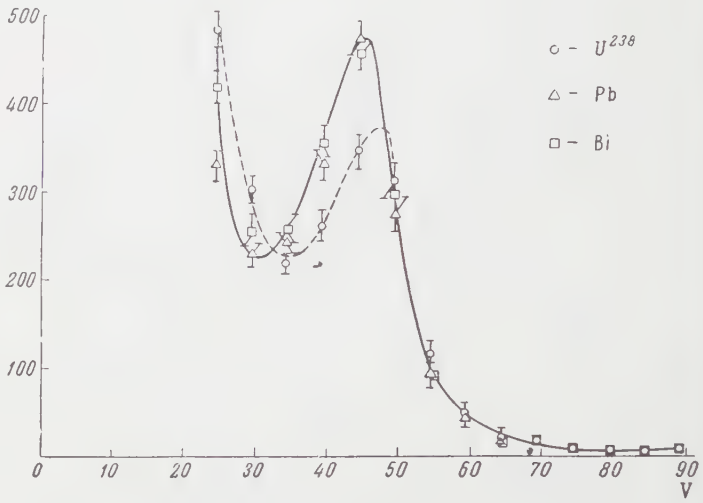

FIG. 1. Spectra of mesic x-ray photons from a lead target (4.46 g/cm²), bismuth (4.46 g/cm²), and U^{238} (4.60 g/cm²) targets. The abscissas represent the amplitude of the pulse in volts. The ordinates represent the number of pulses within a 5-volt interval. The curves are normalized to an equal number of muons stopped in the target. The spectra of lead and bismuth are indistinguishable.

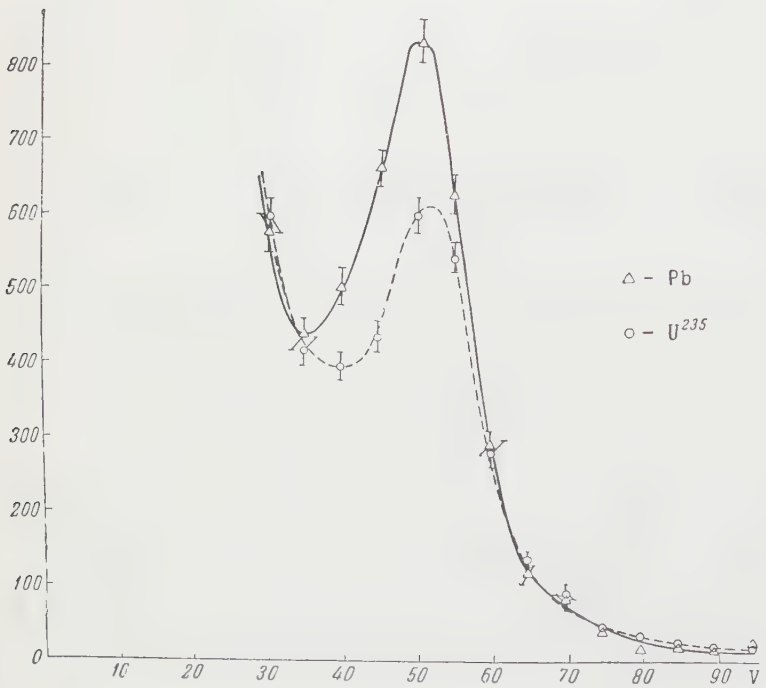

FIG. 2. The same as Figure 1, for a lead (5.56 g/cm²) and U^{235} (5.59 g/cm²) targets.

	Intensity of mesic x-ray 2P-1S radiation	Fraction of nonradiative 2P-1S transitions
Pb	1	—
Bi	1±0.06	0±0.06
Th	0.85±0.07	0.15±0.07
U_{235}	0.71±0.05	0.29±0.05
U_{238}	0.77±0.04	0.23±0.04

that the different targets were equivalent as regards the muon ionization losses, and consequently differed somewhat from the point of view of photon absorption (different photon energies and different Z).

The table shows that the intensities of the investigated transitions are the same in lead and in bismuth. This is apparently caused by the fact that both in lead and in bismuth the density of the nuclear levels is anomalously small at excitation near 6 Mev, and therefore the fraction of nonradiative transitions in these mesic atoms is almost equal to zero. In the other nuclei we can note the effect of nonradiative transitions.

As a result of the excitation of nuclei by 2P — 1S transitions, we expect a priori: 1) fission, 2) disintegration with emission of a single neutron, and 3) return of the nucleus to the ground state with emission of gamma quanta (a phenomenon analogous to Raman scattering in optics). Apparently, nonradiative fission has low probability, owing to the Coulomb field of the negative muon. Emission of a neutron is impossible for thorium from energy considerations. The neutron photoproduction threshold in U^{235} is much lower than in U^{238} (the thresholds for the emission of photoneutrons are 6.34 ± 0.04, 5.97 ± 0.10, and ~ 5.1 Mev for thorium, U^{238}, and U^{235} respectively, while the 2P — 1S transition energies are close to 6 Mev in all the investigated mesic atoms).

The fact that the intensities of the nonradiative 2P — 1S transitions in U^{238} and U^{235} differ by relatively little suggests that an important role is played in "nonradiative transitions" by mechanism 3 (the "combination" mechanism).

[1] Balats, Kondrat'ev, Landsberg, Lebedev, Obukhov, and Pontecorvo, JETP **37**, 1715 (1960), Soviet Phys. JETP **11**, 1239 (1960).

Translated by J. G. Adashko
220

ON THE PROBABILITY OF MESON CAPTURE IN DIFFERENT MESO-ATOMIC LEVELS

S. S. GERSHTEĬN

Joint Institute of Nuclear Research

Submitted to JETP editor August 16, 1960

J. Exptl. Theoret. Phys. (U.S.S.R.) **39**, 1170-1172 (October, 1960)

THE determination of the probability of capture of negative mesons in different levels of mesic atoms and the investigation of the subsequent transitions to the ground state are very important for the interpretation of the data on the interaction of negative mesons with nuclei. In particular, the initial distribution over the meso-atomic levels determines the average number of Auger electrons observed in the capture of negative mesons in photoplates.[1] Of special interest is the distribution over the levels of the mesic atoms of hydrogen, since it can, apparently, have a considerable effect on the capture of π and K mesons from high orbits[2] and can also determine the time elapsing between the slowing-down of the π mesons and the nuclear reaction[3] and the characteristics of the capture of π and K mesons by nuclei with $Z > 1$.[4]

The probability for the capture of negative mesons in atomic hydrogen was computed recently by Baker.[5] However, the results of Baker, which were obtained in Born approximation, are completely useless for the most interesting case: the capture of mesons slowed down to velocities considerably smaller than the velocity of the atomic electron.

Nevertheless, the probability of capture of slow negative mesons by atomic hydrogen can be easily computed by considering that for distances less than $R_0 \simeq 0.64\, a_e$ ($a_e = \hbar^2/m_e e^2$) between the meson and the proton there exists no bound state for the electron,[6,7] so that the electron makes an adiabatic transition to the continuous spectrum as the meson comes as close to the proton as the distance R_0. This leads to great ionization losses of the mesons up to energies equal to the ionization potential of hydrogen, I, and for energies $\epsilon < I$ to capture in a close-lying meso-atomic level. Since the energy losses for adiabatic ionization are multiples of I and the spectrum of the incident mesons is practically constant over energy intervals of the order I, we may assume that the energy distribution of the slowed-down mesons is

constant in the interval $0 < \epsilon < I$. The probability for the capture of the mesons in levels with $n > n_0 = (\mu/m_e)^{1/2}$ is then

$$f(n) \sim n^{-3}. \quad (1)$$

If we regard the motion of the meson as classical, we see easily that the distribution over l will be proportional to ldl. The maximal value of I is determined from the condition that a meson with energy ϵ reaches the distance R_0 in the presence of the centrifugal barrier $\hbar^2 l^2/2\mu R^2$:

$$\hbar^2 l^2/2\mu R_0^2 - e^2/R_0 \leqslant \varepsilon - I, \quad (2)$$

so that

$$l_{max} = n_0 \{1.28 [1 - 0.32 (n_0/n)^2]\}^{1/2} \simeq n_0. \quad (3)$$

In the capture in levels with large n the angular momenta are therefore not bounded by the condition $l < n - 1$, but by condition (3). The cross section for capture in levels with $n < n_0$ is smaller than the cross section corresponding to (3) approximately by the factor $(m_e/\mu)^2$ (reference 5).

The large capture cross sections connected with the adiabatic ionization can, of course, be observed not only for hydrogen, but also for any element Z, if the element $(Z - 1)$ does not form negative ions. In particular, these considerations can, for example, explain why the capture probability for Li in the compound LiF is considerably smaller than for F.[8] Indeed, F in the compound LiF represents a negative ion, and the extra electron cannot be retained by the screened nucleus as the negative meson approaches. Thus adiabatic ionization must occur. It is clear that the presence of the neighboring Li atoms, or of the other hydrogen atom in the H_2 molecule, may cause the electron forced out of one atom to go over to another atom during the time of collision, from where it then returns to the first atom after the meson has receded to a sufficiently large distance. In this case the meson does not lose its energy, and the above considerations are therefore not entirely convincing. If the atom $(Z - 1)$ forms a negative ion, it is known that adiabatic ionization will not occur during the capture of mesons by the atom Z. In this case a slow meson ($v < v_0$, where v_0 is the velocity of the atomic electrons) can cause ionization only if it is accelerated by the nuclear Coulomb field to such a degree that the perturbation which it applies to the electrons contains frequencies of the order of the frequency of the transition to the continuous spectrum. A simple estimate on the basis of the Massey criterion shows that meson capture occurs most effectively for $l \sim (\mu/m_e)^{1/3}$ and becomes rapidly less probable for large l. The effective values of l for μ mesons are $l = 6$ to 7. The calculations of Borde[1] show that the assumption that the μ mesons are captured with $l = 7$ (as opposed to the usually accepted $(2l + 1)$ distribution) leads to good agreement with the experimentally observed number of Auger electrons.

In conclusion I express my deep gratitude to Academican L. D. Landau and Ya. A. Smorodinskiĭ for valuable comments, and also to T. E. Belovitskiĭ for a discussion of the experimental data.

[1] A. H. de Borde, Proc. Phys. Soc. **A67**, 57 (1954).

[2] Day, Snow, and Sucher, Phys. Rev. Lett. **3**, 61 (1959); and **118**, 864 (1960).

[3] T. Fields et al., Bull. Am. Phys. Soc. **4**, 402 (1959); J. E. Russel and G. L. Shaw, Phys. Rev. Lett. **4**, 369 (1960).

[4] Panofsky, Aamodt, and Hadley, Phys. Rev. **81**, 565 (1951); W. H. Barkas et al., Phys. Rev. **112**, 622 (1958).

[5] G. A. Baker, Phys. Rev. **117**, 1130 (1960).

[6] E. Fermi and E. Teller, Phys. Rev. **72**, 399 (1947).

[7] A. S. Wightman, Phys. Rev. **77**, 521 (1950).

[8] M. B. Stearns and M. Stearns, Phys. Rev. **105**, 1573 (1957).

Translated by R. Lipperheide
221

MAGNETIC CHANGE IN RESISTIVITY OF FERROMAGNETS ABOVE THE CURIE POINT

I. K. KIKOIN, N. A. BABUSHKINA, and T. N. IGOSHEVA

Submitted to JETP editor August 20, 1960

J. Exptl. Theoret. Phys. (U.S.S.R.) **39**, 1172-1174 (October, 1960)

THE aim of this work is to determine the relation between the change of electrical resistivity in a magnetic field and the magnetic susceptibility of ferromagnets above the Curie point. This question arises because the corresponding relation has been determined for the Hall effect in ferromagnets above the Curie point.[1,2] It was shown that in the paramagnetic state, as in the ferromagnetic state,

the Hall emf contains a term proportional to the magnetization $\sigma = \kappa H$ (κ is the magnetic susceptibility of the specimen and H is the strength of the external magnetic field).

A chromium-tellurium alloy was chosen, having a sufficiently low Curie temperature $\Theta \approx 50°$ C and a paramagnetic susceptibility varying with temperature according to the Curie-Weiss law $\kappa = c/(T - \Theta_p)$ with $\Theta_p = 86°$ C[2].

The temperature dependence of $\Delta r/r$ is shown in Fig. 1 for this alloy (r is the resistivity in the absence of a field and Δr is the change in resistivity produced by the field). The change in resistivity was found to be negative over the whole temperature range studied, although one might have expected that it would have become positive far from the Curie point, as in normal non-ferromagnetic metals.

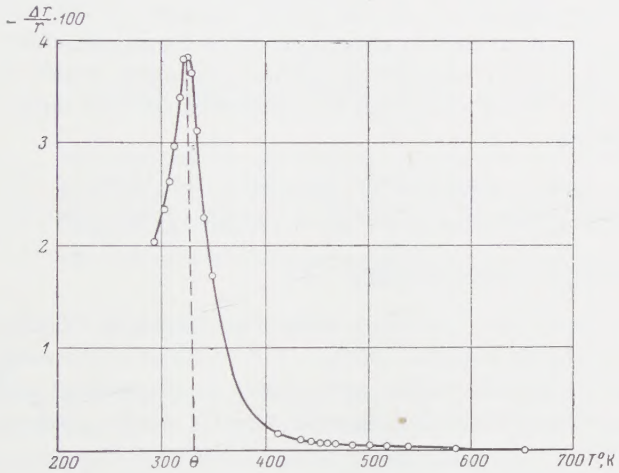

FIG. 1

Figure 2 shows the relation between the values of $\Delta r/r$ measured for the Cr-Te alloy and the square of the magnetic susceptibility κ^2 at the corresponding temperature. Over the temperature range studied, this dependence is linear.

In addition, $\Delta r/r$ varies as the square of the field at a given temperature. This indicates that the magnetic change in resistivity in the paramagnetic state is connected with the magnetization by the relation

$$-\Delta r/r = a(\varkappa H)^2 = a\sigma^2. \qquad (1)$$

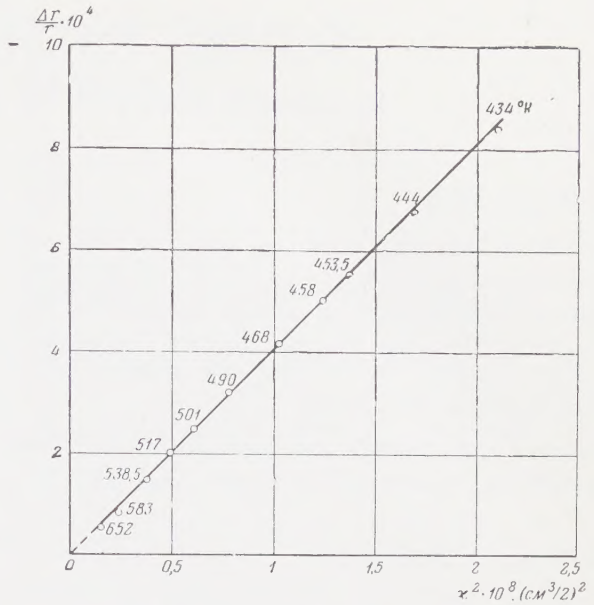

FIG. 2

Preliminary measurements made on the same specimen below the Curie point showed that the magnetic change in resistivity in a transverse field follows the well known relation[3]

$$-\Delta r/r = b(\sigma^2 - \sigma_s^2), \qquad (2)$$

where σ is the resultant magnetization, σ_S is the spontaneous magnetization, and b is a constant almost independent of temperature.

If we put $\sigma_S = 0$ above the Curie point, the results show that the relation between the magnetic change of resistivity and the magnetization remains the same in the ferromagnetic and paramagnetic states of the specimen. It is remarkable that the coefficients a and b in Eqs. (1) and (2) agree to within 20%.

[1] I. K. Kikoin, JETP 10, 1242 (1940).

[2] Kikoin, Buryak, and Muromkin, Dokl. Akad. Nauk SSSR 125, 1011 (1959), Soviet Phys.-Doklady 4, 386 (1959).

[3] E. Englert, Z. Phys. 74, 748 (1932).

Translated by R. Berman
222

SOVIET PHYSICS JOURNALS

Published in English by the American Institute of Physics

Soviet Physics—JETP

A translation, beginning with 1955 issues of "Zhurnal Eksperimental'noi i Teoreticheskoi Fiziki" of the USSR Academy of Sciences. Leading physics journal of Soviet Union. Similar to "The Physical Review" in quality and range of topics. Outstanding new work is most likely to appear in this journal.

Twelve issues, approximately 4000 pages. $75 domestic, $79 foreign. Libraries $35 domestic, $39 foreign. Single copies, $8.*

Soviet Physics—SOLID STATE

A translation, beginning with 1959 issues of "Fizika Tverdogo Tela" of the USSR Academy of Sciences. Offering results of theoretical and experimental investigations in the physics of semiconductors, dielectrics, and on applied physics associated with these problems. Also publishes papers on electronic processes taking place in the interior and on the surface of solids.

Twelve issues, approximately 2000 pages. $55 domestic, $59 foreign. Libraries $25 domestic, $29 foreign. Single copies, $8.*

Soviet Physics—TECHNICAL PHYSICS

A translation, beginning with 1956 issues of "Zhurnal Tekhnicheskoi Fiziki" of the USSR Academy of Sciences. Contains work on plasma physics and magnetohydrodynamics, aerodynamics, ion and electron optics, and radio physics. Also publishes articles in mathematical physics, the physics of accelerators, and molecular physics.

Twelve issues, approximately 2000 pages, $55 domestic, $59 foreign. Libraries $25 domestic, $29 foreign. Single copies, $8.*

Soviet Physics—ACOUSTICS

A translation, beginning with 1955 issues of "Akusticheskii Zhurnal" of the USSR Academy of Sciences. Devoted principally to physical acoustics but includes electro-, bio-, and psychoacoustics. Mathematical and experimental work with emphasis on pure research.

Four issues, approximately 500 pages. $12 domestic, $14 foreign. (No library discounts.) Single copies, $4.

Soviet Physics—DOKLADY

A translation, beginning with 1956 issues of the physics sections of "Doklady Akademii Nauk SSSR," the proceedings of the USSR Academy of Sciences. All-science journal offering four-page reports of recent research in physics and borderline subjects.

Six issues, approximately 1500 pages. $35 domestic, $38 foreign. Libraries $15 domestic, $18 foreign. Single copies Vols. 1 and 2, $5; Vol. 3 and later issues, $7.*

Soviet Physics—CRYSTALLOGRAPHY

A translation, beginning with 1957 issues of the journal "Kristallografiya" of the USSR Academy of Sciences Experimental and theoretical papers on crystal structure, lattice theory, diffraction studies, and other topics of interest to crystallographers, mineralogists, and metallurgists.

Six issues, approximately 1000 pages. $25 domestic, $27 foreign. Libraries $10 domestic, $12 foreign. Single copies, $5.*

SOVIET ASTRONOMY—AJ

A translation, beginning with 1957 issues of "Astronomicheskii Zhurnal" of the USSR Academy of Sciences. Covers various problems of interest to astronomers and astrophysicists including solar activity, stellar studies, spectroscopic investigations of radio astronomy.

Six issues, approximately 1100 pages. $25 domestic, $27 foreign. Libraries $10 domestic, $12 foreign. Single copies, $5.*

Soviet Physics—USPEKHI

A translation, beginning with September, 1958, issue of "Uspekhi Fizicheskikh Nauk" of the USSR Academy of Sciences. Offers reviews of recent developments comparable in scope and treatment to those carried in "Reviews of Modern Physics." Also contains reports on scientific meetings within the Soviet Union, book reviews, and personalia.

Six issues, approximately 1700 pages. (Contents limited to material from Soviet sources.) $45 domestic, $48 foreign. Libraries $20 domestic, $23 foreign. Single copies $9.*

*For libraries of nonprofit academic institutions.
Subscription prices subject to annual variation, depending on size of Russian originals.

Please send orders and inquiries to

American Institute of Physics

335 East 45 Street, New York 17, N.Y.